CHEMICAL REACTION and REACTOR DESIGN



Edited by

Hiroo Tominaga and Masakazu Tamaki

Chief Editor

Hiroo Tominaga Professor Emeritus

University of Tokyo

Masakazu Tamaki Chairman

Chiyoda Corporation

Editors

This edition was produced by the following editors from Chiyoda.

Yasuo Morimura

Munekazu Nakamura

Hideki Hashimoto

Yoshimi Shiroto

Koji Watanabe

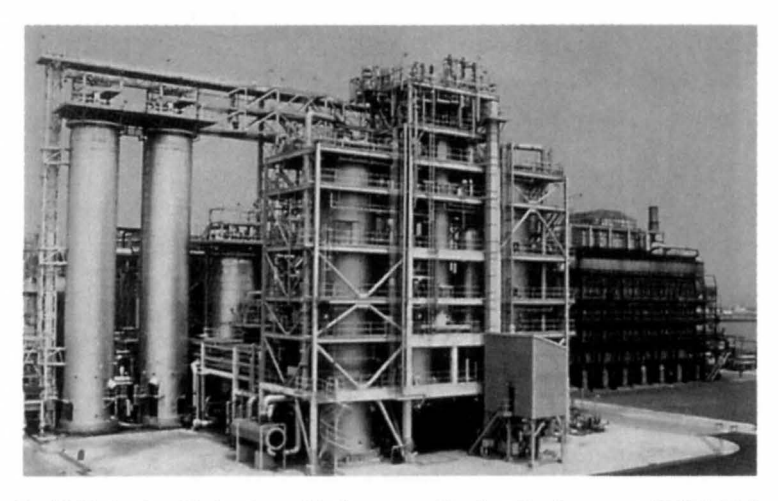
Masato Tauchi

Takafumi Kuriyama

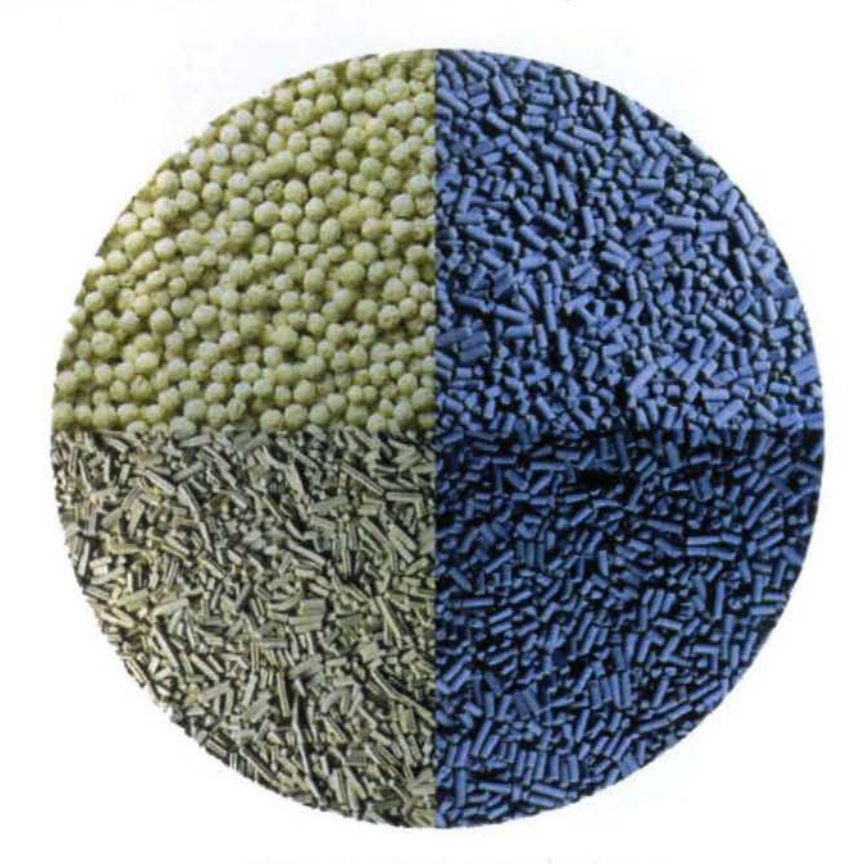
Akio Shindo



Resid Fluid Catalytic Cracking (RFCC) Unit (By courtesy of Tohoku Oil Co., Ltd. Licenced by The M.W. Kellog Company)



Resid Hydrodesulfurization with Onstream Catalyst Replacement (OCR) Unit (By courtesy of Idemitu Kosan Co., Ltd. Licenced by Chevron Products Company – Technology Marketing)



Catalysts for Hydroprocessing (By courtesy of Nippon Ketjen Co., Ltd.)



Industrial Catalyst Types
(By courtesy of Sued Chemie AG & Nissan Girdler Catalyst Co., Ltd.)

Chemical Reaction and Reactor Design

Edited by

HIROO TOMINAGA

Professor Emeritus, University of Tokyo, Japan

and

MASAKAZU TAMAKI

Chairman, Chiyoda Corporation, Yokohama, Japan

JOHN WILEY & SONS

 $Chichester \cdot New\ York \cdot Weinheim \cdot Brisbane \cdot Singapore \cdot Toronto$

Authorized Translation from Japanese language edition published by Maruzen Co., Ltd. Tokyo

Copyright © 1997 John Wiley & Sons, Ltd.

Baffins Lane, Chichester,

West Sussex PO19 1UD, England

National 01243 779777
International (+44) 1243 779777
e-mail (for orders and customer service enquiries): cs-books@wiley.co.uk
Visit our Home Page on http://www.wiley.co.uk
or http://www.wiley.com

All Rights Reserved. No part of this book may be reproduced, stored in a retrieval system, or transmitted, in any form or by any means, electronic, mechanical, photocopying, recording or otherwise, except under the terms of the Copyright, Designs and Patents Act 1988 or under the terms of a licence issued by the Copyright Licensing Agency, 90 Tottenham Court Road, London, UK WIP 9HE, UK, without the permission in writing of the Publisher. Published under the Co-publishing Agreement between Wiley and Maruzen, the English translation published by John Wiley and Sons Ltd, Chichester.

Other Wiley Editorial Offices

John Wiley & Sons, Inc., 605 Third Avenue, New York, NY 10158-0012, USA

VCH Verlagsgesellschaft mbH, Pappelallee 3, D-69469 Weinheim, Germany

Jacaranda Wiley Ltd, 33 Park Road, Milton, Queensland 4064, Australia

John Wiley & Sons (Asia) Pte Ltd, 2 Clementi Loop #02-01, Jin Xing Distripark, Singapore 129809

John Wiley & Sons (Canada) Ltd, 22 Worcester Road, Rexdale, Ontario M9W 1LI, Canada

British Library Cataloguing in Publication Data

A catalogue record for this book is available from the British Library

ISBN 0-471-97792-6

Typeset by Dobbie Typesetting Limited, Tavistock, Devon Printed and bound by Antony Rowe Ltd. Eastbourne

Contents

Pref			
	_	Chemical Reactions and Design of Chemical Reactors	1
1.1		luction	
1.2		the and Engineering for Reactor Design	_
1.3		y of Chemical Reaction	
1.4			3
1.5			8
1	1.5.1	Naphtha Cracking	
	1.5.2	Tubular Steam Reforming	
	1.5.3		1
	1.5.4		2
	1.5.5		3
	1.5.6	Flue Gas Desulphurization	4
	-	Equilibrium and Reaction Rate	7
піге	osni Koi	· · · · · · · · · · · · · · · · · · ·	
2.1	Natur		7
	2.1.1		7
	2.1.2		8
	2.1.3		9
2.2		1	1
	2.2.1		1
	2.2.2		2
	2.2.3		4
	2.2.4	-1	:5
	2.2.5	Operating Conditions and Energy Efficiency of Chemical Reactions	26

2.3	The R	Rate of Reaction	28
	2.3.1		30
2.4	Comp	olex Reaction System	36
	2.4.1		36
	2.4.2		
	2.4.3	Relations with Other Transfer Processes	38
Cha	pter 3	Fundamentals of Heat and Mass Transfer	
Koi	chi Asar	no	39
3.1	Rate	Equations	39
		Conduction of Heat	39
	3.1.2		40
	3.1.3		42
3.2		and Heat Transfer Coefficients	43
J. L	3.2.1		43
	3.2.2		44
	3.2.3		48
	3.2.4		
3.3		and Mass Transfer in a Laminar Boundary Layer	
5.5		ng a Flat Plate	49
	3.3.1	Governing Equations of Heat and Mass Transfer	
	3.3.2	Physical Interpretation of the Dimensionless Groups	• ,
	5.5.2	used in Heat and Mass Transfer Correlation	50
	3.3.3	Similarity Transformation	
	3.3.4	Numerical Solutions for Heat and Mass Transfer	
	3.3.5	High Mass Flux Effect	
3.4		Transfer inside a Circular Tube in Laminar Flow	
5.4	3.4.1	Heat Transfer inside a Circular Tube with	50
	5.1.1	Uniform Velocity Profile	57
	3.4.2	Heat Transfer inside a Circular Tube with	51
	3.1.2	Parabolic Velocity Profile (Graetz problem)	58
3.5	Mass	Transfer of Bubbles, Drops and Particles	
0.0	3.5.1	Hadamard Flow	
	3.5.2	Evaporation of a Drop in the Gas Phase	
	3.5.3	Continuous Phase Mass Transfer of Bubbles or	00
	2.2.2	Drops in the Liquid Phase	62
	3.5.4	Dispersed Phase Mass Transfer	
	3.5.5	Heat and Mass Transfer of a Group of Particles and	J.
		the Void Function	63
3.6	Radia	ant Heat Transfer	
-	3.6.1	Heat Radiation	
	3.6.2	Governing Equations of Radiant Heat Transfer	66
	5.6.2	Governing Equations of Radiant Heat Transfer	66

CONTENTS	VII

Chaj	pter 4	Fundamentals of Reactor Design	69			
4.1	or Types and Their Applications					
	Shinte	aro Furusaki	71			
	4.1.1	Homogeneous Reactors	71			
	4.1.2		74			
4.2	Design	n of Homogeneous Reactors				
		iro Shimogaki	83			
	4.2.1	Material and Heat Balances in Reaction Systems	83			
	4.2.2	Design of Batch Stirred Tank Reactor	84			
	4.2.3	Design of Continuous Stirred Tank Reactors	91			
	4.2.4	Design of Tubular Reactors	94			
	4.2.5	Homogeneous and Heterogeneous Complex Reactions	97			
4.3	Plann	ing and Design of Multiphase Reactors				
		yuki Horio	105			
	4.3.1	Features of Planning and Design of Multiphase				
		Reaction Processes	105			
	4.3.2	Model Description of Multiphase Processes	108			
	4.3.3	Concepts of Multiphase Reaction Processes	135			
	4.3.4	Development and Scale-up of Multiphase Reactors	170			
4.4		mic Analysis of Reaction System	1,0			
7.7						
	4.4.1	Dynamics of Reactors	183 183			
	4.4.2	Stability of Reactors	185			
	4.4.3	Control of Reactors	188			
	4.4.4	Optimization of Reactor Systems	194			
-	pter 5	Design of an Industrial Reactor	211			
5.1		tha Cracking				
	Hiros	hi Yagi	213			
	5.1.1	Petrochemical Complex in Japan	213			
	5.1.2	Cracking Furnace for Naphtha	217			
	5.1.3	Treatment of a Cracked Gas	221			
	5.1.4	Quench and Heat Recovery	222			
	5.1.5	Thermodynamics of Thermal Cracking Reaction	224			
	5.1.6	Mechanism of Thermal Cracking	226			
	5.1.7	Reaction Model for Yield Estimation	230			
	5.1.8	Design Procedure of Cracking Furnace	236			
	5.1.9	Results of Thermal Cracking Simulation	239			
	5.1.10	Technology Trend of a Cracking Furnace	243			
5.2		ar Steam Reforming				
	J. R.	Rostrup-Nielsen and Lars J. Christiansen	247			
	5.2.1	The Reactions				
	5.2.2	The Tubular Reformer	252			

viii CONTENTS

	5.2.3 The Catalyst and Reaction Rate	259
		262
	5.2.5 Carbon Formation	264
		267
		269
		269
5.3	Epoxy Resin Production	
5.5		273
		273
		274
		275
		276
		279
	5.3.6 The Reaction Model	281
		282
		283
		285
		292
5.4	Hydrotreating Reactor Design	
		297
		298
		304
		310
	5.4.4 VGO Hydrotreating Catalysts	314
		317
	5.4.6 VGO Hydrotreating Reactor Design	317
		328
		331
		332
5.5	Fluid Catalytic Cracking	
		335
		339
		345
		352
	5.5.4 Practice of FCC Reactor Design	365
	The second secon	369
5.6	Wet Flue Gas Desulphurization	507
0.0		377
	5.6.1 Process Description	378
	5.6.2 Structure of JBR	380
	5.6.3 Chemical Reactions in JBR	
	5.6.4 Heat and Material Balance around the Reactor	381 388
	5.6.6 Applicable Materials for the Wet FGD Plant	391
		393
	Index	205

Preface to the English Edition

Now that the Cold War is over, the next hurdle for mankind is the wealth gap between north and south. We must cooperate with developing countries to generate sustainable development programmes that bring true prosperity while protecting the environment. The engineers in engineering firms hope that the chemical engineering skills they refine daily will contribute to international economic development and to richer lives for all mankind. We believe engineering stands alongside agriculture, commerce, and manufacturing as one of the four pillars of national strength. These four words are engraved in the pedestals of the four columns of the Albert Memorial in London, which was built in 1876 when the British Empire was at its zenith. And these four words connote the source of Britain's tremendous strength during the reign of Queen Victoria.

Chemical Reaction and Reactor Design commemorates the 50th anniversary of the foundation of the Chiyoda Corporation, and was published in Japanese by Maruzen Co., Ltd in January 1996. This book was created for colleagues in the design departments of engineering companies, and for students who hope to pursue careers in engineering. The Japanese edition immediately prompted many requests for an English version. Now, thanks to John Wiley & Sons Ltd, the English edition is available.

In the course of their daily work, chemical engineers come in contact with various reactions, catalysts, and reactors. They constantly encounter new technologies, such as residue fluidized catalytic cracking (RFCC), continuous catalyst recirculation (CCR) reforming and heat exchanger type reactors and consistently meet the challenge of using them effectively. This experience helps them to unify systems and equipment into a smoothly operating entity, achieving greater precision in design standards and more efficient design systems for better operation of reactors, separators, heat exchangers, and other hardware. Systems and equipment operate as an organic whole in petroleum refining, petrochemical processes, and environmental protection procedures, combining many individual processes at very high levels of precision. These processes are vital to industry because so many manufacturers use them. In the first four chapters, Chemical Reaction and Reactor Design deals with the fundamentals of chemical engineering. Then it gives six case studies in reaction and reactor design in Chapter 5.

We hope this book will make it possible to develop reliable reactors without relying on expensive, time-consuming tests with pilot or bench plants.

Dr Hiroo Tominaga, professor emeritus at the University of Tokyo, supervised the editing of the book and wrote the first chapter. Dr Shintaro Furusaki, a professor at the University of Tokyo, along with other authorities in the field, wrote the sections on basic theory. The sections of Chapter 5 that deal with tubular steam reforming, hydrotreating, and polymerization, were prepared in cooperation with licensors of the applicable technologies, i.e., Haldor Topsøe A/S of Denmark, Chevron Research and Technology Company of the United States, and Asahi Denka Kogyo K.K. of Japan. The other sections of Chapter 5 were written and edited by Chiyoda Corporation engineers. We wish to thank the many companies that provided invaluable assistance for this book, and Maruzen Co., Ltd and John Wiley & Sons Ltd, without whose help and cooperation it could never have been published.

I hope and believe that this English version will help the technological development of reaction engineering and reactor design worldwide and serve as a springboard to bigger and better things for individual engineers.

March 1997, Masakazu Tamaki

This book presents a wealth of knowledge on reaction kinetics and its application to chemical reactor design and operation; and intended as a text for students in technical college and graduate school, and also for scientists and engineers engaged in chemical research and development.

In the second half of the twentieth century, the chemical industry has made remarkable progress based on the developments of petroleum chemistry and polymer science, representing the innovations in both chemical process and product, respectively. Recently, a deliberate shift in paradigm from process to product innovation seems to be emphasized in the chemical industry. Since no chemical product can be manufactured without a properly designed process to produce it, the significance of process innovation should also be noted. In this connection, reactor design and its operation, which both play a key role in the chemical process, may be considered the key to chemical technology.

Perfection of chemical reactor design may be realized based upon the relevant science and engineering. The scientific approach to understanding chemical reaction kinetics and mechanism, however, is now mostly concerned with a simple reaction in order to identify the basic principles in terms of molecular dynamics. On the other hand, chemical reaction engineering aims at computations of a complex system, involving a large number of variables not only of chemistry but also of mass and heat transfer, to select the reactor type, to determine its size and to optimize its operation. There remains much, however, to be supplemented by technical know-how obtained through experience in practice, some of which will be generalized, systematized and integrated as engineering science for reactor design in future.

This book is comprised of two parts; reviews of science and engineering as bases for chemical reactor design; and several examples of specific reactor design practised in petroleum refining, petroleum chemistry, polymer industry or air pollution abatement. All of these are contributed by experts in the related academic discipline or industry. The editors take sole responsibility for any shortcomings in this volume, but hope it will stimulate new ideas in academia and technical advances in industry.

We are indebted to the Chiyoda Corporation, Maruzen Co. Ltd., and John Wiley & Sons Ltd for their continued support and encouragement in the publishing of this book.

March 1997, Hiroo Tominaga

CHAPTER 1

Chemical Reactions and Design of Chemical Reactors

HIROO TOMINAGA

University of Tokyo, Japan

1.1 INTRODUCTION

The Chemical industry is a branch of the industry that produces highly valueadded chemicals from a variety of natural resources used as basic raw materials. Science and technology in the chemical industry centre around the chemical transformation of materials, i.e. chemical reaction, and therefore the design and operation of chemical reactors as ways and means of realizing the chemical reaction, are so important that they may be said to be the key technology of the chemical industry.

Theoretical approaches to the design of chemical reactors have thus been developed systematically, utilizing the knowledge of science and engineering about chemical reactions. However, it is not well known to the public how the theories are put into practice by chemical engineers.

The book summarizes the fundamental theory of reactor design and the practice of its applications in the industrial processes, such as petroleum refining, petroleum chemistry and others.

The book is largely divided into two parts: the fundamentals in Chapters 2-4, and the applications in Chapter 5. This chapter outlines the scope of respective chapters as an introduction to chemical reactions and reactor design.

1.2 SCIENCE AND ENGINEERING FOR REACTOR DESIGN

The science and engineering related to reactor design are shown in Figure 1.1, demonstrating how diversified knowledge and information are essential to the design and operation of chemical reactors. Among these, the

2 H. TOMINAGA

fundamental chapters deal with chemical reactions and reaction engineering theories.

1.3 THEORY OF CHEMICAL REACTION

This theme is treated in Chapter 2.

Why and how does a chemical reaction take place? What factors govern the selectivity and the rate of reaction? The specific field of science dealing with these issues is termed as the theory of chemical reaction, which is comprised of chemical equilibrium, kinetics and mechanisms.

The equilibrium of chemical reactions is discussed by chemical thermodynamics, which reveals whether a given chemical reaction will take place or not and if so, to what extent. In more detail, the change in standard free energy of formation accompanied by a chemical reaction gives an equilibrium constant at a given temperature, which provides the equilibrium conversion of

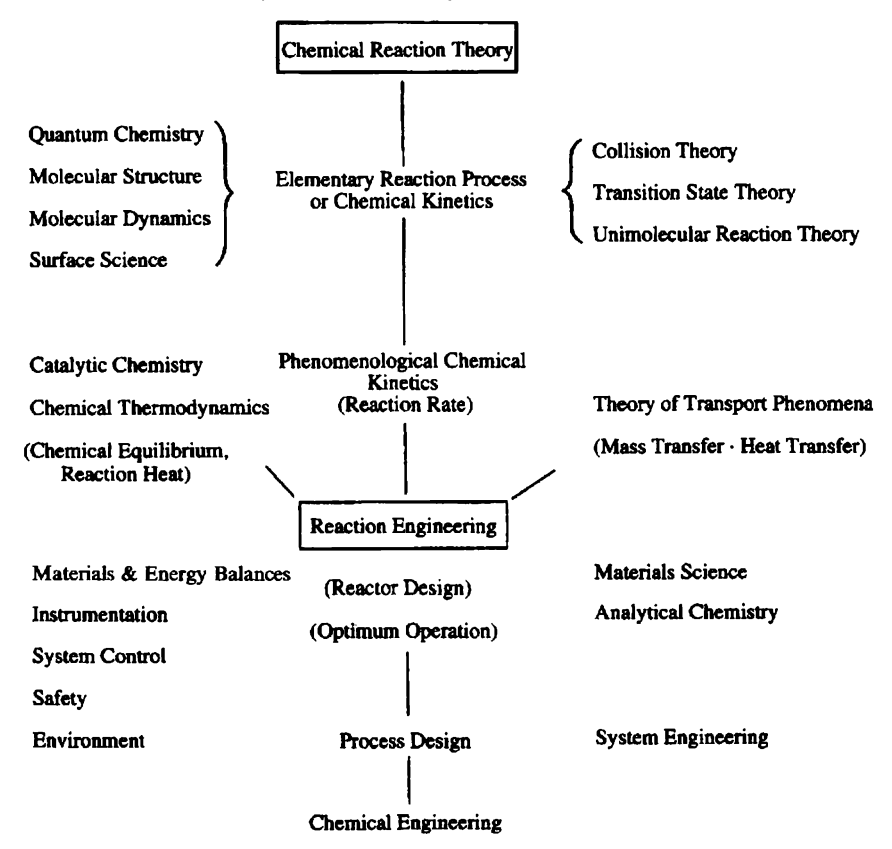


Figure 1.1 Science and engineering related to reactor design.

reactants under their particular initial pressure and composition. In addition, chemical thermodynamics enables the calculation of the heat balance associated with a reaction which is either endothermic or exothermic. This thermodynamic information is indispensable for reactor design.

The rate of chemical reaction is another critical factor in reactor design. The progress of rate theory, however, is so far behind meeting the need to predict precisely any particular rate of reaction that it has to be observed by experiment.

Chemical kinetics deals with the rate of a chemical reaction to reach its equilibrium. It originated from careful observation of the rate of a chemical reaction through experiments, followed by a mathematical expression of the rate of the chemical reaction. This approach is called phenomenological kinetics. Subsequently, theoretical studies on the rate of a chemical reaction have emerged. The discussions were centred on the microscopic mechanism of chemical reaction and the factors affecting the rate of the chemical reaction. Comparisons were made between the rate observed by experiment and the theoretical prediction. This approach includes collision theory, absolute reaction rate theory, transition-state theory, and unimolecular reaction theory.

Recently, academic interest has been focused on molecular dynamics, which discusses the rate of elementary reaction as a function of the quantum state of the reacting molecules (or chemical species such as free radicals and ions).

In spite of such progress in chemical kinetics, the general theory has not yet been established that can accurately predict, a priori, the rate of chemical reactions that are thermodynamically favourable. At this stage, analysis of carefully obtained experimental results is the only way to obtain the accurate rate of a chemical reaction.

On the other hand, the systematic acquisition of a database is now in progress with respect to the kinetic parameters of elementary reactions in gas/liquid-phase homogeneous systems. Utilizing this database, techniques have already been developed to compute the overall reaction rate consist for a network of elementary reactions. This has led to success in designing and controlling chemical reactors. Combined with the progress of a priori and/or semi-empirical prediction theory of the rate of elementary reaction, hopefully it will not be long before predications of reaction rates are practicable, with a satisfactory degree of accuracy.

1.4 CHEMICAL REACTION ENGINEERING AND REACTOR DESIGN

This theme is treated in Chapters 2–4.

The scientific or academic study for chemical kinetics is interested mostly in clarifying fundamental principles on a molecular scale that governs the rate of

4 H. TOMINAGA

a chemical reaction, preferably a simple one. However, the objective of the study on kinetics in engineering, or chemical reaction engineering, is to establish the practical methodology of reactor design and operation not only for simple but also for complex reaction systems, where mass and heat transfer have crucial effects on the rates of the chemical reaction.

Examples of the reactors where mass transfer of reactants in heterogeneous phases plays an important role, include the bubbling column reactor in which a gas is blown into a liquid, and the catalytic reactor in which a gas passes through a porous granular catalyst bed. In the former case, the mass transfer on the gas/liquid interface, and in the latter case, the diffusion rate of gaseous molecules in the pores of the catalyst, respectively, govern the reaction rate and the product distribution significantly.

Examples of heat transfer-controlled reaction systems include high-temperature thermal cracking and partial oxidation of hydrocarbons. Since the former case is accompanied by a large amount of heat absorption, the heat transfer rate through the reactor tube wall substantially governs the reaction rate, while in the latter case, elimination of the large amount of heat generated and control of the reaction temperature are the keys to the reactor design in order to minimize the side reaction, namely complete oxidation of hydrocarbons.

To resolve the dynamics of mass and heat transfer (as well as momentum transfer) in association with chemical reaction, multidimensional analyses are required in terms of time and space. In this respect, the use of a capable computer is indispensable.

The conception of reactor design is first to specify the preferable reaction conditions so as to carry out the intended chemical reaction efficiently, and then to determine the type and size of the reactor.

In more detail, to achieve the specified goals set for both production scale and product quality, the reactor operating conditions should be optimized from both economical and technical viewpoints. Configuration of the process scheme, selection of the reactor type and determination of its size and structure are made so as to minimize the costs for both operation and investment.

The economical viewpoint means the minimization of the product manufacturing cost consisting of the variable and fixed expenses of the whole process. On the other hand, the technical standpoint implies the adaptability or flexibility of the process, safety of operation, and social acceptance with respect to environmental issues.

Chemical reactions are classified from various viewpoints with individual characteristics. Similarly, reactors can be classified on the basis of their kinetic behaviour as follows

- (1) Batch type
- (2) Continuous flow type

- (a) Tubular reactor, plug flow
- (b) Tank reactor, mixed flow.

The basic concepts of these reactors are shown in Figure 1.2 and Table 1.1. In the case of the batch type reactor, its operation starts by feeding the raw materials into the reaction vessel, followed by sealing or heating if necessary. When the reacting system is in the heterogeneous phase of liquid-solid (or gas), it is desirable to stir well to improve the contact of reactants and the diffusion of product. In several hours or days of operation, the reaction proceeds nearly to completion, and it is terminated by cooling the reactor, followed by the recovery of the product from the reactor.

The batch type reactor is generally used for liquid-phase systems with relatively slow reaction rate. In commercial applications, this type of reactor is suitable for small-scale plants such as those producing dyes and pharmaceuticals. In addition, the reactor has the advantage of multi-purpose use; a variety of products may be manufactured using only one reactor, by scheduled batch operation.

The continuous flow type reactor, wherein raw materials are continuously fed and from where the product is taken out, is suitable for large-scale chemical processes with relatively high reaction rate at substantially constant operating conditions.

In the case of the tubular reactor, the concentration of raw materials is highest at the inlet of the reactor tube and gradually decreases toward the outlet, while product concentration gradually increases along the reactor. In this type of reactor, there is no back-mixing or diffusion of reacting molecules along the direction of the material flow. In other words, a sector of reaction zone in a plug (or a piston) form travels through the reaction tube, but the reacting molecules remain in that plug. For this reason, the residence time (reaction time) of the molecules passing through the reactor are equal for all.

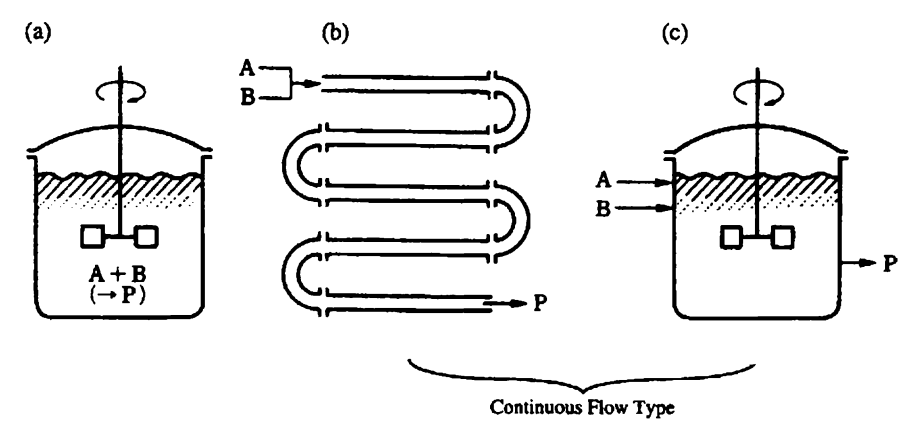


Figure 1.2 Types of Reactor. (a) Batch type tank reactor. (b) Tubular reactor. (c) Tank reactor.

H. TOMINAGA

Table 1.1 Comparison of characteristics of reactors

			Contin	uous flow	
Comparison item Reactor		Batch	Tubular type	Tank type	
Ideal conditions	Temperature, pressure, composition in reactor	Uniform at each moment	 Concentration changes in the direction of flow No gradient of reaction rate and temperature in radial direction No mixing and diffusion in axial direction 	 Complete mixing Composition in the reactor is uniform and equal to that at the outlet 	
Ide	2. Residence time distribution of reactant	None	None	Yes	
stics	1. Required reactor volume (Equal conversion basis)	Relatively small	Relatively small	Large	
Kinetic characteristics	2. Distribution of products (Consecutive reaction)	Large yield of intermediate product	Large yield of intermediate product	Small yield of intermediate product	
Kinetic	3. Probability of reaction with specific composition ratio	Impossible	Impossible	Possible	
S.	1. Flexibility	Large	Small	Medium	
Features	2. Application	Multi-purpose and small- scale production	Mass production	Medium	

Table 1.2 Examples of industrial chemical processes

Process	Reactor	Chemical reaction	Design issues
Naphtha cracking	Vapour phase, homogeneous, tubular furnace	Endothermic, consecutive reaction	Product yield, rapid heating and cooling
Tubular steam reforming	Vapour solid phase, heterogeneous, fixed bed	Endothermic, reversible reaction chemical equilibrium	Heat balance, heat
Epoxy resin production	Liquid phase, complete stirred tank reactor	Exothermic reaction polymerization	Heat removal, control of polymerization
Hydrotreating	Liquid and vapour phases, heterogeneous, fixed bed	Exothermic, high pressure reaction	Hydrogen consumption, heat removal, catalyst
Fluid catalytic cracking	Vapour-liquid-solid phases, heterogeneous, continuous fluidized bed	Endothermic, consecutive reaction	Product distribution, continuous catalyst regeneration
Wet-type flue gas desulphurization	Vapour-liquid-solid phases, heterogeneous, bubbling tank	Acid-base reaction	Mass transfer, saving power energy

The tank reactor, which is another continuous flow type of reactor is equipped with a stirrer that vigorously agitates the reactants. In this completely mixed reactor, if ideally operated, the chemical composition and temperature are kept constant throughout the reaction vessel. This is the key difference between the tank and tubular reactors.

The residence time of reacting molecules in the tank reactor is not equal. The average residence time can be calculated by dividing the reactor volume by the feed rate in volume under the reacting conditions, but the residence times of each of the reacting molecules are very different. Some of the reacting molecules remain in the reactor for a long time and others remain only for a short time. That is, their residence times are widely distributed. This is the second key difference between the tank and tubular reactors.

These characteristics of the tubular and tank reactors lead to significant differences in the reactor volume required to attain the desired raw material conversion (production rate), the selectivity (yield) of intermediate products in consecutive reactions and so on. Compared with the tubular reactor of the same volume and feed rate, the tank reactor gives lower conversion and lower selectivity of the intermediate product. Despite these disadvantages, as seen in

8 H. TOMINAGA

the cases of *auto-oxidation* reactions, tank reactor is preferred for those reacting systems where the reaction proceeds smoothly only in a narrow range of specific composition.

1.5 REACTOR DESIGN FOR INDUSTRIAL PROCESSES

This theme is dealt with in Chapter 5.

This chapter introduces practical approaches where the theories of chemical reaction engineering are applied to the design of commercial reactors. The selected six subjects are selected from the chemical processes playing important roles in the industrial fields of oil refinery, petrochemistry, pollution abatement and so on. Table 1.2 summarizes the types of reactors, characteristics of chemical reactions, and major design considerations for such chemical processes.

The engineering issues to be considered in designing these reactors vary greatly depending on the characteristics of chemical reactions as described in the relevant sections of Chapter 5, and hence provide a good method of learning the variety of reactor designs.

Subsequent sections present a brief introduction to both the chemical processes and the characteristics of the chemical reactions involved which are reflected in the design of individual reactors.

1.5.1 NAPHTHA CRACKING

Naphtha cracking constitutes the most fundamental process for conversion of petroleum into olefins such as ethylene and propylene, and aromatic hydrocarbons such as benzene, toluene and xylene, which are the basic materials for the petrochemical industry. For the cracking process, light naphtha, a distillate fraction from petroleum, is used exclusively as feed stock in Europe and Japan.

Decomposition reactions of paraffins, the principal components of naphtha, are significantly endothermic, and therefore a sufficient supply of the reaction heat is of primary importance. Moreover, the decomposition must be performed at high temperature where the equilibrium is favourable thermodynamically. At high temperatures, olefins, the primary products of decomposition, may change into more stable aromatics and then into carbon and hydrogen consecutively. The carbon, or coke, thus formed is deposited on the inner surface of reactor tubes, hindering heat transfer, and results in the clogging of reactor tubes. The prevention of such carbon deposition is a second crucial requirement. Another consideration is to adjust the ratio of by-product olefins and aromatics to ethylene, the main product, so as to meet their demands in the down-stream petrochemical industry.

In order to control the product distribution, it is necessary to understand the reaction kinetics and mechanism. Fortunately, fundamental studies have been extensively done on the thermal cracking reaction of hydrocarbons. It has been established that the reaction is carried out by a free radical chain mechanism initiated by the unimolecular decomposition of paraffin. The kinetic parameters of the elementary reactions involved are fairly well known. In order to obtain the optimum reacting conditions based on the reaction network comprised of hundreds and thousands of elementary reactions, a number of computer programs have been developed.

To obtain a high olefin yield, it is desirable to conduct the thermal cracking reaction at a high temperature, in a short residence time and at a low pressure. The decomposition of paraffin into olefin is a first-order reaction with a high activation energy, on the other hand the subsequent aromatic formation from the olefin is a second-order reaction with a relatively low activation energy.

For the above reasons, a tubular reactor, which is intrinsically free from back-mixing, is used for the naphtha cracking reaction. Since the reaction requires a large amount of heat, the feed must rapidly be heated up to the desired temperature as fast as possible. On the other hand, decomposed products, olefin and aromatics, must be rapidly cooled down to minimize the loss by their cooking. The structure of the quencher is crucial to the enhanced heat recovery and also to the convenience of decoking. Low pressure operation can be realized by feeding a large amount of superheated steam into the reactor tubes together with naphtha. The steam also plays the role of supplying reaction heat and suppressing coke deposition.

In order to achieve rapid heating of naphtha and steam, it is crucial to increase the heat flux. For product distribution control, the temperature profile along with reactor tube should be optimized. These can be achieved by designing the diameter and type of the tubes and their arrangement. As one example of a tube arrangement, a stepwise reduction from the inlet to the outlet in the number of reaction tubes, e.g. by putting two tubes into one, can effect a shorter residence time in the down-stream and thus prevents undesired consecutive reactions.

In the advanced naphtha cracking unit, the following reacting conditions have been attained in the cracking furnace: outlet temperature 850°C; outlet pressure 0.2 MPa; residence time 0.2 s.; steam-naphtha ratio 0.5, with these conditions the olefin yield versus naphtha has largely been improved up to 33%, also the energy consumption per unit production of olefin has successfully decreased to 65% compared with that in the 1970s.

1.5.2 TUBULAR STEAM REFORMING

Steam reforming is a process for producing syngas to be used for methanol synthesis or hydrogen used for ammonia synthesis and petroleum refining. The

10 H. TOMINAGA

synthesis gas formation, reaction of hydrocarbons with steam, to form hydrogen and carbon monoxide (reforming reaction) is accompanied by significant heat absorption. The CO shift reaction, wherein hydrogen is formed by reaction of carbon monoxide with steam, is a slightly exothermic reaction. A nickel catalyst is used generally for steam reforming reaction. Both the reforming reaction and the CO shift reaction are reversible reactions; in the presence of an excellent catalyst at a high temperature, the reaction rates are very large in both the forward and reverse directions. Therefore, the composition of the gas produced is inherently determined by thermodynamic equilibrium, being entirely dependent on the feed gas composition, temperature and pressure, and can thus be well estimated by theoretical calculations without any experiment.

In the steam reforming reaction that is endothermic as a whole, supply and recovery of the reaction heat are crucial, therefore, heat balance calculations are carefully performed for improvement of thermal efficiency. The catalyst-packed tubular reactor is placed in the heating furnace and operated under an appropriate high temperature and pressure. The temperature of the feed gas at the inlet of the reactor tube usually ranges from 450 to 650 °C, whereas the outlet temperature is from 700 to 950 °C depending on the final usage of product. The material of the reaction tubes restrains the maximum tube wall temperature and hence as the maximum heat flux, and the life of the reaction tubes is largely dependent on the maximum tube wall temperature, a careful design consideration is required for the material selection.

The reforming catalyst, one of the most important factors in reactor design, must be durable enough for severe reacting conditions. A decrease in the catalytic activity is due to a reduction of the surface area caused by nickel sintering. This is prevented by providing the catalysts, which are made of porous carriers impregnated with nickel, with a suitable pore distribution and sufficient thermal resistance. The catalyst particle size and shape should be optimized to achieve maximum activity and maximum heat transfer, while minimizing the pressure drop. The high mass velocities in steam reforming reactor necessitate a relatively large catalyst particle size to obtain a low pressure drop across the catalyst bed; but the particle size is limited by another requirement for effective packing. The pressure drop depends strongly on the void fraction of the packed bed and decreases with the size of the packed particle.

In addition, carbon deposition on the catalyst surface can be a serious problem, thus its prevention is essential. Carbon tends to be formed under high temperatures and low hydrogen partial pressures. Unless the product gas is recycled, no hydrogen exists in the reacting gas at the inlet of the reactor. This raises the technical issue of what inlet temperature should be set to prevent carbon deposition. The problem can be solved by consideration based on chemical thermodynamics.

In the case of hydrogen manufacturing, the demand for the product purity varies depending on its application. If CO is undesirable by reason of its catalyst poison or for other reasons, CO shift reaction is firstly applied at a high-temperature, a kinetically favourable but thermodynamically unfavourable condition, which is followed by a low-temperature CO shift reaction to convert the remaining CO into hydrogen. A very small amount of CO still remaining can further be transformed into methane by a methanation reaction. Instead of these catalytic processes, the purity of hydrogen may be improved through a physical separation method such as the PSA.

1.5.3 EPOXY RESIN PRODUCTION

Typically epoxy resin is obtained by polycondensation of bisphenol A and epichlorohydrin, giving various grades of the product with their average molecular weights ranging from 350 through to 20000. Depending on their respective characteristics, a wide range of applications epoxy resin include paints such as adhesives, electrical insulating materials, etc.

In order to produce multiple types of products in small amounts, it is generally known that a liquid-phase stirred-tank batch reactor is useful. In this case, it is crucial to determine the optimum reaction conditions based on a systematic production schedule in view of a reasonable combination of various batch operations.

It is therefore important to understand the complicated networks of polycondensation reactions composed of various elementary reactions, and the effects of various operating factors on various quality parameters of the product. These relations are formulated in a simulation program to produce the desired products efficiently.

The process consists of first-stage azeotropic reactor and second-stage solvent reactor. The first-stage reactor is a batch type reactor with stirrer. This reactor is operated to carry out the epoxidation reaction to an extent not causing over gelation, and excessive epichlorohydrin, alkali salt and also gel substances formed as byproducts are eliminated. In the second-stage reactor, a solvent is added to lower the viscosity, and then the required amount of alkali is charged for reaction at a low temperature to reduce the hydrolyzable chlorine.

The first-stage reactor runs an exothermic reaction. But heating of the reactor is required, since the water produced is to be removed in an azeotropic mixture with epichlorohydrin, so that the external circulatory heating system is adopted to secure a sufficient heating surface area. The second-stage reaction is carried out in a continuous flow type reactor, namely a stirred tank with one column and three stage chambers is used, in view of economics.

Running a process system using a combination of the reactors—batch and continuous flow type in series—to its best performance, requires a balanced time sequence based on their STY (space time yield) and other factors.

12 H. TOMINAGA

1.5.4 HYDROTREATING

Hydrotreating is one of the key technologies in petroleum refining, covering a series of processes with different objectives. Various petroleum fractions are treated with hydrogen in the presence of catalyst, to decompose and eliminate unfavourable impurities such as sulphur, nitrogen and metals or to hydrogenate olefin and aromatics into saturated hydrocarbons. Detailed discussion is given on the hydrotreating of vacuum gas oil with distillate obtained from atmospheric residue oil in a vacuum tower.

The purpose of hydrotreating the vacuum gas oil is to remove such compounds as sulphur, nitrogen and others in order to produce clean fuel oil or feed stock for fluid catalytic cracking. The rates of the hydrotreating reactions of those compounds vary largely with their chemical structure. Hence the order of reaction of hydrodesulphurization is higher than first and near to second order with respect to sulphur concentration. This implies that an infinite reaction time is required for complete removal of those impurities, provided other reaction conditions are held constant. From the economic viewpoint, it is desirable to save the consumption of hydrogen by minimizing hydrogenation of the aromatic. Under pressures from 5 to 10 MPa and at temperatures of 360 °C or higher, hydrogenation of aromatics is thermodynamically unfavourable.

Commercial hydrogenation catalysts are generally composed of cobalt-molybdenum supported on alumina, and if larger hydrogenation activity is required, then nickel is employed instead of cobalt. In addition to the above metal oxides (sulphides in practical usage) as active components, control of pore diameter and acidity of the alumina as carrier are the important factors for preparation of the catalyst with excellent performance.

Typical conditions of hydrotreating are: liquid hourly space velocity (LHSV) 1-3; temperature 340-450 °C; pressure 7-14 MPa; and hydrogen consumption 50-100 m³ per kl of feedstock. The catalyst is charged into a fixed-bed reactor. The reactor structure is designed in such a way that the reaction fluid is uniformly distributed over the catalyst bed with a low and uniform pressure drop. Particular attention is paid to avoid any local temperature rise due to the reaction heat. To this end, the catalyst bed is sometimes divided into several stages to introduce quenching streams into the reactor. Because hydrotreating is an exothermic reaction, every safety measure is taken against possible accidents: temperature runaway, formation of hot spots, and accidents such as shutdown of the recycling compressor.

Since the reactors are operated at high temperature under high pressure, they are designed to meet the legal standards for pressure vessels. Regarding the reactor materials, since hydrogen and hydrogen sulphide coexist, austenite stainless steel is selected for the inner surface of the reactor.

The catalyst activity degrades gradually during the operating time because of metals and carbon produced from the heavy ends in the feed. To supplement its

activity loss, the reactor is operated at temperatures which are increased gradually, and finally shut down either for replacement of the catalyst or regeneration of the catalyst while holding it within the reactor (in situ). Catalyst regeneration is carried out by adding air little by little into the inert gas which is charged into the reactor to burn (carefully) the carbon deposited on the catalyst.

1.5.5 FLUID CATALYTIC CRACKING

Fluidized catalytic cracking process is an important petroleum refining technology for increased production of gasoline from a given barrel of crude oil.

In response to the increasing demand of automobile gasoline, what first developed was thermal cracking technology of a heavy distillate from crude. However, the thermal cracking process had many disadvantages: low yield of gasoline; large amount of byproducts such as gas and coke; low octane value of gasoline; large amounts of unstable olefin with conjugated double bond; and a bad smell.

Later, the catalytic cracking process was invented. This process was found rather incidentally in the lubricating oil refining experiment through the use of activated clay. Namely gasoline was formed as byproduct when the treating temperature was increased. Conversion of the heavy distillate into gasoline could be achieved at a lower temperature by using catalyst with much less side reactions producing gas and coke, as well as significant improvement in the gasoline qualities such as octane number, odour, stability, etc.

The thermal cracking had been replaced by the advanced catalytic cracking process. The first commercial application was Houdry catalytic cracking process developed in the 1930s where a fixed-bed reactor was employed.

The biggest technical challenge to the success of the catalytic cracking process was coke deposition over the solid acid catalyst which quickly caused the cracking activity to deteriorate. However, the activity of the catalyst is recovered after the coke is burnt and eliminated; the Houdry process had multiple reactors in parallel, and cyclic operations of cracking, purge and regeneration were carried out to permit continuous operation as a whole.

Following this, a more advanced technology-moving bed process was developed, from which an innovation shortly emerged; namely the fluid catalytic cracking process. In this process, catalysts in powder form are fluidized and continuously circulated between a cracking reactor and a regenerator. This process was successfully industrialized after a joint R&D project undertaken by major U.S. and British petroleum companies in 1942 in the middle of World War II. In the half-century since the birth of the first FCC unit, FCC technologies have made significant progress in reactor design and

14 H. TOMINAGA

processing technologies. In the 1990s, the most modern FCC units are in use worldwide.

Along with the engineering progress of the FCC reactor, a special mention is warranted of the advancement of the catalysts for cracking. In the early stages, activated clay manufactured from natural montmorillonite clay served as the catalyst. Later on, this was replaced by synthetic silica/alumina. Further, in the 1960s, a catalyst composed of synthetic zeolite (Faujasite type etc.) came on the scene. This novel catalyst has the excellent advantages of extremely high cracking activity and high gasoline selectivity.

It is truly 'epoch-making', since the advent of this catalyst completely changed the structure of the fluidized bed reactor. The remarkably high activity of the catalyst ensures the completion of the cracking reaction, within an extremely short residence time, in a small-diameter riser that had acted just as a catalyst transport pipe, and so former reactors are now playing the role of separator of the cracked products from catalyst. This new process, where the cracking reaction proceeds so rapidly in a riser tube that has little back-mixing, inhibits over-cracking of gasoline and improves the selectivity for gasoline.

This is a good example of the success where development of an excellent catalyst has changed the structure of reactors. The history of the fluidized catalytic cracking process being developed in line with the progresses of chemical reaction engineering and catalyst science, includes many useful suggestions for developing new technology.

In the 1980s, residual oil fluidized catalytic cracking (RFCC) had been developed permitting direct processing of asphaltene containing residual oil in the FCC unit, where special considerations need to be paid to the catalyst formulation. It should be stressed that an idea to use the heat generated by catalyst regeneration for the reaction heat and also for recovery as electric power, is excellent, turning the disaster of coke deposition into an asset.

1.5.6 FLUE GAS DESULPHURIZATION

Flue gas desulphurization is a process for eliminating sulphur dioxide in the flue gas generated when fossil fuel, such as heavy oil and coal, containing sulphur is burnt in a boiler or heating furnace. Along with the technology of desulphurization of the fossil fuel, the importance of this process is increasing in the fight against air pollution in the industrial and municipal areas, and recently for conservation of the global environment or abatement of acid rain.

Among various flue gas desulphurization processes, the wet lime and gypsum process introduced here can attain a high-level desulphurization with excellent economics, using less expensive limestone as the neutralizer to produce useful gypsum as a byproduct. The JBR (Jet Bubbling Reactor), an example of the reactors of this process, fires flue gas into water to form a fine bubble bed, and sulphur dioxide and dust are eliminated while passing through this bed.

Sulphur dioxide is absorbed into water a sulphurous ions, oxidized to sulphate ions by oxygen in the air subsequently injected, and then neutralized by limestone powder slurry for recovery as gypsum. The desulphurized flue gas is discharged from the funnel after being pressurized and reheated.

These reaction systems have three phases: gas, liquid and solid, and the analyses of equilibrium and rates of mass transfer and chemical reactions on the interface of those heterogeneous systems form the bases of reactor design. It was demonstrated that the JBR efficiently treats a large amount of flue gas (e.g. 2000000 N m³ of 800 ppm per hour) discharged from a thermal electric power station (capacity: 700 MW) with a stable high desulphurization rate of 95% or more. The volume of the JBR in this case was about 2000 m³ and the amount of limestone used was 6200 kg per hour.

CHAPTER 2 Equilibrium and Reaction Rate

HIROSHI KOMIYAMA

Department of Chemical System Engineering, University of Tokyo, Japan

2.1 NATURE OF CHEMICAL REACTION

There are many different types of chemical reactions in the natural world. Any of these phenomena, such as: iron turning into iron oxide in the air; food decomposing into nutrients in a human body; and plants synthesizing carbohydrates from carbon dioxide and water, are due to chemical reactions. Also in industrial processes, various chemical reactions are used to synthesize substances. Among various factors for classifying chemical reactions, this chapter summarizes points to be considered in designing a reaction process and reactor.

2.1.1 SUPPLY OF ACTIVATION ENERGY

First of all, an important point is how to supply the activation energy for a reaction. In the most typical case, a chemical reaction is excited by thermal energy. In general, the mass we experience is thermally at equilibrium, in which molecules with various different energies coexist. Only a small number of molecules have a high energy, causing a reaction beyond a barrier of activation energies. The ratio of molecules with a high energy, exceeding a certain value increases with temperature exponentially; thus, thermal reaction rates increase sharply with temperature.

Reactions in which activation energies are supplied in the form of light are called photochemical reactions. They are in most cases activated by ultraviolet rays. For example, sunburn is the result of a photochemical reaction by ultraviolet rays, but you never get suntanned by a stove. It is the effect of infrared rays that makes you feel hot. Because the quantum mechanical photon energy 'hv' of infrared ray is smaller than the activation energies for many reactions, it cannot excite any reaction. That is why infrared rays cannot cause sunburn. Light is costly compared with the heat of the same amount of energy,

18 H. KOMIYAMA

there are therefore not so many cases where photochemical reactions are used in industrial processes. As an example of its large-scale application, caprolactam as a raw material of nylon is synthesized using ultraviolet light from mercury lamps.

A type of reaction which gives energy through voltage, i.e. electrostatic potential is called an electrochemical reaction. A familiar example is the electrolysis of NaCl and water, which is used for industry in areas where electric power is available at low cost. Another type of reaction which causes electrons to collide directly with molecules in order to feed the activation energies, is called a plasma chemical reaction. Amorphous silicon acting as the material of solar cells is produced by depositing silane (SiH₄) on a substrate after cracking in plasma.

Although the energy available from light, electricity and electrons is used, most reactions in commercial usage are from thermal reactions. For example, in the petrochemical industry, basic materials such as ethylene and propylene are synthesized by cracking naphtha at a temperature as high as 800 °C. Also, a catalyst is often used. Catalysts do not change before or after a reaction, and neither give energy to raw molecules, but reduce the value of the activation energy. Since the activation energy is fed as heat, catalytic reactions are a kind of thermal reaction. The list of examples of catalytic reactions is endless: hydrogenation of the unsaturated hydrocarbons using palladium as a catalyst; synthesis of polymers from olefins using the Ziegler-Natta catalyst; and production of gasoline by zeolite. It is more likely that catalysts are used in the majority of industrial reaction processes. Enzymes are also a kind of catalyst. In the process that converts cane sugar into glucose through hydrolysis, either sulphuric acid or an enzyme called α-amylase is available for accelerating the reaction; thus processes using either of them as a catalyst become widespread in industrial applications. Figure 2.1 shows the types of chemical reactions classified by the method of excitation.

2.1.2 ELEMENTARY AND COMPLEX REACTIONS

Single reactions such as occur when fast argon molecules collide with hydrogen molecules to decompose into hydrogen atoms are called elementary reactions. However, it is very rare that a single reaction takes place independently. It occurs only in the case where the possibility is very low that the formed molecules collide with other molecules because of extremely low pressure in a high vacuum reactor or in space. Those reactions which are observed by us are mostly results of a series of sequential elementary reactions. For example, a seemingly simple reaction of burning methane takes place by way of more than one hundred intermediates before yielding water and carbon dioxide. Table 2.1 shows the mechanisms of a combustion reaction simplified up to major reaction paths. Also, in the case of a catalytic

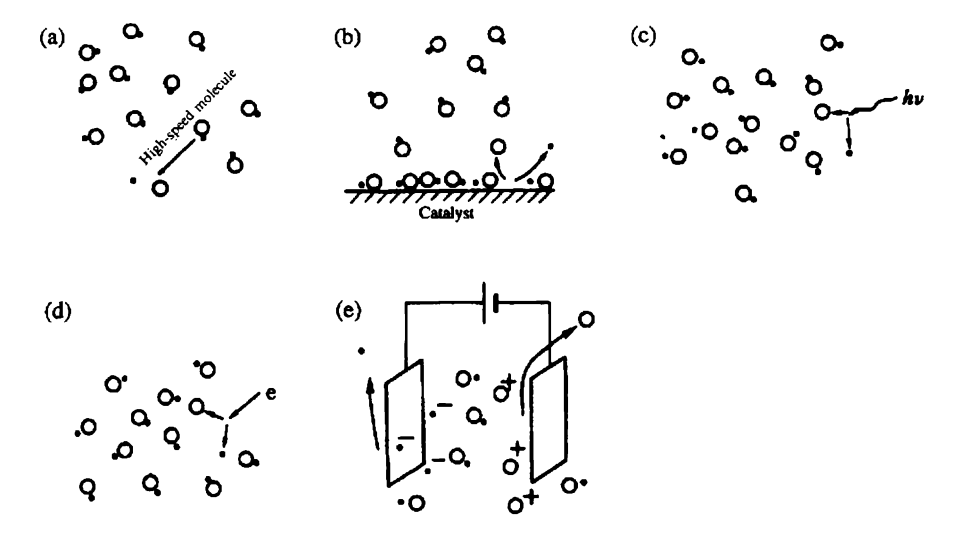


Figure 2.1 Classification of chemical reactions with activation means. (a) Homogeneous thermochemical reaction. High-energy molecules (state) existing at a particular probability in a thermal equilibrium substance, bring about the reaction. (b) Heterogeneous thermochemical reaction. Adsorption increases the reactivity of a molecule. Increased concentration of molecules by adsorption enhances the probability of their reacting thermochemically. (c) Photochemical reaction. High-energy photons like ultraviolet light collide to cause the molecules to react. (d) Plasmachemical reaction. High-energy electrons collide to cause the molecules to react. (e) Electrochemical reaction. Molecules (or ions) accept (or release) overpotential electrons to react at the electrodes.

reaction, for example, many chemical species are formed on the catalyst surface before methanol is synthesized from carbon monoxide and hydrogen by the catalyst of zinc oxide.

The fact of the rare occurrence of an independent elementary reaction is also important for reactions excited by energies other than heat, as mentioned in Section 2.1.1. Even if the excited reaction is one elementary reaction, it triggers a series of sequential reactions. If collisions of electrons in plasma form SiH₂ and SiH₃ from SiH₄, subsequent chemical reactions are accelerated as those radicals react with SiH₄ to form other molecules, and further formed molecules form more new molecules, etc.

It must be noted that most of the chemical reactions, irrespective of industrial or laboratory levels, are complex reactions.

2.1.3 OTHER FACTORS IN REACTOR DESIGN

Supply and removal of heats for a large reactor are not easy because of a small specific surface area.

20 H. KOMIYAMA

Table 2.1 Elementary reactions occurring in the combustion reaction of methane with oxygen

1) $H + H + M = H_2 + M$	47) CH ₂ O + CH ₃ = CH ₄ + HCO
2) $CH_3 + H + M = CH_4 + M$	48) $CH_2O + M = HCO + H + M$
3) $CH_4 + H = CH_3 + H_2$	49) $CH_2O + OH = HCO + H_2O$
4) $CH_4 + CH_2 = CH_3 + CH_3$	50) $CH_3O + M = CH_2O + H + M$
5) $CH_3 + CH_3 = C_2H_5 + H$	51) $CH_3O + O_2 = CH_2O + HO_2$
6) $CH_3 + H = CH_2 + H_2$	52) $HCO + M = HCO + M$
7) $CH_3 + CH_2 = C_2H_4 + H$	53) $HCO + H = CO + H_2$
8) $CH_3 + M = CH_2 + H + M$	54) $HCO + OH = CO + H_2O$
9) $CH_2 + H = CH + H_2$	55) $HCO + O_2 = CO + HO_2$
10) $CH + CH_4 = C_2H_4 + H$	56) HCO + O = CO + OH
11) $CH + CH_3 = C_2H_3 + H$	57) $HCO + O = CO_2 + H$
12) $C_2H_6 + H = C_2H_5 + H_2$	58) $HCO + CH_3 = CO + CH_4$
13) $C_2H_6 + CH_3 + C_2H_5 + CH_4$	59) $CH_4 + O = CH_3 + OH$
14) $C_2H_6 = CH_3 + CH_3$	60) $CH_4 + OH = CH_3 + H_2O$
15) $C_2H_5 = C_2H_4 + H$	61) $CH_4 + HO_2 + CH_3 + H_2O_2$
16) $C_2H_5 + CH_3 = C_2H_4 + CH_4$	62) $CH_3 + OH = CH_2O + H_2$
17) $C_2H_4 + M = C_2H_2 + H_2 + M$	63) $CH_3 + OH = CH_3O + H$
18) $C_2H_4 + M = C_2H_3 + H + M$	64) $CH_3 + O_2 = CH_3O + O$
19) $C_2H_4 + H = C_2H_3 + H_2$	65) $CH_3 + O_2 = CH_2O + OH$
20) $C_2H_3 + H = C_2H_2 + H_2$	66) $CH_3 + O = CH_2O + H$
21) $C_2H_3 + H = C_2H_2 + H_2$	67) $CH_3 + HO_2 = CH_3O + OH$
22) $C_2H_3 + M = C_2H_2 + H + M$	68) $CH_3 + HO_2 = CH_4 + O_2$
23) $C_2H_3 + CH_3 = C_2H_2 + CH_4$	69) $CH_2 + O_2 = CO + OH + H$
24) $C_2H_2 + M = C_2H + H + M$	70) $CH_{2}CO + OH = CH_{2}O + HCO$
25) $C_2H_2 + H = C_2H + H_2$	71) $CH_2CO + H = CH_3 + CO$
26) $H_2 + OH = H_2O + H$	72) $CH_2CO + O = HCO + HCO$
27) $H_2 + O = H + OH$	73) $CH_2CO + M = CH_2 + CO + M$
28) $H + O_2 = OH + O$	74) $C_2H_6 + O = C_2H_5 + OH$
29) $H + OH + M = H_2O + M$	75) $C_2H_6 + OH = C_2H_5 + H_2O$
$30) H + HO_2 = OH + OH$	76) $C_2H_6 + O_2 = C_2H_5 + HO_2$
31) $H + HO_2 = H_2 + O_2$	77) $C_2H_6 + HO_2 = C_5H_5 + H_2O_2$
32) $H + HO_2 = H_2O + O$	78) $C_2H_5 + O_2 = C_2H_4 + HO_2$
33) $H + O_2 + M = HO_2 + M$	79) $C_2H_4 + O = CH_3 + HCO$
34) $HO_2 + OH = H_2O + O_2$	80) $C_2H_4 + OH = C_2H_3 + H_2O$
35) $HO_2 + O = O_2 + OH$	81) $C_2H_4 + O_2 = C_2H_3 + HO_2$
36) $HO_2 + HO_2 = H_2O_2 + O_2$	82) $C_2H_3 + O_2 = HCO + CH_2O$
37) $H_2O_2 + OH = H_2O + HO_2$	83) $C_2H_2 + O = CH_2 + CO$
38) $H_2O_2 + H = HO_2 + H_2$	84) $C_2H_2 + O = HCCO + H$
39) $H_2O_2 + M = OH + OH + M$	85) $C_2H_2 + OH = C_2H + H_2O$
40) $OH + OH = H_2 + O$	86) $C_2H_2 + OH = CH_2CO + H$
41) $CO + OH = CO_2 + H$	87) $C_2H_2 + OH = CH_3 + CO$
42) $CO + HO_2 = CO_2 + OH$	88) $C_2H_2 + O_2 = HCO + HCO$
43) $CO_2 + O = CO + O_2$	89) $C_2H + O_2 = HCO + CO$
44) CH2O + O = HCO + OH	90) $C_2H + O_2 = HCCO + O$
45) $CH_2O + H = HCO + H_2$	91) $HCCO + H = CH_2 + CO$
46) $CH_2O + HO_2 = HCO + H_2O_2$	92) $HCCO + O = HCO + CO$

There are types of reactions that generate and absorb heat. In industrial processes, how to remove and supply the reaction heat is a significant problem. The number of moles produced by a chemical reaction is proportional to the reaction volume. On the other hand, the heat transfer rate is proportional to the wall area of the reactor. The specific surface area is different between a small beaker and a large reaction vessel. This is the essence that heat is critical in industrial processes. For small experimental reactors, it is easy to start a reaction by heating externally and remove heat during the process of an exothermic reaction. However, for the case of large reactors, a special device, e.g. installation of water-cooled jacket is required so as to keep the temperature constant while removing the heat of reaction.

It is also critical to reactor design whether the reacting materials and products are gas, liquid, or solid, and whether the 'phase' is a solid or liquid-phase catalyst. These factors are reflected on the selection of reactor: solid packed bed, liquid phase stirred tank, or fluidized bed.

2.2 DIRECTION OF THE REACTION PROGRESS AND CHEMICAL EQUILIBRIUM

2.2.1 DIRECTION OF REACTION PROGRESS

A chemical reaction has two directions: one in which it proceeds naturally and one in which it does not. In order to determine, specifically and quantitatively, whether a certain reaction will proceed or not, the equilibrium constant can be obtained by calculating the change in the Gibb's standard formation free energy. Let us try to calculate whether it is possible to synthesize NH_3 from N_2 and H_2O at room temperature and atmospheric pressure.

The reaction formula is

$$N_2 + 3H_2O \rightarrow 2NH_3 + 3/2O_2$$
 (2.1)

Obtain the values of $\Delta G_{\rm f}^{\circ}$ for each component from a handbook and subtract the left $\Delta G_{\rm f}^{\circ}$ from the right $\Delta G_{\rm f}^{\circ}$ to obtain the reaction $\Delta G_{\rm f}^{\circ}$

$$\Delta G_{\rm f}^{\circ} = (16.67) \times 2 - (-228.94) \times 3 = 720 \,\text{kJ/mol}.$$
 (2.2)

The equilibrium constant K_P is given by

$$RT \ln K_P = \Delta G_{\rm f}^{\circ} \tag{2.3}$$

Thus

$$K_P = \frac{P_{\text{NH}_3}^2 \cdot P_{\text{O}_2}^{3/2}}{P_{\text{N}_2} \cdot P_{\text{H}_2\text{O}}^3} = \exp(-301.3).$$

22 H. KOMIYAMA

If nitrogen, water and oxygen are at a pressure of 1 atm (bar*), then the equilibrium partial pressure of NH_3 is $e^{-301.3}$ atm, i.e. nearly 0. This indicates that it is substantially impossible to form NH_3 from nitrogen and water at room temperature and atmospheric pressure.

Now, some people may think that the reaction of $\Delta G_f > 0$ has progressed. since a small amount of NH₃ could have been produced. In other words, the equilibrium partial pressure is $e^{-301.3}$ but not 0, meaning that even if the value of ΔG_f is positive, there should be some minor progress. However, this is wrong. The free energy change $\Delta G_{\rm f}^{\circ}$ by Eq. (2.3) is called the standard formation free energy change, which is calculated from the free energy of formation of each component at standard conditions. Specifically, the value represents the ΔG_f required to produce ammonia at a pressure of 1 atm and oxygen at a pressure of 1 atm from nitrogen at a pressure of 1 atm and water at a pressure of 1 atm. To clearly indicate that it is the value for substances at standard conditions at a pressure of 1 atm, ΔG_f is expressed by adding the superscript ",' i.e. $\Delta G_{\rm f}$ ". If the change in the free energy of formation of each component at a pressure of 1 atm has been calculated at a specific temperature, the extent of the reaction progress at the temperature can be calculated from K_P even under the different pressure conditions of raw materials and products. This is the significance of calculating the free energies of reacting systems.

Equation (2.3) means that at room temperature, nitrogen at a pressure of 1 atm and water at a pressure of 1 atm can only produce NH₃ at a pressure of $e^{-301.3}$ atm with oxygen at a pressure of 1 atm, and the ΔG_f of its change is 0. In the end, formation of NH₃ up to a pressure of $e^{-301.3}$ atm indicates that the process $\Delta G_f > 0$ does not take place at all.

Some people may think that a low concentration could be covered by compression: i.e. this problem could be solved by compressing the pressure to 1 atm since synthesis is possible even at a low concentration, whereby it may be considered that a process of $\Delta G_{\rm f} > 0$ made some progress. The answer to this question can be found by calculating the work required for compression. The minimum work required to compress 2 mol of NH₃ at a pressure of $\exp(-301.3)$ atm down to 1 atm is a reversible work of isothermal compression, i.e. $2RT\ln(1/\exp(-301.3)) = 720 \, \text{kJ/mol}$. This value is equal to the free energy required to synthesize NH₃ at a pressure of 1 atm according to Eq. (2.2). To obtain NH₃ at a pressure of 1 atm, work corresponding to at least $\Delta G_{\rm f}^{\circ}$ must be done. Needless to say, the agreement between the reversible compression work and $\Delta G_{\rm f}^{\circ}$ is not a coincidence. This is one of the principles learned in thermodynamics. Figure 2.2 summarizes what is described in this section.

2.2.2 ROLE OF THE CATALYST

A catalyst controls the rate of reaction without affecting an equilibrium relation such as calculated above. For example, even if C_2H_4 and O_2 are mixed,

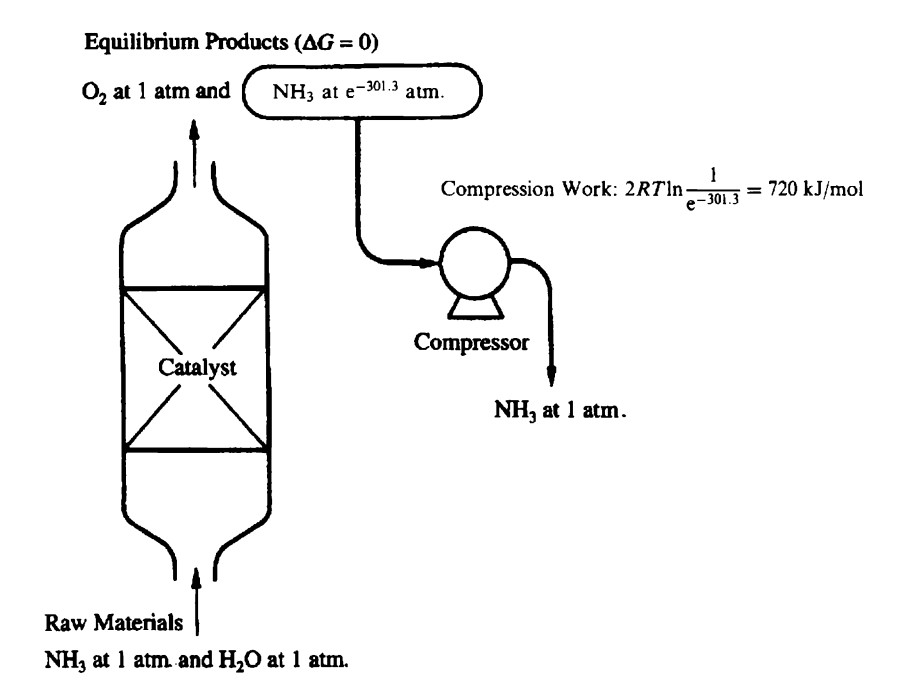


Figure 2.2 The Gibbs free energy relationship when N_2 and H_2O react until equilibrium is reached, and the extremely low pressure NH_3 produced in the equilibrium mixture is compressed up to 1 atm. ΔG° is the minimum energy required to produce a product at 1 atm from a raw material at 1 atm.

no reactions will take place with no sparks. A catalyst is provided to prompt reactions. However, from the aspect of equilibrium, there are many reactions which can proceed with C_2H_4 and O_2 as raw materials. In industrial processes, C_2H_4O (ethylene oxide) and CH_3CHO (acetaldehyde) are synthesized, and completely oxidized to CO_2 and H_2O in exhaust treatment.

$$C_2H_4 + (1/2)O_2 \xrightarrow{\text{Ag catalyst at 250 °C}} C_2H_4O$$
 (2.4)

$$C_2H_4 + (1/2)O_2 \xrightarrow{Pd^2 \text{ catalyst at } 120 \text{ °C}} CH_3CHO$$
 (2.5)

$$C_2H_4 + 3O_2 \xrightarrow{\text{Pt catalyst at } 300 \,^{\circ}\text{C}} 2CO_2 + 2H_2O$$
 (2.6)

A chemical reaction proceeds in directions where free energies decrease, these directions are countless, thus it is possible to proceed anywhere. It is the role of industrial catalyst technology to accelerate the desired reaction selectively, according to the catalyst and to the reacting conditions such as

24 H. KOMIYAMA

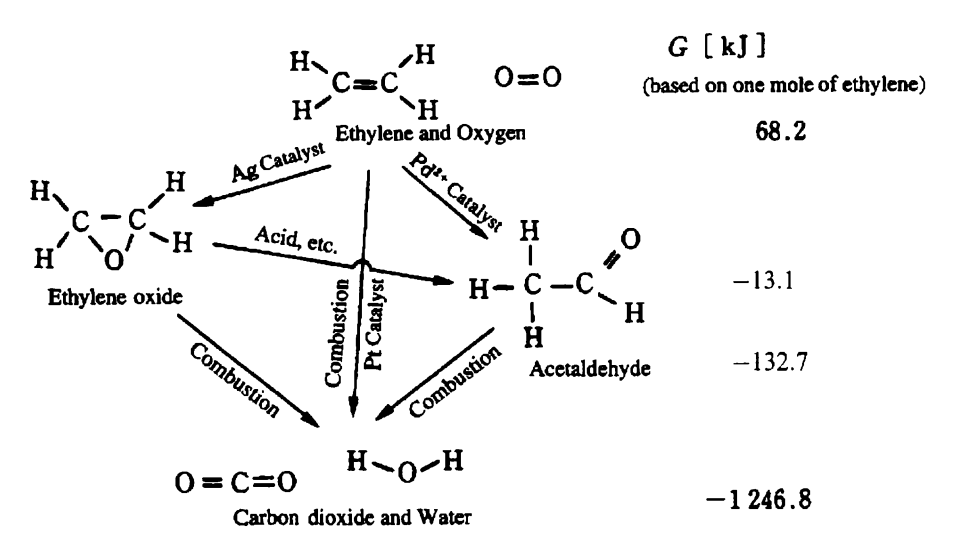


Figure 2.3 Several reaction paths from ethylene and oxygen and the Gibbs free energy relationship.

temperature and pressure. Figure 2.3 shows the relations between the reaction paths and the changes in free energies.

2.2.3 REVERSIBLE AND IRREVERSIBLE REACTIONS

Section 2.2.1 showed that there is no substantial progress of ammonia synthesis from nitrogen and water, because the free energy is $\Delta G_{\rm f}^{\circ} = 720 \,\mathrm{kJ/mol}$, and the equilibrium constant is $K_P = \exp(-301.3) \cong 0$. This indicates that a reversible reaction to oxidize ammonia into nitrogen and water, proceeds almost completely with a free energy of 720 kJ/mol and an equilibrium constant of $K_P = \exp(-301.3)$. Those reactions which are called irreversible reactions, requiring no consideration of reversible reactions, refer to those with a large negative standard formation free energy.

The ammonia synthesis is an epoch-making industrial process that enabled mankind to rapidly increase the production of foodstuffs. Let us discuss its meaning.

$$N_2 + 3H_2 \xrightarrow{\text{Fe catalyst}} 2NH_3 \tag{2.7}$$

The change in the standard formation free energy of this reaction is $\Delta G_f^{\circ} = -32.9 \,\mathrm{kJ/mol}$, and the equilibrium constant is $K_P = \exp(\Delta G_f^{\circ}/RT) = \exp(-6.9)$ at 300 °C. Compared to the oxidation of ammonia, the equilibrium constant is close to the order of 1. That is, this reaction may proceed in the direction of synthesis of NH₃ from N₂ and H₂ and also in the

reverse direction. This indicates that the selected reaction temperature and total pressure sensitively affect the existence of ammonia in the product under partial pressure. Accordingly, such reactions with a small standard free energy change are called reversible reactions.

2.2.4 HOW TO CALCULATE THE HEAT OF REACTION AND THE EQUILIBRIUM CONSTANT

2.2.4.1 The Heat of Reaction

The heat of reaction can be calculated by subtracting the enthalpies of raw materials from those of products. Since an enthalpy is one form of energy, only the difference is required but not the absolute value with respect to engineering calculations. It is therefore unnecessary to determine the absolute value if a single compound is considered, i.e. in the case where the subject is only about physical operations such as evaporation, heating, etc. However, if a chemical reaction occurs and the heat of this reaction is to be obtained, the absolute value must be determined. Such enthalpies, which assume that the enthalpy of the single most stable element at 298 K and a pressure of 1 atm is 0 and that the enthalpy of a substance is the heat of the reaction which forms the substance from the most stable elements, are 'standard formation enthalpies'. Enthalpies of respective compounds shall be determined so that the difference of the enthalpies between different substances becomes the heat of reaction at the same temperature and pressure. Enthalpies cited in handbooks usually refer to the standard formation enthalpies ' $\Delta H_{\rm f}^{\circ\circ}$ '.

If the heats of reaction of respective compounds at $298 \, \text{K}$ and a pressure of 1 atm are known from the differences in the standard formation enthalpies, the heat of reaction under different conditions can be obtained. For example, the heat of reaction at temperature T can be obtained by applying the law of conservation of energy that 'the total calorific value of a reaction remains the same irrespective of the paths' as shown in Figure 2.4. Specifically, the heat of reaction can be calculated by

$$\Delta H_{\rm f}^{\circ}(T) = \Delta H_{\rm f}^{\circ}(T_{\rm f}) \int_{T_{\rm f}}^{T} \Delta c_P dT$$
 (2.8)

where Δ_{CP} is the difference between the specific heats of products and raw materials. The heat of reaction can be obtained from a handbook by checking $\Delta H_{\rm f}^{\circ}$ of the raw materials and products in standard condition. Then the heat of reaction under any conditions can be calculated by obtaining the specific heat data of each substance as the function of temperature. Once one has calculated Eq. (2.8) for some reactions, they will be convinced that any variation in the heat of the condition affected by the temperature is not normally too significant.

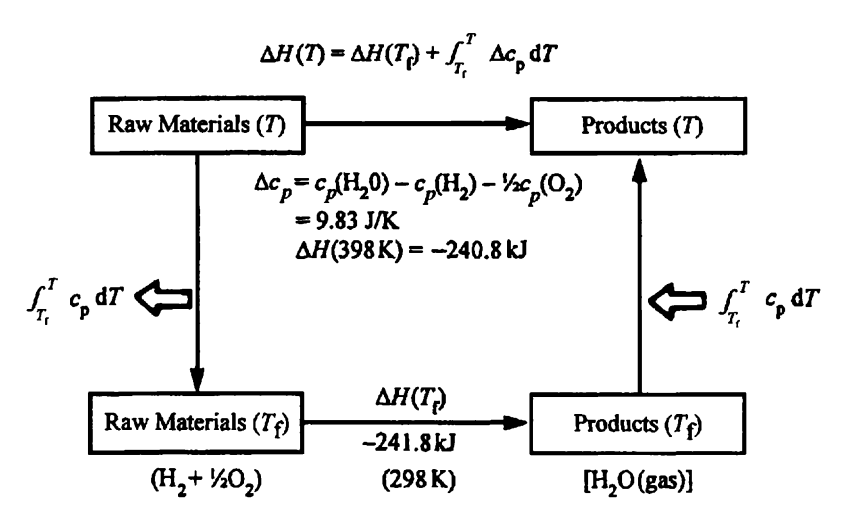


Figure 2.4 Reaction heat at an arbitrary temperature given the reaction heat at a particular temperature. Cooling, reacting and warming, will produce the same total heat. Enthalpy is a state function. An example of the reaction $H_2 + (1/2)O_2 \rightarrow H_2O$ (gas) is shown numerically.

2.2.4.2 The Equilibrium Constant

The equilibrium constant of a certain reaction at whatever temperature can be calculated from the difference between the Gibbs standard formation free energies of products and materials at a pressure of 1 atm by Eq. (2.3). However, the standard formation free energies contained in handbooks are in standard states at a temperature of 25 °C. The free energy at any given temperature can be obtained from the value at the standard condition and the specific heat data using the following equation.

$$\Delta G_{\rm f}^{\,\circ}(T) = \Delta G_{\rm f}^{\,\circ} + \int_{298}^{T} \Delta c_P dT - (T - 298) \Delta S_{\rm f}^{\,\circ} - T \int_{298}^{T} \Delta c_P d\ln T \qquad (2.9)$$

2.2.5 OPERATING CONDITIONS AND ENERGY EFFICIENCY OF CHEMICAL REACTIONS

Someone may falsely assume that proceeding toward room temperature is a way of enhancing the energy efficiency in a reaction process. It is in many cases wrong. For example, the reaction of adding chlorine to ethylene is an important step in the process of vinyl chloride synthesis; however we are striving to enhance energy efficiency by raising the reaction temperature as high as possible for the following reasons.

This is an exothermic reaction that proceeds even close to room temperature in the presence of iron ions. To begin this reaction at room temperature, heat must be removed from the reactor by cooling with water. In this case, the reaction heat is discarded to the water. The reaction temperature for a process pursuing energy efficiency is up to about 130 °C. The reaction heat is removed together with steam when the cooling water is boiled, and this steam is usable as energy such as a heat source for distillation of products. In short, the heat of reaction is recovered as high quality heat by raising the reaction temperature. The problem with higher reaction temperatures is the increase in byproducts such as polychlorides.

This example is consistent with the conclusion of thermodynamics that 'a reversible process is most efficient'. A reversible process is a process developed at equilibrium throughout the process. As known by the Le Chatelier-Braun law, in an exothermic reaction, the equilibrium constant decreases with temperature, leading to a lowered equilibrium conversion. In the above case, however, the equilibrium conversion at about 130 °C is still about 100%. A reaction at a high temperature provides high efficiency as it comes closer to a reversible reaction. The point beyond which the reaction does not proceed is the equilibrium temperature, where the theoretical limit of the energy efficiency improvement is given. On the contrary, the temperature for an endothermic reaction should be minimized as the equilibrium conversion and reaction rate are not largely restricted. Athermal reactions which generate little reaction heat may be conducted at any temperature. One of the reasons for the commercial success in reactions conducted at close proximity to room temperature using enzymes, as seen in the synthesis of fructose by isomerization of glucose, and synthesis of acetoamide by hydration of acrylonitrile, is that they are close to athermal reactions. The efficiency of processes such as the synthesis of ammonia and methanol performed in close proximity to the equilibrium conditions of a reaction is quite high.

Any desired reaction temperature can be selected. As shown in Figure 2.5, the temperatures of raw materials fed to a reactor can be adjusted as close to the reaction temperature as possible through heat exchange between the raw

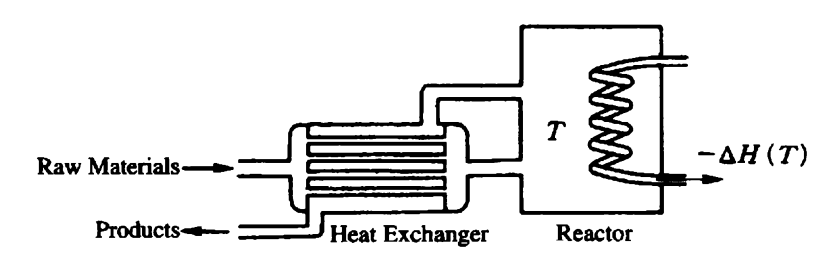


Figure 2.5 Heat exchange allows us to choose the reaction temperature level freely.

materials and products. A reaction at a high temperature does not generate more loss of energy for heating raw materials.

2.3 THE RATE OF REACTION

(a) The rate of elementary reactions is proportional to the concentration. It is common practice to define the rate of reaction based on the unit volume. The reaction rate is expressed as the number of molecules reacting per unit volume in unit time. This unit volume is the basis of finding the concentration. If the probability of a molecule reacting per unit time has been determined, the number of molecules reacting per volume is proportional to the number of molecules per volume, i.e. the concentration.

Let us consider a case in which a product is formed from two kinds of raw molecules A and B.

$$A + B \to C \tag{2.10}$$

From the above argument, it is obvious that the reaction rate is proportional to the probability of the reaction of A per unit time and the concentration of A. Molecule A would react when having an appropriate collision angle, and in contact with molecule B with a certain energy state. No matter what the detailed mechanism is, the probability would be proportional to the concentration of molecule B. Thus, the rate of reaction to form C from A and B is

$$r = k[A][B] \tag{2.11}$$

The reaction rates of A and B are proportional to the concentrations of A and B, respectively, insofar as the electronic state and reaction path of molecule A are not affected by an increase in concentration of A resulting from extremely high concentrations of A and B. Figure 2.6 shows a summary of the concentration dependency of the reaction rate.

(b) The rate of catalytic reactions is proportional to the adsorption concentration. The rate of reaction is proportional to the concentration, but it is not always equal to the concentrations of the gas and liquid phases. For example, in solid catalytic reactions that are crucially important in industrial processes, the factor determining the reaction rate is the concentration of reactants on the catalyst surface, while the concentration on an electrode surface determines the rate of the electrode reactions. That is, the rate of reaction is proportional to the concentration in the field where a reaction proceeds. Because it is difficult to measure the concentration on a solid surface, the relation between gas (or liquid) phase concentration and surface concentration is obtained in order to express the reaction rate as the function of gas (or liquid) phase concentration, i.e. the so called reaction rate equation.

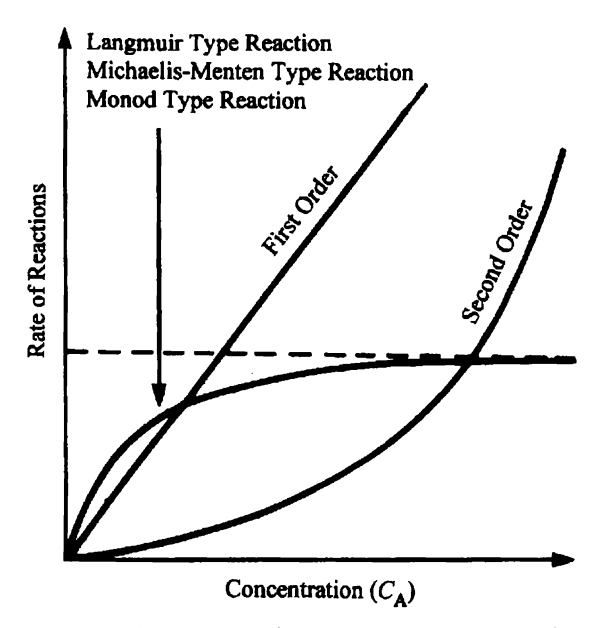


Figure 2.6 Concentration dependency of the rate of chemical reactions.

(c) Adsorption equilibrium and Langmuir's model

When in collision with a solid surface, molecules in a gas (or liquid) phase interact with various intermolecular forces. The molecules are absorbed on the solid surface by these forces with a certain probability. This is adsorption. Vibrating on the surface due to the thermal effect, the adsorbed molecules are released to the gas phase with a certain probability. This is desorption. The adsorption equilibrium is a state where the rate of molecular adsorption from a gas phase is equal to the rate of desorption from a solid surface. There are many relational expressions suggested on the adsorption concentration and gas (or liquid) phase concentration. Among them, the most popularly used is the Langmuir model.

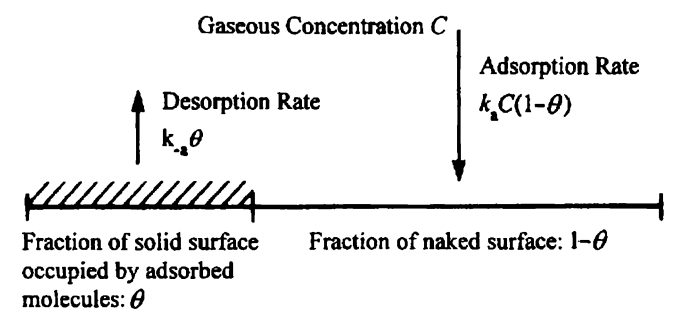


Figure 2.7 Concept of the Langmuir adsorption isotherm.

As shown in Figure 2.7, assume that the total surface on solid for adsorption is 1, the surface fraction θ is covered with adsorbed admolecules, and $1-\theta$ is the uncovered surface fraction. In this case, adsorption occurs if molecules collide with region 1- θ , but not if they collide with region θ . With the concentration in the gas phase being C, the rate of adsorption will be proportional to the product of the ratio $(1-\theta)$ and the number of collisions.

If we let the proportional coefficient be k_a ,

Adsorption rate =
$$k_{\mu}C(1-\theta)$$
 (2.12)

On the other hand, as that the desorption rate will be proportional to θ , expressing the proportional coefficient as k_{-a} leads to

Desorption rate =
$$k_{-a}\theta$$
 (2.13)

$$\theta = KC/(1 + KC) \tag{2.14}$$

where

$$K = k_a/k_{-a} \tag{2.15}$$

When molecules are absorbed on a solid surface at the maximum level, i.e. the saturated adsorption concentration is Q_0 , then the adsorption concentration O with the gas-phase concentration C is

$$Q = Q_0 KC/(1 + KC) (2.16)$$

The concept of Langmuir is simple and clear. Since the concentrations of C in the gas phase and on the solid surface are low, the adsorption concentration increases with the number of collisions from the gas phase, i.e. the gas-phase concentration. When the concentration on the solid surface reaches the saturated absorption concentration, the adsorption concentration will not increase any more even if the gas phase concentration is increased.

2.3.1 FACTORS GOVERNING THE RATE OF REACTION

A reaction rate is proportional to the concentration of molecules. To be more specific, it is dependent on the concentration of the active molecules in all molecules which have energy sufficient for causing a reaction, and also on the frequency of reactions of the active molecules. The factors determining the fraction of active molecules and the frequency of reactions are the temperature for thermal reactions and the luminous intensity for photochemical reactions.

2.3.1.1 The Rate Equation for Homogeneous Reactions (Thermal reactions)

Molecules have degrees of freedom of motion such as translation, rotation and vibration. When molecules are within a substance at thermal equilibrium at temperature T, the average energy of (1/2)kT is distributed to the molecules according to their degrees of freedom, where k is the Boltzmann constant. For example, although vibration energies are proportional to the square of the amplitude, energies vibrate with an amplitude leading to (1/2)kT on average. However, not all molecules have an energy of (1/2)kT. Some molecules have very small amplitudes and some have even larger amplitudes. Molecules with excessively large amplitudes may be decomposed in their directions, and when two different types of molecules come close to each other at a specific angle and in a specific energy state, they may form a high-energy state that can easily result in decomposition or unification. In this way, chemical reactions may occur because of a high-energy state formed at a certain probability among molecules at thermal equilibrium; such reactions are called thermal reactions.

In systems at thermal equilibrium, the probability that the energies of one degree of freedom will become higher than ε is proportional to $\exp(-\varepsilon/kT)$. If we assume that E is a value obtained by multiplying ε by Avogadro's number, i.e. energies per mole, the number of molecules with their energies per mole exceeding E is proportional to $\exp(-E/RT)$. Thus, the rate constant of a thermal reaction and the reaction rate equation for the first-order reaction are

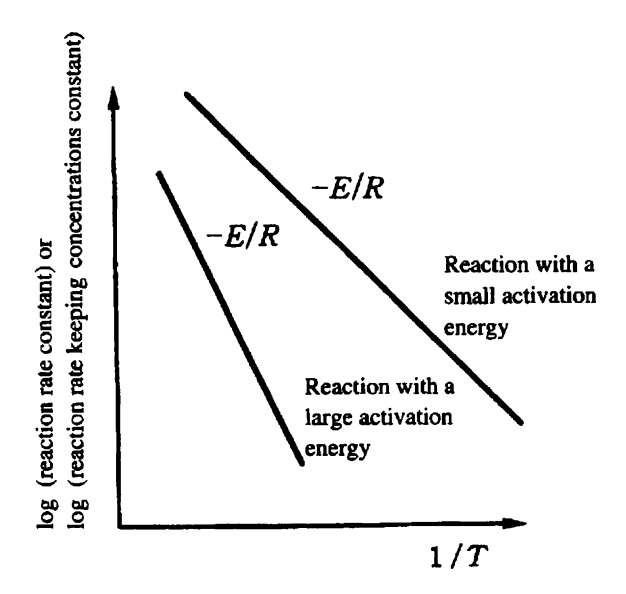


Figure 2.8 Arrhenius plot.

$$k = A \exp(-E/RT) \tag{2.17}$$

$$r = kC \tag{2.18}$$

where E [J/mol] is called the activation energy for a reaction. Equation (2.17) is called the Arrhenius equation. As shown in Figure 2.8, plotting the logarithm of the reaction rate constant versus the inverse of absolute temperature, gives a straight line. Such a method of plotting is called an Arrhenius plot. The activation energy is obtained from (-E/R), the slope of the straight line.

2.3.1.2 Rate Equation for Heterogeneous Reaction (Thermal Reaction)

2.3.1.2.1 Solid Catalytic Reaction

Nothing happens even if the mixture of CO and H_2 is kept at a few hundred degrees, but if an Ni catalyst with ultra-fine Ni particles dispersed on a porous carrier is added to the mixture, CH_4 is formed. This solid catalytic reaction is thought to proceed with CO and H_2 adsorbed on the surface of Ni.

$$CO + 3H_2 \xrightarrow{N_i} CH_4 + H_2O$$
 (2.19)

The rate of reaction is dependent on the reacting conditions such as the activity of the Ni catalyst, the reaction temperature and the concentration. For example, it has been reported that the rate can be expressed by the following equation:

$$r = k[CO]^{-1}[H_2].$$
 (2.20)

This means that the reaction rate decreases with an increase in concentration of CO, but proportional to the concentration of H_2 . The reason why the reaction rate decreases with an increase in concentration of CO is considered to be because a catalytic reaction takes place on a catalyst surface, and the reaction rate is proportional to the adsorption concentration on the catalyst surface. The reaction rate equation that applies Langmuir's adsorption equilibrium to the rate of catalytic reaction is called the Langmuir-Hinshelwood equation. That is, the adsorption equilibrium concentration as expressed by Eq. (2.16) is assumed to be kept even on the catalyst surface.

For example, in the case when molecules of CO and H_2 are absorbed competitively on some active site, it is called competitive absorption, the adsorption concentrations of CO and H_2 and the reaction rate equation are

$$q_{\text{CO}} = K_{\text{CO}} C_{\text{CO}} / (1 + K_{\text{CO}} C_{\text{CO}} + K_{\text{H}_2} C_{\text{H}_2})$$

$$q_{\text{H}_2} = K_{\text{H}_2} C_{\text{H}_2} / (1 + K_{\text{CO}} C_{\text{CO}} + K_{\text{H}_2} C_{\text{H}_2})$$

$$r = k K_{\text{CO}} K_{\text{H}_1} C_{\text{CO}} C_{\text{H}_2} / (1 + K_{\text{CO}} C_{\text{CO}} + K_{\text{H}_3} C_{\text{H}_3})^2$$
(2.22)

Let us assume that the adsorption of CO is much stronger than H_2 , and furthermore that $K_{CO}C_{CO} \gg K_{H_2}C_{H_2} \gg 1$, Eq. (2.22) leads to

$$r = (kK_{\rm H_2}/K_{\rm CO})C_{\rm CO}^{-1}C_{\rm H_2} \tag{2.23}$$

This means that the result agrees with the experiment: the reverse first-order reaction for the concentration of CO and the first-order reaction for that of H₂.

As a physical image, because the Ni surface is mostly covered with CO, the adsorption concentration does not increase even with an increase in concentration of CO in a gas phase. Instead, the concentration of H_2 is rather decreased, which adversely reduces the reaction rate. On the other hand, H_2 is weakly adsorbed; an increase in concentration of H_2 in the gas phase increases the adsorption concentration proportionally.

As above, even if the apparent reaction rate indicates a peculiar concentration dependency, the rate is proportional to the concentration in the reaction field.

2.3.1.2.2 Enzymic Reaction

Enzymes are protein as well as a catalyst existing in a living body. The rate equation for enzymic reactions is called the Michaelis-Menten reaction rate equation. Its conception and the form of the rate equation are completely identical with Langmuir's rate equation with respect to solid catalysts.

$$E + S \Longrightarrow ES$$
 (2.24)

$$ES \longrightarrow E + P \tag{2.25}$$

Where E is an enzyme and S is the substrate for enzymic reactions. ES is a complex in which the enzyme is adsorbed by substrate, and P is the product. For example, in the case of an isomerization reaction of glucose into fructose by invertase, E is invertase, S is glucose and P is fructose. The reaction rate is proportional to the concentration of ES, $C_{\rm ES}$. In the case of steady-state assumption for ES, the reaction rate is

$$r = kC_{\rm E0}C_{\rm S}/(K_{\rm m} + C_{\rm S})$$
 (2.26)

where $K_{\rm m}$ is the Michaelis-Menten constant, and $C_{\rm S}$ and $C_{\rm E0}$ are the substrate concentration and overall enzyme concentration, respectively. Equation (2.26) is the Michaelis-Menten equation that is very similar to the Langmuir-

Table 2.2 Concept of heterogeneous reactions and their rate equations

Reaction	Reaction rate equation	Mechanism that causes non-linear concentration dependency		
Solid catalytic reaction	Langmuir–Hinshelwood equation $\frac{kKC}{1+KC}$	Decreased surface area available fo adsorption		
Enzymic reaction	Michaelis–Menten equation $\frac{k[E_0][S]}{K_m + [S]}$	Decreased concentration of free enzyme		
	Monod's equation $\frac{kC}{K+C}$	Essentially, enzymic reactions occur		

Hinshelwood catalytic reaction rate equation shown in Eq. (2.22) because their conceptual mechanisms are almost identical.

When the substrate concentration C_S is small, most of an enzyme is free, and the concentration of ES is proportional to C_S . However, as C_S becomes higher, the ratio of the free part of the enzyme becomes low, whereby even if C_S is increased, C_{ES} does not increase at that ratio. After that, when the enzyme reaches C_{ES} almost overall, the reaction rate does not increase even if C_S is further increased. Enzymes may be replaced by the surface area of solid catalysts.

2.3.1.2.3 Breeding Reactions of Micro-organisms (extension of the enzymic reaction rate equation)

Although both solid catalytic and enzymic reactions are abiotic reactions, breeding of micro-organisms is a bioreaction that is very complex because of dependence in age and activity of micro-organisms. For the logarithmic growth phase within the ages of micro-organisms, a typical rate equation called Monod's equation is presented, expressing the dependency of the breeding rate on the substrate concentration.

$$r = kC/(K_{\rm M} + C) \tag{2.27}$$

Table 2.3 Kinds of chemical reactions and their kinetic characteristics

	Reaction rate equation	Energy term
Thermochemical reaction	$A \exp\left(-\frac{E}{RT}\right)C$	Temperature: T
Electrochemical reaction	$A\exp\bigg(\frac{azF(V-V^*)}{RT}\bigg)C$	Overpotential: $V-V^*$
Photochemical reaction	AIC APC(n>1) Appreciable in very strong irradiation as laser light intensity	Irradiation: I
Plasmachemical reaction	$(v_e \sigma C_e)_{av} C$ σ : Dissociation cross-section C_e : Electron concentration	Electron velocity: v_e

C refers to concentration. The rate of any kind of reaction is proportional to the concentration in the reaction field

Monod's equation has the same form as the Michaelis-Menten equation, from which it can be understood that Monod's equation is a rate equation governed by reactions in micro-organisms.

As a result, although catalysts vary by reactions: solid catalysts, enzymes and micro-organisms, similar reaction rate equations are proposed based on the similar mechanisms with a reasonable explanation of experimental data. Table 2.2 summarizes the reaction rate equations of those heterogeneous systems.

2.3.1.3 Rate Equations for Other Chemical Reactions

Photochemical, electrochemical and plasma chemical reactions are utilized in industrial applications, in which molecules are not excited by heat, thus their reaction rate constants are different from those obtained from Eq. (2.17). In general, the rate of photochemical reaction is proportional to luminous intensity, but less dependent on temperature. In electrochemical reactions, overvoltage is a critical factor. That is, electrochemical reactions strongly depend on the magnitude of potential difference from the equilibrium potential difference required to start a reaction. Normally, electrochemical reactions depend on overvoltage exponentially. In plasma chemical reactions, the key factor is the behaviour of raw molecules when electrons existing in plasma collide with the molecules. This behaviour is summarized by specific values of

the reaction system called the collision cross-section. Generally, the plasma chemical reaction is evaluated by the yield of radicals.

It is important to note that the rate equations are for elementary reactions. Strictly speaking, the reaction rate equations referred to herein concern elementary reactions. For example, let us assume that radicals are formed in a photochemical reaction. The rate is given as shown in Table 2.3. However, those radicals react with raw molecules to form new species, subsequently repeating reactions to form products. To predict the rates of reduction of raw materials and formation of products, we must recognize that real reactions are the results of complex phenomena.

2.4 COMPLEX REACTION SYSTEM

It is very rare to have an elementary reaction take place independently. For example, let us consider oxidation of methane by burning. This reaction is expressed by

$$CH_4 + 2O_2 \longrightarrow CO_2 + 2H_2O \tag{2.28}$$

This reaction consists of 100 or more elementary reactions as shown in Table 2.1, and those reactions proceed simultaneously. One molecule of CO₂ and two molecules of H₂O are not formed directly by collision of two molecules of oxygen with one molecule of methane. Actually, many species such as stable molecules of CO and C₂H₄ as well as radicals of OH and CH₃ are formed, and methane combustion proceeds with a number of elementary reactions simultaneously. Since it is not easy to analyse a reaction consisting of a number of elementary reactions, we will be well advised to simplify the reaction to attain the purpose of expressing the reaction rate mathematically. Such a procedure is called reaction modelling. The basic concept of reaction modelling is described below.

2.4.1 RATE-DETERMINING STEP

Simply, let us consider a reaction system where A_1 forms A_2 , which then triggers a series of subsequent formations from A_2 to A_3 , and from A_3 to A_4 ...

$$A_1 \iff A_2 \iff \iff A_n \longrightarrow P$$
 (2.29)

From those reactions, we find the slowest reaction compared with other reactions. When the rate of this reaction governs the rate of the overall reaction, this is called the rate-determining step. If this rate-determining step is $A_n \rightarrow P$, the reduction rate of A_1 , i.e. the formation rate of P, is given by

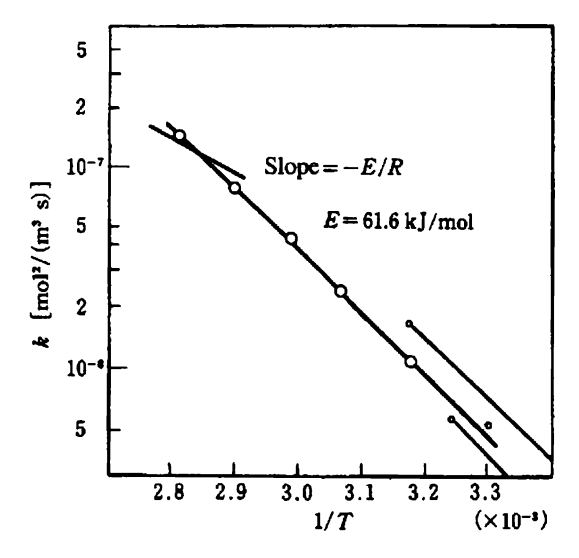


Figure 2.9 Temperature dependency experimentally observed for synthesis of acetaldehyde from C_2H_4 (calculated by the author using the data reported in five publications). The rate of this reaction is expressed as $r=k[Pd^{2+}][C_2H_4]/[Cl^{-}]^2[H^{+}]$, where $[Pd^{2+}]$, $[Cl^{-}]$, $[H^{+}]$ are concentration of the Palladium ion, Chlorine ion and Hydrogen ion, respectively in catalyst solution. This complex reaction rate form reveals the existence of multiple equilibria in the reaction solution.

$$r = kK_1K_2 \cdots K_nC_{A_1}$$

 $K_i = k_i/k_{-i}$ (2.30)

All reactions proceeding to the rate-determining step are at equilibrium. That is, we may approximate all reactions proceeding to the rate-determining step at equilibrium. What is important here is that the reaction rate could be expressed by the concentration of raw material A₁ alone. But, we cannot always find out the rate-determining step. Still, in the case of several reactions having similar degrees of rate constants, we cannot determine the rate-determining step exactly, but we can determine it generally. This is because it is a normal case where the slowest reaction is slower by at least more than 10 times the next slowest reaction. When the rate-determining step is known, the reaction rate can be simplified as Eq. (2.30).

Expressing the reaction rate by Eq. (2.30) means, for example, that even if we try to obtain the activation energy from temperature dependency by measuring the reaction rate, the obtained value does not represent the activation energy of the elementary reaction that controls the over-all reaction. Its example is shown in Figure 2.9.

2.4.2 PATTERNING OF REACTION SYSTEMS

An actual reaction system consisting of a number of elementary reactions has several basic patterns or their combinations.

Parallel reactions A
$$\nearrow$$
 B (2.31)

Consecutive reactions
$$A \longrightarrow B \longrightarrow C$$
 (2.32)

If a reaction system can be expressed by these combinations, this allows simplification of the handling of its reactions along with the concept of the rate-determining step. What is complicated is the case where loops are produced. For example, if reactions forming A from B or C for Eq. (2.32) are not negligible, its mathematical handling will be complicated.

2.4.3 RELATIONS WITH OTHER TRANSFER PROCESSES

So far we have postulated that, however complex they are, reactions proceed freely without restriction of mass transfer and heat conduction in chemical reaction processes. However, chemical reactions rarely proceed without such restrictions in a reactor.

For example, in the case where polymerization is performed in the stirred tank while removing the heat of reaction by externally cooling, the temperature in the centre of the tank is higher than temperatures in the vicinity of the outer wall of the tank. So, the reaction rate in the tank centre is higher; thus, the entire tank cannot be considered to be a field of equal reactions.

In another case, the rates of fast reactions such as combustion may be dependent on the diffusion. For example, burning of fireworks is a combustion reaction of metals and explosive particles in the air. Its reaction rate depends on the rate at which oxygen diffuses from the air onto the surface of the particles.

Although a chemical reaction of the slowest rate is assumed to be the ratedetermining step in Section 2.4.1, the overall rate may be often dependent on the mass feed and heat transfer in the actual processes.

CHAPTER 3

Fundamentals of Heat and Mass Transfer

KOICHI ASANO

Department of Chemical Engineering, Tokyo Institute of Technology, Japan

3.1 RATE EQUATIONS

3.1.1 CONDUCTION OF HEAT

Figure 3.1 shows a physical picture of conduction of heat through a flat plate of surface area A [m²] and thickness δ [m], of which both surfaces are at different temperatures. Transfer of heat takes place from the higher temperature side to the lower one, which is known as conduction of heat. At steady state, a linear temperature profile is established in the direction of heat flow, the y-direction, and the rate of heat transfer Q [W] under such conditions is known to be proportional to the temperature difference between both the surfaces, ΔT [K]:

$$Q \propto A(\Delta T/\delta) \tag{3.1}$$

As δ becomes infinitesimally small, Eq. (3.1) reduces to the following equation to give the heat flux or rate of heat transfer per unit area of the surface q(=Q/A) [W/m²].

$$q = Q/A = -k(dT/dy)$$
 (3.2)

Equation (3.2) is known as Fourier's law of heat conduction, where proportionality constant on the right-hand side of the Eq. (3.2), k, is the thermal conductivity [W/(m K)]. The thermal conductivities of pure substances are physical properties of the substances, which vary with temperatures. The thermal conductivity of mixtures varies with their compositions as well as temperatures.

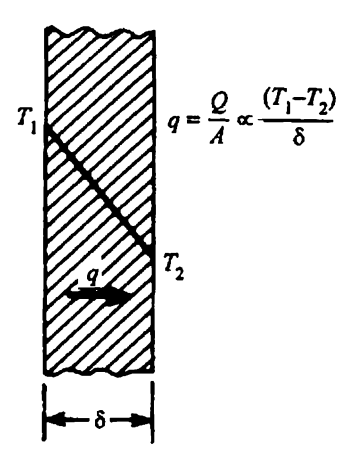


Figure 3.1 Conduction of heat through a solid plate.

3.1.2 DIFFUSION

Figure 3.2 shows a physical picture of evaporation of volatile liquid in a test tube in contact with flow of dry air. At steady state linear concentration profile of evaporated vapour is established in the vapour space of the test tube and steady evaporation of the liquid takes place. The transfer of material, which is caused by non-uniform distribution of concentration, is known as the diffusion. The rates of the diffusion of the component A per unit area of the surface (diffusion flux) J_A [kg/(m²s)] are empirically known to be proportional to their concentration gradients:

$$J_{A} = -\rho D(d\omega_{A}/dy) \tag{3.3}$$

which is known as the Fick's law of the diffusion, where ρ is the density of fluid $[kg/m^3]$, ω_A is the mass fraction of component A [-], y is the distance from the surface [m], and the coefficient D is the diffusivity or diffusion coefficient $[m^2/s]$. The diffusivities of the component A in the fluid or solid are physical properties of the system. The diffusivities in binary systems are usually independent of the concentration, whereas the ones in multicomponent systems are not. The binary diffusion coefficients in the gas phase are dependent on temperature and pressure, while the ones in the liquid phase are dependent on temperature and not on pressure.

The kinetic theory of gases defines the diffusion flux of the component A in the gas phase as relative motion of the component to the centre of mass of the mixture. To simplify the discussions, we assume one-dimensional motion of each component with $v_i[m/s]$. The mass average velocity of the system, V[m/s], or the baricentric velocity is given by:

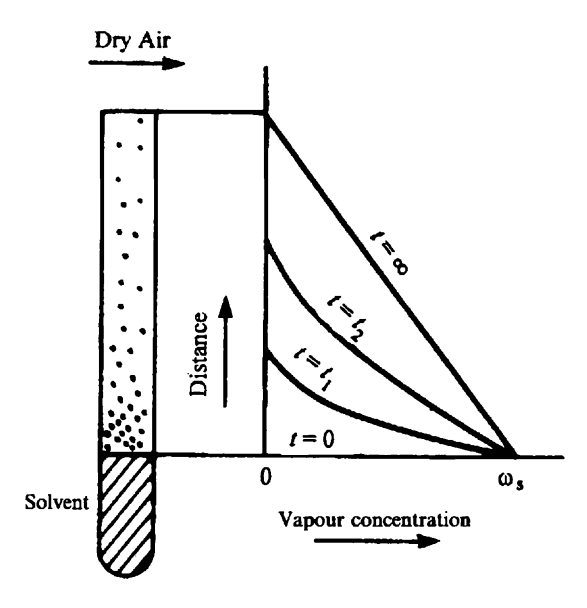


Figure 3.2 Diffusion of vapour⁽¹⁾.

$$V = \sum \omega_i v_i \tag{3.4}$$

Thus, the diffusion flux of component i, J_i [kg/(m²s)], is expressed as:

$$J_{i} = \rho \omega_{i}(v_{i} - V) \tag{3.5}$$

From Eqs (3.4) and (3.5), we obtain an important theorem for the diffusion fluxes:

$$\sum J_{i} = 0 \tag{3.6}$$

After long and tedious calculations, of which the detail is shown in standard textbooks on the kinetic theory of gases, the diffusion flux of component A in a binary system is shown to be identical with the empirical Fick's law,

$$J_{A} = \rho \omega_{A} (v_{A} - V)$$

$$= -\rho D(d\omega_{A}/dy)$$
(3.7)

A similar relation is obtained for the molar diffusion flux, J_i^* [kmol/(m² s)], which is defined in terms of molar average velocity, $V^*(=\sum x_i v_i)$ [m/s]:

$$J_i^* = cx_i(v_i - V^*) = -cD(dx_i/dy)$$
(3.8)

That is,

$$\sum J_i^* = 0 \tag{3.9}$$

For a binary system, the following simple relationship between the two diffusion fluxes, J_A and J_A^* :

$$J_{A}^{*} = (x_{B}/M_{A} + x_{A}/M_{B})J_{A}$$
 (3.10)

is obtained from the definition of diffusion fluxes, but no similar relation is known for multicomponent systems.

3.1.3 DIFFUSION FLUX AND MASS FLUX⁽²⁾

Let us consider a transport phenomenon, which takes place during contact between two immiscible fluids, or contact between fluid and solid. If the concentration of a component is not uniform in either or in both phases, the diffusion of the component from the interface to the bulk, or vice versa, takes place, through which transfer of the component takes place. This phenomenon is called mass transfer.

The mass flux of the component A, or the mass of the component A passing through the unit area of the interface per unit time, N_A [kg/(m²s)], is expressed as the product of the mass fraction of component A at the interface, ω_{As} [-], the velocity of the component A normal to the interface, v_{As} [m/s], and the density of the mixture, ρ_s [kg/m³]

$$N_{\mathsf{A}} = (\rho_{\mathsf{s}}\omega_{\mathsf{A}\mathsf{s}}v_{\mathsf{A}\mathsf{s}}) \tag{3.11}$$

Rearranging the above equation by use of the definition of the diffusion flux, Eq. (3.3), gives the following expression for the mass flux:

$$N_{A} = (\rho_{s}\omega_{As}v_{s}) + \{\rho_{s}\omega_{As}(v_{A} - V)\}$$

$$= (\rho_{s}\omega_{As}v_{s}) + (J_{A})_{s}$$
(convective term) (diffusion term)
$$(3.12)$$

The above equation clearly indicates that the mass flux is composed of two parts: the convective mass flux and the diffusion flux at the interface. This makes a big difference from the heat transfer, where no effect of the convective term is known.

Unidirectional diffusion is a binary mass transfer, in which only one component is transferred through a stagnant fluid, as is the case with gas absorption or evaporation of a pure liquid. If we assume that component A is transferred through the stagnant component B, the mass flux of component B, N_B [kg/(m² s)] is given by:

$$N_{\rm B} = (\rho_{\rm s}\omega_{\rm Bs}v_{\rm s}) + (J_{\rm B})_{\rm s} = 0 \tag{3.13}$$

Rearrangement of Eq. (3.13) by use of the diffusion flux theorem, Eq. (3.6),

gives the following expression for the interfacial velocity, v_s , or the normal component of the interface velocity as:

$$v_{\rm s} = -(J_{\rm B})_{\rm s}/\rho_{\rm s}\omega_{\rm Bs} = (J_{\rm A})_{\rm s}/\{\rho_{\rm s}(1-\omega_{\rm As})\}$$
 (3.14)

Substitution of Eq. (3.14) into Eq. (3.12) gives the following equation for the mass flux of component A:

$$N_{\rm A} = (J_{\rm A})_{\rm s}/(1 - \omega_{\rm As})$$
 (3.15)

This indicates that the mass flux in unidirectional diffusion is $1/(1-\omega_{As})$ times as large as the diffusion flux at the interface.

3.2 MASS AND HEAT TRANSFER COEFFICIENTS

3.2.1 MASS TRANSFER COEFFICIENT

Figure 3.3 shows a schematic picture of the concentration profile near the interface between two fluids. At the interface, the surface concentrations of each phase are at their equilibrium conditions, but the concentrations near the interface are usually different from the one at the interface. As is shown in the figure, the concentration near the interface changes rapidly with distance from

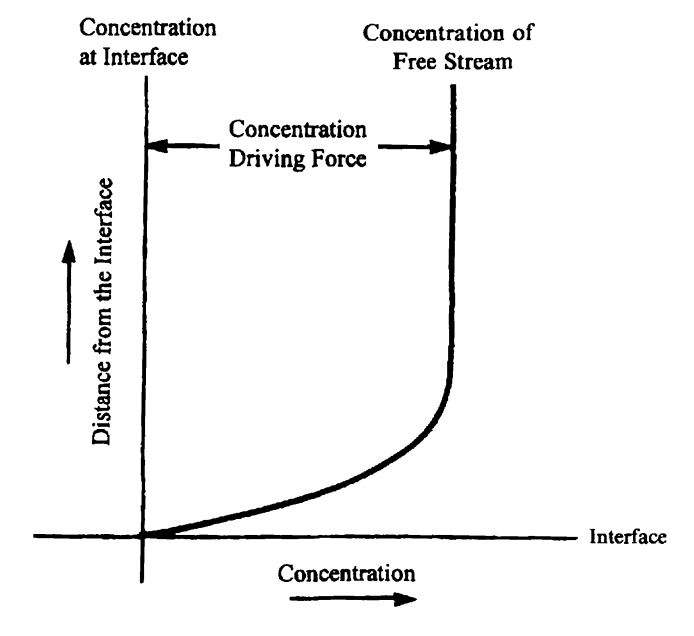


Figure 3.3 Concentration profile near the interface.

the interface and approaches gradually to the bulk fluid concentration. This concentration difference between the interface and the bulk fluid, which causes the diffusion of the component, is called the concentration driving force for mass transfer.

Concentration driving force =

interface concentration – free steam concentration

If we assume that the mass fluxes are proportional to their concentration driving forces, we may define the mass transfer coefficients by the following equation:

Mass flux = (mass transfer coefficient) \times (concentration driving force)

The problem with mass transfer is that we are using a variety of units to express the concentrations, such as mole fraction, mass fraction etc., because of practical convenience. This gives a variety of mass transfer coefficients. Table 3.1 summarizes mutual relationships between various units of the concentrations. Table 3.2 shows various definitions of the mass transfer coefficients and their corresponding dimensionless groups, Sherwood numbers.

3.2.2 OVERALL MASS TRANSFER COEFFICIENT

In the actual mass transfer processes, concentration distributions are usually observed on both sides of the interface except for the special cases such as absorption of pure gases or evaporation of pure liquids. Figure 3.4 shows a physical picture of the concentration profiles near the interface. Under such conditions, the interface concentrations are difficult to determine and evaluation of the rates of mass transfer by use of mass transfer coefficients becomes practically impossible. However, we can evaluate the rates of mass transfer even under such conditions, if we make use of the overall mass transfer coefficients, $K_{0v}[\mathrm{kmol/m^2}\,\mathrm{s})]$ or $K_{0x}[\mathrm{kmol/(m^2}\,\mathrm{s})]$ instead of the individual coefficient.

The mass balance on both sides of the interface can be expressed by the following equations:

$$N_{A}^{*} = k_{y} (y_{\infty} - y_{s})$$

$$= k_{x} (x_{s} - x_{\infty})$$

$$= K_{0y} (y_{\infty} - y^{*})$$

$$= K_{0x} (x^{*} - x_{\infty})$$
(3.16)

If we assume a linear equilibrium relation at the interface (y = mx + b), the following relation between the overall mass transfer coefficient and individual coefficients can easily be obtained:

Table 3.1 Relation between various units of concentration⁽³⁾

	Mass Fraction $\omega_{\rm A}$ [-]	Mole Fraction x _A [-]	Density $ ho_A$ [kg/m ³]	Partial concentration C_A [kmol/m ³]	Absolute Humidity PA [kPa]	Partial pressure H [-]
Mass fraction ω_A	ω_{A}	$\frac{x_{A}M_{A}}{\Sigma x_{i}M_{i}}$	$rac{ ho_{A}}{\Sigma ho_{i}}$	$\frac{c_{A}M_{A}}{\rho}$	$rac{p_{\mathrm{A}}M_{\mathrm{A}}}{\Sigma p_{i}M_{i}}$	$\frac{H}{(1+H)}$
Mole fraction x_A [-]	$rac{\omega_{ m A}/M_{ m A}}{\Sigma\omega_i M_i}$	x_{A}	$\frac{(ho_{\mathrm{A}}/M_{\mathrm{A}})}{\Sigma\left(ho_{i}/M_{i} ight)}$	$\frac{c_{Ai}}{\sum c_i}$	$\frac{p_{A}}{\sum p_{i}}$	$\frac{H}{(M_{\rm A}/M_{\rm B})+H}$
Partial density ρ _A [kg/m ³]	$ ho\omega_{ extsf{A}}$	$\frac{\rho x_{A} M_{A}}{\sum x_{i} M_{i}}$	$ ho_{A}$	$c_{A} M_{A}$	$\frac{M_{\mathrm{A}}p_{\mathrm{A}}}{RT}$	$\frac{\rho H}{(1+H)}$
Concentration c_A [kmol/m ³]	$rac{ ho\omega_{ extsf{A}}}{M_{ extsf{A}}}$	$cx_{\mathbf{A}}$	$\frac{ ho_{A}}{M_{A}}$	c_{A}	$\frac{p_{A}}{RT}$	$\frac{(\rho/M_{\rm A})H}{(1+H)}$
Partial pressure p _A [kPa]	$\frac{(\omega_{A}/M_{A})P}{\Sigma\omega_{i}M_{i}}$	$Px_{\mathbf{A}}$	$\frac{RT\rho_{A}}{M_{A}}$	$c_{A}RT$	$p_{\mathbf{A}}$	$\frac{PH}{(M_{\rm A}/M_{\rm B})+H}$
Absolute humidity H [-]	$\frac{\omega_{A}}{(1-\omega_{A})}$	$\frac{(M_{\rm A}/M_{\rm B})x_{\rm A}}{1-x_{\rm A}}$	$(ho_{\rm A}/ ho_{\rm B})$	$\frac{c_{A}M_{A}}{c_{B}M_{B}}$	$\frac{(M_{\rm A}/M_{\rm B})p_{\rm A}}{(P-p_{\rm A})}$	Н
Mixture	$\rho = \sum \rho_i, c =$	$=\Sigma c_i, P=\Sigma p_i, M=$	$= \sum x_i M_i$			

Table 3.2 Various definitions of mass transfer coefficients and Sherwood numbers

Flux	Phase	Definition	Unit	Sherwood numbers	
	1	$N_{\rm A}^* = k_c(c_{\rm s} - c_{\infty})$	[m/s]	$k_c L/D_{ m G}$	
		$N_{\rm A}^* = k_y (y_{\rm s} - y_{\infty})$	$[kmol/(m^2 s)]$	$k_y L/c_{ m G} D_{ m G}$	
	Vapour	$N_{\rm A}^* = k_{\rm G}(p_{\rm s} - p_{\infty})$	[kmol/m ² s kPa]	$k_{\rm G}RTL/D_{\rm G}$	
Mole flux	$N_{\rm A}^* = k_{\rm Y}(Y_{\rm s} - Y_{\infty})$	$[kmol/(m^2 s)]$	$\frac{k_Y L(Y_s - Y_\infty)}{c_G D_G(y_s - y_\infty)}$	Sh*	
		$ (N_{\rm A}^* = k_{\rm L}(c_{\rm L} - c_{\infty}) $	[m/s]	$k_{ m L}/D_{ m L}$	
Liquid	Liquid	$\langle N_{A}^* = k_x (x_{s} - x_{\infty})$	$[kmol/m^2 s)]$	$k_x L/c_{L} D_{L}$	
		$N_{A}^* = k_{x}(X_{s} - X_{\infty})$	$[kmol/(m^2 s)]$	$\frac{k_x L(X_s - X_\infty)}{c_L D_L(x_s - x_\infty)}$	
	1	$(N_{\rm A}^* = \rho k(\omega_{\rm s} - \omega_{\infty})$	[m/s]	$kL/D_{ m G}$	
Mass flux	Vapour	$\begin{cases} N_{\rm A}^* = k_{\rm H}(H_{\rm s} - H_{\infty}) \end{cases}$	$[kg/(m^2 s)]$	$\frac{k_{\mathrm{H}}L(H_{\mathrm{s}}-H_{\infty})}{\rho D_{\mathrm{G}}(\omega_{\mathrm{s}}-\omega_{\infty})}$	Sh
	Liquid	$\{ N_{\rm A}^* = \rho k(\omega_{\rm s} - \omega_{\infty})$	[m/s]	$kL/D_{ m L}$	

Remarks: c_G = Vapour phase molar density [kmol/m³]: c_L = Liquid phase molar density [kmol/m³]: D_G = Vapour phase diffusion coefficient [m²/s]: D_L = Liquid phase diffusion coefficient: H = Absolute humidity [-]: L = (Characteristic) Length [m]: m_A = Molecular weight [kg/kmol]: N_A = Mass flux [kg/m² s]: N_A^* = molar flux (= N_A/M_A) [kmol/m² s]: p = partial pressure [kPa]: R = Gas constant = 8.3143 [J/(mol K)]: T = Temperature [K]: T = Liquid phase mole fraction [-]: T = Vapour phase m

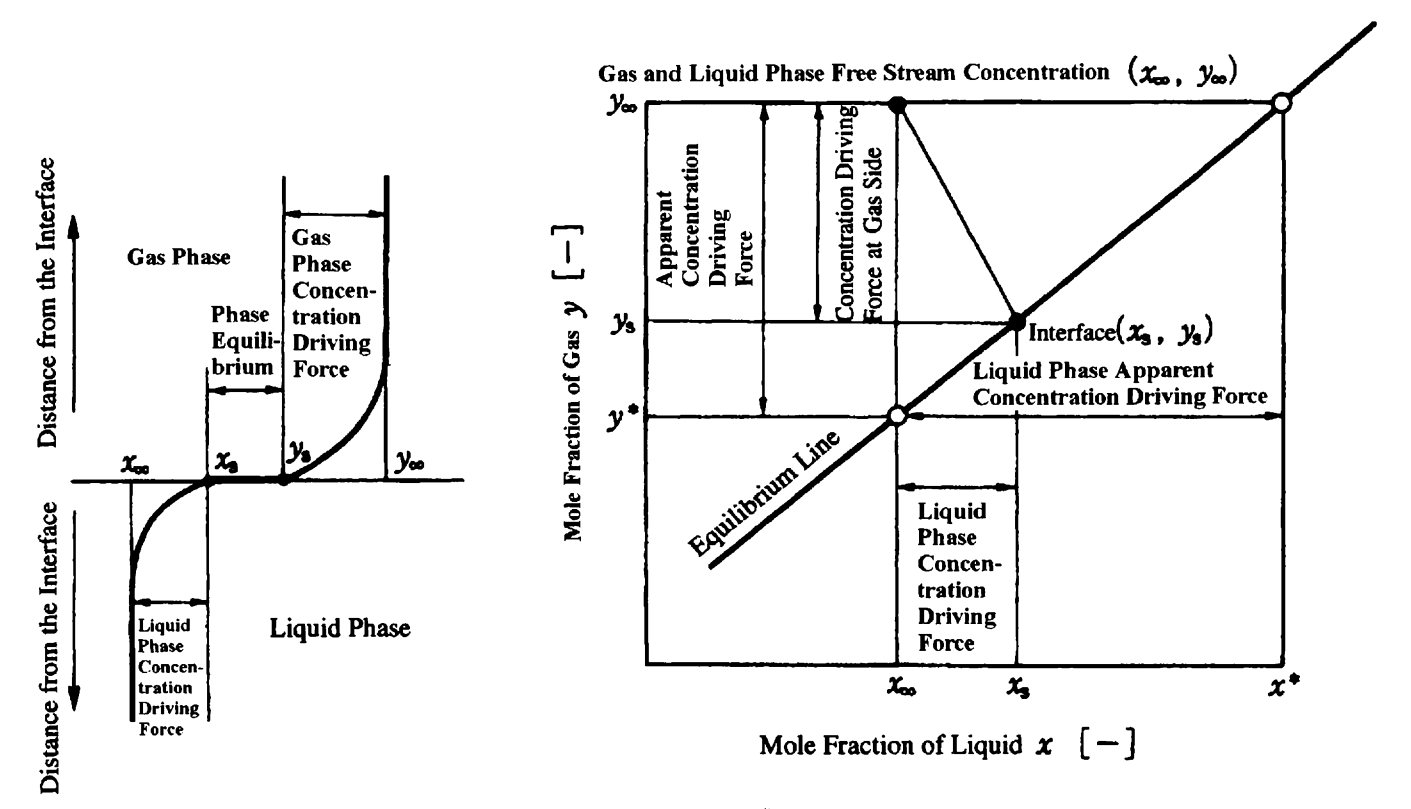


Figure 3.4 Overall mass transfer coefficients and concentration profiles⁽⁴⁾.

$$1/K_{0y} = 1/k_y + m/k_x = m/K_{0x}$$
 (3.17)

Equation (3.17) indicates that we can estimate the overall mass transfer coefficient K_{0y} or K_{0x} , if individual coefficient, k_y and k_x , is known and finally evaluate the rates of mass transfer. Although the above discussions are based on the mass transfer coefficients in terms of the mole fraction concentration driving-force, similar relations are obtained for the mass transfer coefficients based on other definitions of concentration driving-forces.

3.2.3 HEAT TRANSFER COEFFICIENT

In convective heat transfer between the fluid and the solid or the one between the fluid and fluid, a similar temperature distribution to that in Figure 3.3 is observed. If we assume that the heat flux q [W/m²] is also proportional to the temperature difference between the wall and the bulk fluid, ΔT [K], or temperature driving-force, the heat flux q can be expressed as:

$$q = h\Delta T \tag{3.18}$$

where the proportionality constant h [W/(m² K)] on the right-hand side of Eq. (3.18) is called the heat transfer coefficient.

3.2.4 OVERALL HEAT TRANSFER COEFFICIENT

If heat is transferred from the high-temperature fluid to the low-temperature one through a solid wall, such as is the case with heat exchangers, the temperature difference between the wall and the bulk fluid is usually observed on both sides of the heating wall. The heat flux through the wall can be calculated by use of the overall heat transfer coefficient $U[W/(m^2K)]$ in a similar way.

The following equations are obtained from the heat balance:

$$q = h_1(T_1 - T_{w1})$$

$$= (k/\delta)(T_{w1} - T_{w2})$$

$$= h_2(T_{w2} - T_2)$$

$$= U_1(T_1 - T_2)$$
(3.19)

Rearrangement of the above equations gives the following equation for the overall heat transfer coefficient:

$$1/U = 1/h_1 + 1/h_2 + (\delta/k)$$
(3.20)

where h_1 and h_2 are the heat transfer coefficients of phase 1 and phase 2, respectively, k is the thermal conductivity of the wall [W/(m K)], and δ is the thickness of the wall [m].

3.3 HEAT AND MASS TRANSFER IN A LAMINAR BOUNDARY LAYER ALONG A FLAT PLATE

3.3.1 GOVERNING EQUATIONS OF HEAT AND MASS TRANSFER

Heat and mass transfer in a laminar boundary layer along a flat plate are fundamental problems in transport phenomena. Figure 3.5 shows the velocity and the concentration profile in the region near the flat plate which is placed parallel to the direction of flow of uniform velocity. If the free stream velocity, U_{∞} [m/s], is large enough, the effect of viscosity is limited to a narrow region near the plate and the velocity changes rapidly in this region. This is called the (velocity) boundary layer. Under such conditions similar profiles are observed for the temperatures and the concentrations, which are known as the temperature and the concentration boundary layer, respectively. If the flow in the boundary layer is laminar then it is called the laminar boundary layer and, if it is turbulent, then the turbulent boundary layer.

In a laminar boundary layer along a flat plate, the velocity, the temperature and the concentration profiles are given by the following equations:

Continuity equation:

$$\frac{\partial u}{\partial x} + \frac{\partial v}{\partial y} = 0 \tag{3.21}$$

Equation of motion:

$$\rho u \frac{\partial u}{\partial x} + \rho v \frac{\partial u}{\partial y} = \mu \frac{\partial^2 u}{\partial y^2}$$
 (3.22)

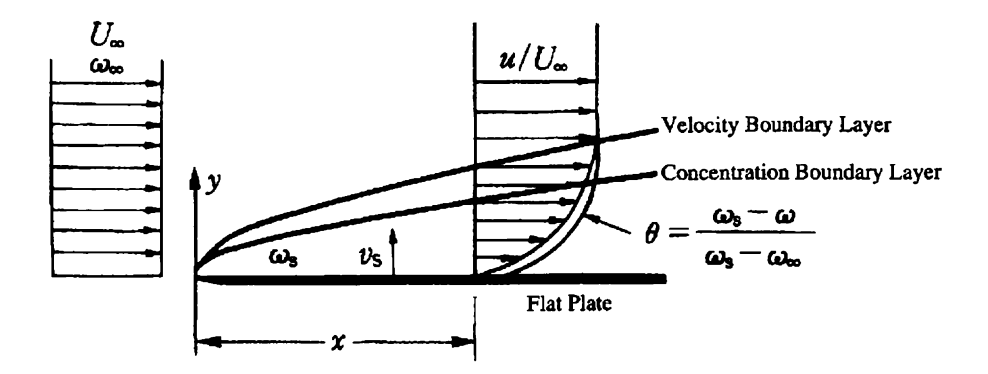


Figure 3.5 Velocity and concentration profile in boundary layer along a flat plate⁽⁵⁾.

Energy equation:

$$u\frac{\partial T}{\partial x} + v\frac{\partial T}{\partial y} = (k/\rho c_p)\frac{\partial^2 T}{\partial y^2}$$
 (3.23)

Diffusion equation:

$$u\frac{\partial\omega}{\partial x} + v\frac{\partial\omega}{\partial y} = D\frac{\partial^2\omega}{\partial y^2}$$
 (3.24)

where μ is the viscosity [Pa s], k is the thermal conductivity [W/(m K)], and c_p is the specific heat at constant pressure [J/(kg K)].

The boundary conditions are

$$y = 0$$
: $u = 0$, $v = 0$, $T = T_s$, $\omega = \omega_s$
 $y = \infty$: $u = U_\infty$, $v = 0$, $T = T_\infty$, $\omega = \omega_\infty$ (3.25)

3.3.2 PHYSICAL INTERPRETATION OF THE DIMENSIONLESS GROUPS USED IN HEAT AND MASS TRANSFER CORRELATION⁽⁶⁾

In a laminar boundary layer along a flat plate of thickness δ [m] shown in Figure 3.5, the relative order of magnitude of the inertia force is nearly equal to the viscous force. Equation (3.22) can be approximated by the following equation:

$$\rho U_{\infty}^2/x = \mu U_{\infty}/\delta^2 \tag{3.26}$$

Rearrangement of the above equation gives the following equation:

$$\delta/x = (\rho U_{\infty} x/\mu)^{-1/2} = Re_{\rm X}^{-1/2}$$
 (3.27)

where Re_X is a dimensionless group known as the Reynolds number, which represents the relative order of magnitude of the thickness of the velocity boundary layer, δ , to the distance from the leading edge. The definition of the Reynolds number can also be rearranged to give another physical interpretation:

$$Re_{\rm X} = \rho U_{\infty}^2/(\mu U_{\infty}/x) = {\rm (inertia\ force)/(viscous\ force)}$$
 (3.28)

If the Reynolds number becomes larger than a certain critical value, known as the critical Reynolds number, the flow of fluid changes from laminar to turbulent flow. For a flow in a circular tube the critical Reynolds number is about 2300, and for a boundary layer along a flat plate, it ranges from 3.5×10^5 to 3.5×10^6 .

If we assume that the thickness of the concentration boundary layer (the region where the concentration is not uniform), δ_D [m], is much smaller than that of the velocity boundary layer, δ [m],

$$\delta \gg \delta_{\rm D}$$
 (3.29)

the velocity profile in the concentration boundary layer can be approximated by the following equation:

$$u = U_{\infty}(\delta_{\rm D}/\delta) \tag{3.30}$$

Substitution of the above equation into Eq. (3.24) gives the following equation:

$$D(\omega - \omega_{\infty})/\delta_{\rm D}^2 = U_{\infty}(\delta_{\rm D}/\delta)(\omega_{\rm s} - \omega_{\infty})/x \tag{3.31}$$

Rearrangement of the above equation by use of Eq. (3.27) gives the following equation for the concentration boundary layer:

$$(\delta_{\rm D}/\delta) = (\mu/\rho D)^{-1/3} = Sc^{-1/3}$$
 (3.32)

where $Sc(=\mu/\rho D)$ is a dimensionless group called the Schmidt number, which represents the relative order of magnitude of the thickness of the concentration boundary layer to that of the velocity boundary layer.

A similar relation is obtained for the thickness of the temperature boundary layer, δ_T [m], as a function of the Prandtl number, $Pr(=c_P\mu/k)$:

$$(\delta_{\mathrm{T}}/\delta) = Pr^{-1/3} \tag{3.33}$$

The Prandtl and the Schmidt numbers are the physical properties of the system as is clear from their definitions. The order of magnitude of these dimensionless groups for gases, is as follows:

$$Pr = Sc \cong 1 \tag{3.34}$$

and they are less affected by temperature.

For liquids, the orders of magnitude of these parameters are as follows:

$$10 < Pr < 10^2 \tag{3.35a}$$

$$4 \times 10^2 < Sc < 10^4 \tag{3.35b}$$

which are usually affected by temperature.

In mass transfer correlation, the rates of mass transfer are usually expressed in terms of a dimensionless group, the Sherwood number, defined by the following equation:

(Sherwood number) =

(mass transfer flux)/(characteristic diffusion flux at the interface)

As was discussed in Section 3.1, we have two different diffusion fluxes, the mass-based diffusion flux, J_A , and the mole-based diffusion flux, J_A^* . We also have two different definitions of the Sherwood numbers, the mass-based one, Sh, and the mole-based one, Sh^* , respectively.

$$Sh_{X} = N_{A}x/\rho_{s}D\left(\omega_{s} - \omega_{\infty}\right) \tag{3.36}$$

$$Sh_{X}^{*} = N_{A}^{*}x/c_{s}D(x_{s} - x_{\infty})$$
 (3.37)

where c is the molar density $[mol/m^3]$, x is the mole fraction [-], and ω is the mass fraction [-].

From the definitions of the Sherwood numbers, the following equation is obtained:

$$(Sh^*/Sh) = \{1 + (M_B/M_A - 1)\omega_\infty\}$$
 (3.38)

As is clear from the above equation, the numerical values of these two Sherwood numbers are not usually identical with each other, except for the special case of the same molecular weight of the diffusing component and the inert medium. Therefore, we must be very careful when defining the Sherwood number, if we are going to correlate mass transfer data in terms of the Sherwood number.

The rates of convective heat transfer, are usually expressed in terms of the Nusselt number, Nu_X , defined by the following equation:

$$Nu_{X} = q_{X}x/k(T_{s} - T_{\infty}) = hx/k$$
(3.39)

where h is the heat transfer coefficient $[W/(m^2 K)]$, q_X is the local heat transfer flux $[W/m^2]$, and k is the thermal conductivity [W/(m K)].

3.3.3 SIMILARITY TRANSFORMATION

If we assume that the velocity profile in the boundary layer is similar, we can make use of a similarity transformation.

$$\eta = y \left(\rho U_{\infty}/\mu x\right)^{1/2} \left(\approx y/\delta\right) \tag{3.40a}$$

$$F = \phi \left(\mu x U_{\infty} / \rho \right)^{-1/2}$$
 (3.40b)

$$\theta_{\rm T} = (T_{\rm s} - T)/(T_{\rm s} - T_{\infty}) \tag{3.40c}$$

$$\theta_{\rm C} = (\omega_{\rm s} - \omega)/(\omega_{\rm s} - \omega_{\infty}) \tag{3.40d}$$

Substitution of the above equations into Eqs (3.21)–(3.24) gives the following ordinary differential equations:

$$F''' + (1/2)FF'' = 0 (3.41)$$

$$\theta_{\mathrm{T}}^{"} + (Pr/2)F\theta_{\mathrm{T}} = 0 \tag{3.42}$$

$$\theta_{\mathcal{C}}^{"} + (Sc/2)F\theta_{\mathcal{C}} = 0 \tag{3.43}$$

From Eq. (3.25) the boundary conditions are transformed as:

$$\eta = 0: \quad F = 0, \quad F' = 0, \quad \theta_{\rm T} = 0, \quad \theta_{\rm C} = 0$$

$$\eta = \infty: \quad F(\infty) = 1 \qquad \theta_{\rm T} = 1, \quad \theta_{\rm C} = 1$$
(3.44)

Then the dimensionless heat and diffusion flux can be expressed as

$$Nu_{\rm X} = q_{\rm X} x / k (T_{\rm s} - T_{\infty}) = Re_{\rm X}^{1/2} \theta_{\rm T}'(0)$$
 (3.45)

$$Sh_{X}(1-\omega_{s}) = N_{AX}(1-\omega_{s})x/\rho D(\omega_{s}-\omega_{\infty}) = Re_{X}^{1/2}\theta_{C}'(0)$$
 (3.46)

The above equations indicate that the rates of heat and mass transfer will be predicted, if the dimensionless temperature or concentration gradient at the interface, $\theta'_{1}(0)$ or $\theta'_{2}(0)$ is known.

3.3.4 NUMERICAL SOLUTIONS FOR HEAT AND MASS TRANSFER

In the calculations of heat and mass transfer, the first step is to get exact solutions for the stream functions by numerical integration of the equation of motion, Eq. (3.41). Substitution of the numerical solutions for the stream functions into the energy, Eq. (3.42), or the diffusion equation, Eq. (3.43), followed by numerical integration, gives the following equation for the temperature or the concentration profile:

$$\theta_{\mathsf{T}} = \theta_{\mathsf{T}}'(0) \int_{0}^{\eta} \exp\left\{ (-Pr/2) \int_{0}^{\eta} F \mathrm{d}\eta \right\} \mathrm{d}\eta \tag{3.47}$$

$$\theta_{\mathrm{T}}'(0) = 1 / \left[\int_0^\infty \exp\left\{ (-Pr/2) \int_0^\eta F \mathrm{d}\eta \right\} \mathrm{d}\eta \right]$$
 (3.48)

$$\theta_{\rm C} = \theta_{\rm C}'(0) \int_0^{\eta} \exp\left\{ (-Sc/2) \int_0^{\eta} F \mathrm{d}\eta \right\} \mathrm{d}\eta \tag{3.49}$$

$$\theta_{C}'(0) = 1/\left[\int_{0}^{\infty} \exp\left\{(-Sc/2)\int_{0}^{\eta} F d\eta\right\} d\eta\right]$$
(3.50)

Figure 3.6 shows the dimensionless concentration profiles obtained by use of the above equations in terms of the dimensionless distance from the wall, η , with the Schmidt number as a parameter. Equations (3.41)–(3.43) clearly indicate that the velocity and the temperature or the concentration profile become identical, if the condition Pr = 1 or Sc = 1 holds.

The numerical solutions for heat and mass transfer for the range:

$$0.6 < Sc, Pr < 10^3$$

are well correlated by the following equations:

$$Nu_{\rm X} = 0.332 Pr^{1/3} Re_{\rm X}^{1/2} \tag{3.51}$$

$$Sh_{\mathbf{X}}(1-\omega_{\mathbf{s}}) = 0.332Sc^{1/3} Re_{\mathbf{X}}^{1/2}$$
 (3.52)

For heat transfer under very low Prandtl number range (Pr < 0.01), the following asymptotic solution is known:

$$Nu_{\rm X} = 0.560 Pr^{1/2} Re_{\rm X}^{1/2} \tag{3.53}$$

Figure 3.7 shows numerical solutions for heat and mass transfer in a laminar boundary layer along a flat plate. Although Eqs (3.52) and (3.53), are obtained for a laminar boundary layer along a flat plate, they are also applicable to gas phase mass and heat transfer with a moving interface such as is the case with

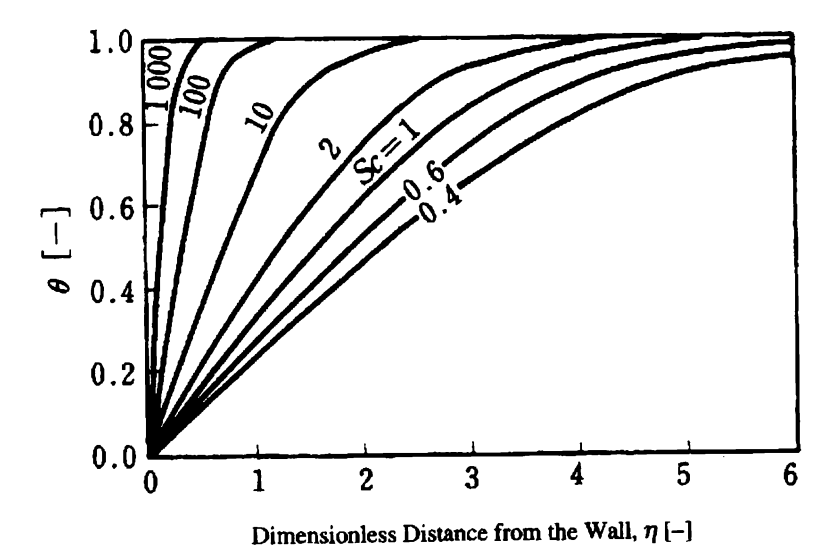


Figure 3.6 Effect of Schmidt number on dimensionless concentration profiles in concentration boundary layer⁽⁷⁾.

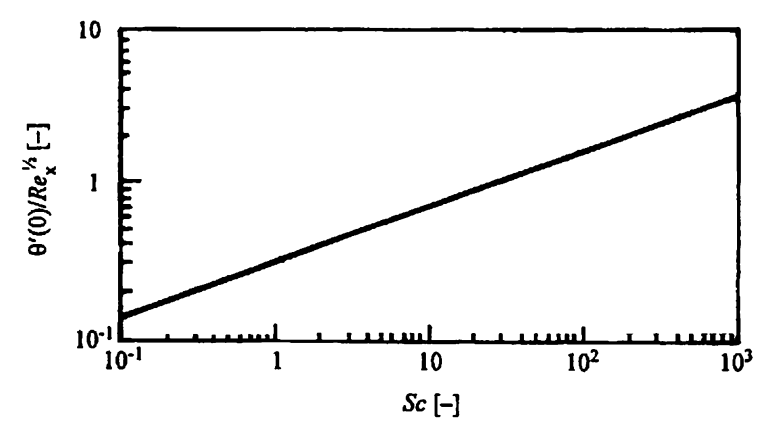


Figure 3.7 Numerical solutions for heat and mass transfer in a laminar boundary layer.

gas absorption, if the relative order of magnitude of the tangential velocity is not large in comparison with the free stream velocity $(u_s/U_\infty < 0.1)$.

3.3.5 HIGH MASS FLUX EFFECT

If the transfer of a component through a stagnant media takes place, as is the case with gas absorption or evaporation of a liquid, the normal component of the surface velocity, v_s , is induced by diffusion of the transferring component, as shown in Section 3.1.3. If, v_s becomes larger than a certain critical value, the velocity profile near the interface is affected by mass transfer, through which heat and mass transfer are also affected. This phenomenon is known as the high-mass flux effect. Figure 3.8 shows the effect of mass injection or suction on the velocity profile in a laminar boundary layer along a flat plate, as a dimensionless stream function as:

$$F(0) = -2(v_{\rm s}/U_{\infty}) Re_{\rm X}^{1/2}$$
 (3.54)

Although detailed discussions are not shown here, a final correlation for mass transfer under high mass flux conditions is given by the following equation:

$$Sh_{X}(1 - \omega_{s}) = 0.332Sc^{1/3} Re_{X}^{1/2} g(B_{M})$$
 (3.55)

$$B_{\rm M} = (v_{\rm s}/U_{\infty}) \{ Re_{\rm X} Sc/Sh_{\rm X} (1 - \omega_{\rm s}) \}$$
 (3.56)

where $B_{\rm M}$ is the transfer number for mass transfer, a dimensionless group representing the effect of high mass flux, and $g(B_{\rm M})$ is the effect of high mass flux on mass transfer.

Similar relations hold for heat transfer under high mass flux conditions as follows:

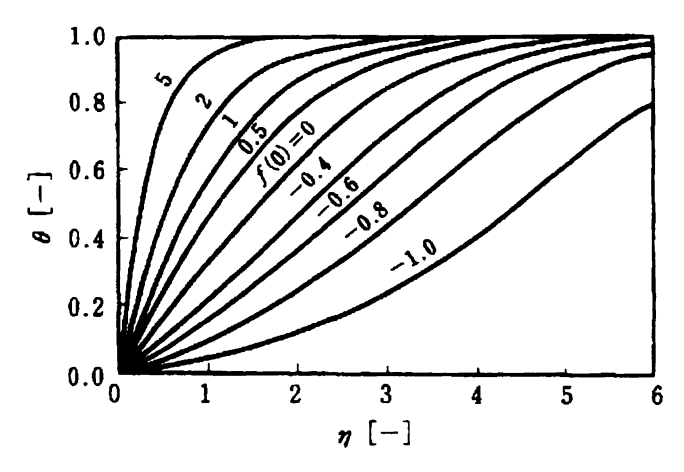


Figure 3.8 Effect of mass injection or suction on the velocity profile in laminar boundary layer along a flat plate $(Sc=1)^{(8)}$.

$$Nu_{\rm X} = 0.332 Pr^{1/3} Re_{\rm X}^{1/2} g (B_{\rm H})$$
 (3.57)

$$B_{\rm H} = (v_{\rm s}/U_{\infty})(Re_{\rm X}Pr/Nu_{\rm X}) \tag{3.58}$$

where $B_{\rm H}$ is the transfer number for heat transfer, and the function $g(B_{\rm H})$ is the effect of high mass flux on heat transfer. The following relation holds between the functions $g(B_{\rm H})$ and $g(B_{\rm M})$:

$$g(B_{\mathsf{M}}) = g(B_{\mathsf{H}}) \tag{3.59}$$

Figure 3.9 shows the variation of $g(B_M)$ with transfer number for flow in a laminar boundary layer along a flat plate.

3.4 HEAT TRANSFER INSIDE A CIRCULAR TUBE IN LAMINAR FLOW

The velocity profile in a circular tube just after the inlet section, is uniform, such as a flow near the junction between the end plate and the heat exchanger tube, where the cross-sectional area of the path contracts suddenly. At large distance from the inlet section (Z/D >> 0.04Re), the velocity is fully developed and a parabolic velocity profile is established, because of the effect of frictional resistance on the tube wall.

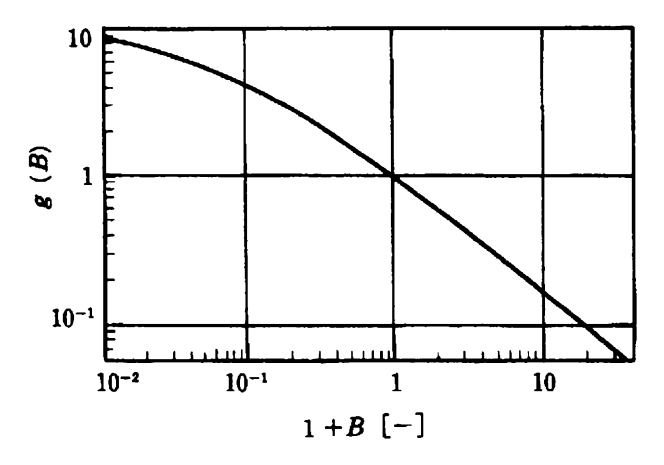


Figure 3.9 Variation of $g(B_M)$ with transfer number for a flow in the laminar boundary layer along a flat plate⁽⁸⁾.

3.4.1 HEAT TRANSFER INSIDE A CIRCULAR TUBE WITH UNIFORM VELOCITY PROFILE⁽¹⁾

Since uniform velocity profile is observed near the inlet section of a tube, the energy equation is expressed as:

$$U\frac{\partial T}{\partial z} = (k/\rho c_p) \left\{ \frac{\partial^2 T}{\partial r^2} + \frac{1}{r} \frac{\partial T}{\partial r} \right\}$$
 (3.60)

The boundary conditions are

$$z = 0$$
: $T = T_0$, $r = D/2$: $T = T_W$ (3.61)

Equation (3.60) is the Bessel differential equation, the solution of which is given by:

$$\theta_{T_{m}} = 4 \sum_{1}^{n} (1/\alpha_{n}^{2}) \exp(-\pi \alpha_{n}^{2}/Gz)$$
 (3.62)

The rate of heat transfer is given by:

$$Nu_{\rm m} = qD/k\Delta T_{\rm lm}$$

= $(-Gz/\pi) \{\ln(4\Sigma (1/\alpha_n^2) \exp(-\pi\alpha_n^2/Gz))\}$ (3.63)

where Gz is the Graetz number $(=\pi\rho c_P UD^2/4kZ)$, T_m is the average temperature over the cross-section of the tube [K], T_w is the wall temperature [K], α_n is the eigenvalue of the Bessel function of zeroth order [-], and ΔT_{1m} is the log-mean temperature driving force between the bulk fluid and wall

temperature at both ends of the tube [K] (= $(T_{\rm m2}-T_{\rm ml})/\ln{(T_{\rm wl}-T_{\rm ml})}/(T_{\rm w2}-T_{\rm m2})$).

3.4.2 HEAT TRANSFER INSIDE A CIRCULAR TUBE WITH PARABOLIC VELOCITY PROFILE (GRAETZ PROBLEM)⁽⁹⁾

If the velocity is fully developed, the energy equation can be written as:

$$U\{1 - (r/R)^{2}\} \frac{\partial T}{\partial z} = (k/\rho c_{p}) \left\{ \frac{\partial^{2} T}{\partial r^{2}} + \frac{1}{r} \frac{\partial T}{\partial r} \right\}$$
(3.64)

The solution of the above equation is usually called the Graetz problem in honour of professor Graetz who first solved the equation. Although detailed discussions are not shown here, the analytical solution of the above equation in terms of the dimensionless temperature is given by:

$$\theta_{\text{Tm}} = (T_{\text{w}} - T_{\text{m}})/(T_{\text{w}} - T_{0})$$

$$= 8\Sigma (G_{n}/\beta_{n}^{2}) \exp(-\pi \beta_{n}^{2}/2Gz)$$
(3.65)

The rate of heat transfer is given by:

$$Nu_{\rm m} = (-Gz/\pi) \ln \left\{ 8\Sigma \left(G_n/\beta_n^2 \right) \exp \left(-\pi \beta_n^2/2Gz \right) \right\}$$
 (3.66)

where T_0 is the inlet temperature [K], and $T_{\rm m}$ is the average temperature over the cross-section of the tube [K]. Table 3.3 shows the eigenvalues for Eqs (3.63) and (3.66), which are necessary for calculation of the heat fluxes. Figure 3.10 shows the theoretical values for the Sherwood numbers for the case of uniform

Table 3.3 Eigenvalues for Eq. (3.63) and (3.66)

Case with uniform velocity profile eigenvalues for Eq. (3.63)		Case with parabolic velocity profile eigenvalues for Eq. (3.66) ⁽¹⁰⁾		
n	α_n	β_n	G_n	
1	2.40483	7.312	0.749	
2	5.52008	44.62	0.544	
3	8.65373	113.8	0.463	
4	11.79153	215.2	0.414	
5	14.93092	348.5	0.382	
6	18.07106			
7	21.21164	n >	> 3	
8	24.35247	$\beta_n = 4(n -$	-1) + 3/8	
9	27.49348	$\beta_n = 4(n - G_n) = 1.01$	$276/\beta_n^{1/3}$	
10	30.63461			

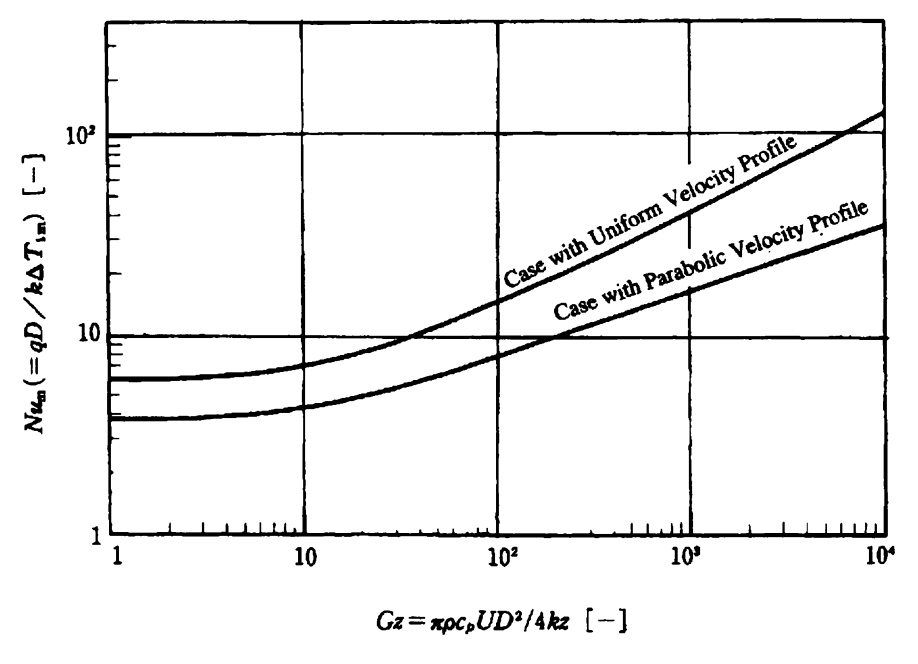


Figure 3.10 Laminar heat transfer in a circular tube.

velocity profile and parabolic velocity profile, as a function of Graetz numbers, respectively.

3.5 MASS TRANSFER OF BUBBLES, DROPS AND PARTICLES

3.5.1 HADAMARD FLOW(12)

Figure 3.11 shows a physical picture of a flow field around a small bubble or a drop in relatively slow laminar flow. On the surface of the bubble or the drop, there is observed a circulation of flow caused by continuity conditions of normal and tangential stress at the interface. Such a slow laminar flow with internal circulation flow inside the drop or bubble is known as the Hadamard flow, of which details are shown in the text book⁽¹²⁾. The internal circulation flow takes a maximum at the surfaces, of which the magnitude is given by:

$$v_{\rm s}(\theta) = U(\mu_{\rm C}/\mu_{\rm D})\sin\theta/2(1 + \mu_{\rm C}/\mu_{\rm D})$$
 (3.67)

The terminal velocity of a drop or a bubble in Hadamard flow is usually larger than that of a solid particle for the reason that the surface circulation flow

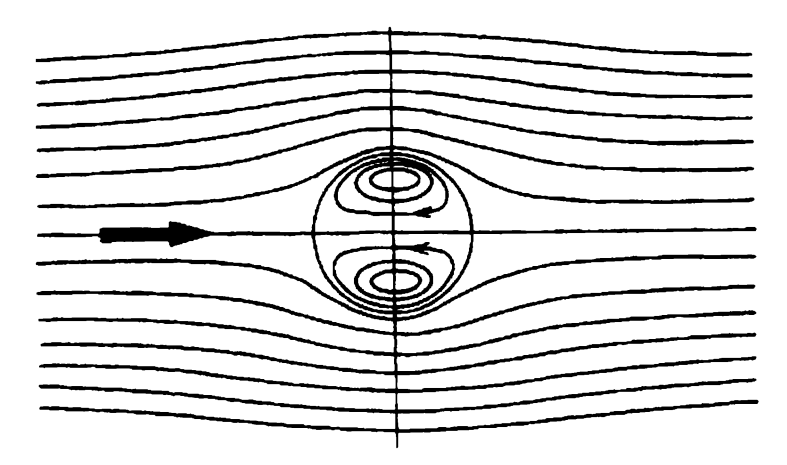


Figure 3.11 Hadamard flow.

retards the continuous phase velocity gradients at the drop or bubble interface. That is,

$$U = \{(1 + \mu_{\rm C}/\mu_{\rm D})/(1 + 2\mu_{\rm C}/3\mu_{\rm D})\}\{\rho_{\rm D} - \rho_{\rm C}\}gD_{\rm P}^2/18\mu_{\rm C}\}$$

= \{(1 + \mu_{\mathcal{C}}/\mu_{\mathcal{D}}\)/(1 + 2\mu_{\mathcal{C}}/3\mu_{\mathcal{D}}\)\\\ U_{\mathcal{S}T} (3.68)

where D_P is the drop diameter [m], g is the gravitational acceleration [m/s²], U is the terminal velocity of bubbles or drops [m/s], U_{ST} is the terminal velocity of solid particles [m/s], v_s is the tangential velocity at the interface [m/s], ρ_C is the density of the continuous phase (medium) [kg/m³], ρ_D is the density of the dispersed phase (bubbles or drops), μ_C is the viscosity of the continuous phase [Pa s], and μ_D is the viscosity of the dispersed phase [Pa s].

3.5.2 EVAPORATION OF A DROP IN THE GAS PHASE

For a droplet in the gas phase, the condition $\mu_D \gg \mu_C$ usually holds. Equation (3.68) suggests that the motion of a liquid drop in the gas phase can safely be approximated by that of a solid sphere.

If a drop is placed in a stationary gas, the governing equation and boundary conditions are as follows:

$$\frac{\mathrm{d}}{\mathrm{d}r} \left(r^2 \left(\frac{\mathrm{d}\omega}{\mathrm{d}r} \right) \right) = 0 \tag{3.69}$$

$$r = R$$
: $\omega = \omega_s$, $r = \infty$: $\omega = \omega_\infty$ (3.70)

Integration of Eq. (3.69) in terms of the radius r by considering the boundary conditions gives the following analytical solution for the concentration profile around the drop:

$$(\omega - \omega_{\infty})/(\omega_{\rm s} - \omega_{\infty}) = R/r \tag{3.71}$$

The rate of evaporation of the drop per unit surface area, $NA [kg/(m^2S)]$ is given by:

$$N_{A} = \{-\rho_{C} D_{C}/(1 - \omega_{s})\} (d\omega/dr)_{r=R}$$

$$= \{-\rho_{C} D_{C}/(1 - \omega_{s})\} (\omega_{s} - \omega_{\infty})/R$$

$$(3.72)$$

The above equation is made dimensionless by:

$$Sh_{P}(1 - \omega_{s}) = N_{A} D_{P}(1 - \omega_{s}) / \rho_{C} D_{C}(\omega_{s} - \omega_{\infty}) = 2$$
 (3.73)

A similar relation is obtained for the heat transfer of a drop in stationary gas:

$$Nu_{\rm P} = qD_{\rm P}/k_{\rm C}(T_{\rm s} - T_{\infty}) = 2$$
 (3.74)

where $D_{\rm C}$ is the diffusion coefficient in the continuous phase [m²/s], $D_{\rm P}$ is the drop diameter [m], $\rho_{\rm C}$ is the density of the continuous phase [kg/m³], and $k_{\rm C}$ is the thermal conductivity of the continuous phase [W/(m K)].

For heat and mass transfer of drops moving in the gas phase, the exact solutions are generally obtained by solving simultaneously the equations of motion and energy or the diffusion equation in terms of spherical coordinates, but the calculation is not easy in comparison with the one in a stationary fluid. Although detailed discussions are not shown here, the numerical solutions for the range Re < 1000, are well correlated by the following equation, which together are known as the Ranz-Marshall correlation:

$$Sh_{\rm P}(1-\omega_{\rm s}) = 2 + 0.6 \, Sc_{\rm C}^{1/3} Re_{\rm P}^{1/2}$$
 (3.75)

$$Nu_{\rm P} = 2 + 0.6Pr_{\rm C}^{1/3}Re_{\rm P}^{1/2} \tag{3.76}$$

where Pr_C is the continuous phase Prandtl number (= $c_{PC}\mu_C/k_C$), Re_P is the drop Reynolds number (= $\rho_C D_P U/\mu_C$), and Sc_C is the continuous phase Schmidt number (= $\mu_C/\rho_C D_C$). Since the Ranz-Marshall correlations are applicable for prediction of heat and mass transfer of drops for wide ranges of Reynolds and Schmidt or Prandtl numbers, the correlations are used as the standard equations for spray drying. Figure 3.12 shows the Ranz-Marshall correlation.

62 K. ASANO

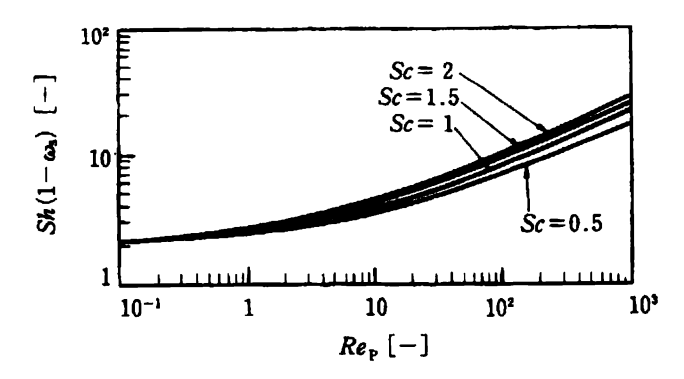


Figure 3.12 Ranz-Marshall's correlation⁽¹²⁾.

3.5.3 CONTINUOUS PHASE MASS TRANSFER OF BUBBLES OR DROPS IN THE LIQUID PHASE

For bubbles or drops dispersed in liquid phase the following conditions hold:

$$\mu_{\rm D} \ll \mu_{\rm C}$$
 or $\mu_{\rm D} \approx \mu_{\rm C}$

which causes circulation flow at the bubble or drop surface. Heat and mass transfer under such conditions is much more different from those of solid sphere. The following approximate solution is obtained for continuous phase mass transfer of a small bubble or a drop in Hadamard flow by Levich:

$$Sh_{\rm P}(1-\omega_{\rm s}) = 0.651Sc_{\rm C}^{1/2}Re_{\rm P}^{1/2}(1+\mu_{\rm D}/\mu_{\rm C})^{-1/2}$$
 (3.77)

Although Eq. (3.77) is applicable for mass transfer of a small bubble or a droplet in a clean system or a system not contaminated with surface-active agents, however; the equation is not applicable for industrial operations, where contamination with trace surface-active agents is usually accompanied, and accumulation of such materials at the interface retards the surface circulation flow.

The nature of mass transfer for large bubbles or drops is much more complicated where the shapes are deformed from spherical to spheroidal or to spherical-cap. The detailed discussion is given in the textbook⁽¹¹⁾.

3.5.4 DISPERSED PHASE MASS TRANSFER

For mass transfer in gas absorption with liquid drops of relatively low solubility, the rate controlling resistance is the mass transfer inside the drop (dispersed phase mass transfer). The Hadamard's condition, Eq. (3.67), suggests that the internal circulation flow is completely retarded inside the drop on the reason that the liquid viscosity (dispersed phase) is usually much larger

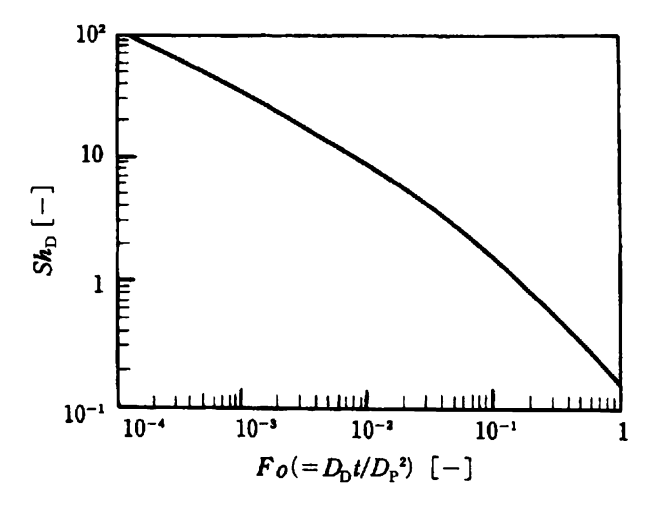


Figure 3.13 Dispersed phase mass transfer by Eq. (3.78) solid sphere penetration model⁽²⁾.

than that of the gas (continuous phase). For mass transfer under such conditions, the following solid sphere penetration model can be applicable:

$$Sh_{\rm D} = \frac{1}{6Fo} \left\{ 1 - \frac{6}{\pi^2} \sum_{n=1}^{\infty} \frac{1}{n^2} \exp\left(-4n^2\pi^2 Fo\right) \right\}$$
 (3.78)

where Fo is the Fourier number $(=D_{\rm D}t/D_{\rm P}^2)$, $Sh_{\rm D}$ is the dispersed phase Sherwood number $(=N_{\rm A}D_{\rm P}/\rho_{\rm d}D_{\rm D}(\omega_{\rm s}-\omega_{\rm 0})$, and t is the contact time [s]. Figure 3.13 shows the dispersed phase mass transfer by Eq. (3.78) in terms of the Fourier number.

3.5.5 HEAT AND MASS TRANSFER OF A GROUP OF PARTICLES AND THE VOID FUNCTION

Heat and mass transfer of a group of particles are usually lower than those of single particle because of the effect of interactions between neighbouring particles. In practical purposes, heat and mass transfer of a group of particles are related to those of single particle by use of void function defined below:

Heat and Mass Transfer Rate of a Group of particles = (Void function) × (Heat and Mass Transfer Rate of Single Particle)

64 K. ASANO

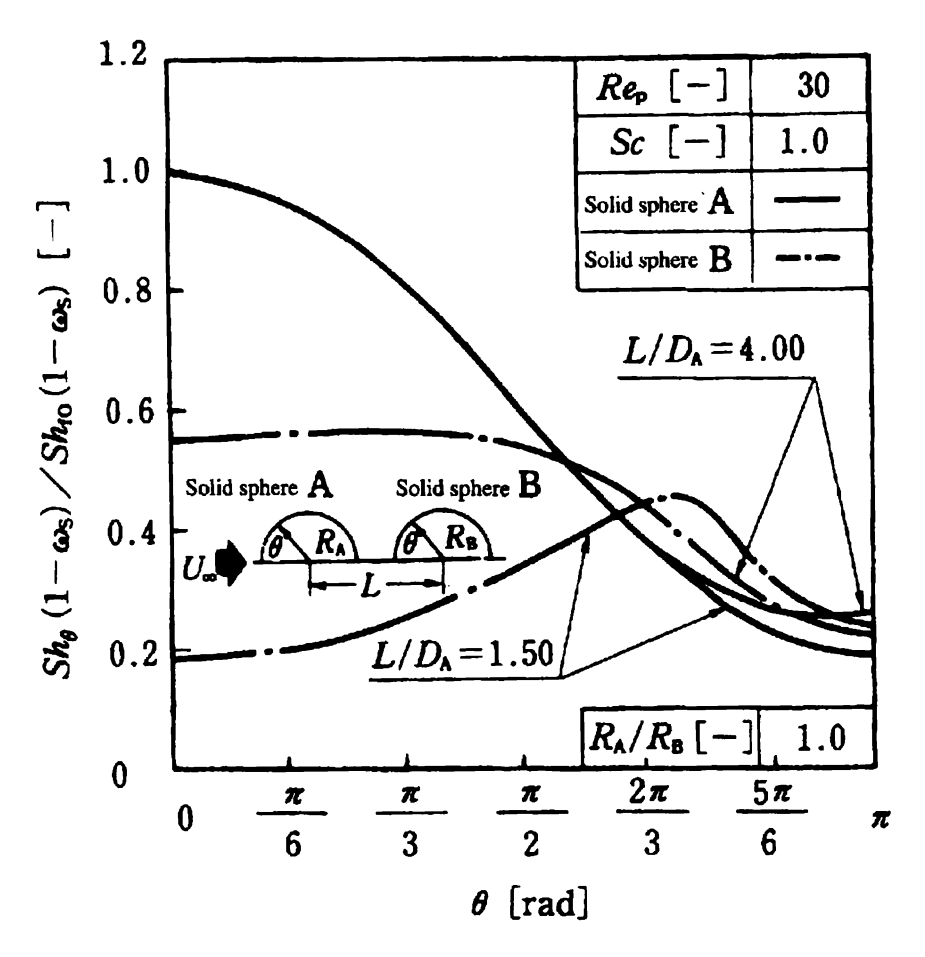


Figure 3.14 Distributions (angular distributions) of the local mass fluxes of the two coaxially arranged solid spheres of equal diameter⁽¹⁴⁾.

Figure 3.14 shows the distributions (angular distributions) of the local mass fluxes of the two coaxially arranged solid spheres of equal diameter. The figure clearly indicates that the local mass fluxes of the upper hemisphere of the down stream sphere are much decreased by the effect of wake caused by the upstream sphere. Considering this fact, Taniguchi and Asano proposed the following numerical correlation for the void function by computer simulation:

$$F(\varepsilon) = 1/\{1 + 1.32(1 - \varepsilon)^{0.76}\}$$
 (3.79)

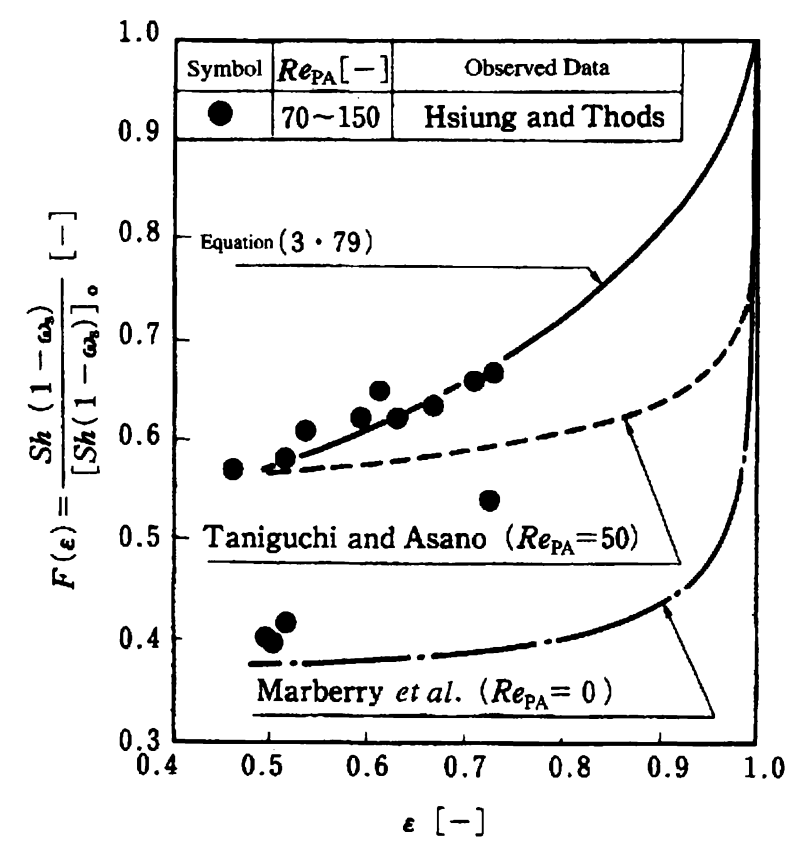


Figure 3.15 Void function, comparison of simulation and observed data(15).

3.6 RADIANT HEAT TRANSFER

3.6.1 HEAT RADIATION

Radiation is the phenomenon in which a substance emits and absorbs energy in the form of electromagnetic waves. A special type of radiation in which emission and absorption of electromagnetic waves are caused by thermal motion of the molecules is called thermal radiation. A black body is defined as the one which absorbs all the irradiated energies to the surface. The thermal radiation from a black body is called the black body radiation. The energies emitted by the thermal radiation from a body are comprised of energies of various wavelengths and a small fraction of the energy around the wavelength λ is called the monochromatic radiation. The monochromatic emissive power is the derivative of the total emissive power with respect to wavelength. The total

66 K. ASANO

emissive power of a black body per unit surface of the black body, E_b [W/m²] is given by the Stefan-Boltzmann law:

$$E_{\rm b} = \sigma T^4 \tag{3.80}$$

where σ is the Boltzmann constant (5.6687 × 10⁻⁸) [W/(m²K⁴)].

The monochromatic radiation of a non-black body is usually less than that of the black body of the same temperature, and the ratio of monochromatic emissive power of a non-black body to that of a black body of the same temperature, is called the monochromatic emissivity. A body in which monochromatic emissivities are independent of wavelengths, is called a grey body. The thermal radiation of a grey body is expressed as:

$$E = \varepsilon \sigma T^4 \tag{3.81}$$

where ε [-] is the emissivity.

For a surface exposed to radiant energy at thermal equilibrium, a fraction of the radiant energy is reflected, transmitted and absorbed, called the reflectivity, r [-], the transmissivity, t [-], and the absorptivity, α [-], respectively. The following relation holds.

$$r + t + \alpha = 1 \tag{3.82}$$

If a body is at thermal equilibrium, the absorbed energies are re-emitted as radiant energies; thus the following relation holds:

$$\varepsilon = \alpha$$
 (3.83)

This is called Kirchhoff's law.

3.6.2 GOVERNING EQUATIONS OF RADIANT HEAT TRANSFER

Consider the radiation heat transfer between the two black body surface elements, dA_1 and dA_2 a distance s[m] apart, as shown in Figure 3.16. The total radiant energy $dQ_1[W]$ transferred to the surface element dA_2 per unit time from the surface element dA_1 with solid angle of $d\omega_1$ (= $dA_2\cos\phi_2/s^2$), is given by:

$$dQ_1 = I_{b1}dA_1\cos\phi_1d\omega_1 = I_{B1}(\cos\phi_1\cos\phi_2/s^2) dA_1dA_2$$
 (3.84)

where I_{b1} [W/m²] is the radiant energy of the surface per unit solid angle $(=E_{\rm B}/\pi=\sigma T_1^4/\pi)$.

Conversely, the radiant energy from the surface element dA_1 to dA_2 is

$$dQ_2 = I_{b2}(\cos\phi_1\cos\phi_2/s^2) dA_1 dA_2$$
 (3.85)

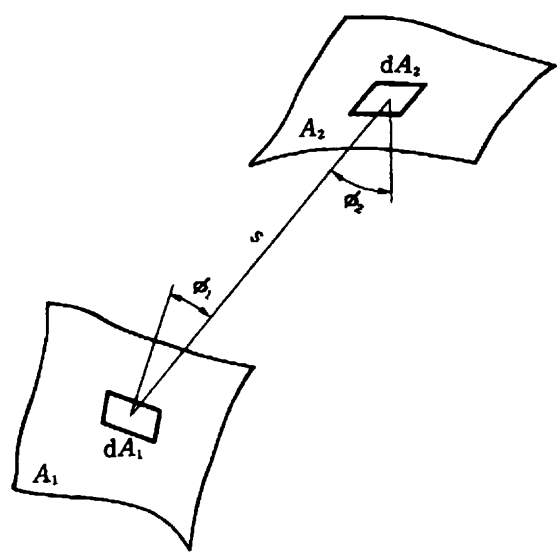


Figure 3.16 Radiation heat transfer between the two black body surface elements⁽¹⁶⁾.

Thus, the net rate of radiant heat transfer from the surface elements dA_1 to dA_2 , dQ_{12} [W], is given by:

$$dQ_{12} = \sigma(T_1^4 - T_2^4)(\cos\phi_1\cos\phi_2/\pi s^2) dA_1 dA_2$$
 (3.86)

Integration of the above equation gives the rate of radiant heat transfer between the two surfaces, A₁ and A₂, as:

$$dQ_{12} = \sigma(T_1^4 - T_2^4) A_1 F_{12} = \sigma(T_1^4 - T_2^4) A_2 F_{21}$$
(3.87)

where

$$A_1 F_{12} = A_2 F_{21} = \int_{A_1} \int_{A_2} (\cos\phi_1 \cos\phi_2 / \pi s^2) \, \mathrm{d}A_1 \, \mathrm{d}A_2 \tag{3.88}$$

The F_{12} and F_{21} are shape factors (view factors), which are functions of geometrical relations such as size, shape and angle between the two surfaces.

REFERENCES

- (1) K. Asano, Busshitsu Ido-Ron (Fundamentals of Mass Transfer), p. 6, Kyoritsu Shuppan (1976).
- (2) K. Asano, Busshitsu Ido-Ron (Fundamentals of Mass Transfer), p. 11, Kyoritsu Shuppan (1976).
- (3) K. Aano, Bunri-Seisei Gijutsu Handobukku (Handbook of Separation and Purification Technology), p. 42, Maruzen (1993).

68 K. ASANO

(4) K. Aano, Bunri-Seisei Gijutsu Handobukku (Handbook of Separation and Purification Technology), p. 43, Maruzen (1993).

- (5) K. Aano, *Pasokon-de-toku Kagakuk-Kogaku* (Application of Personal Computer to Chemical Engineering), p. 208, Maruzen (1993).
- (6) K. Asano, Busshitsu Ido-Ron (Fundamentals of Mass Transfer), p. 14, Kyoritsu Shuppan (1976).
- (7) K. Aano, Bunri-Seisei Gijutsu Handobukku (Handbook of Separation and Purification Technology), p. 45, Maruzen (1993).
- (8) K. Aano, Bunri-Seisei Gijutsu Handobukku (Handbook of Separation and Purification Technology), p. 46, Maruzen (1993).
- (9) W. M. Kays and M. E. Crawford, Convective Heat and Mass Transfer, 2nd Ed., p. 103, McGraw-Hill (1980).
- (10) J. R. Sellars, M. Tribus and J. S. Klein, Trans ASME, 78, 491 (1956).
- (11) K. Asano, Busshitsu Ido-Ron (Fundamentals of Mass Transfer), p. 47, Kyoritsu Shuppan (1976).
- (12) R. Clift, J. R. Grace and M. E. Weber, *Bubbles, Drops and Particles*, p. xx, Academic Press (1978).
- (13) K. Aano, *Bunri-Seisei Gijutsu Handobukku* (Handbook of Separation and Purification Technology), p. 50, Maruzen (1993).
- (14) I. Taniguchi and K. Asano, J. Chem. Eng. Jpn, 20, 287 (1968).
- (15) I. Taniguchi and K. Asano, J. Chem. Eng. Jpn, 25, 321 (1968).
- (16) Japan Society for Mechanical Engineers, Natsu-Kogaku (Heat Transfer), Kikai-Kogaku Benran (Mechanical Engineers' Handbook), 6th Ed., A6, p. 100 (1985).

CHAPTER 4 Fundamentals of Reactor Design

CHAPTER 4.1

Reactor Types and Their Applications

SHINTARO FURUSAKI

Graduate School of Engineering, University of Tokyo, Japan

In this chapter, we introduce reactors used for industrial chemical reactions. There are various reactor types depending on phases like gas, liquid and solid with respect to reactants and products, or on catalytic and non-catalytic types. We classify reactors into homogeneous and heterogeneous reactors in view of their internal states. The former contains a homogeneous phase (gas, liquid or solid), and the latter has two or more phases (gas—liquid, gas—solid, liquid—solid or gas—liquid—solid). This classification may facilitate the generalized design strategy of reactors. The reactor types and applications are introduced in subsequent sections.

4.1.1 HOMOGENEOUS REACTORS

Reactors which handle reacting systems of a homogeneous phase such as gas or liquid are classified as homogeneous reactors. In many cases, materials are mixed uniformly before they are supplied to the reactor, so changes in behaviour involving mass transfer do not normally take place. Instead, longitudinal mixing and heat transfer are crucial operating considerations. Reactors of this type can be explained typically by tubular and stirred tank categories.

4.1.1.1 Tubular Reactors

Figure 4.1 shows tubular reactors and their operational modes. The major differences in the modes are the inlet and outlet locations for reactants and products. For heat transfer, two methods can be considered: one is transferring heat through the tube wall and the other is transferring heat through heat exchanger tubes into or out of the reactor. The latter method is used when relatively large diameters are used. For tubular reactors, the larger the aspect ratio (length/diameter), the closer the flow generally turns to piston flow. This

72 S. FURUSAKI

promotes ideal reactions and normally provides better selectivity. In addition, small tube diameters offer good heat transfer as well as easy control. However, if the diameter is too small, resistance to the flow increases, which results in a large pressure drop between the inlet and outlet. So the energy consumption will become large. A reactor must be designed in line with the flow velocity appropriate to the property of a substance.

Reactors of this type are used for continuous homogeneous reactions such as thermal cracking in a gas phase, neutralization in a liquid phase, esterification with an acid catalyst, saponification and acid hydrolysis.

4.1.1.2 Stirred Tank Reactors

This type of reactor is a mixing tank with perfectly mixed flow. The liquid phase is normally used in this reactor. The reactor is operated with a batch or continuous process, or semi-continuous process (also called the fed batch) in which reactants are continuously fed in and products are discharged batchwise.

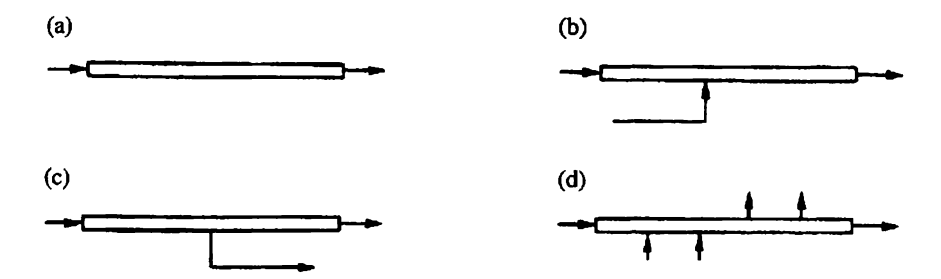


Figure 4.1 Tubular reactors and their operational modes. (a) Single inlet and outlet. (b) Multi-inlets and single outlet. (c) Single inlet and multi-outlets. (d) Multi-inlets and outlets.

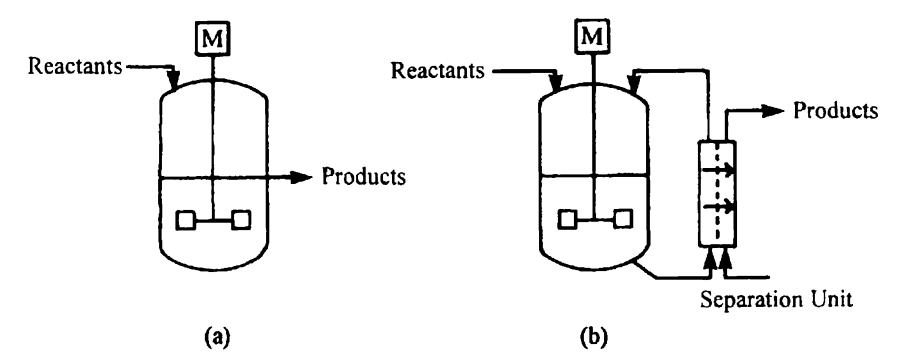


Figure 4.2 Typical types of systems using stirred tank reactors. (a) Continuous stirred tank reactor. (b) Stirred tank reactor combined with separation unit.

In combination with separation, reactants are fed by batch, while products can be discharged continuously. There are slight differences in stirred tank structure depending on the heat exchange method, stirring method and size of the reactor. A mixing blade must be carefully designed when the reactants contain solid particles, when solids are formed by reactions, or when the viscosity of the materials is increased.

Figure 4.2 shows typical types of systems using these stirred tank reactors. Due to its good mixing performance and high capacity, this type of reactor is best suited to regulate reactions which might succumb to runaway, or for the careful control of reacting conditions. These reactors are used for neutralization, hydrolysis, esterification, amide formation, chelate formation etc. They are also applied to polymerization, in which case the baffle plate, mixing blade and heating element must be simple in structure because of increased viscosity.

4.1.1.3 Other Homogeneous Reactors

Although homogeneous reactors are generally classified into tubular and stirred tank reactors as described above, there is another classification lying between the two as a column reactor with an aspect ratio of about 3–20. This reactor may often be placed horizontally. In this case it is called a lateral reactor. Generally, the distributor must be devised to allow uniform fluid feed. Since longitudinal mixing of the flow through the reactor is not negligible, perforated plates or packings may be set in place. Circulation in the reactor is sometimes preferred to control reacting conditions such as temperature and pH (Figure 4.3).

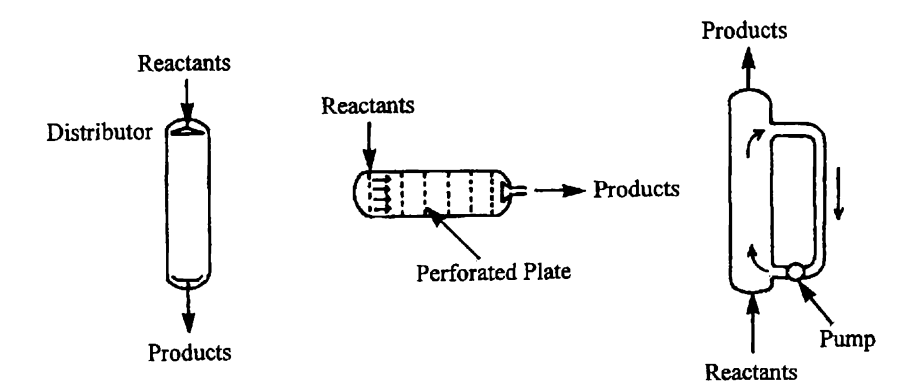


Figure 4.3 (a) Column reactor. (b) Lateral reactor. (c) Column reactor with circulation.

74 S. FURUSAKI

4.1.2 HETEROGENEOUS REACTORS

Heterogeneous reactors are those which contain more than one phase. These reactors are often used for non-catalytic reactions. They also play an important role when used for catalytic reactions. In this section, we explain those reactors which are used for both catalytic and non-catalytic reactions. For liquid phase reactions using fine particles as a catalyst, mixing tanks such as those described in Section 4.1.1.2 are used in many cases.

4.1.2.1 Fixed Beds

Fixed beds are formed by packing solid particles in a reactor. Although catalysts are usually applied, there may be cases in which solids react with fluids, i.e. not the catalyst bed. Figure 4.4 shows several types of fixed bed reactors. These are presented just as typical types, because in practical cases reactors are often designed by modifying the typical types.

In a fixed bed, fluid flows joining or branching at the solid particles are packed randomly. This will make distribution of the residence time small, similar to that of the cascaded equipment. In other words, the fluid flow behaves similarly to piston flow, offering high conversion and good reaction selectivity. Assuming piston flow, if we replace the fluid residence time by the elapsed reaction time, we can then handle the reaction in the same way as that of a batch reaction. The reaction feed should be well designed in a fixed bed to disperse the feed of reactant uniformly over the cross-section. In addition to mass flow, temperature control is also critical. Radial heat transfer is realized by radial fluid flow (convection) and by heat conduction through solids. However, full attention must be devoted to temperature control, as the rate of heat transfer is relatively low in fixed beds.

Fixed beds are used for many catalytic reactors: the gas phase sytheses of ammonia, methanol and sulphuric acid; liquid phase catalytic reactions such as hydration and hydrogenation; and bioreactions using immobilized enzymes. Fixed beds are also used for the reactor, reducing NO_x contained in automobile exhaust fumes. In addition, they are used for reactions such as ion exchange and as a heat reservoir using solids as the heating medium. The fixed bed reactors are most commonly used as catalytic reactors.

4.1.2.2 Moving Beds

Although fixed beds offer fluid mixing close to that of piston flow with good reaction performance, solid particles cannot be removed from the reactor. If the catalyst deteriorates or solid—gas reactions are performed, the solid particles must be supplied and removed continuously or semi-continuously in order to perform steady state operations. Solid particles then move slowly in

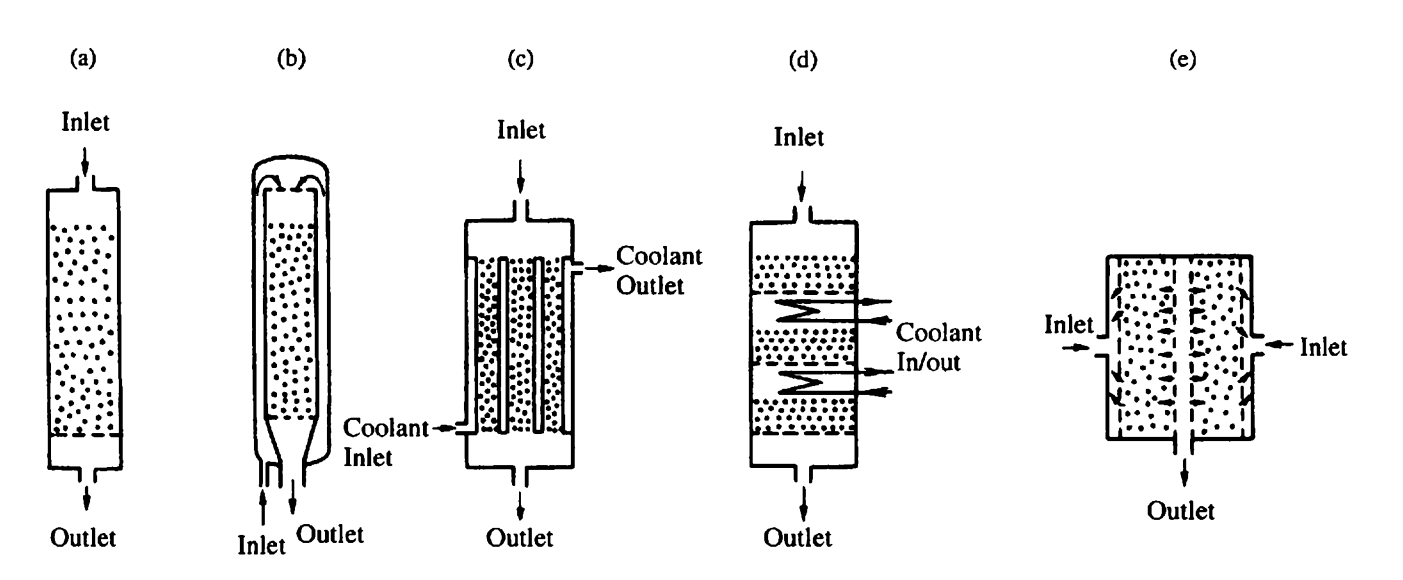


Figure 4.4 Several types of fixed bed reactors. (a) Down flow type. (b) Self-thermal-exchange Type. (c) Cooling Type. (d) Intermediate Cooling Type. (e) Radial Flow Type.

76 S. FURUSAKI

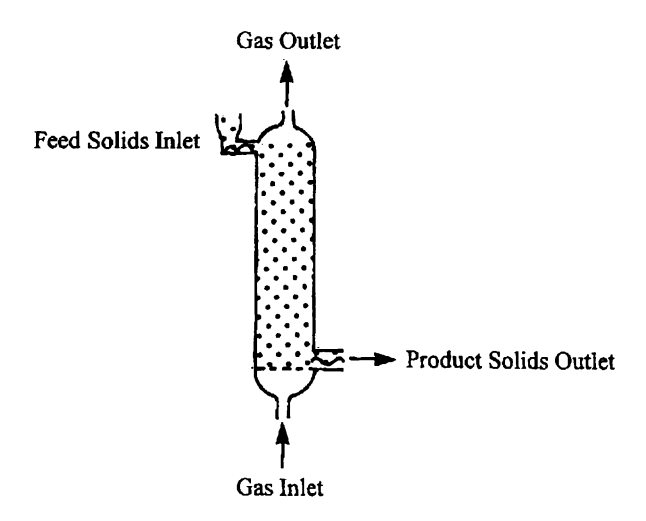


Figure 4.5 Moving bed.

the reactor toward the outlet. This is a moving bed (Figure 4.5). It is, however, rather difficult to remove solids from small-scale equipment. In this respect, a rotary valve, vibrator and screw type of solid-transporting equipment are considered. In many cases, it may be easier to remove solids intermittently.

The fluid property of a moving bed is almost identical to that of the fixed bed. Typical examples of its application are seen in reactions which require removal of solids, e.g. blast furnaces used for iron refining and calcinators for production of cement and lime.

4.1.2.3 Fluidized Beds

Fluidized beds are useful when solid particles which are involved in reactions must be removed frequently. In a fluidized bed, particles move freely floated by the fluid flowing upward. This motion of particles allows their easy removal from the bed.

Fluidized beds fall into gas-solid and liquid-solid systems. In gas-solid systems, the fluid state varies depending on the particle properties. Within the range of relatively low gas velocity where particle elutriation is not significant, the bed is called a bubbling fluidized bed, in which gas moves upward in the bed in bubble form. The bubbling bed has two regimes, i.e. fluid bed and teeter bed^{(1),(2)}. A fluid bed consisting of relatively fine particles provides a smooth flow and is used for catalytic reactions. Particles with sizes of $44 \mu m$ or less have an especially smooth flow effect, which are often referred to as 'good fraction'.

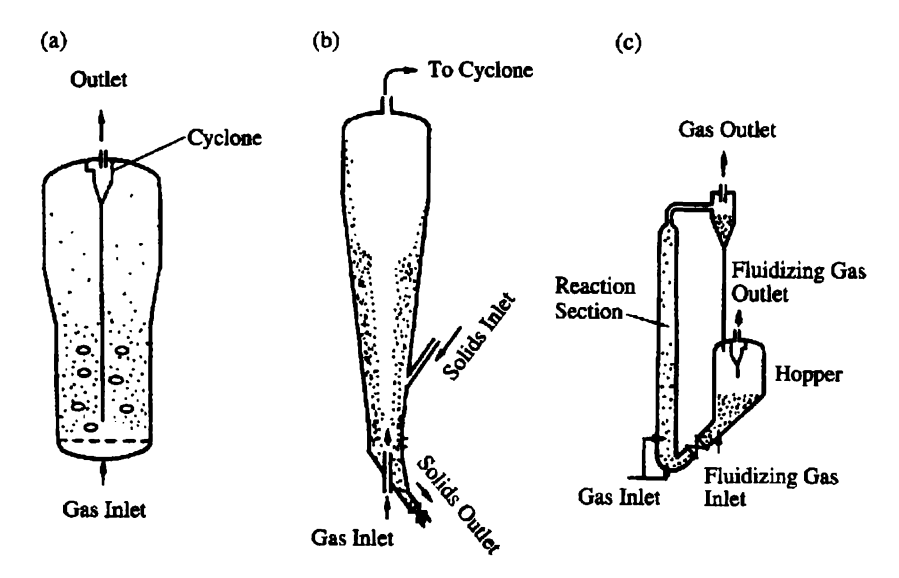


Figure 4.6 Fluidized beds. (a) Bubbling fluidized bed. (b) Spouted bed. (c) Circulating fluidized bed.

In this sense, it is desirable to have particles in this range occupying 10%-30%. In a fluid bed, because of significant turbulence, the bubble sizes are relatively small, and bubbles do not grow much larger while rising. In this region, bubbles split and coalesce vigorously as they are manipulated in a rather turbulent flow area. On the other hand, relatively large particles (ranging from hundreds of μ m to several mm) cause slugging which results in a vibrating and slightly unstable bed (teeter bed). In the teeter bed, bubbles grow as they move upward, forming large bubbles up to dozens of centimetres. This is the cause of slugging.

If gas is blown in high speed into a bed that has particles of poor flowability, paths of gas (channels) develop, forming a so called spouted bed. A relatively long bed turns into a transport bed if particles placed inside it are fluidized by gas with much higher velocity. Those particles can be circulated when captured by a cyclone. This is called a fast fluidized bed or circulating fluidized bed. The fluidized beds introduced here are illustrated in Figure 4.6.

In general, fluid beds are used for catalytic reactions including a typical example of fluidized catalytic cracking (FCC) as well as syntheses of acrylonitrile, ethylene dichloride, maleic anhydride and melanine. Teeter beds are used for coal gasification and combustion as well as thermal treatment, drying and granulation of solids. Spouted beds are also used in similar applications. Recently, FCC is often carried out in a transport bed (riser reactor). This is a kind of circulating fluidized bed. In this case, the circulating amount of the catalyst is very large at a level of 500–800 kg/(m²s). Application of the circulating fluidized bed to coal gasification is also under

78 S. FURUSAKI

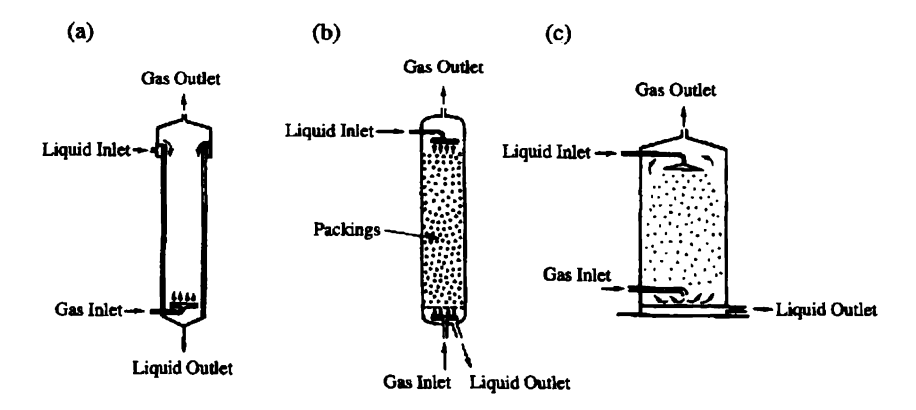


Figure 4.7 Gas-liquid contactor (for the case when the gas phase is continuous).
(a) Wetted-wall column. (b) Irrigated packed column. (c) Spray column.

study. The circulating amount of solid for this application is $20-50 \, \text{kg/(m}^2 \, \text{s})$. On the other hand, gas-phase polymerization equipment using a fluidized bed for polyethylene and polypropylene has large-sized particles with low density which rather belongs to the teeter bed.

The liquid fluidized bed shows a very smooth flow with small particles. But the larger the particle size or the bed diameter, the more the flow turns into circulation because of channelling, which enlarges longitudinal mixing of liquid and particles. Liquid fluidized beds are used for reactions and for adsorption that uses ion exchange resins, activated carbon etc., and are also used as bioreactors using immobilized enzymes and immobilized cells.

The three-phase fluidized bed consisting of vapour, liquid and solid phases is described in Section 4.1.2.5.

4.1.2.4 Gas-liquid Contactor

This equipment handles reactions including gas and liquid. If the gas phase is continuous, the contactor form will be a wetted-wall column, packed column or spray column as shown in Figure 4.7. In general, a mixing tank or bubble column that turns the gas phase into a dispersed phase is used as the gas—liquid reactor. Absorption of reactive gas may also be performed through the tubing or by using a mixer (Figure 4.8). Whenever a gas phase is turned into a dispersed phase, bubbles are formed. In this respect, the sizes of those bubbles must be reduced to ensure effective mass transfer between bubbles and liquid. To do this, an increase in the rate of rotation is effective for the case of stirred tank, but an excessive rotation demands high energy consumption.

In the bubble column, gas flows into liquid to form bubbles, and then mass transfer across the bubble interface proceeds to accomplish a reaction between

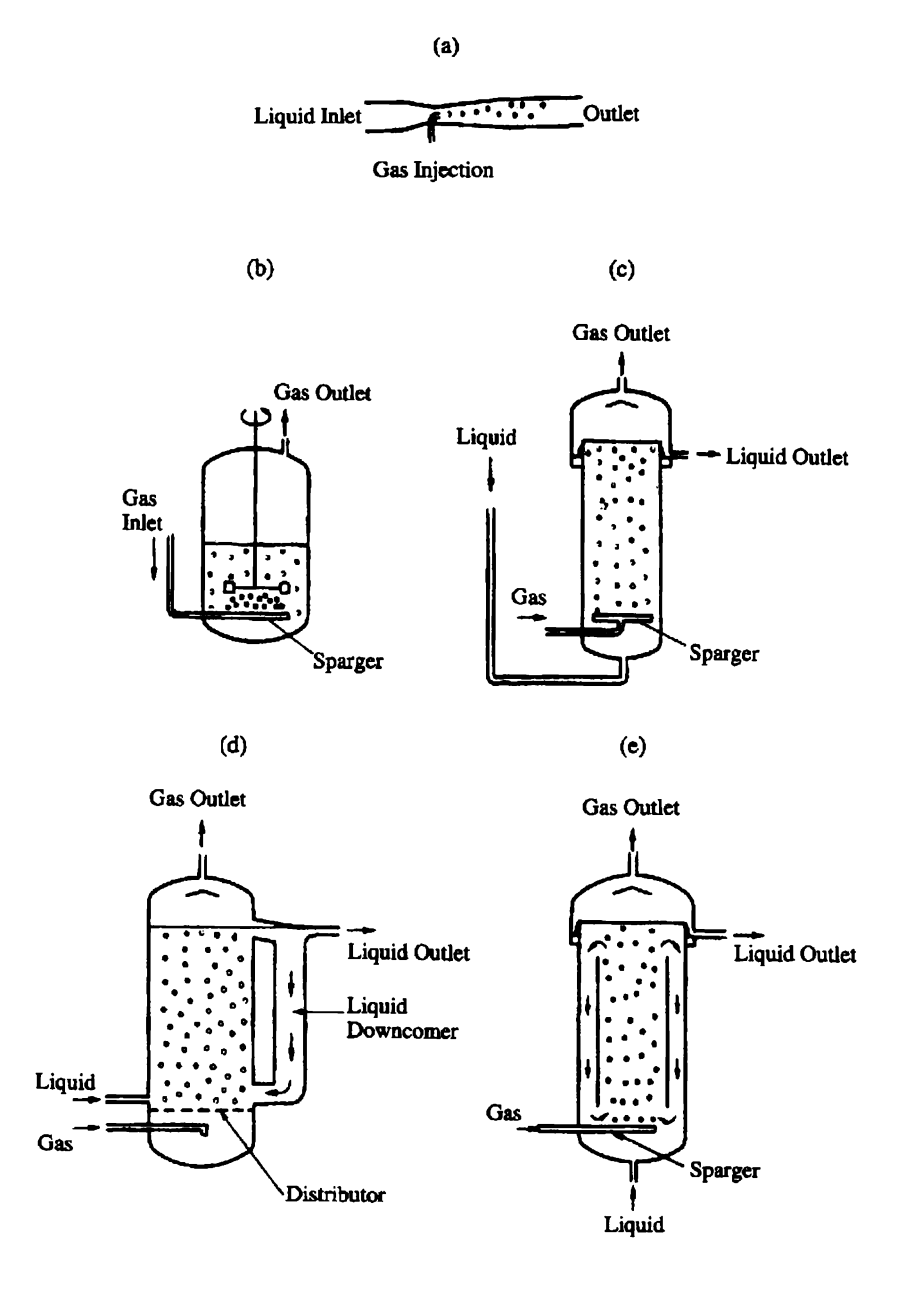


Figure 4.8 Gas-liquid contactor (for the case when the gas phase is dispersed). (a) Gas-liquid tubular reactor (Venturi mixer). (b) Stirred tank. (c) Bubble column. (d) Bubble column with outside circulation. (e) Circulating bubble column (draft-tube type).

80 S. FURUSAKI

the gas and liquid. With a low superficial velocity of gas, the column can be operated under a smooth flow regime called the bubble flow. In this case, bubbles do not coalesce, and therefore the small bubbles formed rise up in the column as they are formed, without growth. With increasing superficial velocity, bubbles accumulate in the centre of the column, creating circulation of solid particles. In the column, the flow turns into a turbulent state, and the bubbles rise up in the column while growing by repeated splitting and coalescence. When split and coalescence reach a balance, the bubbles will no longer grow, and finally settle down at a constant bubble size. This bubble size is not so large as that in a fluidized bed (teeter bed). Also, a draft tube may be installed to accelerate circulation, in order to encourage liquid mixing (Figure 4.8). This method keeps the concentration and temperature distribution of the liquid phase uniform.

4.1.2.5 Three-phase Contactor

This is a system that carries out a reaction by contacting the three phases: gas, liquid and solid. Basically, the behaviour is similar to a gas-liquid contactor. The gas-liquid contactor is operated with particles suspended in the mixing vessel or bubble column. An example of this can be seen when catalyst particles are suspended in a liquid. The chemical reaction proceeds as reactants in a gas phase are transferred into the liquid phase through the gas-liquid interface to be dissolved, and the reactants dissolved in the liquid are transferred to the solid surface in order for reaction to occur. In the so called solid-suspended bubble column, the solid particles should be dispersed uniformly in the column. This requires perfect mixing by bubbles. This type is often called a three-phase fluidized bed, when the bed has relatively large solid particles as well as a large hold-up of solids.

These apparatuses are also used for bioreactors such as fermenters that suspend micro-organisms and for reactors that use immobilized biocatalysts.

4.1.2.6 Membrane Reactors

These reactors are operated while separating catalysts from reactants and/or products using a membrane, and often used as bioreactors. For example, a system that holds enzymes or tissue culture cells of micro-organisms, animal or plant cells (these are called biocatalysts) inside a part of the reactor divided by a membrane to separate them from reactants or products may be considered as a kind of immobilized biocatalyst. This reactor offers a variety of immobilizing methods: mixing biocatalysts with reactants or products; contacting reactants with biocatalysts through a membrane; and reacting by biocatalysts immobilized inside a membrane.

Figure 4.9 shows the above types of membrane reactors. In (a) and (b) of the figure, the catalysts are dissolved or suspended in the liquid. The membrane is

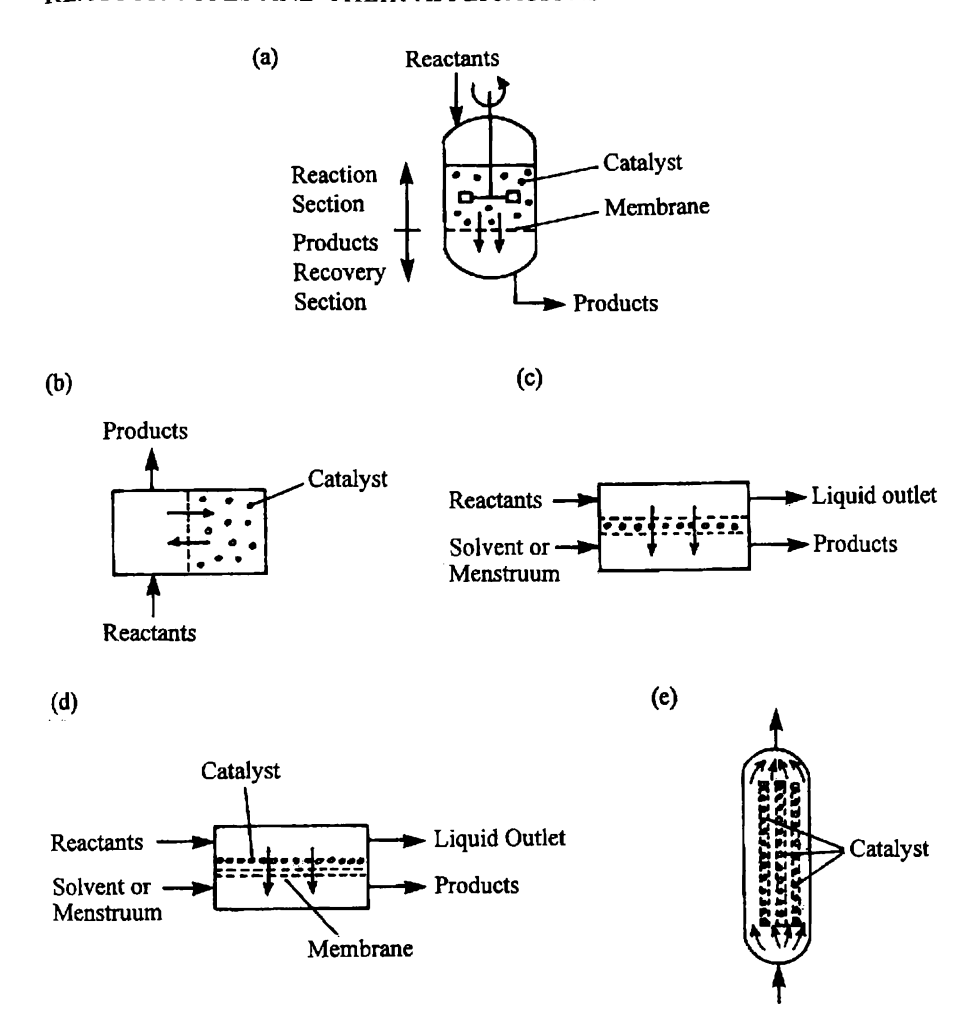


Figure 4.9 Typical membrane reactors (o: Catalyst). (a) Products filtration. Catalysts are suspended. (b) Diffusion through membrane. Catalysts stay in the right side of the column. To accelerate residual diffusion, membrane transmission is possible by pressure swing as well. (c) The catalyst is immobilized inside the membrane. Reaction occurs when reactants permeate through membrane. (d) The catalyst accumulates and is attached on the membrane. (Dynamic membrane). (e) The membrane serves as the carrier of the catalyst. Reactants diffuse into the membrane.

used here to separate the catalysts from the liquid input and output. In (c), the catalyst is immobilized inside the membrane. In (d), the catalyst accumulates and is attached on the membrane surface. In the cases of (c) and (d), reactions proceed when the liquid passes through the membrane or catalyst bed. In (e), the membrane serves as the carrier of the catalyst, forming a kind of fixed bed.

82 S. FURUSAKI

In these reactors, flat membranes are shown. Hollow fibres may be used instead, or a membrane module may be attached to the reactors to obtain a larger membrane surface area.

4.1.2.7 Other Reactors

In the preceding sections, we described reactors of typical types. This section introduces other useful reactors.

A very fast catalytic reaction is sometimes performed by depositing a catalyst on the tube wall of a tubular reactor. This reactor is called a tube-wall reactor, featuring easy temperature control of the tube wall. When using a metal catalyst, the catalyst is used in the form of wire gauze. In this case, a fast reaction like, or similar to, combustion is performed by passing a gas through the meshes in the wire gauze. With a slower reaction rate, the reaction is carried out by passing gas along the wire mesh or through the packing of the wire mesh in the reactor to ensure larger contact time.

In a liquid-phase reaction when the conversion is restricted by equilibrium, and when the product has a high vapour pressure, simultaneous reaction and distillation (reactive distillation) may promote the reaction efficiently. The reactor used in this case is a distillation column. A plate distillation column is used because a high liquid hold-up is favoured. This example is seen in esterification.

As mentioned briefly, a mixing tank or tubular reactor is used for polymerization. It is better to use a reactor of simpler structure because of very high viscosity, and its temperature control must be carefully designed, as the heat transfer coefficients are small. In the mixing tank, the heat generated by mixing must also be considered. For the effects of longitudinal mixing on molecular weight distribution, Denbigh⁽³⁾ gives a theoretical consideration.

References

- (1) A. M. Squires, Chem. Eng. Prog., 58 (4), 66 (1962).
- (2) T. Miyauchi, S. Furusaki, S. Morooka and Y. Ikeda. Advan. Chem. Eng., 11, 275 (1981).
- (3) K. Denbigh, Chemical Reactor Theory, Cambridge University Press (1965).

CHAPTER 4.2

Design of Homogeneous Reactors

YUKIHIRO SHIMOGAKI

Department of Chemical System Engineering, University of Tokyo, Japan

As described in Section 4.1, the forms of homogeneous reactor can be classified into tubular reactors and stirred tank reactors. Because of its form, the tubular reactor is the plug-flow type. On the other hand, the stirred tank reactor is sufficiently mixed and it is operated as a batch type reactor or continuous stirred tank reactor (CSTR). However, as described later, attention must be paid to the fact that perfect mixing flow can be assumed even for the tubular reactor, depending on the balance of mass transfer rate due to longitudinal diffusion compared with the rate due to the fluid flow.

The target of reactor design is the optimization of production rate and yield of the desired product. To achieve this aim, it is necessary to optimize the form and volume of the reactor, reaction time, and the feed rate of reactants. Such information can be obtained by examining the material and heat balances in the reactor, provided that kinetic information, such as the reaction mechanisms and the reaction rates, are obtained from the rate analysis. Let us describe the reactor design method for the reaction systems that have been well studied from the kinetic point of view.

4.2.1 MATERIAL AND HEAT BALANCES IN REACTION SYSTEMS

The basic equations for reactor design of isothermal operation systems can be obtained by making the mass balance in the reacting system. In non-isothermal operations, energy balances must be used in conjunction with mass balances, which is normally covered by the heat balance equation considering only the enthalpy. If we make the mass balance, assuming a closed space in a reactor (reactor element), the following expression holds:

(Rate of reactant inflow)—(rate of reactant outflow) + (rate of reactant loss due to chemical reaction within reactor element)

$$=$$
 (rate of accumulation of reactant within reactor element) (4.1)

Similarly, the following expression holds for the heat balance:

(Rate of heat flow into reactor element by fluid)—(rate of heat flow out of reactor element by fluid)+(rate of production of heat within reactor element)—(rate of disappearance of heat within reactor element)

= (rate of accumulation of heat within reactor element)
$$(4.2)$$

Selection must be made on the reactor element so that the concentration and temperature within the element are both uniform. For example, since concentration distribution does not exist in a perfect mixing tank, the entire reactor is assumed to be one reactor element. However, in the case of a tubular reactor, a concentration distribution exists from the reactor inlet through to the outlet, so a balance must be made for the infinitely small volume of the reactor. In either case, the governing equations for reactor design can be obtained from Eq. (4.1), and in conjunction with Eq. (4.2) as necessary. Some examples of those equations and the analytical solutions for different types of reactor will be described below.

4.2.2 DESIGN OF BATCH STIRRED TANK REACTOR

4.2.2.1 Governing Equations for Constant Volume Operation

For the batch reactor as shown in Figure 4.10, only the balance in the entire reactor has to be considered. In this case, both inflow and outflow are '0', therefore

For reacting component A,

Rate of reactant loss due to chemical reaction within reactor element = $r_A V$ (4.4)

Rate of accumulation of reactant within reactor element =
$$\frac{dN_A}{dt}$$
 (4.5)

$$r_{\rm A}V = \frac{{\rm d}N_{\rm A}}{{\rm d}t} \tag{4.6}$$

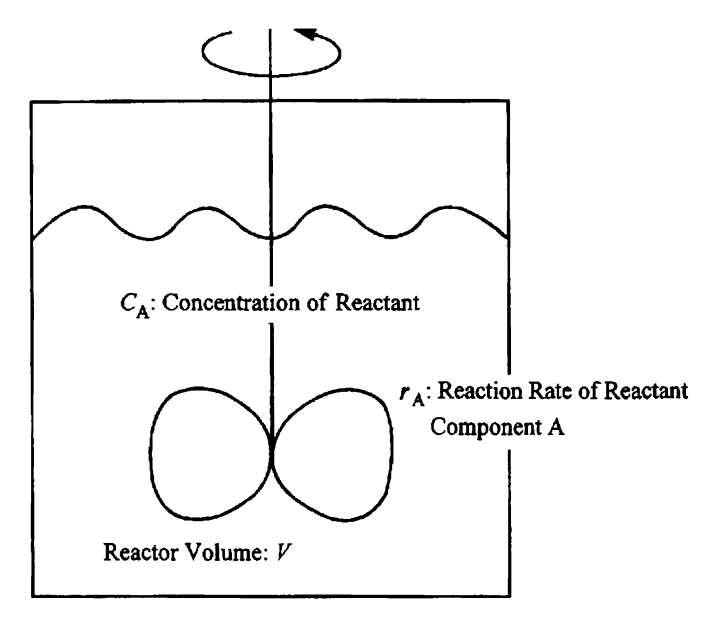


Figure 4.10 Constant-volume batch stirred tank reactor.

Since the fluid volume V is constant in constant-volume reactions, Eq. (4.6) can be modified as

$$\frac{\mathrm{d}(N_{\mathrm{A}}/V)}{\mathrm{d}t} = \frac{\mathrm{d}C_{\mathrm{A}}}{\mathrm{d}t} = r_{\mathrm{A}} \tag{4.7}$$

The following initial conditions at the start of reaction

$$t = 0, C_{A} = C_{A_0} (4.8)$$

used to integrate Eq. (4.7) to obtain

$$t = \int_{C_{A_0}}^{C_A} \frac{dC_A}{r_A} = \int_{C_A}^{C_{A_0}} \frac{dC_A}{-r_A}$$
 (4.9)

gives the time required for reacting component A to change from the initial concentration C_{A_0} to C_A . Rewriting Eq. (4.9) using the conversion x_A of A leads to

$$t = C_{A_0} \int_0^{x_A} \frac{\mathrm{d}x_A}{-r_A} \tag{4.10}$$

If the reaction is first order with respect to the reacting component A, meaning that the rate equation given by

$$r_{\rm A} = kC_{\rm A} = kC_{\rm Ao}(1-x)_{\rm A}$$
 (4.11)

Table 4.1 Integration forms of governing equations for constant-volume batch stirred tank reactor⁽¹⁾

Quantum equation	Equation for reaction rate	Integration form
Arbitrary quantum equation	$-r_{A} = k$ (0 order)	$C_{A_0} - C_A = C_{A_0} x_A = kt \ (t < C_{A_0}/k)$ $C_A = 0 \qquad (t \ge C_{A_0}/k)$
	$-r_{A} = kC_{A}$ (1st order)	$-\ln(C_{A}/C_{A_{0}}) = -\ln(1-x_{A}) = kt$
	$-r_{A} = kC_{A}^{n}$ (nth order)	$C_{A}^{1-n} - C_{A_0}^{1-n} = C_{A_0}^{1-n}[(1-x_A)^{1-n} - 1]$ = $(n-1)kt$
$A + bB \stackrel{k}{\longrightarrow} C$	$-r_{A} = kC_{A}C_{B}$	$\ln \frac{C_{A_0}C_B}{C_{B_0}C_A} = \ln \frac{\theta_B - bx_A}{\theta_B(1 - x_A)} = C_{A_0}(\theta_B - b)kt$
$A + B \xrightarrow{k} C$	$-r_{A} = kC_{A}\sqrt{C_{B}}$	$\ln \left[\left(\frac{\sqrt{\theta_{B}} - \sqrt{\theta_{B} - 1}}{\sqrt{\theta_{B}} + \sqrt{\theta_{B}} - 1} \right) \left(\frac{\sqrt{\theta_{B} - x_{A}} + \sqrt{\theta_{B} - 1}}{\sqrt{\theta_{B}} - x_{A}} - \sqrt{\theta_{B} - 1} \right) \right]$
		$=k\sqrt{C_{A_0}(\theta_B-1)}t \ (\theta_B\neq 1)$
$A \underset{k^{-1}}{\overset{k}{\rightleftharpoons}} C$	$-r_{A} = k(C_{A} - C_{C}/K_{C})$	$\ln\left[\frac{1-\theta_{\rm C}/K_{\rm C}}{(1-\theta_{\rm c}/K_{\rm C})-(1+1/K_{\rm C})x_{\rm A}}\right] = k\left(1+\frac{1}{K_{\rm C}}\right)t$
		$K_{\rm C} = \frac{k}{k^{-1}}$

 $[\]theta_{\rm B}=C_{\rm B_0}/C_{\rm A_0}\neq b,~\theta_{\rm c}=C_{\rm C_0}C_{\rm A_0}$

is substituted in Eqs (4.9) and (4.10), then the integral form

$$kt = -\ln(C_A/C_{A_0}) = \ln(1 - x_A)$$
 (4.12)

can be obtained. In this way, an analytical solution is given to single reacting systems having a relatively simple formulation on r_A . Table 4.1 shows integral forms of governing equations for typical reaction rate equations.

For complex reactions, a similar sequence can be made to have the basic equations. The mass balance equations will be made for the number of

components equivalent to those in the rate equations. First, let us consider the first order parallel reactions.

$$\mathbf{A} \longrightarrow \mathbf{P}_1, \quad r_1 = k_1 C_{\mathbf{A}} \tag{4.13}$$

$$A \longrightarrow P_2, \quad r_2 = k_2 C_A$$
 (4.14)

The governing equations for the reactions expressed as above are given by

$$\frac{dC_{A}}{dt} = -(k_1 + k_2)C_{A} \tag{4.15}$$

$$\frac{\mathrm{d}C_{\mathbf{P}_1}}{\mathrm{d}t} = k_1 C_{\mathbf{A}} \tag{4.16}$$

$$\frac{\mathrm{d}C_{\mathrm{P}_2}}{\mathrm{d}t} = k_2 C_{\mathrm{A}} \tag{4.17}$$

Using the initial condition $C_A = C_{A_0}$ at t = 0, the following expression can be obtained from Eq. (4.15)

$$\frac{C_{A}}{C_{A_0}} = \exp\{-(k_1 + k_2)t\}$$
 (4.18)

Substituting Eq. (4.18) into Eqs (4.16) and (4.17), and assuming that $C_{\rm P_1} = C_{\rm P_2} = 0$ at t = 0, we obtain the following expressions showing changes in the concentrations of P_1 and P_2 with time

$$\frac{C_{P_1}}{C_{A_0}} = \frac{k_1}{k_1 + k_2} \{1 - e^{(-k_1 + k_2)t}\}$$
 (4.19)

$$\frac{C_{P_2}}{C_{A_0}} = \frac{k_2}{k_1 + k_2} \{1 - e^{-(k_1 + k_2)t}\}$$
 (4.20)

There is no change in selectivity since the ratio of the formation rate between P_1 and P_2 is kept constant. In the case of consecutive reactions, the formation rate of final and intermediate product components changes with time, therefore the selectivity varies depending on the operating conditions.

$$A \longrightarrow R$$
, $r_1 = k_1 C_A$ (4.21)

$$R \longrightarrow P, \quad r_2 = k_2 C_R$$
 (4.22)

The governing equations for the above consecutive reactions can be written as

$$\frac{\mathrm{d}C_{\mathrm{A}}}{\mathrm{d}t} = -k_1 C_{\mathrm{A}} \tag{4.23}$$

$$\frac{\mathrm{d}C_{\mathrm{R}}}{\mathrm{d}t} = k_1 C_{\mathrm{A}} - k_2 C_{\mathrm{R}} \tag{4.24}$$

$$C_{\rm P} - C_{\rm P_0} = C_{\rm A_0} + C_{\rm R_0} - C_{\rm A} - C_{\rm R} \tag{4.25}$$

Eq. (4.23) can be simply solved, and the following expression can be obtained

$$\frac{C_{\rm A}}{C_{A_0}} = e^{-k_1 t} \tag{4.26}$$

An equation obtained by substituting this in Eq. (4.25) is the first-order linear differential equation. Thus, by solving this equation in accordance with the formula, the concentration of the intermediate product components for $k_1 \neq k_2$ is

$$\frac{C_{\rm R}}{C_{\rm A_0}} = \frac{k_1}{k_1 - k_2} (e^{-k_2 t} - e^{-k_1 t}) + \frac{C_{\rm R_0}}{C_{\rm A_0}} e^{-k_1 t}$$
(4.27)

The concentration of the final product components can simply be obtained from Eq. (4.25). Figure 4.11 shows changes in concentration of each reactant with time. Intermediate product component R has the maximum value determined by the ratio between rate constants k_1 and k_2 . The yield of R is defined as

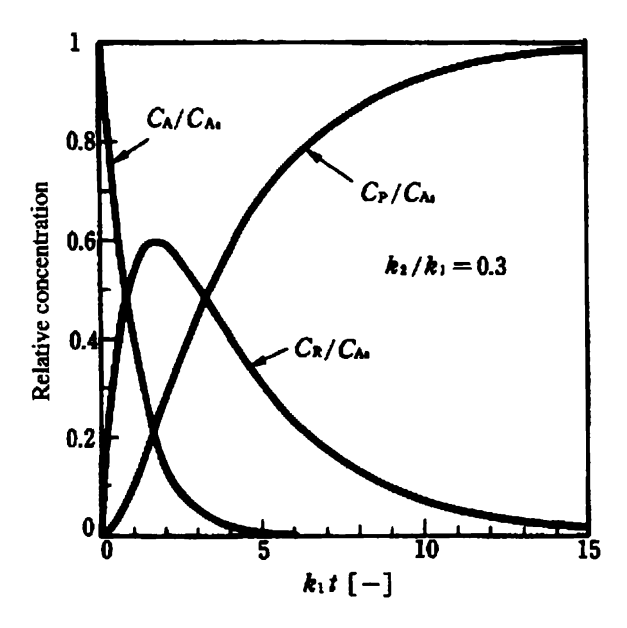


Figure 4.11 Changes in concentration of each reactant with time for the consecutive reactions $(A^{\underline{k_1}}, R^{\underline{k_2}}, P)$.

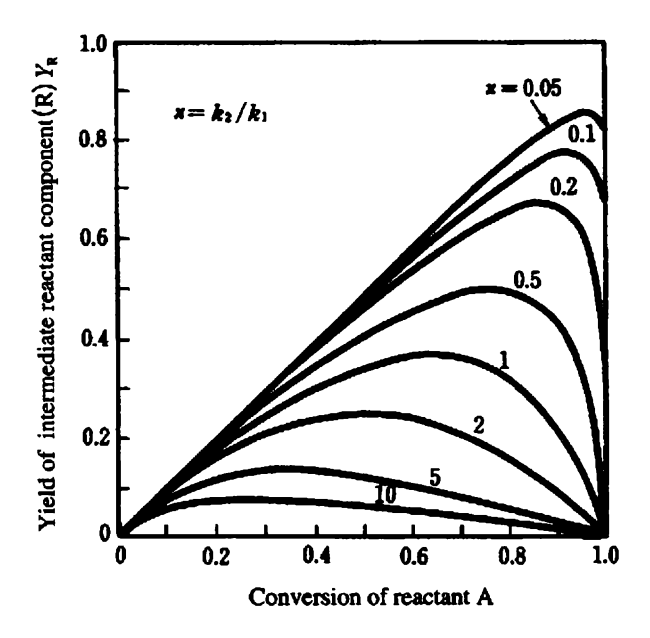


Figure 4.12 Relation between the yield of the intermediate reactant component (R) and the conversion of reactant A for the consecutive reactions $(A \xrightarrow{k_1} R \xrightarrow{k_2} P)^{(1)}$.

$$Y_{R} = \frac{C_{R} - C_{R_{0}}}{C_{A_{0}}} \tag{4.28}$$

and its relation with the conversion of A is illustrated in Figure 4.12. As is apparent from the figure, the conversion optimizing the yield of the intermediate product components and its yield vary depending on the k_1/k_2 ratio.

If integration cannot be made easily because of more complex rate equations, graphic integration or numerical integration can be used. Basically, the procedure is the same as described above. First, write the mass balance expressions for each component as in Eqs (4.15)–(4.17) and then solve them using the aid of computers or graphics. In general, gas-phase reactions such as combustion consist of a number of gas-phase elementary reactions, and it is not unusual that the number of aimed components is more than one hundred. Therefore, non-linear simultaneous differential equations covering more than one hundred elements must be solved, which is difficult practically, even by computer. The Runge-Kutta Method is famous as a numerical analysis method for differential equations, but it cannot be used for the gas-phase reactions. Particularly when numerous reaction species are considered, there may be a case in which the reaction rate disperses by more than ten digits, which indicates that solutions obtained by an extrinsic type of solution method

like the Runge-Kutta Method may diverge in many cases. Basically, such divergence can be minimized by shortening the time count intervals in the calculation. However, too short time count intervals require an enormous time for calculations and may also cause intrinsic errors on the computer such as digit omission. For this reason, the intrinsic method of solution such as the Gear Method must be adopted to ensure stability in solutions even with large time-count intervals.

4.2.2.2 Governing Equations for Non-constant Volume Operation

When a gas-phase reaction is performed at a constant temperature and pressure, the fluid volume changes as the reaction proceeds. In such a case, Eq. (4.7) can be rewritten as

$$\frac{dN_{A}}{dt} = \frac{dN_{A_{0}}(1 - x_{A})}{dt} = r_{A}V_{0}(1 + \varepsilon_{A}x_{A})$$
 (4.29)

where ε_A is the increased amount of moles of the system when 1 mole of the reactants react. Arranging this gives

$$\frac{C_{A_0}}{(1 + \varepsilon_A x_A)} \frac{\mathrm{d}x_A}{\mathrm{d}t} = -r_A \tag{4.30}$$

The integral form is

$$t = C_{A_0} \int_0^{x_A} \frac{\mathrm{d}x_A}{(1 + \varepsilon_A x_A)(-r_A)} \tag{4.31}$$

4.2.2.3 Non-isothermal Operation of Constant Volume System

If the operation is non-isothermal because of the effect of reaction heat, the heat balance must be considered in addition to the mass balance. For batch operation:

Rate of production of heat within reactor element =
$$Q_A r_A V$$
 (4.32)

Rate of accumulation of heat within reactor element = $US(T - T_C)$ (4.33)

Rate of disappearance of heat within reactor element = $Vc_P \rho dT/dt$ (4.34)

where Q_A is the reaction heat, U is the overall heat transfer coefficient, S is the heating surface area, T is the temperature in the reactor and T_C is the coolant temperature. Thus, the heat balance equation is

$$Vc_{P}\rho \frac{\mathrm{d}T}{\mathrm{d}t} = Q_{A}r_{A}V - US(T - T_{C}) \tag{4.35}$$

Eq. (4.35) is solved simultaneously with the mass balance expressed with respect to the reacting component A. However, since it cannot always be solved analytically, numerical analysis, with the aid of computer software, is normally employed.

4.2.3 DESIGN OF CONTINUOUS STIRRED TANK REACTORS

4.2.3.1 Governing Equations for Constant Volume Operation

In this section, we consider constant-volume reactions performed in the stirred tank reactor that handles continuous operation as shown in Figure 4.13. In such a reactor, reaction mixtures are well stirred inside and the concentration of each component is uniform throughout the reactor. Thus, the mass balance for component j can be expressed as

$$F_{V}(C_{ii} - C_{i0}) = r_{i}V (4.36)$$

Similarly, the mass balance expression for component A is

$$F_{V}(C_{A_{0}} - C_{A}) = -r_{A}V (4.37)$$

Expressing this using the conversion

$$x_{\rm A} = 1 - C_{\rm A}/C_{\rm A_0} \tag{4.38}$$

gives the expression

$$\tau = \frac{V}{F_{V}} = \frac{C_{A_0} - C_{A}}{-r_{A}} = \frac{C_{A_0}, x_{A}}{-r_{A}}$$
(4.39)

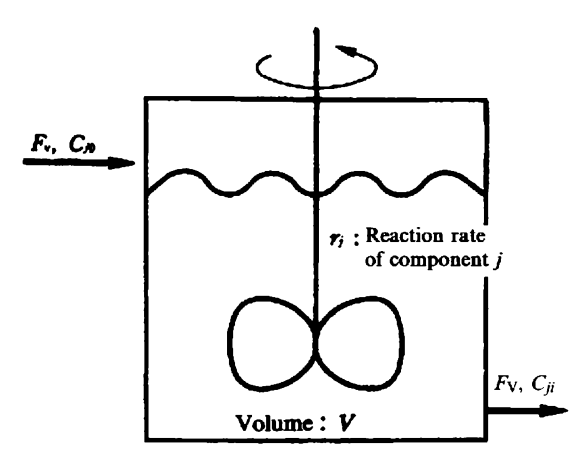


Figure 4.13 Continuous stirred tank reactor.

For a perfect mixing flow reactor as shown in Figure 4.13, part of the components which simultaneously feed into the reactor is discharged immediately, but another part remains in the reactor for a long time, so the above τ is assumed to be the mean value of the residence times, called the mean residence time.

If the reaction rate of a constant-volume reaction is expressed by the nthorder reaction of reactants, the above expression leads to

$$k\tau C_{A_0}^{n-1}(C_A/C_{A_0})^n + (C_A/C_{A_0}) - 1 = 0$$
(4.40)

This is an algebraic equation with C_A unknown. For n=1 and 2, the analytical solutions can be simply obtained by

$$C_{\rm A}/C_{\rm A_0} = 1 - x_{\rm A} = \frac{1}{1 + k\tau}$$
 (4.41)

$$C_{\rm A}/C_{\rm A_0} = 1 - x_{\rm A} = \frac{\sqrt{1 + 4k\tau C_{\rm A_0}}}{2k\tau C_{\rm A_0}}$$
 (4.42)

For more complex generic reaction rates, non-linear algebraic equations must be solved. This can be done by performing a numerical analysis such as the Newton-Laphson method.

In the case when N units of stirred tank reactors are connected in a series as shown in Figure 4.14, the mean residence time is expressed by the following expression from the mass balance expression of reacting component A in the ith tank:

$$\tau_i = \frac{V_i}{F_v} = \frac{C_{A_{i-1}} - C_{A_i}}{-r_{A_i}} = \frac{C_{A_0}(x_{A_{i-1}} - x_{A_i})}{-r_{A_i}}$$
(4.43)

where r_{A_i} and τ_i are the rate of consumption and the mean residence time of A in the *i*th tank, respectively. At this time, the ratio between the outlet concentration of Nth tank C_{A_N} and the inlet concentration of the first tank C_{A_0} is given by

$$\frac{C_{A_N}}{C_{A_0}} = 1 - x_A = \frac{C_{A_1}}{C_{A_0}} \frac{C_{A_2}}{C_{A_1}} \cdots \frac{C_{A_{\text{iti}}}}{C_{A_{i-1}}} \cdots \frac{C_{A_N}}{C_{A_{N-1}}}$$
(4.44)

Then the conversion x_{A_N} of the entire N tank can be determined. For first-order reactions, the ratio can be obtained by using Eq. (4.41) that is applicable to each tank as follows:

$$\frac{C_{A_N}}{C_{A_0}} = 1 - x_A = \frac{1}{(1 + k_1 \tau_1)(1 + k_2 \tau_2) \cdots (1 + k_N \tau_N)}$$
(4.45)

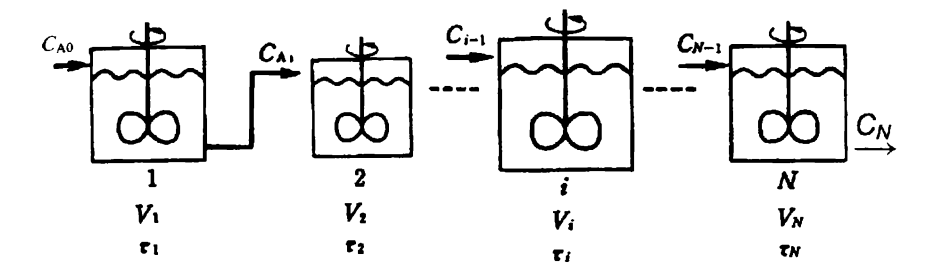


Figure 4.14 Continuous multi-stage stirred tank reactors.

Under conditions in which the rate constants and mean residence times are equal in all tanks, the concentration of the reacting species at the last tank can be obtained as,

$$\frac{C_{A_N}}{C_{A_0}} = 1 - x_A = \frac{1}{(1 + k_1 \tau_1)^N}$$
 (4.46)

It is difficult to obtain these analytical solutions from non-linear rate equations, in which case Newton-Laphson's method needs to be applied.

4.2.3.2 Graphic Solution

Next we introduce a method for obtaining the conversion of the abovementioned N units of continuous stirred tank reactors by means of the graphic solution. First, modification of Eq. (4.43) gives

$$-r_{A_i} = (-1/\tau_i)(C_{A_i} - C_{A_{i-1}}) \tag{4.47}$$

The left side represents the reaction rate, and its concentration dependency can be obtained from kinetic studies. C_{i-1} is the concentration at the inlet of i tank. Therefore, plotting by taking the concentration on the abscissa and the reaction rate on the ordinate as shown in Figure 4.15 represents the right side of Eq. (4.47) as a straight line where the slope of $-1/\tau_i$ and the ordinate axis intercept of C_{i-1} cross each other. The point of intersection of this straight line and the curve indicating the concentration dependency of the experimentally obtained reaction rate shown on the left side of Eq. (4.47) represents the concentration C_i at the outlet of the ith tank. Thus, the concentration of each tank can be simply obtained by repeating this graphic solution from the first tank. By repeating this procedure up to the Nth tank, the conversion at the outlet of the entire reactor system can be obtained. In addition, if you want to set the conversion at the outlet to a certain value or set the concentration of

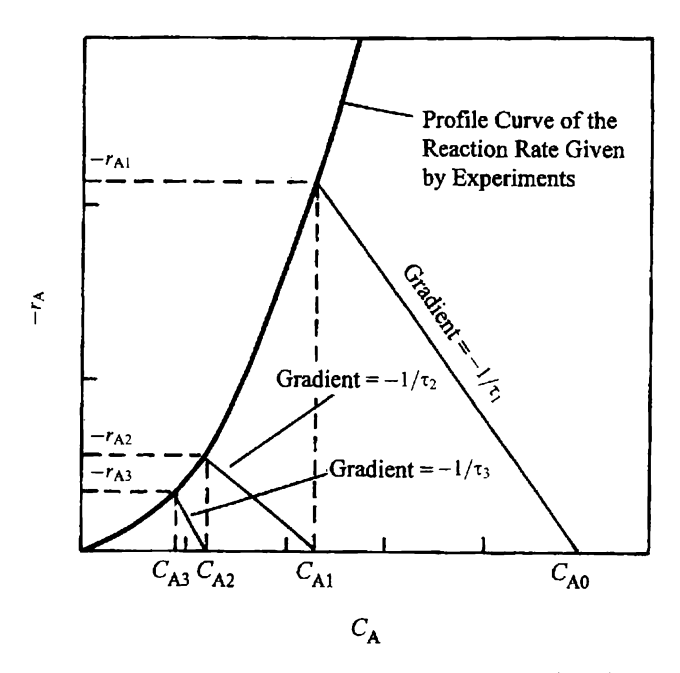


Figure 4.15 Design method of continuous multi-stage stirred tank reactor (complete mixing flow) by graphical solution.

each tank, optimum solutions can be obtained by adjusting the slope of the straight line to appropriate values by changing the residence time, so as to obtain the desired conversion and concentration.

4.2.4 DESIGN OF TUBULAR REACTORS

4.2.4.1 Governing Equations for a Tubular Reactor

Let us consider the equations to design tubular flow reactors as shown in Figure 4.16. First consider the infinitely small volume element dV in the reactor and then examine the mass balance in a steady state in this part to obtain

$$\frac{\mathrm{d}F_j}{\mathrm{d}V} = r_j \tag{4.48}$$

Focusing on the reacting component A, if we express the above expression using the conversion x_A

$$F_{A_0} \frac{dx_A}{dV} = -r_A (4.49)$$

Integration of this expression gives

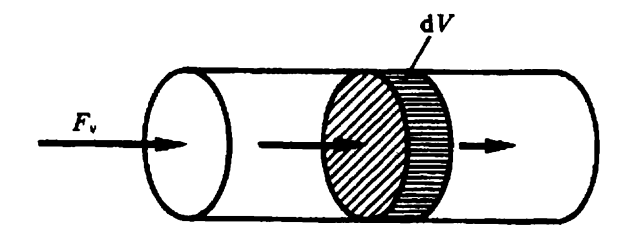


Figure 4.16 Tubular flow reactor.

$$\frac{V}{F_{A_0}} = \int_0^{-x_A} \frac{\mathrm{d}x_A}{-r_A}$$
 (4.50)

or

$$\tau = \frac{V}{F_{\nu}} = C_{A_0} \int_0^{r_A} \frac{\mathrm{d}x_A}{-r_A}$$
 (4.51)

Integral forms of Eq. (4.51) for typical reaction rate equations are given in Table 4.2.

4.2.4.2 Comparison of Tubular and Continuous Stirred Tank Reactors

The relation between $C_{A_0}/(-r_A)$ versus x_A generally gives a curve as shown in Figure 4.17. As apparent from Eqs (4.10) and (4.51), the mean residence time in the batch stirred tank and tubular reactors corresponds to the area enclosed by the curve and the abscissa. In other words, the time required to obtain the same conversion with respect to the same reaction rate equation is identical for the batch stirred tank and tubular reactors. For the continuous stirred tank reactor, the mean residence time corresponds to the quadrilateral area shown in the figure as apparent from Eq. (4.39). This indicates that, as compared with the continuous stirred tank reactor, the tubular reactor requires less time to achieve the same conversion. This is because the continuous stirred tank reactor has a residence time distribution with some components discharged in a time shorter than the mean residence time.

In contrast to this, if the backmixing effect by diffusion is added to the flow direction of the reacting fluid in the tubular reactor, its characteristics are assumed to be close to those of the continuous stirred tank reactor. The governing equation for the tubular reactor considering such a longitudinal diffusion is given by

$$E_{z}\frac{d^{2}C}{dz^{2}} - u\frac{dC}{dz} - kC = 0 {(4.52)}$$

Table 4.2 Integration forms of Eq. (4.51) for gas-phase reactions with constant pressure in tubular reactors⁽¹⁾

Quantum equation	Equation for reaction rate	Integration form
$A \longrightarrow cC$	$-r_{A}=kC_{A}$	$k\tau = \frac{kC_{A_0}V}{F_{A_0}} = (1 + \varepsilon_A)\ln\frac{1}{1 - x_A} - \varepsilon_A x_A$
$ \begin{array}{c} A + B \longrightarrow cC \\ (C_{A_0} = C_{B_0}) \\ 2 A \longrightarrow cC \end{array} $	$-r_{A} = kC_{A}C_{B}$ $-r_{A} = kC_{A}^{2}$	$k\tau C_{A_0} = \frac{kC_{A_0}^2 V}{F_{A_0}} = 2\varepsilon_{A}(1 + \varepsilon_{A})\ln(1 - x_{A}) + \varepsilon_{A}^2 x_{A} + (1 + \varepsilon_{A})^2 \frac{x_{A}}{1 - x_{A}}$
$A + bB \longrightarrow cC$	$-r_{A} = kC_{A}C_{B}$ $(\theta_{B}/b \neq 1)$	$k\tau C_{A_0} b = \frac{kC_{A_0}^2 bV}{F_{A_0}} = \varepsilon_A^2 x_A + \frac{(1 + \varepsilon_A)^2}{(\theta_B/b) - 1} \ln \frac{1}{1 - x_A} + \frac{(1 + \varepsilon_A \theta_B/b)^2}{(\theta_B/b) - 1} \ln \left[\frac{(\theta_B/b) - x_A}{(\theta_B/b)} \right]$
		$k_1 \tau = \frac{k_1 C_{A_0} V}{F_{A_0}} = \frac{\theta_c + c x_{A_\infty}}{\theta_c + c} \left[- (1 + \varepsilon_A x_{A_\infty}) \right]$

$$A \rightleftharpoons cC \qquad -r_{A} = k_{1}C_{A} - k_{2}C_{c} \qquad \times \ln\left(1 - \frac{x_{A}}{x_{A\infty}}\right) - \varepsilon_{A}x_{A}$$

$$(\theta_{c} = C_{c_{0}}/C_{A_{0}}, x_{A_{\infty}} \text{ is equilibrium conversion})$$

Where ε_A is the increasing rate of moleculars in the reaction system. In the case of the liquid-phase reaction with constant volume, ε_A is regarded as zero.

where E_z is the longitudinal diffusion coefficient and u is the linear velocity of the fluid. Figure 4.18 shows the calculations made with respect to the fraction of reactant unconverted and $k\tau$ from the analytical solution of Eq. (4.52), using various Péclet numbers in first-order reactions. In the case when the backmixing effect by diffusion applies in this way, the conversion becomes the function of the mean residence time and uL/D (= Péclet number). It corresponds to perfect plug flow when the Péclet number is infinite, and to the perfect mixing tank when the Péclet number is zero. You will find that when the backmixing effect is applied to plug flow through the tubular reactor, its reactor characteristics gradually transform into those of the perfect mixing tank.

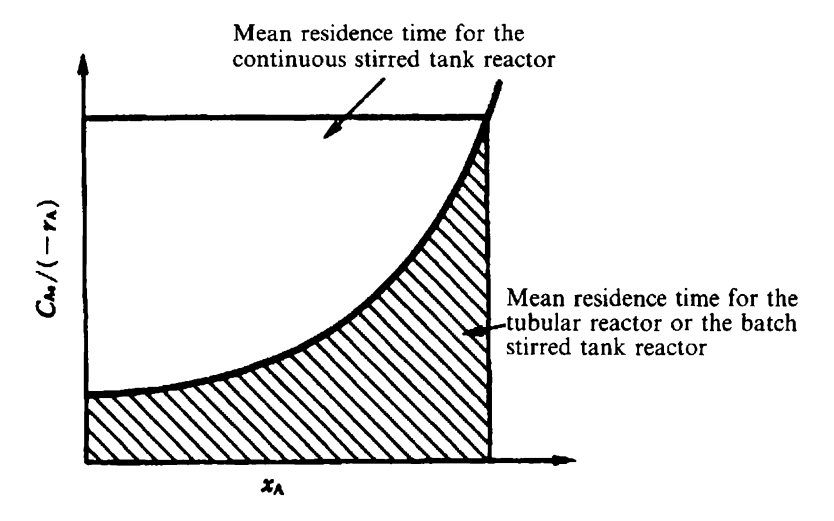


Figure 4.17 Comparison of tubular reactor and continuous stirred tank reactor (required residence time to obtain the same conversion).

4.2.5 HOMOGENEOUS AND HETEROGENEOUS COMPLEX REACTIONS

So far we have discussed the basic equations to design the reactors considering only the homogeneous reactions. However, the heterogeneous reactions may affect the reactor performance and should be considered together with the homogeneous reactions. In this section, we briefly summarize the mixing of gas-phase and surface reactions.

Let us assume a case in which a reaction proceeds on the reactor wall in addition to the gas-phase reaction in a tubular reactor. If reacting component A is consumed through first-order reactions in the gas phase and at the surface to yield the product, the governing equation for the reactants basically given by Eq. (4.49), can be written as

$$F_{\rm A}\frac{\mathrm{d}x_{\rm A}}{\mathrm{d}V} = -r_{\rm A} = \left(k_{\rm g} + \frac{4}{d}k_{\rm s}\right)C_{\rm A} \tag{4.53}$$

where d is the diameter of the reaction tube, k_g is the first-order reaction rate constant in the gas phase, and k_s is the surface reaction rate constant. Since the surface reaction rate is proportional to the surface area (S), and the concentration change accompanied by the surface reaction is inverse to the volume (V), the reaction rate of component A can be written as

$$-V\frac{\mathrm{d}C_{\mathrm{A}}}{\mathrm{d}t} = Vk_{\mathrm{g}}C_{\mathrm{A}} + Sk_{\mathrm{s}}C_{\mathrm{A}} \tag{4.53a}$$

98 Y. SHIMOGAKI

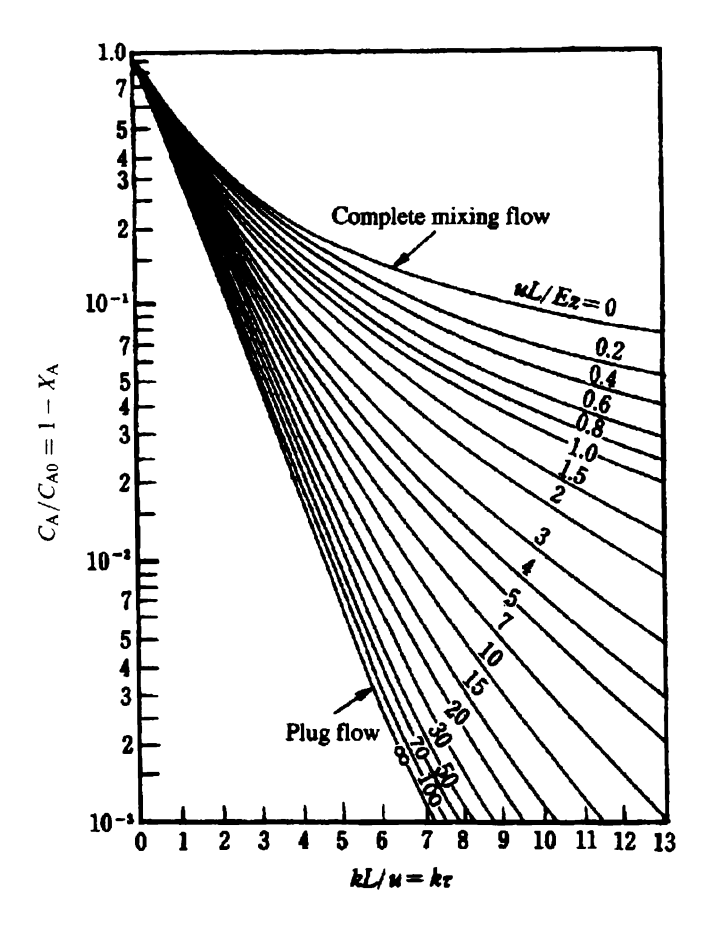


Figure 4.18 Effect on the longitudinal diffusion on the reaction rate of the tubular reactor⁽²⁾.

$$r_{\rm A} = -\frac{{\rm d}C_{\rm A}}{{\rm d}t} = (k_{\rm g} + S/V)C_{\rm A}$$
 (4.53b)

therefore, S/V ratio must be correlated with respect to k_s . It is obvious that the S/V ratio of the circular tube reactor is 4/d. In a reaction rate analysis, the overall reaction rate constant can be calculated from the outlet conversion using Eq. (4.50). The reaction rate constants of the gas-phase and surface reactions can be obtained individually by evaluating the overall reaction rate constant while changing the inner diameter of the tubular reactor using the relation shown in equation (4.53b). In other words, when reactions are performed in reactors that have reaction tubes of different diameters, the

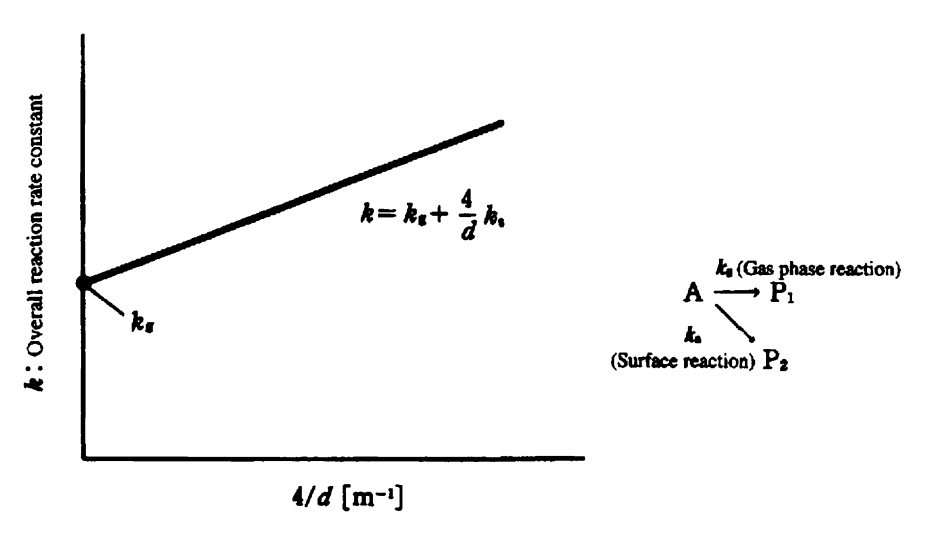


Figure 4.19 Relation between the overall reaction rate constant and the diameter of the reaction tube in the case of a gas-phase reaction with surface reaction.

overall rate constants obtained from their conversions based on Eq. (4.50) are different. As shown in Figure 4.19, plotting the overall rate constant with respect to the S/V ratio (4/d) for the tubular reactor) gives a straight line, representing the value of intercept on the y coordinates intercept as the homogeneous reaction rate constant, and the slope is the heterogeneous reaction rate constant.

If the reaction rate constant of the surface reaction is sufficiently large, the transfer rate of reactants to the inner wall surface by diffusion is the rate determining step. This indicates that the rate constant of heterogeneous reactions represents the mass transfer coefficient but not the surface reaction rate constant. Using the diffusion coefficient (D) and the Sherwood number (Sh), the mass transfer coefficient is given by

$$k_{\rm d} = Sh \frac{D}{d} \tag{4.54}$$

This k_d may be used instead of k_s in Eq. (4.53). If the flow through the circular tube is laminar flow, Sh = 3.657 is fixed. Thus, the overall reaction rate constant increases inversely with the square of the tube diameter of the reactor when the mass transfer is the rate determining step, and is inverse to the tube diameter as shown in Figure 4.19 when the surface reaction is rate-controlling. From this, the factor that controls the heterogeneous reaction rate can be found by examining the tube diameter dependency of the overall reaction rate constant. For example, Figure 4.20 shows an example that identifies the mass

100 Y. SHIMOGAKI

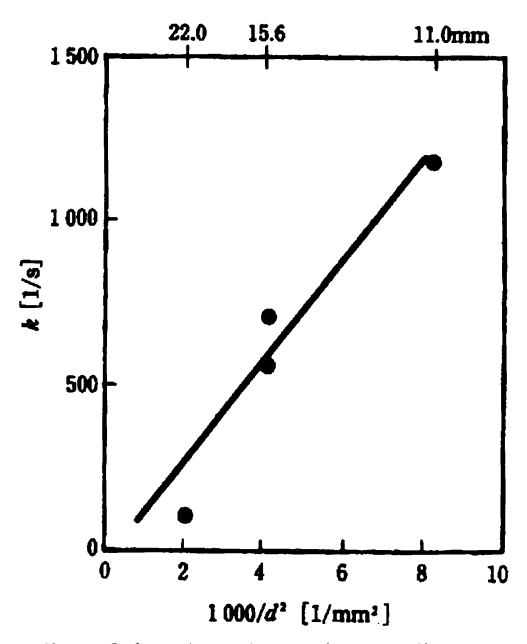


Figure 4.20 The effect of the S/V ratio on the overall rate constant when the mass transfer is the rate determining step. Plotted data were obtained for the WSi_x film synthesis by reactions with WF_6 and

SiH₂Cl₂ (Ref ⁽³⁾).

transfer as rate-controlling, since the overall rate constant is inverse to the square of the reaction tube diameter. In the case when the mass transfer is rate controlling, the rate determining step can also be identified by examining the total pressure dependency of the overall reaction rate constant, because the diffusion coefficient D is in inverse proportion to pressure⁽⁴⁾.

In many cases, the surface reaction at the reactor wall surface also contributes the chain termination medium for radical chain reactions such as combustion. For example, suppose that radicals are de-activated because of a collision with the reactor wall in simple radical chain reactions as shown by

$$\begin{array}{c}
A \longrightarrow R \\
A + R \longrightarrow R + R
\end{array} \tag{4.55}$$

If the deactivation rate of radicals at the reactor wall is higher than the formation rate of radicals in the gas phase, the radical chain reaction decreases gradually and does not continue further. However, if this balance is lost, the reaction proceeds explosively. Figure 4.21 shows the circumstances of combustion of the H₂-O₂ system⁽⁵⁾. For example, if the pressure of gas is increased from the low pressure side at 500 °C, the reaction shifts from the moderate state to the explosive area. This is due to the fact that de-activation

of radicals at the wall surface has a significant effect on the low-pressure side where the mean free path of gas is long.

To explain such a phenomenon simply, let us model the balance between the radical formation rate in the gas phase and the de-activation rate. The radical formation rate in the gas phase is expressed as

$$\frac{\mathrm{d}C_{\mathrm{R}}}{\mathrm{d}t} = k_{\mathrm{g}}C_{\mathrm{R}} \tag{4.56}$$

On the other hand, in consideration of the volume and area of the reactor wall, the de-activation rate on the wall is expressed as

$$-\frac{\mathrm{d}C_{\mathrm{R}}}{\mathrm{d}t} = k_{\mathrm{s}} \frac{S}{V} C_{\mathrm{R}} \tag{4.57}$$

In general, since reactions in a gas phase have higher activation energy, the temperature dependence on the respective rates is as illustrated in Figure 4.22. Here, the points where both lines cross each other respectively indicate the temperatures at which the gas-phase radical chain reactions proceed explosively in the reactor. The important point is that the initiating temperature of reaction varies by changes in the S/V ratio of the reactor. Table 4.3 shows the relations between the initiating temperature and diameter of the reaction tube for a CVD (Chemical Vapour Decomposition) reaction

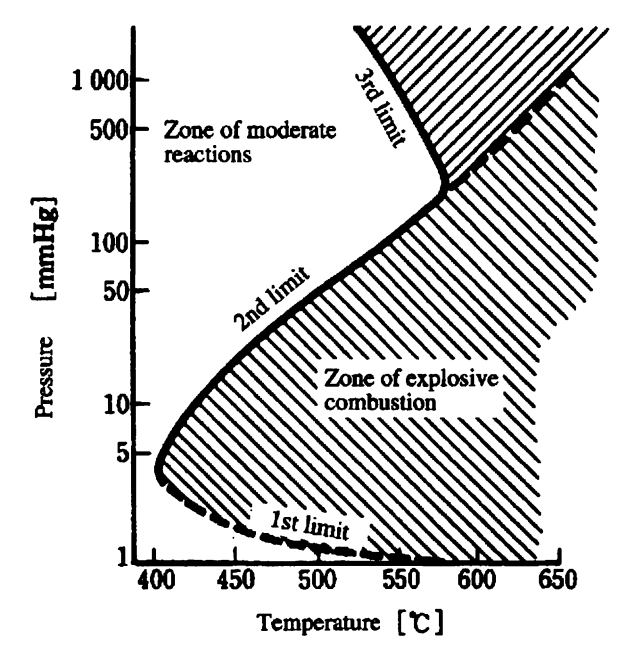


Figure 4.21 Circumstances of combustion of the H₂-O₂ system⁽⁴⁾.

102 Y. SHIMOGAKI

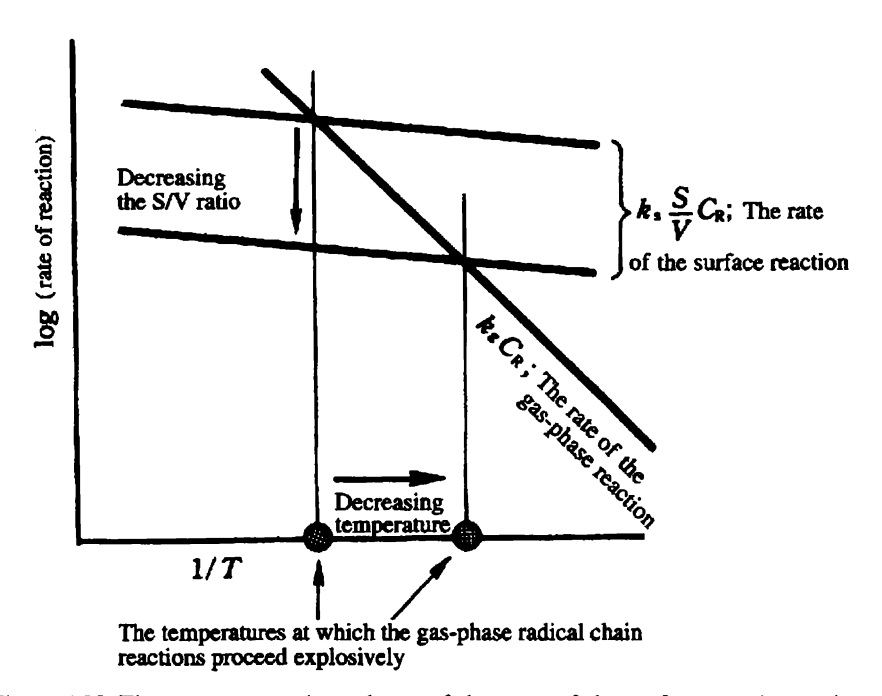


Figure 4.22 The temperature dependency of the rates of the surface reaction and gasphase reactions.

governed by radical chain reactions. The larger the reactor size, i.e. the smaller the S/V ratio, the more homogeneous reactions become dominant, so reactions proceed even at a low temperature.

Accordingly, it should be given consideration to design reactors so that heterogeneous reactions on the reactor wall are not always negligible, even for homogeneous reactions.

Table 4.3 Relation between the initiation temperature and inner diameter of the reaction tube for a Chemical Vapour Decomposition (CVD) reaction governed by the radical chain reaction.

The circle indicates that WSi_x film deposition occurred in the experimental period. The cross indicates that WSi_x film deposition could not be observed in the experimental period $^{(6),(7)}$.

Inner diameter of the tubular reactor	S/V ratio	Initiation temperature			
		80 °C	100 °C	120°C	140 °C
4.0	1.0	_		×	0
11.0	0.364	_	×	0	_
16.5	0.242	×	0	Ö	_

References

- (1) K. Hashimoto, Hannou-Kogaku (Chemical Reaction Engineering). Baifukan (1983).
- (2) T. Otake, Kagaku-Kogaku part 3 (Chemical Engineering, Part 3). Iwanami Syoten (1983).
- (3) T. Saito, Y. Shimogaki, Y. Egashira, H. Komiyama, K. Sugawara, K. Takahiro, S. Nagata and S. Yamaguchi, *Proceedings of Advanced Metallization for ULSI Applications in 1994*, pp. 415 (1995).
- (4) R. C. Reid, J. M. Prausnitz, T. K. Sherwood, *Properties of Gases and Liquids*, McGraw-Hill Book Company (1977).
- (5) Y. Shimogaki, H. Komiyama, *Chemical Engineering* (in Japanese), Vol. 40, 445 (1995).
- (6) T. Saito, Y. Shimogaki, Y. Egashira, H. Komiyama, Y. Yuyama, K. Sugawara, S. Nagata, K. Takahiro and S. Yamaguchi, *Appl. Phys. Lett.*, **62**, 1606 (1993).
- (7) T. Saito, Y. Yuyama, Y. Egashira, Y. Shimogaki, K. Sugawara, H. Komiyama, S. Nagata, K. Takahiro and S. Yamaguchi, *Jpn J. Appl. Phys.*, 33, 275 (1994).

CHAPTER 4.3

Planning and Design of Multiphase Reactors

MASAYUKI HORIO

Department of Chemical Engineering, Tokyo University of Agriculture and Technology, Japan

4.3.1 FEATURES OF PLANNING AND DESIGN OF MULTIPHASE REACTION PROCESSES

4.3.1.1 Multiphase Reaction Processes and Chemical Engineering

Multiphase reaction processes are mostly involved in complex industrial networks chained by a variety of materials, products and byproducts and impose various loads on the environment. Multiphase processes are also complex systems subject to non-linear and multibody problems. Accordingly, the design of such processes cannot remain the routine task of repeatedly applying the existing methods established by our predecessors. We have already viewed various multiphase reactors in Section 4.1.2. Their variety has not been developed unintentionally but has been created from natural requirements and social needs.

As a new methodology, Chemical Engineering, which includes multiphase reaction engineering as a significant part of it, made its debut together with the petrochemical industry right after World War II and has become widely accepted in many industrial fields. As a matter of course, applications of multiphase reaction engineering which were initially intended for petrochemical processes have diversified rapidly into electronics, metal, ceramics, bio, energy and environmental processes in the last few decades. Octave Levenspiel⁽¹⁾, the author of the insightful textbooks 'Chemical Reaction Engineering' and 'Chemical Reactor Omnibook', used the words 'The Chemical Engineers' Grand Adventure', at the end of his Dankwerts Commemorative Lecture in 1989, to express the feeling of that time.

Chemical engineers' delight exists in planning and conducting big projects which involve the development of complex systems through smart approximations in situations where phenomena of different levels of scale and issues of

different disciplines coexist in relation to chemical reactions, fluid flows, configuration of process systems and various social demands. Chemical reaction engineering should provide unique and sophisticated strategies to produce new processes which meet the needs of society and which solve complicated problems created by the conflict between human desires and nature.

4.3.1.2 Reasons for Adopting Multiphase Reactors

Irrespective of the heterogeneity of a system, the type of reactor should be determined by taking into account the reaction rate, degrees of exothermic or endothermic heat of reaction, reaction temperature and pressure, side reactions and strictness of control of the reaction temperature, etc. At present, we consider the factors involved in both homogeneous and multiphase systems as the 'common factors' in reactor planning.

There are two situations where adoption of a multiphase reaction process is unavoidable:

- (1) in the case where phase difference occurs among reactants, impurities in feed, heterogeneous catalysts and micro-organisms, and
- (2) in the case where phase difference occurs amongst products and byproducts.

Let us see some examples of these cases:

(1) The multiphase nature of reactants including impurities in feed, heterogeneous catalysts and micro-organisms is seen in: (a) gas-solid or liquid-solid reactions; (b) gas-liquid reactions; (c) reactions between immiscible liquids; (d) solid-solid reactions; and (e) gas or liquid reactions with immobilized catalysts, immobilized enzymes or micro-organisms.

In any case, selection of a contact scheme for phases involved in the system is crucial in order to achieve efficient operation. In processes involving solids, it is common that reactants are either intentionally ground for easy transport and good contact with other phases or granulated to avoid uncontrolled cohesion and agglomeration in further processing. In gas-liquid and liquid-liquid systems, if phase separation occurs, the interface between phases is enlarged by dispersing one phase into another phase in the form of bubbles (e.g. stirred tanks, bubble columns or three-phase fluidized beds) or droplets (e.g. stirred tanks, liquid-jet columns or spray columns) or by packing solids to form a liquid film on their surfaces (e.g. irrigated packed columns). Once the contact scheme has been selected, the method of introducing each feed into the reactor, the flow regime and the phase-coexisting condition in the reactor, (i.e. which phase disperses into which phase), are determined in conjunction with the common factors mentioned above (i.e. rapidness of reaction rates, types of side reactions, extent of strictness of the reaction temperature control and maintenance conditions of catalysts or micro-organisms).

(2) The multiphase nature of products and byproducts is seen in: (a) reactions forming gases or solids from liquids; (b) reactions forming liquids or solids from gases; and (c) reactions forming gases or liquids from solids.

In these cases, the morphology control of products (i.e. particulates or films) is quite important. Depending on the product properties, planning should be done to permit easy separation for the postprocess and easy handling of materials after separation. When deposition of a solid or liquid phase is probable, it should be minimized so as not to occur on the reactor wall or conduit wall, regardless of whether the depositing phase is the intended product or an unnecessary byproduct. Even if the depositing phase is a liquid, it can be quite harmful because the deposits may solidify and other solid particles may then be bound further to the deposits causing plugging of the reactor.

Here, let us briefly examine the fundamental feature of each phase in a multiphase system. Out of the three phases, the gas and liquid phases are called fluids. The fluid is defined as 'a continuum in which the normal stress is pressure (i.e. not tension) and the tangential stress does not exist in a stationary state'⁽²⁾. By this definition, 'gases and liquids' can be distinguished from solids. This is because in solid phases the normal stress may turn into tension, and the tangential stress may remain even in a stationary state. This also applies to unfluidized powder beds.

In the meantime, the distinction between gas and 'liquid or solid' is based on the fact that the latter two are condensed phases. For a gas, the mean free path of the molecules is about one hundred times the diameter of the molecules, while the mean free path of the molecules in a liquid is about the same as the diameter of the molecules, since it is a condensed phase. Naturally, there are significant volume changes in a gas caused by pressure changes, but the corresponding volume changes are minor in condensed phases.

It has been the role of 'fluid mechanics' to describe the behaviour of gases and liquids in multiphase reactors. Nevertheless, fluid mechanics has not been given a decent position in chemical engineering and chemical reaction engineering. This may be because the complete fluid mechanic description of multiphase systems is not yet established since most of their flow is turbulent. So far, studies have focused on macroscopic equations and correlations for flow regimes of multiphase systems, transition conditions and transport properties, which are only sufficient for the basic design of ordinary multiphase reactors. However, if the pressure, temperature and substances in a reactor to be constructed are beyond our previous experience, the reliability of the data obtained from empirical methods and approximate solutions is limited. In almost all cases, experimental tests are still essential.

Rapid developments in computer fluid mechanics and computer graphics are now heralding a big change in this situation. It must be noted that most of the existing numerical fluid simulation codes are still limited to single-phase

systems or very dilute suspensions. Many of the existing codes for multiphase systems are still quite weak at handling the interactions between dispersed solids and between the dispersed phase and the continuous phase. Nevertheless, it is expected that direct simulation will increasingly exert its power in reactor development as a tool to examine the conditions not covered by available correlations or sections with a large temperature gradient, and to determine the reactor shape, particularly the entrance and exit designs. However, it is important for a reactor designer not to place too much confidence in computations, but to try to find some experimental evidence to the computed results, and also to take part in modelling and coding for modifications and improvements.

The countless factors involved in the planning and design of a multiphase reactor make it possible to be very creative. In other words, if we develop our own scenario for things such as flow, heat transfer and reactions, the cost and risk of development and construction for a given scenario can be reduced substantially. This enables us to realize competitive processes through innovation of the reaction mode or the reactor type (Section 4.3.4). To come up with such a scenario, knowledge of the phenomenological versatility of multiphase systems themselves (Section 4.3.3.1) and on alternatives in the configuration of reacting systems (4.3.3.2) is necessary. Of course, the power of mathematical analysis is essential. So, let us first set up mathematical tools as our common language.

4.3.2 MODEL DESCRIPTION OF MULTIPHASE PROCESSES

4.3.2.1 Governing Equations for State Variables of Each Phase

Mathematical expressions for multiphase systems are basically given by combining those for homogeneous systems. Depending on the flow and mixing conditions of the respective phases, we have continuous and batch systems and systems of complete mixing, incomplete mixing and plug flow (or non-mixing).

Here let ε_i represent the local volume fraction of phase i in a rector, a_{ij} the specific surface area of the interface between phases i and j, X_{im} the capacity per unit volume (specific capacity) of the m-th quantity Q_m subject to a conservation law (i.e. mass of material, number of particles or enthalpy), u_i the velocity vector of phase i, $k_{ij}a_{ij}$ ($X_{ijm,eq} - X_{jm}$) the exchange rate of Q_m with other phases per unit reactor volume, $X_{im,eq}$ the equilibrium composition on the phase i side of the interface ij, R_{im} the generation rate of Q_m per unit volume by reaction, and E_{ii} the eddy diffusivity in the x_l -direction. k_{ij} is the mass transfer coefficient based on the concentration on the phase i side of the interface ij, and $k_{ij}a_{ij}$ may generically be called the capacity coefficient. Then the equations of conservation of mass or heat for an infinitesimally small section of phase i shown in Figure 4.23 can be written as follows:

$$\frac{\partial \varepsilon_{i} X_{im}}{\partial t} + u_{i} \operatorname{grad}(\varepsilon_{i} X_{im}) = \frac{\partial}{\partial x_{i}} \left(E_{ii} \varepsilon_{i} \frac{\partial X_{im}}{\partial x_{i}} \right)$$
Accumulation Convection Diffusion term
$$+ \Sigma_{j} k_{ij} a_{ij} (X_{ijm, eq} - X_{im}) + R_{im} \varepsilon_{i}$$
Exchange term Reaction rate

where the diffusion term is the sum of those in each direction of x_1 , x_2 and x_3 . Specifically, X_{im} is substituted with the concentration C_{im} of component M_m or with the enthalpy per unit volume of phase $i, \rho_i c_i T_i$ (c_i : mean specific heat of phase i, T_i : temperature and ρ_i : density).

If the eddy diffusivity E_i is sufficiently large as in the case of a well mixed stirred tank, we can assume complete mixing. Then, expressing the reactor volume as V, and the flow rates of phase i into and out of the reactor as F_{i0} and F_i , respectively, leads to

$$V\frac{\mathrm{d}\varepsilon_{i}X_{im}}{\mathrm{d}t} + F_{i}X_{im} - F_{i0}X_{im0} = \Sigma_{j}k_{m,ij}a_{ij}V(X_{ijm,eq} - X_{im}) + R_{im}\varepsilon_{i}V \qquad (4.59)$$
Accumulation Convection terms Exchange term Reaction rate

where X_{im0} denotes the value at the inlet, and X_{im} is either the concentration of chemical species M_m or the enthalpy in the reactor. When $X_{im} = C_{im}, k_{ij}$ should be $k_{f,ij}$ (mass transfer coefficient with respect to phase i) and when $X_{im} = \rho_i c_i T_i, k_{ij}$ should be $h_{ij}/\rho_i c_i$ (h_{ij} : heat transfer coefficient between phases i and j), the enthalpy corresponding to temperature T_j of phase j is substituted for $X_{iim,eq}$. That is,

(1) For the material balance of component $M_{m'}$

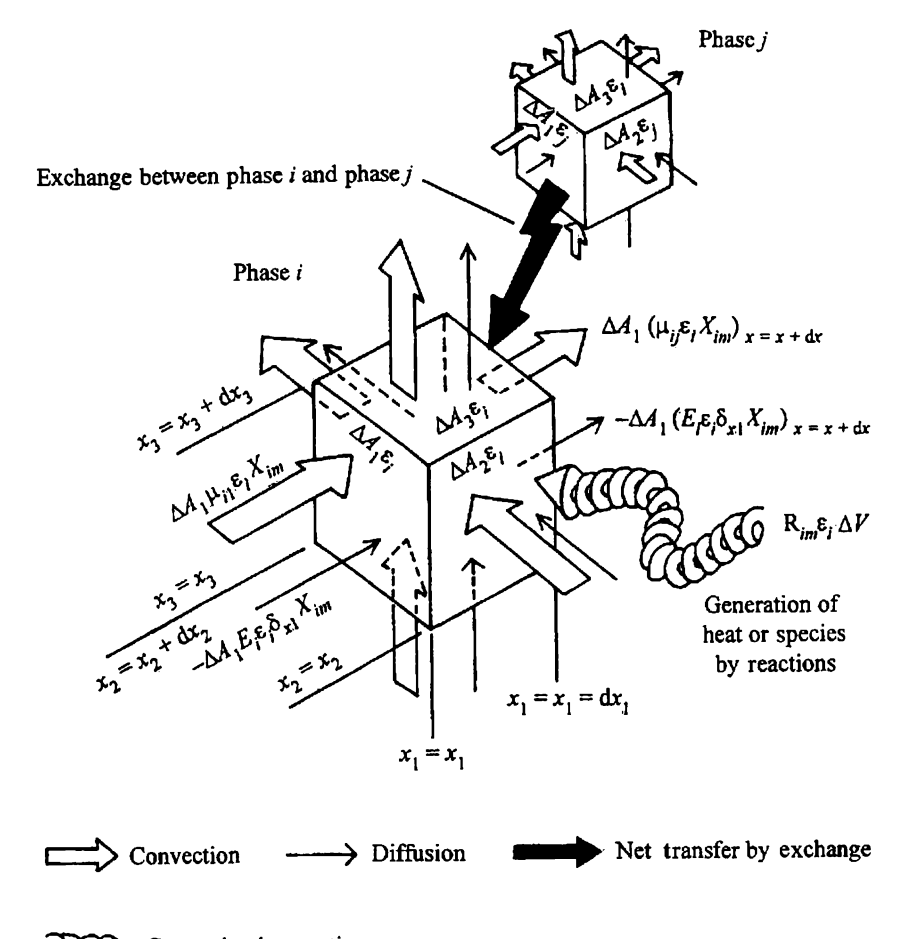
$$X_{im} = C_{im'}, k_{m,ij} = k_{f,ij,m'}, X_{ijm,eq} = C_{ijm',eq}$$

(2) For the heat balance

$$X_{im} = \rho_i c_i T_i, k_{m,ij} = h_{ij} l \rho_i c_i, X_{ijm,eq} = \rho_i c_i T_j$$

Almost all multiphase systems can be described by Eq. (4.58) or Eq. (4.59). However, in dispersed phases such as particulate phases, the mixing of particles, droplets or bubbles does not immediately mean mixing at the molecular level. In such cases a population balance must be made as described in Section 4.3.2.2.

Once the conservation equations are written for all phases and all the process variables we are concerned with, including population balances, it can be said that the multiphase system is completely expressed in a mathematical sense. Of course, along with these expressions, it is necessary to estimate all the process



Generation by reactions

Figure 4.23 Mass and heat balances for an infinitesimally small section to derive governing equations for a multiphase process.

parameters, i.e., area occupied by phase i A_i , flow rate F_i , diffusivity E_i , specific surface area at phase ij, interface mass or heat transfer parameter k_{ij} and reaction rate R_{im} . Note that the first five variables are all related to the flow regime and turbulence. This indicates that in the case of multiphase reactors we have to put a heavier focus on the fluid mechanical factors than in the case of homogeneous reactors.

Let us further consider this point by taking a first-order irreversible reaction as an example. Suppose that X_i is the reactant concentration C, and Eqs (4.58) and (4.59) are applied to a homogeneous system in a steady state. Since we can assume $\varepsilon_1 = 1$, the exchange term = 0 and the reaction rate term $R_1 = -kC$ (k:

reaction rate constant), we obtain Eqs. (4.60) and (4.61) as the governing equations for a plug flow reactor (PFR: $E_1 = 0$) and a continuous stirred tank reactor (CSTR), respectively.

$$u\frac{dC}{dx} = -kC \text{ (at } x = 0 - L \text{ and } x = 0, C = C_0) \text{ (PFR)}$$
 (4.60)

$$F(C - C_0) = -kVC (C_0 : inlet concentration) (CSTR)$$
 (4.61)

The conversion η for each reactor can be expressed as a function of mean residence time $\bar{t} = V/F = L/u$, as follows:

$$\eta_{\rm PFR} = 1 - \exp(-k\bar{t}) \tag{4.62}$$

$$\eta_{\text{CSTR}} = \frac{k\bar{t}}{1 + k\bar{t}} \tag{4.63}$$

In homogeneous systems, the conversion for the case of incomplete mixing lies in between the above two conversions. For example, let us consider the case where a reactor has two regions: the complete mixing region in which fraction q' of the total flow rate flows, and the plug flow region in which the remaining 1-q' of the total flow rate flows. Expressing the residence times in these regions with t_{CSTR} and t_{PFR} , respectively, the conversion η can be written as

$$\eta = \frac{qk\bar{t}_{\text{CSTR}}}{1 + k\bar{t}_{\text{CSTR}}} + (1 - q)(1 - \exp(-k\bar{t}_{\text{PFR}}))$$
 (4.64)

However, such a simple addition rule does not hold for heterogeneous reactors because the phase contacting modes vary in different regions. As an example, consider a catalytic reaction system shown in Figure 4.24.

In this case, the reaction proceeds in the completely mixed region (phase 2) where catalyst particles are dispersed, whereas the whole gas flows through the plug flow region (phase 1) where there is no catalyst. This corresponds to the bubbling fluidized bed reactor described later. Accordingly, reactants are supplied to the reacting region only via gas exchange with the plug flow region. The governing equations of the system are as follows:

$$F\frac{\mathrm{d}C_1}{\mathrm{d}x} = k_{12}a_{12}A_1(C_2 - C_1) \tag{4.65}$$

$$k_{12}a_{12}(\langle C_1 \rangle - C_2) = kC_2 \tag{4.66}$$

where F is the total flow rate, A_t is the cross-sectional area of the reactor, and $\langle C_1 \rangle$ is the mean value of C_1 in the plug flow region. Integration of Eq. (4.65) under the condition of $C_1 = C_0$ at x = 0 gives

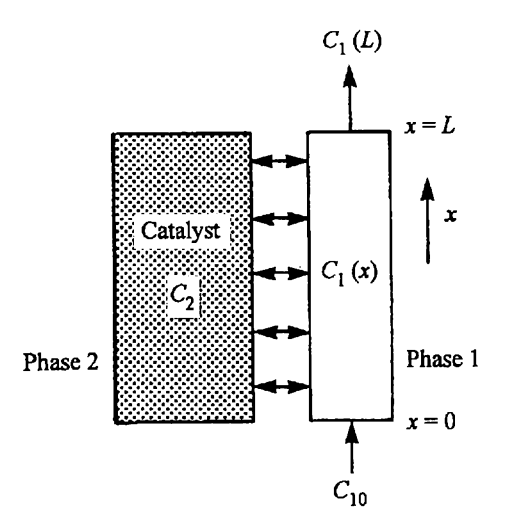


Figure 4.24 A catalytic reaction system with a completely mixed region with catalyst (phase 2) and a plug flow region without (phase 1).

$$C_1 = C_0 \exp(-N_{12}x/L) + C_2(1 - \exp(-N_{12}x/L)) \tag{4.67}$$

Integrate the above equation for x = 0 to L to obtain the mean value (C_1) . Then, substitute it into Eq. (4.66) to determine C_2 . Finally, the following expression can be obtained:

$$\frac{C_2}{C_0} = \frac{1}{N_R + 1 - \exp(-N_{12})} \tag{4.68}$$

where N_{12} and N_R are defined as

$$N_{12} = k_{12}a_{12} V/F = k_{12}a_{12}\bar{t} (4.69)$$

$$N_{\rm R} = kV/F = k\bar{t} \tag{4.70}$$

 N_{12} is the number of transfer unit obtained by dividing the bed height L by H.T.U., the height of the transfer unit $u/k_{12}a_{12}$. Similarly, N_R is the number of reaction units, which is also called the Damköhler number.

Thus, the conversion at the reactor exit is given by

$$\eta = \frac{(1 - \exp(-N_{12}))(N_{R} - \exp(-N_{12}))}{N_{R} + 1 - \exp(-N_{12})}$$
(4.71)

The above expression indicates that η converges to η_{CSTR} when the gas exchange unit N_{12} becomes infinite. The relation between the conversion and the number of reaction units N_R for various cases is shown in Figure 4.25. A

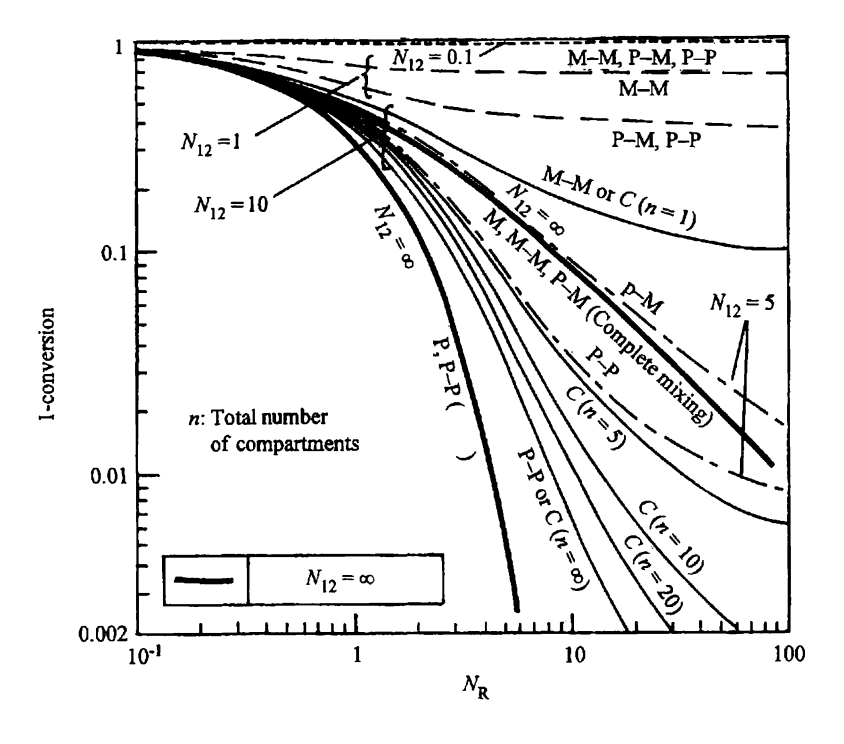
significant point drawn from this figure is that, in regions with high conversions (i.e. economically important regions), there turns out to be several orders of magnitude of difference in the values of the number of the reaction unit (i.e. the reactor volume) required to realize a given conversion depending on the mixing condition or contacting mode. For example, for $\eta = 0.99$, we have $(kt)_{PFR} = \ln 100 = 4.6$ for plug flow and $(kt)_{CFTR} = 99$ for complete mixing. Since the reaction rate constant should be identical, a CSTR requires a residence time 21.5 times as large as that of a PFR.

Now it is easily understood that the residence time required for a non-ideal reactor would be a value in between those for the PFR and CSTR or even longer than the one for the CSTR. Accordingly, chances are that a designer faces a critical failure if he is blind to this aspect. This illustrates the importance of chemical engineers and chemical reactor engineering. In addition, the mixing conditions and contacting modes are far more important with complex reaction systems than those in the so far discussed first-order irreversible reaction systems.

4.3.2.2 Dispersed Phase Modelling and Population Balance

Elements of the dispersed phase such as particles, bubbles and droplets, which are hereafter represented as 'particles' in the broad sense, are independent of each other, and accordingly, they are not easily mixed up at the molecular level. For this reason, the microscopic distribution of state variables exists in a local space of the dispersed phase. Similar to stochastic mechanics and molecular dynamics in molecular systems there are two methods of handling such a case: (i) the number balance or population balance method that expresses the distribution of particle properties in the form of a probability distribution by handling particles as a sufficiently large set for stochastic treatment; and (ii) the discrete element method that tracks the behaviour of individual particles. The discrete element method can also be combined with the Monte Carlo Method. where variations of particle properties at the time of formation and the directions of particle motion may be treated stochastically using random numbers. Of course, the discrete element method requires larger computer capacity due to the increased number of elements. In the following, we briefly, but rigorously, introduce the population balance method as a typical macroscopic expression for complex systems, but readers who are not interested in the derivation may skip the mathematics.

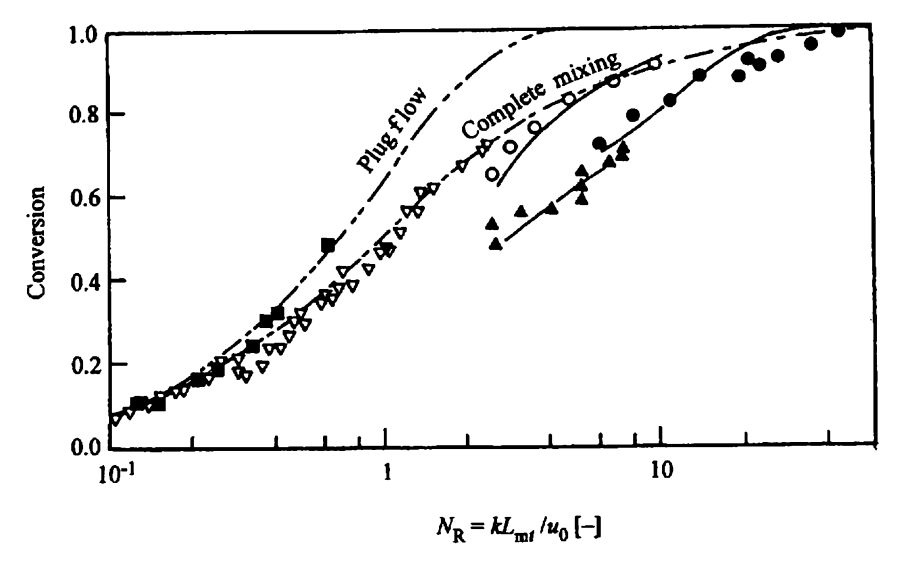
First, assume that the particles have n_p kinds of properties such as particle size, density, composition and shape. Let us call these properties the state variables of the particle phase. These state variables are expressed by a vector Y_p . Because Y_p has n_p kinds of elements, Y_p is an n_p -dimensional vector. The k-th element of Y_p is written as Y_{pk} . The infinitesimally small section of the state variables Y_{p1} to $Y_{p1} + dY_{p1}$, Y_{p2} to $Y_{p2} + dY_{p2}$, and Y_{pn_p} to $Y_{pn_p} + dY_{pn_p}$ is simply



Symbol	Description	1-conversion
P	Bubble free plug flow model	$\exp(-N_{\mathbf{R}})$
M	Bubble free complete mixing model	$1/(1+N_{\rm R})$
P-P	Two-phase plug flow model)*	$\exp\left(-\frac{N_{\rm R}}{N_{12}+N_{\rm R}}\right)$
Р-М	Two-phase model (plug flow in bubble phase and complete mixing in emulsion phase)*	$\frac{1 + N_{\rm R}e^{-N_{12}} - e^{-2N_{12}}}{1 + N_{\rm R} - e^{-N_{12}}}$
М-М	Two-phase complete mixing model*	$\frac{N_{\rm g}+N_{12}}{N_{\rm R}+N_{12}+N_{\rm g}N_{12}}$
С	Two-phase compartment model*	$\left[\frac{(N_{12}/N_{\rm R})+1}{(1+N_{\rm R}/n)(N_{12}/N_{\rm R})+1}\right]^n$

^{*}gas flow in emulsion phase is assumed negligible.

Figure 4.25 Relation between the conversion and number of reaction units N_R for various cases. (a) Conversions from various models⁽³⁾.



- ▲ Cooke et al. (1968)
- Shen and Johnstone (1965)
- ▼ Massimilla and Johnstone (1961)
- Lewis et al. (1959)
- O Kobayashi et al. (1969)
- Ogasawara et al. (1959)
- calculated from B.A. Model

(b)

Figure 4.25 (cont.) Relation between the conversion and number of reaction units N_R for various cases. (b) Comparison of observed conversion with calculated conversion based on plug-flow, complete mixing and bubble assemblage models.

expressed as $dV_{\gamma p} = dY_{p1} dY_{p2} \dots dY_{pn_p}$. Note that $dV_{\gamma p}$ is the infinitesimally small volume of the state space but not of the actual space dV. Using $dV_{\gamma p}$ we can define the probability density function ϕ (Y_p, x, t) as follows, in which $x = (x_1, x_2, x_3)$ is a position in the actual space and t is time:

Number of particles whose state is included in the infinitesimally small state space $\mathrm{d}V_{\mathrm{Yp}}$ out of those particles which are within the volume $\mathrm{d}V$ at a certain moment $= \phi(Y_{\mathrm{p}}, x, t) \mathrm{d}V_{\mathrm{Yp}} \rho_{\mathrm{bN}} \mathrm{d}V$

where ρ_{bN} is the number density of particles, i.e. the number of particles in the unit volume, and $dV = dx_1 dx_2 dx_3$ for three-dimensional models. If the flow is unidirectional and the distribution of state variables in the cross-section of area A_i is negligible, then $dV = A_i dx$.

Since ϕ is the probability density function, the value integrated over the entire space of state variables V_{Yp} must be 1. That is,

$$\int_{VY_p} \phi(Y_p, x, t) dV_{Y_p} = 1 \text{ (normalization condition)}$$
 (4.73)

In addition, the number flux of particles [number/ m^2 s] is expressed by the symbol n.

The population balance is now made as illustrated in Figure 4.26 in accordance with the above-mentioned notation. For 'those particles existing in the infinitesimally small section dV in the actual space having their properties in $dV_{\gamma p}$, which are hereafter abbreviated as 'such particles', the following number balance or population balance expression can be written:

- (1) [Changes in the number of such particles with time]
 - = (2) [Number of such particles 'flowing in and out' entrained by continuous phase flow]
 - +(3) [Number of such particles 'flowing in and out' by diffusion]
 - + (4) [Number of such particles 'coming in and out' by direct feed (f), discharge (d), coalescence (c) and splitting (s)]
 - + (5) [Number of such particles 'coming in and out' due to changes in the properties or state of individual particles with time]

(4.74)

where the number of particles flowing (or coming) out is expressed with the negative sign and the number of those particles 'flowing (or coming) in and out' is determined by taking the difference between them.

In the above expression terms (1)–(5) can be written as below, in which, a small change in vector variable (x_1, x_2, x_3) to $(x_1 + dx_1, x_2, x_3)$ is expressed simply as x to $x + dx_1$. The partial differential operator with respect to time $(\partial/\partial t)$ is abbreviated as ∂_t , and the one with respect to x_i is as ∂x_i . Furthermore, in the following (2), (3) and (5), Σ indicates the sum over i = 1 to 3. x_i and $x_{i'}$ are the two coordinates orthogonal to x_i .

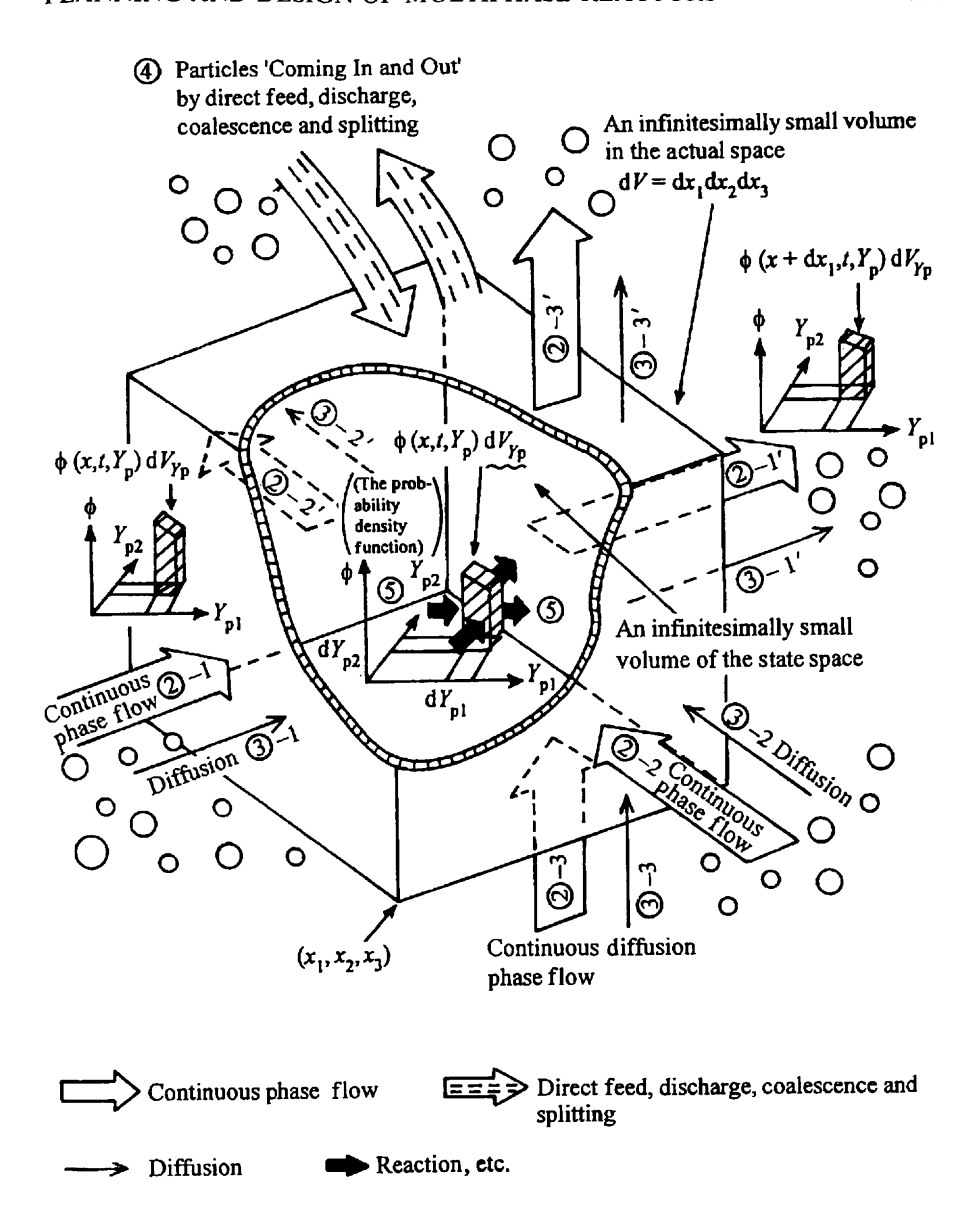


Figure 4.26 Population balance for particles existing in the infinitesimally small volume dV in the actual space having their properties in the small section dV_{γ_p} in the state space (cf. Eq. (4.74)).

$$(1) = \partial_t [\phi(Y_p, x, t) \rho_{bN}(x, t)] dV_{Yp} dV dt$$

$$(2) = \sum [n_i(x,t) dx_j dx_j \phi(Y_p,x,t) dV_{Yp} - n_i(x+dx_i,t) dx_j dx_j \phi(Y_p,x+dx_i,t) dV_{Yp}] dt$$

$$(3) = \sum [-E_{N}(Y_{p}, x, t)\partial_{xi}\{\rho_{bN}(x, t)\phi(Y_{p}, x, t)\}dx_{j}dx_{j'}dV_{Y_{p}} + E_{N}(Y_{p}, x + dx_{i}, t)\partial_{xi}\{\rho_{bN}(x + dx_{i}, t)\phi(Y_{p}, x + dx_{i}, t)\} dx_{j'}dx_{j'}dV_{Y_{p}}]dt$$

where $E_{\rm N}$ is the particle diffusivity defined with the number concentration.

$$(4) = n_{f/d/c/s}(x,t)\phi_{f/d/c/s}(Y_p,x,t)dVdV_{Yp}dt$$

where the subscripts f, d, c and s correspond to the direct *feed* to place dV, direct *discharge* from dV, and *coalescence* and *splitting* in dV, respectively, with the implication of taking the sum of all of them.

$$(5) = \sum \rho_{bN}(x,t) [r_k^*(Y_p, x,t) \ \phi(Y_p, x,t) - r_k^*(Y_p + dY_{pk}, x,t) \phi(Y_p + dY_{pk}, x,t)] \ dt dV dV_{Yp} / dY_{pk}$$

Substitution of the above expressions into the balance (4.74) gives the following governing equation:

$$\partial_t(\phi \rho_{\rm bN}) + \operatorname{div}(n\phi) = \nabla E_{\rm N} \nabla (\rho_{\rm bN} \phi) + n_{\rm f/d/c/s} \phi_{\rm f/d/c/s} - \rho_{\rm bN} \operatorname{div}_{\rm p}(r^*\phi) \tag{4.75}$$

where ∂_t is the abbreviation of $(\partial/\partial t)$ as noted above, div is the divergence (i.e. sum of partial derivatives) in the directions (x_1, x_2, x_3) , and div_p is the divergence in the state space. In addition, E_N is the diagonal matrix of particle diffusivities in the x_1 , x_2 and x_3 directions and r^* is the rate of change in the state vector Y_p when individual particles are tracked (indicated by *), defined as

$$r^* = \partial_t (Y_p)^* \tag{4.76}$$

If all particles are uniformly entrained by the flow with no segregation, i.e. no separation between large and small or heavy and light particles, the number flux n_i of particles in the x_1 direction in (ii) may be replaced by $u_i \rho_{bN}$. Furthermore, if the particle diffusivity is assumed to be isotropic, the governing equation becomes as simple as follows:

$$\partial_t(\phi \rho_{bN}) + \operatorname{div}(u \rho_{bN} \phi) = E_N \nabla^2(\rho_{bN} \phi) + n_{f/d/c/s} \phi_{f/d/c/s} - \rho_{bN} \operatorname{div}_p(r^* \phi) \quad (4.77)$$

For a completely mixed cell where the distribution function ϕ should be same everywhere and

$$V\frac{\mathrm{d}(\phi\rho_{\mathrm{bN}})}{\mathrm{d}t} + n_{\mathrm{d}}\phi = n_{\mathrm{f/c/s}}\phi_{\mathrm{f/c/s}} - V\rho_{\mathrm{bN}}\,\mathrm{div}_{\mathrm{p}}(r^*\phi) \tag{4.78}$$

Combined with the normalization condition of Eq. (4.73), it can be confirmed theoretically that the population balance equation completely satisfies the material balance.

Now, let us consider a simple example. Assume a steady state of particles where there is no splitting or aggregation but a single reaction that accompanies particle size reduction. For simplicity, let us take only one state variable for the particle, i.e. let $Y_p =$ particle size, and for the feed, $Y_p = Y_{p \text{ max}}$, i.e. the maximum value of Y_p . Suppose particles are completely consumed by the reaction, they do not have to be discharged. Accordingly, $n_d = 0$. Then the governing equations and boundary conditions are reduced to

$$V\rho_{bN}\frac{dr^*\phi}{dY_p} = n_f\phi_f - n_d\phi \tag{4.79}$$

$$\phi(Y_{\text{p min}} - 0) = \phi(Y_{\text{p max}} + 0) = 0 \tag{4.80}$$

$$\phi_{\rm f} = \delta(Y_{\rm p} - Y_{\rm p \, max}) \tag{4.81}$$

$$r^* \equiv \frac{\mathrm{d}Y_p}{\mathrm{d}t} = -kC$$
 (C: reactant concentration in gas phase) (4.82)

 $k = k_s$ (reaction rate control), $k = D/Y_p$ (mass transfer control)

When the reaction rate is controlled by chemical reaction, $k = k_s$, and when it is by mass transfer, $k = k_f = D/Y_p$ (if $Sh = k_f Y_p/D = 2$), where k is the apparent reaction rate constant, k_s is the chemical reaction rate constant, D is the diffusivity, and δ is Dirac's δ -function having the following properties:

$$\int_{-\infty}^{+\infty} \delta(Y) dY = 1$$

$$\delta(0) = \infty, \ \delta(Y \neq 0) = 0$$
(4.83)

Equation (4.79) can be expressed for the chemical reaction rate control case (CRC) and mass transfer control case (MTC) as follows:

$$\frac{\mathrm{d}\phi}{\mathrm{d}Y_{\mathrm{p}}} + \frac{n_{\mathrm{d}}}{V\rho_{\mathrm{bN}}k_{\mathrm{s}}C}\phi = \frac{n_{\mathrm{f}}}{V\rho_{\mathrm{bN}}DC}\phi_{\mathrm{f}} \tag{CRC}$$

$$\frac{\mathrm{d}(\phi/Y_{\mathrm{p}})}{\mathrm{d}Y_{\mathrm{p}}} + \frac{n_{_{d}}Y_{\mathrm{p}}}{V\rho_{\mathrm{bN}}DC} \left(\frac{\phi}{Y_{\mathrm{p}}}\right) = \frac{n_{\mathrm{f}}}{V\rho_{\mathrm{bN}}DC} \phi_{\mathrm{f}} \tag{MTC}$$

In accordance with the solution of the linear first-order ordinary differential equation, integrating the coefficient of the second term on the left hand side of the above equations, multiplying both sides by the exponential function of it,

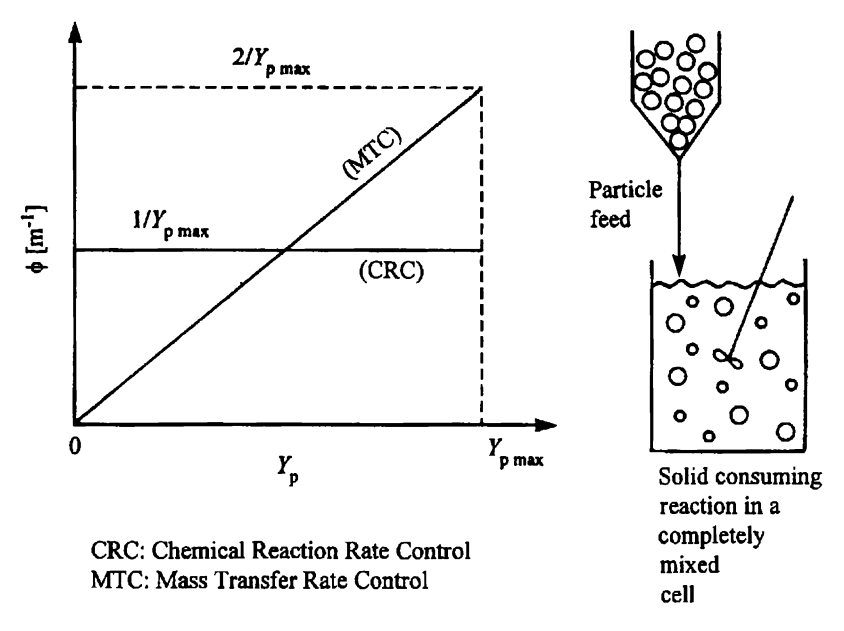


Figure 4.27 Particle size distribution density function ϕ for a solid consuming reaction in a completely mixed cell.

performing definite integration over the range between Y_p and $Y_{p max} + 0$ and taking into account Eq. (4.83), we finally obtain ϕ and ρ_{bN} as

$$\phi = 1/Y_{\text{p max}} \quad \text{(CRC)} \tag{4.85a}$$

$$\phi = 2Y_{\rm p}/Y_{\rm p \ max}^2$$
 (MTC) (4.85b)

$$\rho_{\rm bN} = n_{\rm f} Y_{\rm p max} / V k_{\rm s} C \quad (CRC) \tag{4.86a}$$

$$\rho_{\rm bN} = n_{\rm f} Y_{\rm p max}^2 / 2VDC \quad (MTC) \tag{4.86b}$$

The above solutions for the particle size distribution density function ϕ are shown in Figure 4.27.

As demonstrated above, the solution of the population balance expression can be obtained quite easily. In this example, the shape of the particle size distribution changes largely due to controlling mechanisms. Roughly speaking, if we neglect the size or conversion distribution, we may overestimate or underestimate the reactor size by up to 30%.

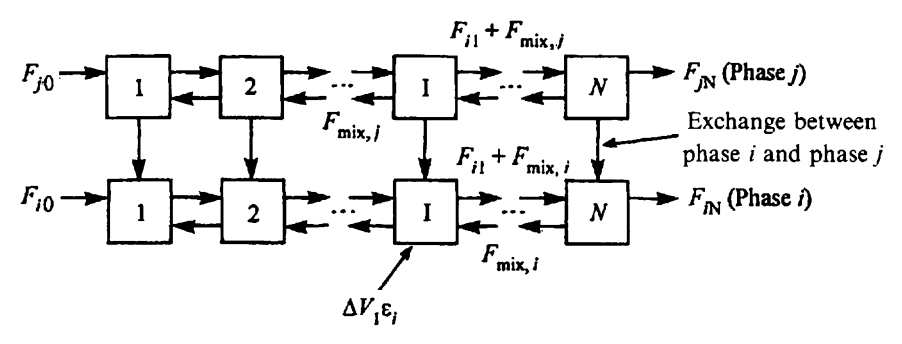


Figure 4.28 Tanks in series model with back mixing.

4.3.2.3 Relationship between the Multi-stage Cell model and the Continuous model

For the multi-stage stirred tank reactor, the tanks in series model with complete mixing cells can be written as shown in Figure 4.28. From material balance for Cell I of volume $\Delta V_{\rm I}$ with backmixing between adjacent cells (flow rate: $F_{\rm mix}$), the 'tanks in series model with backmixing' can be derived as follows:

$$\Delta V_{\rm I} \left(\frac{\mathrm{d}\varepsilon_{i1} X_{im1}}{\mathrm{d}t} \right) + (F_{i1} X_{im1} - F_{i1-1} X_{im1-1})^{*}$$

$$= F_{\mathrm{mix},i} (X_{im1-1} - 2X_{im1} + X_{im1+1})^{**} + \Delta V_{\rm I} [\Sigma_{i} k_{ii1} a_{ii1} (X_{iim.eq1} - X_{im1}) + \varepsilon_{i1} R_{im1}]$$
(4.87)

Where, X_{iml} is the specific capacity of component m in phase i in Cell I (similar to Section 4.3.2.1), ε_{i1} is the volume fraction of phase i in Cell I and F_{i1} is the volume flow rate in phase i from Cell I to Cell I+1. Therefore, the convection term marked with * is effective only when F_i is positive. If F_i is negative, process variables of Cell I must be accompanied by the real outgoing flow as $(F_{i1-1}X_{im1} - F_{i1-1}X_{im1})$ instead of $(F_{i1}X_{im1} - F_{i1-1}X_{im1-1})$. This is the so called upwind method. For three-dimensional network systems, the terms marked with * and ** represent the sum in all x_1 , x_2 and x_3 directions.

Now, even a continuous system expressed by the partial differential equation Eq. (4.58) can be described by the tanks in series model. Between the two models there exists a relationship between model parameters which makes the two models almost identical, i.e. for the backmixing flow rate, the diffusivity E_i and the cell size Δx_1 we have:

$$F_{\min,i} = E_i \varepsilon_{i1} \Delta A_1 / \Delta x_1 \tag{4.88}$$

where ΔA_1 is the cross-sectional area of the side of the cell normal to the x_1 direction.

Now let us see how Eq. (4.88) is derived. First, the difference expression of the diffusion term in Eq. (4.58) can be written as:

$$\frac{\partial}{\partial x_1} \left(E_i \varepsilon_i \frac{\partial X_{im}}{\partial x_1} \right) = E_i \varepsilon_i [(X_{iml+1} - 2X_{iml} + X_{iml-1})/(\Delta x_1)^2]$$
 (4.89)

If we apply Eq. (4.88), we can write $E_i \varepsilon_i / (\Delta x_1)^2 = F_{\text{mix},i} / \Delta V$ since $\Delta x_1 = \Delta V / \Delta A_1$. Then, it is easy to see that the above expression corresponds to the result obtained by dividing the backmixing term in Eq. (4.87) by $\Delta V = \Delta x_1 \Delta x_2 \Delta x_3 = \Delta x_1 \Delta A_1$.

Similar correspondence holds for $F_{\text{mix}, i} = 0$ with no backmixing in Eq. (4.87). In short, to make Eq. (4.58) equivalent to the following multi-stage tanks in series model, Eq. (4.90), the cell size may be determined by Eq. (4.91).

$$\Delta V_{I} \left(\frac{\mathrm{d}\varepsilon_{i1} X_{imI}}{\mathrm{d}t} \right) + (F_{i1} X_{imI} - F_{iI-1} X_{imI-1})^{*}$$

$$= \Delta V_{I} \left[\sum_{i} k_{iiI} a_{iiI} (X_{iim.eq1} - X_{imI}) + \varepsilon_{iI} R_{imI} \right]$$
(4.90)

$$\Delta x_1 = E_i/u_{i1} \text{ (or } N_1 \equiv L_1/\Delta x_1 = 1/Pe_{i1})$$
 (4.91)

where N_1 is the total cell number in direction 1, and $Pe_{i1} \equiv u_{i1}L_1/E_i$ is the Péclet number for diffusion in direction 1 in phase i.

Here, let us quickly see how Eqs (4.90) and (4.91) are derived. Subtracting the convection term on the left hand side of Eq. (4.58) from the diffusion term on the right hand side of Eq. (4.58) we can approximately write the following difference expression:

$$\left[\frac{\partial}{\partial x_{1}} \left(E_{i} \varepsilon_{i} \frac{\partial X_{im}}{\partial x_{1}}\right) - u_{i} \left(\frac{\partial \varepsilon_{i} X_{im}}{\partial x_{1}}\right)\right] \Delta V
= \left[E_{i} \varepsilon_{i} (X_{im1+1} - 2X_{im1} + X_{im1-1}) / (\Delta x_{1})^{2} - u_{i1} \varepsilon_{i} (X_{im1+1} - X_{im1}) / \Delta x_{1}\right] \Delta V$$
(4.92)

Thus, when the condition of Eq. (4.91) is satisfied, the above expression leads to Eq. (4.93) (note $\Delta V = \Delta x_1 \Delta A_1$ and $u_{i1} \Delta A_1 = F_i$), from which Eq. (4.90) can be obtained.

$$\left[\frac{\partial}{\partial x_1} \left(E_i \varepsilon_i \frac{\partial X_{im}}{\partial x_1} \right) - u_i \left(\frac{\partial \varepsilon_i X_{im}}{\partial x_1} \right) \right] \Delta V
= -u_{i1} \varepsilon_i (X_{im1} - X_{im1-1}) \Delta A_1$$
(4.93)

As we have examined, (i) different reactors may exhibit similar performance in spite of their different appearances and (ii) there may be equivalent models in the reactor calculation. It is worth noting here that cell models provide more practically feasible expressions than the difference expressions directly obtained from differential equations. Cell models ensure stable and physically realizable solutions in numerical calculation. For this reason the authors recommend cell models in reactor calculations including non-linear equilibrium relations and rate expressions. Similar cell models can also be derived for population balances.

4.3.2.4 Mechanical and Morphological Variety of Each Phase and Contacting Mode Parameters

For a quantitative description of multiphase reaction systems we need to determine the contacting mode parameters such as volume fraction of phase i, ε_i , specific surface area of the contacting face of interface ij, a_{ij} , mass or heat transfer coefficient, k_{ij} (or volumetric coefficient k_{ij} a_{ij}), the flow allotment rate to each phase, $u_i \varepsilon_i A_i$, and the eddy diffusivity of each phase, E_i . In the following, correlations for model parameters mainly for bubble columns and fluidized beds are introduced just as an example. Readers who need more detailed data, please refer to literature⁽⁵⁾⁻⁽¹⁰⁾.

4.3.2.4.1 Relations between Parameters

The following relations hold between the velocity u_i , total flow rate F_i , volume fraction ε_i of phase i and the reactor cross-sectional area A_i , where F_i/A_i , denoted by u_{0i} is called the superficial velocity of phase i:

$$u_i \varepsilon_i = F_i / A_t \equiv u_{0i} \tag{4.94}$$

$$\therefore \varepsilon_i = u_{0i}/u_i \tag{4.95}$$

In most multiphase systems, ε_i is a parameter dependent on operating conditions and accordingly it is unknown in many cases unless measured. Thus, the superficial velocity u_{0i} is commonly used instead of u_i in correlating contacting modes with fluid mechanical properties.

Expressing the volume equivalent diameter of 'particles' (let us include bubbles and droplets) in phase i as d_i , the particle number density ρ_{bNi} and the specific surface area a_i are written as follows:

$$\rho_{\mathsf{bN}i} = \varepsilon_i / ((\pi/6)d_i^3) \tag{4.96}$$

$$a_i = 6\varepsilon_i/d_i\phi_s \tag{4.97}$$

where ϕ_s is the sphericity defined by (surface area of spheres of the same volume)/(real external surface area of particles).

4.3.2.4.2 Behaviour of an Isolated Particle (Solid Particle, Bubble and Droplet)

For an isolated spherical solid particle, a motion of constant velocity is attained when the drag force acting on the particle, which is the sum of viscous force and inertia force, is proportional to the gravity of the particle and buoyancy (i.e. the integrated pressure acting on the particle surface). The constant velocity is called the terminal velocity u_t . From the force balance, u_t can be obtained as

$$u_{\rm t} = [4gd_{\rm p}(\rho_{\rm p} - \rho_{\rm f})/3\rho_{\rm f}C_{\rm D}]^{1/2}$$
(4.98)

For a spherical solid particle, the drag coefficient $C_D = (Drag force)/(Inertia force)$ is correlated as

$$C_{\rm D} = \begin{cases} 24/Re & \text{(Stokes' law)} & Ar \le 104\\ 10/Re^{0.5} & \text{(Allen's law)} & 104 \le Ar \le 8.78 \times 10^4\\ 0.44 & \text{(Newton's law)} & 8.78 \times 10^4 \le Ar \le 3 \times 10^9 \end{cases}$$
(4.99)

where Ar is the Archimedes number, which is defined as

$$Ar = d_{\rm p}^{3} \rho_{\rm f}(\rho_{\rm p} - \rho_{\rm f}) g / \mu_{\rm f}^{2}$$
 (4.100)

Thus, the terminal velocity of a spherical solid particle becomes

$$u_{t} = \begin{cases} g(\rho_{p} - \rho_{f})d_{p}^{2}/18\mu_{f} & Ar \leq 104 \\ d_{p}[4g^{2}(\rho_{p} - \rho_{f})^{2}/225\mu_{f}]^{1/3} & 104 \leq Ar \leq 8.78 \times 10^{4} \\ [3g((\rho_{p} - \rho_{f})/\rho_{f})]^{1/2} & 8.78 \times 10^{4} \leq Ar \leq 3 \times 10^{9} \end{cases}$$
(4.101)

The rising velocity of an isolated bubble in an infinitely wide space, $u_{b\infty}$, is given by the following expression:

$$u_{b\infty} = \alpha (gD_b)^{1/2} \ (\alpha = 0.5 - 0.7)$$
 (4.102)

where D_b is the volume equivalent diameter of the bubble and g is the gravitational acceleration. The above expression can be confirmed immediately by applying Bernoulli's equation for a streamline on the bubble surface where the pressure is constant, taking into account the zero relative velocity at the top of the bubble and the fact that the velocity at the sides of the bubble is approximately equal to $u_{b\infty}$.

By using the definition of C_D and Eq. (4.102) for $u_{b\infty}$, the drag coefficient of a bubble can be calculated as:

$$C_{\rm D} = \frac{(\pi/6)D_{\rm b}^3 \rho_i/g}{\frac{1}{4}\pi D_{\rm b}^2 \frac{1}{2}\rho_i u_{\rm boo}^2} = \frac{8}{3}$$
 (4.103)

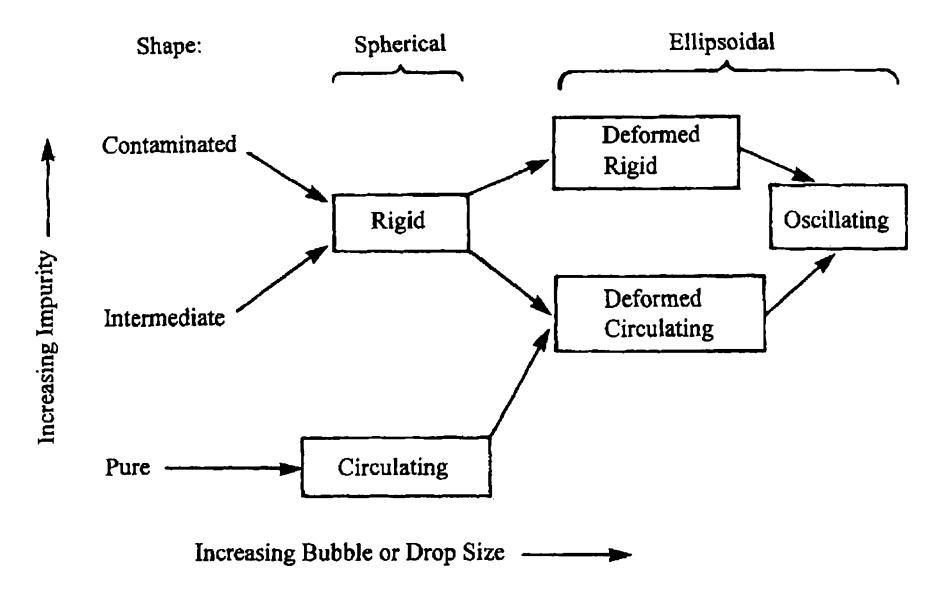


Figure 4.29 Flow transitions for bubbles and drops in liquids (schematic). Reproduced with permission from Academic Press Inc. Orlando, Florida⁽¹⁾.

For a droplet, the drag coefficient is higher by about 50% than the above result because of the drag reduction by the circulation in the droplet. However, the above result is applicable if the droplet diameter becomes smaller or if its surface is covered with surfactants or impurities so that such a circulation cannot be formed so easily. On the other hand, as the bubble and droplet diameters become larger, their shapes deviate far from a sphere as shown in Figure 4.29.

In the case where a circulation occurs inside a droplet, the drag coefficient is represented by the following expression from the Hadamard–Rybczynski theory⁽¹²⁾⁽¹³⁾.

$$C_{\rm D} = \frac{2+3\beta}{1+\beta} \frac{8}{Re} \tag{4.104}$$

 $\beta = \mu_p/\mu$ is the viscosity ratio between the two fluids, where the subscript p denotes the 'fluid in the particle (droplet)'.

4.3.2.4.3 Behaviour of Multi-particle Systems

In multi-particle systems, particles behave differently from an isolated particle system because of the interaction among particles and the entrainment effect accompanied by the continuous phase motion.

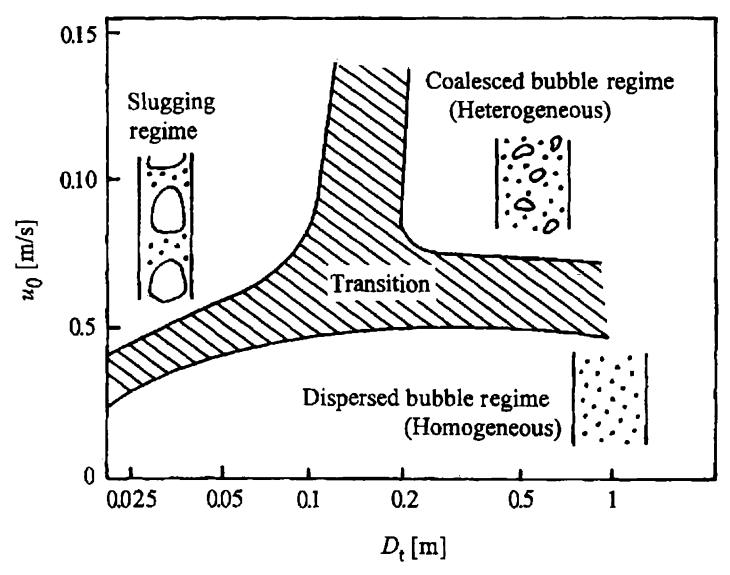


Figure 4.30 Flow regimes of bubble column and slurry bubble column (from Deckwer et al. (1980))⁽¹⁴⁾.

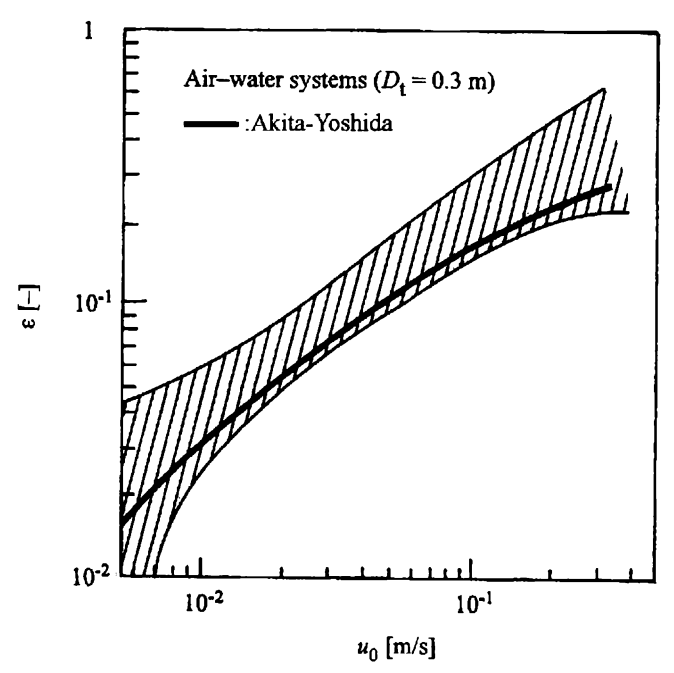


Figure 4.31 Comparison of the Akita-Yoshida correlation with the available data for the gas hold-up in bubble columns. Reproduced by permission of the publisher, Butterworth-Heinemann, Oxford and Boston⁽¹⁶⁾.

Figure 4.30 is an illustration of flow regimes of multi-bubble systems. The following Akita-Yoshida expression⁽¹⁵⁾ is as an example of the correlation for volume fraction of bubbles:

$$\frac{\varepsilon_{g}}{(1 - \varepsilon_{g})^{4}} = c \left(\frac{D_{t}^{2} \rho_{l} g}{\gamma}\right)^{1/8} \left(\frac{D_{t}^{3} \rho_{l}^{2} g}{\mu_{f}^{2}}\right) \left(\frac{u_{g}^{2}}{g D_{t}}\right)^{1/2}$$

$$c = \begin{cases}
0.2 & \text{(Non-electrolytic pure liquid)} \\
0.25 & \text{(Electrolytic solution)}
\end{cases}$$
(4.105)

where D_t is the column diameter, γ is the surface ternsion, and subscripts g and l are gas and liquid phases, respectively.

Figure 4.31 shows the comparison of the above expression with the available data for air-water systems.

4.3.2.4.4 Behaviour of Solid Dispersed Systems

Depending on their sizes, fine solid particles are called aerosol or ultrafine particles ($\sim 1 \mu m$), powder ($1 \mu m \sim 1 mm$) or granules ($\sim 1 mm$). However, the size references differ depending on the field of application. Except for very special cases, powders and granular materials coexist with the fluids in the space between the particles. The pressure gradient in the fluid yields fluid flow which then creates drag force in the flow direction in the bed. On the other hand, the external forces such as gravity, centrifugal force and magnetic force act across the whole powder bed and create stresses in the bed i.e. powder pressure and shear stress.

The pressure gradient grad P of the fluid in the powder bed, which acts as the drag force on the particles, can be expressed well by Ergun equation⁽¹⁷⁾:

$$-\operatorname{grad} P = \frac{1 - \varepsilon}{\phi_{s} d_{p} \varepsilon^{3}} \left[150 \frac{(1 - \varepsilon) \mu_{f}}{\phi_{s} d_{p}} + 1.75 \rho_{t} u_{0} \right] u_{0}$$
 (4.106)

In the case of a multi-dimensional flow, u_0 in the above expression is a vector variable. ϕ_s is the sphericity, ε is the void fraction, μ_f is the fluid viscosity, and ρ_f is the fluid density. If there is a particle size distribution, the following surface-to-volume mean diameter for d_p should be used for Eq. (4.106).

$$d_{\rm p} = \sum_{i} d_{\rm p}i/x_{\rm p}i \qquad (x_{\rm p}: {\rm mass\ fraction}) \tag{4.107}$$

When the drag force balances with the external forces, the pressure and the shear stresses in the bed disappear and individual particles are released from constraint. At this time, the powder bed starts behaving like a liquid. This is

called the fluidization of a powder bed. The minimum superficial velocity to maintain the fluidized state is called the minimum fluidization velocity $u_{\rm mf}$. Accordingly, if u_0 is greater than $u_{\rm mf}$ we have a sort of liquid state in the powder. On the other hand, if u_0 exceeds $u_{\rm t}$ of Eq. (4.98), particles are entrained in the fluid. This is a sort of gas state in the powder.

The void fraction at the minimum fluidization is written as $\varepsilon_{\rm mf}$. Wen and Yu⁽¹⁸⁾ discovered that relations $1/(\phi_s \varepsilon_{\rm mf}^3) = 14$ and $(1 - \varepsilon_{\rm mf})/(\phi_s^2 \varepsilon_{\rm mf}^3) = 11$ hold for most powders, and further, by substituting these relations and the condition of fluidization into Ergun's equation, derived the following correlation for $u_{\rm mf}$:

$$Re_{\rm mf} = d_{\rm p}\rho_{\rm f}u_{\rm mf}/\mu_{\rm f} = [(33.7)^2 + 0.0408Ar]^{1/2} - 33.7$$
 (4.108)

where Ar is the Archimedes number defined by Eq. (4.100). In a viscosity-dominant regime with a small Ar, the above formula is reduced to

$$Re_{\rm mf} = Ar/1650 \quad (Ar < 1.9 \times 10^4)$$
 (4.108')

Thus, fixed bed or moving bed state, fluidized bed state, and entrained bed or pneumatic transport state emerge as basic states of powder beds as shown in Figure 4.32. These can be regarded as solid, liquid and gas states in suspended powder and granular materials.

In solid-gas systems, a suspension is further divided into dense and lean phases. When gas velocity is low, a bubbling fluidized state is created where the lean phase is dispersed in the dense phase. If the gas velocity is high with a high particle loading, a fast fluidized state is created where the dense phase is dispersed into the lean phase. In these cases, Eq. (4.94) and (4.95) can be written for each phase. Also, for bubbles inside the bed Eq. (4.102) can be applied with $\alpha = 0.71$. In a bubbling fluidized bed, roughly speaking, the amount of gas required for fluidization, i.e. $u_{\rm mf}A_t$, flows through the dense phase, and the excess gas $(u_0 - u_{\rm mf})A_t$ flows as bubbles. This is called the two-phase theory of Toomey and Johnstone⁽²⁰⁾.

According to Geldart⁽²¹⁾ bubbling fluidized beds have four fluidization modes.

In Mode A, the dense bed of particles well expands above the minimum fluidization velocity, which allows the homogenous fluidization with no bubbles. Above minimum bubbling velocity, a bubbling bed is formed but in Mode A bubbles split and recoalesce quite often, fluidization keeping their size rather small.

In Mode B, bubbles are formed immediately above the minimum fluidization velocity; thus, no homogeneously fluidized bed is created. Bubble splitting is negligible in Mode B, allowing the formation of large bubbles.

In Mode D, the minimum fluidization velocity is significantly larger than the bubble rise velocity. Gases flow through bubbles (bubble throughflow). Bubbles coalesce easily causing slugging.

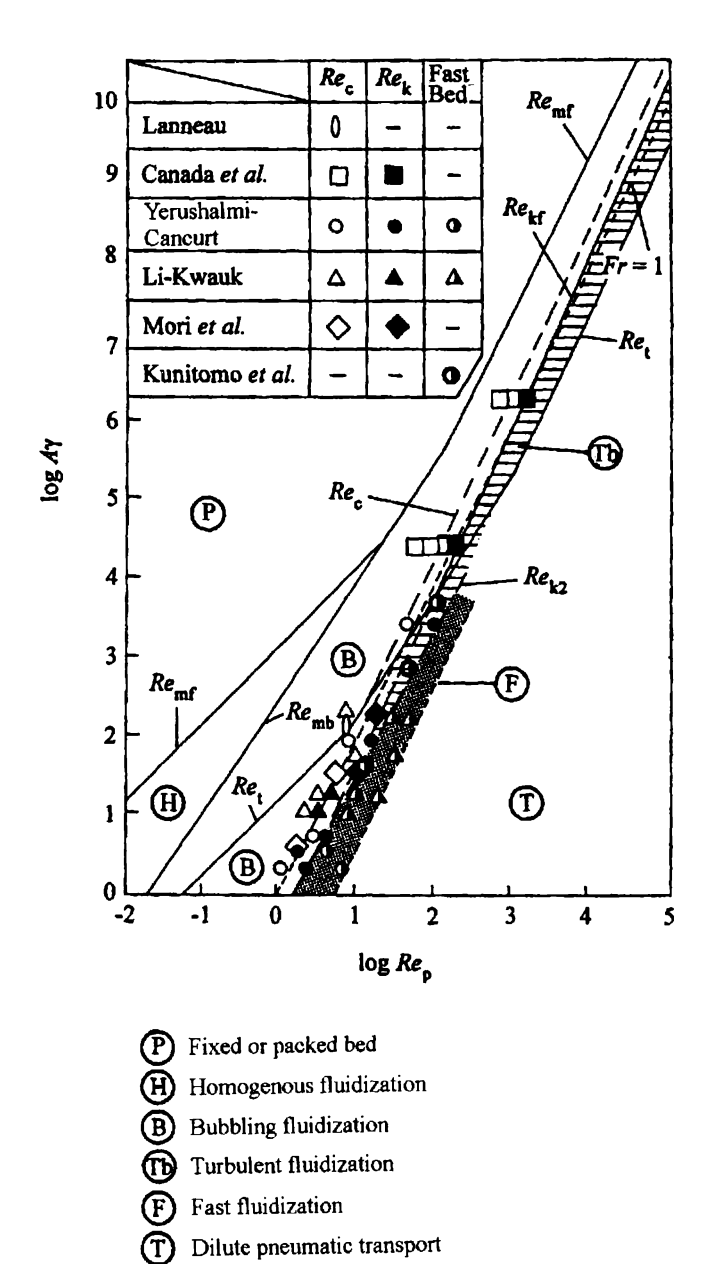


Figure 4.32 Flow regimes of gas-solid dispersed systems(19).

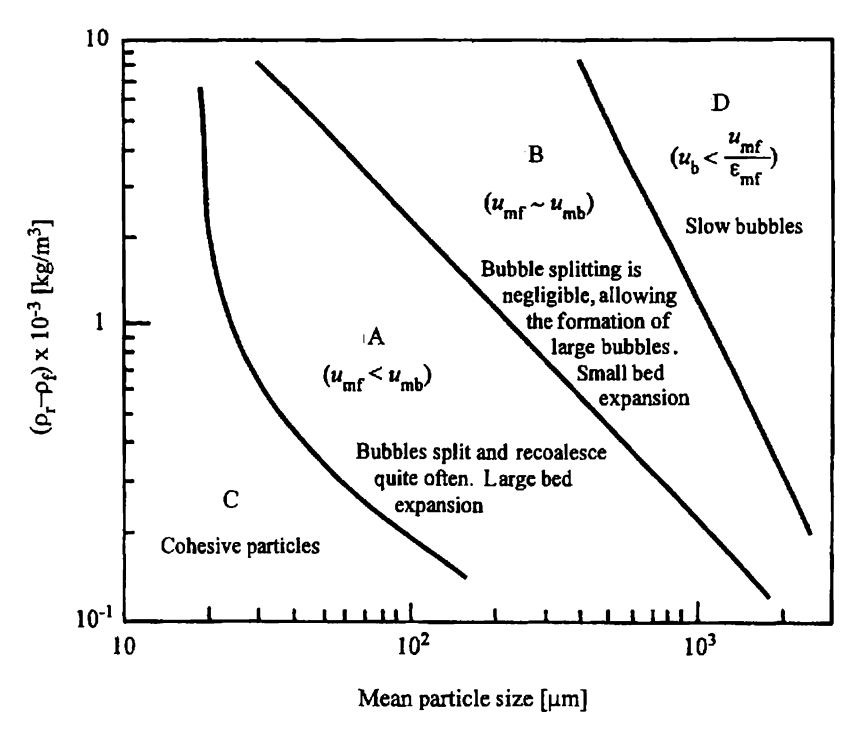


Figure 4.33 Geldart's diagram for powder classification for fluidization by air at ambient conditions⁽²¹⁾.

The mode that is not immediately defined based on bubbling characteristics is Mode C, in which difficulties associated with the cohesiveness of particles such as agglomeration and defluidization easily occur.

Figure 4.33 is a powder classification map defined corresponding to the above fluidization modes at normal temperature and normal pressure.

4.3.2.4.5 Mass Transfer Volumetric Coefficient $(k_{ij}a_{ij})$ and Gas Exchange Coefficient (K_{ij})

In a multiphase operation in which the interface is disturbed intensely, there is little significance in treating the mass transfer coefficient and specific surface area separately, therefore, they are often correlated in the form of a 'volumetric coefficient'.

As a typical equation for the liquid-side mass transfer volumetric coefficient for bubble columns, Akita and Yoshida's⁽¹⁵⁾ correlation is shown below:

$$\frac{k_{lg}a_{lg}D_{t}^{2}}{D} = 0.6 \left(\frac{D_{t}^{2}\rho_{l}g}{\sigma}\right)^{0.62} \left(\frac{D_{t}^{2}\rho_{l}g}{\mu_{l}^{2}}\right)^{0.31} \left(\frac{\mu_{l}}{\rho_{l}D}\right)^{0.5} \varepsilon g^{1.1}$$
(4.109)

where D is the molecular diffusivity of the liquid component in which we are interested.

Also in gas fluidized beds, k and a cannot be obtained separately. Since calculation of fluidized bed reactions is often based on bubble volume, the concept of the gas exchange coefficient $K_{\rm BE}$ is more useful than the volumetric coefficient ka. $K_{\rm BE}$ is defined as,

(Mass transfer rate in volume from bubble phase to dense phase per unit volume of bubbles phase)

$$= K_{\rm BE}(C_{\rm B} - C_{\rm E}) \tag{4.110}$$

The mass transfer rate in the unit volume of the bed can be obtained by multiplying this coefficient by the bubble fraction ε_b . Thus, we have the following relationship between $(ka)_{FB}$ and K_{BE} :

$$(ka)_{\rm FB} = K_{\rm BE} \, \varepsilon_{\rm b} \tag{4.111}$$

For $K_{\rm BE}$, Davidson's⁽²²⁾ theoretical expression considering both the gas circulation between the bubble and emulsion phases and molecular diffusion from the bubble wall is given by

$$K_{\rm BE} = [4.5u_{\rm mf} + 5.85D^{1/2}(g/D_{\rm b})^{1/4}]/D_{\rm b}$$
 (4.112)

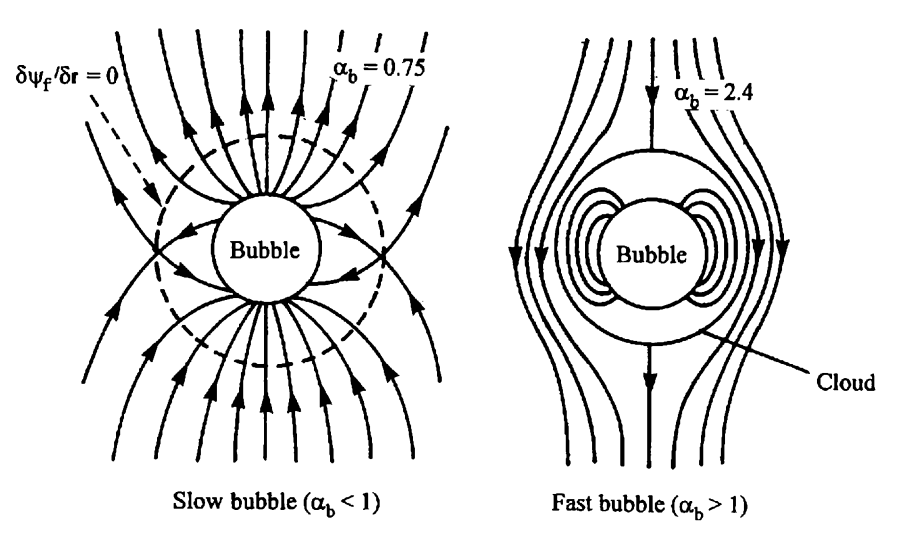


Figure 4.34 Stream lines of gas around a bubble. Reproduced with permission from Fluidized Particles Davidson and Harrison, 1963; Cambridge University Press. $^{(22)}a_b \equiv u_b \varepsilon_{mf}/u_{mf}$. Ψ_f : stream function.

where D is the molecular diffusivity of the component.

In fact, the dense phase may be further divided into two regions: one where the circulation of gas with the bubble phase exists, i.e. the cloud phase, and one where the circulation gas does not penetrate, i.e. the emulsion phase, as shown in Figure 4.34. Since the reactant gases in the bubble phase can penetrate only within the cloud phase, the cloud fraction is an important factor which significantly affects the contact efficiency of a fluidized bed reactor.

4.3.2.4.6 Eddy Diffusivity

Axial eddy diffusivities in liquid and gas phases in a bubble column E_{lz} and E_{gz} are correlated by (4.113) and (4.114), as shown in Figure 4.35.

$$(E_{lz}/\sqrt{D_1^3 g}) (\mu_l^4 g/\rho_l \sigma^3) = 0.037 + 0.188 Fr_g^{0.36}$$
 (Hikita and Kikukawa⁽²⁴⁾) (4.113)

where $Fr_g \equiv u_{g_0}^2/gD_t = 1.6 \times 10^{-3} \sim 0.16$, $u_l^4 g/\rho_l \sigma^3 = 2.6 \times 10^{-11} \sim 2.5 \times 10^{-6}$ and

$$E_{\rm gz} = 50D_{\rm t}^{1.5} (u_0/\varepsilon_{\rm g})^{3.0} \qquad \text{(Mangartz and Pilhofer}^{(25)}) \tag{4.114}$$

for $D_1 = 0.092 \sim 1.067$ m, $u_{g_0} = 0.015 \sim 0.13$ m/s, $u_{l_0} = 0.0072 \sim 0.0135$ m/s. With respect to mixing in a packed bed, Lapidus *et al.*⁽²⁶⁾ showed that the mixing process can be well reproduced by a cell model with a cell size of

mixing process can be well reproduced by a cell model with a cell size of roughly the particle diameter. In a packed bed, the flow is always branched due to the presence of particles. Furthermore, a velocity distribution is formed in the clearance between adjacent particles as shown in Figure 4.36. This causes dispersion both in the flow direction and in directions perpendicular to it. According to Levenspiel⁽²⁸⁾, the corresponding Péclet numbers are correlated as

$$1/Pe_{r} \equiv E_{r}/ud_{p} = 0.1$$
 (4.115)

$$1/Pe_2 \equiv E_z/ud_p = \begin{cases} 2 & \text{(liquid system, } Re_p = d_p u \rho_f/\mu_f = 0.1 \sim 500) \\ 0.5 & \text{(gas system, } Re_p = 4 \sim 400) \end{cases}$$
(4.116)

In packed beds the convection term in the axial direction is negligible as it is smaller than the diffusion term. Let us briefly verify this by subtracting the diffusion term from the convection term and further approximating $\partial_z C$ with respect to $\Delta C/d_p$, in which ΔC is the concentration difference over a small increment in the axial direction as large as the particle diameter d_p . Then,

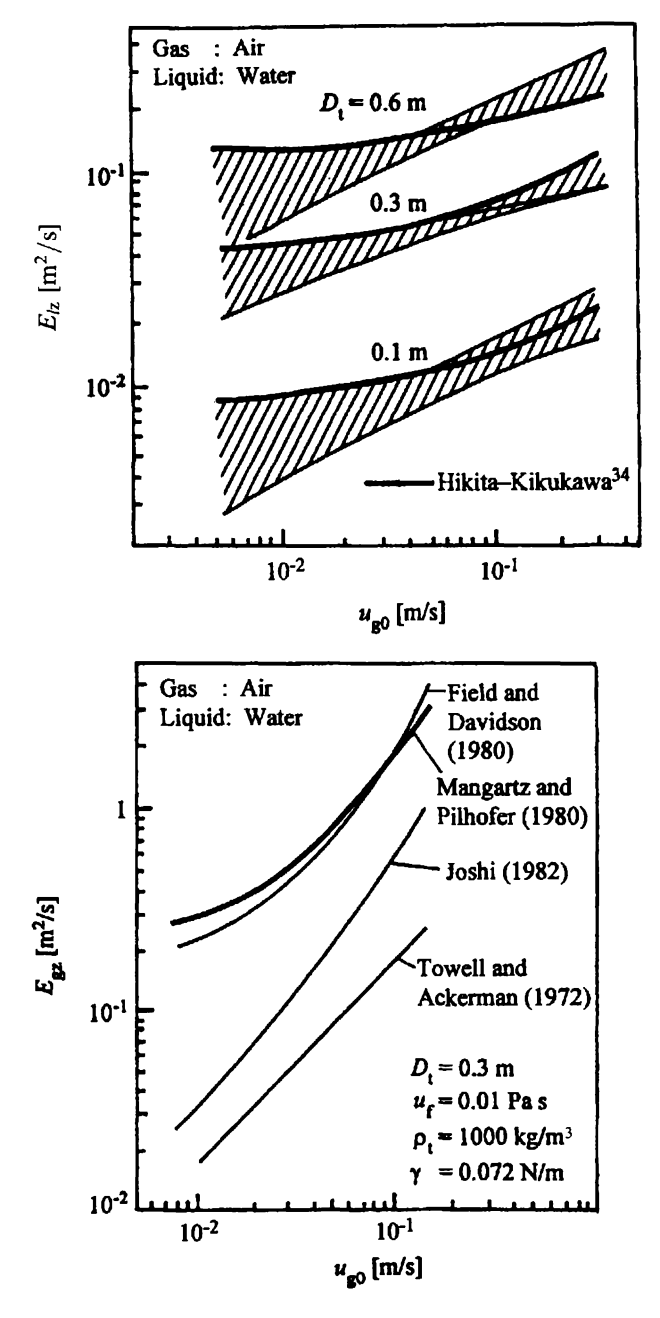


Figure 4.35 Axial eddy diffusivities in liquid and gas phases in bubble columns⁽²³⁾. Reproduced by permission of the Publisher, Butterworth-Heinemann, Oxford and Boston.

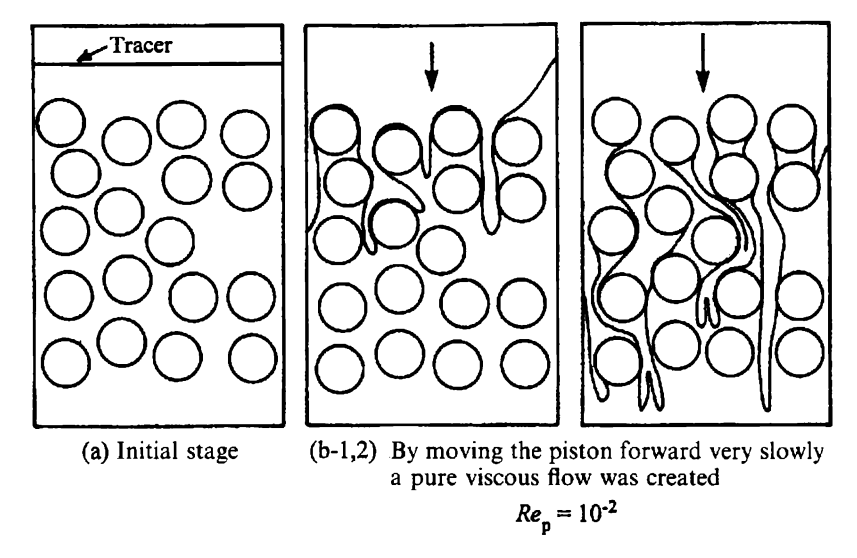


Figure 4.36 Demonstration of axial and lateral dispersions in packed bed flow and the reversibility of viscous flow⁽²⁷⁾ (liquid: 98% Glycerine solution).

Convection term – Diffusion term =
$$\partial_z (u_0 C - \varepsilon E_z \partial_z C)$$

= $\partial_z \left[\frac{\varepsilon E_z C}{d_p} \left(\frac{u_0 d_p}{\varepsilon E_z} - \frac{\Delta C}{C} \right) \right]$ (4.117)
= $\partial_z \left[\frac{\varepsilon E_z C}{d_p} \left(Pe - \frac{\Delta C}{C} \right) \right]$

From Eq. (4.116), the value of Pe in the above expression is 0.5-2. Thus, if the relative concentration change over a section equivalent to about one particle layer $\Delta C/C$ is sufficiently smaller than 0.5-2, the axial mass flux should dominate the convection—or the flow is approximately equivalent to plug flow in the axial direction. Since this condition is almost always satisfied, except for the case of extremely rapid reactions where only a few layers of particles would be enough for completion of the reaction (but this would be quite an unusual packed bed), the assumption of 'convection-dominant' in the axial direction is allowed for any ordinary packed bed reactor.

For mixing in bubbling fluidized beds, bubbles may be used as an approximate scale of the mixing length. Kato and Wen⁽²⁹⁾ proposed the Bubble Assemblage Model for fluidized bed reactor modelling where the bed is expressed as a series of well mixed tanks of the same thickness as the mean height of a bubble. This model is applicable for the gas-phase description. However, for the particle phase the mixing effects of particle

circulation due to the wake lifting by bubbles must be taken into account. It is also known that a similar circulation is created in bubble columns, but for more details please refer to the relevant literature.

4.3.2.4.7 The importance of the State of the Interface

In multiphase reactors the 'interface' is nothing but the place where multiphase reactions occur. The 'interface' is a phase-to-phase boundary at which different phases directly contact each other. Interfaces in contact with a gas phase, i.e. gas-solid and gas-liquid interfaces, are specifically called the 'surface'. However, an interface does not always exist between phases. In supercritical fluids, which have recently been used for extraction of aromatic components, molecules cluster and no uniform condensed phase or clear surface is formed.

An interface is not only a partition between different phases. A solid surface acts as a place where the electric charge is localized by bond breakage and by lattice defects. Furthermore, -OH, -COOM and peroxides are formed by reaction with H₂O, CO₂ and O₂ in air. On the surface of zeolite, for example, there exists a Brønsted acid giving and receiving protons and a Lewis acid receiving base and electron pairs. Also, on the surface of alkaline earth metal oxides such as MgO, dioxides of various coordination numbers exists, turning the surface into a base.

Gas-liquid and liquid-liquid interfaces are, in many cases, stabilized by adsorption of amphiphilic molecules such as surfactants, which create a dispersed phase whose breakdown is not easy, or a specific electrostatic state which prohibits other molecules or particles approaching the interface. The lipid film covering the outer surface of a micro-organism has a structure made of a protein complex called 'the channel' that permits specific ions and substances to penetrate selectively. In multiphase reactors, the micro—or nano—structures of interfaces and surfaces and accordingly their functions will change drastically in the future.

4.3.3 CONCEPTS OF MULTIPHASE REACTION PROCESSES

4.3.3.1 Alternatives to the State of the Interface

There is a variety of modes of phase coexistence and types of interface in multiphase reaction processes. If a specific type of interface is adopted in a reactor, there must be sufficient reasons or causes. Let us examine several cases and see what leads us to a particular selection.

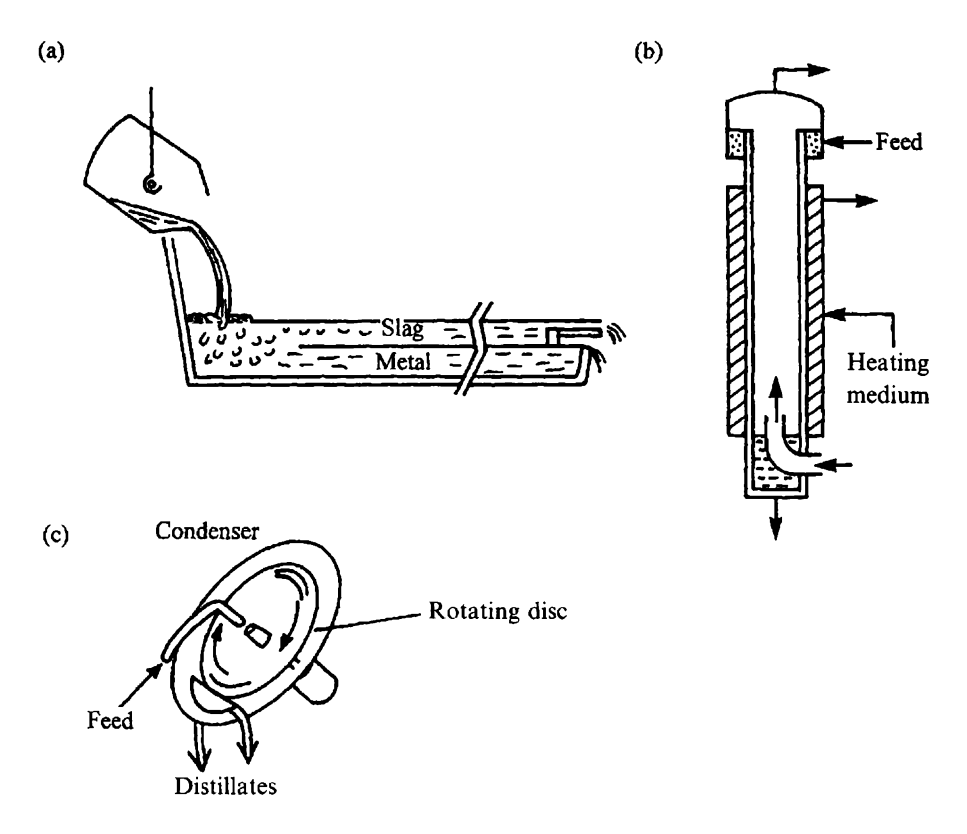


Figure 4.37 Systems with flat interfaces. (a) Open hearth furnace used in the past for metal smelting. (b) Wetted wall column. (c) Rotating molecular distillation plant.

4.3.3.1.1 Systems with Flat Interfaces (Figure 4.37)

These are the simplest in structure and least turbulent. There, contact between the two continuous phases is made at a single stationary interface. Examples of this type of system include wetted-wall columns, open hearth furnaces, molecular distillation plants and reactors with honeycomb catalysts.

Now the reader may wonder why such an interface is still adopted in spite of the fact that the transfer rate becomes higher with increased interfacial area. In the case of the slag-metal reactions, for example, the necessity was to prevent the dispersion of fine droplets of molten slag into the metal phase which brings about inclusions in the product steel. However, what was found afterwards was that, when placed in a strong turbulent field, the fine slag droplets could grow through collisions and were subject to rather easy separation by buoyancy. Today open hearth furnaces are completely replaced by LD converters that feature intense stirring by oxygen blowing in a short operating time. In the

molecular distillation plant, a thin liquid film is created to heat the feed liquid rapidly and uniformly enough not to decompose those thermally sensitive compounds.

In gas-solid systems, catalyst honeycombs can be another example, where the porous catalyst support walls are placed in parallel with the pass so as to minimize the pressure drop.

4.3.3.1.2 Systems with One or More Phases Dispersed (Figure 4.38)

In general, this is a type of system in which rate processes are intensified by the large contacting surface area created by the dispersion of one phase into another.

Examples of such systems containing a liquid phase are those with bubbles blown into a continuous liquid phase (e.g. bubble columns), those with liquid droplets into continuous gas phase (e.g. spray columns), those with powder and granular materials dispersed in a continuous liquid phase, and dispersions of an immiscible liquid phase into another (e.g. extraction columns). In gas—liquid systems, the liquid phase is turned into a dispersed phase (1) when the main purpose is to evaporate the liquid phase (e.g. cooling towers, liquid fuel burners, spray dryers and gas phase olefin polymerization equipment where liquid state monomer may be fed to the reactor to remove the heat of polymerization effectively) or (2) when the main purpose is to treat a gas phase where high inlet pressure cannot be expected (e.g. flue gas scrubbers).

In systems of suspended solids, particles are either suspended in a fluid (e.g. fluidized beds and entrained beds) or not where a fluid passes through a non-suspended bed (e.g. fixed beds and moving beds).

Entrained beds can be used only in rapid processes in which fine powders of less than about $100\,\mu\mathrm{m}$ are used with no requirement for strict temperature uniformity and no risk of reaction runaway. Examples of such systems are riser reactors for fluid catalytic cracking with zeolite catalyst, suspension preheaters for preheating raw cement powders, pulverized coal fired (PCF) boilers, high temperature coal gasifiers and reactors to produce some fine ceramic powders from metals (e.g. high-temperature nitridation of metal powders). In fast reactions product compositions are quite sensitive to the contact time. Accordingly, not only the mean value, but also the distribution of the residence time is often very critical.

Fluidized beds are widely adopted because of the uniformity and stability of bed temperature which is brought about by the high heat capacity of bed materials and by good solids mixing. This ensures rapid heating of the feed, prevention of runaway or side reactions (e.g. catalytic partial oxidation such as acrylonitrile production, thermal decomposition, gasification, combustion, and heat treatment of resins) and prevention of various problems such as fusion, solid adhesion and/or plugging of catalyst pores by overheating (e.g. catalyst regeneration and fluidized bed combustion). Furthermore, by utilizing the

liquid-like nature of fluidized beds, stirring, mixing and gravity sorting can be done easily. For instance, agglomeration is prevented by dispersing cohesive materials into a non-cohesive fluidized bed in heavy oil cracking and/or spray coating; a mixture of various materials of different sizes and densities are treated in fluidized bed waste incineration, where fluidized beds provide a condition for in-bed combustion of combustibles and selective discharge of non-combustibles. In fluidized bed dryers, granulation proceeds through tumbling of in-bed particles. A fluidized bed can be also used as a rate controllable fine powder feeder. Note that these operations are possible only when the level of shear force in the fluidized bed is greater than the inter-particle cohesion force. Understanding the cohesive limit of each operation is quite important to avoid problems such as defluidization.

Moving beds are used for slower reactions where the bed volume must be sufficiently large to ensure the time for reactions. To achieve a low pressure drop and a uniform fluid penetration in tall moving beds, large particles of equal size are recommended. In the blast furnace process, crushed iron ore is first sintered and then their sizes are made uniform (to about 20 mm) for the feed. In moving beds of large and heavy particles, the cohesion of particles is a relatively small problem. The moving bed may be recognized as a method for treating solids in large grains whose adhesive properties are largely increased if finely ground. Furthermore, in a blast furnace iron ore and coke are charged layer-by-layer so that metallic coke can prevent permeability reduction and gas maldistribution which is possibly caused by adhesion and fusion of iron ore in the course of reduction.

Nevertheless, the criteria for selecting an entrained bed, a fluidized bed or a moving bed are not simple. If pulverized particles can be used instead of large granules by improving the catalyst or increasing the reaction temperature, reactions can be completed in a short time. This then allows the use of a fluidized or an entrained bed. For coal gasification, as an example, all three types such as Lurgi's moving bed, the NEDO Yubari type and TEXACO, Shell and other entrained beds are available. The different choices have been made based on solid properties such as the de-volatization and de-ashing characteristics of coal accompanied by heating and melting characteristics of the ash. Of course the heat utilization efficiency and the requirements for reactor material should be considered.

For powders with low cohesiveness, a gas-particle trickle flow reactor is available where gas and particles trickle after colliding with baffles in the column. (Figure 4.38(k)).

4.3.3.1.3 Systems with Stabilized Dispersions (Figure 4.39)

If we make the size of the particles smaller, the surface energy of the particles or their cohesiveness becomes larger. Accordingly, reaction, evaporation or

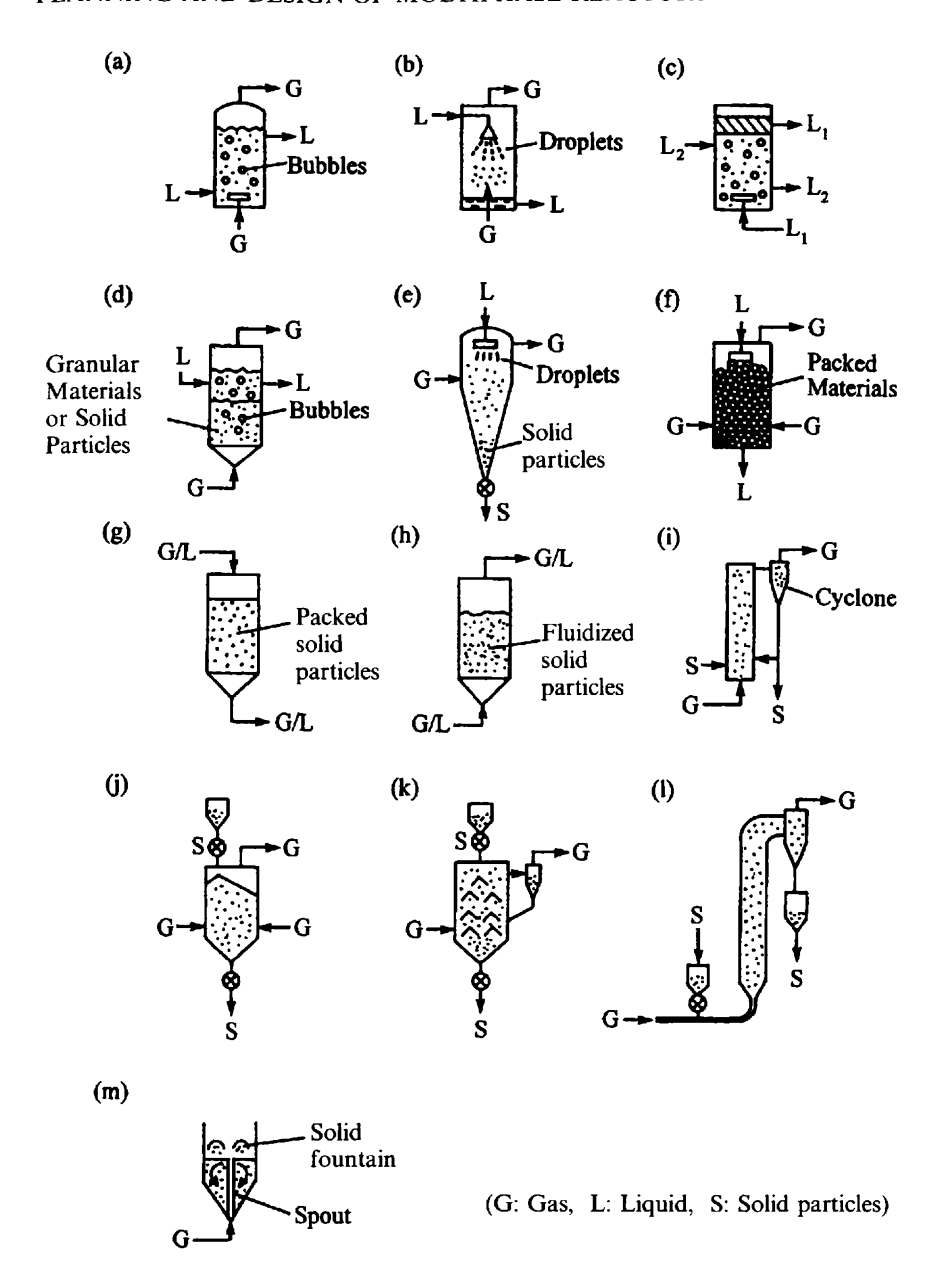


Figure 4.38 Systems with one or more phases dispersed: (a) bubble column; (b) Spray column; (c) extraction column; (d) suspended bubble column; (e) spray dryer; (f) trickle bed; (g) fixed bed; (h) fluidized bed; (i) circulating fluidized bed; (j) moving bed; (k) solid trickle bed; (l) entrained bed and (m) spouted bed.

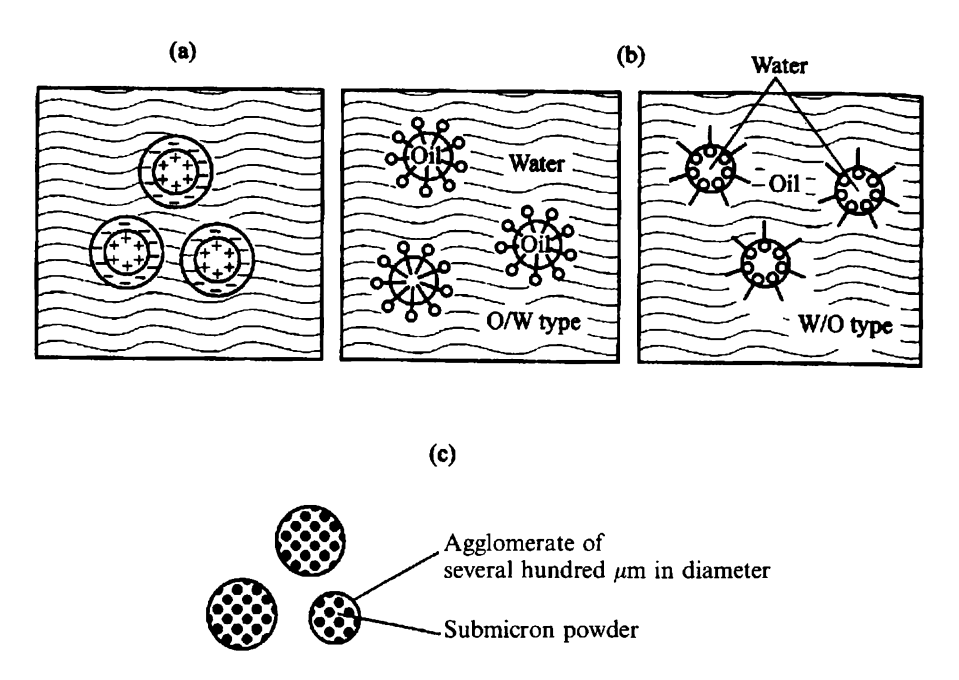


Figure 4.39 Systems with stabilized dispersions. (a) Stabilization by electric double layers. (b) Stabilization by surfactants. (c) Relative reduction of cohesiveness by formation of agglomerates.

dissolution rates become much more rapid but at the same time agglomeration or coalescence rate increases. This is why agglomeration is one of the key issues of particle technology. For example, in the manufacture of various monodispersed particles, it is common to enlarge particles preventing their mutual agglomeration. In these cases, colloid technology is applied to create interparticle repulsion forces with adsorbed ions or surfactants. Such methods are also applied to the synthesis of plastic pigment particles and production of microcapsules by emulsion polymerization, or decomposition of fats and oils by water-soluble enzymes. Also in fluidized beds, sub-micron particles can be produced in well controlled pores within porous particles which can be regarded as microreactors.

Fine powders with high agglomeration properties may be better treated after being granulated to a certain larger size. Such pre-granulation is used in many manufacturing processes of materials, pigments and chemicals of various kinds. This prevents dust generation, deposition on the wall, sintering and formation of agglomerates too large to handle.

For the case of dilute solid dispersions with a small solvent-to-crystal refractive index, care must be taken to distinguish them from other transparent

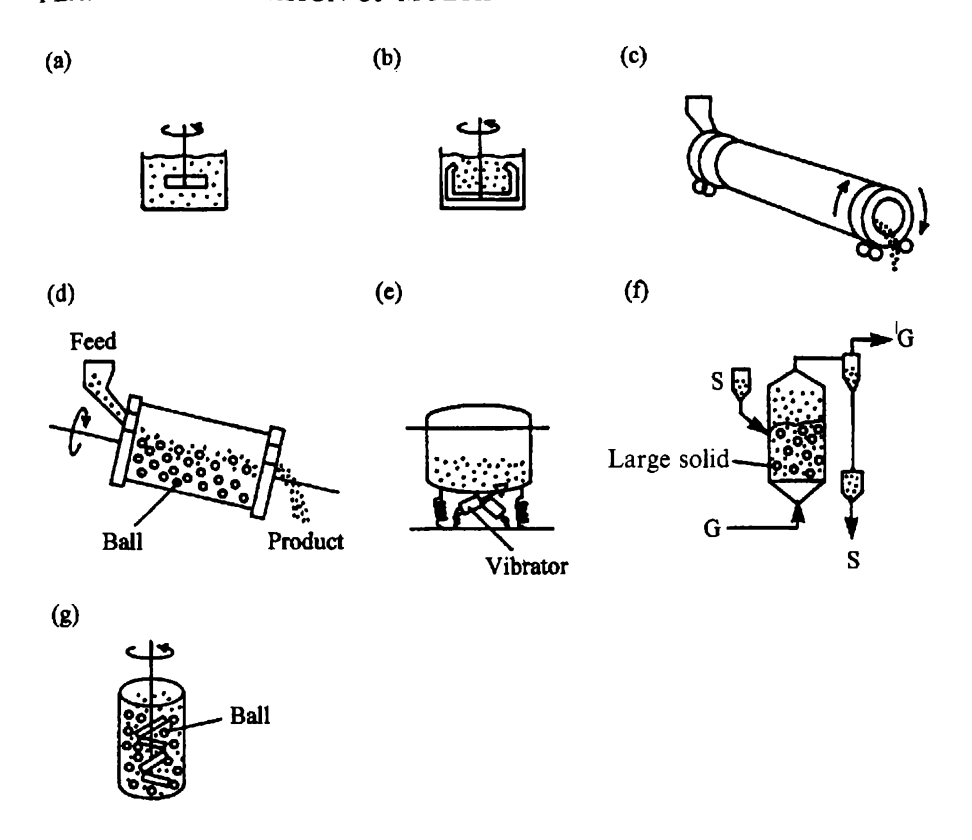


Figure 4.40 Systems with forced mechanical dispersion. (a) Stirred tank reactor. (b) Reactor with scraper. (c) Rotary kiln. (d) Ball mill. (e) Vibrated bed. (f) Multi-particle fluidized bed. (g) Attriter.

solutions. Such 'solutions' may cause wear on the stirrer even though they look like pure liquids.

4.3.3.1.4 Systems with Forced Mechanical Dispersion (Figure 4.40)

When suspensions cannot be sufficiently stabilized by chemical methods only, it is worth applying some mechanical ones to prevent agglomeration. Such examples are those reactors fitted with a stirrer or a scraper, rotary kilns, ball mills, vibrated beds and multi-particle fluidized beds. Rotary kilns are most suitable for easy handling of otherwise difficult-to-handle solids of odd shapes and an adhesive nature. This is why rotary kilns are often used for material processing and waste treatment. However, rotary kilns have disadvantages such as difficulty of sealing, significant heat loss through the kiln wall in high-

temperature reactions, and utilization of only a very small portion of the crosssectional area. It is accordingly appropriate to consider that even if a rotary kiln is adopted at an early stage of a commercial process, there remains a high potential for its replacement by another contact scheme.

The forced renewal of microscopic surfaces of solids can be achieved with ball mills, attriter or vibrated mills. Accordingly, they are used in kneading and in manufacture of various composite ceramics or metal—ceramic composites. Multi-solid fluidized beds are also of a similar kind where easy-to-agglomerate fine powders can be treated while they are decomposed by the milling effect of coarse granules. These operations are intended for mixing and/or mechanochemical reactions at the primary particle level.

4.3.3.1.5 Contacting Systems with a Porous Material (Figure 4.41)

Finer catalyst particles can have higher activity but particles of sizes down to the nanometer scale are usually too active and unstable to avoid sintering and therefore to maintain their activity. In the case of solid-gas or solid-liquid contact the increase in surface area does not always require the creation of a dispersed system of microscale particles. As described in 4.3.3.1.3, the use of pre-granulated agglomerates or porous particles can keep a relatively stable internal surface area tens of thousands of times as large as their external surface area. Let us compare the specific surface area of a variety of materials.

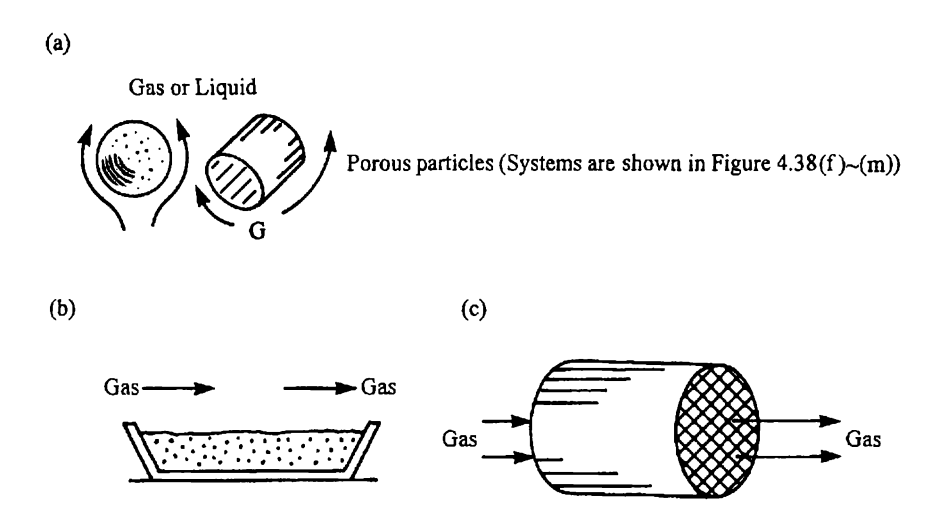


Figure 4.41 Contacting systems with a porous material. (a) Fixed, moving, fluidized and entrained beds (particles are porous). (b) Non-percolation fixed bed. (c) Honeycomb tube reactors (Porous honeycomb walls).

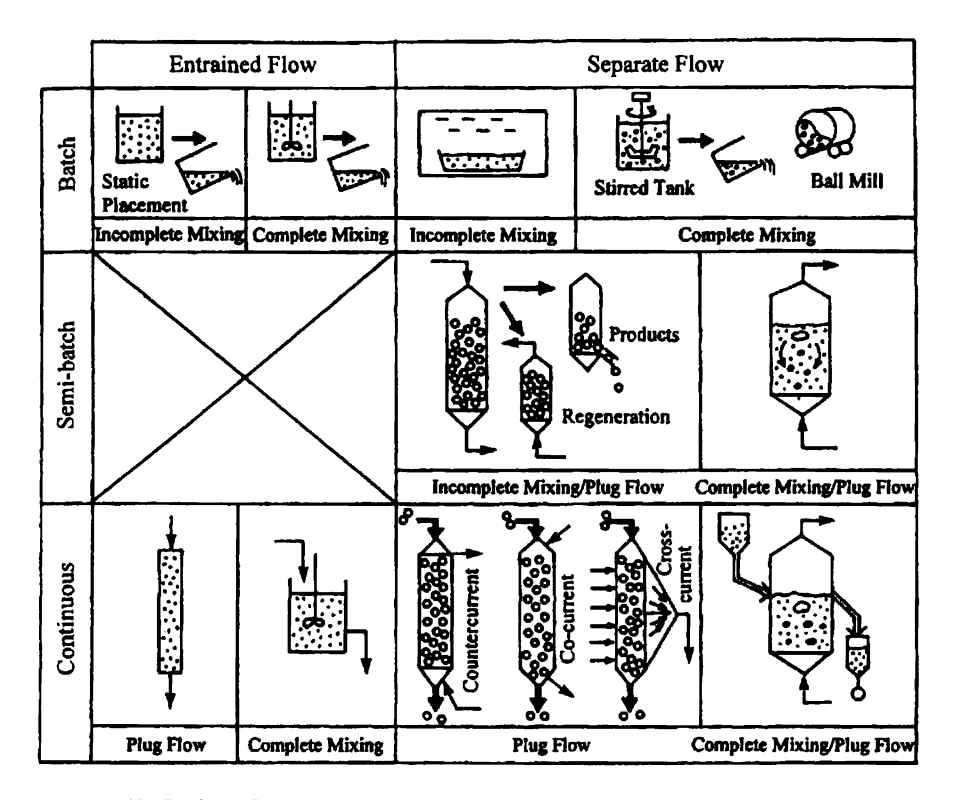


Figure 4.42 Options for reacting systems and reactor structures.

If the particle size d_p ranges from 100 μ m to 5 mm, the specific surface area of the external surface $a_{\text{ex}} \equiv (\pi d_3^2 p)/(\pi d_p^3/6) = 6/d_p$ is 6×10^4 to 1.2×10^3 m⁻¹, while if we assume that the micro-pore diameter is 5 nm and the porosity is 0.25, the specific surface area of the internal surface is $a_{\text{int}} = (\text{porosity}) \times$ (specific surface area of a circular tube) = $0.25 \cdot 4/(5 \times 10^{-9}) = 2 \times 10^8 \text{ m}^{-1}$. This demonstrates that the internal surface area is much more important for porous materials with fine pores of the nanometer scale. The internal surface areas are $10^7 - 10^9 \,\mathrm{m}^{-1}$ for industrial catalysts, $10^9 \,\mathrm{m}^{-1}$ for adsorbents such as activated carbon, 10^5-10^6 m⁻¹ for calcined limestone, and about 10^8 m⁻¹ for char particles (i.e., fixed carbon formed by pylorisis) in coal gasfication or combustion. Under elevated temperature conditions, however, coalescence of fine pores and growth of crystal grains may even take place at a temperature significantly lower than the melting point of solids, resulting in loss of internal surface area. Thus, we have to determine the external size of the porous materials and the fluid-solid contact scheme such as fixed, moving, fluidized or entrained bed or honeycomb tube, taking into account the reaction rate and thermal characteristics of solids.

So far, we have reviewed the morphological varieties of phases as well as the reasons of adopting and combining particular phases in particular forms. In the following section we examine the options for multiphase reactors from the standpoint of the modes of reacting systems and the structure of reactors.

4.3.3.2 Options for Reacting Systems and Reactor Structures

Groups of options: batch or semi-batch, semi-continuous or continuous, entrained flow or separate flow, complete mixing or plug flow, co-current, counter-current or cross-current, uniform reaction, zone reaction or surface reaction, micro mixing, macro mixing or eddy diffusion and static, dynamic and stability.

Some of the above classifications are illustrated in Figure 4.42. We will deal with them group by group below.

4.3.3.2.1 Batch/Semi-batch (Semi-continuous)/Continuous

In batch or semi-batch systems reactions are initiated either by elevating temperature and adjusting pressure to a desired condition or further by supplying gas reactants into the reactor where powders or liquids are charged beforehand. A 'semi-batch process' is a continuous process in terms of the gas phase. In this configuration, it is relatively easy to prevent the migration of impurities. A batch or semi-batch system is adopted in (1) processes producing small amounts of materials and many different products, such as pharmaceutical and functional materials to avoid excessive costs for equipment and space, (2) mass production processes such as for foods, pharmaceutical products, and metal refining which do not allow heat loss or mixing of impurities, and (3) processes under extreme conditions such as high temperature, high vacuum and high corrosiveness where continuous systems cannot be adopted because of material restrictions or sealing technology. High pressure crystallizers, CVD reactors and/or the countercurrent regenerative heat exchangers for hot blast stoves are some of the examples of (3).

Batch systems require a production-support system including skilled workers, well trained robots or computers for feed, product discharge, shutdown and cleaning. Thus, the continuous system is undoubtedly useful in ordinary mass production processes because of longer operating times with less labour.

4.3.3.2.2 Entrained Flow/Separate Flow

In reactions with a homogeneous dispersion such as colloids or fine powders in an entrained-bed state, one flowing phase entrains the other phases. Such a system may be classified as a system of the entrained type. Phases are handled in a similar way to homogeneous flows until one fluid phase is separated at the final stage. To decompose a dispersion, coagulating agents might be applied for the colloid and filtration for an aerosol. Entrained flow reactors pose only minor hydrodynamic problems. Nevertheless, in the development and design of an entrained flow reactor, attention must always be paid to the original nature of the dispersion. If a proper reaction condition is not satisfied even at local spots in a reactor, separation and deposition may immediately take place causing some unexpected problems.

The slip between phases is common in many continuous heterogeneous systems. An extreme example is the one having a flat interface described in Section 4.3.3.1.1 which stands opposite to homogeneous suspensions. An almost continuous spectrum of heterogeneous systems exists between a completely separated system and a well dispersed entrained system.

4.3.3.2.3 Complete Mixing/Incomplete Mixing/Plug Flow

For (1) good contact of reactants with those in other phases or with catalysts, (2) uniformity in reaction temperature and (3) improvement in external heating or cooling rate, we often apply direct stirring and mixing. Although ordinary bubble columns and fluidized beds have no stirring apparatus, their continuous phase can be put into a complete mixing condition through the mixing effect of bubbling. For a continuous system, the conversion and heat exchange efficiency of a 'complete mixing system' are lower than those of a plug flow system of the same mean residence time. However, despite such a disadvantage, there are many situations where priority should be given to the above three reasons. On the other hand, batch and semi-batch systems, which have no such disadvantages, correspond to completely mixed conditions.

Here, let us briefly examine the meaning of 'complete mixing' in multiphase systems. Even in a well-stirred system, a concentration distribution may occur inside the tank when the reaction rate exceeds the mixing rate. In contrast to this, there are cases equivalent to complete mixing. Even in a flow system with recycle or circulation, the flowing phase can be practically regarded as completely mixed, if the probability of the flowing phase contacting any infinitesimally small section of the counterphase is uniform over the entire volume.

In a similar manner, the concept of 'plug flow' for multiphase systems should be slightly different from that for single phase systems. Continuously rising bubbles or droplets may be treated as phases in plug flow even though they are dispersed phases. However, once droplets or bubbles are collected at the exit, substantial mixing should take place due to the distribution of their rise velocity. But, mixing in such a dispersed phase in the reactor may not be mixing at the molecular scale but the one only in the bubble/droplet scale. This is the background of the 'mixing' issue discussed later in 4.3.3.2.6. Furthermore, we have another mixing phenomenon quite unique to

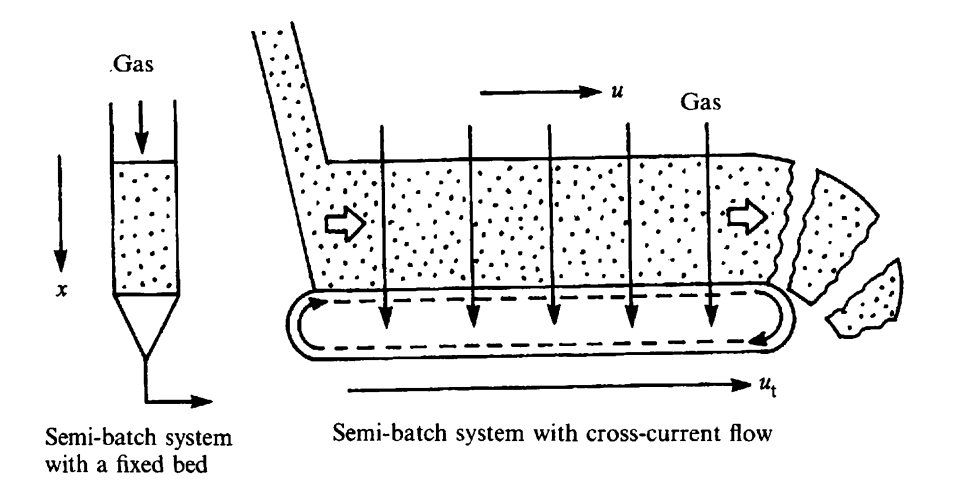


Figure 4.43 Comparison of semi-batch system with fixed bed and semi-batch system with cross-current flow.

heterogeneous systems, the one due to the exchange of material or heat with other phases, which will be discussed in 4.3.3.2.5.

4.3.3.2.4 Co-current/Countercurrent/Cross Current

The classification of co-current, counter-current and cross-current systems basically is effective in plug flow systems and not in stirred systems. Entrained flow systems, where one phase entrains another phase, occur naturally in co-current systems since otherwise it would be well mixed. Counter-current contacting is adopted intentionally in heat exchange reactors for effective use of the heat of reaction. In such a counter-current contacting system the preheating zone of one flow serves as the cooling zone of another flow. Thus, by sandwiching the reaction zone with such heat exchange zones, a process with a high heat utilization efficiency can be constructed, where only the reaction zone is placed at a high temperature.

In cross-current systems, two phases contact flowing in a right angle so that one phase is treated continuously by another in its course of horizontal or vertical movement. Examples of gas-solid cross-current systems are iron ore sintering and moving bed filtration. In iron ore sintering, the particle bed on the grate moves laterally and the gas flows downward from the top of the bed. In the moving bed filter, filtrate particles move downward by gravity between

the two guide plates with slits called louvers and the gas flows through laterally. In gas—liquid systems the cross-current contact occurs in plate columns where liquid flows laterally and gas flows upward in the form of bubbles. In solid—liquid systems there is cross-current solid—liquid extraction, i.e. leaching, where liquids sprayed over the laterally moving bed flowing down in irrigating (i.e. trickled flow) mode. If mixing in the flow direction is not strong, one-to-one correspondence can hold between an unsteady semi-batch system (a batch reactor for phase 1 as shown in Figure 4.43) and a steady cross-current system.

Now, let us analyse the above three cases. For easy understanding, assume that the following reaction takes place between two phases.

A(Phase 1: dispersed) + bB(Phase 2: continuous)

$$\rightarrow$$
 cC(Phase 1) + dD(Phase 2) (4.118)

The reaction rate here is assumed to be first order with respect to the reactant concentration of phase 2, C_{2B} [kmol/m³], with apparent reaction rate constant k which is a function of the reactant composition of phase 1, C_{1A} [kmol/m³]. Furthermore, let us use ε_1 for the volume fraction, d_1 [m] for particle size and T_1 [K] for the temperature of phase 1. We also assume that the reaction takes place at the phase interface, and the heat of reaction $(-\Delta H)$ [J/kmol] is given to phase 1. Mixing in the flow direction is supposed to be negligible (i.e. plug flow), and velocities u_1 and u_2 [m/s], and flow rates F_1 and F_2 [m³/s] are positive for upward flows. Then, the material balances for components A and B and the heat balances of phases 1 and 2, respectively can be written as:

$$A_1 \frac{\partial C_{1A}}{\partial t} + F_1 \frac{\partial C_{1A}}{\partial x} = -A_1 k C_{2B} \tag{4.119}$$

$$A_2 \frac{\partial C_{2B}}{\partial t} + F_2 \frac{\partial C_{2B}}{\partial x} = -bA_t k C_{2B} \tag{4.120}$$

$$A_{1}\rho_{1}c_{1}\frac{\partial T_{1}}{\partial t} + \rho_{1}c_{1}F_{1}\frac{\partial T_{1}}{\partial x} = A_{1}a_{12}h(T_{2} - T_{1}) + (-\Delta H)A_{1}kC_{2B}$$
 (4.121)

$$A_{2}\rho_{2}c_{2}\frac{\partial T_{2}}{\partial t} + \rho_{2}c_{2}F_{2}\frac{\partial T_{2}}{\partial x} = A_{1}a_{12}h(T_{1} - T_{2})$$
(4.122)

Here, we introduce the following dimensionless parameters:

$$\tau \equiv t/t_0$$
: dimensionless time (4.123a)

$$\xi \equiv x/L$$
: dimensionless distance (4.123b)

 $X_{ij} \equiv C_{ij}/C_{ij,in}(j: A, B)$: dimensionless concentration of component i in phase i

component
$$j$$
 in phase i (4.124)

 $\alpha_i \equiv u_i/(L/t_0)$ (i = 1,2): dimensionless velocity of

phase
$$i$$
 (non-conversion of j) (4.125)

$$K \equiv kt_0/\varepsilon_2$$
: dimensionless reaction rate constant (4.126)

$$N_1 \equiv a_{12}ht_0/(\varepsilon_1\rho_1c_1)$$
: number of heat transfer units (4.127)

$$\phi_{21} \equiv 1/\phi_{12} \equiv \varepsilon_2 C_{2\text{Bin}}/\varepsilon_1 C_{1\text{Ain}}$$
: capacity ratio (4.128a)

$$\phi_{\rm H21} \equiv 1/\phi_{\rm H12} \equiv \varepsilon_2 \rho_2 c_2/\varepsilon_1 \rho_1 c_1$$
: thermal capacity ratio (4.128b)

$$\Delta T_{\rm ad} \equiv (-\Delta H)C_{1\rm Ain}/\rho_1 c_1 \tag{4.129}$$

where t_0 is the reference time.

The adiabatic temperature rise $\Delta T_{\rm ad}$ is a virtual temperature rise in an adiabatic condition if the heat of reaction is given only to phase 1 after the reaction is completed.

Then, governing equations (4.119)–(4.122) can be made dimensionless as follows:

$$\frac{\partial X_{1A}}{\partial \tau} + \alpha_1 \frac{\partial X_{1A}}{\partial \xi} = -K\phi_{21}X_{2B} \tag{4.119'}$$

$$\frac{\partial X_{2B}}{\partial \tau} + \alpha_2 \frac{\partial X_{2B}}{\partial \xi} = -bKX_{2B} \tag{4.120'}$$

$$\frac{\partial T_1}{\partial \tau} + \alpha_1 \frac{\partial T_1}{\partial \xi} = N_1 (T_2 - T_1) + \Delta T_{ad} \phi_{21} K X_{2B}$$
 (4.121')

$$\frac{\partial T_2}{\partial \tau} + \alpha_2 \frac{\partial T_2}{\partial \xi} = N_1 \phi_{\text{H}12} (T_1 - T_2) \tag{4.122'}$$

(1) Counter-current/co-current contacting systems

For $\alpha_1 \neq 0$ and $\alpha_2 \neq 0$, the reactor shall be of continuous counter-current or co-current type among the systems in Figure 4.42. At a steady state, the governing equations reduce to the following set of ordinary differential equations:

$$\alpha_{1} \frac{dX_{1A}}{d\xi} = -K\phi_{21}X_{2B} \tag{4.130}$$

$$\alpha_2 \frac{\mathrm{d}X_{2B}}{\mathrm{d}\xi} = -bKX_{2B} \tag{4.131}$$

$$\alpha_1 \frac{dT_1}{d\xi} = N_1(T_2 - T_1) + \Delta T_{ad} \phi_{21} K X_{2B}$$
 (4.132)

$$\alpha_2 \frac{dT_2}{d\xi} = N_1 \phi_{H12} (T_1 - T_2) \tag{4.133}$$

Among the dimensionless groups specifying the system performance the following capacity flow ratios for material and heat are the dominant parameters concerning concentration and temperature profiles:

$$G_{12} \equiv (\alpha_1/\alpha_2)\phi_{12} = \varepsilon_1 C_{1Ain} u_1/\varepsilon_2 C_{2Bin} u_2$$
 (4.134)

$$G_{\rm H12} \equiv (\alpha_1/\alpha_2)\phi_{\rm H12} = \epsilon_1 \rho_1 c_1 u_1/\epsilon_2 \rho_1 c_2 u_2$$
 (4.135)

From Eqs. (4.130)–(4.133) the following relations hold between X_1 and X_2 , and T_1 and T_2 :

$$G_{12}\frac{\mathrm{d}X_{1A}}{\mathrm{d}X_{2B}} = 1/b \tag{4.136}$$

$$G_{\rm H12} \frac{dT_1}{dT_2} = -1 + \frac{\Delta T_{\rm ad} \phi_{21} K X_{2B}}{T_1 - T_2}$$
 (4.137)

 $|G_{\rm H12}|$ is the thermal capacity flow ratio which specifies the shape of the temperature profile in the heat exchange reactor. $G_{\rm H12}>0$ represents cocurrent flow, and $G_{\rm H12}<0$ represents counter-current. If $G_{\rm H12}=-1$ and K=0 (no reaction), ${\rm d}T_1/{\rm d}T_2$ becomes unity from Eq. (4.137), i.e. the temperature profiles become linear.

Figure 4.44 shows examples of temperature and concentration profiles in cocurrent and counter-current moving beds. The co-current system requires preheating to a temperature above the ignition temperature so that the reaction rate becomes appreciable. Processes of high thermal economy can be realized only with a counter-current system.

Figure 4.45 shows the inlet temperature of phase 1 (particles) T_{11} as a function of the particle outlet temperature T_{10} . T_{11} was predicted by integrating the equation of a counter-current moving bed, Eqs (4.130)–(4.133), for assumed T_{10} . Three types of steady states emerge depending on the relative intensity of heat-exchange (N), the temperature dependency of the reaction rate (K) and the inlet temperature of phase 1 (see Figure 4.45(d)). An intermediate steady state solution corresponds to an unstable steady state, in which gas (phase 2) is cooled down halfway through the reaction because of the

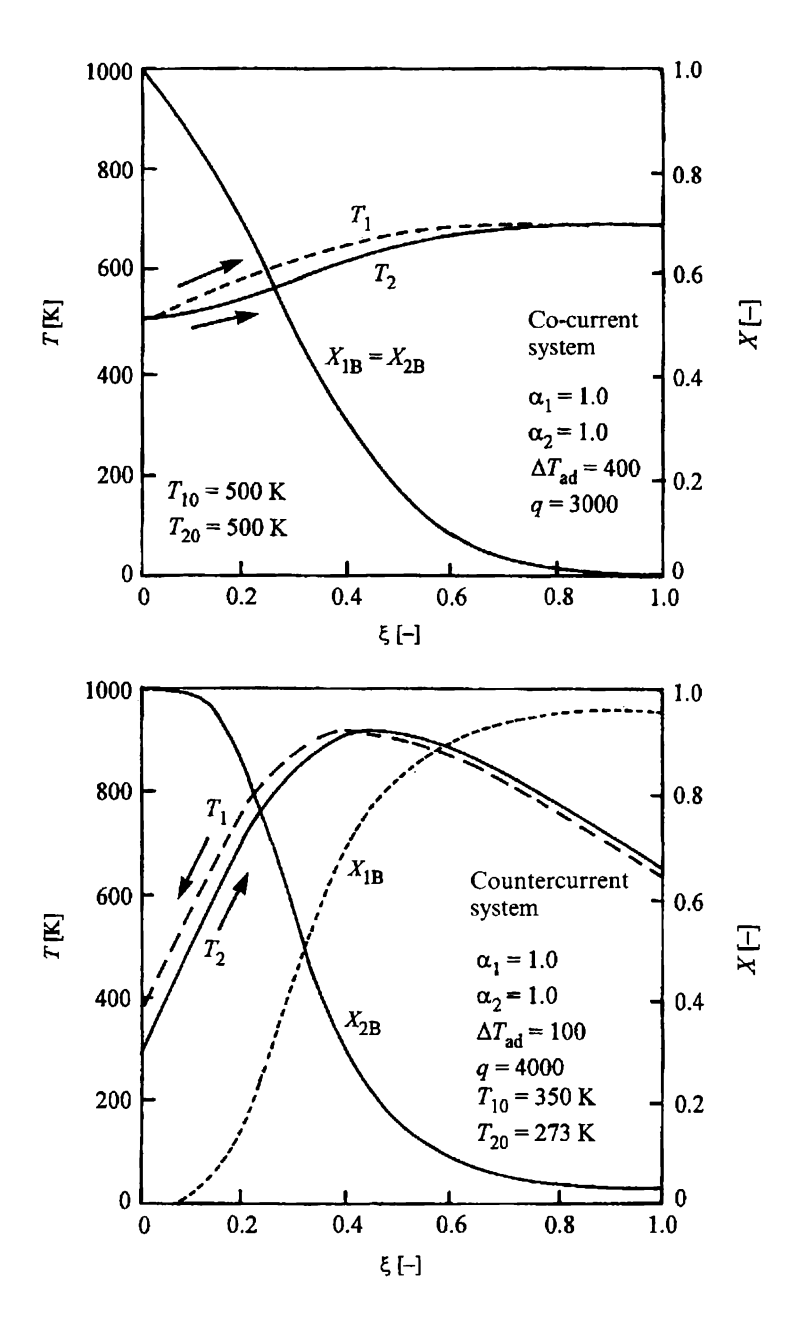


Figure 4.44 Temperature profiles for co-current and countercurrent systems. $\phi_{21} = 1.0, b = 1.0, N_1 = 30.0, \phi_{H12} = 1.0, K_0 = 500.0.$

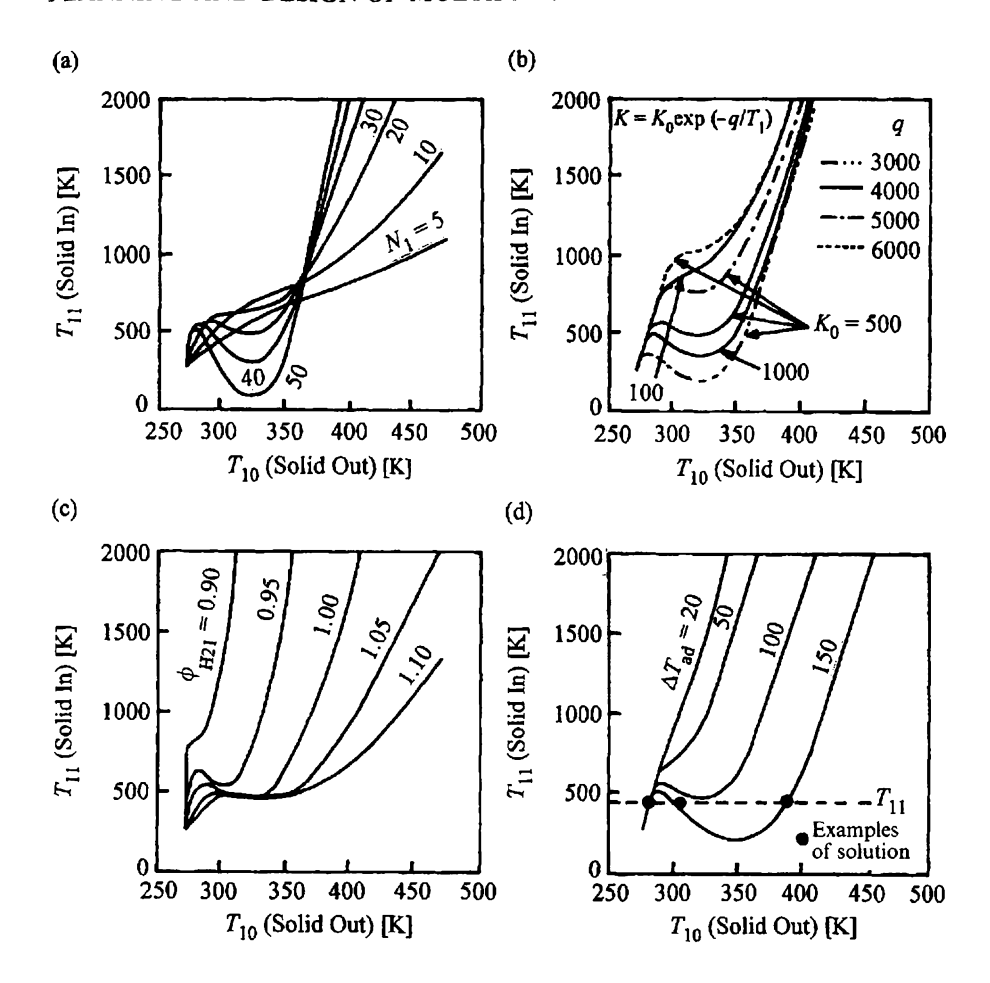


Figure 4.45 The inlet temperature T_{11} predicted by integrating the equation for a cocurrent moving bed, Eqs (4.130)–(4.133), for the assumed outlet temperature of phase 1 (particles) T_{10} at the inlet of phase 2 (gas)⁽³⁰⁾. Parameters not designated above: $\phi_{\text{H}12} = 1$, $N_1 = 30$, q = 4000, b = 1, ΔT_{ad} , $\phi_{12} = 1$, $K_0 = 500$.

insufficient preheating of the particles. Since the reaction is suspended in this way, it can be either re-ignited with a small positive disturbance in temperature or completely quenched by a negative disturbance. Such a steady state cannot be maintained, as confirmed by transient calculations. In any case, a unique heat exchange process can be realized by a moving bed.

(2) Semi-batch/cross-current contacting

As a special case of Eqs (4.118)–(4.121) we have a semi-batch or cross-current contacting system illustrated in Figure 4.43. If we adopt a coordinate system that

moves along with phase 1 in cross-current contact, the horizontal position of phase I corresponds to the time t that has passed since phase I entered the system. Therefore, a cross-current system is equivalent to the unsteady operation of a semi-batch system. Accordingly, the second term on the left hand side of Eqs (4.119) and (4.121) for phase I can be neglected. Now if phase 2 is gas, the density is so small that the time delay due to its passage is negligible compared with the timescale of changes in phase I and a pseudo-steady state can be approximated for phase 2. Then, the governing equations can be reduced to

$$\frac{\partial X_{1A}}{\partial \tau} = -K\phi_{21}X_{2B} \tag{4.138}$$

$$\frac{\partial X_{2B}}{\partial \xi} = -b(K/\alpha_2)X_{2B} \tag{4.139}$$

$$\frac{\partial T_1}{\partial \tau} = N_1(T_2 - T_1) + \Delta T_{ad} \phi_{21} K X_{2B}$$
 (4.140)

$$\frac{\partial T_2}{\partial \xi} = (N_1 \phi_{\text{H}_{12}} / \alpha_2) (T_2 - T_1) \tag{4.141}$$

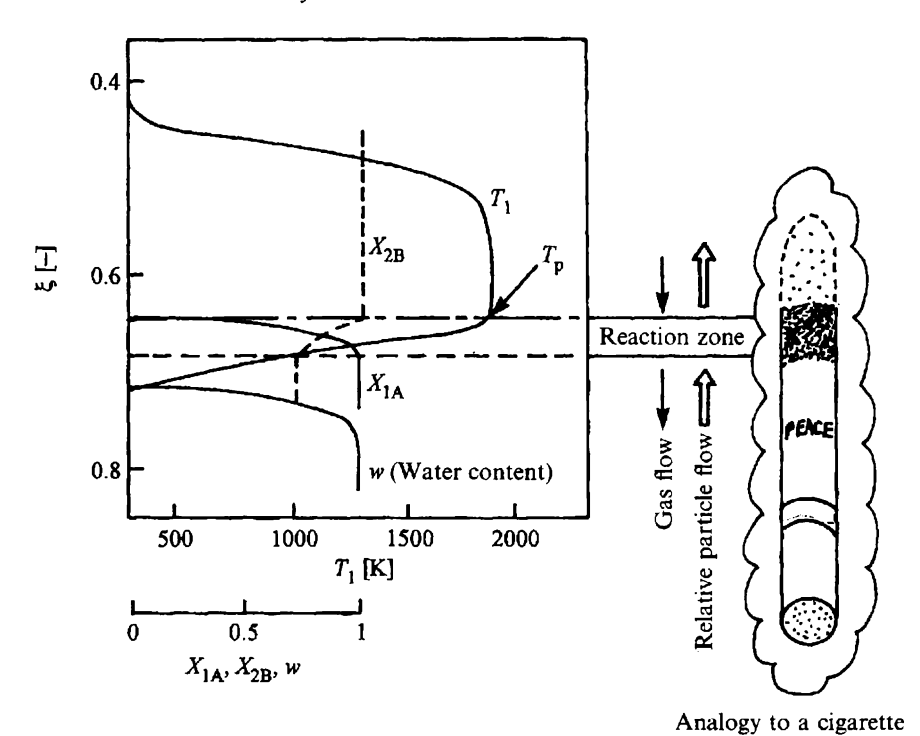


Figure 4.46 Formation and progress of reaction zone at semi-batch/cross-current contacting operation⁽³¹⁾.

In a semi-batch or cross-current contactor for exothermic reactions a reaction zone and a high-temperature isothermal zone or a thermal plateau are formed. These zones in phase 1 move toward the flow direction of phase 2. The moving hot spot of a cigarette practically creates a counter-current system as shown in Figure 4.46. Assuming that the velocity of the moving reaction zone is u_a , we obtain the following equation from the heat balance around the reaction zone between two isothermal zones:

$$u_{a}\varepsilon_{1}c_{1p}\rho_{1}T_{p} + (u_{2} - u_{a})\varepsilon_{2}c_{2}\rho_{2}T_{0} + u_{a}C_{1Ain}(-\Delta H)$$

$$= u_{a}\varepsilon_{1}c_{1}\rho_{1}T_{0} + (u_{2} - u_{a})\varepsilon_{2}c_{2p}\rho_{2}T_{p}$$
(4.142)

where T_p is the peak or plateau temperature, and c_{ip} is the specific heat of phase i for $T_i = T_p$. Arranging the above equation with respect to u_a using Eqs (4.128) and (4.129), we have

$$\frac{u_{\rm a}}{u_2\phi_{\rm H21}} = \frac{(c_{\rm 2p}/c_2)\,T_{\rm p} - T_0}{\phi_{\rm H21}[(c_{\rm 2p}/c_2)\,T_{\rm p} - T_0] + (c_{\rm 1p}/c_1)\,T_{\rm p} - T_0 + \Delta T_{\rm ad}} \tag{4.142'}$$

For isothermal reactions, since a reaction zone is moving at a velocity of u_a placed between unreacted and reacted zones, we can write

$$u_a \varepsilon_1 C_{1A} = (u_2 - u_a) \varepsilon_2 C_{2B} \tag{4.143}$$

Arranging this with respect to u_a and using Eq. (4.128a), we have

$$\frac{u_{\rm a}}{u_2\phi_{21}} = \frac{1}{1+\phi_{21}} \tag{4.143'}$$

In both cases, the moving velocity of the reaction zone is given by a simple function of the velocity of the flowing phase (phase 2) u_2 and the capacity ratio ϕ_{21} . When an exothermic reaction takes place in a bed of a sufficient height, the maximum temperature of the moving reaction zone always remains almost constant, and only the thickness of the temperature plateau increases with time as shown in Figure 4.47. With a fixed bed or a cross-current moving bed, high temperatures can easily be attained from exothermic reactions. However, in catalyst regeneration in cracking processes or sorbent regeneration in high-temperature dry desulphurization, micropores may be damaged in the hot spot by sintering. The maximum temperature must be controlled by regulating the reactant concentration of gas. In summary, a cross-current or semi-batch configuration can be adopted to design processes with good thermal economy and a well controlled maximum temperature.

4.3.3.2.5 Uniform Reactions/Zone Reactions/Surface Reactions

(1) Formation of the reaction zone in a reactor As described in Section 4.3.3.2.4, reactions do not always take place uniformly

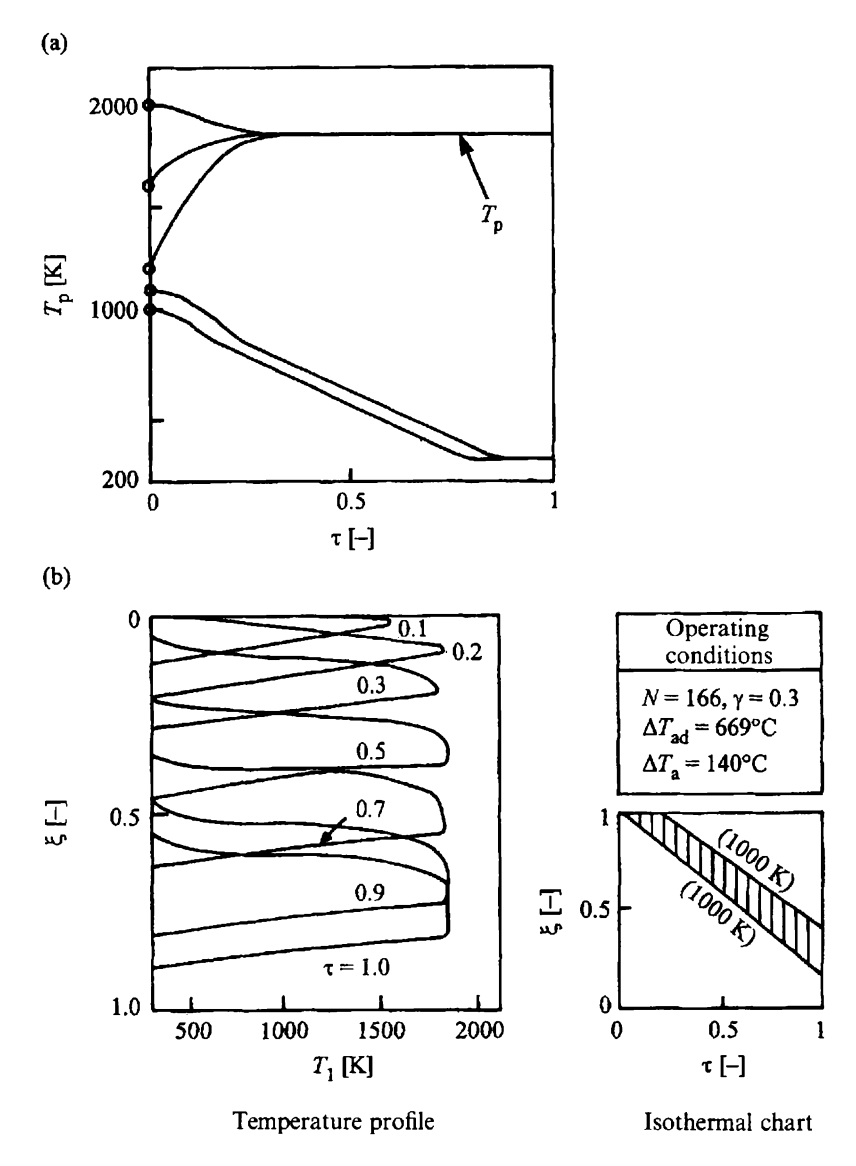
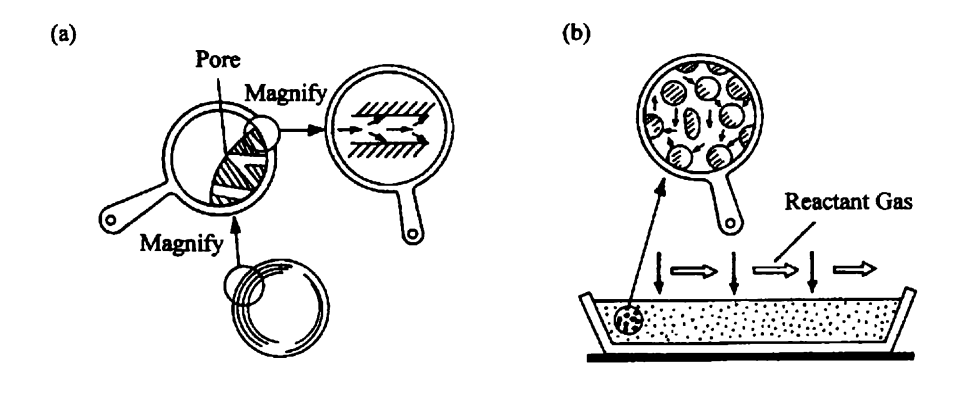


Figure 4.47 Stabilities of exothermic solid reaction in a fixed bed⁽³¹⁾. (a) Changes of various initial temperatures with time. (b) An example of the moving temperature profile.

throughout a reactor. Accordingly, it is important to distinguish zone reactions from uniform reactions. The concept of heat exchange reactors described above is intended for zone reactions by forming a reaction zone utilizing temperature distribution. Its typical examples include self-heat exchange



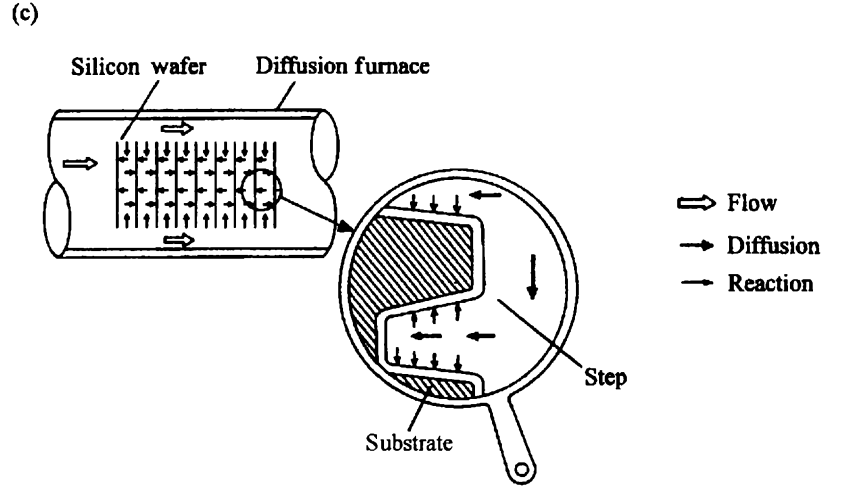


Figure 4.48 Systems of parallel diffusion and reaction. (a) Catalyst pellet, solid reaction particles. (b) Fixed bed with no flow. (c) Chemical vapour deposition.

reactors for ammonia synthesis, counter-current and cross-current moving beds, e.g. blast furnaces for iron production and iron ore sintering machines, respectively. We can also name the chromato-reactor which utilizes the difference of adsorption and desorption rates, the zone melting process in smelting, diffusion flame and multi-stage aeration for low NO_x burners.

(2) Systems of diffusion and reaction in parallel

Examples of parallel reaction and diffusion systems in solid—gas reactions are shown in Figure 4.48. In these systems, reactions proceed either uniformly or locally, forming zones depending on the balance between reaction and

diffusion rates. In such a diffusion field the following equation can be written for concentration C of a component in gas, where n = 1 for a slab, n = 2 for a cylinder, and n = 3 for a sphere.

$$\varepsilon \left(\frac{\partial C}{\partial t}\right) = \left(\frac{1}{r^{n-1}}\right) \left(\frac{\partial}{\partial r} r^{n-1} D_{e} \left(\frac{\partial C}{\partial r}\right)\right) + R_{v}$$
 (4.144)

The boundary conditions are

$$C = C_0 \text{ at } x = x_l$$
 (4.145)

$$\partial C/\partial x = 0$$
 at $x = 0$ (4.146)

where ε is the porosity, D_e is the effective diffusivity, and R_v is the generation rate of the component of interest per unit volume of the porous material.

In solid-gas reactions the solid-to-gas density ratio is roughly a thousand and, moreover, gas molecules are moving at quite a high velocity. Accordingly, the time for significant changes in composition or structure of the solid phase is much longer than the relaxation time of the gas phase concentration profiles, i.e. the time to recover a steady state after a disturbance has occurred. Thus, the unsteady term on the left hand side of Eq. (4.144) can be neglected. Thus, the ordinary differential equation for a pseudo-steady state is sufficient for describing the system.

The reaction rate is dependent both on the composition of the gas and the structure of the solid phase. However, in most cases, the latter can be assumed uniform in the early stage of reaction. Assuming such a situation, let us consider a 'volume reaction' where reaction rate per unit volume of the porous material is proportional to the reactant concentration similar to first order irreversible catalytic reactions. Then,

$$R_{\rm v} = -k_{\rm v}C\tag{4.147}$$

Solutions for a slab and a sphere are

$$C/C_0 = \begin{cases} \frac{\cosh m\xi}{\cosh m} & \text{(slab)} \\ \frac{\sinh m\xi}{\xi \sinh m} & \text{(sphere)} \end{cases}$$
 (4.148a)

where the Thiele number m and dimensionless coordinate ξ are defined as

$$m = (k_{\rm v}/D_{\rm e})^{1/2}l_0 \tag{4.149}$$

$$\xi = x/l_0 \tag{4.150}$$

Integration of the reactant concentration thus obtained, multiplied by k_v , over the volume of porous material gives the total reaction rate. The ratio of

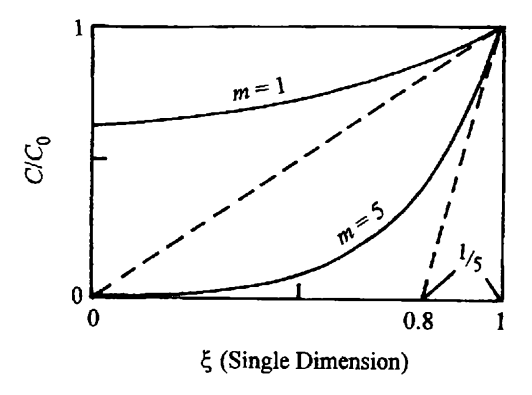


Figure 4.49 Concentration profile of reactant gas in the porous material.

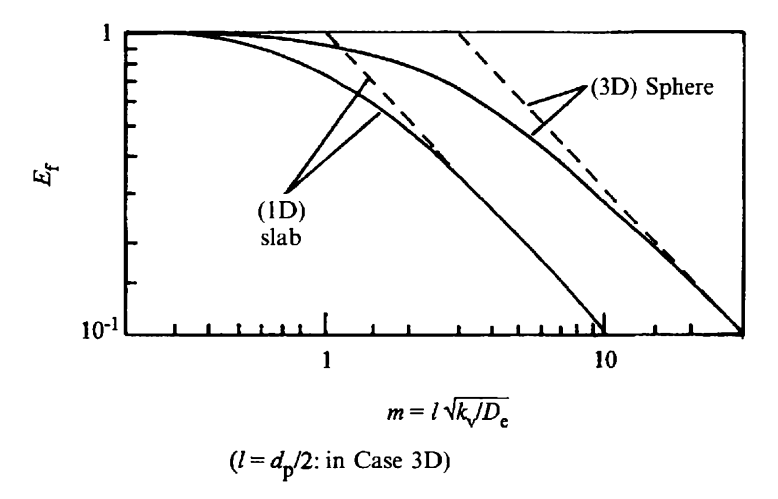


Figure 4.50 Effective numbers with Thiele numbers.

the total reaction rate to the fictitious rate for $C(\xi) = C_0$ gives the effectiveness factor E_f . E_f indicates how efficiently the volume of the porous material is utilized for the reaction.

Then.

$$E_{\rm f} = \begin{cases} \frac{1}{m} \tanh m & \text{(slab)} \\ \frac{3}{m} \left(\frac{1}{\tanh m} - \frac{1}{m} \right) & \text{(sphere)} \end{cases}$$
 (4.151a)

Figures 4.49 and 4.50 show the concentration profile of the gas in the porous material and effectiveness factors as a function of Thiele number, respectively.

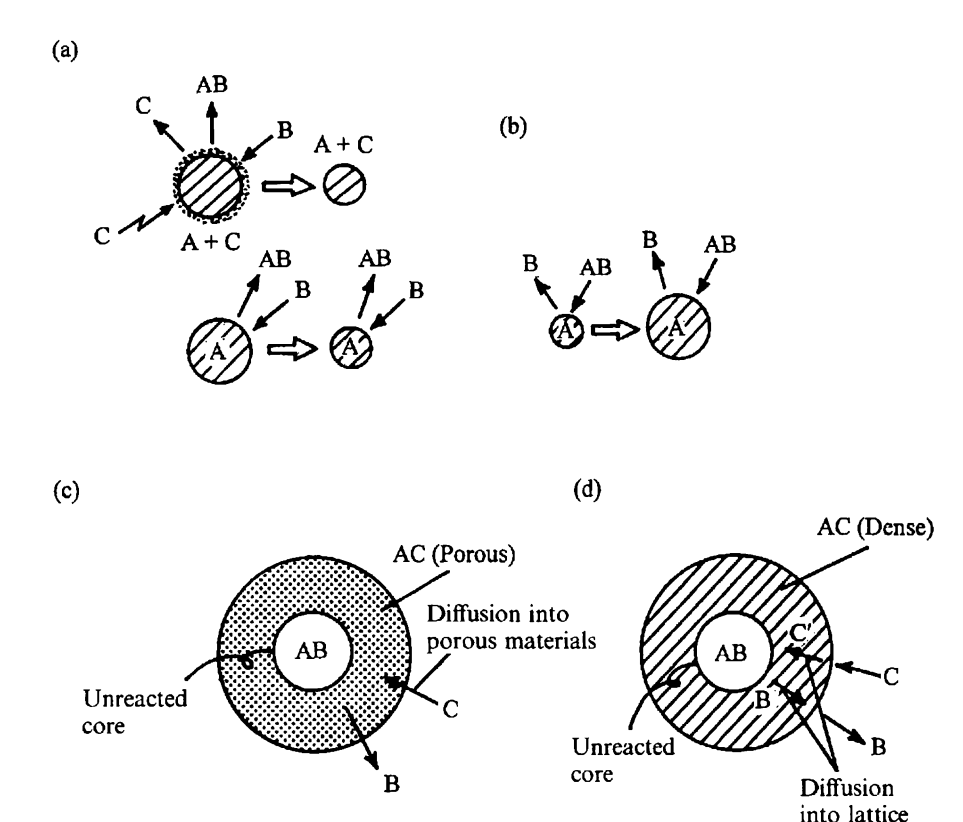


Figure 4.51 Surface reaction systems. (a) Reactions with no product layer (combustion, chlorination). (b) Reactions forming dense product solid (various CVD). (c) Reactions with a porous product layer. (d) Reactions with a dense product layer.

A rule of thumb understanding is that for a slab the reactant gas can diffuse roughly the dimensionless depth of 1/m (when m > 1) from the external surface. Only 1/m of the whole volume of the porous material is then utilized. For a sphere 3/m (when m > 3) is utilized effectively.

In process handling of adhesive particles, we often have static operations with no gas percolation. Then, the concept of effectiveness factor can be also applied to a 'bed' of particles because gas penetrates only by diffusion into the bed. In such cases, m, and accordingly the bed thickness l can be determined to achieve $E_{\rm f}=1$.

(3) Systems of diffusion and reaction in series

When m is extremely large for a reaction field of porous material, the thickness of the reaction zone becomes so thin that the reaction takes place at the

interface or boundary between the reactant phase and product phase in the solid.

Since, in such a case, the reaction takes place after gaseous reactants are transported to the reaction interface by diffusion, a system of 'diffusion and reaction in series' or a 'surface reaction system' is obtained. As shown in Figure 4.51, there are a variety of surface reaction systems depending on solid shapes i.e. sphere, cylinder, flat plane etc. and on conditions of the product layer as discussed in the following (a), (b) and (c):

(a) Reactions with no product layer, i.e. solid consuming reactions: rapid gasification reactions such as combustion and chlorination or reactions of the peeling product layer, and reactions forming dense solid products such as CVD reactions.

In this case diffusion in the outer shell need not be considered. A kinetic description of the reaction is then possible taking into account the resistances of the surface reaction and film diffusion in series. Here, since both rates of surface reaction and film diffusion are equal in a pseudo-steady state, for a spherical particle we write

$$R^* = \pi d_p^2 k_s C_p (4.152)$$

$$= \pi d_{\rm p}^2 k_{\rm f} (C_{\infty} - C_{\rm p}) \tag{4.153}$$

where R^* [kmol/s] is the reaction rate per particle, d_p is the particle diameter, k_s is the surface reaction rate constant [m/s], k_f is the mass transfer coefficient [m/s], C_p is the concentration of the gas phase reactant at the external surface of the particle [kmol/m³], and C_∞ is the concentration of the gas phase reactant in the bulk [kmol/m³]. Then, from the above two expressions the following expressions can be derived for the overall reaction rate:

$$R^* = \pi d_p^2 \bar{k} C_\infty \tag{4.154}$$

$$\bar{k} = \frac{1}{1/k_{\rm s} + 1/k_{\rm f}} \tag{4.155}$$

If particles are placed in a slowly flowing gas phase, k_f is inversely proportional to d_p since the Sherwood number Sh equals 2. Then,

$$k_{\rm f} = 2D/d_{\rm p} \tag{4.156}$$

Since R^* can be expressed in terms of the rate of the particle volume change,

$$R^* = \frac{(-1)^i \rho_p X_i}{2M_i} \pi d_p^2 \frac{dd_p}{dt}$$
 (4.157)

In the above expressions, let i = 1, $M_i = \text{molecular weight of solid reactants}$ [kg/kmol] and $X_1 = \text{mass fraction of solid reactants in solids for a solid consuming reaction. For a solid deposition reaction, let <math>i = 2$, $M_2 = \text{molecular}$

weight of solid product and $X_2 = 1$. ρ_p is the density of either reactant or product solid.

Equating Eqs (4.154) and (4.157) and substituting Eq. (4.156) into it we have

$$\frac{dd_{p}}{dt} = \frac{2M_{i}}{(-1)^{i}\rho_{p}X_{i}} \cdot \frac{C_{\infty}}{1/k_{s} + d_{p}/2D}$$
(4.158)

Then, integrating it under the initial conditions $d_p = d_{p0}$ at t = 0

$$\left(\frac{1}{k_{\rm s}} + \frac{d_{\rm p}}{4D}\right) d_{\rm p} - \left(\frac{1}{k_{\rm s}} - \frac{d_{\rm p0}}{4D}\right) d_{\rm p0} = \frac{2M_i C_{\infty}}{(-1)^i \rho_{\rm p} X_i} t \tag{4.159}$$

Thus, in a solid consuming reaction (i = 1), the time for complete reaction t_c can be obtained as

$$t_{\rm c} = \frac{\rho_{\rm p} X_1 d_{\rm p0}}{2M_1 C_{\infty}} \left(\frac{1}{k_{\rm s}} + \frac{d_{\rm p0}}{4D} \right) \tag{4.160}$$

The dependency of t_c on the initial particle size is different for the two extreme cases shown in the following:

$$t_{\rm c} = \begin{cases} (\rho_{\rm p} X_1/2M_1k_{\rm s}) d_{\rm p0} & \text{(chemical reaction control: CRC)} \\ (\rho_{\rm p} X_1/8DM_1) d_{\rm p0}^2 & \text{(film diffusion control: FDC)} \end{cases}$$
(4.161a)

Reactions of coarse particles are controlled by film diffusion in many cases. However, the smaller the particle size, the larger becomes $k_{\rm f}=2D/d_{\rm p}$ and the system gets closer to chemical reaction control. If the particle size becomes even smaller, the Thiele number also becomes smaller and the mode of reaction shifts from surface reaction to volume reaction. This is why it has been said that the combustion of solids starting in the surface reaction mode ends in the volume reaction mode.

In the above analysis, we have been concerned with a single particle. For multi-particle systems a population balance discussed in Section 4.3.2.2 is applied with Eq. (4.158) for the kinetic expression Eq. (4.76).

(b) Reactions with a porous product layer.

If the product phase is a porous solid, gas phase reactants and by-products move through the porous product layer by diffusion. For spherical particles the rate of reactant diffusion in particles R^* can be expressed by Fick's diffusion law as follows:

$$R^* = 4\pi r^2 D_e \frac{\mathrm{d}C}{\mathrm{d}r} \tag{4.162}$$

where C and D_e are the reactant concentration in the gas phase in pores and the effective intra-particle diffusivity, respectively. In a pseudo-steady state R^* is

constant at any radial location r, and the above expression can be integrated from the reaction interface $r = d_s/2$, where $C = C_s$ to the outer surface $r = d_p/2$, where $C = C_{p-}$. Then, rearranging the expression with respect to R^* , we obtain

$$R^* = \frac{\pi d_p^2 (2D_e/d_p)}{(d_p/d_s) - 1} (C_{p-} - C_s)$$
 (4.163)

where d_s is the diameter of the unreacted core and $C_{\rm p-}$ is the reactant concentration in particles at $r=d_{\rm p}/2_0$ just inside the particle surface. For porous materials, $C_{\rm p-}$ coincides with the concentration at the outer surface $C_{\rm p-}$ Rates of surface reaction and film diffusion, can be treated as in case (a) and

$$R^* = \pi d_s^2 k_s C_s \tag{4.164}$$

$$= \pi d_{\rm s}^2 k_{\rm f} (C_{\infty} - C_{\rm p}) \tag{4.165}$$

Eliminating the unknowns C_s and $C_p = C_{p-}$ in Eqs (4.163)–(4.165), and considering the unreacted core shrinking rate similar to Eq. (4.157), we obtain the following overall reaction rate:

$$R^* = -\frac{\rho_{\rm p} X_1 \pi d_{\rm s}^2 d_p}{2M_1} \cdot \frac{\mathrm{d}(d_{\rm s}/d_{\rm p})}{\mathrm{d}t} = \frac{\pi d_{\rm p}^2 C_{\infty}}{\frac{1}{k_{\rm s}} \left(\frac{d_{\rm p}}{d_{\rm s}}\right)^2 + \left(\frac{d_{\rm p}}{2D_{\rm e}}\right) \left(\frac{d_{\rm p}}{d_{\rm s}} - 1\right) + \frac{1}{k_{\rm f}}}$$
(4.166)

If the particle diameter d_p does not change during reaction, it is easy to integrate the above expression within the range of t = 0 to t under the initial condition of $d_s = 0$ at t = 0. First, let us integrate Eq. (4.166) as

$$\int_{d_{s}/d_{p}}^{1} \left[\frac{1}{k_{s}} + \frac{d_{p}}{2D_{e}} \left(\left(\frac{d_{s}}{d_{p}} \right) - \left(\frac{d_{s}}{d_{p}} \right)^{2} \right) + \frac{1}{k_{f}} \left(\frac{d_{s}}{d_{p}} \right)^{2} \right] d\left(\frac{d_{s}}{d_{p}} \right) = \int_{0}^{t} \frac{2M_{1}C_{\infty}}{\rho_{p}X_{1}d_{p}} dt \quad (4.166')$$

Then, conducting the above integration, we obtain

$$\left[\frac{1}{k_{s}} + \frac{d_{p}}{2D_{e}} \left\{ \frac{1}{2} - \frac{1}{3} \left(\frac{d_{s}}{d_{p}} \right) \right\} \left(\frac{d_{s}}{d_{p}} \right) + \frac{1}{3k_{f}} \left(\frac{d_{s}}{d_{p}} \right)^{2} \right] \left(\frac{d_{s}}{d_{p}} \right) \\
= \left[\frac{1}{k_{s}} + \frac{d_{p}}{12D_{e}} + \frac{1}{3k_{f}} \right] - \frac{2M_{1}C_{\infty}}{\rho_{p}X_{1}d_{p}} t \tag{4.167}$$

Thus, the time for a complete reaction t_c is given as follows (to derive it substitute $d_s/d_p = 0$ into the above equation):

$$t_{\rm c} = \frac{\rho_{\rm p} X_1 d_{\rm p}}{2M_1 C_{\infty}} \left[\frac{1}{k_{\rm s}} + \frac{d_{\rm p}}{12D_{\rm e}} + \frac{1}{3k_{\rm f}} \right]$$
(4.168)

If D_e and k_f are sufficiently large, it is natural that the above expression is identical with Eq. (4.160) of case (a). The effective diffusivity D_e is expressed by

$$D_{\rm e} = \frac{\varepsilon}{\tau} \frac{1}{1/D + 1/D_{\rm K}} \tag{4.169}$$

where D is diffusivity in the gas phase, D_K is the Knudsen diffusivity, ε is the porosity, and τ is the tortuosity factor of the pores. τ is a function of $\varepsilon^{(32)}$ larger than unity and varying material by material. Therefore, in many cases we are forced to determine τ from the experimentally determined D_{ε} .

(c) Reactions with a dense solid product layer, i.e. inorganic reactions: metal oxidation and carbonization, nitriding, sulphidation and sulphation of metal oxides.

In these cases, the rate processes are basically in the same scheme as those in the above case (b). In the solid phase, however, reactants supplied from the gas phase diffuse as atoms or ions that substitute the lattice in the solid (Schottky diffusion) or that enter the free space in the lattice (Frenkel diffusion). Here, the concentrations, diffusivities and reaction rate constants of diffusing species are marked with *. As before, the following rate expressions can be written for the surface reaction, solid state diffusion and film diffusion:

$$R^* \equiv -\frac{\rho_p X_1 \pi d_s^2}{2M_1} \frac{dd_s}{dt}$$

= $\pi d_s^2 k_s^* C_s^*$ (4.170)

$$= \frac{\pi d_{\rm p}^2 (2D^*/d_{\rm p})}{(d_{\rm p}/d_{\rm s}) - 1} (C_{\rm p}^* - C_{\rm s}^*)$$
 (4.171)

$$= \pi d_{\rm p}^2 k_{\rm f} (C_{\infty} - C_{\rm p}) \tag{4.172}$$

At the particle surface $r = d_p/2$, the following equilibrium relation is assumed, in which K is the equilibrium constant:

$$C_{\rm p}^* = KC_{\rm p} \tag{4.173}$$

Replacing k_s by k_s^*K and D_e by D^*K in Eqs (4.166)–(4.168), we have the overall reaction rate expression, its integral expression and the time for complete reaction for those reactions forming a dense product layer, as

$$-\frac{\rho_{p}X_{1}\pi d_{s}^{2}}{2M_{1}} \cdot \frac{dd_{s}}{dt} = \frac{d_{p}^{2}\pi C_{\infty}}{\frac{1}{k_{s}^{*}K} \left(\frac{d_{p}}{d_{s}}\right)^{2} + \left(\frac{d_{p}}{2D^{*}K}\right) \left(\frac{d_{p}}{d_{s}} - 1\right) + \frac{1}{k_{f}}}$$

$$\left[\frac{1}{k_s^* K} + \frac{d_p}{2D^* K} \left\{ \frac{1}{2} - \frac{1}{3} \left(\frac{d_s}{d_p}\right) \right\} \left(\frac{d_s}{d_p}\right) + \frac{1}{3k_f} \left(\frac{d_s}{d_p}\right)^2 \right] \left(\frac{d_s}{d_p}\right)$$
(4.174)

$$= \left[\frac{1}{k_s^* K} + \frac{1}{12D^* K} + \frac{1}{3k_f} \right] - \frac{2M_1 C_\infty}{\rho_p X_1 D_p} t \tag{4.175}$$

$$t_{\rm c} = \frac{\rho_{\rm p} X_1 d_{\rm p}}{2M_1 C_{\infty}} \left[\frac{1}{k_{\rm s}^* K} + \frac{d_{\rm p}}{12D^* K} + \frac{1}{3k_{\rm f}} \right]$$
(4.176)

It is now obvious that cases (b) and (c) have similar mathematics. The particle conversion η_s in a shrinking core reaction is related to the core diameter d_s by

$$1 - \eta_{\rm s} = (d_{\rm s}/d_{\rm p})^3 \tag{4.177}$$

To determine the kinetic parameters of these systems one should conduct thermogravimetric analysis or chemical analysis by sampling particles at different η_s vs. time relationships but adjusting the gas velocity so that k_f becomes sufficiently large the gas film resistance may be neglected.

Eq. (4.166) or Eq. (4.174) with negligible $1/k_f$ leads to

$$\frac{6M_1C_{\infty}}{\rho_p X_1 d_p} \cdot \frac{(1 - \eta_s)^{2/3}}{(d\eta_s/dt)} = \frac{1}{k_s} + \frac{d_p}{2D_e} \left[1 - (1 - \eta_s)^{1/3} \right] (1 - \eta_s)^{1/3}$$
(4.178)

Based on the above expression, data can be analysed by the mixed resistance plot as shown in Figure 4.52. From this k_s and D_e can be determined simultaneously. However, since Figure 4.52 is based on the time derivative of the conversion data, it is recommended to confirm that the validity of the parameters thus determined by checking the integrated conversion-time curve.

The above discussion applies to first-order irreversible reactions. For reversible reactions or for reactions with the hindering effect of adsorbed products, just replace C_{∞} with the difference from equilibrium composition $(C_{\infty} - C_{\infty,eq})$ or with

$$(C_{\infty} - C_{\infty, eq})/(1 + K_{\mathsf{A}}P_{\mathsf{A}} + K_{\mathsf{B}}P_{\mathsf{B}})$$

where K_A and K_B are adsorption equilibrium constants and P_A and P_B are partial pressures of reactant and product, respectively.

(4) Systems of grain aggregates (intermediate systems between (2) and (3)) In realistic situations we find many solids having a fractal structure, which can

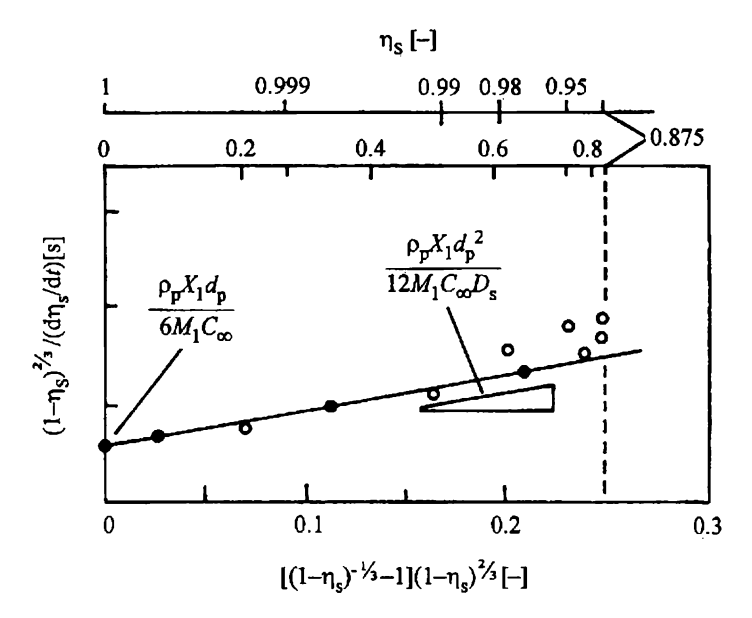


Figure 4.52 k_s and D_c can be determined at the same time by composite rate control plot.

be classified as an intermediate system between (2) and (3). For instance, coarse particles often contain micro particles which are usually called grains as shown in Figure 4.53. Thus, even if the reaction for a whole coarse particle is volumetric, it may actually be a surface reaction for grains. This picture applies to the powder bed with stagnant gas phase and/or porous particles containing polycrystallite. In such cases, kinetic parameters can be determined by the following procedures:

(a) Determination of kinetic parameters for grains

For particles pulverized approximately to the grain diameter, determine $D_{\rm e}$ and $k_{\rm s}$ or D^*K and $k_{\rm s}^*K$, and other necessary variables using the method described above in case (3). Let us distinguish such grain parameters by adding the subscript G, like $D_{\rm G}$, $k_{\rm sG}$, $\rho_{\rm pG}$, $\varepsilon_{\rm G}$, $X_{\rm G}$ and $d_{\rm pG}$. Thus, the reaction rate per one single grain shall be written as $R_{\rm G}^*$.

- (b) Determination of kinetic parameters for grain aggregates For grain aggregates (coarse particles, grain agglomerates or packed beds), obtain the porosity or void fraction ε , and effective diffusivity $D_{\rm e}$.
- (c) Prediction of the reaction rate of grain aggregates
 On the basis of the parameters introduced above, let us derive the reaction rate

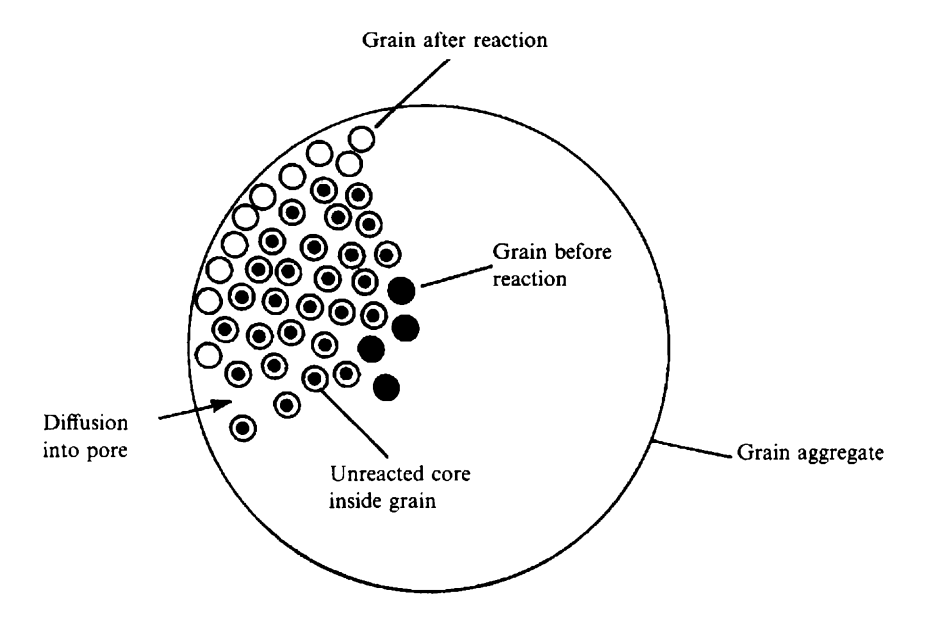


Figure 4.53 System of grain aggregates.

per unit volume of a grain aggregate R_v using the rate per grain R_G^* . The particle number per unit volume is given by dividing the particle volume fraction $(1 - \varepsilon)$ by the volume of one particle, thus

$$R_{\rm v} = \frac{1 - \varepsilon}{\frac{\pi}{6} d_{\rm pG}^3} \cdot R_{\rm G}^* \tag{4.179}$$

$$\therefore R_{v} = \frac{\left(\frac{6}{d_{pG}}\right)(1-\varepsilon)C}{\frac{1}{k_{sG}(1-\eta_{s})^{2/3}} + \left(\frac{d_{pG}}{2D_{G}}\right)\left(\frac{1}{(1-\eta_{s})^{1/3}} - 1\right)}$$
(4.180)

The equation for the gas concentration C(r, t), the pseudo-steady state version of Eq. (4.144), is written as:

$$\left(\frac{1}{r^{n-1}}\right)\left(\frac{\partial}{\partial r}\,r^{n-1}D_{\rm e}\left(\frac{\partial C}{\partial r}\right)\right) + R_{\rm v} = 0 \tag{4.181}$$
(flat plate: $n = 1$, cylinder: $n = 2$, sphere: $n = 3$)

The equation for the solid conversion $\eta_s(r, t)$ can be written as:

$$\frac{\partial \eta_{\rm s}}{\partial t} = \frac{M_1}{2\rho_{\rm pG}X_{\rm lG}(1-\varepsilon)} R_{\rm v} \tag{4.182}$$

Initial condition: $\eta_s = 0$ at t = 0

Boundary condition: $C = C_{\infty}$ at r = 1 (film resistance is assumed to be negligible)

For the initial reaction rate the following can be substituted into Eq. (4.181):

$$R_{\rm v} = \frac{6(1-\varepsilon)}{d_{\rm pG}} k_{\rm sG} C$$
 at $t = 0$ (4.183)

The apparent volume reaction rate constant k_v can be related to the surface rate constant k_{sG} for a grain by

$$k_{\rm v} = \frac{6(1-\varepsilon)}{d_{\rm pG}} k_{\rm sG} \tag{4.184}$$

On the other hand, the overall initial reaction rate $R_{v,t=0}$ can be written as follows with the effectiveness factor E_f :

$$\bar{R}_{v,t=0} = k_v E_f C_{\infty} \tag{4.185}$$

$$E_f = f(m)$$
 (see Eq. (4.151)) (4.186)

$$m \equiv \sqrt{\frac{k_{\rm v}}{D_{\rm e}}} l$$
 (see Eq. (4.149)) (4.187)

To determine k_G from the initial reaction rate $R_{v,t=0}$, we first determine k_v by an iteration for E_f , i.e. by calculating E_f from Eqs (4.186) and (4.187) from an assumed value of k_v until it converges.

4.3.3.2.6 Micro Mixing/Macro Mixing, and Molecular Diffusion/Eddy Diffusion

When collision, splitting or coalescence occurs frequently among particles in dispersed phases, it can be assumed that the mixing in the dispersed phase would reach the molecular level, i.e. the micro mixing condition. For powder and granular materials however, their mixture can never reach the molecular level because those particles are normally in complete separation no matter how hard they are mixed. In many cases, bubbles and droplets are also mixed only to the macroscopic level, and concentrations are different in individual bubbles and droplets. This is called the macro mixing condition.

These two mixing conditions may be identified strictly as follows. The micro

mixing condition is a condition where uniformity in concentration holds for samples containing about 1000 molecules (imagine a cube where 10 molecules are lined up on its side). In contrast to this, the macro mixing condition is defined as a condition where such a microscopic concentration uniformity does not exist but a sort of uniformity exists over a space containing about 1000 elements of the dispersed phase (or fluid lump elements).

For a mathematically linear system, where reaction rates should be proportional to the first order of the concentration of a respective reactant, the issue of the macro and micro mixing is insignificant because the mean conversion is not affected at all by the mixing scale no matter how severe the segregation is. However, since the reaction rates of many heterogeneous reactions, and rates of solid reactions (solid–gas, solid–liquid and solid–solid) in particular, are proportional to the product of the reactant concentrations or area of relevant phases, it is rare that their reaction rate equations are linear. In such systems, handling the conversion of solids using the mean value is inefficient. Instead, the reaction process must be expressed by considering their probability distributions in terms of population balance (balance with respect to discrete solids). This may also apply to gas—liquid and liquid—liquid systems such as the growth of aerosol particles.

Problems of micro- and macro-mixing exist even in the continuous phase. When a rapid reaction takes place in a turbulent diffusion field, marked concentration and temperature non-uniformities may occur in terms of the microscopic scale, even if they are uniform in terms of the macro scale. This is because mixing at fluid lump level is different from that at the molecular level. A turbulent diffusion flame is an example of it. Another example can be found in packed beds, where mixing is made by the fluid velocity distribution around each particle, which is also very different from mixing at the molecular level. The diffusion phenomenon at the macro-mixing level is called 'eddy diffusion' or 'dispersion' to distinguish from that at the molecular level.

4.3.3.2.7 Statics/Dynamics/Stability

Statics, dynamics and stability of steady states are all essential for the stable operation of a system with a certain degree of fluctuation in normal operating conditions. Statics is the characteristics of a steady state, while dynamics is the characteristics of output changes with time. The maximum time constant of a system can be obtained approximately by dividing the maximum mass and heat capacities of a reactor by respective flow rates. In natural feedstock processing or waste management, the feed composition changes frequently. In such cases if the maximum time constant is made sufficiently larger than the predicted cycle of the change, and if materials are mixed well, such changes can be

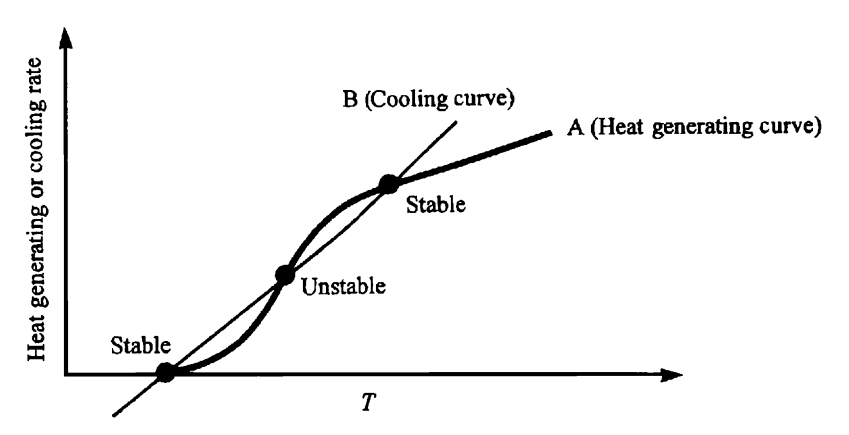


Figure 4.54 More than one steady solution and stability can exist in an exothermic reaction system.

absorbed, and the system output can be made stable. Otherwise, a proper control scheme has to be introduced.

In non-linear systems there may exist unstable steady state solutions accompanying the hysteresis phenomenon shown before in Figure 4.45. To prevent undesirable side and runaway reactions, it is important to set the steady operating conditions on the sufficiently safe side at the design stage.

The stability issue is also crucial in the chemical kinetics of heterogeneous systems. The reaction temperature is the most important kinetic parameter, but the actual reaction temperature can be often different from the prescribed temperature of the reactor. The actual reaction temperature is determined by the balance between the rate of heat generation by reactions and the rate of cooling by heat transfer. Let us briefly examine this issue for the case of solid fuel combustion (4.3.3.2.5 (3)).

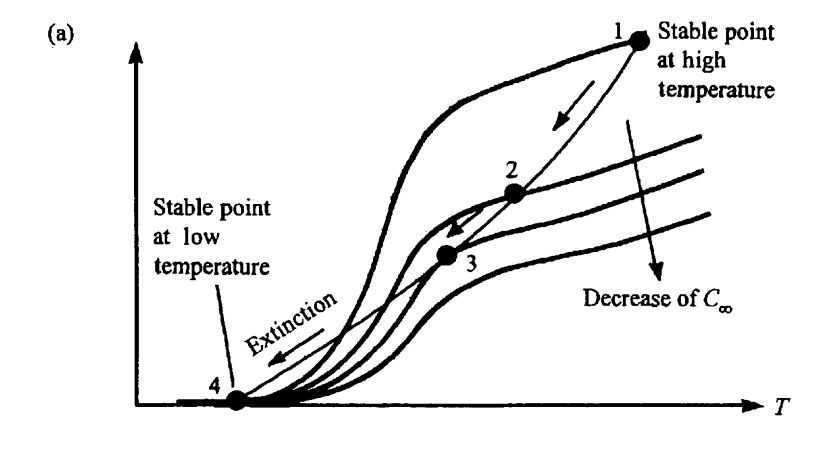
The heat balance of a single burning particle can be written as

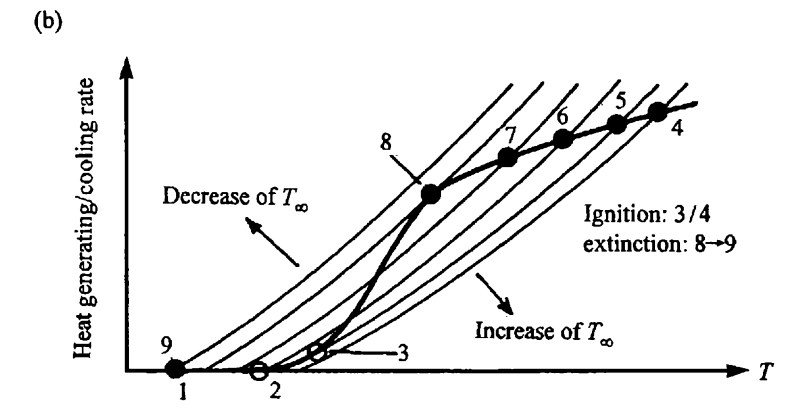
$$\frac{\pi}{6} d_{\rm p}^{3} \rho_{\rm p} c_{\rm p} \frac{\mathrm{d}T}{\mathrm{d}t} = \frac{\pi}{4} d_{\rm p}^{2} [(-\Delta H) \bar{k} C_{\infty} - h(T - T_{\infty})]$$
 (4.188)

where \bar{k} is the overall reaction rate constant defined by Eq. (4.155). In a pseudo-steady state the first term, i.e. the heating rate due to the reaction equals the second term i.e. the cooling rate.

Concerning the temperature dependency of the heat generating and cooling curves, it must be noted that the overall reaction rate constant is asymptotic to the chemical reaction rate constant k_s at low temperatures and to the mass transfer coefficient k_f at high temperatures. k_s is expressed by the following Arrhenius equation:

$$k_{\rm s} = k_{\rm s0} \exp(-E/RT)$$
 (4.189)





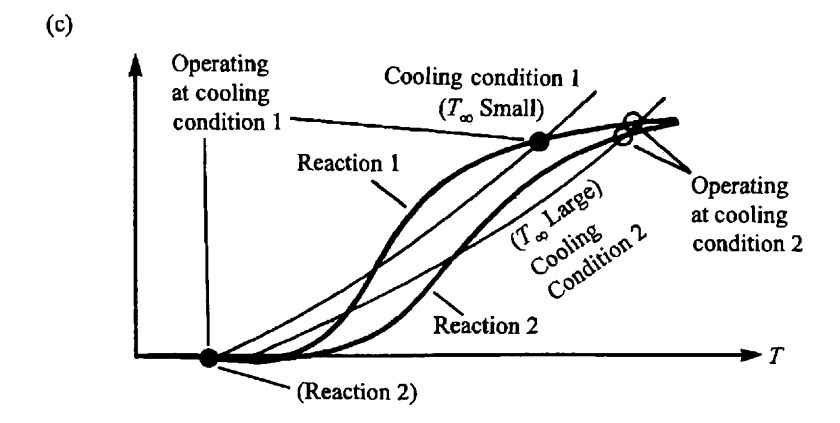


Figure 4.55 Hysteresis in exothermic reaction systems.

Then, the heat generating curve is given by curve A in Figure 4.54. On the other hand, the cooling curve is given by curve B in Figure 4.54, where both convection and radiation heat transfer are taken into account. The heating and cooling curves make one to three intersections for the steady state solutions. Out of these solutions, the one whose cooling curve has a slope in the vicinity of the intersection steeper than that of the heating curve is a steady state solution stable against small temperature perturbations around it. In the reverse case, a small perturbation would be amplified and thus, such a steady point is unstable.

From this diagram we can understand the mechanisms behind ignition and extinction phenomena easily. Ignition and extinction take place by changing the concentration of gas phase reactants C_{∞} or the coolant temperature T_{∞} as shown in Figure 4.55(a) and (b). Furthermore, it is apparent from Figure 4.55(c), that when the heat of reaction is too high, it is difficult to treat two reactions separately by using their largely different activation energies. Once both of the reactions become out of control, they proceed in a similar rate to the mass transfer rate controlling conditions. The thermal stability issue is also relevant in volume reaction systems.

4.3.4 DEVELOPMENT AND SCALE-UP OF MULTIPHASE REACTORS

4.3.4.1 The Nature of Development and Scale-up Issues

The development or scale-up of a multiphase reactor is nothing more than a task to achieve a new combination of flow, heat transfer and reaction so that a desired function is realized in a new system or in an expanded scale not previously experienced. In other words, it is an issue concerned with how the configuration and scale of a reactor affect the performance of a system of phenomena with different hierarchies.

Since the chemical reaction rate is determined based on molecular mechanisms, it is independent of a change in scale of the reactor. However, when the real reactions proceed they are affected by all the conditions: the supply of reactants and removal of products by convection and diffusion; and activation by heating and temperature control with cooling, including convection, conduction and radiation. Thus, by scaling-up a process it is quite possible to lose the balance of flow, diffusion, heat transfer and reaction which was once achieved in the small-scale system. In other words, one of the major technical issues in the development and scale-up of multiphase chemical reactors is to realize the increased production rate maintaining its quality by increasing the reactor size and by adjusting phenomena of different sensitivities to the scale change.

4.3.4.2 Methodology of Development and Scale-up

Now, if a complete set of mathematical expressions has been already obtained for a reactor, the problem of scale-up can be settled by directly solving the equations and determining the design variables such as the column diameter and height to reach the required performance. However, in practical cases, especially those of multiphase reactors, it will still take some more time until such a direct solution becomes feasible because of their complicated multiphase fluid mechanics and reactions. For the time being, the most feasible reactor simulations are those based on mass and heat balance expressions with correlations for macroscopic transport and hydrodynamic parameters (e.g. for a gas-liquid system Eq. (4.105) for hold-up, Eq. (4.98) for relative velocity and Eq. (4.113) for diffusivity).

The limitation of such a reactor simulation basically results from the applicable limits of the correlations caused by simplified hydrodynamics. If the operating conditions exceed their applicable limit, additional experiments must be performed to extend the applicable range of the correlations. Furthermore, since ordinary correlations have been developed for cylindrical columns, a special examination would be required if a significant deviation from a cylinder is to be introduced in the reactor shape. A small-scale test rig (often called a scale model) geometrically similar to a larger reactor concept can be applied to find the effect of shape changes. Here, it should be stressed that in most cases such a scale model can provide a hydrodynamic similarity but not heat transfer and reaction similarities. Accordingly, we first intend to examine hydrodynamics by similarity and then other factors by different approaches. For the reaction rates, it is recommended to develop rate expressions with wide applications through examination of kinetic factors of the diffusion-reaction systems discussed in 4.3.3.2.5.

To conduct development and scale-up successfully it is further recommended that tests are conducted on all aspects, i.e. experiments for kinetics, scale model experiments for hydrodynamics, overall reactor simulation based on the data on flow and mixing obtained from scale models and cold models, and then pilot plant testing to validate these predictions, as illustrated in Figure 4.56. The risks in developments and scale-up may well be reduced by such an approach.

In addition to the general understanding mentioned above, let us briefly examine the scaling law applicable to scale model experiments on multiphase systems. In multiphase flow, there exist levels of hierarchy starting from the macroscopic scale structures almost equivalent to the equipment scale, then the mesoscale structures of dispersed particles (bubbles and droplets) and the microscale structures around and in-between individual dispersed particles. It can be easily recognized that it is very difficult to make the flow phenomena of all hierarchy levels similar at the same time. This is why the sacrifice of the

172 M. HORI

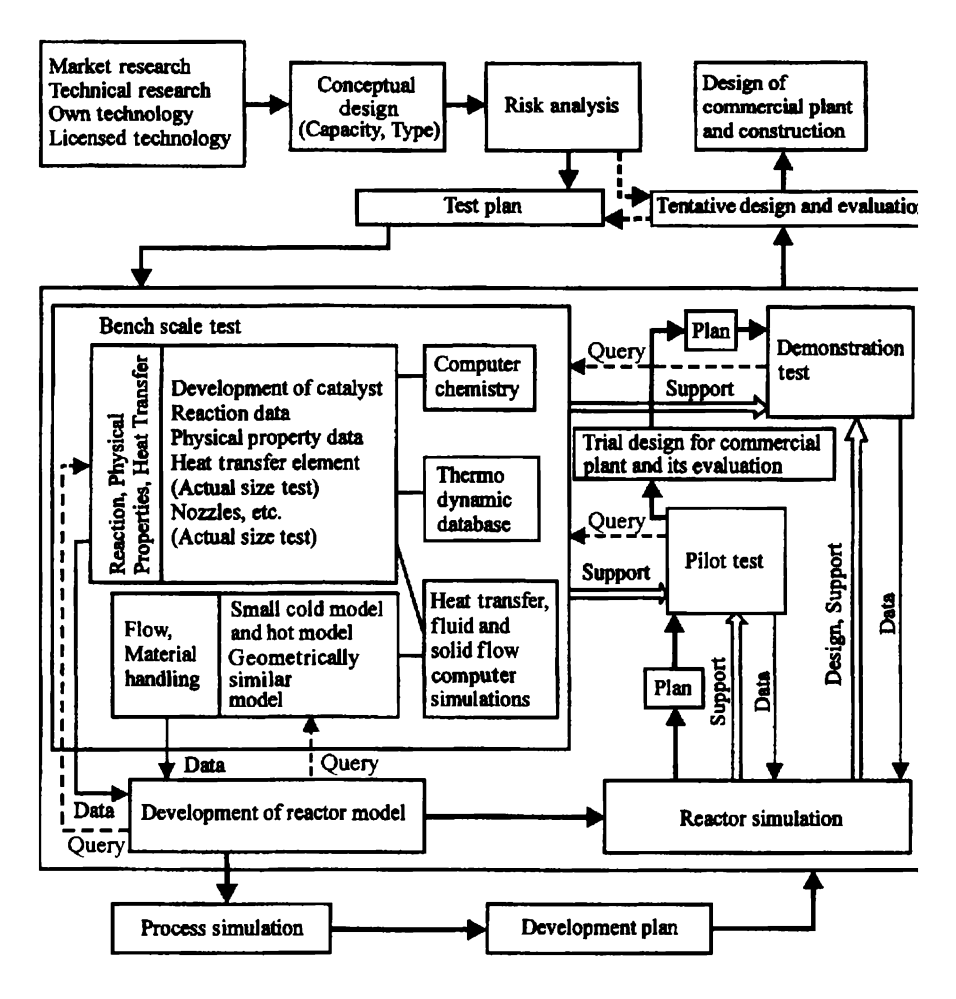


Figure 4.56 Rational scale-up procedure.

similarity of phenomena of minor scale levels is required in order to obtain information on specific industrial scale phenomena. For detailed design issufull-scale testing is always desirable at least for those items which are leaffected by the entire equipment size and structure.

On the scaling issue, fluidized beds provide us with a good example. I bubbling fluidized beds, there are three different levels of hierarchy: (1) bubb distribution in the bed; (2) gas flow through the dense phase of particle surrounding bubbles; and (3) gas flow around individual particles. Characte istic lengths governing these levels of hierarchy are the column diameter for (1 bubble diameter for (2) and particle size for (3). Now, let us assume that the are two fluidized bed plants of completely similar flow conditions, one is the

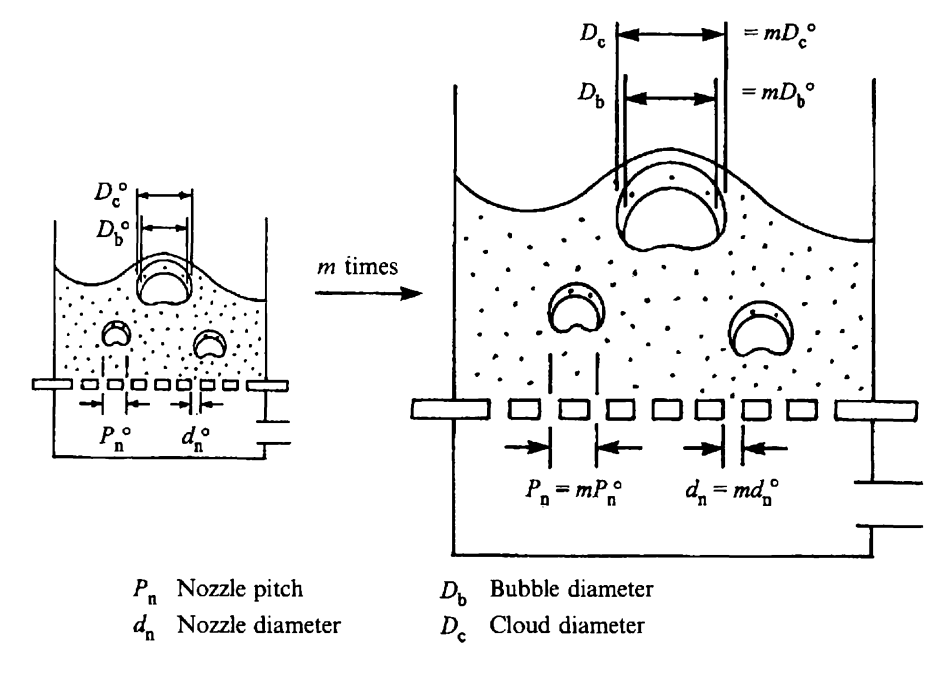


Figure 4.57 Completely similar flow conditions of two fluidized bed reactors.

reference plant or model and another is a plant or model m times larger than the former as shown in Figure 4.57, where the variables of the reference equipment are expressed by the superscript "". Their similar geometry condition can be expressed by the following relations for the column diameter D_1 and the bed height L_1 :

$$D_{t} = mD_{t}^{\circ} \tag{4.190}$$

$$L_{\rm f} = mL_{\rm f}^{\circ} \tag{4.191}$$

Hereafter, the dimensionless coordinates ξ , η and ζ of the following definitions are used to describe parameter distributions in each bed. In the following

$$\xi = \frac{x}{D_1} = \frac{x^\circ}{D_1^\circ} \tag{4.192a}$$

$$\eta = \frac{y}{D_1} = \frac{y^{\circ}}{D_1^{\circ}} \tag{4.192b}$$

$$\zeta = \frac{z}{D_0} = \frac{z^{\circ}}{D_0^{\circ}} \tag{4.192c}$$

174 M. HORIO

Now that the time-averaged bubble diameter in both models must be similar, we write:

$$D_{\mathbf{b}}(\xi, \eta, \zeta) = mD_{\mathbf{b}}^{\circ}(\xi, \eta, \zeta) \tag{4.193}$$

Nevertheless, the bubble fraction ε_b remains identical at similar positions in both models and

$$\varepsilon_{\rm b}(\xi,\,\eta,\,\zeta) = \varepsilon_{\rm b}^{\circ}(\xi,\,\eta,\,\zeta) \tag{4.194}$$

In fluidized beds the 'two-phase theory' of Toomey and Johnstone⁽²⁰⁾ holds approximately, i.e. the gas in excess of that required to fluidize the solids, $u_0 - u_{\rm mf}$ to flow as bubbles, where u_0 is the superficial velocity and $u_{\rm mf}$ is the minimum fluidization velocity. On the other hand, the product of the bubble rise velocity $u_{\rm b}$ and $\varepsilon_{\rm b}$ represents the bubble flow rate per local unit cross-sectional area and its average over the cross-section must be equal to $u_0 - u_{\rm mf}$. Since ξ and η vary within a circle of radius 0.5 and an area of $\pi/4$, the following relationships can be written for the scale model and the reference scale model, respectively:

$$u_0 - u_{\rm mf} = \frac{4}{\pi} \iint_{\xi^{\mathbf{E}} + \eta^2 \leq 1/4} u_{\mathbf{b}} \varepsilon_{\mathbf{b}} d\xi d\eta \qquad (4.195)$$

Similarly,

$$(u_0 - u_{\rm mf})^{\circ} = \frac{4}{\pi} \iint_{\xi^8 + \eta^2 \le 1/4} u_b^{\circ} \varepsilon_b^{\circ} d\xi d\eta \qquad (4.196)$$

Since from Eq. (4.98) $u_b = \alpha (gD_b)^{1/2}$ and $u_b^{\circ} = \alpha (gD_b^{\circ})^{1/2}$, substitution of these into Eq. (4.193) gives

$$u_{\rm b} = \sqrt{m}u_{\rm b}^{\circ} \tag{4.197}$$

Substituting Eqs (4.194) and (4.197) into Eq. (4.195) you find that the integrals of Eqs (4.195) and (4.196) are different only \sqrt{m} times.

Accordingly, the following first condition of Horio et al. (33) is derived as the requirement for bubble distribution:

$$u_0 - u_{\rm mf} = \sqrt{m} \left(u_0 - u_{\rm mf} \right)^{\circ} \tag{4.198}$$

Their second condition concerns the flow around bubbles. The velocity of gas in the dense phase around a bubble is under the minimum fluidization condition, thus $u_{\rm mf}/\varepsilon_{\rm mf}$ is the average interstitial gas velocity. Note that $u_{\rm mf}$ is the superficial velocity, which must be divided by $\varepsilon_{\rm mf}$ to obtain the interstitial velocity.

Depending on the ratio of bubble velocity u_b to the reference gas velocity around bubbles $u_{\rm mf}/\varepsilon_{\rm mf}$, chances are that the closed gas circulation around a bubble called the 'cloud' is formed as already shown in Figure 4.34. That is, the cloud is formed for:

$$\frac{u_{\rm b}}{u_{\rm mf}/\varepsilon_{\rm mf}} > 1$$

and the cloud is not formed, or the gas circulation cannot be closed, for:

$$\frac{u_{\rm b}}{u_{\rm mf}/\varepsilon_{\rm mf}}$$
 < 1

Now, when the bubble diameter is used as a reference scale in the Davidson⁽²²⁾ model, the flow field around a bubble becomes a function of only $u_b/(u_{\rm mf}/\varepsilon_{\rm mf})$ and a dimensionless position. Thus, to attain similarity of the gas and solid flow in the emulsion phase around a bubble, we need:

$$\frac{u_{\rm b}^{\circ}}{u_{\rm mf}^{\circ}/\varepsilon_{\rm mf}} = \frac{u_{\rm b}}{u_{\rm mf}/\varepsilon_{\rm mf}} \tag{4.199}$$

Substituting Eq. (4.197) into the above equation, we obtain the following condition on $u_{\rm mf}$ for the similar flow field around a bubble (the second condition of Horio *et al.*'s scaling law⁽³³⁾):

$$u_{\rm mf} = \sqrt{m} \, u_{\rm mf}^{\circ} \tag{4.200}$$

In the viscosity-dominant regime, $u_{\rm mf}$ is correlated from Eq. (4.108) as $(Ar < 1.9 \times 10^4)$:

$$u_{\rm mf} = \frac{d_{\rm p}^2(\rho_{\rm p} - \rho_{\rm f})g}{1650\,\mu_{\rm f}} \tag{4.201}$$

Thus, Eq. (4.200) can be rewritten for the particle diameter as:

$$d_{\rm p} = d_{\rm p}^{\circ} m^{1/4} (\mu_{\rm f}/\mu_{\rm f}^{\circ})^{1/2} [(\rho_{\rm p}^{\circ} - \rho_{\rm f}^{\circ})/(\rho_{\rm p} - \rho_{\rm f})]^{1/2}$$
 (4.202)

Finally, for similarity of the flow around a particle, the particle size itself must be similar. Thus, instead of Eq. (4.202) the following condition is required:

$$d_{p} = md_{p}^{\circ} \tag{4.203}$$

Thus, we obtain the following from Eqs (4.200), (4.201) and (4.203):

$$\mu_{\rm f}(\rho_{\rm p} - \rho_{\rm f}) = m^{1.5} \mu_{\rm f}^{\circ} / (\rho_{\rm p}^{\circ} - \rho_{\rm f}^{\circ})$$
 (4.204)

M. HORIO

Test series A: Bubble size distribution and the gas flow around a bubble are similar.

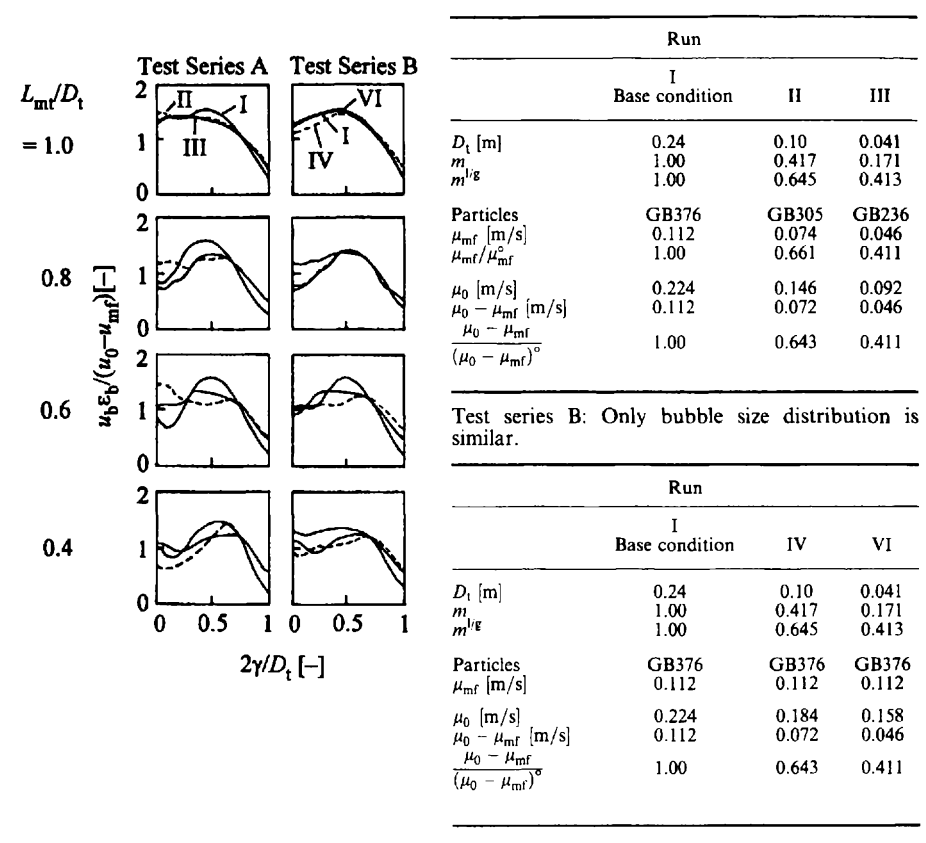


Figure 4.58 Experimental results for two fluidized beds of different diameters with completely similar geometry⁽³³⁾.

Summarizing the above, we obtain

(1) Conditions to make only the bubble size and its distribution similar:

$$u_0 - u_{\rm mf} = \sqrt{m}(u_0 - u_{\rm mf})^{\circ}$$

 $u_{\rm mf} = u_{\rm mf}^{\circ}$ (same particles can be used)

(2) Conditions to make the bubble size and its distribution and the gas flow around a bubble similar $(Ar < 1.9 < 10^4)$:

$$\begin{split} u_0 - u_{\rm mf} &= \sqrt{m} (u_0 - u_{\rm mf})^{\circ} \\ u_{\rm mf} &= \sqrt{m} u_{\rm mf}^{\circ} \\ d_{\rm p} &= d_{\rm p}^{\circ} m^{1/4} (\mu_{\rm f}/\mu_{\rm f}^{\circ})^{1/2} [(\rho_{\rm p}^{\circ} - \rho_{\rm f}^{\circ})/(\rho_{\rm p} - \rho_{\rm f})]^{1/2} \end{split}$$

(3) Conditions to make the bubble size and its distribution, the gas flow around a bubble and the gas flow around individual particles similar $(Ar < 1.9 < 10^4)$:

$$u_0 - u_{\rm mf} = \sqrt{m}(u_0 - u_{\rm mf})^\circ$$

$$u_{\rm mf} = \sqrt{m}u_{\rm mf}^\circ$$

$$d_{\rm p} = md_{\rm p}^\circ$$

$$\mu_{\rm f}/(\rho_{\rm p} - \rho_{\rm f}) = m^{1.5}\mu_{\rm f}^\circ/(\rho_{\rm f}^\circ - \rho_{\rm f}^\circ)$$

For case (1), the same particles can be used in the scale model experiment. For case (2), the particle size must be changed slightly (with $m^{1/4}$) when the same kind of material (the same ρ_p) is needed. For case (3), the scaling experiment is impossible without finding particles of a different but proper density. Instead, in case (1) similarities in the gas flow fields around bubbles and around particles are sacrificed, in case (2) similarity in the gas flow around a particle is sacrificed and although no such sacrifice exists in case (3), the degree of freedom in choosing experimental conditions is largely restricted. Figure 4.58 demonstrates examples of the similarity of radial distribution of bubble flow rate in the above cases (1) and (2).

As is apparent from the above discussions, the issue of the scale model experiments can be reduced to the question 'to what extent do we need to make the phenomena similar?'. However, scale model experiments are limited to the fluid mechanic phenomena. Instead, reactions must be examined with actual reactants and catalysts under actual temperature and pressure conditions.

So far, we have studied the major issues which we encounter in the development of multiphase reactors. They may, however, be only the tip of the iceberg. The nature of the problem exists in a range of about 10¹⁰ times from the nanometre scale to the ten metre scale. On concluding this section, I would like to emphasize that what is most important for a chemical engineer is the power of thinking about phenomena at different scales, different hierarchies and priorities, of course with the aid of physical and chemical knowledge.

Acknowledgements

The author would like to thank Ph.D. students Yuki (Ms Iwadate) of Tokyo University of A&T and John (Mr P. J. Sanderson) of Monash University for their assistance.

Notation

 A_i cross-sectional area orthogonal to the flow in phase i [m²] Ar Archimedes number [-] 178 M. HORIO

4		r 21
A_{t}	cross-sectional area of column	$[m^2]$ $[m^2/m^3]$
a_{ij} C_0	specific area of interface <i>ij</i> inlet concentration	[kmol/m ³]
-		
$C_{\mathbf{D}}$	drag coefficient	[~]
	concentration	$[kmol/m^3]$
c_i	specific heat of phase i	[J/kg·K]
D_{b}	bubble diameter	[m]
$D_{\rm e}$	effective diffusivity in porous material	$[m^2/s]$
$D_{\mathbf{G}}$	diffusivity in grains	$[m^2/s]$
D_{K}	Knudsen diffusivity	$[m^2/s]$
D_{t}	column diameter	[m]
d_{p}	particle diameter	[m]
	grain diameter in grain model	[m]
div	(,,,	[1/m]
dV	$= dx_1 dx_2 dx_3$	$[m^3]$
$\mathrm{d}V_{\mathrm{YP}}$	$= dY_{p1} \dots dY_{pn_p}$	
$\boldsymbol{\mathit{E}}$	activation energy	[J/kmol]
E_{f}	effectiveness factor	[-]
E_{i1}	eddy diffusivity in the x_1 direction in phase i	$[m^2/s]$
E_{N}	eddy diffusivity of particles based on the number	
	concentration	$[m^2/s]$
\boldsymbol{F}	total flow rate	$[m^3/s]$
F_i	flow rate of phase i	$[m^3/s]$
F_{i0}	feed rate of phase i	$[m^3/s]$
Fr	Froude number (Eq. (4.113))	[-]
G_{12}	capacity flow ratio of material of phase 1 against	
- 12	phase 2 (Eq. (4.134))	[-]
$G_{\rm H12}$	heat capacity flow ratio of phase 1 against	. ,
-1112	phase 2 (Eq. (4.135))	[-]
g	graviational acceleration	$[m/s^2]$
_	$= (\partial_{x1}, \partial_{x2}, \partial_{x3}), \text{ gradient}$	[1/m]
h	heat transfer coefficient	$[J/m^2 s K]$
h_{ij}	heat transfer coefficient at interface <i>ij</i>	$[J/m^2 s K]$
K_{BE}	bubble phase (B)-to-emulsion phase (E) gas exchange	[3/111 3 14]
ABE	coefficient (Eq. (4.111))	[1/s]
K	dimensionless reaction rate constant (Eq. (4.126)) or	[1/3]
Λ	equilibrium constant (Eq. (4.173))	[-]
k		
	reaction rate constant, apparent rate constant	[1/s]
$k_{\mathrm{f},ij}$	mass transfer coefficient at interface ij	[m/s]
k_{ij}	transfer coefficient at interface ij surface reaction rate constant	[m/s]
$k_{\rm s}$		[m/s]
k_{sG}	surface reaction rate constant for reaction in grain	[m/s]
L	column height	[m]

l	thickness or radius of porous material	[m]
M_i	molecular weight of component i	[kg/kmol]
m	Thiele number (Eq. (4.149)) or scale ratio (Eq. (4.190))	[-]
N_{12}	number of mass transfer or gas exchange units at	
	interface 1-2 (defined by Eq. (4.69)	[-]
N_i	number of heat transfer units with respect to phase i	
	(defined by Eq. (4.127))	[-]
$N_{ m R}$	number of reaction units (defined by Eq. (4.70))	[-]
n_i	particle number flux in x_i -direction	$[1/m^2 s]$
Pe	Péclet number	[-]
Q	quantity subject to a conservation law (mass of	•
_	chemical species, enthalpy etc.)	[kg, kmol or J]
q	$\equiv E/R\Delta T_{\rm ad}$	
Ŕ	gas constant	[J/kmol K]
R*	reaction rate per particle	[kmols/s]
Re	Reynolds number	[-]
R _G *	reaction rate per grain	[kmol/s]
$R_{\rm v}$	reaction rate per unit volume	[kmol/m ³ s]
R_{im}	generation rate of Q_m in phase i	[kmol/m ³ s]
r	radius	[m]
r*	= (r_1^*, r_2^*, \ldots) , rate of change in particle-side state Y_{pk}	[***]
•	for a single particle (Eq. (4.76)) (Eq. (4.82))	
Sh	= $k_f d_p/D$, Sherwood number	[-]
T	temperature	[K]
T^*	$= T/\Delta T_{\rm ad}, \text{ dimensionless temperature}$	[IX]
	$= I/\Delta I_{ad}$, difficulties temperature time	[a]
1		[s]
t	mean residence time	[s]
t_0	reference time	[s]
и	$= (u_1, u_2, u_3)$, velocity vector	[m/s]
u_0	superficial velocity	[m/s]
$u_{\rm b}$	bubble rise velocity	[m/s]
$u_{\mathrm{b}\infty}$	rise velocity of a single isolated bubble	[m/s]
$u_{\mathrm{g}0}$	superficial velocity of gas	[m/s]
u_{l0}	superficial velocity of liquid	[m/s]
$u_{\rm mf}$	minimum fluidization velocity	[m/s]
u_t	terminal velocity	[m/s]
V	reactor volume	$[m^3]$
V_{Yp}	whole domain of Y_p	
X_{ij}	dimensionless concentration of component j in	
	phase i (Eq. 4.124)	[-]
X_{im}	specific capacity Q_m in phase i (abundance per volume)	
x	x coordinate or coordinate vector	[m]
x_i	x_i coordinate	[m]

180 M. HORIO

x_{pi}	mass fraction of particles whose average diameter is $d_{\rm pi}$	[-]
Y_{p}	state variable in population balance	f1
y	y coordinate	[m]
Z	z coordinate	[m]
α	bubble rise velocity coefficient	[-]
α_i	$= u_i/(L/t_0)$, dimensionless velocity of phase i	[-]
γ	surface tension	$[N/m^2]$
δ	Dirac delta function	[-]
ϵ_{b}	bubble fraction	[-]
$\epsilon_{ m mf}$	void fraction at the minimum fluidization condition	[-]
3	void fraction, porosity	[-]
ϵ_{i}	volume fraction of phase i	[-]
ϕ	particle number density function	[1/m]
ϕ_{21}	= $\varepsilon_2 C_{2Bin}/\varepsilon_1 C_{1Ain}$, reactant capacity ratio	[-]
$\phi_{ m H2I}$	$= \varepsilon_2 \rho_2 c_2 / \varepsilon_1 \rho_1 c_1$, heat capacity ratio	[-]
ϕ_{s}	shape factor (sphericity)	[-]
$ ho_{ m bN}$	bulk density of particle number	$[1/m^3]$
$ ho_{ m f}$	fluid density	$[kg/m^3]$
$ ho_{ m p}$	particle density	$[kg/m^3]$
ρ_1	liquid density	$[kg/m^3]$
η	liquid-side conversion	[-]
η_{g}	particle-side conversion	[-]
μ_{f}	fluid viscosity	[Pa s]
μ_1	liquid viscosity	[Pa s]
ΔA_i	area of cell plane perpendicular to x_i -direction	$[m^2]$
	adiabatic temperature rise (defined by Eq. (4.129))	[deg]
ΔH	heat of reaction	[J/kmol]
Δx_i	infinitesimally small section in x_i	[m]
$\Delta V_{\rm I}$	volume of cell I	[m ³]
∂_{t}	$= \partial/\partial t$, partial differential operator by t	[1/s]
∂_{x_i}	$= \partial/\partial x_i, \text{ partial differential operator by } x_i$	[1/m]
∇	$= (\partial_{x_1}, \partial_{x_2}, \partial_{x_3}), \text{ nabla (operator)}$	[1/m]
τ	$\equiv t/t_0$, dimensionless time	[-]
η	$\equiv x_1/L$, dimensionless distance	[-]
ξ	$\equiv x_2/L$, dimensionless distance	[-]
ζ	$= x_2/L$, dimensionless distance $= x_3/L$, dimensionless distance	[-]
•	— 33, 2, differentiation distante	L J

References

- (1) O. Levenspiel, 'Chemical Engineering's Grand Adventure', 3rd Dankwerts Memorial Lecture, Chem. Eng. Sci., 43, 427 (1988).
- (2) I. Imai, Ryutai-rikigaku (Fluidmechanics), p. 12, Shohkabo (1973).
- (3) M. Horio and C. H. Wen, AIChE Symp. Series. vol. 73, Number 161, 9 (1977).

- (4) S. Mori and C. Y. Wen, Fluidization Technology, ed. Keairns, vol. 1, p. 171, McGraw-Hill (1976).
- (5) H. Kobayashi (ed.), Shokubai Souch oyobi Sekkei (Catalytic Reactors and their Design), Chijin-Shokan (1965).
- (6) R. Clift, J. R. Grace and M. E. Weber, Bubbles, Drops and Particles, Academic Press (1978).
- (7) Y. T. Shah, Gas-Liquid-Solid Reactor Design, McGraw-Hill (1979).
- (8) I. Muchi, S. Mori and M. Horio, Ryudousou-no-Hannou Kougaku (Fluidized Bed Reaction Engineering), Baifu-Kan (1984).
- (9) L. S. Fan, Gas-Liquid-Solid Fluidization Engineering, Butterworths (1989).
- (10) D. Kunii and O. Levenspiel, *Fluidization Engineering*, 2nd Ed., Butterworth-Heinemann (1991).
- (11) R. Clift, J. R. Grace and M. E. Weber, *Bubbles, Drops and Particles*, p. 190 (Fig. 7.13), Academic Press (1978).
- (12) J. S. Hadamard, C. R. Acad. Sci., 152, 1735-1738 (1911).
- (13) W. Rybezynski, Bull. Int. Acad. Pol. Sci. Lett., Cl. Sci. Math. nat., Ser. A, p. 40 (1911).
- (14) W.-D. Deckwer, Y. Louisi, A. Zaidai and M. Ralek, I & EC Process Des. & Dev., 19, 699 (1980).
- (15) K. Akita and F. Yoshida, I & EC Process Des. & Dev., 12, 76 (1973).
- (16) L. S. Fan, Gas-Liquid-Solid Fluidization Engineering, p. 256 (Fig. 4.2), Butterworths (1989).
- (17) S. Ergun, Chem. Eng. Progr., 48, 89 (1952).
- (18) C. Y. Wen and Y. H. Yu, AIChE J., 12, 610 (1966).
- (19) M. Horio, Funtaikougaku kaishi (J. Soc. Powd. Tech. Japan) 23, 80 (1986).
- (20) R. D. Toomey and H. F. Johnstone, Chem. Eng. Progr., 48, 220 (1952).
- (21) D. Geldart, Powder Technol., 7, 285 (1973).
- (22) J. F. Davidson and D. Harrison, *Fluidized Particles*, Cambridge Univ. Press (1963).
- (23) L. S. Fan, Gas-Liquid-Solid Fluidization Engineering, p. 269 (Fig. 4.9), p. 277 (Fig. 4.10), Butterworths (1989).
- (24) H. Hikita and H. Kikukawa, J. Chem. En. Japan, 8, 412 (1975).
- (25) K. H. Mangartz and T. Pilhofer, Verfahrenstechnik, 14, 40 (1980).
- (26) H. A. Deans and L. Lapidus, AlChE J., 6, 656 (1960).
- (27) Hiby J. W. Proc. Symp. on the Interaction between Fluids & Particles, 312 (1962).
- (28) O. Devenspiel, Chemical Reaction Engineering—An Introduction to the Design of Chemical Reactors, 1st Ed. p. 275. John Wiley & Sons (1962).
- (29) K. Kato and C. Y. Wen, Chem. Eng. Sci., 24, 1351 (1969).
- (30) M. Horio, S. Mori and I. Muchi, Preprints of 34th Annual Meeting of JCEJ, B108, 158 (1969).
- (31) M. Horio, T. Otake and I. Muchi, Tetsu-to-Hagane, 60, 465 (1974).
- (32) C. N. Satterfield and T. K. Sherwood, *The Role of Diffusion in Catalysis*, Addison-Wesley (1963).
- (33) M. Horio, A. Nonaka, Y. Sawa and I. Muchi, AIChE J., 32 (9) 1466 (1986).

CHAPTER 4.4

Dynamic Analysis of Reaction System

HISAYOSHI MATSUYAMA

Department of Chemical Engineering, Kyushi University, Japan

4.4.1 DYNAMICS OF REACTORS

4.4.1.2 Definition and Classification

Those variables which express the state of a reactor, such as the temperatures in the reactor and concentrations of reactant and catalyst, are called 'state variables'. The state variables are affected by 'controlled variables' to be freely set during operation and 'design variables' to be set at the design stage. The former includes the temperature, flow rate and composition of fluids fed to the reactor, and the external heating or cooling rate. The latter includes the heat transfer area of the jacket and the reactor volume. The characteristics of the reactor are represented by the 'equation of state' expressing the relationships between the state variables and controlled or design ones.

The reactors are generally classified into 'lumped-parameter reactors' and 'distributed-parameter reactors'. The former are reactors whose state variables are independent of the position inside the reactors such as stirred tank reactors and fluidized beds with uniform internal state. The latter are reactors whose state variables are functions of the position inside the reactors, such as tubular reactors, fixed beds, and moving beds.

4.4.1.3 Mixing and Dynamic Characteristics in a Reactor

The dynamics of a reactor are strongly affected by the mixing characteristics of the fluid in the reactor. In particular, the dynamics of homogeneous phase systems are determined only by their mixing characteristics, reaction rate, and the heating or cooling rate in the reactor. Since the mixing characteristics of a stirred tank reactor are simple, its dynamics are accurately expressed in the form of a transfer function, with a given reaction rate and a heating or cooling rate as described below.

The mixing characteristics of the stirred tank reactor are expressed as a residence time distribution function:

$$f(t) = \exp(-t/\theta) \tag{4.205}$$

where t is the residence time of a fluid particle in the reactor and θ is a mean residence time. The Laplace transform of f(t) is as follows:

$$F(s) = 1/(s + 1/\theta) \tag{4.206}$$

The reaction rate r is given as the function of the reactant concentration C and the temperature T in the reactor.

If the temperature in the reactor can be easily kept constant because of the small heat of reaction, the dynamics concerning the temperature are not taken into consideration. Therefore, the dynamics of a continuous stirred tank reactor (CSTR) in the neighbourhood of a steady state are represented by a transfer function from inlet to outlet concentration of the reactant, $G_{\rm CC}(s)$, which is expressed by the following equation with the residence time distribution function and reaction rate:

$$G_{\rm CC}(s) = (1/\theta)/(s + 1/\theta + r_{\rm C})$$
 (4.207)

where r_C is $\partial r/\partial C$ at steady state.

If a control system is required to keep the reactor temperature constant because of the large heat of reaction, the dynamics concerning the temperature should be considered. In this case, a suitable cooling (or heating) system should be chosen, corresponding to the magnitude of the heat of reaction. To express the dynamics of stirred tank reactors with the jacket, the jacket cooling rate is needed in addition to the mixing characteristics and reaction rate.

The cooling rate of the jacket, Q_C is given by

$$Q_{\rm C} = UA(T_{\rm J} - T) \tag{4.208}$$

where T_J is the temperature in the jacket, U is the overall heat transfer coefficient between the reactor and the jacket, and A is the heat transfer area.

The dynamic characteristics of a CSTR in the neighbourhood of a steady state are represented by the transfer function from the reactant inlet to the outlet concentration $G_{CC}(s)$, the transfer function from the reactant inlet concentration to the outlet temperature $G_{TC}(s)$, the transfer function from the inlet temperature to the reactant outlet concentration $G_{TC}(s)$, the transfer function from the jacket temperature to the reactant outlet concentration $G_{JC}(s)$, and the transfer function from the jacket temperature to the outlet temperature $G_{JT}(s)$, which are given by

$$G_{CC}(s) = (1/\theta)[s + 1/\theta + (UA/c_P\rho V) - (-\Delta H/c_P\rho)r_T]/(s^2 + As + B)$$

$$G_{CT}(s) = (1/\theta)(-\Delta H/c_B\rho)r_C/(s^2 + As + B)$$

$$G_{TC}(s) = -(1/\theta)r_{T}/(s^{2} + As + B)$$

$$G_{TT}(s) = (1/\theta)(s + 1/\theta + r_{C})/(s^{2} + As + B)$$

$$G_{JC}(s) = -(UA/c_{P}\rho V)r_{T}/(s^{2} + As + B)$$

$$G_{TT}(s) = (UA/c_{P}\rho V)(s + 1/\theta + r_{C})/(s^{2} + As + B)$$
(4.209)

where c_P is the specific heat of the fluid in the reactor, ρ is the density of the fluid in the reactor, $-\Delta H$ is the heat of the reaction, V is the reactor volume, r_T is $\partial r/\partial T$ at steady state, and A and B are constants given by

$$A = 2/\theta + (UA/c_P \rho V) + r_C - (-\Delta H/c_P \rho)r_T$$
 (4.210)

$$B = (1/\theta)^{2} + \{(UA/c_{P}\rho V) + r_{C} - (-\Delta H/c_{P}\rho)r_{T}\}(1/\theta) + (UA/c_{P}\rho V)r_{C}$$
(4.211)

Since the dynamics of the stirred tank reactor are accurately expressed as above, its control system is designed much more easily than control systems for other types of reactors. When the heat of reaction is large or high product quality is required, reaction conditions should be tightly controlled. In these cases, stirred tank reactors are generally used.

The dynamics of tubular reactors are also determined theoretically by the mixing characteristics, the reaction rate, the heating or cooling rate. However, it is difficult to express the dynamics accurately by using transfer functions because of the complexity of mixing characteristics in the tubular reactors. For heterogeneous reactors, the dynamics cannot be determined only by their mixing characteristics, reaction rate, and heating or cooling rate, because the mass and heat transfer in phase and between phases must be considered.

4.4.2 STABILITY OF REACTORS

4.4.2.1 Unstable Phenomena in a Reactor

Stability is the most important characteristics of a reactor. Reactors may be unstable (runaway) due to the following positive feedback:

- (1) In the case of an exothermic reaction, with increasing temperatures, the rate of reaction rises. Consequently, the heat of reaction is generated rapidly and increases the temperature more and more.
- (2) In the case of an autocatalytic reaction, with increasing product concentration, the rate of reaction rises. Consequently, the product amount increases rapidly and increases the product concentration more and more.

(3) In the case of polymerization, with increasing degrees of polymerization, the viscosity of the reacting liquid increases and gelation occurs. Consequently, the temperature in the reactor rises because of insufficient cooling due to decreasing of the heat transfer rate. Then the rate of reaction increases and the degree of polymerization increases more and more.

Since the above case (2) and (3) take place rarely, an unstable state caused only by case (1) is described below.

If the activation energies of secondary reactions are much larger than that of the main reaction, the reactor can be operated at a relatively low temperature under which the secondary reactions proceed little. However, if any secondary reactions is an exothermic reaction, the reactor temperature increased by some reason may trigger the secondary reaction, and the temperature, further increased by the exothermic reaction, makes the secondary reaction become dominant, which results in temperature runaway. There are many examples of reactions causing problems in industrial processes, such as complete oxidization reactions in partial oxidation reactors and decomposition reactions in ethylene polymerization reactors.

It must be noted that the existence of an exothermic reaction is not always the cause of instability. In an exothermic reaction, there is positive feedback in which a temperature rise in a reactor increases the reaction rate and the heat of reaction, which in turn increases the reactor temperature, as shown in Figure 4.59. On the other hand, there is negative feedback in which an increase in the rate of reaction reduces the reactant concentration, which in turn lowers the rate of the reaction. In the case of an isolated fluid particle without mass and heat exchange with its surroundings, its temperature cannot be kept at a higher level, since the reactant in the fluid particle is consumed by the increase in the reaction rate, even if its temperature increases for some reason. A necessary condition for an exothermic reaction leading to unstable phenomena is the existence of a reaction zone, where the reactant is continuously fed at high temperature, or heat is supplied to the reactant with high concentration. The above mentioned phenomena are as follows:

- (1) Mixing of a fluid in a stirred tank reactor
- (2) Backmixing during flow in a tubular reactor

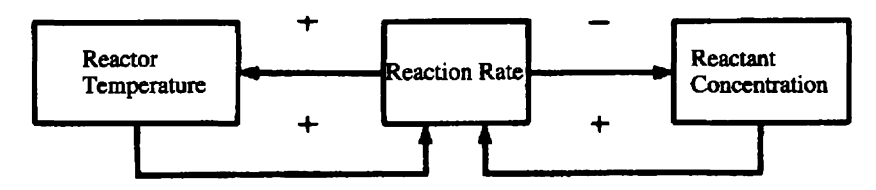


Figure 4.59 Cause and effect relationships in an exothermic reaction.

- (3) Flow velocity distribution in a tubular reactor
- (4) Mixing of fluids in fluidized beds
- (5) Backmixing during flow in fixed and moving beds
- (6) Slip velocity between gas and solid phases, and interphase mass and heat transfer
- (7) Heat transfer by conduction or radiation in the solid phase in gas-solid reactors, and interphase heat transfer
- (8) Recycling
- (9) Autothermal operation.

4.4.2.2 Mixing of the fluid in a Stirred Tank and a Tubular Reactor

(1) Mixing of fluid in a stirred tank reactor and (2) backmixing during flow in a tubular reactor are basically the same phenomenon as mixing by turbulence. When (i) a fluid with a high temperature and a low reactant concentration accompanying reaction and (ii) a fluid with a low temperature and a high reactant concentration, owing to less reaction are mixed, a high temperature in the reactor is maintained by feeding reactant into the reaction zone, kept at high temperature, or supplying heat into the zone, kept at high reactant concentration.

Since mixing in a stirred tank reactor is more intense than that in a tubular reactor, the tubular reactor is more stable than the stirred tank reactor if no generation of gases or turbulent flow occurs with the temperature rise in the tubular reactor. Also, in comparing single stirred tank reactors with multistage stirred tank reactors with the same residence time, the latter are more stable, as the mixing inside the single stirred tank reactor is more intense than the entire mixing in the multi-stage stirred tank reactor.

4.4.2.3 Flow Velocity Distribution in a Tubular Reactor

Even if the flow in a tubular reactor is laminar with no backmixing, unstable phenomena can occur in a case (3) with flow velocity distribution. A zone with low flow velocity becomes a state of low reactant concentration and high temperature accompanying reaction. On the other hand, a zone with high flow velocity becomes a state of high reactant concentration and low temperature, owing to less reaction. In other words, the tubular reactor contains two zones: one with a high temperature and another one with a high reactant concentration within the same cross-section. Radial heat transfer by heat conduction supplies heat to the zone at high reactant concentration, and radial reactant transfer by diffusion supplies the reactants to the zone at high temperature, which results in unstable phenomena.

4.4.2.4 Gas-Solid Reactors

In cases (4) and (5) only the influence of the mixing of fluids in the reactor may be considered. But, in cases (6) and (7), both the influences of mass and heat transfer should be considered. The latter cases have the possibility of generating a phenomenon feeding reactants to a high temperature zone or supplying heat to a high reactant concentration zone.

Fluidized bed reactors have less influence caused by the above phenomena due to relatively low relative velocities between the gas and solid phases and small heat conduction in the solid phase. On ther other hand, fixed and moving bed reactors have a large influence by the above phenomena due to high relative velocities between gas and solid phases and large heat conduction or radiant heat transfer in the solid phase.

In gas-solid reactors, the local temperature rise may degrade the catalytic activity and/or may cause crushing of solid particles. The former does not lead to runaway, but causes undesirable results such as movement of the reaction zone and shortening of the catalyst replacement cycle time. The latter causes channelling and dead space in the reactor, which often results in unstable phenomena by increasing the reactant concentration and temperature differences in the reactor.

4.4.2.5 Recycle and Autothermal Operation

In the case of (8) (Recycle Operation), a part of the high-temperature reactor effluent is recycled to the reactor entrance and mixed with fresh feed with high reactant concentration. This means that heat is supplied to the fluid with high reactant concentration. However, since the recycling operation also has the effect of lowering the reactant concentration, the effect of positive feedback is relatively small.

On the other hand, in case (9) (Autothermal Operation), a high-temperature reactor effluent supplies heat to the fresh feed with high reactant concentration, without lowering its concentration. This case easily leads to an unstable condition by the large influence of positive feedback.

4.4.3 CONTROL OF REACTORS

4.4.3.1 Purpose of Reactor Control and Design of a Control System

The purpose of reactor control is to keep the production rate of the desired product and the composition of the effluent fluid at specified values. It is obvious that the production rate of the objective product is the purpose of control. The reason for controlling the composition of the effluent fluid is that

the control heavily affects raw material consumption and the separation cost of the objective product.

The design procedure for a reactor control system is divided into the following three steps:

- Step (1) determination of the heating or cooling method
- Step (2) determination of the control system structure
- Step (3) determination of the control parameter.

Step (1) determines the structure of the reactor required to produce the control system. As described in the foregoing section, an exothermic reaction proceeding in a reactor may cause unstable phenomena by increasing the temperature. Therefore, it is important to determine the structure for such reactors so as not to run short of the cooling capacity. It is necessary to select reactor structures corresponding to the magnitude of the reaction heat. For the reactor structure, refer to Sections 4.1–4.3.

This section mainly focuses on Step (2). Determination of the structure of a control system is to select the 'controlled variables' to be controlled, and the 'manipulated variables' to be directly manipulated to maintain the controlled ones at their set-point values, and to determine the functional relationships between the controlled and the manipulated variables. The controlled and manipulated variables should meet the following requirements:

- (1) Controlled variables are measurable and controlling these variables at their set-points enables the production rate of the objective product and the composition of the effluent fluid to be kept at their target values.
- (2) Manipulated variables are directly adjusted and affect the controlled variables.

Since the production rate of the objective product and the composition of the effluent fluid cannot be directly measured, the controlled and manipulated variables which meet the above conditions are selected, and the target values of the production rate of the objective product and the composition of the effluent fluid are converted to the target values of controlled variables, and then the functional relationships between the deviations of the controlled values from their set-point ones and the manipulated variables are determined.

Step (3) determines the parameters of the control system considering its stability and quick response after determining the control system structure. Various methods have been proposed depending on the structure of the control system, but this step is not discussed here.

4.4.3.2 Selection of Controlled Variables

First, the controlled variables should be selected to determine the structure of a control system. The controlled variables are determined according to the following procedure:

- (1) List all variables determining the production rate of the desired product and the composition of the effluent fluid.
- (2) Take the measurable variables in the list to be the controlled variables.
- (3) For unmeasurable variables in the list, list all variables determining them.
- (4) Repeat steps (2) and (3) so that all variables listed in steps (2) and (3) are determined by the controlled variables.

The example of the continuous stirred tank reactor with a jacket for a liquidphase reaction between two kinds of liquids, is used to explain the above procedure. Figure 4.60 shows the cause and effect relationships among variables in the reactor.

Those variables that determine the production rate of the desired product are the flow rate and composition of the effluent liquid as shown in Figure 4.60. The flow rate of the effluent liquid is a controlled variable because it is measurable.

The composition of the effluent liquid is equal to that in the reactor, but the composition in the reactor can rarely be measured. So, the composition of the effluent liquid cannot be a controlled variable. As shown in Figure 4.60, the variables determining the composition in the reactor are the temperature in the reactor, the composition of feed liquids and the residence time.

The temperature in the reactor can be selected as a controlled variable because it is measurable. The composition of feed liquids can be accurately adjusted by batch-type mixing of the feed liquids after analysis of their composition and measurement of their charge quantity, or the continuous-type mixing of the feed liquids using a flow rate control to keep the flow ratio of the feed liquids at a specified value. The residence time cannot be directly measured, but is determined by the liquid level and flow rate of the effluent liquid. Both liquid level and discharge liquid flow rate are chosen as controlled variables because they are measurable.

In summary, all the above mentioned variables can be determined as the controlled variables when the composition of feed liquids is adjusted at constant value. Namely, the production rate of the objective product and the effluent liquid composition can be kept at each target value, respectively, by the control system consisting of the reactor temperature, the liquid level in the reactor and the effluent liquid flow rate as the controlled variables.

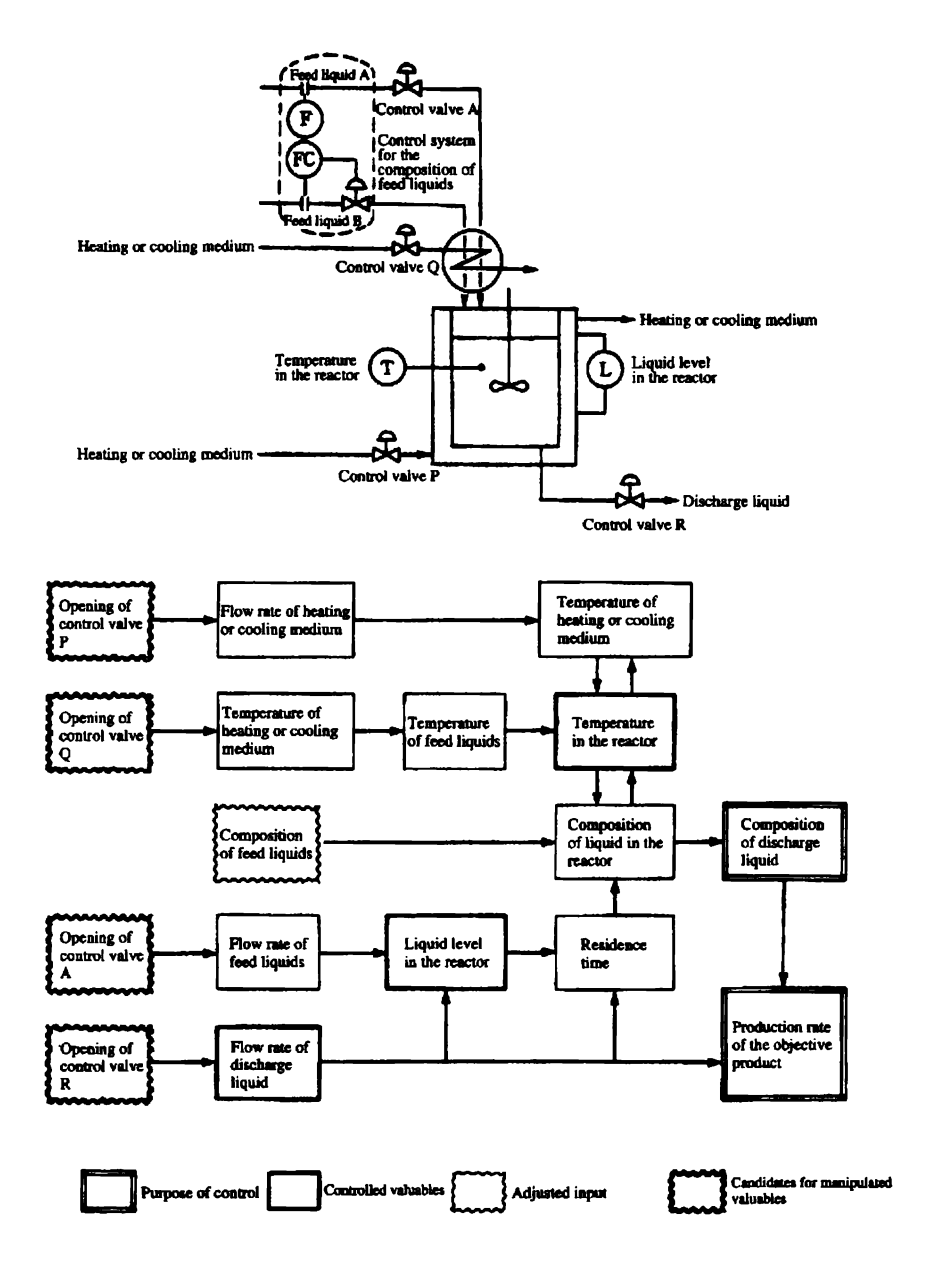


Figure 4.60 Cause and effect relationships among variables in a reactor.

4.4.3.3 Selection of Manipulated Variables

When the number of manipulated variables is larger than that of controlled variables, there are multiple combinations of manipulated variables. A procedure for selecting the manipulated variables is shown below:

- (1) List all directly operable variables as the candidates for manipulated variables.
- (2) Select the same number of variables out of the above candidates as that of the controlled variables, and list all combinations of these variables which directly affect all of the controlled variables.
- (3) Select an optimal combination out of those of manipulated variables listed in step (2).

The search for manipulated variables for a control system whose controlled variables are the reactor temperature, liquid level in the reactor and effluent liquid flow rate is shown below. Taking the aforementioned stirred tank reactor with jacket. Since the directly operable variables are only the four control valve openings, as shown in Figure 4.60, these are taken as the candidates for manipulated variables.

There are four combinations in selecting three out of those variables. When the control valve opening on the feed liquid line is not included, there are no manipulated variables directly affecting the liquid level in the reactor. And if the control valve opening on the effluent liquid line is not included, there are no manipulated variables affecting the effluent liquid flow rate. Thus, the combinations of manipulated variables meeting the requirement in step (2) include the control valve openings on the feed and effluent liquid lines, and the remaining combination is only (A): control valve openings on the heating or cooling medium lines of the jacket or (B): control valve openings on the heating or cooling medium lines for feed liquid.

The combination which is optimal becomes apparent at the stage of determining the functional relationships between the controlled and manipulated variables.

4.4.3.4 Determination of Functional Relationships

In general, control systems consisting of multiple controlled and multiple manipulated variables are called multivariable control systems. Since the design method for multivariable control systems has not yet been established, we should determine plural functional relationships between a control deviation (difference between the process and the set-point value of the controlled variable) and a manipulated variable. As functional relationships, the PID control employing linear combination of proportional, integral and differential relations is most widely used.

The structure of the PID control system for the above mentioned stirred tank reactor with jacket is determined below. For two combinations: (a) one combination of the control valve openings in the heating or cooling medium lines of the jacket as the manipulated variables, and (b) the other combination of the control valve openings in the heating or cooling medium lines for feed liquid as the manipulated variables are briefly illustrated in Figure 4.61.

Since the effluent liquid flow rate is affected only by the control valve opening in the effluent liquid line in both combinations, a PID control system is built, employing the effluent liquid flow rate as the controlled variable, and the control valve opening in the effluent liquid line as the manipulated one, respectively. Also, the liquid level in the reactor is affected by the control valve openings in both feed and effluent liquid lines in both combinations. However, since the control valve opening in the effluent liquid line is alrady used, a PID control system is built, employing the liquid level in the reactor as the controlled variable and the control valve opening in the feed liquid line as the manipulated one.

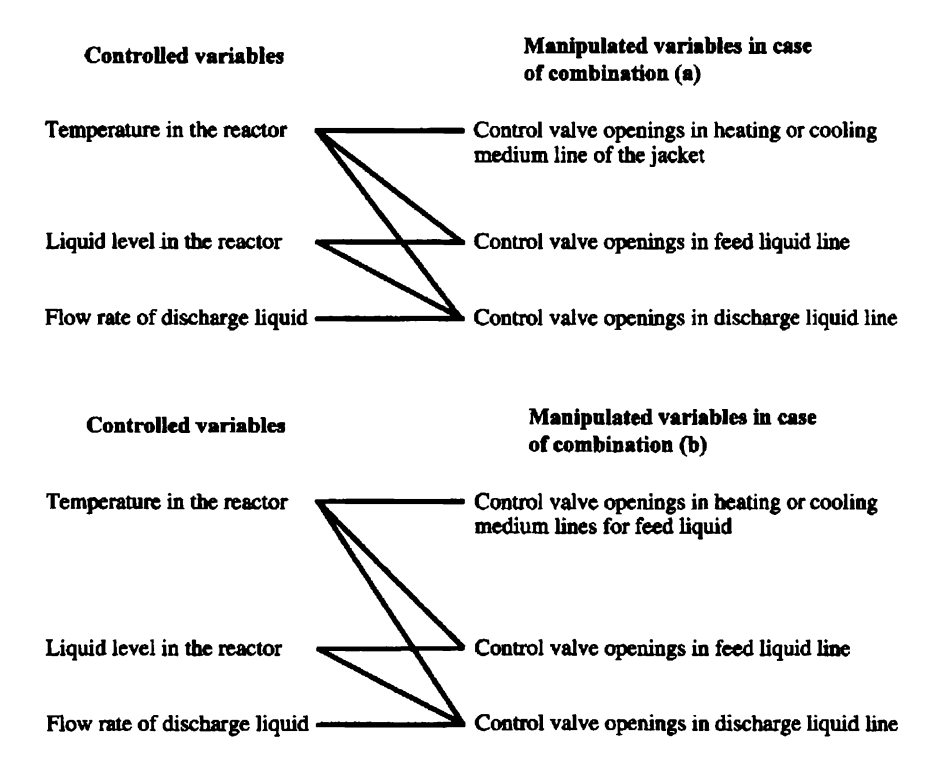


Figure 4.61 Relationships between manipulated and controlled variables for a stirred tank reactor with jacket.

Accordingly, for the manipulated variable for the PID control system, the reactor temperature is used as the controlled variable, in the combination (A), control valve openings in the heating or cooling medium lines of the jacket, while in the combination (B), control valve openings in the heating or cooling medium lines for feed liquid are used for the manipulated variable. From the viewpoint of higher stability of the former with wider ranges of heating or cooling rates, combination (A) is generally adopted for the manipulated variables. The control system structure is determined as shown in Figure 4.62(a).

However, since there are the flow rates and temperatures of the heating or cooling medium between the control valve openings on the heating or cooling medium lines to the jacket and the reactor temperature as shown in Figure 4.60, we have the following problems:

Problem (1):

A long time delay from the flow rate to the temperature of heating or cooling medium, and from the temperature of heating or cooling medium to that in the reactor, respectively.

Problem (2):

Strong non-linear relationships between the control valve openings and the flow rates of the heating or cooling medium.

To solven problem (1), a cascade control system is applied by combining two PID feedback control loops as shown in Figure 4.62(b). One is a primary control loop using the reactor temperature as the controlled variable, and the set-point for the temperatures of heating or cooling medium as the manipulated variables. The other is a secondary control loop using the temperatures of heating or cooling medium as the controlled variables, and the control valve openings as the manipulated variables. Furthermore, to solve problem (2), as shown in Figure 4.62(c), a cascade control system is used by combining three PID control loops. One using the reactor temperature as the controlled variable, and the set-point for the temperatures of the heating or cooling medium, another using temperatures of heating or cooling medium as the controlled variables, and the set-point for flow rates of the heating or cooling medium, and the other using the flow rates of heating or cooling medium as the controlled variables, and the control valve openings as the manipulated variables.

4.4.4 OPTIMIZATION OF REACTOR SYSTEMS

4.4.4.1 Classification of Reactor Optimization Problems

Reactor optimization problems are classified into the optimal design problems of designing an optimal reactor and the optimal control problems of searching for optimal operating conditions for the reactor.

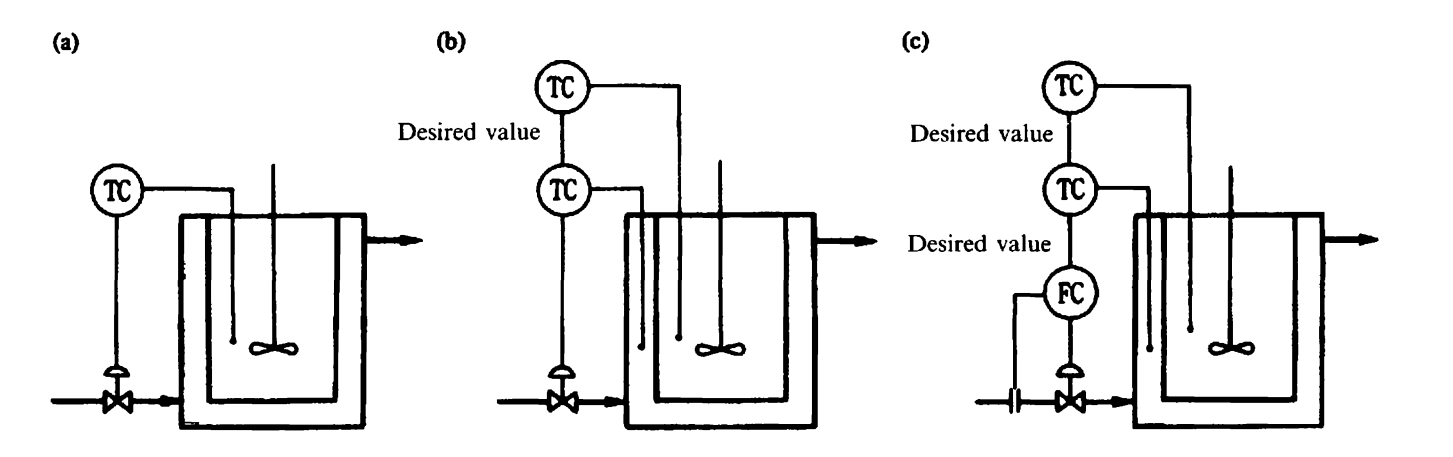


Figure 4.62 Temperature control systems for a stirred tank reactor. (a) PID control system. (b) A cascade control system (combination of two PID control systems). (c) A cascade control system (combination of three PID control systems).

The optimal design problems address the optimization of reactor structure, operation mode (continuous, semi-batch or batch operation), and values of the design variables. Since these problems handling the reactor structure and operation mode cannot be expressed numerically, it is difficult to formulate the problems mathematically and there is no general solution for them. As for an optimal design problem for maximizing the selectivity of the desired product, various 'Optimal Design Guidelines' are available from the properties inherent in the problem, as described in Section 4.4.4.2. It is possible to design a suboptimal reactor by using the guidelines.

As a special case of the optimal design problem, we have the optimal allocation problem of measuring instruments to maximize the estimation accuracy for internal conditions in the reactor. An exact dynamic reactor model is required to determine strictly the optimal allocation of measuring instruments. For the optimal allocation problem of thermometers, 'Optimal Allocation Guidelines' are available as described in Section 4.4.4.3 from the properties inherent in the problem. In addition, an optimal design problem to optimize only the values of design variables, after determination of the reactor structure and operation mode, can be formulated as a constrained minimization problem as below:

Minimize
$$f(x_1, x_2, ..., x_n; u_1, u_2, ..., u_r)$$
 (4.212)

subject to
$$g_i(x_1, x_2, ..., x_n; u_1, u_2, ..., u_r) \le 0 (j = 1, 2, ..., p)$$
 (4.213)

$$h_k(x_1, x_2, ..., x_n; u_1, u_2, ..., u_r) = 0 (k = 1, 2, ..., n)$$
 (4.214)

where x_i ($i=1, 2, \ldots, n$) are state variables and u_k ($k=1, 2, \ldots, r$) are design variables. Eq. (4.212) is an objective function (cost, selectivity×(-1), conversion×(-1), etc.). Eq. (4.213) gives constraints for the state and design variables. Eq. (4.214) gives the state equations. A general solution described in Section 4.4.4.4 is obtained for this problem, when Eq. (4.212) is a single model function, and Eqs. (4.213) and (4.214) are differentiable.

An optimal control problem is the problem of optimizing the functional relationships between control variables and time, being formulated as a variation problem. Since the state equations of lumped parameter reactors are ordinary differential equations using time as an independent variable, its optimal control problem is as follows:

Minimize
$$\int_{t_0}^{t_1} f_0(x_1, x_2, \dots, x_n; u_1; u_2, \dots, u_r) dt$$
 (4.215)

subject to
$$dx_i/dt = f_i(x_1, x_2, ..., x_n); u_1, u_2, ..., u_r) (i = 1, 2, ..., n)$$
 (4.216)

$$x_i(t_0) = a_0 \ (i \in I_0) \tag{4.217}$$

$$x_i(t_1) = a_1 \ (i \in I_1) \tag{4.218}$$

$$u_k \in U_k \tag{4.219}$$

where t_0 and t_1 are the reaction start and end times, respectively, x_i (i = 1, 2, ..., n) are the state variables of reactor, u_k (k = 1, 2, ..., r) are the control variables, I_0 is a set of initial conditions for state variables, I_1 is a set of end conditions for state variables, and U_k is the ranges of u_k . This problem is called a 'variational problem with constraints'. Since the state equations of distributed parameter reactors are expressed by either partial differential equations or differential integral equations, its optimal control problems are formulated as higher order variational problems with constraints, where the constraints are either partial differential equations or differential integral equations. For the variational problems with constraints, their solutions utilizing the properties inherent in the problems are used for individual problems, as a general method of solving them has not been developed. The optimal control problems for the reactors are described in Section 4.4.4.5.

4.4.4.2 Guidelines for Optimal Reactor Design^(1,2)

As described in the foregoing section, it is difficult mathematically to formulate optimal design problems handling the reactor structure and operation mode, which cannot be expressed in numerical form. Therefore, there are no general solving methods for these problems. In the case of maximizing the selectivity of the desired product, 'Optimal Design Guidelines' are available as described below, based on the properties inherent in the problem, and provide a suboptimal solution.

4.4.4.2.1 Effect of Reactant Concentration in Parallel Reactions

Consider the case where two reactions as shown below proceed in parallel in a reactor.



where, P is a desired product, while Q is an unwanted product. If the reaction rate is expressed by the exponential of the concentration of reactant, those rates are formulated as follows,

$$r_{\rm P} = k_{\rm P} C_{\rm A}^p \tag{4.220}$$

$$r_{\mathbf{Q}} = k_{\mathbf{Q}} C_{\mathbf{A}}^{q} \tag{4.221}$$

The following guidelines are given regarding the reactor structure and operation mode:

Guideline 1

For p > q, the higher the concentration of reactant, the higher the selectivity of the desired product. Thus, the batch stirred tank reactor or tubular reactor is better than the continuous stirred tank reactor.

Guideline 2

For p < q, the lower the concentration of reactant, the higher the selectivity of the desired product. Thus, the continuous stirred tank reactor is more advantageous than the batch stirred tank reactor or tubular reactor.

In a more complicated case with two reactants involved, the following guidelines are given regarding the reactor structure and operation mode:

$$A + B \xrightarrow{r_{\mathsf{P}}} P$$

$$r_{\rm P} = k_{\rm P} C_{\rm A}^p C_{\rm B}^r \tag{4.222}$$

$$r_{\rm O} = k_{\rm O} C_{\rm A}^q C_{\rm R}^s \tag{4.223}$$

Guideline 3

As shown in Figure 4.63, the operation modes for the batch stirred tank reactor are given as follows:

- (a) p > q, r > s: both A and B are fed to the reactor from the beginning of the reaction.
- (b) p > q, r < s: A is fed to the reactor from the beginning of the reaction, and B is added gradually.
- (c) p < q, r > s: B is fed to the reactor from the beginning of the reaction, and A is added gradually.
- (d) p < q, r < s: Both A and B are added gradually into the reactor.

Guideline 4

As shown in Figure 4.64, the structures for a continuous reactor are given as follows:

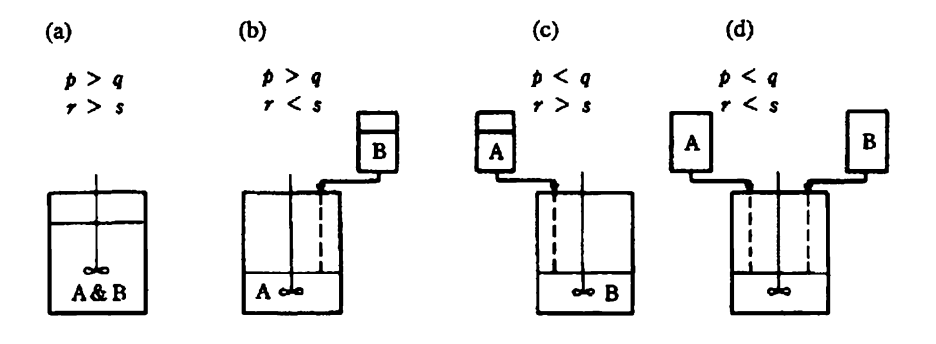


Figure 4.63 Optimal operation modes of a batch stirred tank reactor. (a) Both A and B are fed to the reactor from the beginning of the reaction. (b) A is fed to the reactor from the beginning of the reaction, and B is added gradually. (c) B is fed to the reactor from the beginning of the reaction, and A is added gradually. (d) Both A and B are added gradually into the reactor.

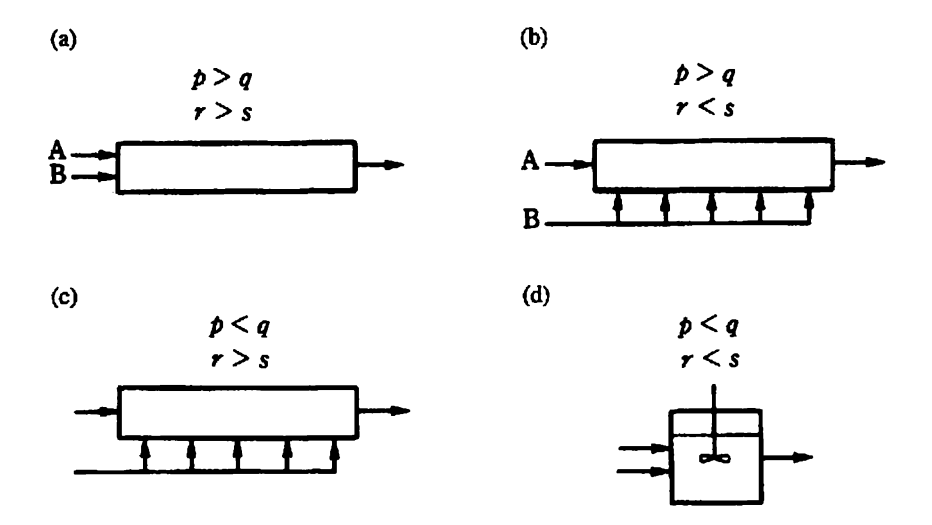


Figure 4.64 Optimal structures for a continuous reactor. (a) The tubular reactor where both A and B are fed to its inlet. (b) The tubular reactor where A is fed to its inlet and B is fed in intermediately through the reaction. (c) The tubular reactor where B is fed to its inlet and A is fed in intermediately through the reaction. (d) The continuous stirred tank reactor.

(a) p > q, r > s: The tubular reactor where both A and B are fed to its inlet.

- (b) p > q, r < s: The tubular reactor where A is fed to its inlet and B fed in intermediately through the reaction.
- (c) p < q, r > s: The tubular reactor where B is fed to its inlet and A fed in intermediately through the reaction.
- (d) p < q, r > s: Continuous stirred tank reactor.

4.4.4.2.2 Effect of the Temperature on Parallel Reactions

The effect of temperature on reaction rate is expressed in the form of activation energy. The temperature dependence of reaction rate constant is represented by Arrhenius type as follows:

$$k_{\rm P} = k_{\rm P}^{\circ} \exp(-E_{\rm P}/RT) \tag{4.224}$$

$$k_{\rm O} = k_{\rm O}^{\circ} \exp(-E_{\rm O}/RT) \tag{4.225}$$

The following guidelines are given regarding the batch stirred tank reactor and multi-stage continuous stirred tank reactor:

Guideline 5

As shown in Figure 4.65(a) and (b), the temperature of the batch stirred tank reactor is set as follows:

- (a) $E_P > E_Q$: set the temperature as high as possible from the beginning to the end.
- (b) $E_P < E_Q$: set the temperature low at the beginning and increase it gradually to higher levels. (The specific temperature profile cannot be obtained unless the variational problems with constraints are solved.)

Guideline 6

The temperature of multi-stage continuous stirred tank reactors are set as follows:

- (a) $E_P > E_O$: set the temperatures of all reactors at the upper limits.
- (b) $E_P < E_Q$: set the temperature of the first reactor low, and gradually raise it with subsequent reactors. (Optimal temperature should be determined by solving the minimization (maximization) problems with the constraints.)

4.4.4.2.3 Effect of the Concentration on Consecutive Reactions

Consider the case where two reactions proceed in series in a reactor as shown below.

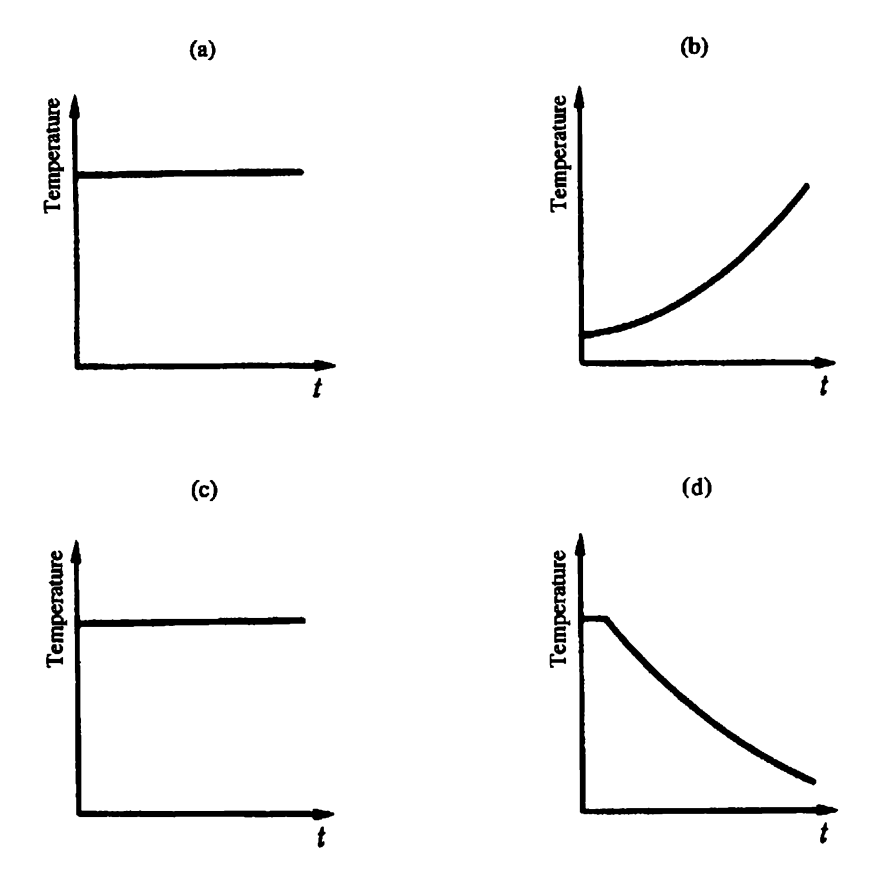


Figure 4.65 Optimal temperature profiles for batch stirred tank reactor. (a) Parallel reactions $E_P > E_q$. Set the temperature as high as possible from the beginning to the end. (b) Parallel reactions $E_P < E_q$. Set the temperature low at the beginning and increase it gradually to higher levels. (c) Consecutive reactions $E_P > E_q$. Set the temperature as high as possible from the beginning to the end. (d) Consecutive reactions $E_P < E_q$. Set the temperature high at the beginning and decrease it gradually to lower levels.

$$A + B \xrightarrow{r_P} P + B \xrightarrow{r_Q} Q$$

Here, P is a desired product, and Q is an unwanted product. Suppose that the effect of the reactant concentration on the reaction rate is expressed by orders of reaction. If the relationship between the reactant concentration and reaction rate is expressed as

$$r_{\rm P} = k_{\rm P} C_{\rm A}^p C_{\rm B}^r \tag{4.226}$$

$$r_{\rm O} = k_{\rm O} C_{\rm P}^{q} C_{\rm B}^{\rm s} \tag{4.227}$$

the following guidelines are given regarding the reactor structure and operation mode:

Guideline 7

The batch stirred tank reactor or tubular reactor is better than the continuous stirred tank reactor.

Guideline 8

The following operation modes are given for the batch stirred tank reactor:

- (a) r > s: both A and B are fed from the beginning of the reaction (Figure 4.63(a)).
- (b) r < s: A is fed from the beginning of the reaction, and B is added gradually (Figure 4.63(b)).

Guideline 9

The following structure and operation modes are given for a continuous reactor:

- (a) r > s: the tubular reactor where both A and B are fed to its inlet (Figure 4.64(a)).
- (b) r < s: the tubular reactor where A is fed to its inlet and B is fed intermediately through the reaction (Figure 4.64(b)).

Guideline 10

When a stirred tank reactor is used for easy control of reaction conditions, the stirred tank reactor with a separator as shown in Figure 4.2(b) is very effective in separating the desired product P.

4.4.4.2.4 The Effect of the Temperature on Consecutive Reactions

The effect of temperature on the reaction rate is expressed in the form of activation energy. The temperature dependence of the reaction rate constant is represented by Arrhenius as follows:

$$k_{\rm P} = k_{\rm P}^{\circ} \exp\left(-E_{\rm P}/RT\right) \tag{4.228}$$

$$k_{\rm Q} = k_{\rm Q}^{\circ} \exp\left(-E_{\rm Q}/RT\right) \tag{4.229}$$

The following guidelines are given regarding the batch stirred tank reactor and multi-stage continuous stirred tank reactor:

Guideline 11

As shown in Figure 4.65(c) and (d), the temperatures of the batch stirred tank reactor are set as follows:

- (c) $E_P > E_Q$: set the temperature as high as possible from the beginning to the end.
- (d) $E_P < E_Q$: set the temperature high at the beginning and decrease it gradually to lower levels. (The optimal temperature profile can be obtained by solving the variational problems with constraints.)

Guideline 12

The temperatures of the multi-stage continuous stirred tank reactor are set as follows:

- (c) $E_P > E_O$: set the temperatures of all reactors at the upper limits.
- (d) $E_P < E_Q$: set the temperature of the first reactor high, and gradually decrease it with subsequent reactors. (Optimal temperature should be determined by solving the minimization (maximization) problems with constraints.)

4.4.4.3 Optimal Allocation of Measuring Instruments

The optimal allocation problem of measuring instruments to maximize the accuracy of estimating the state in the reactor, is one of the main design problems. As the state in the lumped parameter reactor is uniform, the state measured at one point in the reactor may represent the overall state in the reactor. For the distributed-parameter reactor, measuring instruments should be allocated to accurately estimate the distribution of state variables. In particular, when unstable phenomena tend to be generated by an exothermic reaction in the reactor, it is very important to estimate the temperature distribution in the reactor accurately.

A study on the optimal allocation problem of measuring instruments for a distributed-parameter system started early in the 1970s, with the initial study limited to linear systems⁽³⁾. In the 1980s, research on non-linear systems such as the fixed bed reactor was started, and a method to determine the optimal allocation of thermometers was proposed⁽⁴⁾. However, in order to determine the optimal allocation of thermometers in the fixed bed reactor by using the proposed method as it is, it is necessary to develop a rigorous dynamic model for the reactor under consideration.

Since it is quite difficult to develop the rigorous dynamic model for industrial scale reactors at the design stage, the optimal allocation of thermometers in the fixed bed reactor cannot be determined by the proposed method. However, the results of research on the optimal allocation problem of thermometers is summarized in the following 'Guidelines for Optimal Allocation' to be used for determining the thermometer allocation.

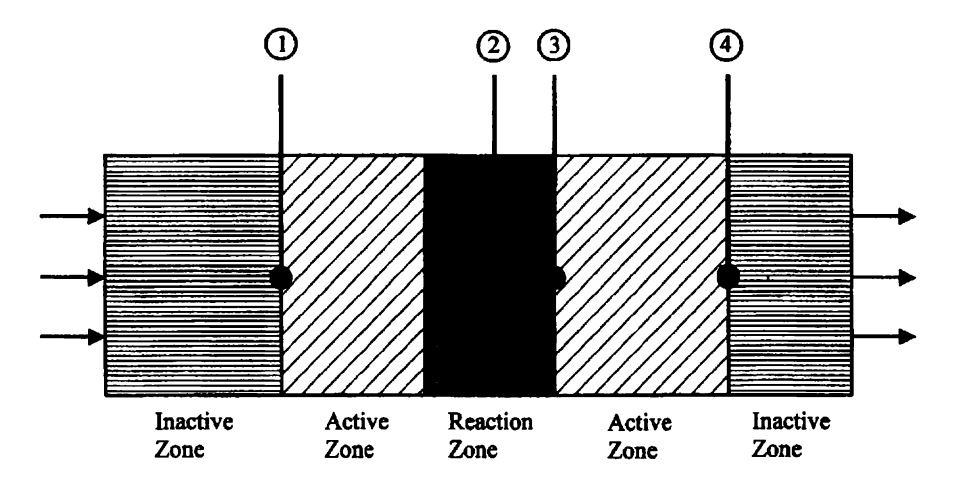


Figure 4.66 Thermometer allocation in a fixed bed reactor.

Guideline 1

At least three thermometers are required to estimate the temperature distribution in a fixed bed reactor.

Guideline 2

Out of the three thermometers, one is placed at the entrance of an active zone in the fixed bed reactor ((1) in Figure 4.66), another in the centre of the reaction zone ((2) in Figure 4.66), and the other at the exit of the active zone ((3) in Figure 4.66).

Guideline 3

If it is allowable to allocate the fourth thermometer, it is placed just behind the reaction zone ((4) in Figure 4.66).

Even if the rigorous dynamic model for the reactor is not obtained, the optimal allocation of thermometers is determined by the above guidelines, with some knowledge of the location of the reaction zone.

4.4.4.4 Solution to the Minimization Problem with Constraints

The optimal design problem of the lumped-parameter reactor after the determination of reactor structure and operation mode, is formulated as the following minimization problem with constraints:

Minimize
$$f(x_1, x_2, ..., x_n)$$
 (4.230)

Subject to
$$g_j(x_1, x_2, ..., x_n) \le 0 \ (j = 1, 2, ..., p)$$
 (4.231)

$$h_k(x_1, x_2, \dots, x_n) = 0 \ (k = 1, 2, \dots, q < n)$$
 (4.232)

Although a penalty function method is well known as a solution to these problems, this method has disadvantages such as slow convergence and numerically poor conditions developed with calculations. The multiplier method⁽⁵⁾ shown below is an improved version of the penalty function method with such disadvantages, and is known to be the most effective solution.

4.4.4.4.1 Algorithm of the Multiplier Method

Define vectors x of state and design variables, vectors λ and μ of Lagrange multipliers, and vectors t and r of penalty parameters as follows:

$$x = (x_1, x_2, \dots, x_n)^T, \lambda = (\lambda_1, \lambda_2, \dots, \lambda_p)^T, \mu = (\mu_1, \mu_2, \dots, \mu_q)^T$$
$$t = (t_1, t_2, \dots, t_p)^T, r = (r_1, r_2, \dots, r_q)^T$$

Also, define the extended Lagrange function $L(x, \lambda, \mu; t, r)$ as

$$L(x, \lambda, \mu; t, r) = f(x) + \sum_{j=1}^{p} [\max\{0, \lambda_j + t_j g_j(x)\}^2 - (\lambda_j)^2] / (2t_j)$$

$$+ \sum_{k=1}^{q} [\mu_k h_k(x) + r_k \{h_k(x)\}^2]$$
(4.233)

then the above minimization problems with constraints can be solved by the algorithm shown below:

Initialization

Let all elements of λ and μ be 0 and all elements of t and r be 10. Let $\alpha = 10$, $\beta = 0.25$, $c = \infty$ and m = 0, and set ε at a small positive constant, necessary to judge the satisfaction degree for the constraints.

Minimization

Obtain x to minimize $L(x, \lambda, \mu; t, r)$.

Selection

Let sets of j and k satisfying the following equations be J and K.

$$|\max\{g_j(x), -\lambda_j/t_j\}| > \beta c \quad (j = 1, 2, ..., p)$$

 $|h_k(x)| > \beta c \quad (k = 1, 2, ..., q)$

Perform the following calculations.

$$a = \max_{j} |\max\{g_{j}(x), -\lambda_{j}/t_{j}\}|$$
$$b = \max_{k} |h_{k}(x)|$$

If a > c or b > c, go to Update 3, otherwise, go to Update 1.

Update 1

$$c \leftarrow \max(a,b)$$
. If $c \le \varepsilon$, go to **End**.

Update 2

$$\lambda_j \leftarrow \max\{0, \lambda_j + t_j g(x)\} \quad (j = 1, 2, ..., p)$$

 $\mu_k \leftarrow \mu_k + r_k h_k(x) \quad (k = 1, 2, ..., q)$

Update 3

$$t_j \leftarrow \alpha t_j \ (j \in J), \quad t_j \leftarrow t_j \ (j \notin J)$$

 $r_k \leftarrow \alpha r_k \ (k \in K), \quad r_k \leftarrow r_k \ (k \notin K)$

Go to Minimization

End

Output x as an optimal solution and end the solving process.

For **Minimization** in the algorithm of the multiplier method, use the algorithm solving the following unconstrained minimization problem:

Minimize
$$f(x_1, x_2, ..., x_n)$$
 (4.234)

The quasi-Newton method is recommended for such an algorithm

4.4.4.4.2 Algorithm of the Quasi-Newton Method

Suppose that H is the square matrix of $n \times n$, define vectors x, y, u and v as follows:

$$x = (x_1, x_2, ..., x_n)^T, y = (y_1, y_2, ..., y_n)^T,$$

 $u = (u_1, u_2, ..., u_n)^T, v = (v_1, v_2, ..., v_n)^T$

Also, let o be the n-dimensional zero vector and E the n-dimensional unit vector to define,

$$\nabla f = (\partial f/\partial dx_1, \partial f/\partial x_2, \dots, \partial f/\partial x_n)^T$$

Initialization

 $H \leftarrow E$, Assume the initial values of x.

Judgment

If $\nabla f(x) = o$, go to **End**.

Gradient

$$v \leftarrow -H\nabla f(x)$$

Check

If $y^T \nabla f(x) \ge 0$, go to **Gradient** with $H \leftarrow E$.

Search

Obtain ξ to minimize $f(x + \xi y)$.

Correction

$$u \leftarrow \xi y, v \leftarrow \nabla f(x + \xi y) - \nabla f(x), x \leftarrow x + \xi y$$

 $H \leftarrow (E - uv^T/u^Tv)H(E - uv^T/u^Tv) + uu^T/u^Tv$
Go to **Judgment**

End

Output x as an optimal solution and end the solving process. For **Search** in the quasi-Newton method, use the following algorithm:

4.4.4.4.3 One-dimensional Minimization Algorithm

Define functions $\phi(\xi)$ and $\psi(\xi)$ as follows:

$$\phi(\xi) = f(x + \xi y) - f(x) - \gamma \xi y^T \nabla f(x)$$

$$\psi(\xi) = y^T \nabla f(x + \xi y) - \delta y^T \nabla f(x)$$

where γ is a constant of 10^{-4} – 10^{-2} , and δ is a constant of 0.1–0.9.

Initialization

Set the values of search step $\nabla \xi$ with respect to γ and δ . $\xi \leftarrow \Delta \xi$

208 H. MATSUYAMA

Range Search

Calculate $\phi(\xi)$. If $\phi(\xi) > 0$, go to Minimum Value Search. Calculate $\psi(\xi)$. If $\psi(\xi) \ge 0$, go to End. Let $\xi \leftarrow \xi + \Delta \xi$, then go to Range Search.

Minimum Value Search

$$a \leftarrow \xi - \Delta \xi, b \leftarrow \xi$$

Average

 $\eta \leftarrow (a+b)/2$ If $\phi(\eta) \le 0$ and $\psi(\eta) \ge 0$, then go to **End** as $\xi \leftarrow \eta$. If $\phi(\eta) > 0$, then go to **Average** as $b \leftarrow \eta$. Otherwise, go to **Average** as $a \leftarrow \eta$.

End

Output ξ as an optimal solution, and end the solving process.

4.4.4.5 Optimal Control Problems for Reactors

The optimal control problems for reactors include optimization of temperature changes in the batch stirred tank reactor, optimization of temperature distribution in the fixed bed reactor, minimization of the amount of off-specification products at the changeover of brand, and minimization of the duration for start-up. The optimal control for the changeover of brand depends on the combination of the brands produced before and after the changeover, and the magnitude of the variations in reactor conditions is significant at the start-up. Therefore, these problems are more difficult than the optimization problems of temperature changes in the batch stirred tank reactor and temperature distribution in the fixed bed reactor.

Studies on optimal control problems of reactors were started at the beginning of the 1960s in order to maximize the selectivity of the objective product. The optimization problems of temperature changes in the batch stirred tank reactor and those of temperature distribution in the fixed bed reactor were formulated in the following constrained variation problems to obtain their solutions by using dynamic programming⁽⁶⁾.

Minimize
$$\int_{t_0}^{t_1} f_0(x_1, x_2, \dots, x_n; u_1, u_2, \dots, u_r) dt$$
 (4.235)

subject to
$$dx_i/dt = f_i(x_1, x_2, \dots, x_n; u_1, u_2, \dots, u_r)$$
 $(i = 1, 2, \dots, n)$ (4.236)

$$x_i(t_0) = a_0 \ (i \in I_0) \tag{4.237}$$

$$x_i(t_1) = a_1 \ (i \in I_1) \tag{4.238}$$

$$u_k \in U_k \tag{4.239}$$

In optimal control problems, the accuracy of the dynamic model of the reactor under consideration largely affects the usefulness of the obtained solutions. Since there were no means of developing complicated reactor models, owing to less capability of computers at that time in the 1960s, studies on optimal control were limited to complete mixing models of stirred tank reactors, or fixed bed reactor models where radial temperature distribution and axial mixing and heat transfer were neglected. Therefore, the study results were applied only to limited ranges of optimal control problem for industrial-scale reactors. In the 1990s, high-speed and large-memory computers are used, and it is possible to develop reactor models on an industrial scale and to realize optimal controls.

For a gas-phase polymerization reactor for polyethylene using lumped parameter reactors, the solution to optimal control problems at the changeover of brand is possible⁽⁸⁾ by developing dynamic reactor models and an on-line estimation method⁽⁷⁾ for the physical properties of polymers. For distributed parameter reactors, the models on industrial-scale tubular reactors have been developed, and it confirms the prediction of variations at the start-up of actual reactors⁽⁹⁾. In the near future, it will be possible to solve the optimal control problems for distributed parameter reactors.

References

- (1) O. Levenspiel, Chemical Reaction Engineering, John Wiley & Sons (1972).
- (2) R. Aris, The Optimal Design of Chemical Reactors, Academic Press (1961).
- (3) T. K. Yu and J. H. Seinfeld, Int. J. Control, 18, 785 (1973).
- (4) J. Alvarez, A. Romagnoli and G. Stephanopoulos, Chem. Eng. Sci., 36, 1695 (1981).
- (5) M. R. Hestenes, J. Optimization and Appl., 4, 303 (1969).
- (6) R. Aris, The Optimal Design of Chemical Reactors, Academic Press (1961).
- (7) K. B. McAuley and J. F. MacGregor, AIChE J., 37, 825 (1991).
- (8) K. B. McAuley and J. F. MacGregor, AIChE J., 38, 1564 (1992).
- (9) J. Verwijs, W. van den Berg and K. R. Westerterp, *AIChE J.*, 38, 1871 (1992).

CHAPTER 5 Design of an Industrial Reactor

This chapter describes the outline of design for industrial reactors applied to six typical processes in the chemical industry. The production facilities in this industry have their own purpose in the social economic system. Various types of reactors are not only designed following scientific fundamentals, but they also are significant in the effort to consider the economic environment as a key function of production facilities. In this sense, before going into the particulars of industrial reactors, the background of the industry in which the production facilities are installed, including the said reactors, is summarized below.

Examples given in some paragraphs are intended so that readers may acquire a better understanding of actual reactor design.

In this chapter it should be observed that the reactor design involved certain assumptions prior to actual reactor design, based on the technological theory, the trade-off between design and economics, cost consciousness, etc.

The outline of six industrial reactors selected is as follows:

Process	Chemical reaction	Type of reactor	Industrial facility
Naphtha cracking	Consecutive thermal cracking reaction, non-catalytic reaction	Heating tubes, continuous vapour phase, atmospheric pressure	Production of ethylene and other olefin stocks
Tubular steam reforming	Reversible reaction, chemical equilibrium, heterogeneous catalytic reaction	Heating tubes, fixed bed, continuous vapour phase, high pressure	Production of reducing gas, hydrogen, and other synthesis gases
Epoxy resin production	Polymerization, homogeneous catalytic reaction	Batch stirred tank, liquid phase, atmospheric pressure	Production of various grades of epoxy resin
Hydrotreating	Hydrogenation and hydro- cracking reaction, heterogeneous catalytic reaction	Fixed bed, high pressure	Upgrading of petroleum heavy fractions, production of gasoline
Fluid catalytic cracking	Cracking reaction heterogeneous catalytic reaction	Fluidized bed, atmospheric pressure	Upgrading of petroleum heavy fractions, production of gasoline
Wet type flue gas desulphurization	Heterogeneous acid-base reaction	Jet bubbling reactor, continuous gas/liquid/solid phase, atmospheric pressure	Flue gas desulphurization for power plant using fossil fuels

CHAPTER 5.1

Naphtha Cracking

HIROSHI YAGI

Chiyoda Corporation, Japan

Thermal cracking is a well known and widely accepted technology for olefin production. This technology is also called steam cracking, since steam is added to hydrocarbons before cracking to reduce the partial pressure of hydrocarbons and to produce a better yield performance. In the petrochemical industry, steam cracking is a core technology for producing olefins, although there are alternative routes from off-gas of fluid catalytic cracking units in oil refineries or by dehydrogenation of propane or butanes. Figure 5.1 is a picture of a typical industrial cracking furnace.

Thermal cracking reactions are basically used to break the C—C bonds of hydrocarbons non-catalytically at a high temperature of around 800–900 °C and at a low pressure of 0.16–0.2 Mpa in the coils located in the radiant sections of furnaces. They finally produce lower molecular weight olefins. In the case of naphtha cracking, the number of elementary reactions reaches 2000, including radical reactions, whereas gas oil cracking is more complex with more than 3000 reactions⁽¹⁾.

Table 5.1 shows the typical yield data of once-through reactions using various feedstocks. In industrial practice, non-reacted ethane or propane is separated in the cold separation section and recycled back to cracking furnaces where ethane and propane are cracked again. Therefore, the ultimate yields of olefins are much higher than those of once-through yields.

5.1.1 PETROCHEMICAL COMPLEX IN JAPAN

Naphtha is used as a base feedstock for petrochemical complexes in Japan. LPG is also used as an alternative feedstock, but accounts for only 2-3% of the total feedstock. In European countries, naphtha accounts for about 60% of such feedstock and the rest of the feedstocks are LPG and gas oil. However, in the United States, ethane and LPG separated from natural gas are major feedstocks, which are used for 70-80% of total demand, while the rest are naphtha and gas oil.

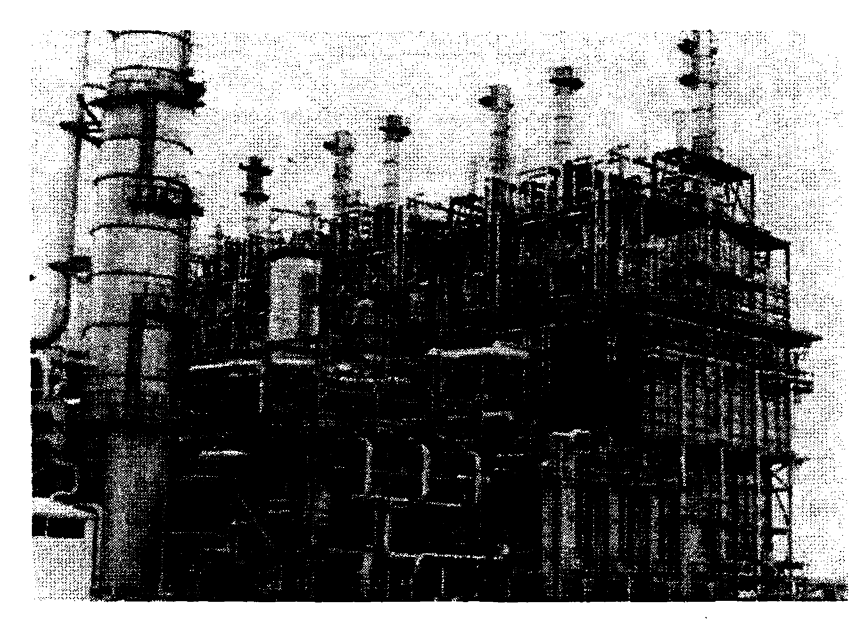


Figure 5.1 Large scale industrial cracking unit (by courtesy of Nigerian National Petroleum Corp./ELEME Petrochemicals Company Ltd. and The M. W. Kellogg Company).

Figure 5.2 shows the product flows in Japanese complexes in the 1990s. Based on naphtha cracking, the product pattern consists of ethylene at 28%, propylene at 17%, butene and butadiene products at 11%, off-gas and pyrolysis heavy oil at 24% and pyrolysis gasoline at 20%.

A typical petrochemical complex consists of an ethylene plant based on a thermal cracking process at the core and associated downstream plants such as polyolefin and aromatic plants using olefin products. The configuration of the complex depends on the final product types and the available feedstocks. A complex based on naphtha-cracking ethylene plants is more elaborate than a complex based on cracking gases such as ethane or propane.

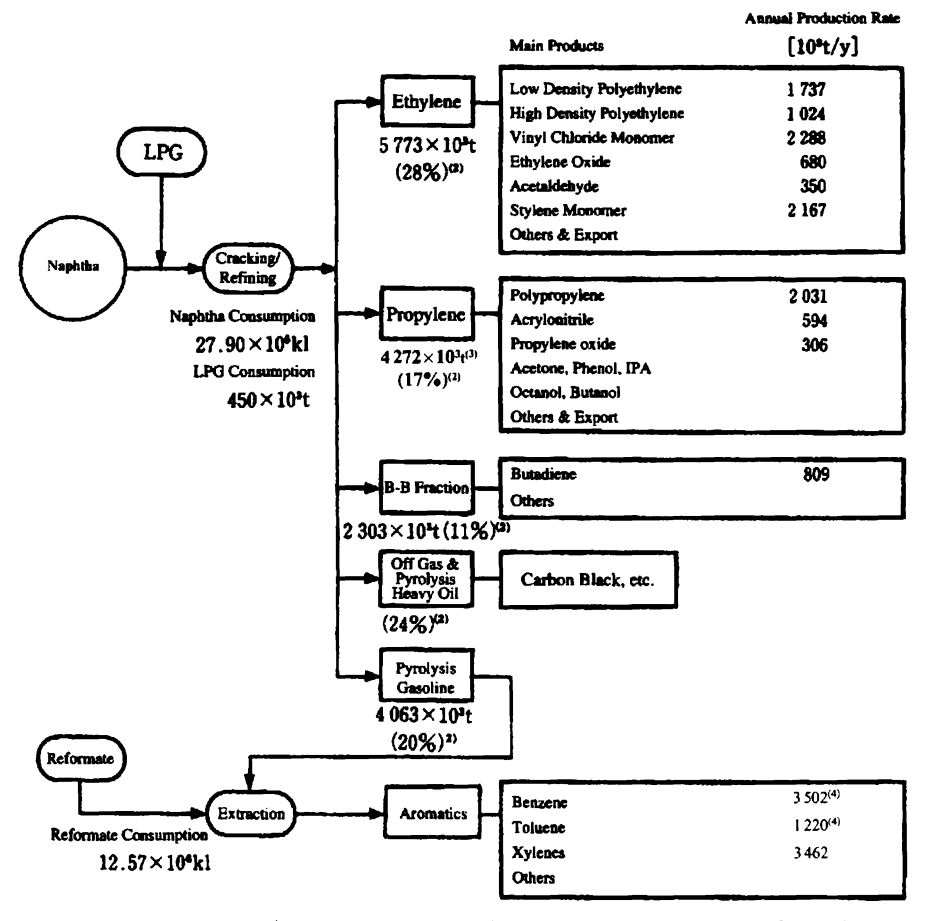
Some 60-70% of pyrolysis gasoline fractions consist of aromatics such as benzene, toluene and xylenes called a BTX fraction. These are recovered by extractive separations at 12-14% based on the feedstock rate. However, in the recent product pattern, the BTX extraction rate tends to decrease due to advances in cracking technology and a paraffinic and lighter naphtha used as the feedstock. In the 1970s, about 50% of BTX demand was supplied from ethylene plants; however, in the 1990s, this has decreased to 40%. The rest of BTX demand is supplied from catalytic naphtha reforming plants.

Figure 5.3 shows the production rate compared to the available capacity of ethylene plants in Japan. The ethylene production rate increased through

Table 5.1 Typical yields of once-through cracking⁽²⁾

Feed Yield [wt%]	Ethane	Propane	<i>n</i> -butane	i-butane	Light naphtha	Full range naphtha	Kerosine
Hydrogen	3.70	1.31	0.90	1.25	0.98	0.86	0.65
Methane	2.80	25.20	20.90	22.60	17.40	15.30	12.20
Acetylene	0.26	0.65	0.55	0.60	0.95	0.75	0.35
Ethylene	50.50	38.90	37.30	10.70	32.30	29.80	25.00
Ethane	40.00	3.70	4.50	0.60	3.95	3.75	3.70
MA/PD*	0.03	0.60	0.80	3.00	1.25	1.15	0.75
Propylene	0.80	11.50	16.40	21.20	15.00	14.30	14.50
Propane	0.16	7.00	0.15	0.30	0.33	0.27	0.40
1,3-butadiene	0.85	3.55	3.85	2.15	4.75	4.90	4.40
Butylenes	0.20	0.95	1.80	17.50	4.55	4.15	4.20
Butanes	0.23	0.10	5.00	8.00	0.10	0.22	0.10
C ₅ S	0.22	1.60	1.60	2.00	3.85	2.35	2.00
$C_6 \sim C_8$ non-aromatics					2.02	2.05	1.55
Benzene	0.20	2.20	2.00	3.06	5.60	6.00	6.20
Toluene	0.05	0.40	0.90	1.40	1.65	4.60	2.90
Xylenes/Ethylbenzen			0.35	0.40	0.72	1.65	1.20
Stylene					0.65	0.85	0.70
C ₉ -200 °C		1.00	1.30	3.25	0.65	3.10	3.10
Fuel oil		1.34	1.70	1.99	3.30	3.95	16.10
Total	100.00	100.00	100.00	100.00	100.00	100.00	100.00

^{*}MA: Methylacetylene, PD: Propadiene



Remarks: (1) All figures from 'Statistics of Chemical Industries' issued by Ministry of International Trade and Industry, except for LPG consumption from MITT's Basic Chemicals Sect Data.

- (2) Figures inside parentheses show the average yields of the entire ethylene centres in Japan.
- (3) Including propylene from FCC units.
- (4) Including tars from coal industries.

Figure 5.2 Gross flow of petrochemical products in Japan.

the first oil embargo in 1973 and the second one in 1978. The process technology in ethylene plants has been changed, and the trend is shown in Table 5.2. During this period, unit capacity of the cracking furnace has also increased and ethylene yield as well as energy efficiency has been significantly improved.

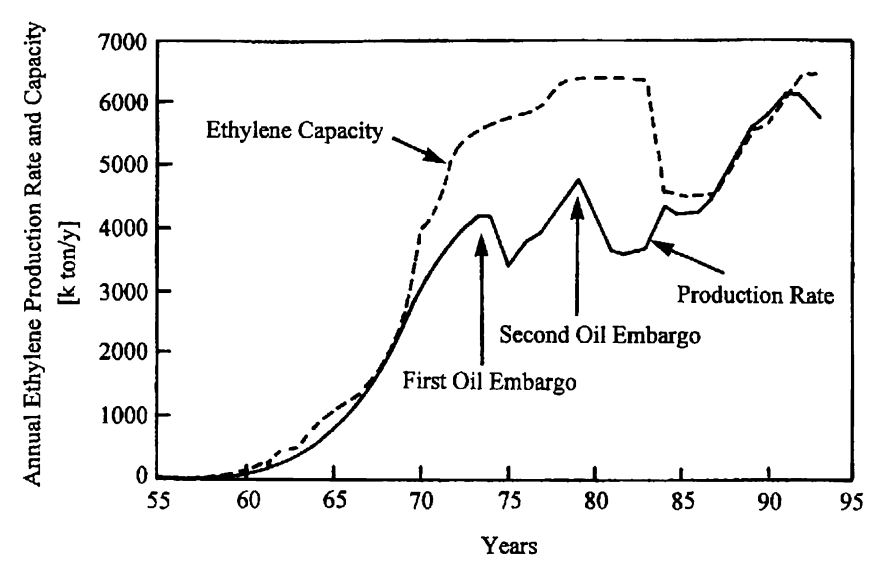


Figure 5.3 Trends in Japanese annual ethylene production rate and the available capacity.

5.1.2 CRACKING FURNACE FOR NAPHTHA

Feed naphtha is preheated at the convection section of a cracking furnace and introduced to the radiation coils, together with dilution steam when the naphtha is thermally cracked into olefin fractions.

5.1.2.1 Type of Cracking Furnace

As shown in Figure 5.4 for a typical configuration of the cracking furnace, it is generally designed as a fire-box type which can be grouped into several subtypes with regard to radiant coils and burner types. In particular, with increasing capacity of the cracking furnace and requirement of high severity operation, the accurate control of heat flux in the radiant coils is important. This is attained by using both floor burners and either radiant wall or stage burners. Fuel gas is mainly used for firing, but fuel oil is also used in some cases. Cracking reactions occur in the radiant coils, and the convection section is used for heat recovery by feed preheating, steam superheating and boiler feed-water preheating. To avoid overcracking of reacted gas, transfer line exchangers for rapid cooling are installed just at the exit of the radiant coil.

The radiant coils are generally located in a single row. The burners are placed on the floor and side wall, or only on the floor. A long-flame type is used for the floor burners, and the flame pattern is formed upward in parallel with

Table 5.2 Technological Trends in a cracking furnace

Items	Years (capacity)	1955–1960 (10–20 k ton/year)	19611964 (100 k ton/year)	1965-1972 (200-300 k ton/ year)	1972–1975	1976–1980
Ethylene yield	[wt%]	16–18	20–25	30	>	33
Thermal efficiency of cracking furnace	[%]	70	80	85	90	95
Material of radiant coil		SUS304	SUS310	HK40 (25Cr- 20Ni)	\rightarrow	HP (25Cr-35Ni)
Constinue tomorphisms	(°C)	750	900	Alloy800, etc. 830		HiSi-HK40, etc. 850–880
Cracking temperature	[°C]		800		\rightarrow	
Residence time	[s]	1–2	0.6–1	0.2 – 0.5	→	0.1-0.3
Coil arrangement		Horizontal	Vertical	→	\rightarrow	→
Yield of $C_6 \sim C_8$ aromatics	[wt%]	15–16	16-17	12-15	\rightarrow	11–12
Flue gas temperature leaving furnace	[°C]	350-400	250–300	about 200	about 150	100–120

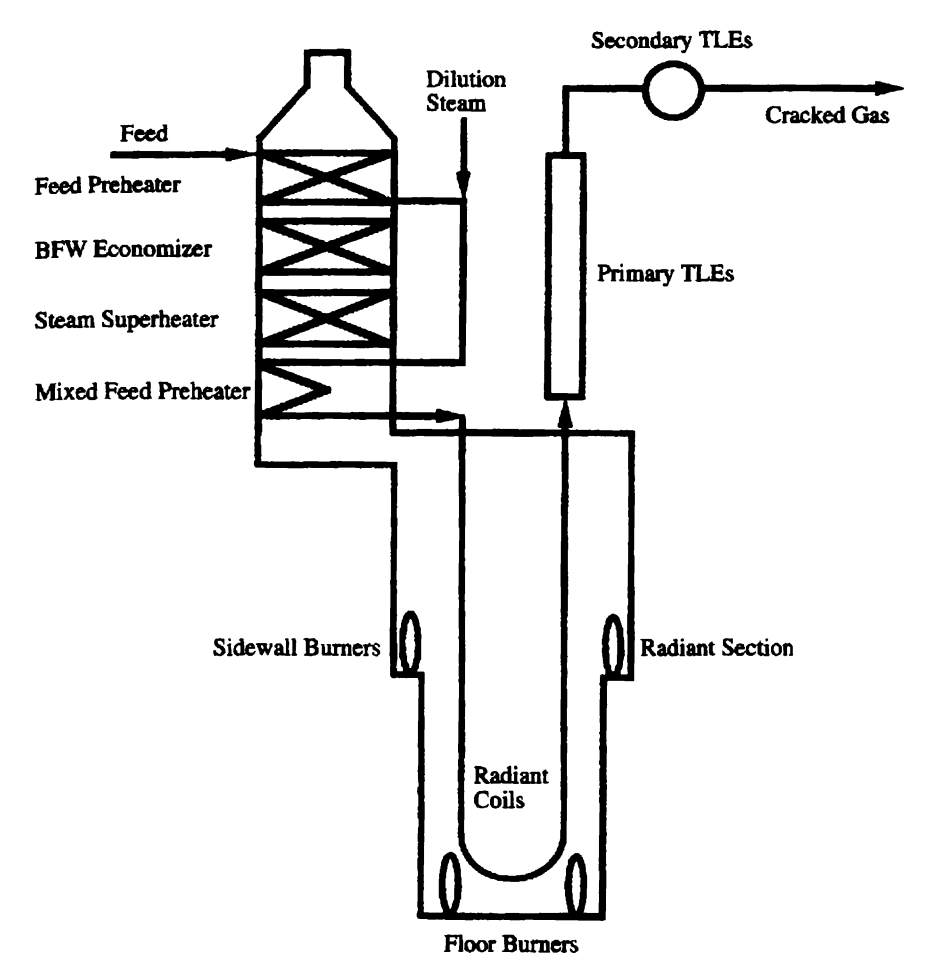


Figure 5.4 Typical configuration of the cracking furnace.

the radiant coils. The side wall burners are generally the radiant wall type and are located at several stages every 1–2 metres. Several sets of side wall burners with long and oval flame may also be installed at the terrace of the radiant wall. The use of side wall burners makes it possible to achieve an accurate control of the heat flux over the radiant coils.

5.1.2.2 Radiant Tube and Coil

In the early days, horizontal straight radiant coils were used, connected with bends at their ends. Along with the requirement of higher severity, the coil skin

temperature rose higher. It caused the deflection of coils so that it was difficult to support the coils horizontally. The coil was therefore set vertically and suspended from the ceiling.

Obtaining better olefin yields requires a short residence time, so coil diameter has been reduced and coil length shortened. The inner diameter of the coil has been reduced to 40–50 mm and the length is now about 10–20 metres. Typical coil arrangements are shown in Figure 5.5.

With respect to coil materials, HK-40 or Incoloy 800 was previously used. With the increase in the severity of operating conditions, the coil skin temperature has risen higher to about 1100 °C. Keeping coil life longer requires carburization-resistance material, and high chomium and high nickel materials

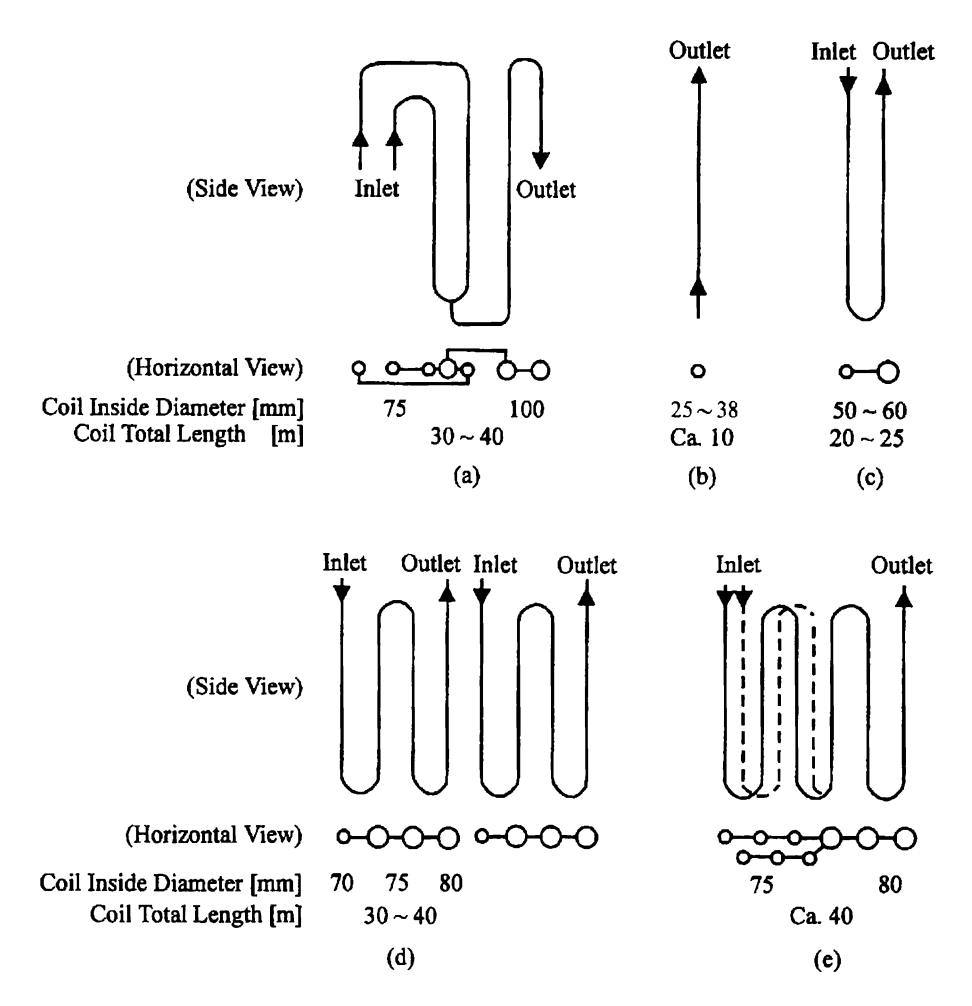


Figure 5.5 Dimension and arrangement of radiant coil.

-	Material	С	Si	Cr	Ni
Cast iron coil	HP MOD			25	35
	XM	0.35-0.45	2.0 Max	32-37	42-46
	XTM	0.40-0.45	1.5 Max	34–37	43-46
Wrought coil	800H	0.06	0.36	20	33
•	HK4M	0.2 - 3.0	0.75 Max	24-26	24-26
	HK4MS	0.1 - 0.2	1.4-2.0	23-26	34-38
	HPM	0.1-0.2	1.4-2.0	23-26	37-40

Table 5.3 Chemical composition of radiant coil materials

with the addition of tungsten, molybdenum or niobium have been developed (refer to Table 5.3). The radiant coils are mainly manufactured by a centrifugal casting method, but this method has a defect in that the inner surface may have casting divots. This causes the acceleration of carburization, so machining on the inner surface requires removal of casting divots, particularly on the surface of the exit part operated at the highest temperature. Wrought coils have been developed to overcome this casting defect.

5.1.3 TREATMENT OF A CRACKED GAS

An ethylene process consists of a hot section, including cracking furnaces, a heat recovery of cracked gas, and a cold section to separate into ethylene, propylene and other olefin products.

The hot section generally consists of the units shown in Figure 5.6. Cracked gas is quenched by a series of transfer line exchangers to recover heat and to terminate cracking reactions. The exchangers generate high-pressure steam (about 10 MPa and 500 °C). Cracked gas is further cooled down in the oil quench tower and the water quench tower, where several levels of heat are recovered. The gas from the top of the water quench tower enters the four to six stage cracking gas compressor to pressurize from 40–50 kPa to 3–3.5 MPa. In the compression stages H₂S and CO₂ are removed from cracked gas by treating caustic soda. The gas is then dried and sent to the cold section, which can be divided into two configurations: the front-end demethanizing system and the front-end depropanizing system. These systems are shown in Figures 5.7(a) and 5.7(b).

Acetylene as the by-product is a catalyst poison for downstream polyethylene productions, so it needs to be removed either by hydrogenation or absorption. Acetylene concentration is up to about 1.5% by volume in an ethylene and ethane mixture in the front-end demethanizing system. Accordingly, controlling the temperature on hydrogenation is relatively difficult. However, the recent advances on the catalyst improve the reaction performance such as the selectivity of acetylene hydrogenation. This

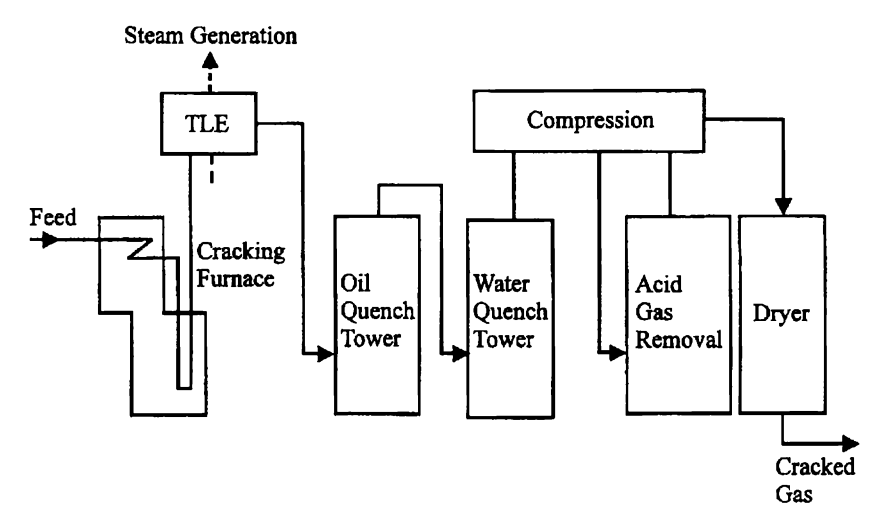


Figure 5.6 Hot section in ethylene process (cracking furnace + heat recovery + gas purification).

hydrogenation system is called 'back-end hydrogenation' because the reactor is sited after the demethanizer. To moderate the reaction and increase selectivity, carbon monoxide may be added as the moderator. However, if high-purity ethylene is required, carbon monoxide is sometimes not used.

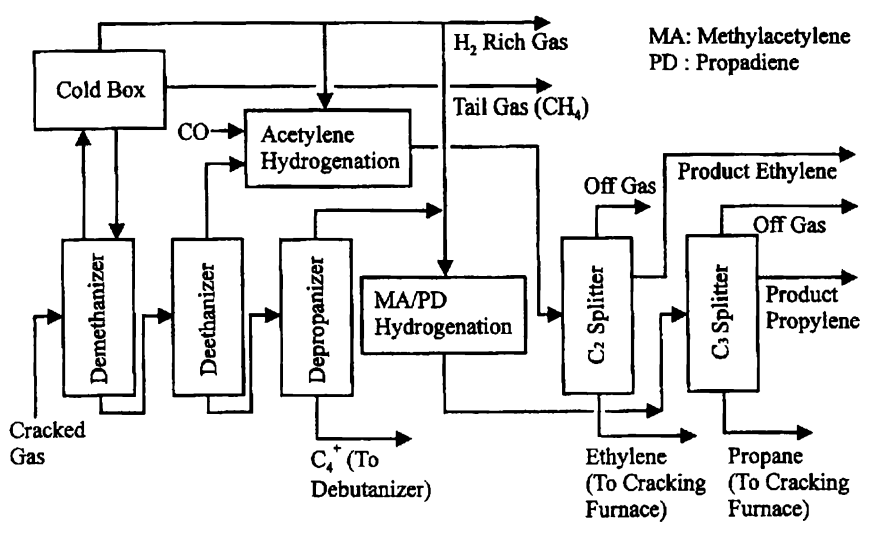
On the other hand, in the front-end demethanizing system, the hydrogenation reactor is sited before the demethanizer, and this system is called 'front-end hydrogenation.' In this case, the acetylene content is relatively low and the hydrogenation reaction is milder than that of the back-end hydrogenation. Hydrogen is contained in the cracked gas, so an additional supply of hydrogen is usually not necessary. Carbon monoxide is also contained in the gas and may improve reaction selectivity. However, the reaction conditions are subject to change due to the furnace operations and hence the cracked gas compositions.

5.1.4 QUENCH AND HEAT RECOVERY

The purposes of the quencher are (1) to terminate the cracking reactions and to prevent the formation of heavy materials by polymerization, and (2) to recover energy at a high temperature. Generally, cracked gas is quenched by the transfer line exchangers, which are directly connected to the radiant coil exit and generate high pressure steam.

In the case of naphtha or gas oil feedstocks, cracked gas may be condensed in the exchanger if the quench temperature is too low. The condensed liquid will accelerate the fouling rate. Therefore, the quench temperature is kept higher and the heat recovery is limited.

In the case of ethane or propane cracking, as less heavier materials are formed by cracking reactions, it is possible to lower the condensing temperature. As the fouling rate may be suppressed, heat is recovered effectively in the transfer line exchangers. Therefore, an oil quench tower is usually not required.



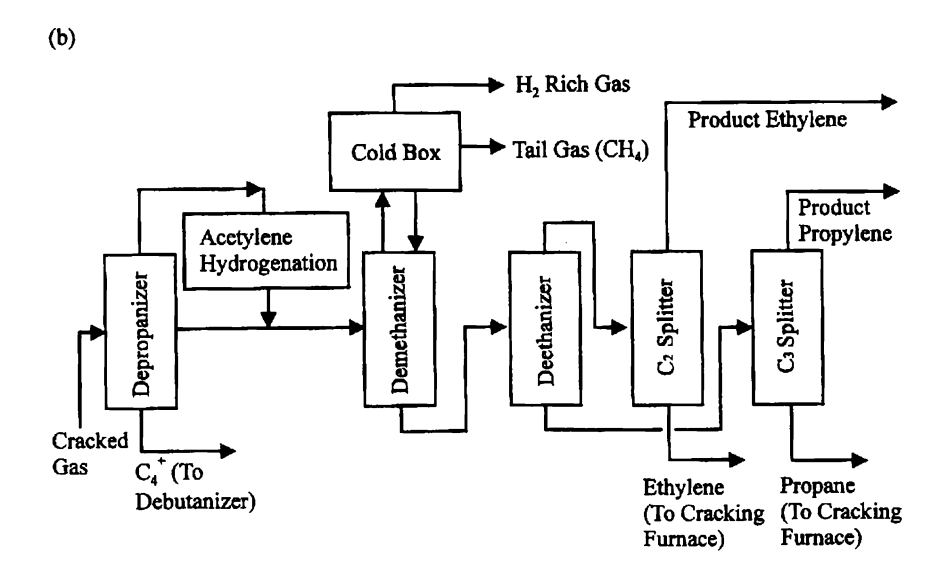


Figure 5.7 Cold section in the ethylene process. (a) Cold section (front-end demethanizer system). (b) Cold section (front-end depropanizer system).

Cracked gas from the transfer line exchangers then enters the oil and water quench towers, and further heat is recovered. At the oil quench tower, cracked gas is cooled down from about 350 °C to 100 °C by direct contact with quench oil. Quench oil is supplied at about 100 °C, and the quench oil temperature is controlled at the bottom of the tower to below about 190 °C to avoid polymerization. However, for heat recovery, a higher temperature is more efficient. If the temperature is too high, it tends to accelerate polymerization. Therefore, an optimal temperature should be selected such as 190 °C. Heat is recovered by generating the dilution steam required for cracking. The purpose of dilution steam is to reduce the partial pressure of hydrocarbons and to facilitate cracking reactions. The heat is also used as reboiler heat in downstream separators. At the water quench tower, heat is recovered at the relatively low temperature of 80–90 °C and is used mainly as reboiler heats for propylene and propane separation and other similar separations.

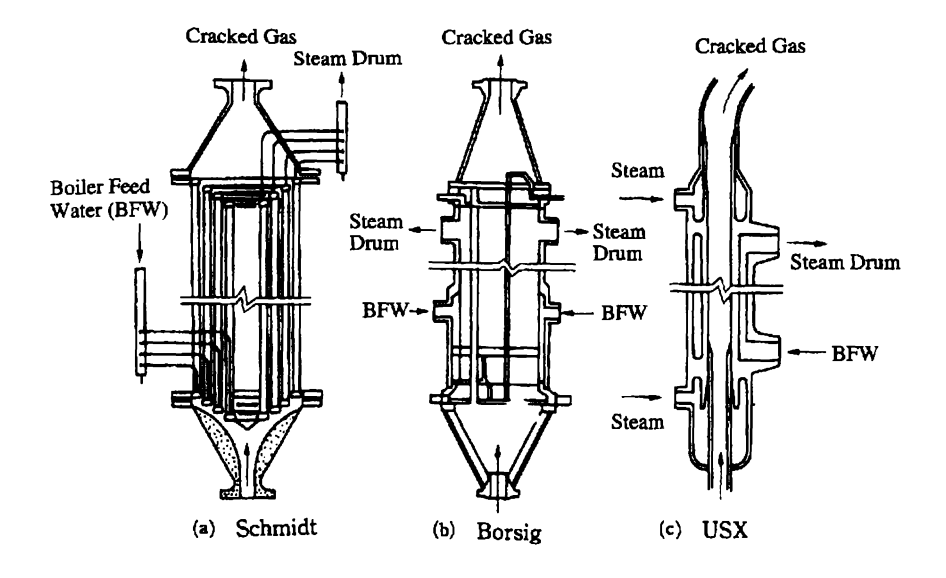
In order to get better olefin yields, the pressure of the cracking reaction is kept as low as possible. On the other hand, the lower suction pressure of the cracked gas compressor requires more power. Therefore, the coil outlet pressure can be lowered only by reducing the pressure drop between the coil outlet and the suction of the cracked gas compressor. It is important to minimize pressure drops in the transfer line exchangers, the oil quench tower and the water quench tower, for higher olefin yields. The coil outlet pressure is mostly designed at 0.16–0.2 MPa.

Figure 5.8 shows typical types of transfer line exchangers, which can be divided into a double-tube exchanger type and a shell-and-tube exchanger type. Generally, the double-tube exchangers are followed by a shell-and-tube exchanger. During operation, fouling of the transfer line exchanger tubes will gradually increase and energy efficiency will drop accordingly. Therefore, easy cleaning of exchanger tubes is needed. The double-tube type has the advantage of easy cleaning, but the shell-and-tube type can also be modified for easier cleaning. Other design criteria are intended to release heat stress, prevent erosion or maintain a low pressure drop.

5.1.5 THERMODYNAMICS OF THERMAL CRACKING REACTIONS

Cracking reactions break the C—C bond of hydrocarbon at a high temperature (800–900 °C) and low pressure (0.16–0.2 MPa) non-catalytically.

A large positive value of the Gibbs free energy means that a system is not stable thermodynamically. According to the standard Gibbs energy of formation per carbon atom for various materials as shown in Figure 5.9, each hydrocarbon tends to be cracked down into hydrogen and carbon atoms above a temperature of 800–900 °C.



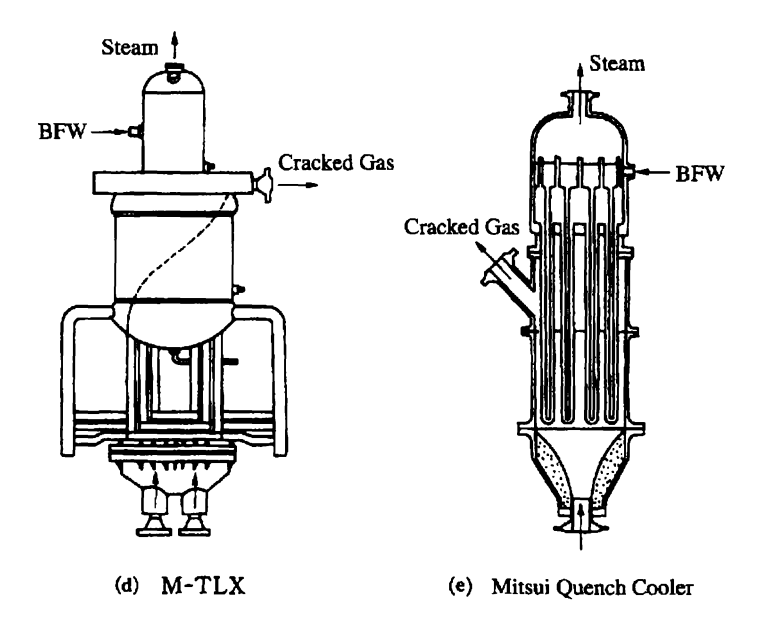


Figure 5.8 Transfer line exchanger (TLE).

Double Tube: (c)

Shell and Tube: (a), (b), (d), (e)

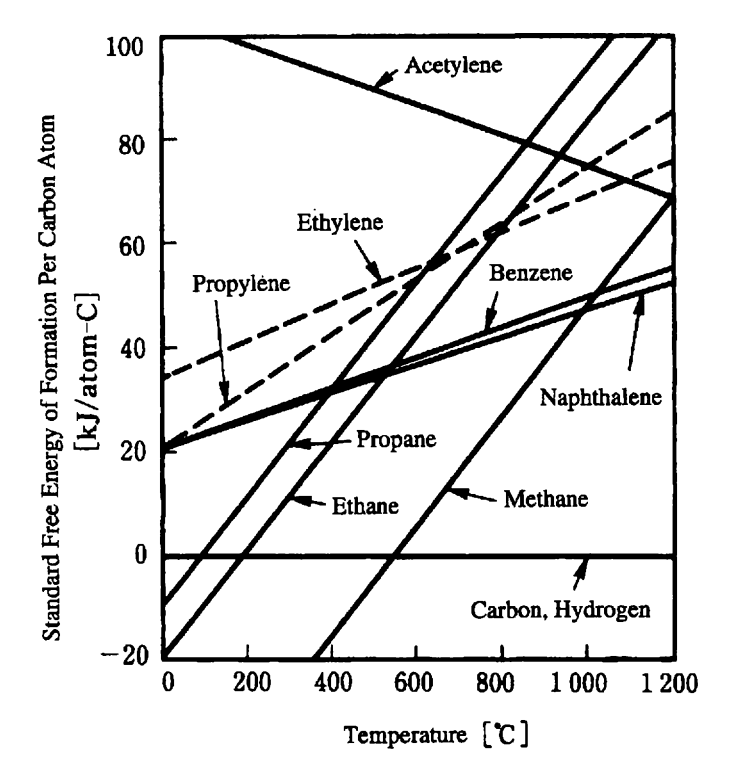


Figure 5.9 Standard free energy of formation for each hydrocarbon vs. temperature.

Therefore, cracking reactions should be terminated by rapid quench control, and residence time kept short to avoid overcracking. This gives higher yields of olefins such as ethylene and propylene. Olefin yields can be predicted quantitatively by a simulator based on the dynamic reaction model for many elementary reactions. But, the following can be explained qualitatively by referring to Figure 5.9:

As the cracking temperature increases:

- (1) pyrolysis of paraffins proceeds,
- (2) more ethylene than propylene is produced,
- (3) more acetylene is produced,
- (4) more hydrogen and carbon deposition are produced, and
- (5) benzene and naphthalene production tends to increase gradually.

5.1.6 MECHANISM OF THERMAL CRACKING

Components included in cracking reactions are so many and reaction paths are also so complicated that the mechanism of thermal cracking is not established theoretically yet. However, Rice and Herzfield first introduced a free radical chain reaction mechanism⁽³⁾⁻⁽⁷⁾. The mechanism has been modified several times by many researchers and is widely accepted as the basis for explaining the mechanism of the cracking reactions.

5.1.6.1 Free Radical Chain Reaction Mechanism

Free radical chain reactions can be divided into three reaction steps, namely initiation, propagation and termination.

(1) Initiation

The reaction is initiated thermally, and pyrolysis initiation of a higher paraffin is caused by homolytic cleavage of a carbon-carbon bond and a carbon-hydrogen bond. It forms free radicals into the reaction system.

(a) Cleavage of carbon-carbon bond

$$C_{n+m}H_{2n+2m+2} \longrightarrow C_nH_{2n+1} + C_mH_{2m+1}$$

(b) Hydrogen transfer between paraffins and olefins

$$C_nH_{2n+2} + C_mH_{2m} \longrightarrow C_nH_{2n+1} + C_mH_{2m+1}$$

(c) Cleavage of C-H bonds

$$C_nH_{2n+2}\longrightarrow C_nH_{2n+1}+H_1$$

Generally, larger molecular weight compounds have less activation energy per carbon bonds and can be reacted more easily. C—C bond energy per molecule is about 300 kJ/mol, which is less than that of C—H bonds of 420 kJ/mol. Therefore, C—C bonds are less stable than C—H bonds. The chain reaction is mainly initiated with the cleavage of the C—C bond that releases two sets of radicals.

- (2) Propagation of free radical chain reactions
- (a) Abstraction of hydrogen

$$C_nH^{\cdot}_{2n+1} + C_mH_{2m+2} \longrightarrow C_nH_{2n+2} + C_mH^{\cdot}_{2m+1}$$

(b) Decomposition of radical

$$C_{n+m}H^{\cdot}_{2n+2m+1} \longrightarrow C_nH_{2n} + C_mH^{\cdot}_{2m+1}$$

(c) Addition of radical

$$C_n H^{\cdot}_{2n+1} + C_m H_{2m} \longrightarrow C_{n+m} H^{\cdot}_{2n+2m+1}$$

(d) Isomerization of radicals

$$C_nH^{\cdot}_{2n+1} \longrightarrow (isomers)$$

Hydrogen abstraction by radicals is an intermolecular and radial-exchange reaction. The low molecular radicals (i.e. CH₃ or H¹) tend to abstract hydrogen radicals from hydrocarbons with relatively lower energy. The activation energy of this hydrogen abstraction is estimated as about 30 kJ/mol.

The radicals generated by hydrogen abstraction are far less stable than the feed hydrocarbons and are easily decomposed into lower molecular olefins and radicals. The activation energy of the decomposition is estimated as about 120–210 kJ/mol, and then lower molecular radicals have a relatively larger activation energy.

Due to the above reasons, larger molecular paraffins are gradually decomposed into lower molecular olefins.

(3) Termination

The radicals generated by the above reactions may react with each other and may disappear.

Termination of radicals is,

$$C_nH^{\cdot}_{2n+1} + C_mH^{\cdot}_{2m+1} \longrightarrow C_{n+m}H_{2n+2m+2}$$

The activation energy of this reaction is so small as to be negligible.

The activation energy of the overall reactions proceeding with the above three steps is theoretically expected to be 230–270 kJ/mol. The smaller molecular weight of hydrocarbon has the larger activation energy. This figure is smaller than the activation energy of C—C bond decomposition of 330 kJ/mol and agrees with the apparent average activation energy acquired by experiments for various hydrocarbons.

5.1.6.2 Intramolecular Decomposition

In thermal cracking reactions, the following well known reactions, which cannot be classified as free radical reactions or decomposition of a carbonium ion, occur intramolecularly, and are so called concerted reactions:

1 - pentane
$$\cdot \longrightarrow C_2H_4 + C_3H_6$$

Cyclohexene $\cdot \longrightarrow C_2H_4 + C_4H_8$

5.1.6.3 Reactions of Olefins with Radicals

Olefins can further react with radicals. When the resident time is too long, the ethylene or propylene produced will be decomposed or polymerized, so the desired yield of olefins cannot be attained. Suppressing these side reactions requires a short residence time, together with higher temperature and low pressure.

5.1.6.4 Formation of Aromatics

Even in the case of paraffinic feed, aromatics are generally produced as byproducts. The main reaction of aromatic formation is the reaction between dienes with conjugated double bond and low molecular weight olefins. This is well known as the Diels-Alder reaction. For example, toluene is produced from butadiene and propylene.

$$CH_3 + C_2H_4 \longleftrightarrow C_3H_7 \longrightarrow C_3H_8 + R$$

 $H_1 + C_3H_6 \longleftrightarrow (C_3H_7)^* \longrightarrow CH_3 + C_2H_4$

where $(C_3H_7)^*$ is an intermediate complex.

5.1.6.5 Mechanism of Coke Formation

Forms of coke can be classified into amorphous, whisker and graphite. Whisker coke is formed over iron particles on the metal surface, generally in the case of ethane or propane feedstocks. The coking mechanism can be explained as follows: at first, hydrocarbons may be decomposed on the heated metal surface and a melted carbon layer is formed. This will disperse on the cold surface and form a solid carbon layer⁽⁸⁾ (refer to Figure 5.10). As the amount of coke formation increases, a thin film of whisker coke will be formed.

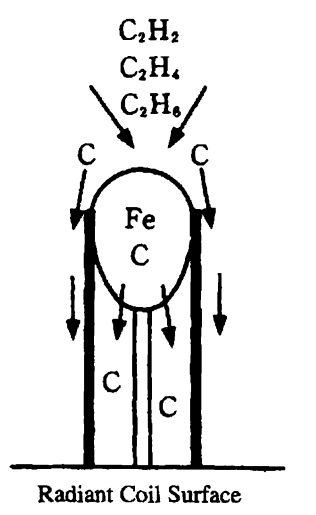


Figure 5.10 Mechanism of whisker coke formation. Exothermic reactions of carbon formation occur on the surface or radiant coils where Fe/FeO acts as the catalyst. Coke is dispersed to the cold surface and cooled down to form a layer. Then, whisker carbon grows. The tip of whisker carbon is covered with deposited carbon. Finally, the catalyst activity of Fe/FeO is lowered and the growth of whisker carbon stops.

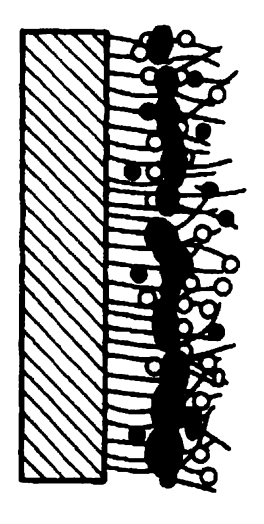


Figure 5.11 Growth mechanism of coke formation. The coke growth mechanism occurs by means of both reaction and adsorption, and a very hard coke is formed. But on the metal surface, relatively soft and porous coke is formed. Liquid drops of tar or radicals generated by thermal cracking are accumulated on the carbon surface close to the metal surface. Coke is gradually accumulated on top of whisker carbon, and covers it with a coke layer.

As the dispersion rate on the surface gradually decreases, the absorption rate and decomposition rate will also decrease. Finally, the surface of metal particles is covered with solid carbon, then decomposition of hydrocarbons and the growth of whisker coke will terminate.

On the other hand, at a high temperature, free radicals with a molecular weight of about 100 are generated from heavy oil such as anthracene oil or oligomer. These may be reacted with whisker coke. This may result in the accumulation of coke uniformly on the surface of whisker coke, where C—H bonds may decompose and free radicals may be formed. This accelerates the coke formation rate. In this case, spherical coke is stacked on the surface of the whisker coke with almost uniform thickness⁽⁹⁾ (Refer to Figure 5.11).

5.1.7 REACTION MODEL FOR YIELD ESTIMATION

5.1.7.1 Method Based on Experimental Data

For simulations of thermal cracking reactions based on the kinetic model, Zdonick proposed a method using a kinetic severity function (KSF) for naphtha cracking⁽⁹⁾.

$$KSF = \int_0^t k d\theta = \int_0^t A \exp(-E/RT) d\theta$$
 (5.1)

where k: reaction rate constant

 θ,t : reaction time

A: reaction frequency factor

E: activation energy

A model compound which is not produced during the thermal cracking of naphtha needs to be selected. *n*-pentane is generally selected as a model compound for naphtha cracking. Its cracking reaction is of first order. By measuring the concentration of *n*-pentane in both feed gas and cracked gas experimentally, the KSF value can be determined. The following first-order reaction equation is substituted into Eq. (5.1) and integrated so that the KSF can be estimated.

$$\frac{\mathrm{d}Y}{\mathrm{d}\theta} = kY\tag{5.2}$$

$$KSF = \int_0^t k d\theta = -\int_{Y_1}^{Y_t} \frac{dY}{Y} = \ln\left(\frac{Y_1}{Y_t}\right)$$
 (5.3)

where Y_i : *n*-pentane concentration in feed gas Y_f : *n*-pentane concentration in cracked gas

The KSF in Eq. (5.3) can become a summarized parameter for the experimental data. The cracking temperature is the main operating factor, and feedstock properties, residence time, coil outlet pressure and steam/hydrocarbon ratio also affect the cracking yields. These operating conditions can be summarized as KSF.

Figure 5.12 shows the charge of cracking yield against KSF. Increasing the KSF also causes ethylene yields and the yields of by-product methane to rise. On the other hand, the propylene yield has a maximum value at KSF of 1.5. The gasoline fraction is decomposed up to KSF of about 3.0, but above this its severity pyrolysis gasoline with a higher molecular weight is produced by the recombination of radicals as side reactions. This pyrolysis gasoline contains olefins, dienes and BTX (benzene, toluene and xylenes).

As described above, KSF is a useful and powerful parameter to estimate the yields of products by thermal cracking. An *n*-pentane is used as a model compound for naphtha cracking, so it cannot be applied to cracking ethane or propane. In such cases, a model compound other than *n*-pentane needs to be selected.

5.1.7.2 Simulation Method Based on the Reaction Model

Thermal cracking mechanisms are very complicated, and the number of elementary reactions reaches about 2000 in the case of naphtha cracking as described earlier. Therefore, simulators are very useful and important to predict cracking yields as well as performance. In particular, KTI's SPYRO simulator is well known. A detailed analysis can be done by using such

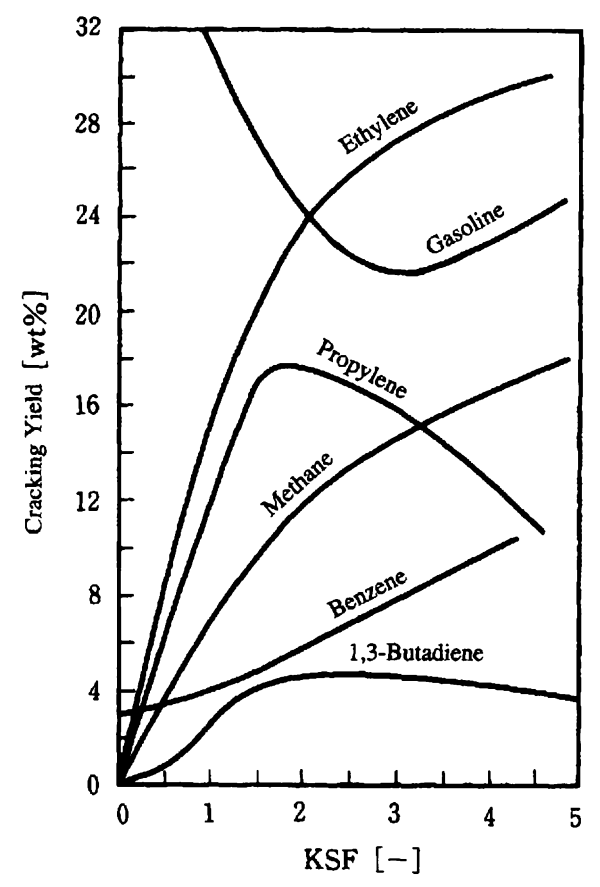


Figure 5.12 Kinetic severity factor (KSF) vs. cracking yield(10).

simulators. Here, using a simple model⁽¹¹⁾, the yields of thermal cracking will be estimated.

(1) Assumptions

The following are assumptions needed to build the simulation model:

- steady state
- direct fire heating
- tubular reactor
- constant heat flux along the tube length
- plug flow in axial direction
- first-order reaction

(2) Simulation Model(11)

Material balance equation:

$$r_{\rm A} = -\frac{\mathrm{d}_{n\mathrm{A}}}{\mathrm{d}V} = n_{\rm A}^{\circ} \frac{\mathrm{d}x}{\mathrm{d}V} = \frac{n_{\rm A}^{\circ} \mathrm{d}x}{A\mathrm{d}z}$$

Energy balance equation:

$$W_{Cp}\frac{\mathrm{d}T}{\mathrm{d}z} + r_{\mathrm{A}}A\Delta H_{r} - D\pi q = 0$$

Momentum balance equation (pressure drop equation):

$$\frac{\mathrm{d}P}{\mathrm{d}z} = \frac{2fG^2}{D\rho}$$

where f is a friction factor obtained by the Fanning equation.

$$f = \frac{Bf_o}{(N_{\rm Re})^{0.2}}$$

where f_0 is a friction factor for straight pipes and B is a correction factor for bending pipes in the Fanning equation and can be obtained by the following equation:

$$B = \frac{L_{\rm ep}}{L_{\rm s} + L_{\rm b}}$$

where L_b and L_{ep} are expressed as follows:

$$L_{\rm b} = 4D$$
$$L_{\rm ep} = L_{\rm s} + 60D$$

Therefore,

$$B = \frac{L_{\rm s} + 60D}{L_{\rm s} + 4D}$$

However, the average heat flux is defined as follows considering the heated part of the reaction coil:

$$q = q_a \left[\frac{L_{\rm h}}{L_{\rm s} + L_{\rm b}} \right]$$

Using the equation of state for real gas PV = zRT and the above equations, the momentum balance equation can be summarized as follows:

$$-P\frac{\mathrm{d}P}{\mathrm{d}V} = \beta T \frac{n_{\mathrm{T}}}{n_{\mathrm{T}}^{\circ}}$$

$$\beta = 3.934 \left[\frac{R}{M_{\rm w}} \right] \left[\frac{zBf_o}{D^{6.8}} \right] (W)^{1.8} m^{0.2}$$

Here, assuming the thermal cracking is a first-order reaction, the following equation can be used:

$$r_{\rm A} = kP_{\rm A} = kP\frac{n_{\rm A}}{n_{\rm T}}$$

If a reactant is of component A and its conversion is x, moles of the component A and total components will be changed as follows:

$$n_{\mathbf{A}} = n_{\mathbf{A}}^{\circ} (1 - x) \tag{5.4}$$

$$n_{\rm T} = n_{\rm T}^{\circ} + \delta n_{\rm A}^{\circ} x \tag{5.5}$$

From the equations of the material balance and the reaction rate,

$$n_{A}^{c} \frac{\mathrm{d}x}{\mathrm{d}V} = kP \frac{n_{A}}{n_{T}}$$

Therefore, substituting Eqs (5.4) and (5.5) into the above equation, the following equation can be derived:

$$n_{\mathsf{T}}^{\circ} \frac{\mathsf{d}}{\mathsf{d}V} = \frac{k(1-x)P}{(1+\delta y_{\mathsf{A}}^{\circ} x)} \tag{5.6}$$

Substituting $dz = (4/\pi D^2) dV$ into the energy balance equation and arranging the expression, the following equation will be derived:

$$\frac{dT}{dV} = m - s \frac{dx}{dV}$$

$$m = \frac{4q}{DW_{Cp}}$$

$$s = \frac{y_A^{\circ} \Delta H_r}{M_{wCp}}$$
(5.7)

[m]

where : cross-section area in reaction coil $[m^2]$ specific heat at constant pressure [kJ/kgK]inside diameter of reaction coil [m] : mass flow rate per cross-sectional area $[kg/s m^2]$ ΔH_r : heat of reaction [kJ/kmol] k : reaction rate constant [-] L_b: equivalent length of bend [m]equivalent length of reaction coil for pressure

drop estimation

$L_{\rm h}$:	heated length of straight part of reaction	[m]
<i>L</i> s :	length of straight part of reaction coil	[m]
M :	molecular weight	[kg/kmol]
n_A :	mole flow rate of component A	[kmol/s]
$n_{\mathbf{A}}^{\circ}$:	mole flow rate of component A at inlet	[kmol/s]
$n_{\rm T}/n_{\rm T}$	$=1+\delta y_{\mathbf{A}}^{\circ}x$	[-]
N_{Re} :	Reynolds number $(=DG/\mu)$	[-]
P :	pressure	[Pa]
q_{a} :	heat flux at heated part	$[kJ/m^2 s]$
q:	average heat flux based on inside diameter	$[kJ/m^2 s]$
R :	gas constant $(=8.3143)$	[kJ/kmol K]
r_{A} :	reaction rate of component A	[kmol/m ³ s]
T :	temperature	[K]
V :	reactor volume (tube volume)	$[m^3]$
W:	mass flow rate	[kg/s]
x :	conversion $(=(n_A^{\circ}-n_A)/n_A^{\circ})$	[-]
$\begin{array}{ccc} x & : \\ y_{\mathbf{A}}^{\circ} & : \end{array}$	mole fraction of component A at inlet	
••	$(=\mathring{n_{A}}/\mathring{n_{T}})$	[-]
z	axial distance in coil	[m]
δ	mole change with reaction	[-]
μ	viscosity	[Pas]
ρ	density	$[k/m^3]$

Example 5.1

The following simple first-order reaction is assumed for thermal cracking:

$$A \longrightarrow 2B$$

and the reaction rate equation is given by

$$r_A = kP_A$$

A feed containing component A of 95 mol% is charged into the cracker at the rate of $10\,kg/s$. The coil inlet temperature (T_i) is $600^\circ C$ and the pressure in the coil is a constant of 0.2 MPa. The heat flux is also constant at $110\,kJ/m^2\,s$ and the coil diameter is specified as $0.085\,m$. The other physical properties required are shown as follows:

$$c_p = 3.0 \, kJ/kg \, K$$

 $k = 2.7 \times 10^{10} exp \, (-25\,800/T)$
 $M_w = 60 \, kg/kmol$
 $\Delta H_r = 100\,000 \, kJ/kmol$

Obtain the change of the conversion and the reaction temperature through the coil. Also estimate the number of tubes at a conversion of 95%, where the coil is assumed to be 10 m long.

Solution

As the reaction rate constant depends on a temperature, the differential equations of 5.6 and 5.7 become non-linear and their numerical integration will be required. Here, for the sake of brevity, the rate constant is assumed as constant in an infinitesimal distance of coil length, so Eqs (5.6) and (5.7) can be solved analytically. Assuming that the reaction coil consists of a number of small isothermal reactors, the integration of Eqs (5.6) and (5.7) for each small reactor result in the following equation:

$$V = \frac{n_T^o}{kP} \{ (1 + \delta y_A^o) \ln(1 - x) + \delta y_A^o \}$$

$$T = \frac{mn_T^o}{kP} \{ (1 + \delta y_A^o) \ln(1 - x) + \delta y_A^o x \} - sx + T_I$$

where m and s can be obtained as follows:

$$m = \frac{4q}{DW_{Cp}} = \frac{(4) (110)}{(0.085) (10) (3.0)} = 172.6 [°C/m^3]$$

$$s = \frac{y_A^o \Delta H_r}{M_{HCp}} = \frac{(0.95) (100000)}{(60) (3.0)} = 527.8 [°C]$$

$$\delta = \frac{2-1}{L} = 1$$

Using the above equation, the changes of the conversion and the reaction temperature through the coil volume are solved as shown in Figure 5.13.

At a conversion of 95%, the required coil volume can be obtained as $3.85 \, \text{m}^3$ at a pressure of 0.2 Mpa from Figure 5.13. As the coil length is 1.0 m, the required number of coils can be calculated as $3.85/(10\times(\pi/4)\times0.085^2)=68$ (coils).

However, for the design of an industrial cracking furnace, the estimation of cracked yield should be made out more distinctly using a detailed simulator such as SPYRO, instead of the simple model described above.

5.1.8 DESIGN PROCEDURE OF A CRACKING FURNACE

In design of cracking furnaces, it is important to consider the feedstock availability, product demands and, furthermore, the overall plan for the

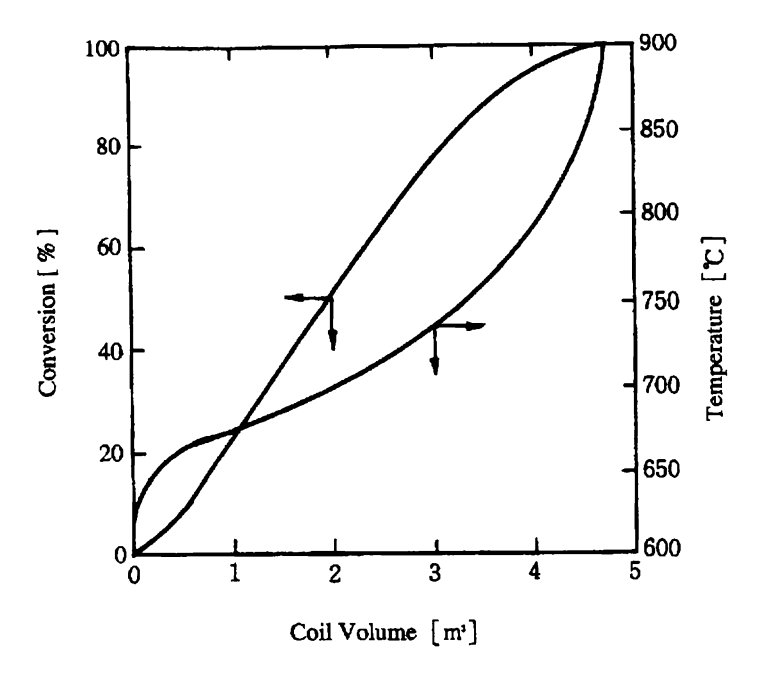


Figure 5.13 Changes of conversion and temperature through coil volume.

petrochemical complex. At first, the feedstock is selected and the determination of cracking specifications follows. Figure 5.14 shows a typical design procedure for a cracking furnace.

Once the feedstock properties are given, the cracking conditions (temperature, pressure, residence time, steam/hydrocarbon ratio, etc.) should be studied to obtain the optimum yield pattern. In the case of naphtha cracking, the coil outlet temperature is generally selected as about 820–850 °C and the outlet pressure is determined at the lowest one as possible. However, the outlet pressure is related to the suction pressure of the cracked gas compressor, as described in Section 5.1.4. Therefore, 0.16–0.2 MPa is generally chosen for the coil outlet pressure. The residence time and the steam/hydrocarbon ratio are usually selected as 0.2 and 0.5 s, respectively, for naphtha cracking.

After the cracking conditions are specified, the number of cracking furnaces, and the arrangements of the cracking coil will be determined through the process and mechanical design. Cracking conditions can be optimized by the simulator incorporating parameters to be adjustable with actual operation data. In general, input data for the simulator are the coil geometry, such as coil equivalent length, coil diameter and transfer line volume, in addition to the process conditions. The practical design of the cracking furnace should be carried out based on the output obtained by the simulator and very valuable knowledge from many years' experience.

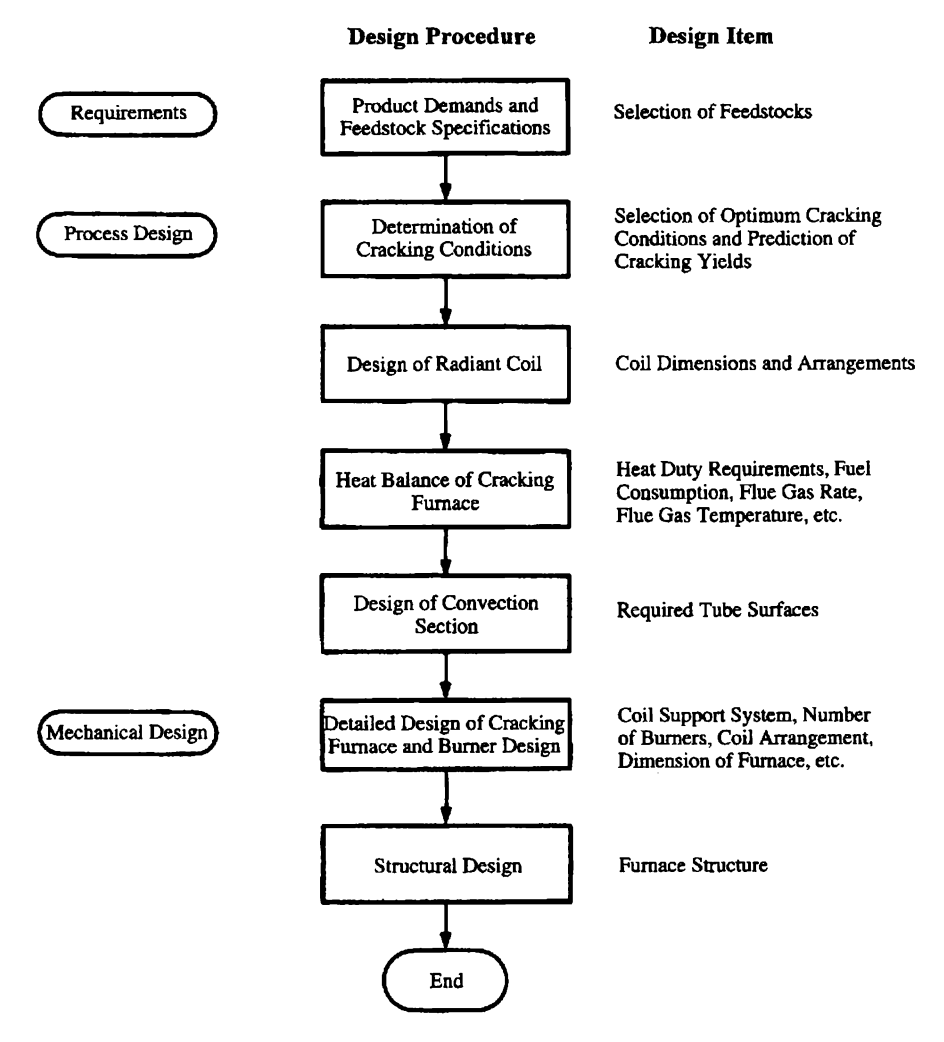


Figure 5.14 Typical design procedure for a cracking furnace.

The cracking section usually consists of more than three cracking furnaces operated in parallel. The number of cracking furnaces is determined considering the operability, including the shut-down period for the de-coking and/or the mechanical cleaning, the flexibility of feedstocks and the stability at low load operation.

The unit capacity of cracking furnaces is about 60 000-80 000 annual tons of ethylene, since the larger capacity has the advantages of being much more economical and requiring less de-coking operation. On the other hand, during

Specific gravity (15/4°C)	0.70
ASTM distillation (ASTM) [°C]	
IBP	30
5%	40
10%	50
50%	95
90%	140
95%	150
EP	170
Total sulphur [wt ppm]	100
Composition [wt%]	
n-paraffin	38.0
i-paraffin	38.0
Naphthenes	16.0
Aromatics	8.0

Table 5.4 Typical properties of feedstock naphtha

downtime, due to de-coking or mechanical cleaning of transfer line exchangers, the production rate is decreased intermittently.

The number of coils and their geometry are designed on the basis of the capacity of each coil, and the number of 2^n per cracking furnace is selected because of better distribution and control of flow from the main heater to each coil and more simple connection to the transfer line exchangers.

5.1.9 RESULTS OF THERMAL CRACKING SIMULATION

5.1.9.1 Feed property

Typical properties of feed naphtha for a simulation are shown in Table 5.4.

5.1.9.2 Reaction Parameters and Yields

As described above, the major parameters of reaction are (1) residence time, (2) coil outlet pressure (COP), (3) coil outlet temperature (COT) and (4) feed naphtha properties. Change of the ethylene and propylene yields, methane yield rate, and the C_{5+} yield vs those parameters are shown in Figures 5.15 and 5.22.

5.1.9.2.1 Residence Times vs Yields

Figure 5.15 and 5.16 show the yield changes versus the residence time while keeping other parameters constant. As the residence time decreases, methane formation and the C_{5+} yield decrease and the ethylene yield increases accordingly. To obtain a higher ethylene yield, the residence time should be

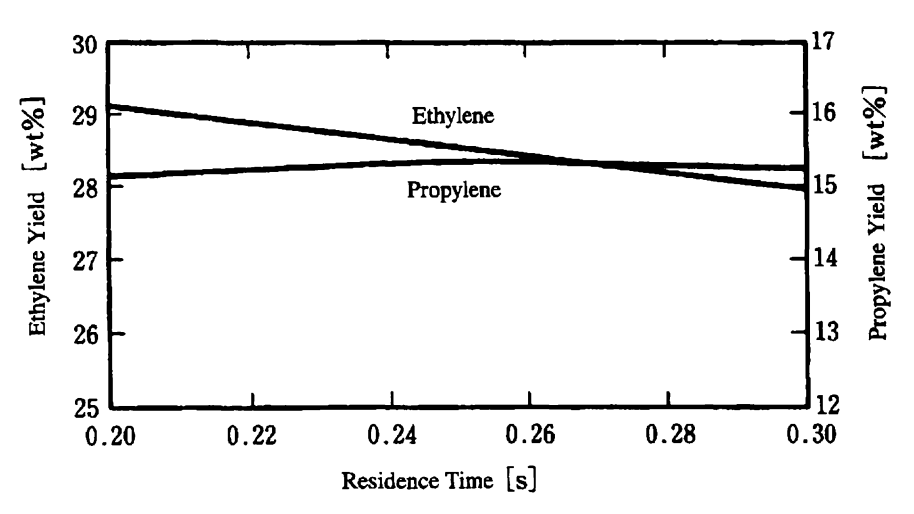


Figure 5.15 Change of ethylene and propylene yield vs. residence time.

short enough, while a higher heat flux needs to apply enough heat to the process gas in a very short time. Therefore, small-diameter coils with a large number are required but they cause the metal skin temperature to rise and increase the coking rate, which in turn shortens the de-coking interval.

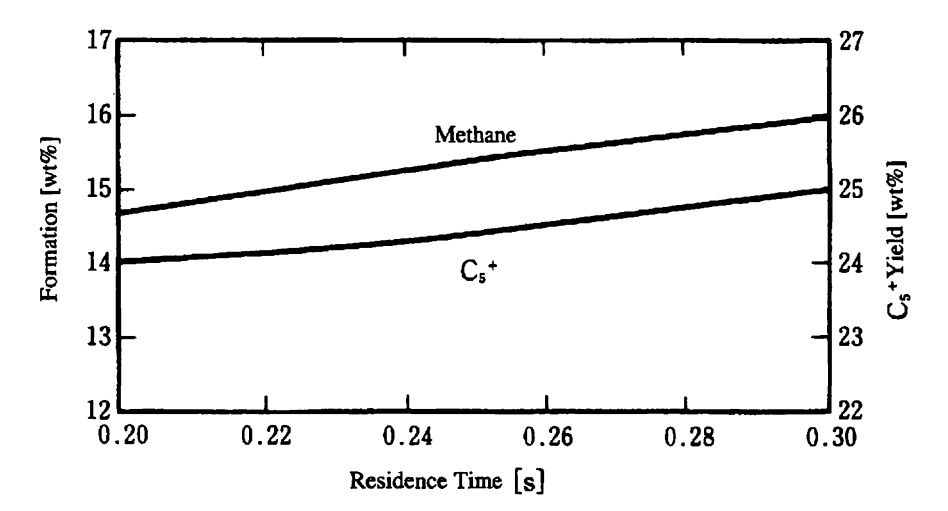


Figure 5.16 Change of methane yield rate and C₅₊ yield vs. residence time.

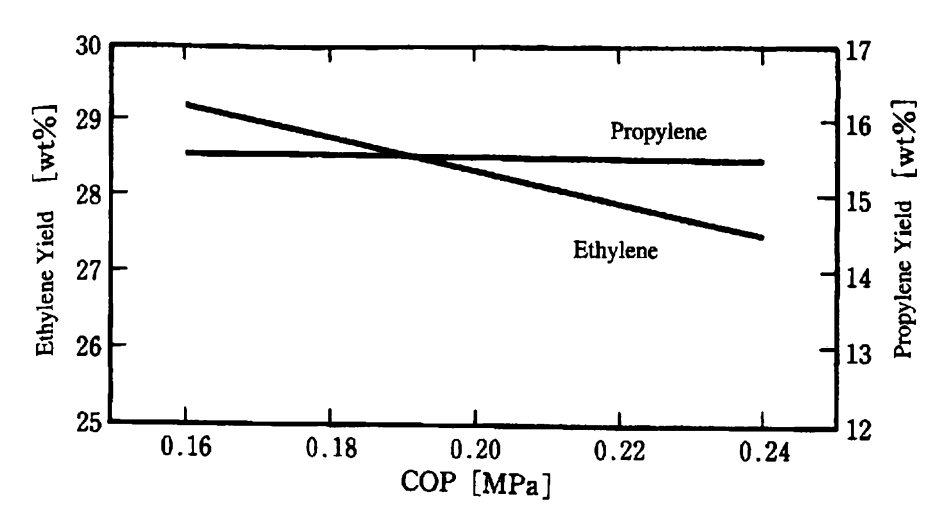


Figure 5.17 Change of ethylene and propylene yield vs. COP.

5.1.9.2.2 COP vs Yields (refer to Figures 5.17 and 5.18)

Decreasing CO results in suppressing polymerization of olefins and converting to heavier fractions, causing the C_{5^+} yield to decrease, while olefin yields also increase, especially the ethylene yield. The propylene yield is kept almost constant. To increase the propylene yield, decreasing COT is the most effective. Decreasing COP causes the coking rate to decrease and extends the de-coking interval.

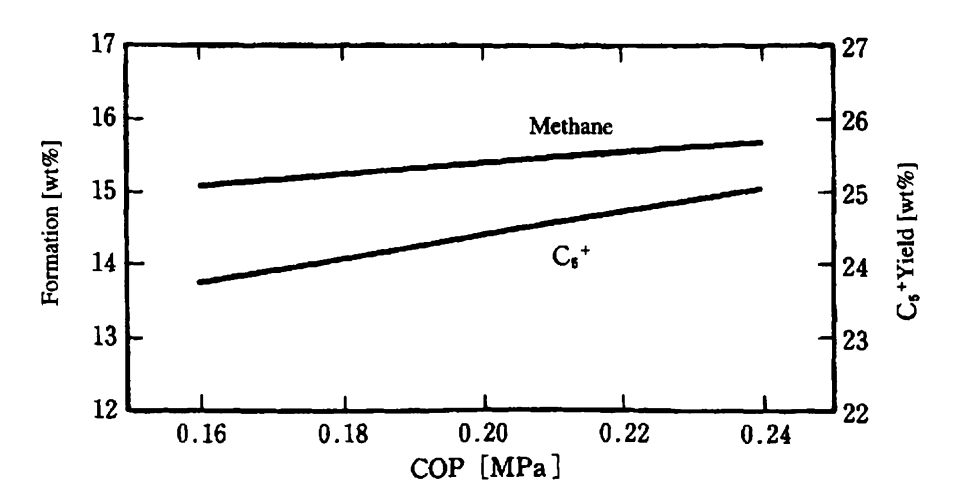


Figure 5.18 Change of methane yield rate and C_{5+} yield vs. COP.

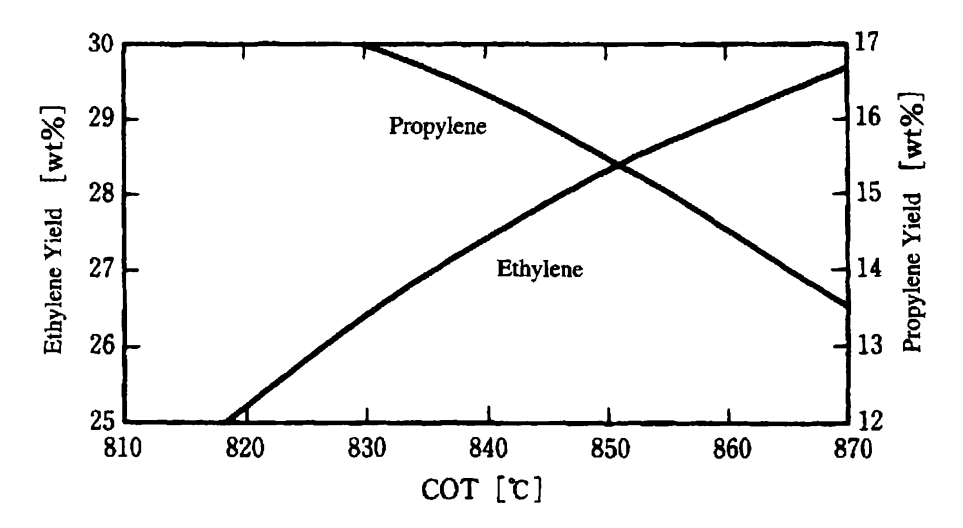


Figure 5.19 Change of ethylene and propylene yield vs. COT.

5.1.9.2.3 COT vs Yields (refer to Figures 5.19 and 5.20)

As the COT increases, the ethylene yield increases but the propylene yield decreases. The methane formation increases monotonically with the increase in COT. At lower COT, the C_{5+} yield increases because of loss of decomposition of heavier fractions. On the other hand, the C_{5+} yield decreases at higher COT.

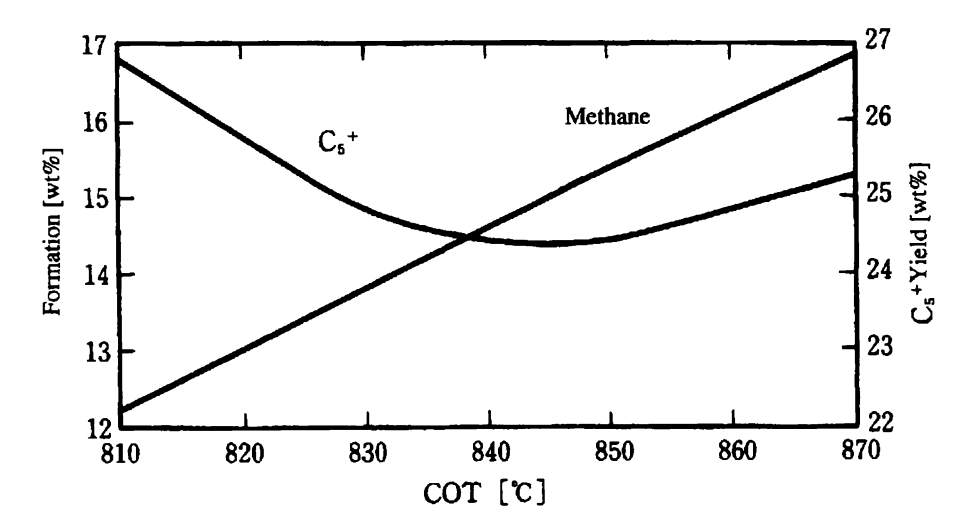


Figure 5.20 Change of methane yield rate and C₅₊ yield vs. COT.

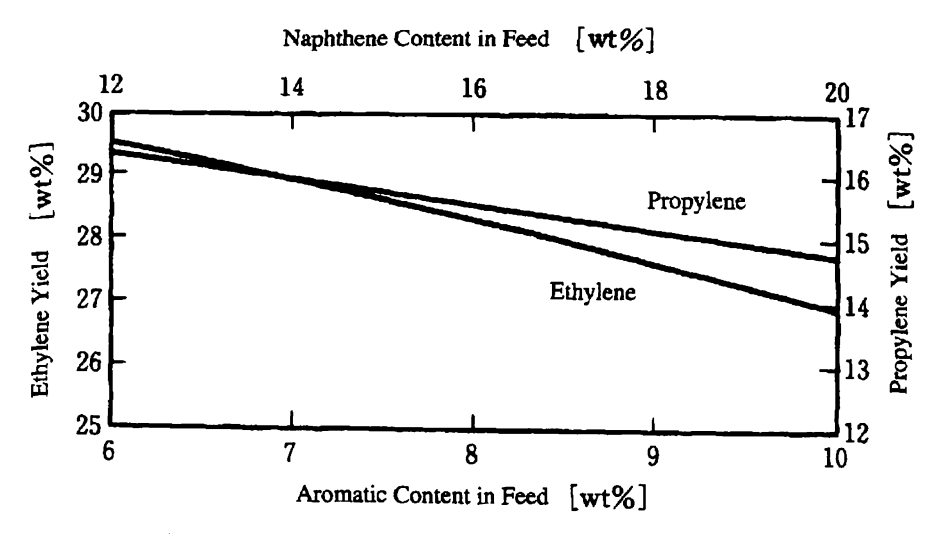


Figure 5.21 Change of ethylene and propylene yield vs. feed properties.

Over 840-850 °C, dimerization and/or polymerization of radicals or olefins may occur, and the C_{5^+} yield increases, while the propylene yield decreases. The COT should be determined by considering the required yields of ethylene and propylene and the feedstock properties.

5.1.9.2.4 Feedstock Properties vs Yields (refer to Figures 5.21 and 5.22)

Olefin yields may be affected by feedstock properties, particularly the contents of aromatics and naphthenics. It is assumed that the ratio of aromatics to naphthenics in feed is constant for this simulation, with the increase in aromatic and naphthenic contents, both ethylene and propylene yields decrease. Methane formation is kept constant, but the C₅⁺ yield increases as the aromatic content increases, and thus production of benzene and toluene increases. Cracked gasoline obtained by thermal cracking of heavy oil contains a large amount of aromatics and naphthenics, so such feed is not preferable for olefin production as shown in Figure 5.21.

5.1.10 TECHNOLOGY TREND OF A CRACKING FURNACE

The technological requirements for a cracking furnace to improve olefin yields are summarized as follows:

(1) A lot of small-diameter coils have been used to reduce the residence time in cracking coils. Uniform heating is one of the key technologies.

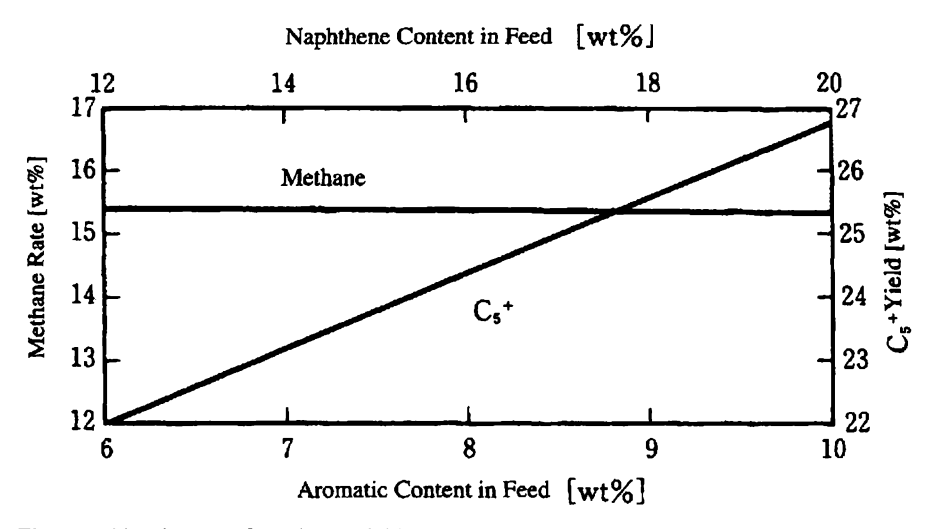


Figure 5.22 Change of methane yield rate and C_{5+} yield vs. feed properties.

- (2) Coil outlet pressure (COP) is selected to be as low as possible. For this purpose, a one-stage shell-and-tube transfer exchanger has often been used.
- (3) Coil outlet temperature (COT) is selected in order to maximize ethylene yield. In this case, as the coking rate increases, the de-coking interval is shortened and the carburization rate is increased. To protect the coils from carburization, new materials for heating coil are expected. The temperature in the cracking furnace should become higher, so mechanical design is crucial. In accordance with the above requirements, the change in design conditions is shown below:

Residence time : $0.4-0.6 \text{ s} \longrightarrow 0.1-0.2 \text{ s}$

Coil inside diameter : $3-4 \rightarrow 1-2$ in

Coil outlet temperature : $800 \,^{\circ}\text{C} \longrightarrow 850-880 \,^{\circ}\text{C}$ Coil metal temperature : $1000 \,^{\circ}\text{C} \longrightarrow 1100 \,^{\circ}\text{C}$ Fire-box temperature : $1050 \,^{\circ}\text{C} \longrightarrow 1200 \,^{\circ}\text{C}$

New coil materials and advanced simulators have contributed to the improvement of olefin yield; for example, ethylene yield has been achieved up to 3% increment of yield for light naphtha feed. Energy consumption has also been improved from 7 000 kcal/kg-ethylene in the 1970s to 4500–5000 kcal/kg-ethylene in the 1990s.

A millisecond furnace with a residence time of less than 0.1s has been developed for higher olefin yields. However, a residence time of about 0.2s and a de-coking interval of 45-60 days are generally selected. The key technological

issue for the design of a cracking furnace is how to shorten the residence time in future without sacrificing the de-coking intervals.

References

- (1) M. E. Dente, E. M. Ranzi, S. J. Piercucci, G. M. Bussani and S. Mullick, 'Evolution of a Fundamental Kinetic Model for Industrial Application of Steam Cracking Process,' paper presented at AIChE Annual Meeting, Chicago, Illinois, November 1990.
- (2) Encyclopedia of Chemical Technology, Vol. 9, p. 393, John Wiley & Sons (1980).
- (3) F. O. Rice, J. Am. Chem. Soc., 53, 1959 (1931)
- (4) F. O. Rice, J. Am. Chem. Soc., 54, 3529 (1932)
- (5) F. O. Rice, J. Am. Chem. Soc., 55, 3035 (1933)
- (6) F. O. Rice, J. Am. Chem. Soc., 55, 4245 (1933)
- (7) F. O. Rice, J. Am. Chem. Soc., 56, 284 (1934)
- (8) R. T. K. Baker and P. S. Harris, *Chemistry and Physics of Carbon*, Vol. 14, p. 83, Dekker (1978)
- (9) L. F. Albright and J. C. Marek, Ind. Eng. Chem. Res., 27 (5), 755 (1988)
- (10) L. E. Chambers and W. S. Potter, *Design of Ethylene Furnaces*, Hydrocarbon Processing, Jan. (1974) and Mar. (1974)
- (11) C. D. Holland and R. G. Anthony, Fundamentals of Chemical Reaction Engineering, 2nd Edn., Prentice-Hall (1989)

CHAPTER 5.2

Tubular Steam Reforming

J. R. ROSTRUP-NIELSEN and LARS J. CHRISTIANSEN

Haldor Topsøe A/S, Copenhagen, Denmark

Industrial processes for manufacture of hydrogen include:

- Electrolysis of water
- Gasification of coal and coke
- Partial oxidation of hydrocarbons
- Steam reforming of hydrocarbons
- Steam reforming of methanol.

Electrolysis has been feasible only for small-scale production. Gasification and partial oxidation were the preferred routes for large-scale production until the conversion of hydrocarbons with steam, called steam reforming, became the dominant process from the mid-1960s with natural gas as the typical feedstock. Today, the choice between steam reforming and partial oxidation depends on the scale of operation and the availability of cheap oxygen. For small-scale production, steam reforming of methanol is also an option.

In refineries, hydrogen is available as a by-product from other refinery processes, primarily the catalytic reforming (plat-reforming) process for high octane gasoline. The main reactions are conversion of *n*-paraffins into isoparaffins, aromatics and hydrogen. The reduced severity of catalytic reformers caused by the requirement of lower contents of aromatics in gasoline, results in less hydrogen at the same time as there is a need for more hydrotreating of diesel and heavy oil fractions. Steam reforming is the obvious choice to fill the hydrogen gap. In general, there is a need for more hydrogen to provide the optimum fuel products. The transportation fuels have an H/C ratio close to two whereas the oil resources have a still decreasing H/C ratio.

The steam reforming process was introduced to industry around 1930 in the USA, where cheap natural gas was available as feedstock. The first plants operated close to atmospheric pressure. During the 1960s, mechanical developments made it possible to design reformers operating at high pressure

(3-4 MPa) and catalyst development made it possible to use naphtha as feedstock. This resulted in a widespread use of the process.

This chapter deals with the tubular reforming of natural gas which is still the most common application of steam reforming. The use of higher hydrocarbons (naphtha) in tubular reformers or in adiabatic prereformers as well as the use of heat exchange reformers will not be discussed in detail. Reference is made to the literature list at the end of the chapter.

5.2.1 THE REACTIONS

Steam reforming is an essential process for the manufacture of synthesis gas and hydrogen from hydrocarbons:

$$CH_4 + H_2O = CO + 3H_2 - 205 \text{ kJ/mol}$$
 (5.8)

$$CO + H_2O = CO_2 + H_2 + 42 \text{ kJ/mol}$$
 (5.9)

Higher hydrocarbons in natural gas, LPG or liquid hydrocarbons will react in a similar way:

$$C_n H_m + nH_2 O = nCO + \left(n + \frac{m}{2}\right) H_2$$
 endothermic (5.10)

Steam may be replaced by CO_2 , which gives a much more favourable H_2/CO ratio for many syntheses:

$$CH_4 + CO_2 = 2CO + 2H_2 - 247 \text{ kJ/mol}$$
 (5.11)

Reactions (5.8)–(5.11) require a catalyst, which typically is supported nickel. The applications of the reforming technology are widespread in the petrochemical industry as well as in the energy related industries. Most of the world ammonia production is based on steam reforming of hydrocarbons, with natural gas being the preferred feedstock.

Oil refineries use hydrogen from steam reforming for desulphurization and hydrocracking. In the petrochemical industry, steam reforming is used for production of synthesis gas for methanol and oxo-alcohols and for C₁-chemistry reactions such as synthesis of acetic acid, etc. The steam reforming process is an important element in solving the problem of the huge amounts of associated gas produced jointly with oil production. The gas may be converted either into methanol or into synthetic liquid hydrocarbons. Other applications include gases for direct reduction of iron ore, conversion of hydrocarbons for fuel cells, and advanced energy transfer systems, in which nuclear heat or solar energy are absorbed by the endothermic steam reforming process.

The methane reforming reaction (5.8) and the water gas shift reaction (5.9) are reversible at reforming temperatures. Reaction (5.11) is the difference of

Tubular Reformer

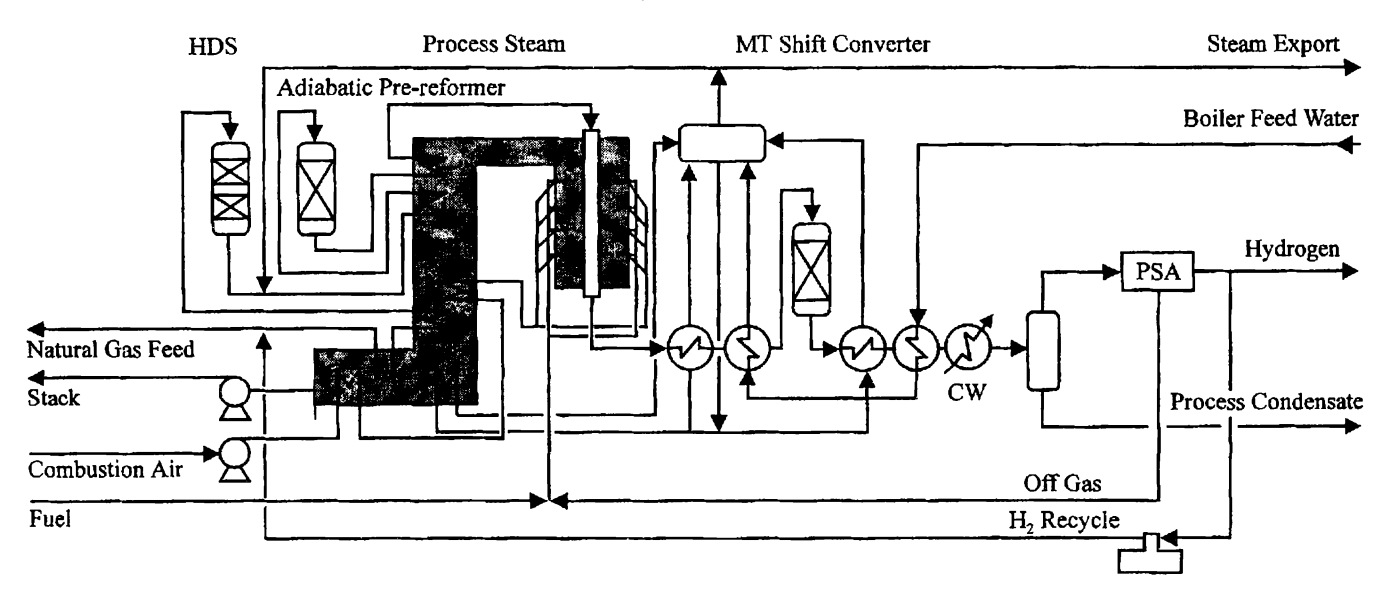


Figure 5.23 Typical process flow diagram of large-capacity hydrogen plant.

			-	$\ln K_{\rm P} = A +$	$-\frac{B}{T}$
Reactions	500 °C	700 °C	900°C	Α	В
$CH_4 + H_2O = CO + 3H_2$	9.945 10 ⁻³ (9.59 10 ⁻³)	12.71 (12.95)	1493 (1497)	30.4197	-27 106.2
$CO + H_2O = CO_2 + H_2$	4.999 (4.872)	1.576 (1.612)	0.7694 (0.7776)	-3.79762	4159.54
$2CO = C + CO_2$, ,		
– graphite	232.1 (227.5)	0.9563 (0.9797)	$2.668 \ 10^{-2}$ (2.704 10^{-2})	-21.0754	20 486.4
$CH_4 = C + 2H_2$					
- graphite	0.4617 (0.4480)	7.715 (7.873)	51.76 (52.05)	13.1413	-10778.8
whisker	(0.2828)	(4.969)	(32.86)	12.6812	-10778.8

Table 5.5 Equilibrium constants (standard conditions 25 °C, 0.101325 MPa)

Note: (1) The above equilibrium constants are defined at ambient pressure (0.101325 MPa). Accordingly, all pressure figures in the examples should be divided by 0.101325 for solution.

reaction (5.8) and reaction (5.9). It is evident, from the principle of Le Chatelier, that at higher temperatures less methane and more carbon monoxide are present in the equilibrium gas, and that the methane content increases with pressure and decreases with increasing ratio of steam to carbon.

In practice, the pressure is often determined by the overall lay-out of the process. This leaves the steam-to-carbon ratio and the catalyst exit temperature as the major parameters determining the gas composition.

Equilibrium constants for reactions (5.8) and (5.9) at selected temperatures are listed in Table 5.5, and an approximate analytical expression, which can be used in the examples, is also shown.

The product gas composition from a reformer can be estimated from thermodynamic calculations because it will in most cases be close to that of the equilibrated gas. In industrial practice, the 'approach to equilibrium' at reformer outlet for the reforming reaction is expressed by a temperature difference defined as:

$$\Delta T_{\rm R} = T({\rm exit\ catalyst}) - T(Q_{\rm R})$$
 (5.12)

in which $T(Q_R)$ is the equilibrium temperature corresponding to an equilibrium constant equal to the reaction quotient Q_R , which is the product of the partial pressures of the individual components raised to the power of their stoichiometric coefficients. The rate of the shift reaction (5.9) is so fast that it can be assumed to be at equilibrium in the major part of the reformer.

⁽²⁾ Figures in parentheses are calculated at each temperature using the formula ($\ln K_p = A + B/T$) with constants A and B.

Equilibrium calculations for reactions (5.8) and (5.9) in the following examples are complex. It is recommended to establish a spread sheet for computer calculations. The program should calculate equilibrium compositions from equilibrium constants in Table 5.5 and enthalpies of gas mixtures from the component data in Table 5.6.

Example 5.2: Equilibrium calculations

An ammonia plant reformer operates on methane at $P_{out} = 3.033 \, MPa$ and $T_{out} = 787^{\circ}$. A small amount of hydrogen is also added in order to keep the catalyst in a reduced state. An analysis of the dry exit gas shows the following composition (vol%): H_2 68.8, CO 8.8, CO 2 10.2, CH_4 12.2.

- (a) Estimate the approach to equilibrium, ΔT_R for reaction (5.8) assuming that the shift reaction is in equilibrium.
- (b) Calculate the steam-to-carbon ratio of the feed gas and the amount of hydrogen in the feed gas.

Solution

(a) The shift reaction (5.9) is assumed to be in equilibrium at T_{out} . Then, the equilibrium constant (K_{P_2}) at T_{out} is calculated from the data in Table 5.5.

$$lnK_{P_2} = -3.79762 + 4159.54/(787 + 273.15)$$

$$\therefore K_{P_3} = 1.134$$

Assume total number of mol of a dry exit gas is equal to 100, then the number of mol of H_2O (X_{H_2O}) is derived from the shift reaction (5.9) and chemical equilibrium as follows:

$$K_{P_2} = \frac{P_{CO_2} P_{H_2}}{P_{CO} P_{H_2O}}$$

$$= (10.2 \times 68.8) / (8.8 \times X_{H_2O})$$

$$= 1.134$$

$$\therefore X_{H_2O} = 70.3$$

$$\therefore X_{OUT} = H_2O 70.3 + H_2 68.8 + CO 8.8 + CO_2 10.2 + CH_4 12.2$$

$$= 170.3$$

This results in a wet exit gas (vol%): H_2O 41.2, H_2 40.4, CO 5.2, CO_2 6.0, CH_4 7.2.

The reaction quotient Q_R for reaction (5.8) at $P_{OUT} = 3.033$ MPa (29.23 atm) is then:

$$Q_R = \frac{P_{CO} P_{H_2}^3}{P_{CH_4} P_{H_2O}}$$

$$= \frac{(29.93 \times 0.052)(29.93 \times 0.404)^3}{(29.93 \times 0.072)(29.93 \times 0.412)}$$

$$= 103.5$$

This corresponds to K_P for reaction (5.8) at 778°C (Table 5.5) i.e. $\Delta T_R = 9$ °C.

(b) Mass balances for O, C and H in inlet and outlet gases are as follows:

$$O: H_2O_{in} = CO_{out} + 2CO_{2 out} + H_2O_{out}$$
 $C: CH_{4 in} = CO_{out} + CO_{2 out} + CH_{4 out}$
 $H: 2H_{2in} + 4CH_{4in} + 2H_2O_{in} = 2H_{2 out} + 4CH_{4 out} + 2H_2O_{out}$

Using the wet exit gas composition derived in solution (a), the steam to carbon ratio (H_2O/C) is calculated as follows:

$$(H_2O/CH_4)_{in} = (O/C)_{out} = \frac{CO_{out} + 2CO_{2out} + H_2O_{out}}{CO_{out} + CO_{2out} + CH_{4out}}$$
$$= \frac{0.052 + 2 \times 0.060 + 0.412}{0.052 + 0.060 + 0.072} = 3.17$$

From a mass balance.

$$(H/C)_{in} = (H/C)_{out} = \frac{2H_{2out} + 4CH_{4out} + 2H_2O_{out}}{CO_{out} + CO_{2out} + CH_{4out}}$$
$$= \frac{2 \times 0.404 + 4 \times 0.072 + 2 \times 0.412}{0.184} = 10.44$$

and also

$$(H/C)_{in} = \frac{4CH_{4in} + 2H_2O_{in} + 2H_{2in}}{CH_{4in}} = 10.44$$

The hydrogen to methane ratio in the feedgas in then calculated as follows:

$$(H_2/CH_4)_{in} = 0.05$$

5.2.2 THE TUBULAR REFORMER

In order to supply the heat for the overall endothermic steam reforming reaction, the process is carried out inside a furnace equipped with burners.

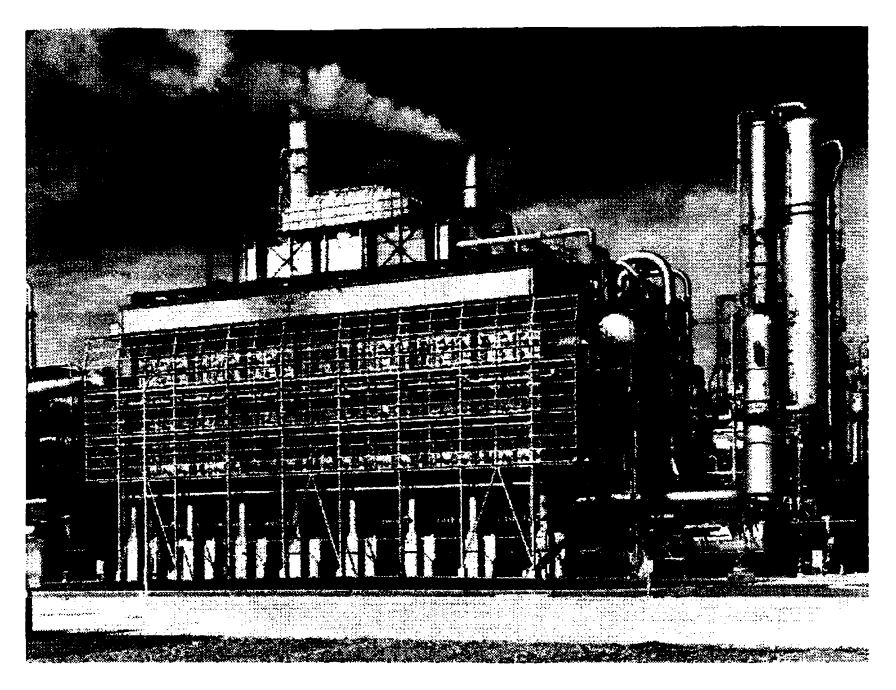


Figure 5.24 Large-capacity tubular reformer (courtesy of Idemitsu Kosan K.K. and Haldor Topsøe A.S.).

Figures 5.24 and 5.25 show examples of Topsøe's typical reformer furnace. The furnace consists of a box-type radiant section including the burners and a convection section to recover the waste heat of the flue gases leaving the radiant section. In the radiant section, the catalyst is loaded in a number of high alloy reforming tubes placed in a row along the furnace. Typical inlet temperatures to the catalyst bed are 450–650 °C, and product gas leaves the reformer at 700–950 °C depending on the applications. The thermal expansions of the catalyst tubes are absorbed either by fixing them at the top or at the bottom depending on the application and then hairpin tubes are used for connecting the catalyst tubes to the feed transfer line at the top and to the product transfer line at the bottom. The outer diameter of the tubes ranges typically from 100 to 150 mm and the length is from 10 to 13 m.

Reforming tubes are connected with high alloy (for example Alloy 800H) sub-collectors through hairpin tubes to collect reformed gases to the transfer line, placed on the ground and insulated inside with high aluminium castables.

In a Topsøe reformer furnace, the tubes are arranged in a single row, and the burners are placed in the furnace walls at 6–7 levels. With this arrangement, it is possible to adjust and control the heat input along the length of the tube, thus ensuring an optimum temperature profile at all operating conditions, and

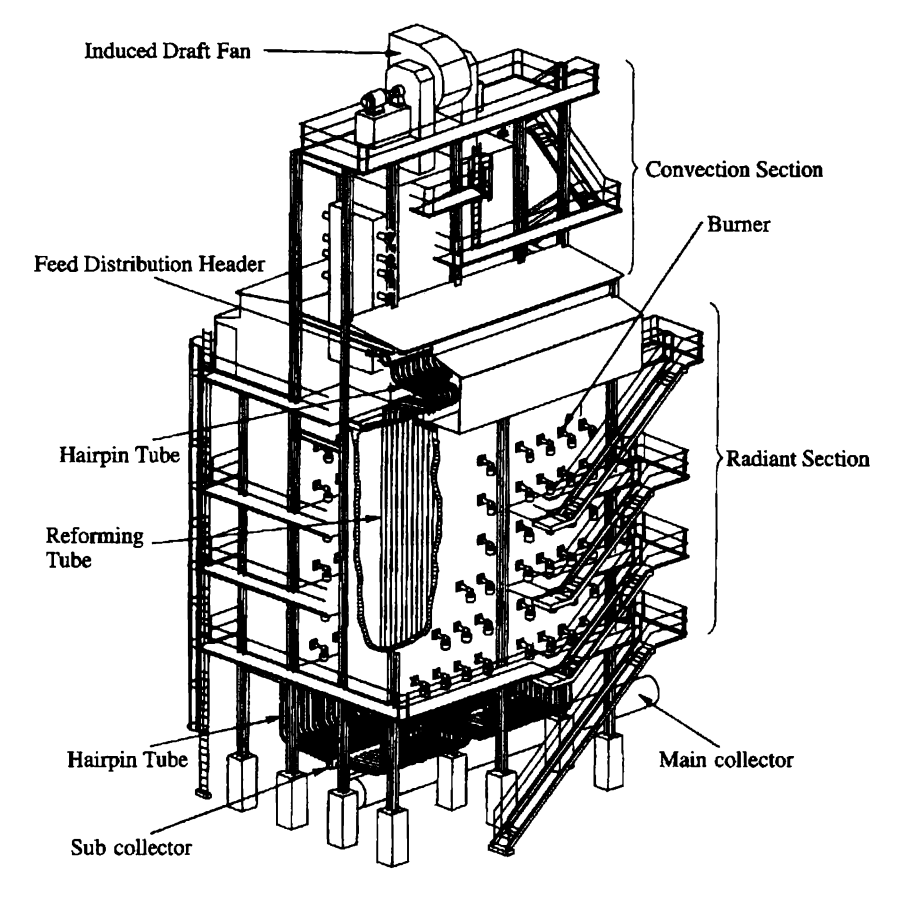


Figure 5.25 Birds-eye view of tubular reformer (Topsøe type).

also permitting control of the flue gas exit temperature at the top. Other furnaces have burners placed at the top of the furnace (Kellogg, ICI), or at terraces at the side walls (Foster Wheeler).

Tube coils for preheating of feed, steam superheating, and eventually combustion air preheating, are installed in the waste heat convection section to recover the heat from the flue gases leaving the radiant section. The flue gas is exhausted by an induced draft fan or through a stack. The overall thermal efficiency achieved by the above system is generally around 90%, and the addition of an air preheat system can increase the efficiency by up to approximately 95%.

Figure 5.26 shows the characteristic temperature, conversion, reaction rate, and catalyst effectiveness factor profiles along the tube. It is seen that the bulk gas arrives rapidly at a composition close to equilibrium when passing down

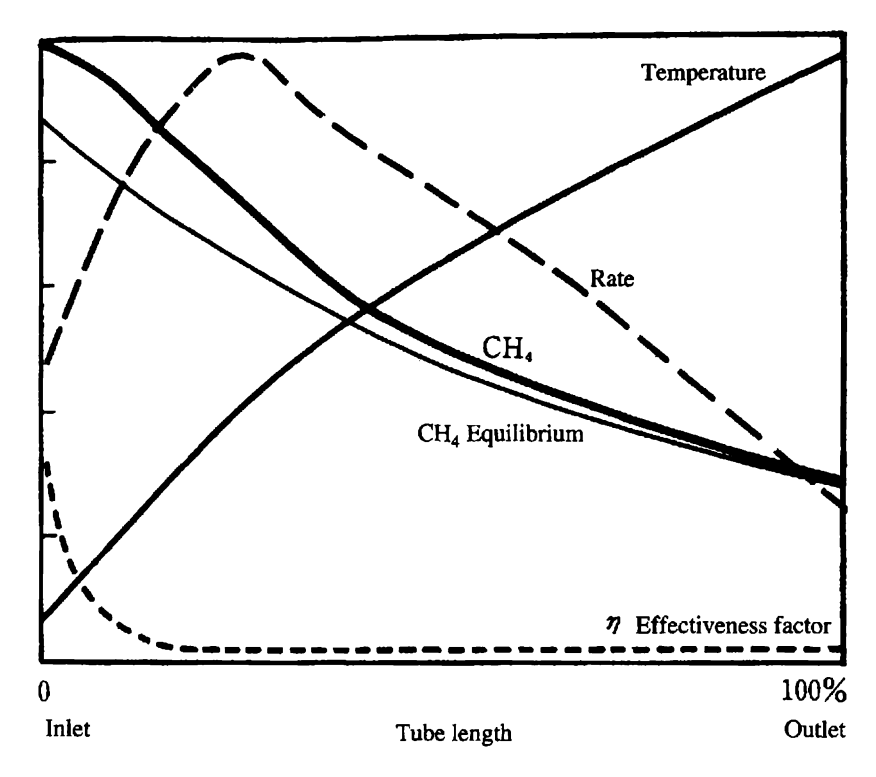


Figure 5.26 Tubular steam reformer. Conversion and rate profiles.

the reformer tube which then results in a reaction rate proportional to the axial temperature gradient, dT/dz, as a driving force.

The required heat input, also called the reformer duty, Q, is the difference between the enthalpies of the exit and the inlet gases, and it can easily be calculated from enthalpy tables, such as the one shown in Table 5.6.

Table 5.6 Enthalpy of formation (standard conditions 25 °C, 0.101325 MPa)

				H = A + BT [kJ/kmol]; T [K]	
Temperature [°C]	500	700	900	A	В
H ₂ O	-224 877	-216953	-208 531	-256 555	40.87
H ₂ O H ₂	13 908	19878	25 974	-9435	30.17
CO	-96207	-89734	-83036	-121704	32.93
CO ₂	-372071	-361548	-350498	-413856	53.93
CH₄	-51752	-38468	-23522	-106592	70.58
$C_7 \vec{H}_{16}$	-64 764	6644	85 462	-356368	375.6

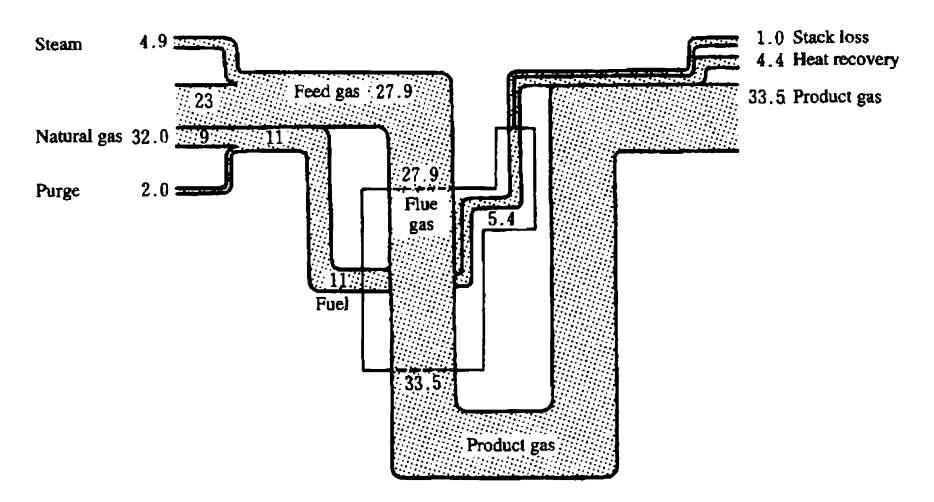


Figure 5.27 Heat balance for tubular reformer in ammonia production (unit: GJ per ton of NH₃).

The duty consists of the heat of reaction as well as the heat required to raise the temperature to the level of the reformer exit. This duty can be calculated directly from the approximate formulas in Table 5.6, since they incorporate the enthalpies of formation of the gases present.

In a typical tubular reformer furnace, about 50% of the heat produced by combustion in the burners is transferred through the reformer tube walls and absorbed by the process (in an ammonia plant: 60% for reaction, 40% for temperature increase). This is illustrated in Figure 5.27. The other half of the fired duty is available in the hot flue gas and recovered in the waste heat section of the reformer for preheat duties and for steam production. In this way, the overall thermal efficiency of the reformer approaches 95%.

The balance between heat input through the reformer tube walls and the heat consumption in the endothermic reforming reaction is a central problem in steam reforming. The maximum allowed stress value in the tubes is strongly influenced by the maximum tube wall temperature and by the maximum heat flux. Even a slight increase in the maximum tube wall temperature may result in a serious decline of the expected tube lifetime.

The reformer tubes are subject to very large stresses since they operate at high temperatures with very large temperature gradients. Reformer tubes are normally designed for an average expected lifetime of 100 000 hours, and great care must be taken when choosing heat flux, tube dimensions, design temperatures and tube materials. New materials which have superior creep rupture characteristics, allow a design with a considerable reduction in tube wall thickness and a corresponding increase in maximum temperature and heat flux.

The heat transferred per unit time and unit volume of catalyst can be obtained from a one-dimensional pseudo-homogeneous reactor model.

$$HQ = \frac{4}{d_t}U(T_W - T_{CAT}) = (-\Delta H)r_v + u_s \rho_g c_P \frac{dT}{dz}$$
 (5.13)

The two terms on the right-hand side represent the heat absorbed by the reforming reactions and that used for increasing the gas temperature, respectively.

The heat input through the reformer tube wall results in radial temperature and concentration gradients in addition to the axial gradients. The radial temperature gradients are significant with high values of dT/dr at the tube wall, whereas radial concentration gradients are insignificant. This means that close to the tube wall, there would be significant deviation from equilibrium as illustrated in Figure 5.29 on page 265. This phenomenon is important for the formation of carbon as explained in Chapter 5.2.5.

Therefore, a two-dimensional reactor model is required when a detailed knowledge of the conversion and temperature profile is necessary.

The heat is transferred from the tube wall in the radial direction of the catalyst bed and then across the gas film surrounding each catalyst particle. The catalyst effectiveness factor, η decreases from the reactor inlet with typical values below 0.1 as illustrated in Figure 5.26. Mass transport restrictions are related mainly to pore diffusion, whereas the heat transfer restrictions are located in the gas film around the particle. The strong endothermic reaction results in a temperature drop of 5–10 °C over the gas film in spite of a high mass velocity, corresponding to Reynolds numbers of say 100 000.

Example 5.3: Design of a Hydrogen Plant Reformer

A methane based reformer should produce $105\,000\,Nm^3H_2+CO$ per hour and a study has shown that the optimum operating parameters are $H_2O/CH_4=2.5$, $H_2/CH_4=0.05$, $T_{in}=500^{\circ}C$, $T_{out}=850^{\circ}C$, $P_{out}=2.145\,MPa$. Mechanical considerations have resulted in selection of tubes with heated length = 11 m and an internal diameter = 71.4 mm for an average heat flux $91.64\,kW/m^2$. Assume $\Delta T_R=10^{\circ}C$.

- (a) Estimate the number of tubes.
- (b) What will be the maximum capacity of the reformer if methane is replaced by naphtha represented as (nC_7H_{16}) while maintaining the same heat flux and hydrogen flow, but increasing the steam to carbon ratio to 3.5?

Solution

(a) Assume that the reforming equilibrium temperature is equal to $T_{out} - 10^{\circ}C$, and the shift equilibrium is established at T_{out} .

(i) Given the relative conversions for reactions (5.8) and (5.9) are F and G, respectively, the overall mass balance is:

	Inlet	Outlet
H_2O	2.5	2.5 - F - G
CH_4	1	1-F
H_2	0.05	0.05 + 3F + G
CO	0	F-G
CO_2	0	G
	3.55	3.55 + 2F

Accordingly, each composition at outlet is equated as follows:

$$X_{H_2O} = \frac{2.5 - F - G}{3.55 + 2F}$$

$$X_{H_2} = \frac{0.05 + 3F + G}{3.55 + 2F}$$

$$X_{CH_4} = \frac{1 - F}{3.55 + 2F}$$

$$X_{CO} = \frac{F - G}{3.55 + 2F}$$

$$X_{CO_2} = \frac{G}{3.55 + 2F}$$

(ii) The equilibrium constants for reaction (5.8) and (5.9) are calculated from the data in Table 5.5 as follows:

$$K_{P1} = \frac{(X_{H_2^3} X_{CO})P^2}{X_{CH_4} H_{H_2O}} = 432.2$$

$$K_{P2} = \frac{X_{CO_2} X_{H_2}}{X_{CO} X_{H_2O}} = 0.910$$

From the above results of (i) and (ii), the exit gas composition (vol%) is calculated by solving the two equations by iteration in the two variables F and G:

H₂O 29.2, H₂ 51.1, CO 9.9, CO₂ 5.1, CO₂ 5.1, CH₄ 4.7.

The total exit gas flow including (H_2+CO) : $105\,000/(0.51+0.099) = 172\,131\,\text{Nm}^3/\text{h}$, from which the feed flow: CH_4 1 513, H_2O 3 786, H_2 77 (kmol/h).

The enthalpy balance is calculated from the data in Table 5.6. The transferred duty;

$$O = H_{out} - H_{in} = 94.6 \times 10^3 \, kJ/s$$

whereafter

Number of tubes =
$$\frac{94.6 \times 10^3}{(91.64)\pi(0.714)(11)} = 418.6 \approx 420$$

(b) The feed flow is guessed as C_2H_{16} flow = 1/7 of 1513 kmol/h = 216 kmol/h from reactions (5.8) and (5.10).

The exit gas composition is calculated as above taking the increase in H_2O/C into account (vol%): H_2O 39.6, H_2 42.2, CO 8.9, CO_2 7.6, CH_4 1.7. Using the carbon flow, the total exit gas flow is (1513)/(0.182) = 8313 kmol/h and $H_2 + CO = 95$ 213 Nm³/h. The absorbed duty = $H_{out} - H_{in} = 85.3 \times 10^3$ kJ/s, which is less than that with methane feed as in case (a). For unchanged absorbed duty, the reformer can produce 95 213 × (94.6/85.3) = 105 594 Nm³ $CO + H_2/h$.

5.2.3 THE CATALYST AND REACTION RATE

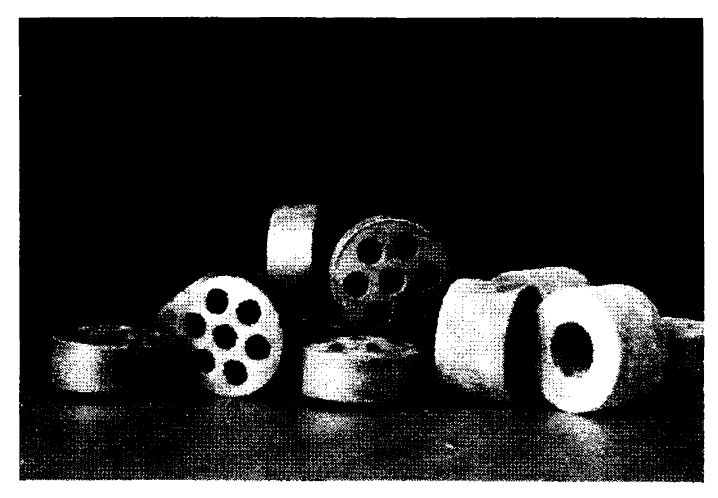
The steam reforming catalyst is normally based on nickel. Cobalt and the noble metals are also active, but more expensive. Attempts to use non-metallic catalysts have not had commercial success, because of low activity.

The catalyst properties are dictated by the severe operating conditions, i.e. temperatures of 450–950 °C and steam partial pressures of up to 3 MPa. The activity depends on the nickel surface area. The nickel crystals will sinter quickly above the Tammann temperature (590 °C). This may be partly prevented by a stable micropore system because the nickel particles may hardly grow larger than the pore diameter of the support.

The activated chemisorption of methane is the rate determining step in steam reforming. There is general agreement on first-order kinetics with respect to methane, but the impact of steam and hydrogen on the rate is complex. The rate of the shift reaction (5.9) can be assumed to be so fast that in practice it is at equilibrium in the major part of the reformer.

For normal steam reforming catalysts, the utilization of the activity as expressed through the effectiveness factor, is smaller than 10% because of transport restrictions. The low effectiveness factor (Figure 5.26) means that for a given catalyst type, the activity is roughly proportional to the external surface area.

The low effectiveness factor means (when assuming first-order kinetics) that the effective reaction rate on a bed volume basis for the methane reforming reaction can be written as:



Activity
$$\propto \frac{1-\varepsilon}{d_{\rm P}}$$

$$\Delta P \propto \frac{1-\varepsilon}{\varepsilon^3} \cdot \frac{1}{d_{\rm p}}$$

Figure 5.28 Steam reforming catalyst (Topsøe R-67-7HR).

$$r_{\rm V} = \frac{6(1-\varepsilon)}{d_{\rm DS}} \sqrt{D_{\rm eff} k_{\rm i}} (C_{\rm CH_4} - C_{\rm CH_{4,eq}})$$
 (5.14)

The catalyst particle size and shape should be optimized to achieve maximum activity and maximum heat transfer while minimizing the pressure drop. The high mass velocities in steam reforming plants necessitate a relatively large catalyst particle size to obtain a low pressure drop across the catalyst bed; but the particle size is limited by the requirement for effective packing. The pressure drop depends strongly on the void fraction of the packed bed and decreases with particle size (Figure 5.28).

Also, the particle size has a minor impact on the heat transfer coefficient. The optimum choice is a catalyst pellet with high voidage and high external surface area.

To summarize, effective catalyst activity is a complicated function of the particle size and shape and the operating conditions. This, however, does not diminish the requirement for a high intrinsic catalyst activity, in particular in those parts of the reformer having a high heat flux.

Example 5.4: Impact of Catalyst Particle Size

Compare the relative activity and relative pressure drop of a catalyst filling consisting of cylinders D/H 16/10 and D/H 9/9, and rings D/d/H = 16/8/10 (D outer diameter, H height, d hole diameter, all dimensions in mm), respectively. It is assumed that the void in the bed is 0.35 for the cylinder without hole.

Solution

The equivalent sphere diameters for cylinders and rings are calculated from $d_{ns} = 6 \times (Vp/Sp)$ as follows:

(a) Cylinders

(i) D/H =
$$16/10$$
; $d_{ps} = 6 \times \frac{\pi}{4} 16^2 \times 10/\{(\pi/4) \ 16^2 \times 2 + \pi \times 16 \times 10\} = 13.33$

(ii)
$$D/H = 9/9$$
; $d_{ps} = 9.0$

(b) Ring catalyst

$$d_{ps} = 6 \times (16^2 - 8^2) / (\pi/4) \times 10 / \{ (16^2 - 8^2) (\pi/4) \times 2 + (16 + 8)\pi \times 10 \}$$

$$= 8.57$$

The void fraction of the ring filling is calculated from the simple geometry as follows:

$$\varepsilon = \varepsilon_{cyl} + (1 - \varepsilon_{cyl}) h$$

where h is the hole fraction

$$\varepsilon = 0.35 + (1 - 0.35) \left(\frac{8}{16}\right)^2 = 0.513$$

The relative activity and pressure drop are estimated by the formulas given in Figure 5.28,

the relative pressure
$$drop = \frac{\Delta P_2}{\Delta P_1} = \frac{(1 - \epsilon_2)/\epsilon_2^3}{(1 - \epsilon_1)/\epsilon_1^3} \frac{d_{P1}}{d_{P2}}$$
the relative activity $= \frac{activity \ 2}{activity \ 1} = \frac{(1 - \epsilon_2)}{(1 - \epsilon_1)} \frac{d_{P1}}{d_{P2}}$

The above results are summarized in the following table.

Catalyst type	d _{ps} [mm]	3	$\frac{1-\varepsilon}{\varepsilon^3}$	The relative pressure drop	The relative activity
Cylinder 16/10	13.33	0.35	15.2	1.0	1.0
Cylinder 9/9	9.0	0.35	15.2	1.5	1.5
Ring 16/8/10	8.57	0.51	3.7	0.4	1.2

It is obvious that the ring filling represents the optimum among the three particles.

5.2.4 POISONING

Sulphur is the most severe poison for steam reforming catalysts. All sulphur compounds in the feed will be converted into hydrogen sulphide at reforming conditions, and hydrogen sulphide will chemisorb on the nickel surface. The Ni/H₂S-chemisorption is well-understood from surface science.

The monolayer of chemisorbed sulphur may be considered as a twodimensional sulphide with about 0.5 S-atom per Ni-atom. The sulphur coverage below saturation is determined by the H₂S/H₂ ratio and temperature.

$$\theta_{\rm S} = 1.45 - 9.53 \times 10^{-5} \ T + 4.17 \times 10^{-5} \ T \ln(\rm H_2S/H_2)$$
 (5.15)

The expression is not valid for θ_S close to zero and close to 1.0. Equation (5.15) demonstrates that there is no fixed limit of sulphur content in the feed below which poisoning will not occur. In practice, well designed hydrodesulphurization systems will result in sulphur contents below about 10 ppb in the dry reformer feed.

In the operating reformer, sulphur poisoning is a dynamic phenomenon, and the pore diffusion restrictions in the catalyst particles have a complex influence on the gradually developing sulphur profiles through the tube.

Example 5.5: Sulphur Poisoning of an Ammonia Plant Reformer

An ammonia plant reformer operates at conditions ($T_{in} = 500 \,^{\circ}C$) as described in Example 5.2. The total sulphur content in the wet methane feed is determined to 0.05 vol ppm.

- (a) Determine the equilibrium coverage on the external surface of the catalyst pellet in the inlet layer.
- (b) What is θ_S at equilibrium in the centre of the pellet at the inlet assuming that the reforming reactions are in equilibrium?
- (c) What is θ_S at equilibrium on the catalyst at the reformer exit? This corresponds to a situation where the sulphur is homogeneously distributed through the pellet.
- (d) What should be the maximum, S-content in the feed if θ_S at equilibrium should not exceed 0.5 at the former exit?

Solution

(a) From the composition of feed gases calculated in the solution for Example 5.2, the feed gas rate at inlet is 77.6 mol/h for the outlet quantity of 100 mol/h. Accordingly,

$$H_2S = 77.6 (0.05 \times 10^{-6}) = 3.88 \times 10^{-6} [mol/h]$$

$$\therefore (H_2S/H_2)_{feed} = 3.88 \times 10^{-6}/0.92 = 4.22 \times 10^{-6}$$

From equation (5.15), $\theta_S = 0.977$ (97.7%).

(b) The centre of the pellet is exposed to equilibrium gas at 500°C.

The gas composition (vol%) at 500° C is calculated using the same method as used in the solution for Example 5.3(a): H_2O 66.0, H_2 11.5, CO 0.1, CO₂ 2.6, CH_4 19.8, then $H_2S/H_2 = 100 \times 0.05 \times 10^{-6}/11.5 = 4.35 \times 10^{-7}$.

From Eq (5.15),
$$\theta_S = 0.904$$
 (90.4%).

(c) Assume that $H_2S_{in} = H_2S_{out}$ at steady state. From the mass balance calculated in Example 5.2 and above (a), H_2 out/ H_2 in = 43.9, $(H_2S/H_2)_{in} = 4.22 \times 10^{-6}$.

Accordingly.

$$(H_2S/H_2)_{out} = (4.22 \times 10^{-6})/43.9 = 9.60 \times 10^{-8}$$

From Eq (5.15), $\theta_S = 0.635$ (63.5%).

(d)
$$\theta_S = 0.5$$
 at $787^{\circ}C$ corresponds to $H_2S/H_2 = 4.57 \times 10^{-9}$.

From the above (c),
$$(H_2S/H_2)_{in} = 4.57 \times 10^{-9} \times 43.9 = 2.01 \times 10^{-7}$$

$$H_2S = 2.01 \times 10^{-7} \times 0.92 = 1.85 \times 10^{-7}$$

$$H_2S$$
 vol ppm = $1.85 \times 10^{-7}/77.6 = 0.00238(2.38 \text{ vol ppb})$

Example 5.6 Effective Activity

A catalyst sample Catalyst A originates from a reformer, in which it was exposed to complete sulphur poisoning. An analysis shows a content of 1200 wt ppm S. The equivalent diameter, $d_{p,s} = 12 \, \text{mm}$ and the effective diffusion coefficient at operating conditions is estimated to 0.0025 m^2/h .

On this basis, make an estimate of the expected effective activity of non-poisoned Catalyst A relative to a bench-mark Catalyst B with the following properties:

Catalyst B: Particle diameter $d_{p,s} = 10 \text{ mm}$

$$D_{eff} = 0.003 \, m^2/h$$

Nickel area = $0.9 \, m^2/g$

Solution

Using S/Ni = 0.5, $N_{av} = 6.02 \times 10^{23}$ and assuming an area of 6.5×10^{-2} nm² per Ni site, the nickel area of Catalyst A is calculated:

$$\alpha_{Ni}(A) = \frac{(1200 \times 10^{-6})(6.02 \times 10^{23})(6.5 \times 10^{-2}(10^{-18})}{(32)(0.5)} = 2.9 \, m^2/g$$

and using equation (5.14):

$$\frac{\mathbf{r}_{v}(A)}{\mathbf{r}_{v}(B)} = \frac{(10)}{(12)} \sqrt{\frac{(0.0025)(2.9)}{(0.0030)(0.9)}} = 1.37 \cong 1.4$$

5.2.5 CARBON FORMATION

Steam reforming involves the risk of carbon formation by the decomposition of carbon monoxide, methane, and other hydrocarbons.

$$2CO = C + CO_2 + 172 \text{ kJ/mol}$$
 (5.16)

$$CH_4 = C + 2H_2 -75 \text{ kJ/mol}$$
 (5.17)

$$C_n H_m \longrightarrow nC + \frac{m}{2} H_2 \tag{5.18}$$

Reaction (5.16) is normally referred to as 'the Boudouard reaction'. At high temperatures (>ca. 650 °C), higher hydrocarbons may react in parallel to reaction (5.10) by thermal cracking (pyrolysis or 'steam cracking') into olefins which may easily form coke via reaction (5.18):

$$C_n H_m \longrightarrow \text{olefins} \longrightarrow \text{polymers} \longrightarrow \text{coke}$$
 (5.19)

Reactions (5.16) and (5.17) are reversible, whereas (5.18) and (5.19) are irreversible for n > 1. Equilibrium constants for reactions (5.16) and (5.17) are listed in Table 5.5

Reactions (5.16) and (5.17) are catalysed by nickel. The carbon grows as a fibre (whisker) with a nickel crystal at the top. The non-ideal whisker structure results in equilibrium constants for reaction (5.17), which are smaller than those calculated on the basis of graphite data (ref. Table 5.5). Reaction (5.18) results in pyrolytic carbon encapsulating the catalyst.

Carbon formation may lead to breakdown of the catalyst, and the build-up of carbon deposits and degraded catalyst may cause partial or total blockage of some tubes resulting in development of 'hot spots' or hot tubes. The uneven flow distribution will cause a self-accelerating situation with further overheating of the hot tubes. Therefore, carbon formation cannot be tolerated in tubular reformers. The important problem is whether or not carbon is formed and not the rate at which it is formed.

For steam reforming of methane, there are two different carbon limits to consider:

'Limit A' is dictated by kinetics. It corresponds to conditions in the reformer where kinetics allow methane to decompose into carbon instead of reacting with steam, even if thermodynamics predicts no carbon formation after equilibrium of reactions (5.8) and (5.9). Carbon formation is then a question of kinetics, local process conditions and reformer design. This is called the 'principle of actual gas'.

In this case, there will be a potential for carbon formation, if the actual gas surrounding the catalyst shows affinity for carbon formation according to the reaction (5.17). This can be expressed by the carbon activity $a_{\rm C}^{\rm eq}$ expressed by:

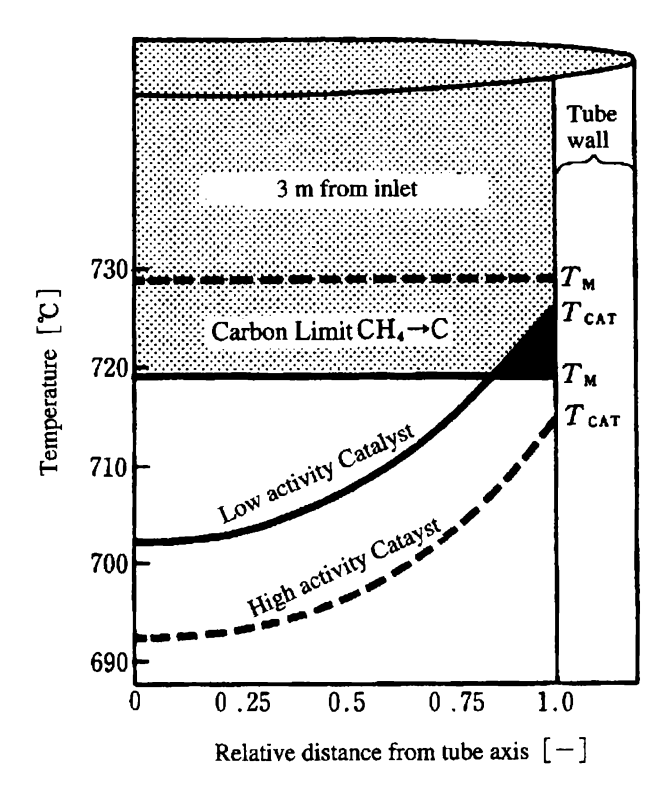


Figure 5.29 Radial gradients in tubular reformer.

$$a_{\rm C}^{\rm eq} = K_{\rm C} \frac{P_{\rm CH_4}}{P_{\rm H_2}^2} \tag{5.20}$$

in which K_C is the equilibrium constant (see Table 5.5) for the methane decomposition (reaction 5.17) and the partial pressures are for the actual gas.

A safe, conservative design would be to require $a_C^{\rm eq} < 1$ at any position in the reformer tube. This is equivalent to require $T_{\rm CAT} < T_{\rm M}$ as shown in Figure 5.29.

 $T_{\rm M}$ is the carbon limit temperature for methane decomposition calculated from the actual gas composition. Carbon formation is expected for $T_{\rm CAT} > T_{\rm M}$.

Figure 5.29 represents two cases for low activity (full lines) and high activity (dotted lines), respectively. With high catalyst activity, the catalyst temperature, $T_{\rm CAT}$ (3 m from inlet) is lower and $T_{\rm M}$ is higher because of higher conversion as compared with low activity.

However, at the inlet of the reformer with almost no hydrogen present, $a_{\rm C}^{\rm eq}$ is much larger than one $(T_{\rm CAT} > T_{\rm M})$, meaning that there is a potential for carbon formation, but in practice no carbon is formed. Therefore, an important question for industrial operation is: what is the maximum inlet temperature allowed before carbon will be formed? A similar situation may exist at other positions in the reformer close to the tube wall as illustrated in Figure 5.29.

Whether carbon-free operation is possible even if $a_{\rm C}^{\rm eq} > 1$, is a question of whether the steady state activity of carbon, $a_{\rm C}^{\rm s} < 1$.

 a_C^s can be expressed by balancing the rate of carbon formation without presence of steam with the rate of gasification of the adsorbed carbon atoms. It can be shown that $a_C^s \leq a_C^{eq}$.

'Limit B' is dictated by thermodynamics. Carbon will be formed if the equilibrated gas shows affinity for carbon. This is called the 'principle of equilibrated gas'. The equilibrated gas composition is achieved by calculating the gas composition with equilibration of reactions (5.8) and (5.9). The principle is justified by the fact that the gas will be at equilibrium in most of the catalyst particle because of the low effectiveness factor.

Example 5.7: Carbon Limits

A reformer is operating at the following conditions: $H_2O/CH_4 = 1.1$, $CO_2/CH_4 = 0.2$, $H_2/CH_4 = 0.15$, P = 2.516 MPa (24.83 atm), $T_{out} = 900^{\circ}$ C. Thermocouples and gas sample line are placed at 3 m from the inlet of the catalyst layer, where carbon formation may be critical. The following measurements are achieved:

Centre catalyst temperature, $708^{\circ}C$ Catalyst temperature at the tube wall, $725^{\circ}C$ Dry gas analysis (vol%): H_2 (43.5), CO (9.1), CO_2 (11.7), CH_4 (35.7). The dry gas analysis is in the centre of the tube, but the same composition can be assumed at the tube wall.

- (a) Estimate risk of carbon formation by graphite carbon from 'principle of equilibrated gas' at the tube wall.
- (b) Has the actual gas potential for carbon formation?

Solution

(a) From a mass balance of C, the feed gas conditions and the dry gas composition which are sampled and analysed, the wet gas composition is derived as follows:

H₂O 27.6, H₂ 31.5, CO 6.6, CO₂ 8.5, CH₄ 25.8 [vol%]

Then the equilibrium gas composition at 725°C is calculated by the same method as the solution for Example 5.3:

H₂O 26.3, H₂ 33.5, CO 7.3, CO₂ 8.3, CH₄ 24.6 [vol%]

For the equilibrated gas at 725°C,

$$P_{H_2}^2/P_{CH_4} = (33.5)^2/24.6 \times \left(\frac{24.83}{100}\right)$$

= 11.3 > K_C (graphite) = 10.4

i.e. the equilibrated gas shows no affinity for carbon formation from reaction (5.17).

(b) For the actual gas:

$$P_{H_2}^2/P_{CH_4} = 9.5 < K_C(graphite) = 10.4$$

 $P_{H_2}^2/P_{CH_4} = 9.5 > K_C(whisker) = 6.6$

i.e. on the basis of graphite, there is potential for C at the tube wall, but not on the basis of whisker carbon. No carbon is expected.

5.2.6 CO₂ REFORMING

The increasing interest for C_1 -chemistry has created a need for synthesis gases with low H_2/CO ratio. This can be obtained by adding CO_2 to the reformer feedstock (reaction (5.11)). The H_2/CO ratio in reaction (5.11) is 1, whereas the H_2/CO ratio is 3 when using steam (reaction (5.8)). The use of CO_2 instead of steam represents no significant change in overall reaction kinetics. However, the presence of CO_2 in the feedstock, results in more critical conditions for carbon formation because of lower H/C ratio.

The ratio of H_2/CO in the reformer exit gas can be estimated by thermodynamic calculations. The results of the calculations may be presented in an equilibrium chart for a given pressure as shown in Figure 5.30.

The selection of process parameters is limited by the potential for carbon formation. The solid curve in Figure 5.30 shows the thermodynamic carbon limit (carbon 'limit B'), considering the deviation of the carbon structure from ideal graphite as so called whisker carbon observed on catalysts. For O/C and H/C ratios on the left side of the curve, there is thermodynamic potential for the formation of carbon.

It is obvious that operation on the left side of the carbon limit curve in Figure 5.30 would result in more economic conditions (lower steam and CO_2 -addition for a given H_2/CO ratio).

One solution may be to carry out the reaction over noble metal catalysts such as a Ru-catalyst, which shows little tendency for carbon formation or the use of a partly sulphur poisoned catalyst on which the sulphur blocks the nickel sites for nucleation of carbon.

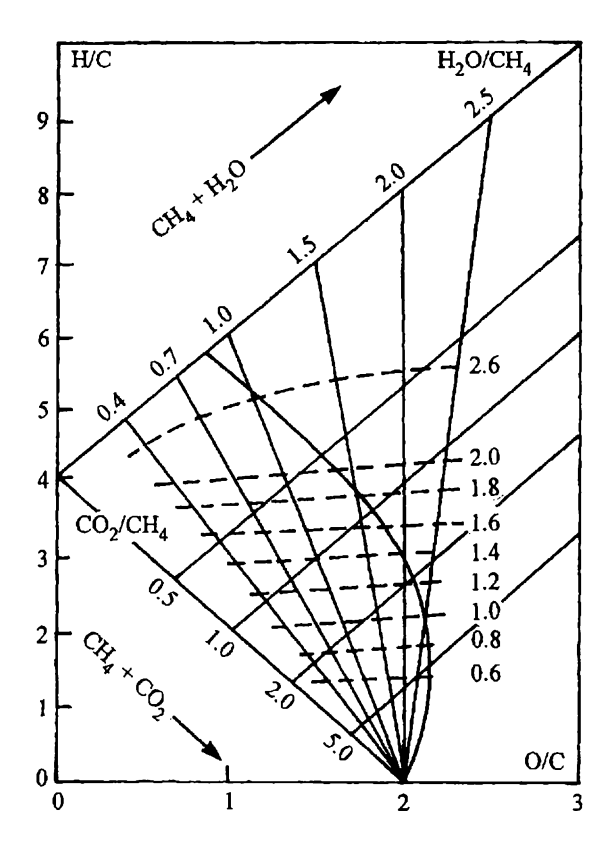


Figure 5.30 Carbon limit diagram (0.6 MPa (5.922 atm). H_2/CO ratios in exit gas indicated by dotted lines. Temperature 900 °C.

Example 5.8

Carbon-free Operation for Low H_2/CO $(H_2/CO=2.0)$ at $P_{out}=6$ MPa, $T_{out}=900$ °C

- (a) Determine from Figure 5.33 the required addition of CO_2 and the exit gas composition for $H_2/CO = 2$ when using $H_2O/CH_4 = 2.5$. Assume that both reactions (5.8) and (5.9) are at equilibrium at 900°C.
- (b) Determine limiting operating conditions for C-free operation when producing a gas of $H_2/CO = 2$ using Figure 5.30. Calculate the exit gas, $\Delta T_R = 0$ °C.
- (c) Compare the total outlet flows, duties, and the Boudouard exit temperatures.

Solution

(a) $(H_2O/CH_4)_{in} = 2.5$, and $(H_2/CO)_{out} = 2.0$ Then, from Figure 5.30, the rate of CO_2 -addition: $(CO_2/CH_4)_{in} = 1.05$ Accordingly the exit gas composition is calculated using the same method as in Example 5.3.

(b) From Figure 5.30; $H_2O/CH_4 = 1.4$, and $CO_2/CH_4 = 0.6$

The exit gas composition (vol%) is derived using the same method as (a) above:

- (c-1) The total product gas volume for each mole of product gas in case (b) is 77% of that in case (a), indicating that the reformer in case (b) will be much smaller.
- (c-2) Transferred duty in case (b) is 91.3% of that in case (a).
- (c-3) Equilibrium constant of the Boudouard reaction for case (a) and case (b) is calculated from each of the two exit conditions (composition and pressure):

$$K_P(a) = 0.451$$

 $K_P(b) = 0.145$

From Table 5.5, the Boudouard exit temperature in case (a) is $737^{\circ}C$ and in case (b) it is $798^{\circ}C$, indicating a higher risk of carbon formation in case (b).

5.2.7 REFORMING OF HIGHER HYDROCARBONS

Higher hydrocarbons give rise to carbon formation more easily than does methane, and special catalysts containing alkali or catalysts based on active magnesia are required for reforming of naphtha and similar feedstocks. The promoters result in enhanced steam adsorption and hence $a_C^s < 1$.

The many steam naphtha reformers designed by Topsøe/Chiyoda use the Topsøe magnesia based catalyst, RKNR. By using an alkali-free catalyst, high activity is achieved. This results in high flexibility in feedstock range, and even kerosene has been used as feedstock for RKNR.

5.2.8 ALTERNATIVES TO STEAM REFORMING TECHNOLOGY

The oxidative conversion of methane into methanol or ethylene has attracted much interest as an alternative route to convert natural gas into useful products:

$$2CH_4 + O_2 = C_2H_4 + 2H_2O + 276 \text{ kJ/mol}$$
 (5.21)

The key question is selectivity, i.e. to minimize the losses originating from CO_2 formation and the corresponding high heat of reaction.

Yields for oxidative coupling appear to approach a ceiling of 25% per pass. Typical selectivities for oxidative coupling of methane to C_2 -hydrocarbons are 80–85% (of which 40–50% as ethylene). Simplified calculations using these data shows that the overall conversion of carbon to CO_2 is ca. 25%.

For comparison, the methanol synthesis has a conversion per pass of ca. 40% with a selectivity of 99.8% resulting in a single pass yield of ca. 40%. The ultimate yield of 94% is obtained by a recycle of unconverted synthesis gas in a recycle ratio of 3-4 vol/vol. The synthesis gas route also consumes methane as fuel in contrast to the direct route. The fuel is converted into carbon dioxide which represents a loss. This results in an overall conversion of carbon to CO₂ of 24%. This illustrates that the two routes have almost the same CO₂ production which may be taken as a rough measure of the process efficiency.

In other words, a direct methane conversion process should have a CO₂-yield substantially lower than 20 C-atom % in order to represent a breakthrough compared to the indirect route.

One argument in favour of the direct oxidative conversion of methane has been that steam reforming requires a large heat input which is only partly recovered in the synthesis—and at lower temperatures. This argument is misleading. The indirect routes are self-sufficient in energy and have no steam export.

In conclusion, the chemistry of the direct oxidative conversion of methane may well be exciting but the process engineering requirements still represent a severe obstacle before these routes may become economic alternatives to the indirect process via steam reforming.

Notation

Carbon activity

$a_{\rm c}$	Carbon activity	
C_{i}	Molar concentration of component i	$(kmol/m^3)$
$C_{i,eq}$	Equilibrium molar concentration of i	$(kmol/m^3)$
C_P	Heat capacity	(kJ/kg/K)
$d_{\rm p}$	Equivalent particle diameter, volume basis	(m)
d_{t}	Inner tube diameter	(m)
$d_{\rm ps}$	Equivalent particle diameter, surface basis	(m)
D_{eff}	Effective diffusion coefficient	(m^2/h)
\boldsymbol{F}	Conversion in reforming	(kmol/h/kmol feed)
\boldsymbol{G}	Conversion in shift	(kmol/h/kmol feed)
HQ	Heat transferred	(kcal/h/m ³ bed)
H	Enthalpy	(kJ/kmol)
ΔH	Heat of reaction	(kJ/kmol)
k_{i}	Intrinsic rate constant, volume basis	(h^{-1})
$k_{ m v}$	Effective rate constant, volume basis	(h^{-1})
$K_{\rm pl}$	Chemical equilibrium constant for steam reforming	

K_{p2}	Chemical equilibrium constant for shift	
P	Pressure	(MPa)
P_{i}	Partial pressure of component i	(MPa)
q	Heat flux	(kW/m^2)
Q	Duty	(kJ/h)
\tilde{Q}_{R}	Reaction quotient for steam reforming	
$r_{\rm v}$	Effective reaction rate, volume basis	(kmol/h/m ³)
S_{p}	External surface area of catalyst particle	(m^2)
Ť	Temperature	(K)
T_{CAT}	Catalyst temperature	(K)
T_{M}	Equilibrium temperature for methane decomposition	(K)
$T_{\mathbf{W}}$	Tube wall temperature	(K)
$\Delta T_{ m R}$	Temperature approach for steam methane reforming	(K)
$u_{\rm s}$	Superficial velocity	(m/h)
$\boldsymbol{\mathit{U}}$	Overall heat transfer coefficient	$(kJ/m^2/h/K)$
V_{p}	Volume of catalyst particle	(m^3)
x_{i}	Mole fraction	
X_{i}	Mole %	
z	Axial distance	(m)
3	Void fraction of catalyst bed	
η	Effectiveness factor	
$ ho_{ extsf{g}}$	Gas density	(kg/m^3)
θ	Sulphur coverage	

References

- (1) J. R. Rostrup-Nielsen, Catalytic Steam Reforming, Springer Verlag, Berlin, 1984, (130 pages).
- (2) J. R. Rostrup-Nielsen, I. Dybkjær and L. J. Christiansen, 'Steam Reforming. Opportunities and Limits of the Technology' in Proc. NATO ASI Study Chemical Reactor Technology for Environmentally Safe Reactors and Products, Aug/Sept. 1991, Ontario, Canada, p. 249-81, Kluwer Academic Publishers.
- (3) J. R. Rostrup-Nielsen, Stud. Surf. Sci. Catal., 81, 25 (1994).
- (4) T. S. Christensen and I. I. Primdahl, Hydrocarbon Process., 73(3), 39 (1994).
- (5) T. S. Christensen, Appl. Catal. A: General, 138, 285 (1996).
- (6) M. A. Pena, J. P. Gómez and J. L. G. Fierro, Appl. Catal. A: General, 144, 7 (1996).
- (7) J. M. Fox III, Catal. Rev.-Sci. Engng., 35(2), 169 (1993).

CHAPTER 5.3

Epoxy Resin Production

GORO SOMA
Asahi Denka Kogyo K.K., Japan
YASUO HOSONO
Chiyoda Corporation, Japan

The batch stirred tank is usd as a general purpose industrial reactor to manufacture many kinds of products on a relatively small scale. In a batch reactor, the time of operation is mainly considered to manipulate the production of respective products according to the required specifications.

A ready-made type reactor available for multi-kind production is often selected in a process, even if there may be some inconvenience in individual productions. The design of such a reactor is of less particular interest in terms of hardware. The important factors are how to determine the reaction time and the operational schedule, and how to allocate the cooling or heating duty in each operation. In the design of such a reaction system, a dynamic model of reactions is utilized to constantly monitor the transient state of the reaction in the batch reactor. Production of epoxy resins is a typical example, since the resins are manufactured in a variety of products with wide usage.

5.3.1. **EPOXY RESIN**^(5,6)

Epoxy resin, which includes two or more epoxy groups in one molecule, is used in combination with a curing agent or hardener. In the 1940s, it was developed in Switzerland and the United States. With subsequent mass production, epoxy resin is widely used in many applications such as paints, adhesives, electrical insulation, and construction materials. BPA-type epoxy resin (diglycidyl ether type) is a most typical one produced by reacting bisphenol A (BPA) with epichlorohydrine (ECH). It accounts for about 70% of all epoxy resins. For reference, BPA⁽⁷⁾ is produced from acetone and phenol, and ECH is from propylene and chlorine.

There are a number of grades of BPA-type epoxy resins depending on the degree of polymerization. These grades range from low-viscosity liquid epoxy

resins with an average molecular weight of about 350 to solid resins with about 20 000. This section describes the most popular liquid epoxy resins.

Typical structure of BPA-type epoxy resins is shown as below:

Epoxy resin, either in a liquid or thermoplastic state at room temperature, turns into a sticky and thermosetting solid, since its structure is changed into a high molecule polymer by reacting epoxy groups on both sides with the hydroxyl group in the resin structure, through curing agents such as amine compounds.

5.3.2 OUALITY PARAMETERS OF EPOXY RESIN(1,5)

The main parameters relevant to the quality of epoxy resin are described as below:

- (1) Average Molecular Weight (AMW)
 Weight-average moelcular weight of an epoxy resin having a molecular weight distribution.
- (2) Degree of polymerization (n) Corresponds to n in Eq (5.22). About 1-5 for the low molecular weight liquid epoxy resins.
- (3) Epoxide Equivalent (WPE)

A key index of additional amounts of curing agent. It corresponds to a value obtained by dividing the average molecular weight by the number of epoxy groups per molecule. In the case of a perfect diepoxide shown in Eq (5.22), the epoxide equivalent is half of the average molecular weight, but is in fact slightly larger than half.

In some cases, the epoxy value (EC) representing the equivalent of epoxy groups existing in a 100 g sample may be used instead of an epoxide equivalent. The relation between them is:

$$EC = 100/WPE \tag{5.23}$$

The higher the epoxy value or the lower the epoxide equivalent, the lower the degree of polymerization.

(4) Viscosity (μ)

In general, the higher the epoxide equivalent, the higher the degree of polymerization, subsequently increasing viscosity.

(5) Colour

In general, much transparency (less hue) is preferable.

(6) Chlorine Content

Hydrolysable chlorine (PCL) as an organic chloride may be contained in the resin. It exists as an intermediate of an epoxidation and disappears with the progress of the reaction. However, a small amount of PCL remains even after the reaction is completed. Too much content of PCL deteriorates the characteristics of cured resins, particularly the electrical characteristics.

Hydrolysable chlorine:
$$\sim$$
O-CH₂-C-CH₂

HO Cl

or \sim O-CH₂-CH-CH₂
 \downarrow
 \downarrow

O- Cl

(5.23)

Unhydrolysable chlorine (NCL) has less effect on the characteristics of cured resins compared with hydrolysable chlorine.

(7) Others

Melting point, density, refractive index, hydroxyl equivalent, volatile matter, etc.

5.3.3 ELEMENTARY REACTIONS FOR EPOXY RESIN PRODUCTION^(1,2,4)

The BPA-type epoxy resins are produced by the condensation reaction of polyhydroxy phenols such as BPA with ECH at 60 °C-120 °C in the presence of an alkaline catalyst (normally NaOH).

(BPA) (ECH)

$$(n+1) HO - CH_{3} - CH_{4} - CH_{4} - CH_{5} - CH_{$$

Q: Heat of reaction + heat of neutralization (about 200 kJ/mol BPA) $n = 0, 1, 2, \ldots$

Main elementary reactions are the oxide ring-opening of ECH and coupling reaction with phenolic anions, expressed in Eq (5.25), and the subsequent epoxidization reaction in Eq (5.26).

In the reaction (5.25), the phenolic anion ($\sim 0^-$) from BPA or intermediate phenolic products react with ECH and chlorohydrin ether is formed. In the reaction (5.26), the epoxide is produced by dehydrochlorination.

Since BPA has two phenol groups, both of the side phenolic anions react with ECH, similar to Eqs. (5.25) and (5.26). Epoxide formed by Eq (5.26) reacts with BPA to produce high molecular compounds. Chlorohydrin formed by Eq (5.25) also reacts with ECH to produce 'epo-hydrin' (cross-linking polymers) by side reactions.

Therefore, these main reactions and their side reactions form a complex reaction network, forming epoxy resins and gel compounds (high polymerized by-products) having a molecular distribution. Other reactions as shown below occur in addition to Eqs (5.25) and (5.26).

$$\begin{array}{cccc}
CH_2-CH^{\sim} + H_2O & \xrightarrow{k_3} & CH_2-CH^{\sim} \\
O & OH & OH
\end{array} (5.27)$$

Oxide ring-opening reaction by water

$$\sim OH + OH^{-} \stackrel{K}{\rightleftharpoons} \sim O^{-} + H_{2}O$$
 (5.28)

Weak acid dissociation equilibrium

This epoxy resin production model is described later in Section 5.3.6.

5.3.4 EPOXY RESIN PRODUCTION PROCESSES

The industrial processes for epoxy resin production are classified as follows:

(1) The One-step Process

This is the most simple process to produce the final product by using a single batch reactor. During reaction, water co-produced with epoxy resin is boiled for removal from the system. However, only ECH, which forms an azeotropic mixture with water, is returned to the reactor after condensation and separation from the condensed two-liquid phase. As the viscosity is increased by the progress of polymerization, the dissociation of weak acids (related to hydrolysable chlorines) is uneven entirely in the reactor. Therefore, the reduction of hydrolysable chlorines is limited and its chlorines remain in the product resin.

(2) The Two-step Process

In the first stage azeotropic reactor, an epoxide reaction proceeds to an extent that does not cause over-polymerization. After discharging the water from azeotropic mixture, excessive ECH and by-produced alkali salt and gel compounds are then removed. In the second stage reactor, a solvent is added to lower the viscosity, and the required amount of alkali is supplied, the reaction then proceeds at a low temperature to reduce the hydrolysable chlorine. In this process, the second stage reactor is ordinarily selected as a continuous type.

(3) The Two-stage Reaction Process

In the first stage reactor, only the oxide-opening and coupling reactions are made to take place with a catalyst and without alkali injection, and in the second stage reactor, the epoxidation is completed by adding alkali and a solvent.

In the past, the one-step process was used, but it has been replaced by the two-step or two-stage reaction process because of the increasing demand of low chlorine epoxy resin for electrical insulation.

This section describes a two-step process consisting of an azeotropic reaction and solvent dissolution units developed and industrialized by Asahi Denka Kogyo K. K. in 1985.

Figure 5.31 shows the block flow diagram of the Asahi Denka process. For typical low-viscosity BPA-type epoxy resins, powdery BPA is dissolved with ECH of 6–12 times of the stoichiometric volume in a dissolver. The dissolved solution is fed to the first stage reactor (batch type) for epoxidation with continuous injection of NaOH. Since the co-produced water prevents the extent of reaction, it is discharged from the reactor through heating and evaporating by a reboiler. ECH is accompanied by the vaporized water as an azeotropy, but is then returned to the reactor by the phase separation after the condensation.

The reaction is completed after an ageing period following the end of NaOH injection. During the ageing, the residual NaOH is consumed and the epoxidation in Eq (5.26) proceeds. After that, the excessive ECH is evaporated and then recovered. The crude epoxy resin, ECH, and NaCl and by-produced

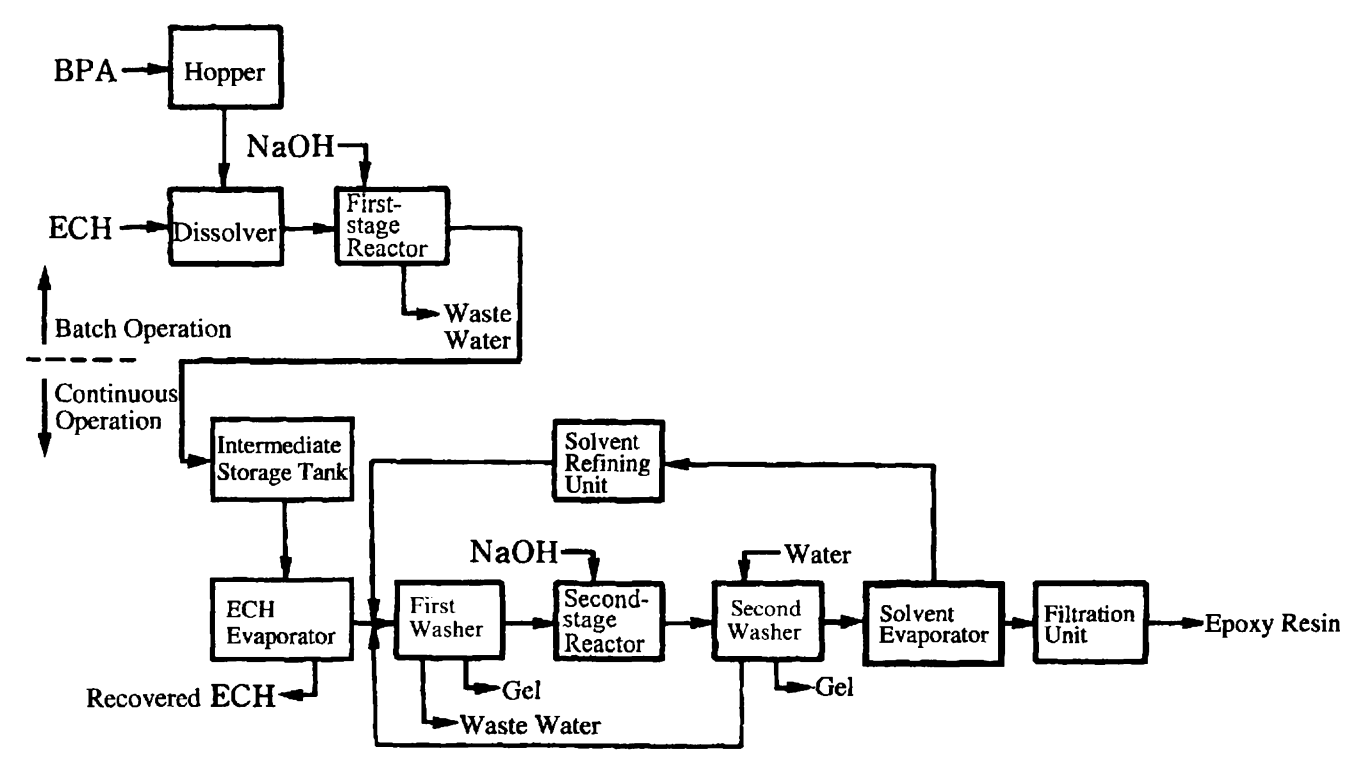


Figure 5.31 Simplified block flow diagram of ADK two-step epoxy resin process.

gel compounds in the reactor are sent to an intermediate storage tank. The gel compounds are a generic name for undissolved polymer produced by overpolymerization. In the first stage process, a sequence-control system is applied to perform the scheduled operation.

The solution from the storage tank is continuously fed to the wiped thin film evaporator which is operated in a vacuum, and ECH is then removed completely. NaCl and gel compounds contained in the crude epoxy resin are removed by washing after a decrease in their viscosities is produced by adding a solvent. The epoxy solution after the washing is fed to the second stage reactor operated as a continuous stirred tank with NaOH injection, where hydrolysable chlorine is reduced and the epoxide reaction is completed. The liquid product is finally obtained from the solution through rewashing, solvent removal and filtration. The recovered ECH and solvent are refined and recycled to the process.

5.3.5 PROCESS OPERATING FACTORS

The main operating factors in the two-step process with the azeotropic reaction and solvent dissociation units are as follows:

For the first stage reaction,

(1) Ratio of ECH/BPA

The degree of polymerization decreases as this value increases, and a low-viscosity epoxy resin is obtained with a smaller epoxide equivalent or a larger epoxy value. Figure 5.32 shows an example of this relation.

(2) Ratio of NaOH/BPA

An increase in this value increases the degree of polymerization and accelerates gelification. If the value is over the allowable range, runaway of polymerization may occur, and the reacting liquid may be solidified. Thus, the injection of NaOH needs to be carefully controlled. On the other hand, if this value is too small, the epoxide reaction is incomplete and a large amount of residual hydrolysable chlorines remains in the product.

(3) Reaction time

If the reaction time is not suitable, undesired side reactions occur and the quality of products deteriorates. The optimal reaction time can be determined by the simulation described later in detail. After the end of NaOH injection, a certain ageing period is necessary to complete the reaction.

(4) Reaction temperature

As shown in Figure 5.32⁽³⁾, the ratio of ECH/BPA varies the epoxy value (EC), according to the reaction temperature. To obtain the product with a

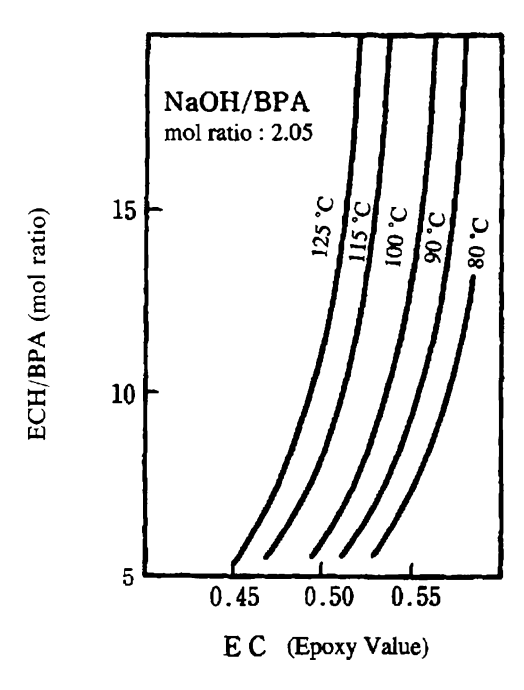


Figure 5.32 Effect of temperature and ECH/BPA mol ratio on epoxy value⁽³⁾.

specified EC, lower ratio of ECH/BPA can be set at a lower temperature, since the lower temperature decreases the side-reactions and over-polymerization, and increases the selectivity of epoxidation. An excessively high reaction temperature, causes less yields of products and plugging trouble from gel compounds. In general, the reaction temperature is set to 100–105 °C.

(5) Reaction pressure

The reaction is normally made to take place at atmospheric pressure or vacuum under boiling conditions.

(6) Water concentration in reacting liquid

The water concentration in the reacting liquid varies according to the following; reaction temperature, water fed from the injected NaOH solution, water co-produced by reaction, water removed through azeotropic evaporation, boiling point raised due to production of epoxy resin, and other factors. The higher water concentration leads to a longer reaction time. With lowered water concentration, the rate of the main reactions increases compared with that of the side-reactions, and the degree of polymerization is low, resulting in less loss of ECH by side-reactions.

(7) Agitation

Appropriate agitation is required to minimize the unevenness of NaOH concentration in the reactor and the non-uniform polymerization in order to obtain a product with a low degree of polymerization and low hydrolysable chlorine, and to prevent precipitation of NaCl particles and gel compounds.

(8) NaOH injection

It is recommended that an adequate injection method is to keep the initial rate at a minimum, to increase the rate in the middle of a reaction, and to reduce it again at the end of a reaction.

In the second stage reaction, solvent such as toluene is used. If ECH is contained in the recycled solvent, hydrolysable chlorine will not be reduced. Methanol is also added to increase the selectivity of reaction, reducing hydrolysable chlorine.

(1) NaOH injection in the second stage reaction

The amount of NaOH injection in the second stage affects the reaction the same as in the first stage. The amount of NaOH injection in the second stage must be determined by subtracting the amount consumed in the first stage reaction from the theoretical chemical equivalent. However, in fact, an amount slightly higher than the theoretical equivalent is injected, since some NaOH is consumed in side reactions.

(2) Temperature in the second stage reaction

The temperature in the second stage may be about 80 °C by the solvent effect, slightly lower than that of the first stage reaction. This reduces the formation of gel compounds.

5.3.6 THE REACTION MODEL

Based on Eqs (5.25)–(5.28) in Section 5.3.3, a reaction model for epoxy resin production is depicted in Figure 5.33 on only one side phenolic group of BPA. In this model, k_1 , k_2 and k_3 are the rate constants of main reactions, and α , β , γ , δ and ε are the correction factors by the respective structures other than the end-groups. K_1 , K_2 , K_3 , K_4 and K_5 are the dissociation equilibrium constants of weak acids. Additional data are required on ion balance and the diffusion equation for injected NaOH, the vapour-liquid equilibrium of the ECH-water system considering the boiling point raised by salt, and so on. The results of simulation using the reaction model are in good agreement with experimental data.

If the concentration of each end-group is known, the quality parameters of epoxy resin (average molecular weight, epoxy value and hydrolysable chlorine content) can be calculated.

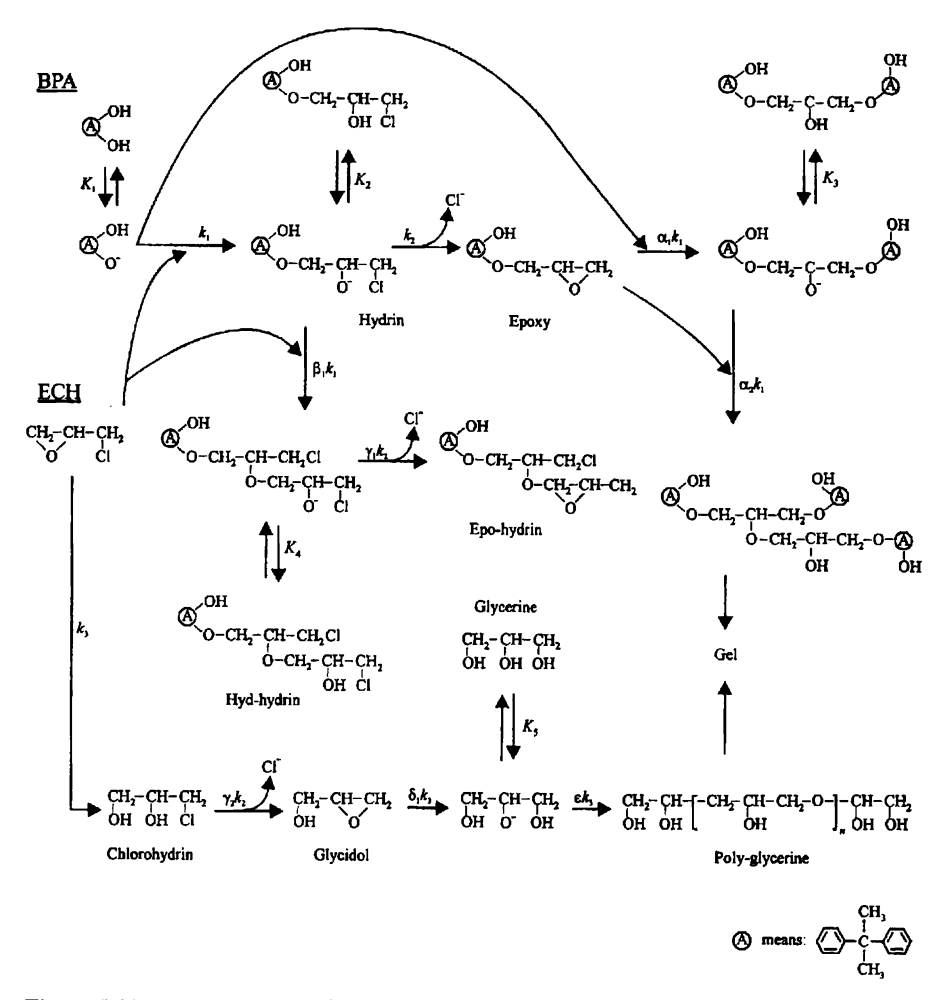


Figure 5.33 Reaction model for epoxy resin production. This figure shows the reaction model only on one side of phenolic group. The other side also reacts following the same reaction routes.

5.3.7 BATCH OPERATION

In the first stage reaction, the following batch operations are performed according to the production schedule:

- (1) Charge of BPA and ECH, and preparation of mixed solution.
- (2) As soon as the reaction starts with injection of an NaOH solution, an increase in water content and a temperature rise are observed. When the

reacting liquid reaches boiling point, evaporation and condensation of ECH and water are carried out.

- (3) Starting the reflux of ECH. Formation of high molecular compounds and salt causes a rise in the boiling point of the reacting liquid, gradually reducing the amount of evaporation. The temperature is decreased as the heat of reaction and neutralization are reduced.
- (4) Heating by supply of steam is started automatically to keep the temperature constant.
- (5) Injection of the NaOH is stopped. At this point, the reaction appears to terminate, whereas, in fact, the reaction has not been completed.
- (6) Ageing is maintained for a short period.
- (7) Unreacted ECH is recovered by increasing the temperature of the reactor.
- (8) Product is discharged from the first stage reaction process.

The state in the reactor is changed with time according to the above operations.

5.3.8 SIMULATION USING THE REACTION MODEL

The logic flow diagram of the simulation for epoxy resin production is shown in Figure 5.34.

Considering the process operating factors in Section 5.3.5 and the batch operations in Section 5.3.7, let us perform a simulation based on the reaction model in Section 5.3.6 to predict the change of state in the reactor with time. Then we can determine the operating schedule and operating factors to meet the required specifications.

For an example, the typical simulation results of the epoxy resin production is presented under the following conditions:

. 10

: 1 hour

Conditions

ECH/RDA male ratio

Second stage reaction time

•	LCH/BI A mole lado	. 10
•	NaOH/BPA mole ratio in the first stage reaction	: 1.95
•	NaOH/BPA mole ratio in the second stage reaction	: 0.065
•	Reaction temperature in the first stage reactor	: 103 °C
•	Reaction temperature in the second stage reactor	: 80 °C
•	Concentration of NaOH solution	: 48%
•	First stage reaction time	: 3 hours
•	Ageing period	: 1 hour 20 minutes

Results

•	Epoxide equivalent	: 185
•	Average molecular weight	: 368

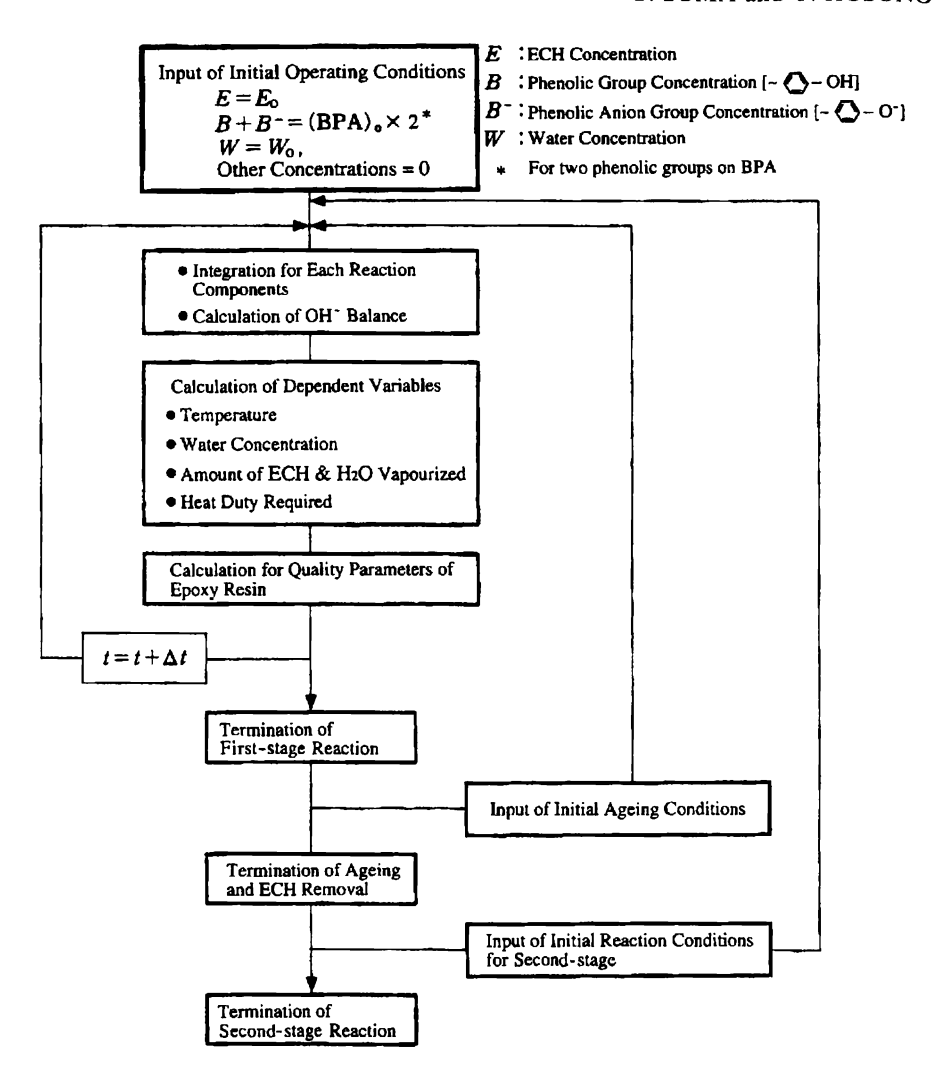


Figure 5.34 Logic flow diagram of the simulation for epoxy resin production.

• Hydrolysable chlorine : 420 wt ppm • Viscosity : 110 cP ECH loss : 1.07% Residual BPA : NIL • Changes in temperature and heat duty around the : Figure 5.35

reactor with time

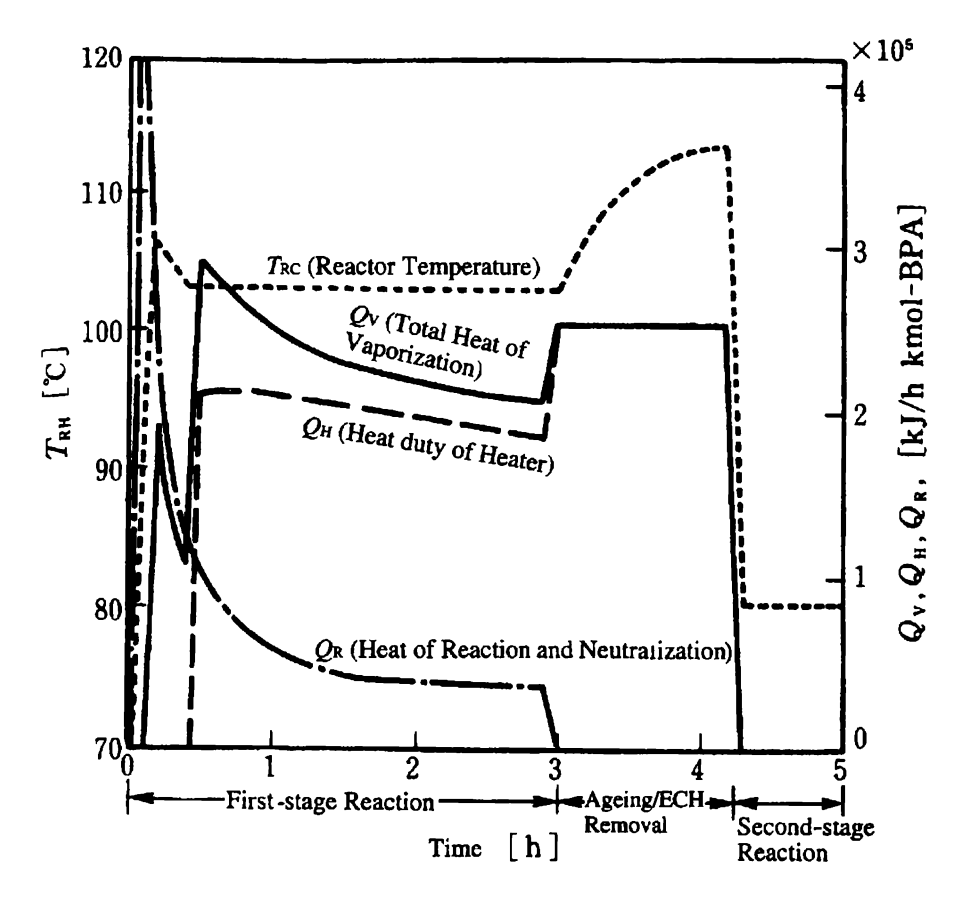


Figure 5.35 Changes in temperature and heat duty around the reactor with time.

- Changes in quality parameters of epoxy resin in the : Figure 5.36 reactor with time
- Changes in component concentrations in the reactor : Figure 5.37 with time

5.3.9 DESIGN OF THE FIRST-STAGE REACTOR

An example of the simulation result for a single product is presented in above section. In this section, a process of multi-kind production is discussed on the following four types of the low-viscosity epoxy resins A, B, C, and D by a single train plant (with a total production capacity of 10 000 tons per year and annual operating time of 7800 hours).

Туре		A	В	С	D
Production	t/y	5000	3500	1400	1000
Epoxide equivalent		185	190	200	240
Average molecular weight		368	375	400	375
Hydrolysable chlorine in product	ppm	300	300	300	2%
Hydrolysable chlorine in product at the first-stage	ppm	4000	3500	3000	2%
Viscosity of product	P(25 °C)	110	140	270	90

The following operating conditions can be obtained from the simulation for the four types of products:

Туре		Α	В	С	D
ECH/BPA	mole ratio	10	8.5	6.1	12.7
NaOH/BPA	mole ratio	1.925	1.95	1.95	1.6
First stage-reaction time	hours	3	2.7	2.5	2
Ageing period	hours	1.2	1.0	0.5	1.0

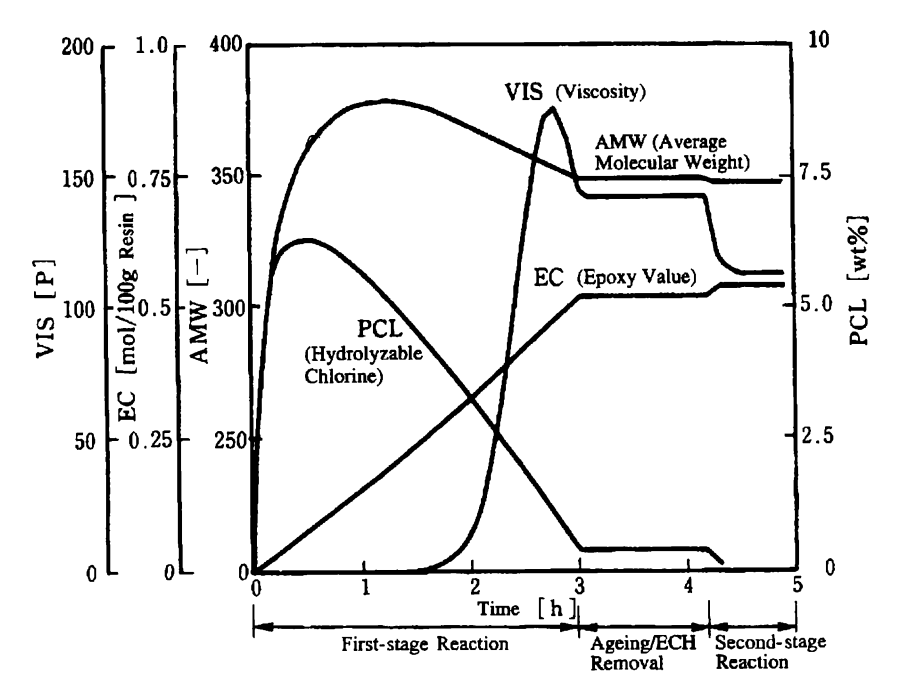


Figure 5.36 Changes in quality parameters of epoxy resin in the reactor with time.

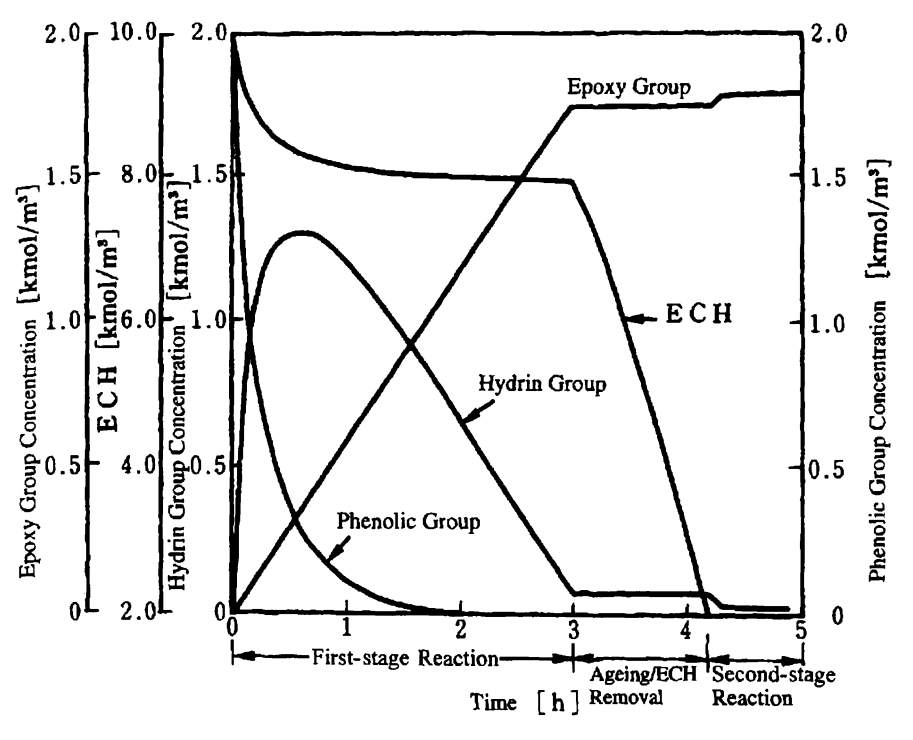


Figure 5.37 Changes in component concentrations in the reactor with time.

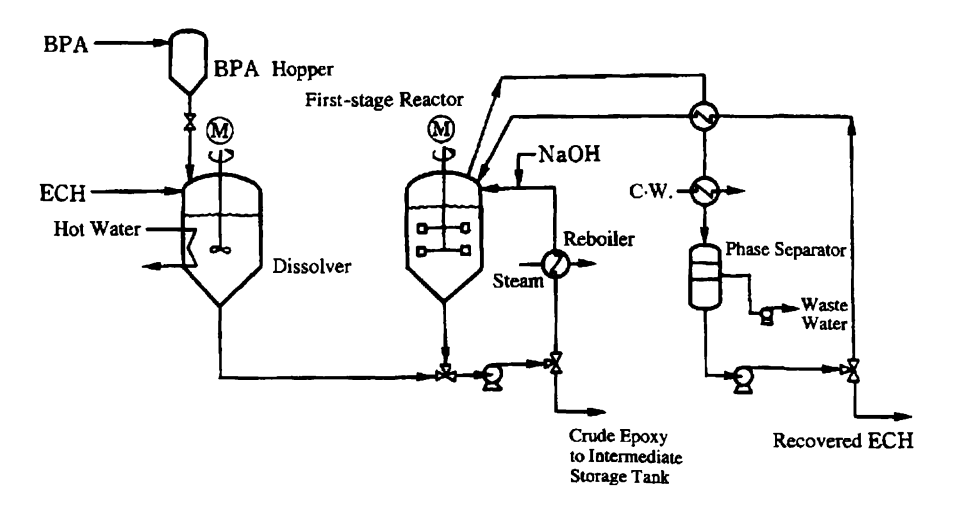


Figure 5.38 Simplified flow diagram of first-stage unit.

Following is the discussion on how to determine the schedule for the batch operations described in Section 5.3.7. The above results indicate that the first stage reaction time is up to three hours for all types. Since the removal time of ECH can be adjusted by the reboiler capacity, the production schedule of the operation may be determined on the basis of Type A with the longest reaction time. A single reactor or multiple reactors in parallel may be used in the first stage process. In this case, as shown in Figure 5.38, the first stage reaction unit consists of a dissolver (feed preparation), a reactor and a separator. Although the treating time requires 12 hours in the dissolver and the reactor for one-batch operation, these operations can be performed by switching each one with batch processing of six hours as shown in Figure 5.39.

The material balance per single batch operation for each type of product is shown below. If the total amount of feed per batch is almost the same for each product, the yearly production rate can be adjusted by the number of batches. The time required for ECH recovery varies for each product, but this variation of time can be dealt with in each bath operation.

Type		A	В	<u>C</u>	D
Production rate	t/y	5000	3500	1400	100
Feed/product weight ratio*		3.908	3.546	2.926	4.380
Production ratio per batch	_	1	1.102	1.320	0.8923
Number of batches	batch/y	694	442	148	16
Production rate per batch	kg	7205	7919	9459	6250
Total amount of feed per batch	kg	28 160	28 083	27 677	27 375
Amount of ECH per batch	kg	19874	18 807	16424	20 965
Amount of BPA per batch	kg	4863	5421	6582	4045
Amount of NaOH (48%) per batch	kg	3423	3855	4671	2365
Amount of ECH recovered per batch	kg	11 482	9347	5084	13 989
ECH recovery time	(min)	80	65	36	98

^{*}The feed/product weight ratio can be obtained as an approximate value by the following equation. The exact value is determined by the simulation. Approximate value of feed/product weight ratio = $\{(ECH/BPA)_{mole\ ratio} \times 92.5 + 226.3 + (NaOH/BPA)_{mole\ ratio} \times 83.3\}/(Average\ molecular\ weight \times 0.90)$

Example 5.9Determine the specifications of the reactor (a stirred tank reactor) used in the first stage reaction unit shown in Figure 5.38.

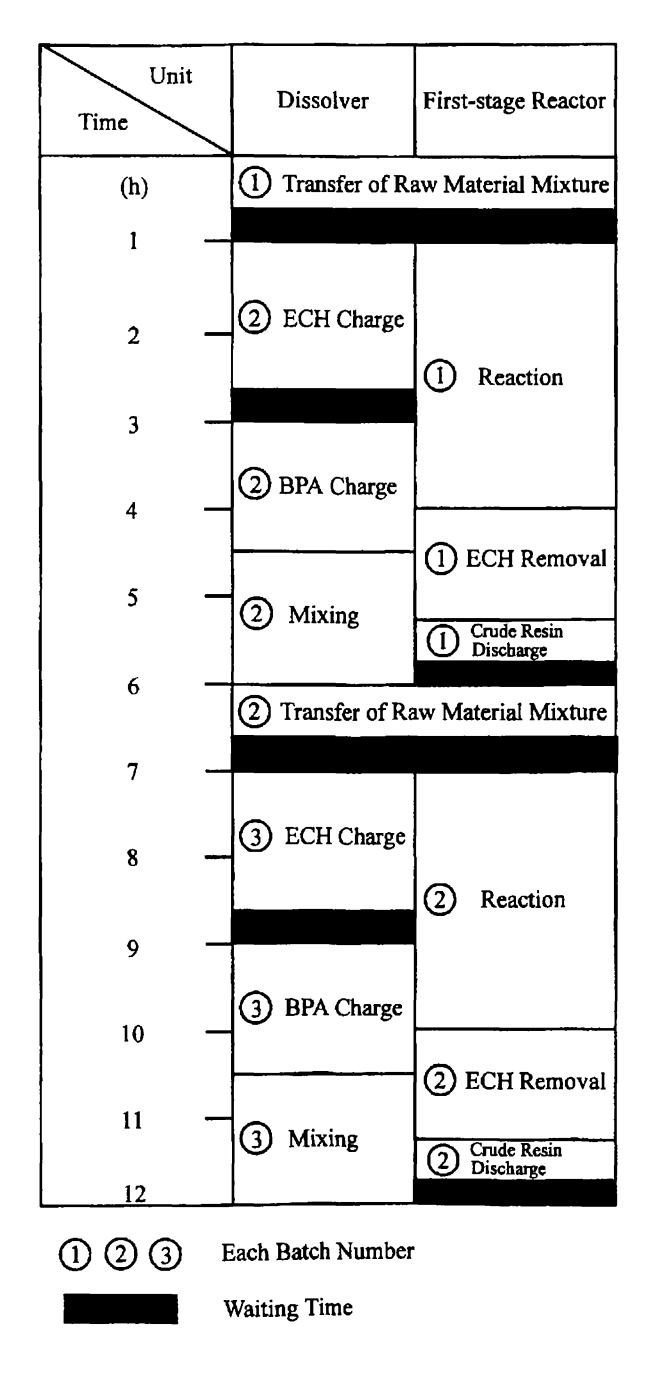


Figure 5.39 Production schedule for first-stage reaction unit.

Solution

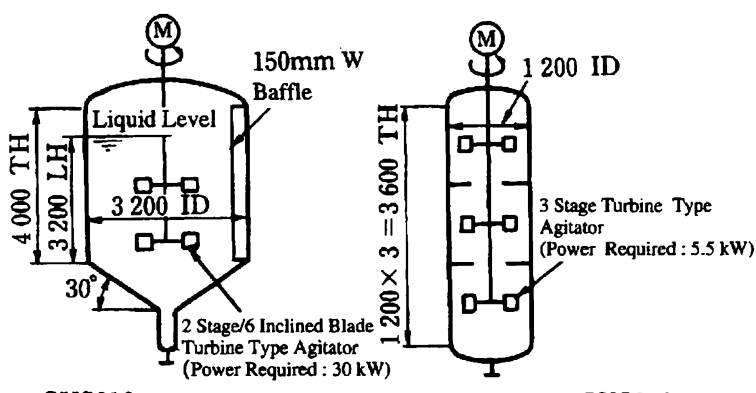
The volume of the liquid phase in the reactor may be the maximum volume (V_L) per batch required for each type of product. V₁ can be obtained as dividing the maximum value of the total amount of feed per batch (W_T) by the minimum density under the reacting conditions (ρ_T).

$$V_L = W_T/\rho_L$$

In this example, W_T is 28 160 kg of the product A and ρ_L is taken as 1090 kg/m³.

$$V_L = (28\ 160)/(1090) = 25.9\ m^3$$

To secure appropriate shear strength and discharging performance in agitation. the ratio of liquid level height to tank diameter (H_1/D) must be appropriately taken and a baffle plate must be installed. For the solid-liquid system with wide ranges of viscosity, the H₁/D ratio may be taken as 0.8-1.2. Assuming $H_I/D = 1.0$, D and H_I are 3200 mm respectively. The baffle plate functions effectively at the ratio of the baffle width B to tank diameter D which is 0.015-0.05. In this case, choosing B/D = 0.05, $B = 150 \, mm$. The height of the vapour phase in the reactor is determined to be 800 mm, which is the height of $0.25 \times D$ in consideration of clearance for entrainment and a fluctuation in the liquid level due to the centrifugal effect caused by agitation. The bottom structure of the tank is the cone type inclined by 30 degrees to prevent solids from settling (Figure 5.40).



Design Press.: 0.7MPa G

Second-stage Reactor

Material : SUS316 : SUS316 Material Design Temp.: 160℃ Design Temp.: 100℃ Design Press.: 0.3MPa G

& Full Vacuum Insulation : 125mm (Hot) : 75mm Insulation

Figure 5.40 Example of reactor design.

First-stage Reactor

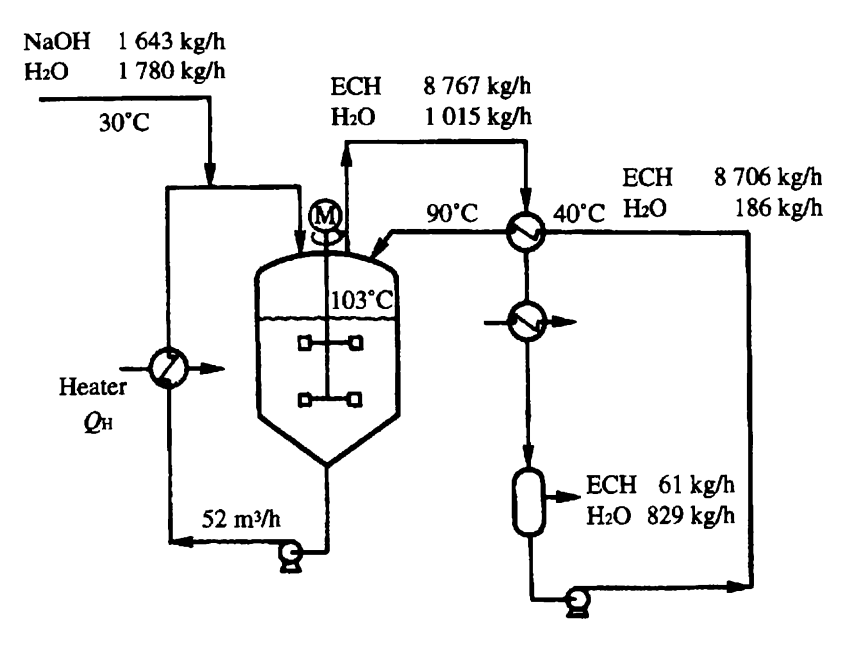


Figure 5.41 Process conditions around a first-stage reactor.

Stainless steel is generally used as a material for the polymerization reactor. In the case of epoxy production, austenitic stainless steel containing Mo is used to prevent pitting corrosion caused by NaCl.

For the type of agitator, multi-stage turbine blades with high shear strength or inclined paddle with excellent discharging performance will usually be selected. In this case, a two-stage, six-inclined turbine blades agitator is adopted with high shear strength and appropriate discharging performance. The power required per unit volume (P_V) is normally about $0.5-2.0\,kW/m^3$ for solid-liquid agitation with medium viscosity. Scale-up of agitators can be done using the P_V value. Since the value of P_V verified in the test for this system was about $1.0\,kW/m^3$, the total required power is $(1.0\,kW/m^3)\,(26\,m^3)=26\,kW$. Thus, the rated power of agitator is determined as $30\,kW$.

Example 5.10

Determine the specifications of the heater equipped with the reactor on the basis of the process conditions as shown in Figure 5.41. As shown in Figure 5.35, the heat duty of the heater reaches a maximum at 30–40 minutes after the start of the reaction. The heater should be designed to meet this condition.

Solution

Heating is required for the purpose of (1): removing water contained in the NaOH solution and formed by reaction step, and (2): evaporating and recovering ECH in the ECH removal step.

In the case of (1) for the reaction step,

$$Q_H = Q_V + Q_X + Q_N - (Q_R + Q_P)$$

when Q_H : heat duty of heater

Q_V: latent heat of ECH and water Q_X: sensible heat of refluxed ECH Q_N: sensible heat of an NaOH solution

 Q_R : heat of reaction + heat of neutralization

 Q_P : heat input from the pump and agitator.

The calculated results are as follows:

 $Q_V = (420.7)(8767) + (2247.9)(1015) = 5970000 kJ/h$

 $Q_X = (1.67 \times 8706 + 4.19 \times 186) (103 - 90) = 199000 \, kJ/h$

 $Q_N = (3.31)(3423)(103 - 30)/(3) = 276000 kJ/h$

 $Q_R = 992\,000\,kJ/h$

 $Q_P = (3.5 + 30)(3600) = 121000 \, kJ/h$

Thus, $Q_H = 5332000 \, kJ/h$ is obtained.

If the heat loss is assumed to be 5%, the heat duty of the heater is permitted to be 5599 000 kJ/h. The heat is selected for a tubular heat exchanger with a forced circulation, controlling the tube-size vaporization below 15%, in consideration of the formation of salt and gel compounds. Using saturated steam at the condition of 0.6 MPaG (165 °C) as a heating medium, the overall coefficient of heat transfer is $2930 \, \text{kJ/(m^2 °Ch)}$, and the heat transfer area of the exchanger is calculated as $35 \, \text{m^2}$. In the case of (2) for the ECH removal step, the required operation time to evaporate the remains of ECH in the reactor is about 60 minutes in the case of using the above $35 \, \text{m^2}$ exchanger. This time is confirmed to be less than 80 minutes which is required for the ECH recovery time for the production of A.

5.3.10 DESIGN OF THE SECOND-STAGE REACTOR

Example 5.11

Determine the specifications of the reactor in the second stage reaction unit for continuous operation as shown in Figure 5.32. The following conditions are premised:

(1) The amount of hydrolysable chlorine in the product resin should be below 200 ppm with a theoretical amount of NaOH injection.

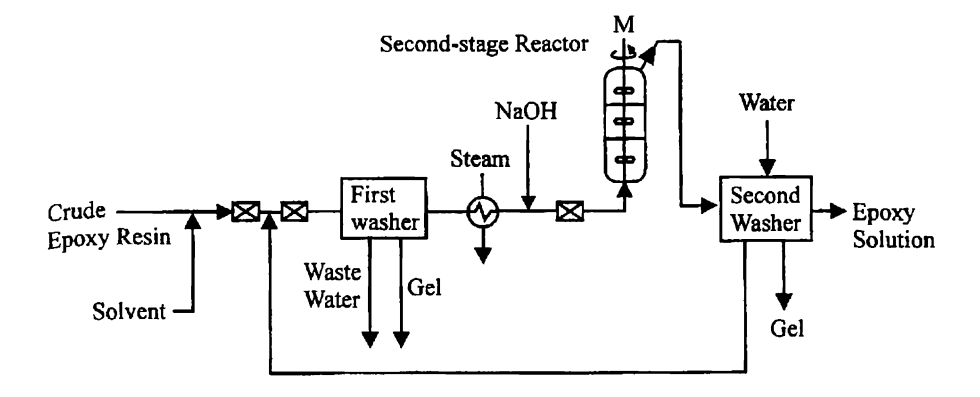


Figure 5.42 Simplified flow diagram of a second-stage reactor unit.

- (2) The feed to the reactor should contain 60% of toluene as a solvent at 80°C and the density of the feed should be 940 kg/m³.
- (3) The feed rate should be 3080 kg/h, and the amount of hydrolysable chlorine in the crude epoxy resins should be 3750 ppm.
- (4) The reduction rate of hydrolysable chlorine -r[wt%/min] may be represented by $-r = 3.17C^2/(1+7.25C)$ with the concentration of hydrolysable chlorine C[wt%]. This equation is derived from the change in the amount of hydrolysable chlorine in batch operation as shown in Figure 5.43 obtained by the simulation.

Solution

In a continuous flow reactor, the residence time of an ideal plug flow reactor is equal to the reaction time of a batch reactor. In this case, however, a single reactor with multi-stage stirred rooms is adopted. The mixing model in this reactor is similar to that in multi-stage continuous stirred tank reactors (CSTRs) in series. Assuming that the reactor corresponds to three-stage CSTRs, obtain the residence time to reach 200 ppm of hydrolysable chlorine by graphic solution.

Figure 5.44 shows the relationship of $-\tau$ against C. The operating line for one CSTR is derived by the material balance from input and output of hydrolysable chlorine, where θ_r is the residence time.

$$-\mathbf{r} = (1/\theta_r)(\mathbf{C}_0 - \mathbf{C})$$

In Figure 5.43, it is expected that the amount of hydrolysable chlorine is reduced under 200 ppm in about 20 minutes in the batch operation. θ_r is assumed to be 20 minutes for each stage of the continuous reactor.

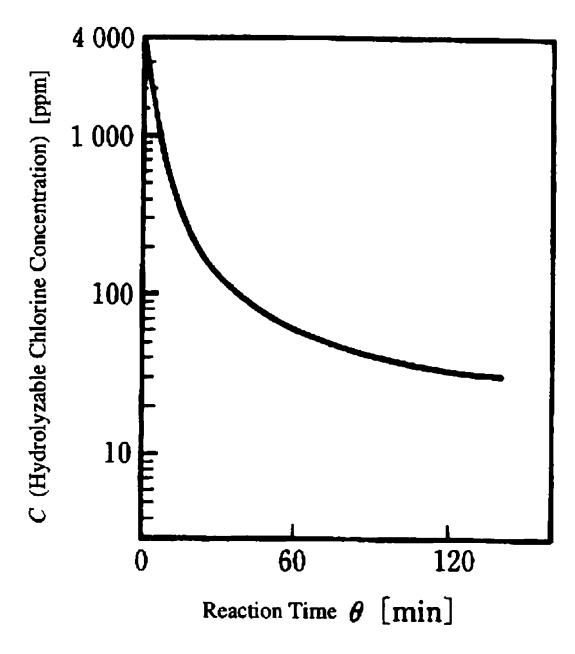


Figure 5.43 Example of change of hydrolysable chlorine concentration in a second-stage batch reaction.

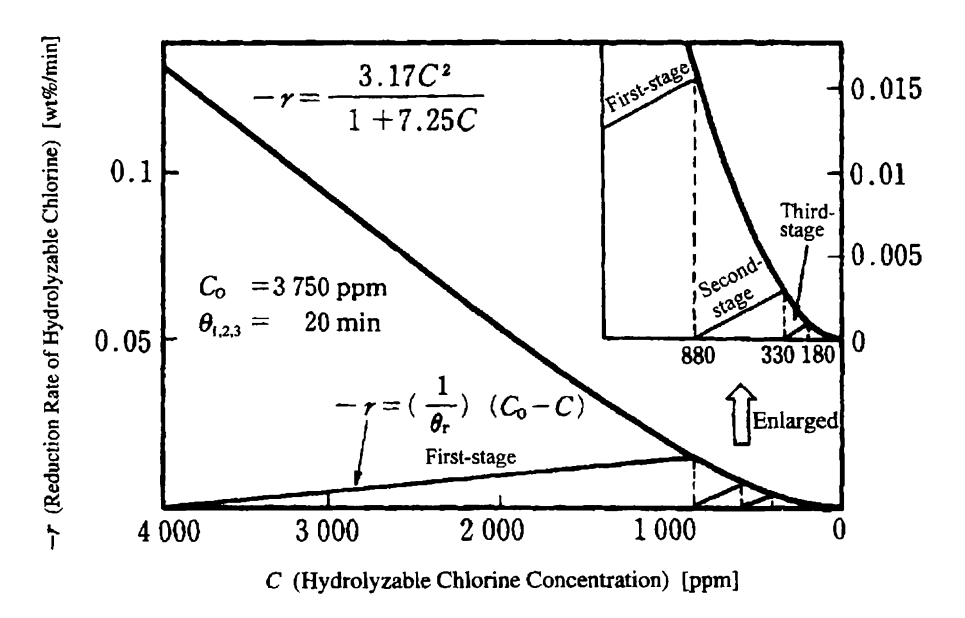


Figure 5.44 Hydrolysable chlorine concentration in a three-stage continuous stirred tank reactor.

In Figure 5.44, the amount of hydrolysable chlorine in the first stage outlet can be determined from the point of intersection with the operating line and the reduction rate curve. Similarly, the amount of hydrolysable chlorine up to the third stage can be obtained by graphic solution. In general, θ_r is found by a trial and error approach. As the result, at $\theta_r = 20$ minutes, the amount of hydrolysable chlorine at the outlet of a three-stage CSTRs is reduced to 180 ppm, which meets the required specification of 200 ppm. Thus, the required volume per one stage (V_I) is:

$$V_I = (3080/940)(20/60) = 1.1 \, m^3$$

Taking L/D=1 for each stage of the reactor, the reactor of 1.2m in inner diameter and 3.6m in tangential height is obtained as shown in Figure 5.40. A three-stage turbine agitator with P_V of $1\,kW/m^3$ for each stage and the rated power of 5.5 kW is adopted.

References

- (1) Z. Brojer, Int. Polym. Sci. Technol., 7, 11, t/70 (1980).
- (2) N. S. J., Enikolopyan, Polym. Sci. Polym. Chem. Ed., 20, 5, 1231 (1982).
- (3) I. Wiesner, Int. Polym. Sci. Technol., 9, 7, t/1 (1982).
- (4) H. Batzer and S. A. Zahir, J. Appl. Polm. Sci., 21, 7, 1843 (1977).
- (5) H. Lee and K. Neville, Epoxy Resins, McGraw-Hill (1957).
- (6) S. A. Zahir and H. Batzer, Epoxy Resin Chem., 13, p. 245, Am. Chem. Soc. (1983).
- (7) K. Sakashita, et al., Proceedings of APCChE & CHEMECA 93 Conference 2, p. 543 (1993).

CHAPTER 5.4

Hydrotreating Reactor Design*

A. G. BRIDGE

Chevron Research and Technology Company, Richmond, CA, USA E. MORSE BLUE

Consulting Chemical Engineer, Walnut Creek, CA, USA

Japan's industries rebounded rapidly after World War II, and energy requirements rose accordingly. With it came increasing air pollution such that, in the 1960's, a pall of blue-grey haze constantly hung over the entire area from Tokyo to Osaka. It was sulphur dioxide in the air, the result of burning fuel oil derived from high sulphur Middle East crude oil. Japan realized that only a reduction in sulphur content of fuel oil could solve the problem. Accordingly, a timetable was set in which sulphur content would be reduced gradually over a period of several years. This was done by hydrotreating fuel oil to remove sulphur. Refineries began installing hydrotreaters in the late 1960's and results showed immediately. Gradually, skies become clearer, such that today, one can frequently see Mt. Fujiyama from Tokyo. This was not possible in 1965.

Hydrotreating involves reactions between hydrogen and petroleum hydrocarbons, and there are many applications. As mentioned above, it is used to desulphurize fuel oil. But, it is also used for the following:

- (1) Removing nitrogen, metals and other contaminants
- (2) Saturating olefins and other unstable compounds
- (3) Conversion of aromatics to cycloparaffins, e.g., producing cyclohexane from benzene, or producing high-quality diesel fuel from lower grades
- (4) Conversion of low-grade lubricating oils to premium quality products.

Another widely used process similar to hydrotreating is called 'hydrocracking' in which large molecules in heavy fractions of crude oil are cracked to

^{*}A typical example for the Chevron OCR (Onstream Catalyst Replacement) hydrotreating unit is shown on the frontispiece.

Chemical Reaction and Reactor Design. Edited by H. Tominaga and M. Tamaki © 1998 John Wiley & Sons Ltd.

make gasoline and other light distillates. Hydrogen is added to the products in this and the above hydrotreating processes. In another, and yet related process, called 'catalytic reforming' hydrogen is removed in converting naphthenes to aromatics. This latter process provides large quantities of hydrogen for hydrotreaters.

5.4.1 HYDROTREATING OBJECTIVES

Hydroprocessing is the general term used to describe all the different processes in which hydrocarbons react with hydrogen. Hydrotreating deals primarily with impurity removal from hydrocarbon feedstocks. Feedstocks consist of petroleum stocks of widely different boiling character—naphthas, atmospheric gas oils, vacuum gas oils (VGOS), and residuum. Within each of these different boiling ranges exist a variety of molecular types depending on both the crude oil source and also, whether or not the material was produced in a cracking reaction or as a straight-run[†] component of the original crude oil. The impurity levels in a variety of crude oils and in their vacuum residua are shown in Table 5.7. The products into which the refiner must convert these and the lighter feedstocks are summarized in Table 5.8.

The introduction of residuum hydroprocessing in the late 1960's was due to an increasing demand for low-sulphur fuel oil (LSFO). More recently, residuum conversion has been the popular goal, and often the hydrotreated product is fed to a fluid catalytic cracking (FCC) unit. In this case the removal of nitrogen, Conradson carbon, and metal contaminants in the hydrotreater are just as important as sulphur removal because they cause FCC catalyst deactivation.

Hydrotreating feedstocks which boil in the VGO range can be straight-run stocks or stocks produced in crackers, visbreakers or residuum hydroprocessing units. Again, these are often processed to produce either LSFO or FCC feed. Sometimes they are hydrocracked to produce diesel, kerosene jet fuel, and/or naphtha. The hydrocracked heavy products are also excellent ethylene plant feedstocks or lube oil base stocks since the process removes heavy aromatic compounds.

Straight-run or cracked stocks boiling in the atmospheric gas oil range can be hydrotreated to produce good quality diesel and jet fuel or ethylene plant feedstock. They can be hydrocracked to produce a naphtha which is an excellent feed for a catalytic reformer. Straight-run or cracked naphthas need to be hydrotreated to remove olefins, sulphur, and nitrogen to produce good catalytic reformer feeds. They can also be hydrocracked to give LPG.

[&]quot;Straight-run" is a term which means the component was produced by distillation of crude oil and has had no further treatment.

Table 5.7 Inspections of crude oils and vacuum residua

		Arabian Light	Arabian Heavy	Kuwait	Iranian Heavy	Sumatran Light	Venezuelan	Alaskan North Slope	North Sea Ninian	Californian
Crude oil										
Gravity	[°API]	33.3	28.1	31.3	30.8	35.3	33.3	26.3	35.1	20.9
Sulphur	[wt%]	1.8	2.9	2.5	1.6	0.07	1.2	1.0	0.41	0.94
Nitrogen	[wt%]	0.16	0.19	0.09	0.18	0.08	0.12	0.22	0.07	0.56
Residuum (1000°F+)										
Yield	[LV%]	17.3	28.6	24.8	21.8	24.4	21.2	23.0	17.8	26.1
Gravity	[°API]	8.0	4.6	7.4	6.3	20.1	10.9	7.4	13.0	5.4
Sulphur	[wt%]	3.7	5.6	5.1	3.2	0.18	2.8	2.1	1.3	1.6
Nitrogen	[wt%]	0.49	0.67	0.38	0.83	0.33	0.56	0.64	0.42	1.33
Asphaltenes	[wt%]	11.3	20.6	12.0	14.7	7.9	16.0	8.1	6.9	12.0
Nickel+Vanadium	[ppm]	96	220	116	462	41	666	130	28	294
Iron	[ppm]		10	0.9	9	13	5	15	<1	90

Table 5.8 Hydroprocessing objectives

Feedstocks	Desired products	Process objectives
Naphthas	Cat reformer feed	Removal of S, N, olefins
•	LPG	Hydrocracking
Atmospheric	Diesel	Removal of aromatics and n-paraffins
gas oils	Kerosene or jet fuel	Removal of aromatics
•	Ethylene feedstock	Removal of aromatics
	Naphtha	Hydrocracking
Vacuum	LSFO	Removal of S
gas oils	FCC feed	Removal of S, N, metals
U	Diesel	Removal of S, aromatics
		Hydrocracking
	Kerosene or jet fuel	Removal of S, aromatics
	J	Hydrocracking
	Naphtha	Hydrocracking
	LPĠ	Hydrocracking
	Ethylene feedstock	Removal of aromatics
	•	Hydrocracking
	Lube oil base stock	Removal of aromatics
		Hydrocracking
Residuum	LSFO	Removal of S
	FCC feedstock	Removal of S, N, CCR and metals
	Coker feedstock	Removal of S, CCR and metals
	Diesel	Hydrocracking

The technical challenge associated with producing these products via hydroprocessing can be illustrated with the use of a chart first proposed by Dr. Bruce Stangeland at Chevron Research and has since been used and modified by many of his colleagues^(2-4,14,17,21). This is a chart relating the hydrogen content of a hydrocarbon to its molecular weight. Figure 5.45 is a Stangeland chart showing the regions in which saleable products fall.

Note that the upper boundary represents the hydrogen content of the paraffinic homologous series. No hydrocarbon exists above this line. The lower line represents aromatic compounds starting with benzene and including the condensed ring compounds, naphthalene, phenanthrene, pyrene, and coronene. These are among the most hydrogen deficient compounds found in petroleum. All the distillable hydrocarbons involved in petroleum refining lie between these two extremes. Even the hydrocarbons present in the residuum—the non-distillable fraction—can easily be represented on this chart, since the molecular weight scale goes up to 10 000 close to the maximum found in crude oil. Lines showing approximate boiling points have been drawn. These show the well known fact that aromatic compounds have much lower molecular weights than paraffinic compounds of the same boiling point.

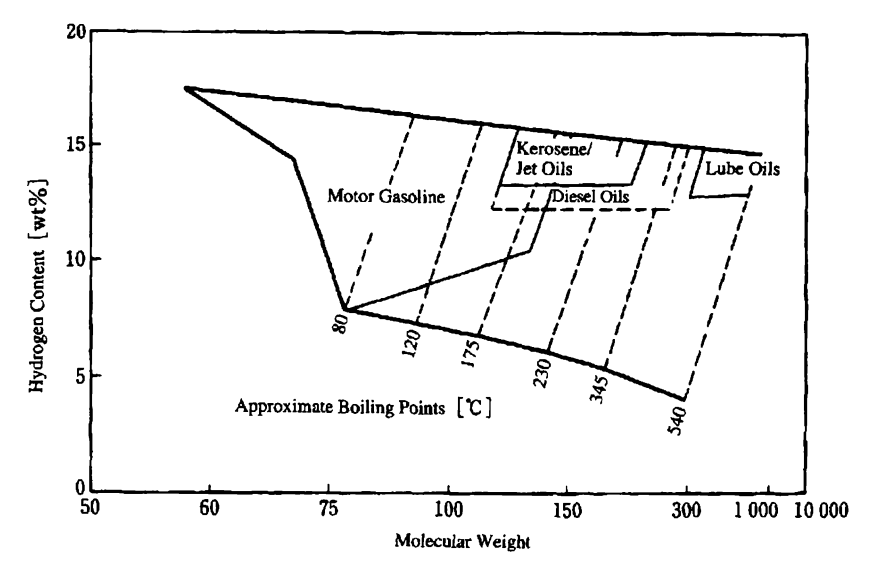


Figure 5.45 Hydrogen contents of refined products.

Specification products are shown as regions. Gary and Handwerk⁽⁷⁾ described all the specifications of the major petroleum products. It is instructive to discuss the important ones with the aid of the Stangeland chart:

5.4.1.1 Motor Gasoline

This region is quite broad since high octane numbers can be achieved with either high aromatic levels or high iso-to-normal paraffin ratios. Catalytic reforming produces aromatics. Isomerization processes convert normal paraffins to isoparaffins. The distillation range of gasoline is set by specifications.

5.4.1.2 Kerosene and Aviation Jet Fuel

Aromatic contents must be low for these products to have clean burning characteristics. The smoke point specification is used to characterize this quality. The front end distillation specification is set by flash point considerations, the back end by freeze point.

5.4.1.3 Diesel Fuels

Similar quality concerns exist for diesel and kerojet products. The cetane number specification limits the aromatic content and the important cold flow property is the pour point, cloud point or cold filter plugging point.

5.4.1.4 Lube Oils

Aromatic compounds have very low viscosity indexes so lube oils must, in general, have limited aromatic levels. Paraffin wax must also be minimized so the more desirable compounds are isoparaffins or molecules containing a combination of naphthenic rings and isoparaffinic side chains. The boiling range of lubricating oils is set by the desired viscosity.

5.4.1.5 Fuel Oils

Hydrogen content is not as important for heating oils or residual fuel oils. Sulphur levels are limited, however, and this often means that hydrotreating is needed for their production. Their boiling range is set by flash point and viscosity considerations.

Having looked at specification products, we now look at feedstock qualities on another Stangeland chart. Figure 5.46 shows regions representing distillable cuts from typical crude oils. Also shown are distillate products from two cracking processes—delayed coking and FCC. Neither of these processes consume hydrogen, but both produce high yields of light products. The liquid products are deficient in hydrogen and some need further hydroprocessing if they are to become transportation fuels. The light liquid products also contain substantial olefin levels. Straight-run distillates are generally easier to upgrade to finished products.

Representing petroleum stocks on a Stangeland chart in this way oversimplifies a very complex situation. Many workers in recent years have improved the

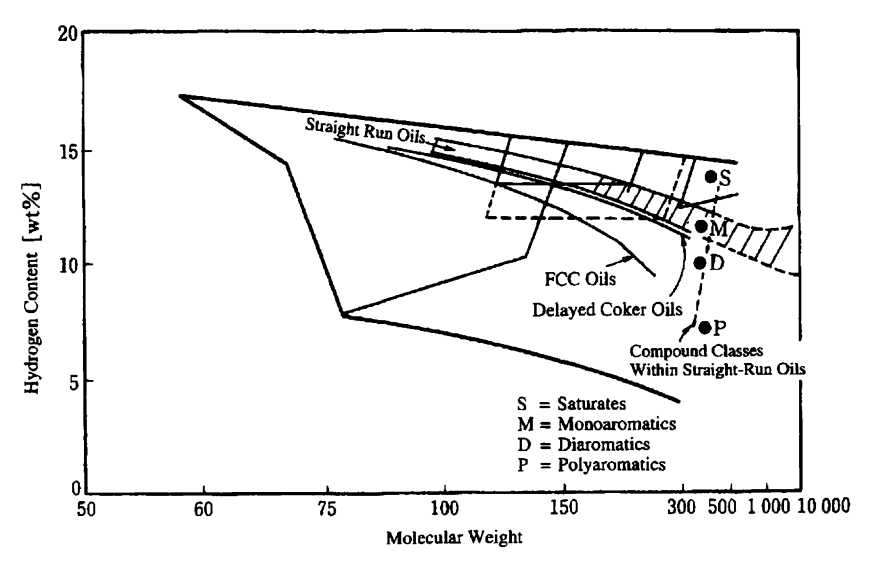


Figure 5.46 Hydrogen content of potential feedstocks.

techniques for characterizing the compounds present in petroleum stocks (for example, Ref (28)). These efforts have helped to understand hydroprocessing reactions, particularly the harmful effects of heavy aromatics. M. F. Ali and coworkers⁽¹⁾ separated the 370–535°C distillate VGO fraction from Arabian heavy crude oil into compound—class fractions, and then made elemental analysis on the four major compound classes—saturates, monoaromatics, diaromatics, and polyaromatics.

These are shown on Figure 5.46. Point P shows the polyaromatics naturally present in this VGO. This compound class amounts to 22.2 wt% of the total VGO and is more aromatic than either of the cracked stocks referred to previously. The sulphur content of the polyaromatics was 9.83%, which means that three-quarters of all sulphur in this VGO resides in the polyaromatics. Every polyaromatic contains, on the average, one sulphur atom. The other compound classes in this VGO are shown as points S, M, and D representing saturates, monocylics, and dicyclics, respectively.

Most modern refineries produce transportation fuels from a blend of components made in different refining processes. Figure 5.47 shows the hydrogen content of a variety of diesel boiling range products from the refining of Arabian crude oils. Those components produced by hydrocracking have much higher hydrogen contents that those produced in non-hydrogen processes. The importance of this is illustrated by Figure 5.48, which shows a rough correlation between jet fuel smoke point and hydrogen content. A 1% change in hydrogen content corresponds to a 10 mm difference in smoke point in the range 20–30 mm. Also, consider the difference in hydrogen content between the

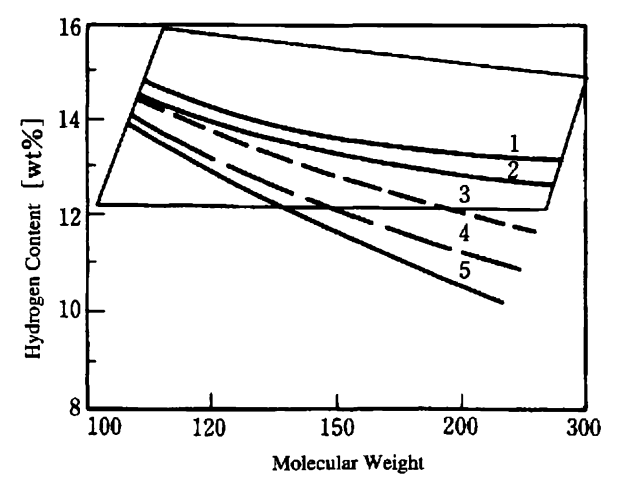


Figure 5.47 Hydrogen content of middle distillates⁽³⁾. Solid boundaries show 121–371 °C diesel range. The processes are: 1, hydrocracker; 2, straight run; 3, delayed coker; 4, fluid coker and 5, fluid catalytic cracker.

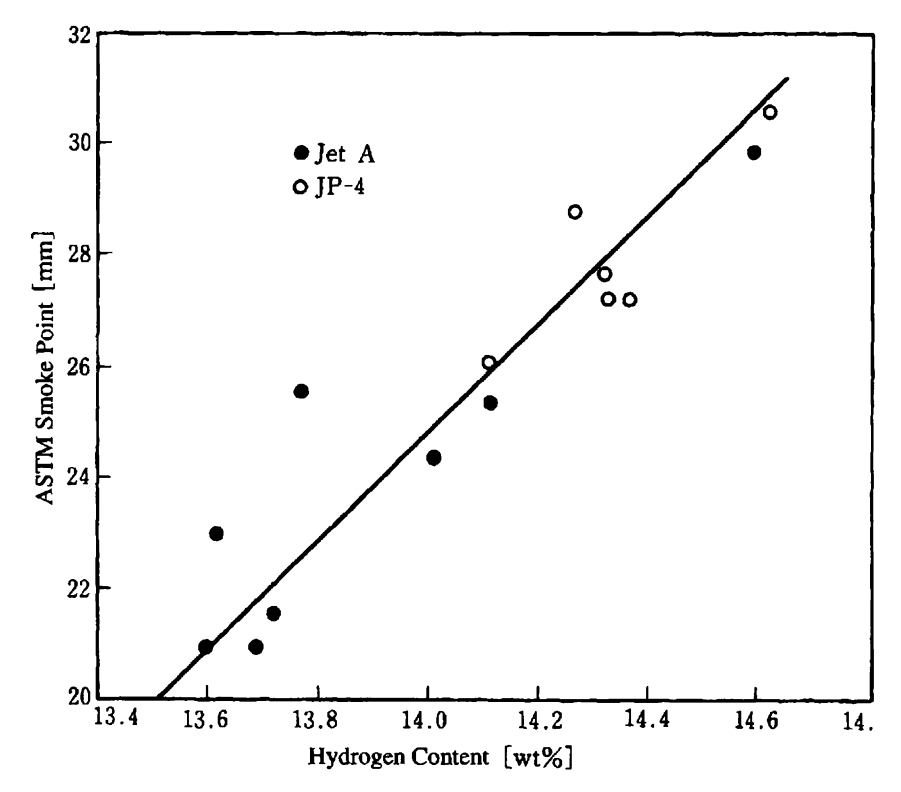


Figure 5.48 The relationship between the jet fuel smoke point and hydrogen conte

components shown in Figure 5.47. A 1% difference in hydrogen content I represents a difference of 125 Nm³/h (700 standard cubic feet (SCF)) hydrogen consumed per barrel when one is trying to upgrade to the sa product specification. Hydrogen is expensive to manufacture and the mod refiner must decide where to invest his hydrogen in order to maximize prod values.

5.4.2 PROCESS FUNDAMENTALS

5.4.2.1 Chemical Reactions

The impurities removed in hydrotreaters are largely concentrated in arom compounds in the feedstocks. Their removal is accomplished by hydrogenal these compounds. Simple examples are shown in Figure 5.49. Note that these examples sulphur is removed without complete saturation of the arom ring, whereas nitrogen removal generally involves saturation and destruct

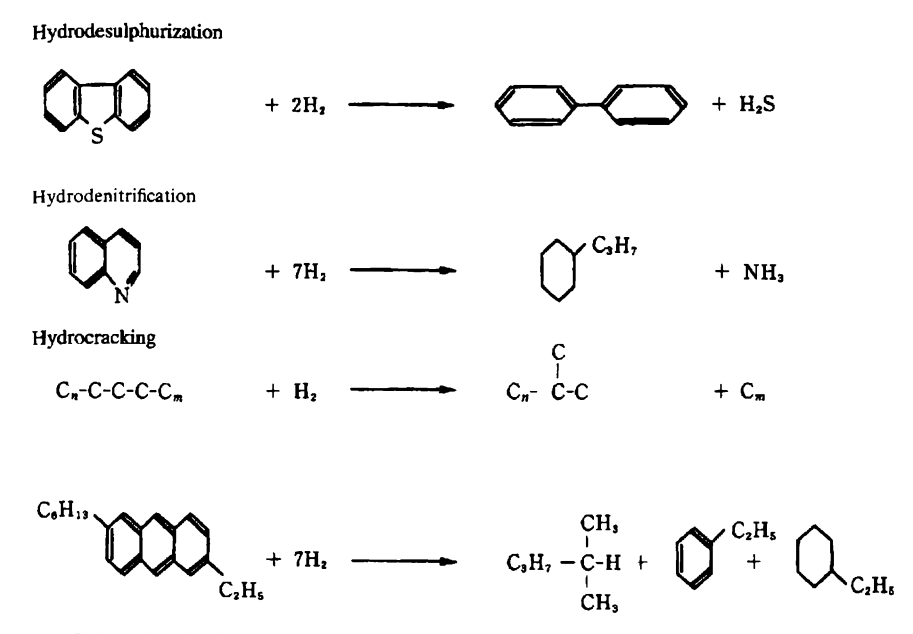


Figure 5.49 Chemical reactions in hydrotreating.

of the aromatic ring. Thus, hydrodesulphurization can be done with low hydrogen consumption at low pressures, whereas nitrogen removal needs high hydrogen partial pressures and consumes more hydrogen.

The reactions in hydrocracking are much more complicated. The chemistry of hydrocracking is essentially the carbonium ion chemistry of catalytic cracking coupled with the chemistry of hydrogenation. Langlois and Sullivan⁽¹³⁾ have reviewed the chemistry of hydrocracking. When the reactants are paraffins, cycloparaffins, and/or alkylaromatics, the products from both hydrocracking and catalytic cracking are similar; but when the reactant is polycyclic aromatics, wide product differences result. Catalytic cracking of phenanthrene over acidic catalysts produced only coke and small quantities of gas while hydrocracking of the same gave low molecular weight cyclic products⁽²⁰⁾. The difference in the product is caused by the hydrogenation component of the catalyst and the excess of hydrogen present in hydrocracking.

The polyaromatic compounds in hydrotreater feeds (represented, for example, by point P in Figure 5.46) play a major role in the process chemistry. Besides containing most of the sulphur contaminants, they are the most polar compounds and, as such, adsorb very strongly on the active catalyst sites. They dominate the coke-forming reactions which cause catalyst de-activation. Removing polyaromatics via hydrogenation and cracking can be accomplished provided operating pressures are sufficiently high to favour the hydrogenation reaction. Under normal desulphurization hydrotreating conditions up to 65%

Table 5.9 Hydroprocessing catalyst types⁽¹⁹⁾

	Catalyst characteristics				
	Acidity	Hydrogenation activity	Surface area	Porosity	
Hydrocracking conversion					
A. Naphthas to LPG	Strong	Moderate	High	Low to moderate	
Gas oils to gasoline	_		Ŭ		
B. HGO to kerosene, jet fuel and/or diesel fuel	Moderate	Strong	High	Moderate to high	
HGO to high V.I. lubricating oils					
Solvent deasphalted oils and residua to lighter pro	ducts				
Removal of non-hydrocarbon constituents					
Sulphur and nitrogen in HGO and LGO	Weak	Strong	Moderate	High	
Sulphur and metals in residua					
Aromatic saturation					
LGO to jet fuel	Weak	Very strong	High	Moderate	

of the polyaromatics are converted to lighter compounds. This results in a slight increase in diaromatics and saturates, and a more substantial increase in monoaromatics. Both hydrotreating and hydrocracking produce high yields of single ring aromatics as a result of this conversion of polyaromatics.

5.4.2.2 Catalysts

Hydrotreating catalysts consist of a hydrogenation component dispersed on a porous, fairly inert, material. Hydrocracking catalysts are dual functional having both hydrogenation and cracking sites. The cracking sites are usually the result of using a porous support of an acidic nature. The best choice of catalyst for a specific situation requires a particular balance between the cracking and hydrogenation functions⁽¹⁹⁾. Table 5.9 shows the families of catalysts that have evolved to accomplish the reactions of industrial importance.

For hydrotreating to remove impurities, catalysts with weak acidity are used since cracking is usually undesirable. Strong hydrogenation activity is needed, particularly with heavy feedstocks containing high molecular weight aromatics.

Note that, besides the chemical nature of the catalyst which dictates the hydrogenation and cracking capabilities, its physical structure is also very important, particularly with heavy feedstocks. With gas oils and residuum, the hydrocarbon feedstock is liquid at reacting conditions so that the catalyst pores are filled with liquid. Both the hydrocarbon and the hydrogen reactants must diffuse through this liquid before reaction can take place at the interior surface of the catalyst particle. At high temperatures, reaction rates can be much higher than diffusion rates and concentration gradients can develop within the catalyst particle. This reduces the overall reaction rate and can lead to costly inefficiencies and undesirable side reactions.

The choice of catalyst porosity is, therefore, very important. A high internal surface area is desirable to give high local reaction rates, but if, in achieving the high surface area, the pore size is reduced to the point where diffusion rates are hindered, then the overall performance will suffer.

Certain generalizations can be made about catalyst porosity⁽¹⁹⁾. For hydrocracking to LPG and gasoline, pore diffusion effects are usually absent. High surface areas (about 300 m²/g) and low-to-moderate porosity are used (from 12 Å pore diameter with crystalline acidic components to 50 Å or more with amorphous materials). With reactions involving high molecular weight impurities, pore diffusion can exert a large influence. Such processes need catalysts with pore diameters greater than 80 Å.

5.4.2.3 Reaction Kinetics

When studying the design of a chemical process, the engineer needs answers to three questions:

- (1) How far will the reaction go?
- (2) What energy changes are involved?
- (3) How fast does the reaction go?

Equilibrium, calculated from free energy data, will determine how far the reaction can go.

The heat of reaction, calculated from heats of formation of the reactants, will determine the energy changes involved.

The rate of reaction is of great interest to the engineer because it determines the size of equipment required. Reaction rate is influenced by several factors including temperature, pressure, concentrations and catalysts. Unfortunately, it cannot be calculated from theoretical data, but must be determined experimentally.

The above information can be obtained fairly easily for a simple chemical reaction. However, as cited earlier, hydroprocessing is not a simple chemical reaction. Not only do the feedstocks contain similar compounds with different boiling points, but there are also widely different compounds with similar boiling points. Knowledge of the rate of the hydroprocessing reaction is vital in the design of a new unit, or in deciding how much feedstock can be processed in an existing unit.

The rate of reaction is obtained in pilot plant experiments by measuring the extent of reaction at different residence times and the same temperature. The rate invariably increases with temperature and this relationship needs to be explored experimentally as well.

Reaction rates can be expressed mathematically. Because hydroprocessing reactions involve many different types of molecules, the overall reaction rate is a combination of many different specific reaction rates which can vary from zero order to second order or higher, in which case it is called an *n*th order rate which is expressed as

$$-\frac{\mathrm{d}C}{\mathrm{d}\theta} = kC^n \text{ which integrates to } k\theta = \frac{1}{n-1} \left(\frac{1}{C^{n-1}} - \frac{1}{C_o^{n-1}} \right)$$
 (5.29)

when n = 1, then $k\theta = \ln(C_0/C)$.

where: C_0 = concentration of reactant in the feedstock

C =concentration of reactant in the product

k = reaction rate constant at a specific temperature

 θ = time of contact

n = reaction order

Although specific reaction rates must be determined experimentally for any new feedstock or type of hydroprocessing, some generalities can be made. In hydrotreating, the reaction rate for denitrification appears to be first order.

	Hydrogen consumption [Nm³/m³ Feedstock]	LHSV [h ⁻¹]	Temperature [°C]	Pressure [MPa]
Naphtha hydrotreating	2–10	2–5	260–350	1.5–3.5
Light oil hydrotreating	15-50	2-5	290-400	1.7 - 3.5
Heavy oil hydrotreating	70-170	1-3	350-425	7–14
Residuum hydrotreating	100-200	0.15-1	350-425	7–14
Residuum hydrocracking	200-270	0.2 - 1	400-425	14-20
Distillate hydrocracking	170-400	0.5 - 10	260-480	3.5-20

Table 5.10 Typical hydroprocessing operating conditions^(5,23)

Desulphurization and de-metallation are higher order, particularly with residuum where the rates approach second order. Considerable work has been carried out on hydrocracking reaction kinetics, and it is generally accepted that the reaction is first order with respect to the hydrocarbon feedstock.

Designing for high temperature operation to take advantage of the high reaction rates must be moderated because the rate of undesirable side reactions (including those which deactivate the catalyst) also increases at high temperature.

5.4.2.4 Process Description

The conditions under which a hydroprocessing unit operates is a strong function of feedstock, as well as the desired product mix. The hydrogen partial pressure must be high enough to partially saturate heavy aromatic molecules. The operating temperature should be sufficiently high to give fast reaction rates but not enough to promote undesirable side reactions or to exceed the metallurgical limits of the high pressure vessels. The amount of catalyst used is that which will give the residence time needed for the reactants to be sufficiently converted at the operating temperature and pressure.

Typical processing conditions are shown in Table 5.10 for a variety of hydroprocesses.

A schematic process arrangement for hydroprocessing is shown in Figure 5.50. Feedstock, recycle gas and hydrogen, at reaction pressure, are heated to reaction temperature in a furnance and then flow through the reactor. The reactor effluent is cooled, after which the liquid and vapour components are separated. The liquid goes to a distillation tower for separation of the liquid products. The separator vapour has a high hydrogen content and most of it is recycled in order to (1) provide the high hydrogen partial pressure needed, (2) to use the hydrogen efficiently and (3) to handle the heat of reaction effectively. A bleed stream of separator vapour is taken as a net product in order to

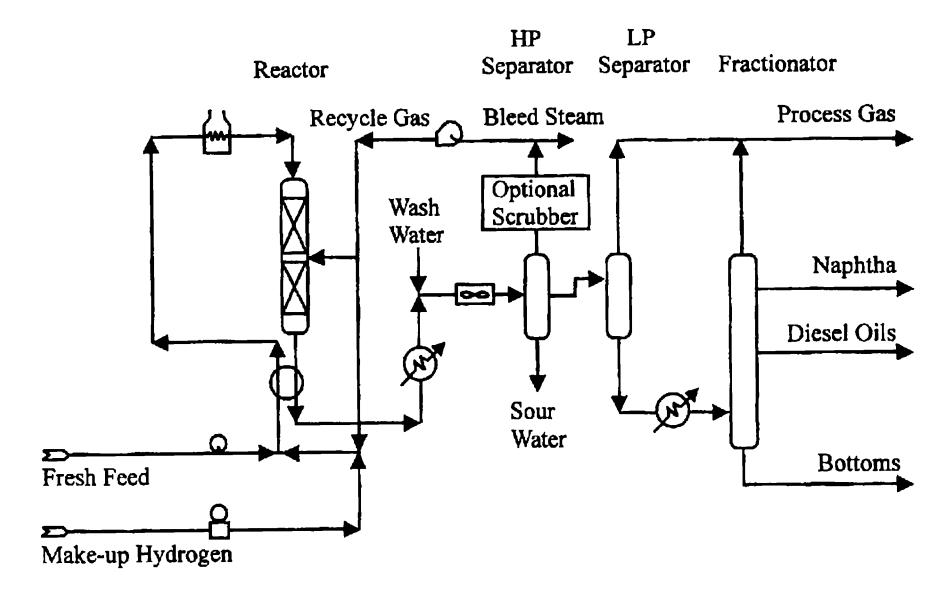


Figure 5.50 Simplified flow diagram for the vacuum gas oil hydrotreating unit.

prevent a build-up of light hydrocarbons which would reduce hydrogen partial pressure in the reaction. Frequently the bleed stream is purified and recycled, thus maximizing the hydrogen partial pressure in the reactor.

The reader will realize that there are several hydroprocesses—hydrotreating, hydrocracking, and catalytic reforming. There are also a wide variety of feedstocks—naphtha, light distillates, vacuum gas oils, and residuum. It would take a separate book to describe each combination in detail. Therefore, in order to stay within the limitations of this book, only one will be used as an example. The following sections will present the chemistry and reactor design issues encountered in hydrotreating vacuum gas oil (VGO).

5.4.3 VGO HYDROTREATING REACTIONS

5.4.3.1 Reaction Kinetics

Despite the complexity of hydroprocesses, reaction kinetics can often be expressed in simple terms. Hydrodesulphurization generally is close to a second order reaction, but can vary depending upon the nature of the sulphur compounds in the raw feed. Figure 5.51 shows desulphurization of a particular VGO in which the rate appears to be 1.7 order.

On the other hand, the hydrodenitrification reaction appears to be first order. Figure 5.52 shows data from a pilot plant processing heavy California

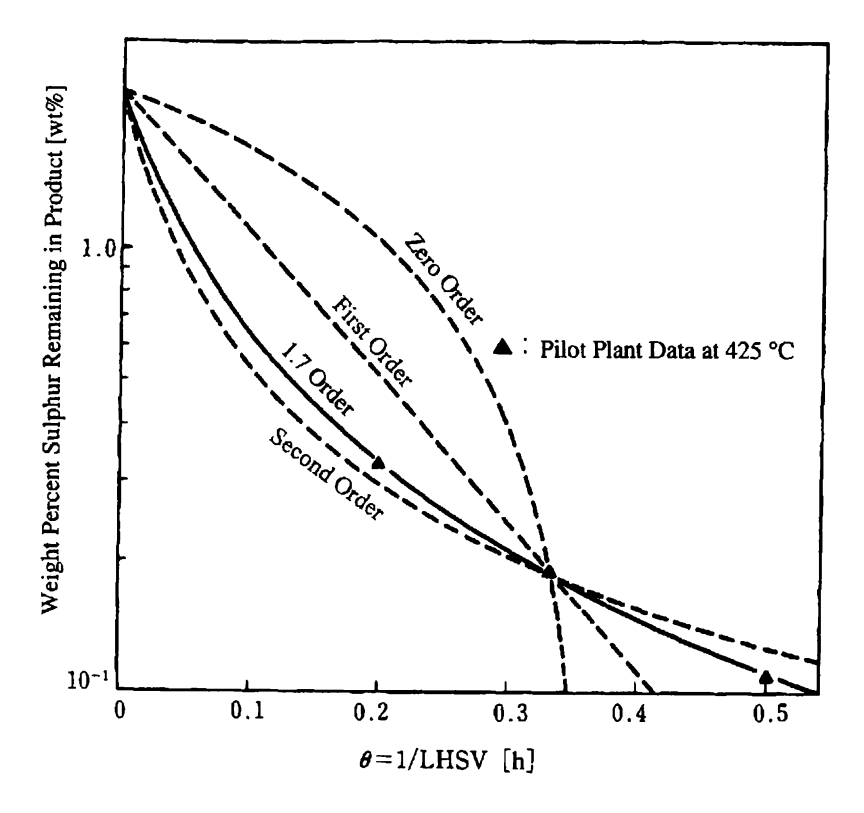


Figure 5.51 Test of pilot plant data for reaction order. (Ref. Table 5.11).

coker gas oil over a weakly acidic catalyst containing both a Group VI and a Group VIII hydrogenation component. First order behaviour describes the data over a range of product nitrogen covering four orders of magnitude.

5.4.3.2 Heats of Reaction

Hydrotreating reactions are exothermic. The design of a process unit must taken maximum advantage of this fact. The feed-effluent exchanger must recover as much heat as is economically practical in order to minimize fuel consumption in the charge furnace. An accurate estimate of the heat release in the reaction is essential to achieve this.

Jaffe⁽¹¹⁾ predicts heat release based on Stull's thermodynamic data⁽¹²⁾ for chemical bonds formed and hydrogen consumed by three important classes of hydrocarbons.

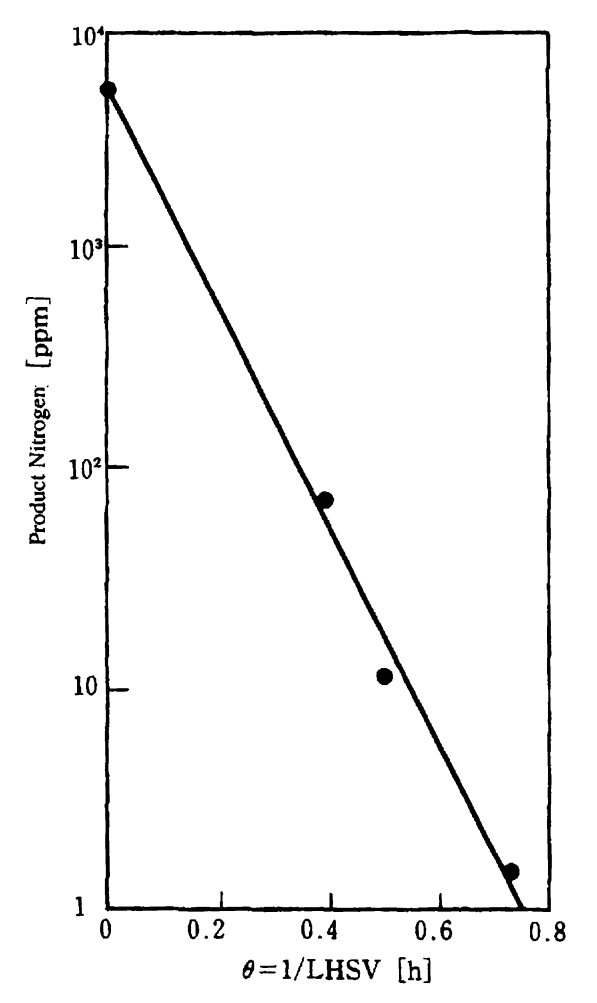


Figure 5.52 Hydrodenitrification kinetics for California coker gas oil⁽¹⁹⁾.

Reaction	kJ per mole of H ₂ consumed
(1) Saturates which consume H ₂	20–45
with cracking or ring opening	
(2) Aromatics saturation	55–70
(3) Olefin saturation	115–125

Modern analytical techniques can be used in small-scale experiments to determine the concentration of bond types in feedstocks and products. Jaffe obtained good agreement between predicted and measured hydrogen consumption by this method.

Shiroto et al. (27) also predict heat release in hydrodesulphurization or hydrodenitrification reactions for hydrocarbons containing N and S, as follows:

Reaction	kJ per mole of H ₂ consumed
(1) Hydrodesulfurization	55–75
(2) Hydrodenitrification	60–85

5.4.3.3 Equilibrium

Saturation of aromatic compounds is important in hydrotreating. This reaction is reversible and the equilibrium between the forward and reverse reaction can hinder the extent of saturation at normal commercial conditions. The hydrogenation reaction is favoured by high hydrogen partial pressures and low operating temperatures. This can be illustrated by considering the simplest aromatic hydrogenation/dehydrogenation reaction, the one between benzene and cyclohexane:

Equilibrium is a function of free energy (ΔG). For this reaction:

$$\Delta G = 200\ 100 - 396T$$
 where $\Delta G = J/\text{mole}$, $T = ^{\circ}\text{kelvin}$

The equilibrium constant, K, is related to the free energy as follows:

$$\Delta G = -RT \ln K$$
 where R is the gas law constant = 8.314 J.K/mol

Partial pressures of the reactants are determined by K as follows:

$$K = \frac{(P_{\rm bz})(P_{\rm H_2})^3}{(P_{\rm ch})} \tag{5.30}$$

Starting with one mole of cyclohexane, and letting x = the fraction of cyclohexane converted, the following table can be made:

	Initial feed	Final product
Cyclohexane	1	1-x
Benzene	0	X
Hydrogen	0	3x
Total	1	3x + 1

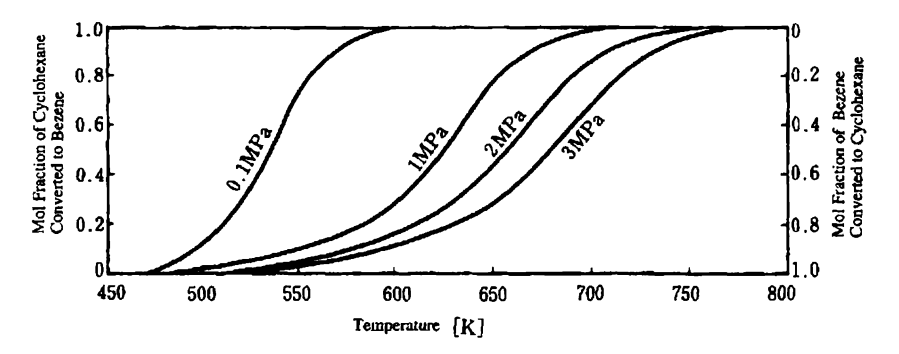


Figure 5.53 Equilibrium relation between benzene and cyclohexane.

$$K = \frac{\left(\frac{x}{3x+1}\right)\prod\left(\frac{3x}{3x+1}\right)^3\prod^3}{\left(\frac{1-x}{3x+1}\right)\prod} \text{ where } \prod = \text{total pressure (Pa)} \quad (5.31)$$

The equilibrium constant, K, and amount of cyclohexane converted can be calculated at several temperatures and pressures as shown graphically in Figure 5.53. As can be seen, hydrogenation of benzene to produce cyclohexane will occur at high pressures and low temperatures, whereas the reverse reaction in which cyclohexane is dehydrogenated to produce benzene will be maximized at high temperatures and low pressures.

Gully and Ballard⁽⁹⁾ summarized the early knowledge on aromatics hydrogenation equilibrium. Hengstebeck⁽¹⁰⁾ proposed a Hydrogenation—Dehydrogenation Index for correlating experimental data. Yui and Sanford⁽²⁵⁾ studied kinetics of aromatics hydrogenation in order to improve the cetane number of an LGO feed. They measured the aromatics hydrogenation at different temperatures, pressures and residence time (LHSV*). Data obtained with Arabian light gas oil (LGO) are shown in Figure 5.54. The results were compared with a kinetic model for aromatics hydrogenation based on a simple first order reversible reaction. Agreement with the model was excellent. This particular reaction is limited by equilibrium at temperatures above 360 °C when operating at pressures of 5–10 Mpa.

5.4.4 VGO HYDROTREATING CATALYSTS

There are a large number of commercial catalysts available for hydrotreating. Typically, the supports are extruded alumina cylinders. Some, as shown on Figure 5.58, are 'shaped', to give extended surfaces.

^{*}Refer to paragraph 5.4.6.3.

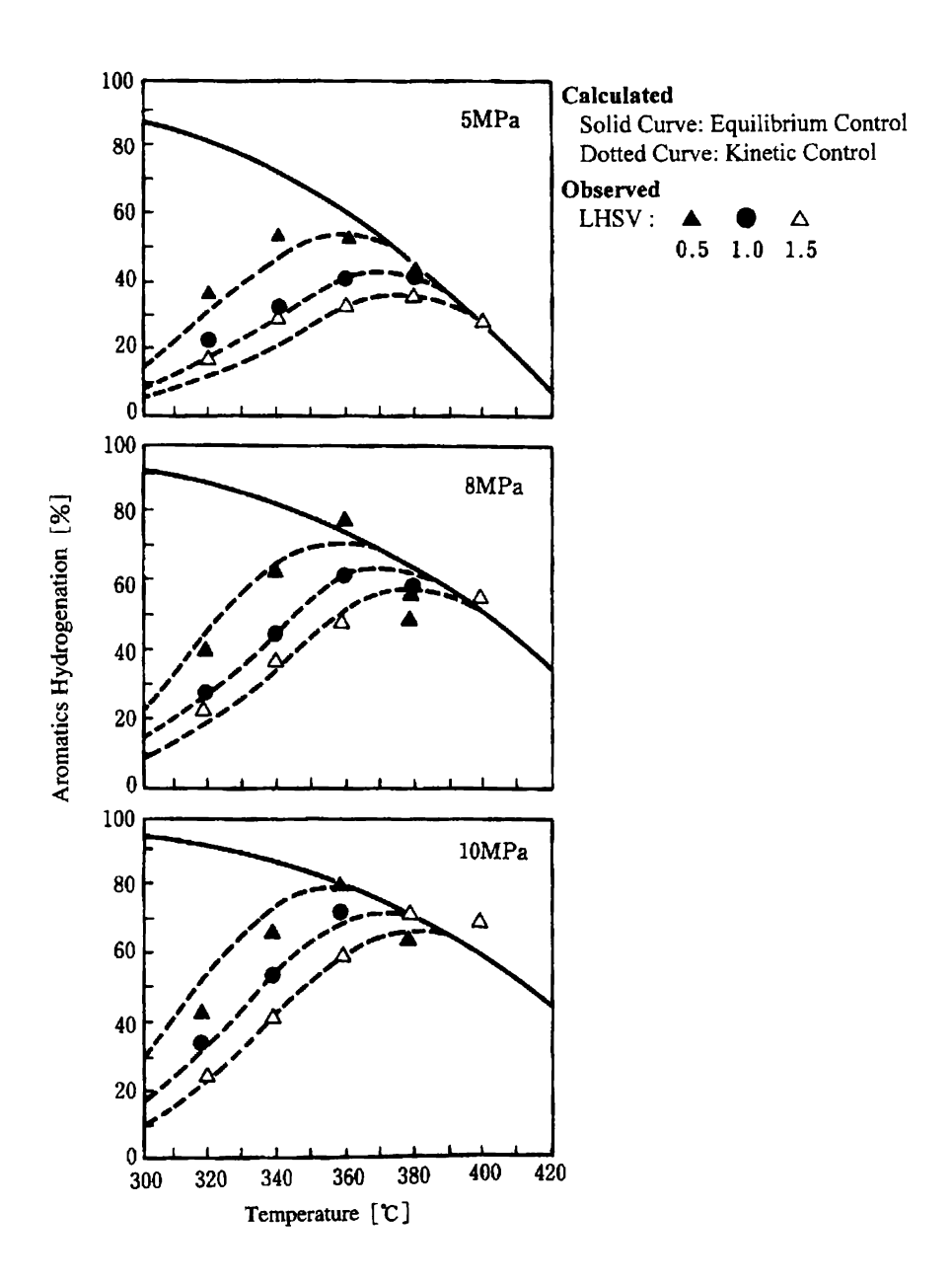


Figure 5.54 Observed and calculated % aromatic hydrogenation at various operating conditions (Arabian light gas oil)⁽²⁵⁾.

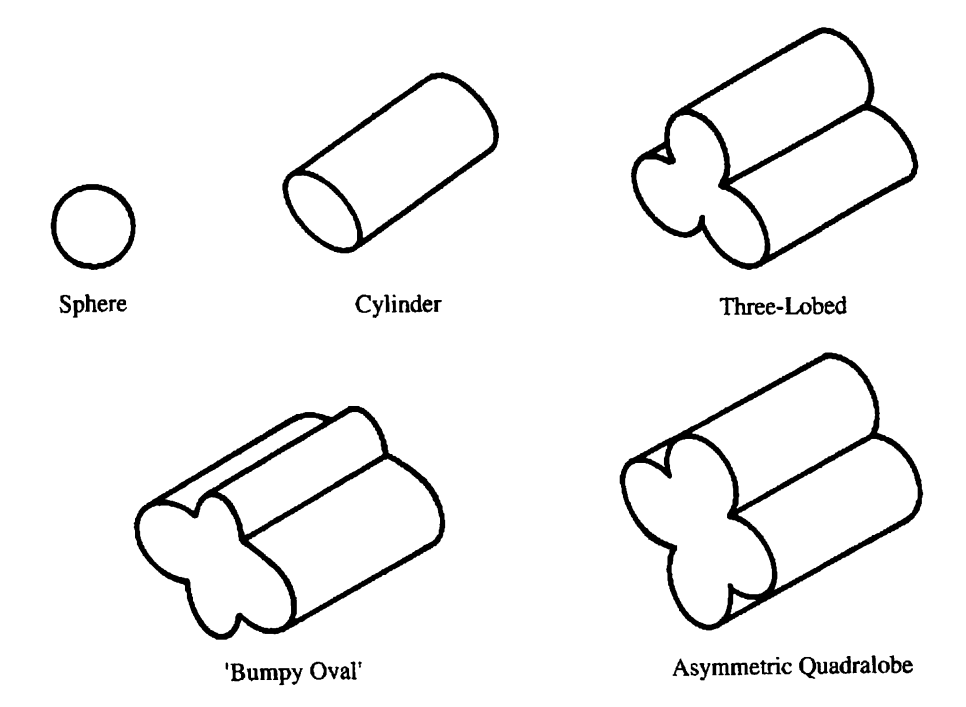


Figure 5.55 Common catalyst shapes.

Diameters of the catalyst particles can vary from 0.8 mm to 5.0 mm. Small diameter catalysts have a larger external surface area per unit volume when compared to large diameter catalysts. However, there are limitations. Very small diameter catalysts can have two serious problems. One is crushing strength, an important catalyst property. Pressure drop through a bed of small diameter catalyst will be greater than that through larger diameter particles, and if too great, can exceed the mechanical strength of the supports. Larger diameter catalysts have greater strength and can resist the crushing effects of pressure drop. The other problem with very small diameter catalysts is their filtering ability, i.e., any discrete solid particles, such as scale, entering the catalyst bed will be trapped at the top of the bed by the fine catalyst. This, in turn, can raise pressure drop over the catalyst bed causing either catalyst crushing or increased operating costs. If scale is a serious problem it can be alleviated by using larger diameter catalyst in the top bed and smaller diameter in the lower bed or beds. Also, external filters are sometimes used on raw feed to remove particulate matter, especially when the stock comes from tankage.

Although the actual composition of commercial hydrotreating catalysts is proprietary information, it can be said that a typical CoMo catalyst will contain about 2-5 wt% Co and 4-8 wt% Mo. A typical NiMo catalyst will

contain about 2-5 wt% Ni and 4-8 wt% Mo. These compositions can vary widely depending on the selectivity desired in the hydrotreating process. One chemical reaction can be encouraged and another discouraged by changes in catalyst components. The products must meet certain specifications, but exceeding them may consume valuable hydrogen that could be used elsewhere in the refinery. Selectivity can be influenced both by variations in catalyst properties and by variations in operating conditions.

5.4.5 VGO HYDROTREATING PROCESS CONDITIONS

Typical hydrotreating operating conditions are shown in Table 5.10. As shown there, hydrogen consumption, temperature and pressure, all increase with increasing boiling range (or molecular weight) of the feedstock, while space rate decreases. Specific operating conditions for a new feedstock are generally determined experimentally in a pilot plant.

As shown in Table 5.10, typical operating conditions for VGO hydrotreating would be with space velocity from 1 to $3\,h^{-1}$, temperature from 350 to 425 °C, pressure from 7 to 14 MPa, and hydrogen consumption of 70–170 Nm³ per kl. Hydrogen partial pressure would be maintained by fresh hydrogen and recycle hydrogen in the ratio of 360 to 540 Nm³ of hydrogen per kl of feed.

In practice, especially in the case of treating an unknown feedstock, process conditions would be determined on the basis of pilot plant test data.

546 VGO HYDROTREATING REACTOR DESIGN

5.4.6.1 Design Basis

The first step in designing a reactor for VGO hydrotreating is the establishment of a design basis. This is the basis for designing the entire process plant. It consists of the following:

- (1) Location of the plant
- (2) Feedstock specification
- (3) Quantity of feedstock to be processed
- (4) Product specification
- (5) Hydrogen source and composition
- (6) Boundary conditions, i.e., temperature and pressure of incoming and outgoing stocks.
- (1) Plant location specifies where the hydrotreating unit is to be located. Ambient air temperature ranges are needed for insulation considerations. Also, types of utilities must be specified.
- (2) Feedstock specification establishes the feedstock, or stocks, that are to be processed—crude oil source, boiling range, specific gravity, wt% contaminants such as sulphur, nitrogen, olefins, metals, etc., and the prior

processing that the stock has received, i.e., whether it is straight run or cracked.

(3) Feedstock quantity states the tons per calendar day (TPCD) and tons per stream day (TPSD) of feedstock to be processed. The difference between the two is the operating factor (OF) expected. The OF is the fraction of time the plant will be on stream. It is normal to expect that plants will be shut down from time to time for catalyst regeneration or changeout, for maintenance, or as required by government regulations for inspections.

Example 5.12: Design Feedstock

25000 BPD is the design feedstock (24°API VGO) rate and the operating factor is expected to be 90%. What is the TPSD rate to be used as the design basis?

Solution

Density (p) of the design feedstock is

$$\rho = \frac{141.5}{^{\circ}API + 131.5} = \frac{141.5}{24 + 131.5} = 0.91$$

Quantity of the design feedstock to be processed is = $25\,000 \times 0.159 \times 0.91/0.9 = 4019$ (TPSD)

Thus, the plant must be designed to process 4019 TPSD in order to allow for the expected downtimes.

- (4) Product specification sets the processing goal. It states maximum contaminants allowable in the product. It sets the boiling range desired in the final product. This is because some cracking will occur and the light products must be removed in the product fractionator.
- (5) Hydrogen source. Hydrogen feed to the process, called make-up hydrogen, can come from various sources. One source is a hydrogen plant (see Chapter 5.2) where fairly pure hydrogen is manufactured from natural gas or other hydrocarbons. Another good source is from catalytic reforming units where naphthenes are dehydrogenated to form aromatics. Gas from catalytic reformers typically contains about 90% hydrogen, but it is usual practice to remove the 10% light hydrocarbons, such that the make-up hydrogen stream to the hydrotreater is essentially pure hydrogen. Also bleed gas from another hydroprocessing plant is sometimes used, although the hydrogen content will be lower than that from catalytic reforming units. When pure hydrogen is required, a separation process such as cold box, PSA or membrane is used.

5.4.6.2 Process Flow Diagram and Material Balance

The next step is the preparation of the process flow diagram which shows the arrangement of all equipment in the VGO hydrotreating plant. It shows the sequence of the processing streams as they enter and exit the various pieces of equipment. It also shows each individual stream quantity, composition, temperature and pressure. Figure 5.50 is a sketch of such a process flow diagram. (Note: A pressure drop profile through the system must be estimated at first. It will be corrected later by economic considerations of the various pieces of equipment in the overall recycle loop.)

The material balance lists the volumes and weights per unit time of each component in each stream. Once it is established, the design of all the individual pieces of equipment in the plant can begin. The quantity and composition of streams entering and exiting each piece is now known, and design of the VGO hydrotreating reactor can start.

5.4.6.3 Space Velocity and Catalyst Volume

Space velocity, particularly for a new feedstock, is determined by a study of experimental data from pilot plant runs which were made using samples of the design feedstock, samples of the intended catalyst, and a simulated hydrogen make-up stream.

Time of actual contact of reactants with the catalyst is difficult to measure. The term 'space velocity' is used to correlate data from pilot plant tests and for reactor design. Space velocity is defined as the volume per hour of raw feed as liquid at 15 °C divided by the volume of space occupied by catalyst in the reactor. This is called the liquid hourly space velocity, or LHSV. LHSV is then the reciprocal of constant time, θ , or LHSV = θ^{-1} .

Table 5.11 and Figure 5.56 show typical data from hydrotreating VGO in a pilot plant. Three tests were made at 425 °C and one was made at 400 °C.

Example 5.13

Using these data, at what space velocity should this VGO be processed if the average catalyst temperature is 415°C and the product is to have a maximum sulphur content of 0.1 wt%?

Solution

The previous section on reactor kinetics (5.2.4.3) covered reaction rate order, and gave equations for zero, first, second and nth order rates. The first step in analysing the pilot plant data is to determine the reaction rate order. Using Eq (5.29) the following rate constants are calculated:

Calculated reaction rate constant, k						
Run no	If zero order	If first order	If second order			
1	4.38	6.08	17.31			
2	6.33	<i>7.48</i>	14.49			
3	9.85	9.78	12.98			

Table 5.11 Typical laboratory pilot plant results

Feedstock Straight run Vacuum Gas	Oil (VGO)	Operating Pressure	5.1	
Specific gravity Molecular weight	0.91 350	H ₂ Part Catalyst	4.3 0.5	
Sulphur [wt%]	2.3			
Boiling range [°C]	270 ~ 555			
Test results:				
Run number	1	2	3	4
Temp. [°C]	425	425	425	400
LHSV [h ⁻¹]	2	3	5	2
Sulphur in product [wt%]	0.11	0.19	0.33	0.29

As none of the possible orders shows a uniform rate constant, it appears this is an nth order reaction rate.

The nth order can be approximated by looking at the ratio of rate constants calculated above. The ratio of rate constants for run 3 to those of run 1 gives the following:

Order	Ratio of k for $\frac{run 3}{run 1}$		
Zero	2.25		
First	1.60		
Second	0.75		

These results are shown graphically in Figure 5.57. As shown thereon, it appears the ratio of rate constants should be 1 at the 1.7 order, i.e., both constants would be the same, indicating the pilot data were showing a 1.7 order reaction rate.

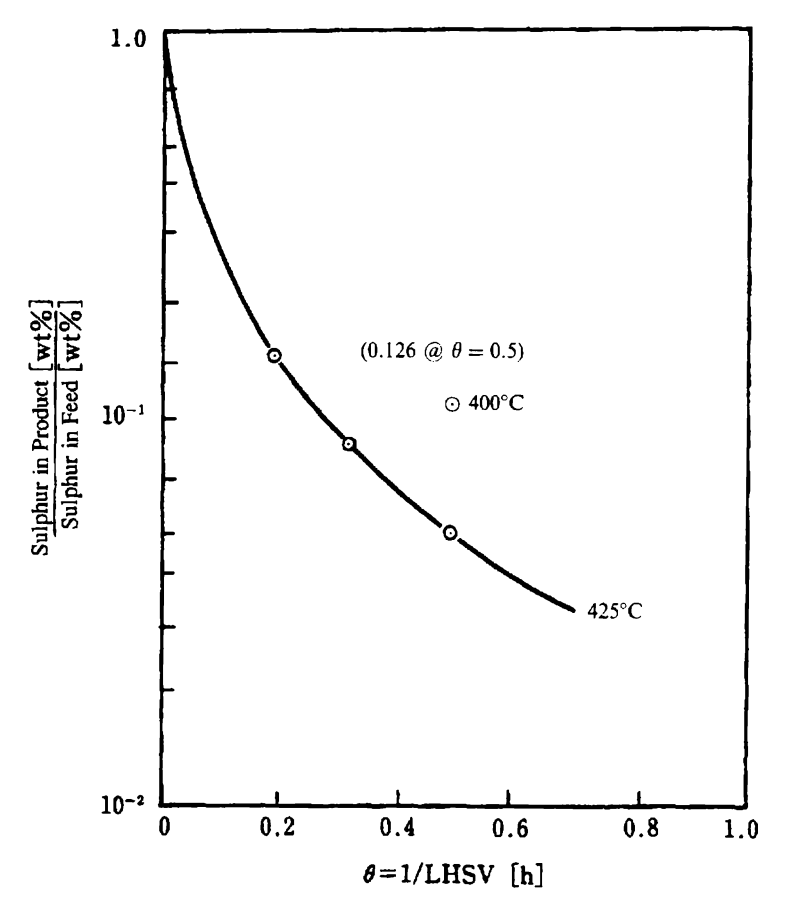


Figure 5.56 Pilot plant results (Table 5.11).

On the other hand, calculating rate constants based on a 1.7 order gives the following:

Run no.	k at 425°C		
1	11.801		
2	11.313		
3	11.534		

Since these values of k are approximately the same, the reaction order can be taken as 1,7. This is further verified in Figure 5.51 where curves for the various

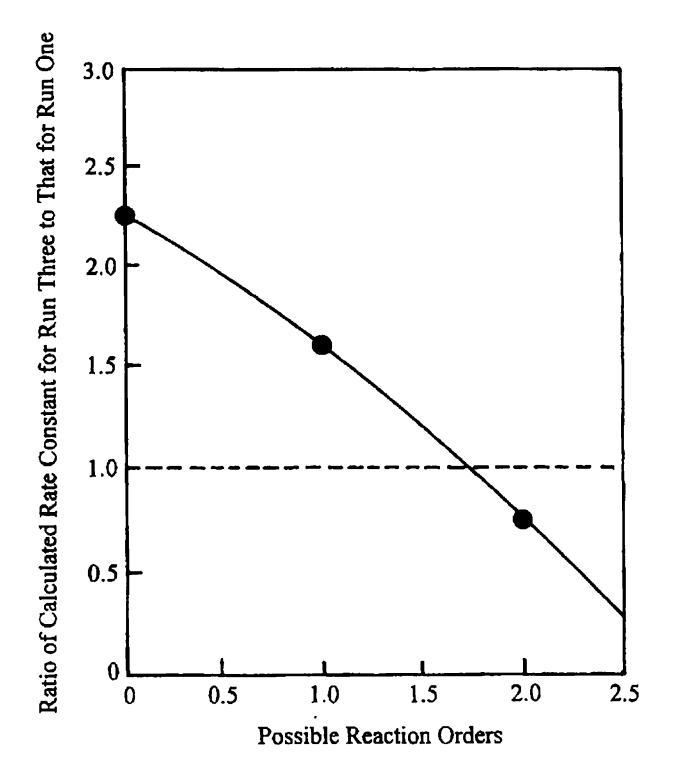


Figure 5.57 Determination of reaction order from calculated orders.

orders are calculated based on average reaction rate, k at $425\,^{\circ}C = 11.549$. This shows data for runs 1, 2 and 3 all fall close to the 1.7 order curve.

Calculating rate constant at 400°C based on data from run 4 gives also the following:

k at
$$400 \,^{\circ} C = 5.201$$
.

Since the design requires operation at 415°C it is now necessary to determine the rate constant for that temperature. This is done using the Arrhenius Equation, which is:

$$k = Ae^{-E/RT}$$
 or $lnk = lnA - \frac{E}{RT}$ (5.32)

where: A = a constant which depends upon activity

E = activation energy

R = a constant

T = absolute temperature, K

A and E are unknowns, but since k is known at both 400°C and 425°C they cm be determined by solving simultaneous equations to give:

$$E/R = 14995$$
 and $lnA = 23.93$

then using Eq (5.29), k at $415 \,^{\circ}C = 8.455$. Equation (5.29) can now be solved for a product sulphur content of 0.10 wt% to give,

$$\theta = 0.75 h \text{ or } LHSV = 1.333 h^{-1}$$

Example 5.14

Now that the space velocity to achieve 0.10 wt% sulphur in the product is known, what catalyst volume is needed to process the design feed rate of 4019 TPSD if the reactor operates at 415 °C and under the same pressure conditions as the plot plant?

Solution

$$4019 TPSD = 167 458 kg/hr = \frac{167 458 [kg/h]}{0.91 \times 1000 [kg/m^3]} = 184.0 m^3/hr$$

$$Catalyst \ volume = \frac{Hourly \ feed \ rate}{LHSV} = \frac{184}{1.33} = 138 m^3$$

5.4.6.4 Reactor Design Considerations

The high-pressure reactor will be one of the most costly items in the plant, so its design requires careful consideration. The quantity of catalyst needed and the pressure level of the reactor are based on knowledge of reaction kinetics, catalyst deactivation rates, and make-up hydrogen purity. The design pressure level is also influenced by product quality considerations. As shown in Table 5.10, heavier feedstocks generally require higher pressures. The quantity of catalyst is chosen to give reasonably low operating temperatures to avoid undesirable side reactions while staying below the reactor metallurgical limit.

The number of reactors required, and the reactor internal configuration is based on a variety of considerations.

The reactor pressure drop must be high enough to promote uniform flows and temperatures but within reason from the point of capital investment and operating costs. Care must be taken not to exceed mechanical strength of the reactor internals, or crushing strength of the catalyst.

The refinery may not be able to accept the largest reactors which a fabricalor can build. Transporting large reactors to the refinery site may not be possible,

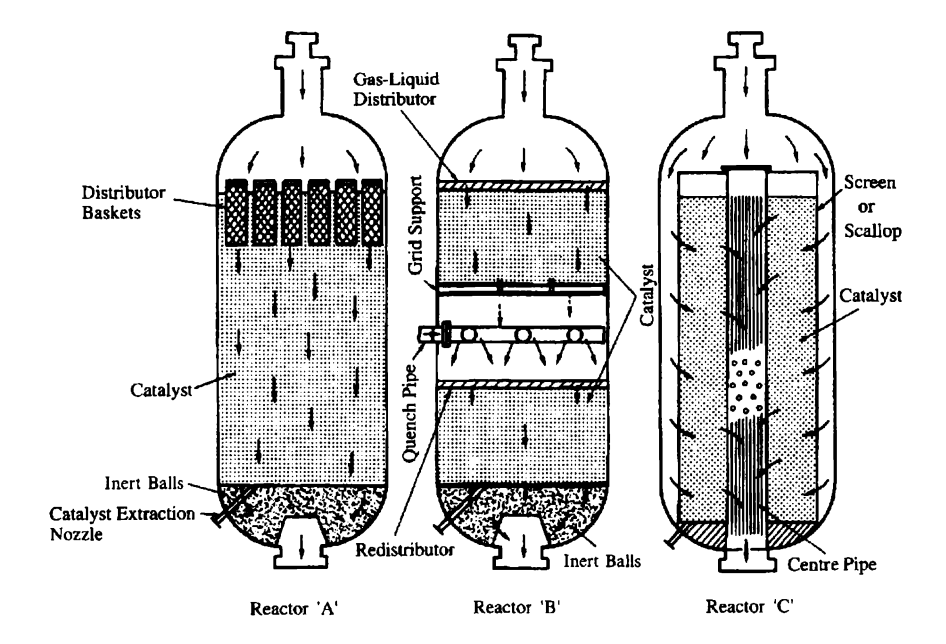


Figure 5.58 Reactor internals.

in which case field fabrication may be necessary. Soil conditions at the refinery may also preclude very heavy reactors.

Reactor internal arrangements will vary depending on the reactant phases, catalyst and type of operation. Figure 5.58 shows typical reactor internals for hydroprocessing units.

- (1) Reactor A with distributor baskets at the catalyst top is used for both single-phase and two-phase operations. The purpose of the baskets is to give uniform distribution of the phase and/or to collect any particulate matter present in the feed which would otherwise clog the top of the catalyst bed and cause increasing pressure drop.
- (2) Reactor B has multiple beds, each requiring support grids. Multiple beds are used to redistribute the liquid phase, and are needed when (1) pressure drop across a single bed would be excessive, or (2), as shown, where a cold quench stream must be introduced to control temperature. Multiple beds are used in hydrotreating units because the exothermic heat of reaction is high. Quench streams are inserted between beds to limit temperature rise. Temperature rise is usually limited to about 25 °C.
- (3) Reactor C is used only for vapour-phase reactions, particularly where a low pressure drop is desired (which is typical in catalytic reforming units).

The reactants distribute over the outer periphery of the catalyst bed (which is contained by a cylindrical screen or perforated sheet metal), then flow radially through a shallow bed into a perforated centre pipe and then out of the reactor bottom.

5.4.6.5 Pressure Drop

Both the capital investment and operating costs of the recycle compressor are a strong function of the reactor loop pressure drop. Designing this loop for too low a pressure drop will result in poor heat transfer coefficients in the heat exchanges and poor flow patterns within the reactor itself. It is important not only to be able to calculate what the individual equipment pressure drops will be, but also what flow regimes exist. This is particularly important in the reactor where a high fraction of the overall loop pressure drop occurs.

However, the pressure drop in hydroprocessing reactors is difficult to calculate or predict. This is because of the complexity of the system, i.e., three phases in which two are flowing under non-isothermal conditions and, further, their volumes are constantly changing. Saez and Carbonel⁽¹⁸⁾ have analysed such systems and present some correlations. Also, Coulson and Richardson⁽⁵⁾ list a number of references for studies of two-phase systems. In practice, most pressure drop calculations for flow-through hydroprocessing reactors are based on experience with similar systems in commercial operation, or on extensive laboratory tests.

Experience shows that pressure drop in a two-phase system will be greater than that for either phase flowing separately, and in fact can be about three times the sum of the individual phase pressure drops.

5.4.6.6 Wall Thickness

Pressure vessels differ from most process plant equipment in that the design criteria are governed by law. All major countries have adopted Codes or Standards which have been developed by technical societies based on engineering experience. These codes are revised periodically in order to incorporate additional experience.

Analysis of the forces in the cylindrical wall of a thin wall pressure vessel (i.e., one thin enough such that forces are uniformly distributed) at equilibrium gives the following relation:

$$t = \frac{PD}{2s} \tag{5.33}$$

where t = wall thickness

P = internal pressure

D = diameter of the vessel

s =tensile stress in the shell.

In the United States this relationship is modified by the ASME Boiler and Pressure Vessel Code to read as follows:

$$t = \frac{PR_j}{SE_j - 0.6P} + C_c \tag{5.34}$$

where t = wall thickness (inches)

P =design pressure (pounds per square inch (psi))

 R_i = inside radius (inches)

S = maximum allowable working stress (psi)

 $E_i = \text{joint efficiency (fraction)}$

 C_c = corrosion allowance (inches).

Note that the thickness calculated by the code takes into account safety, practical and experience factors. The design pressure, P, is greater than the normal operating pressure because allowance must be made for pressure surges and for hydrostatic testing of the vessel before it is placed in operation. The maximum allowable working stress, S, is generally about one-quarter of the ultimate tensile strength of the metal. The joint efficiency, E_j , depends upon the type of weld used in fabricating the vessel. The corrosion allowance is based on tests or experience using the metal in similar services.

Similar codes exist for design of the heads of the vessel, as well as for all the other mechanical features of the reactor.

5.4.6.7 Materials of Construction

Hydrotreating reactors operate under severe conditions; high temperatures, high pressures, corrosive conditions. The refining industry has an excellent safety record for operating high-pressure equipment. Special care is placed on the choice of materials of construction, on monitoring the fabrication of critical pieces of equipment, and on using operating and inspection procedures that protect the equipment.

Hydrogen and the hydrogen sulphide formed in hydrotreating will attack carbon steel and some low-alloy steels under usual operating conditions. At these high temperatures hydrogen can permeate and react with carbon in these steels to form methane which causes the steel to crack and fail. This form of hydrogen embrittlement is called 'High Temperature Hydrogen Attack'. Also, especially in the presence of hydrogen, hydrogen sulphide is extremely corrosive at hydrotreating temperatures. Alloy steels are used to resist these problems. Most hydrotreating reactors are the 'hot wall' type, i.e., insulation is on the outer side of the reactor wall instead of the inner. To resist hydrogen attack the main reactor wall is made of low alloy steel, typically 2-1/4Cr-1Mo. However, at temperatures above 260 °C 18Cr-8Ni stainless steel is needed to protect against hydrogen sulphide attack. This is done by attaching a relatively

thin layer to the inner reactor wall, either by cladding or by weld overlay. Clad steel is made by rolling a thin sheet of stainless steel onto the base metal when the latter is being rolled to its final thickness, thus creating an intimate bond between the two. Weld overlay is done using a stainless steel welding rod and making repeated passes over the base metal until a layer of stainless steel has been built up to the desired thickness. Stabilized grades of 18-8 stainless steel, such as UNS S34700 or UNS S32100, are used. These contain small amounts of columbium or titanium.

Reactor internals (catalyst supports, distributors, piping, etc.) and hot heat exchanger tubes are usually made of stainless steel. High pressure air coolers are subject to corrosion where H_2S and ammonia exit in the presence of water. Piehl⁽¹⁵⁾ has studied this problem and suggested design and operating guidelines to overcome it.

An excellent survey on materials selection for hydroprocessing equipment is given by White and Ehmke⁽²⁴⁾. Included in their publication are the Nelson Charts and other charts showing operating limits for various steels when exposed to hydrogen and hydrogen sulphide. Erwin and Kerr⁽⁶⁾ have written a comprehensive survey on years of experience with 2-1/4Cr-1Mo steel in the thick-wall reactor vessels of the petroleum industry. Start-up and shut-down procedures have been developed to control both temper embrittlement and hydrogen stress cracking in such steels. Hydrogen stress cracking is another form of hydrogen embrittlement associated with hydrogen retained in high strength steels, on cooling from hydrotreating temperatures to below 120 °C. It is avoided by cooling the reactor at a rate slow enough to allow the hydrogen to diffuse out.

5.4.6.8 Optimum L/D Ratio

Reactor dimensions for a given volume of catalyst can be varied over a wide range. The reactor can be tall and narrow, or it can short and wide. As seen in Eqs (5.33) and (5.34), wall thickness is directly proportional to the reactor diameter. A tall narrow reactor will have a thin wall and a long shell compared to a short wide reactor which will have a thick shell. An infinitely tall reactor will have a high cost as will an infinitely wide reactor. Between these two extremes lies an optimum L/D which will be the lowest cost. However, pressure drop and distribution are factors which must be considered as they may be of greater importance than minimum reactor shell cost. Flow through a VGO desulphurizer reactor is both liquid phase and vapour phase. For optimum efficiency both phases must flow together uniformly through the catalyst bed. Uniform distribution of the two phases is a function of mass velocity through the reactor. If the velocity is too low the two phases will separate and each phase will flow through separate channels, nullifying the reactions. On the other hand, if the velocity is too high the pressure drop will become excessive.

A high pressure drop has three bad features; (i) compressor and pumping costs will be high, (ii) many separate catalyst beds would be required to stay within the maximum allowable pressure drop across each bed, and (iii) catalyst churning and breakage can result from high velocities. The optimum superficial velocity is a function of catalyst size and composition of the reactants, and for VGO desulphurizers generally ranges from 0.3 to 0.5 meters per minute.

5.4.7 VGO HYDROTREATING OPERATION

5.4.7.1 Process Control and Instrumentation

Typical instrumentation for a VGO hydrotreater is shown on Figure 5.59.

Temperature is the primary process control in hydrotreating because the reaction rate is temperature dependent. The plant operator adjusts the temperature to give the desired product quality, e.g., the required amount of desulphurization. For example, catalyst activity gradually declines with time so the operator must raise temperature to compensate for the loss of catalyst activity. Also, feedstock quality may change requiring the operator to adjust the temperature in order to meet the product specifications.

Total pressure, or more importantly, hydrogen partial pressure is the other primary process control. Hydrogen partial pressure serves two purposes. It forces the reaction toward equilibrium, and it counteracts catalyst fouling by hydrogenating any unsaturates that form before they have a chance to adhere to the catalyst and form coke. Hydrogen partial pressure is controlled by: (i) the amount of fresh hydrogen make-up; (ii) temperature and pressure in the product separator drum; (iii) the recycle gas rate; and (iv) the amount of net gas bled from the plant. However, the reaction rate is not as sensitive to hydrogen partial pressure as it is to temperature.

Feedstock charge rate and boiling range, and the separation achieved in the product distillation tower, must be controlled in the overall operation of a VGO hydrotreating plant.

5.4.7.2 Catalyst Management

Catalyst activity will decline gradually during operation due to catalyst surface contamination or plugging of the catalyst's pores. This fouling is the result of, (i) metals in the feed, (ii) coke from the complete destruction of heavy compounds which adsorbed on the catalyst surface, (iii) poisons such as arsenic which alloy with active catalyst metal sites, or (iv) particulate matter such as scale from piping in the processing loop that has come loose and is filtered by the first catalyst bed. Normally, the plant operator will raise the process temperature to offset the activity decline. Figure 5.60 shows the history of such operation, called a 'catalyst run' with two different catalysts used for residuum hydrotreating. In this

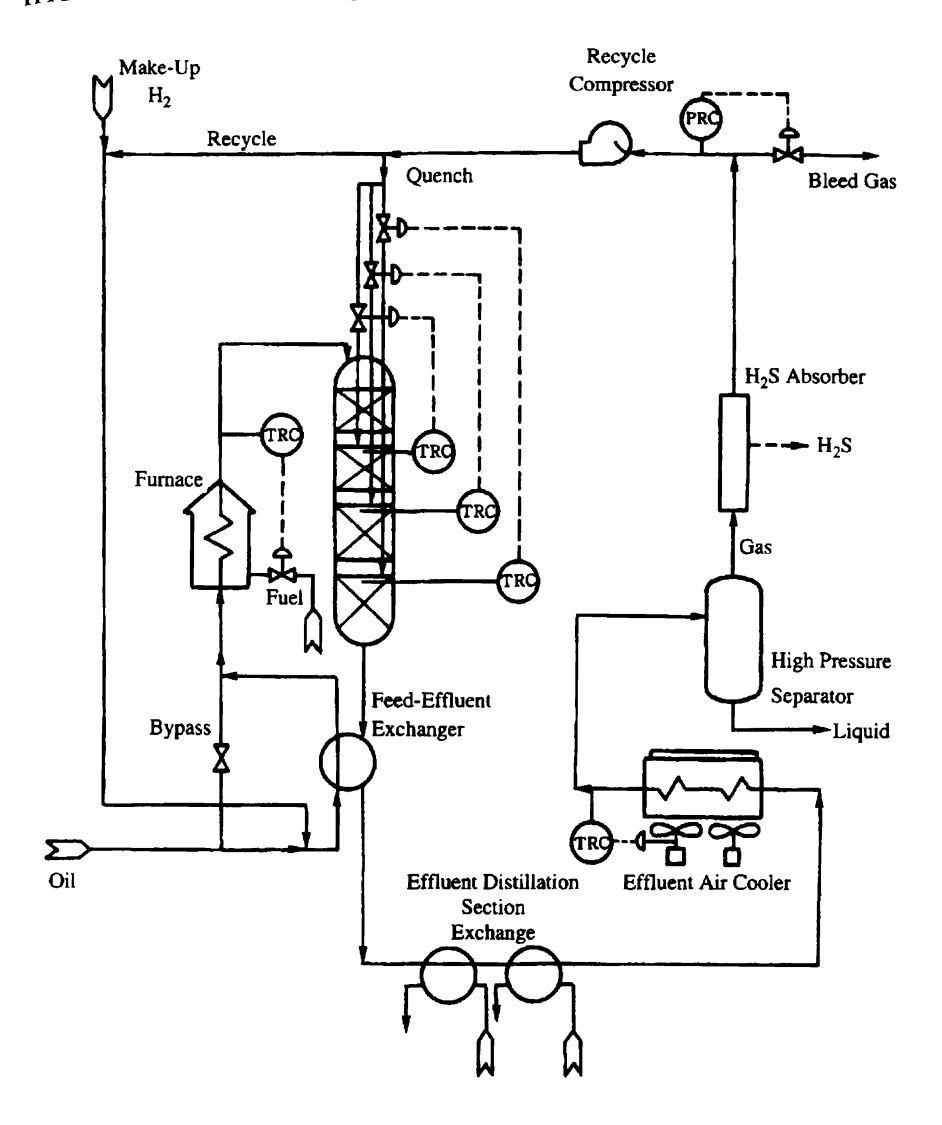


Figure 5.59 Control of a hydrotreater.

example, the smaller catalyst has a much longer life than the larger. This is because catalyst deactivation is caused by metal deposition close to the outside edge of the catalyst particle. The smaller catalyst has a greater surface area per unit volume and therefore can adsorb more contaminants.

This problem of catalyst deactivation in fixed bed reactors has resulted in the development of moving bed catalyst systems in which deactivated catalyst is continuously, or periodically, removed and fresh or regenerated catalyst is

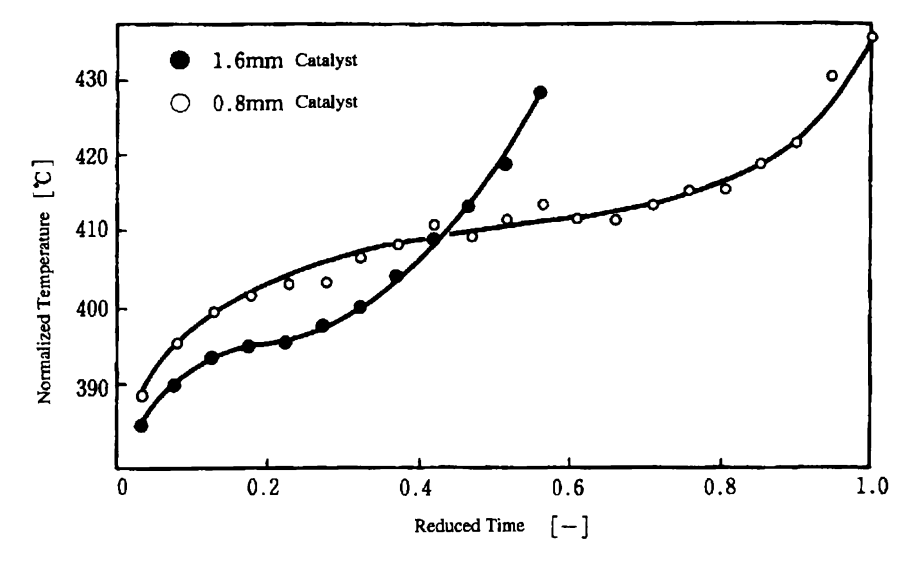


Figure 5.60 The effect of catalyst particle size on catalyst deactivation⁽²²⁾.

added at the same time. This system optimizes catalyst management and provides long on-stream factors. An example of such a process is the Chevron OCR (Onstream Catalyst Replacement). (See frontispiece and Ref. (29))

As shown in Figure 5.60, the temperature is increased rapidly toward the end of the run, and with the higher temperature comes increased undesirable reactions, such as coking, which further increase catalyst fouling. There comes a time, then, when it is no longer economic to operate the process and it must be shut down. The operator must then decide whether to regenerate the catalyst or to remove it and replace with fresh catalyst.

The fouled catalyst can be regenerated if the contaminant is primarily carbon, and this is the usual case with VGO hydrotreaters. The catalyst can be regenerated in situ, although usual practice is to change out the catalyst, in which case the spent catalyst is replaced with new or regenerated material and the spent catalyst is sent to a separate facility for regeneration or disposal.

The spent catalyst must be cool before removal from the reactor because it is in a pyrophoric condition due to metal sulphides on its surface, and these will cause auto-ignition on contact with air if still hot, resulting in release of sulphur dioxide.

In situ regeneration is accomplished by the following steps:

- (1) After shut-down, the reactor and recycle gas loop (including the separator) is purged of hydrocarbons using a hot inert gas such as nitrogen.
- (2) After purging, and with the inert gas still recycling, air is slowly admitted and the temperature raised to the point where combustion of carbon on the

catalyst begins. There will be an immediate rise in temperature at the point of combustion and then a drop in temperature when combustion is completed at that point. This temperature 'wave' will gradually pass the length of the catalyst bed. Initially, the oxygen content of the regeneration gas is very low, but is raised after the first temperature wave has passed through the catalyst. The higher oxygen content is to ensure thorough combustion of any carbon on the catalyst.

- (3) Regeneration gas is purged with inert gas to ensure that all oxygen is removed from the system.
- (4) The plant is restarted with the same procedure used for starting up with new catalyst, except the catalyst must be reduced more carefully because of the presence of sulphates in the regenerated catalyst.

5.4.8 VGO HYDROTREATING SAFETY PROCEDURES

VGO hydrotreaters can encounter serious problems during operation, such as temperature runaways, localized hot spots and unexpected recycle compressor shut-downs.

Temperature runaways can occur if catalyst bed temperatures are not carefully controlled. Hydrotreating is an exothermic reaction, i.e., it gives off heat energy and the reaction rate increases with increasing temperature. Thus, if the catalyst temperature gets too high, the reaction rate will rise rapidly causing further increases in the reaction rate and further increases in the catalyst temperature. If not controlled, the temperature could rise to the point where the reactor metal wall would fail, resulting in an explosion and fire. Temperature runaways are avoided by using cold quench streams to limit temperature rise in each catalyst bed.

Local hot spots will appear if there is poor distribution of reactants through the catalyst bed that results in a region of very low flow in a separate area. In this case there is insufficient flow to carry away the heat generated by the hydrogenation reaction and a localized temperature runaway can occur. If located close to the reactor wall it can cause the reactor wall to bulge or fail with a resultant explosion and fire. Hot spots can be detected by having temperature measurements at several places in the catalyst bed. Reactor exterior walls are often painted with temperature sensitive paints (paints that change colour with increasing temperatures) such that hot spots in the reactor wall can be detected visually. Hot spots are avoided by using a catalyst of uniform size and shape, and by carefully packing the catalyst bed so as to get uniform pressure drop through it. It is also important to provide adequate flow distributors within the reactor.

Jaffe⁽¹²⁾ has studied hot spots and explained them in terms of regions of low flow. He developed a mathematical model which accounts for the temperature rise with rapid reaction of the fluid in the affected region and for a temperature

drop with the eventual mixing of cooler fluid from the surrounding region. By comparing the model with commercial temperature profiles, he estimated the velocity of the low region and its lateral extent. The cause of a low flow region is maldistribution which could be due to presence of catalyst fines or other particulate matter, a physical obstruction, or a failure of the reactor internals.

One of the most serious operating problems for a hydroprocessor is an unexpected recycle compressor shut-down. The loss of gas flowing through the reactor results in a sudden increase in the catalyst temperature since the heat of temperature cannot be transported out of the reactor. Effective procedures have been worked out for handling such a situation. Referring to Figure 5.59 which shows normal VGO hydrotreater controls, they involve bypassing the feed/effluent exchangers, cutting the charge furnace fires, and possibly stopping the make-up hydrogen flow.

5.4.9 FUTURE TRENDS

VGO hydrotreating technology was introduced to the refining industry largely because of the need to remove sulphur, the most common impurity in petroleum stocks. The units were built to operate at relatively low pressures since sulphur can be selectively removed with minimum hydrogen consumption at such conditions. Effective catalysts for this service have been available from a number of suppliers.

Sulphur removal is still a very important objective of modern refiners because of the need to produce fuels which maintain or improve air quality. Other refining objectives, however, have emerged in recent years which have added considerable versatility to VGO upgrading. For example, the process is now often used to prepare fluid catalytic cracking (FCC) feedstocks in order to give low sulphur FCC products, rather than just low sulphur fuel oil (LSFO) components. In this service nitrogen removal is most important since FCC operation is improved substantially when the nitrogen content of the FCC feedstock is reduced.

Also, some refiners want some mild hydrocracking in the units designed originally for VGO desulphurization. Up to 30% conversion, resulting in diesel yields of 15–20% can be achieved by using mild hydrocracking catalysts. This operation and the denitrification operation described earlier are more effective at higher pressures than are typical of most VGO desulphurizing units. New units are therefore being designed for higher pressure operation. Also, more and more large-scale residuum conversion schemes are being implemented worldwide, and there is a need to upgrade coker distillates and other cracked stocks which result from residuum conversion. Higher operating pressures are also needed to hydrotreat these more refractory components.

Finally, environmental regulations now require reduced sulphur and aromatic levels in diesel fuels. The sulphur content of diesel fuel can be reduced quite

effectively in existing VGO hydrotreaters even when the raw diesel fuel is comingled with VGO as a hydrotreater feed blend. However, separate processing is needed if low aromatic levels are desired. Existing VGO hydrotreaters can be converted to low aromatic diesel units to meet this more stringent objective.

All modern refineries now practise VGO hydrotreating. It is an environmentally appealing technology which produces clean products and also helps the refiner to minimize corrosion in his process plants. In the future the operating scope of these units will expand as new catalysts with more capabilities are developed.

References

- (1) M. F. Ali, M. V. Hasan, A. M. Bukhari and M. Saleem, Hydrocarbon Processing, 83 (1985).
- (2) A. G. Bridge, G. D. Gould and J. F. Berkman, Oil Gas J., 85, January (1981).
- (3) A. G. Bridge, J. Jaffe, B. E. Powell and R. F. Sullivan, API Meeting, Los Angeles, May (1983).
- (4) H. C. Chen and A. G. Bridge, Modern Engineering and Technology Seminar, Taiwan. July 3-21 (1978).
- (5) H. G. Cornell and F. J. Heinzelmann, Hydrocarbon Processing, 85, August (1980).
- (5a) J. M. Coulson and J. F. Richardson, Chemical Engineering, Vol. 1, 3rd Ed., p. 95, Pergamon Press (1977).
 - (6) W. E. Erwin and J. G. Kerr, Weld. Res. Council Bull., 275, February (1982).
- (7) J. H. Gary and G. E. Handwerk, Petroleum Refining, Marcel Deker (1984).
- (8) H. G. Geerlings and D. H. Van Nieuwenhuizen, Royal Institute of Engineers in the Netherlands, May 19 (1972).
- (9) A. J. Gully and W. P. Ballard, J. Adv. Petr. Chem. Ref. III (1961).
- (10) R. J. Hengstebeck, Hydrocarbon Processing, 100, August (1970)
- (11) S. B. Jaffe, Ind. Eng. Chem. Proc. Des. Develop, 13, 1 (1974).
- (12) S. B. Jaffe, Ind. Eng. Chem. Proc. Des. Develop, 15, 3 (1976).
- (13) G. E. Langlois and R. F. Sullivan, Adv. Chem. Ser., 97, 38 (1970).
- (14) D. J. O'Rear, H. A. Frumkin and R. F. Sullivan, API Meeting, New York (1982).
- (15) R. L. Piehl, Materials Performance, 15, January (1976).
- (16) F. W. B. Porter and E. C. Housam, *Inst. Chem. Engrs. Yorkshire Meeting*, 9, June (1963).
- (17) J. W. Rosenthal, S. Beret and D. C. Green, API Meeting, Los Angeles (May, 1983).
- (18) A. E. Saez and R. G. Carbonel, AIChE J, 31(1), 52 (1985).
- (19) J. W. Scott and A. G. Bridge, Adv. Chem. Ser., 103, ACS (1971).
- (20) R. F. Sullivan, C. J. Egan, G. E. Langlois and R. P. Sieg, J. Am. Chem. Soc., 83, 1156 (1961).
- (21) R. F. Sullivan, Advances in Catal. Chem. I., Snowbird (1979).
- (22) P. W. Tamm, H. F. Harnsberger and A. G. Bridge, *Ind. Eng. Chem. Proc. Des. Develop.*, **20**, 262 (1981).
- (23) J. W. Ward, Hydrocarbon Processing, 101, September (1975).
- (24) R. A. White and E. F. Ehmke, Materials Selection for Refineries and Associated Facilities, p. 51, National Association of Corrosion Engineers (1991).
- (25) S. M. Yui and E. C. Sandford, API Meeting, Kansas City (May, 1985).

- (26) D. R. Stull, E. F. Westrum, Jr. and G. C. Snike, *The Chemical Thermodynamics of Organic Compounds*, John Wiley & Sons (1969).
- (27) Chiyoda Corporation: In-house Materials.
- (28) M. M. Bonduszynski and K. H. Altgelt, Composition and Analyses of Heavy Petroleum Fractions, Marcel Dekker (1994).
- (29) Rovert A. Meyers (Ed.), Handbook of Petroleum Refining Processes, McGraw Hill (1996).

CHAPTER 5.5

Fluid Catalytic Cracking*

TORU TAKATSUKA and HIDEKI MINAMI

Fluid Catalytic Cracking is called FCC, and is one of the most representative refining technologies, FCC is generally used as a generic term for an FCC process and FCC unit.

The first FCC unit was developed and put into practical use in the United States in the early 1940s, and since then many improvements in catalysts and process technologies have been made. Therefore we can say that FCC is an old, yet new, process.

In the petroleum refining industry, crude oil is first separated into several boiling fractions by atmospheric and vacuum distillation units, and then each boiling fraction is further processed by several kinds of catalytic reaction operation such as hydrotreating, hydrocracking, catalytic reforming and catalytic cracking; by non-catalytic reaction operations such as thermal cracking; and by final treatment operations such as the removal of impurities and fine fractionation.

Through these processes, final refining products such as LPG, gasoline, kerosene, diesel oil, fuel oil, lubricant oil, and asphalt are produced.

Figure 5.61 shows a representative block-flow scheme for petroleum refining. An FCC unit will process feedstocks such as HT VGO (hydrotreated vacuum gas oil) and HDS AR (hydrodesulphurized atmospheric residue) by catalytic cracking reaction in a fluidized bed reactor. This produces high-octane gasoline blending components and cracked gas oil, light olefins (propylene and butylene), and LPG. Propylene and butylenes are furthermore utilized as a feedstock for alkylation and MTBE units to obtain more valuable products such as an alkylate, as a high-octane gasoline blending component, and MTBE (Methyl Tertiary Butyl Ether), which is an oxygen agent containing gasoline also used as a high-octane gasoline blending component.

^{*}A typical example for the M. W. Kellogg Residue FCC unit is shown on the frontispiece.

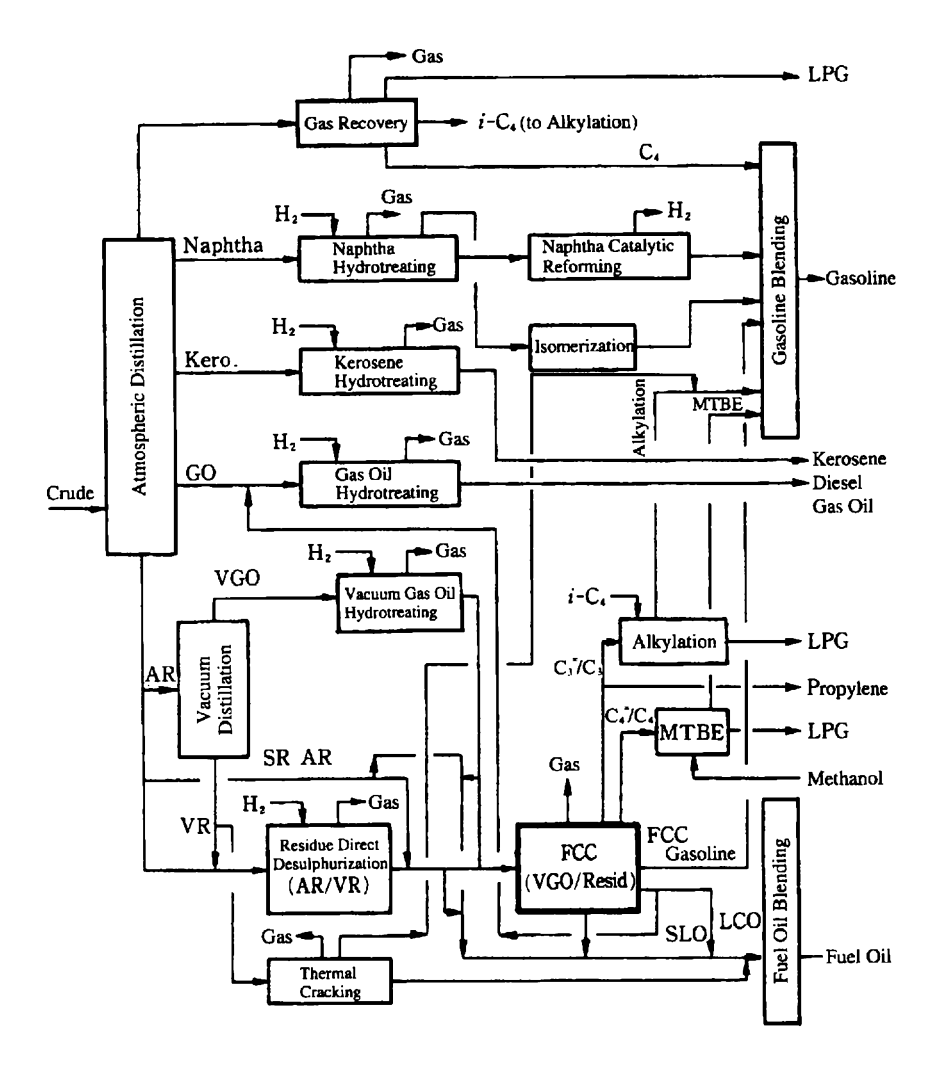


Figure 5.61 Role of FCC in the refining industry (typical refinery block flow).

The first FCC unit, an upflow type, was commercialized in 1942 in the United States, to produce gasoline effectively. It is said that FCC has been the most successful processing development in the history of catalytic cracking processing development, even including types of reactors other than the fluidized catalytic cracking reactor.

Technologies for cracking processes were improved in the following steps, from the thermal cracking process without a catalyst (bath-wise to continuous operation) to the fixed-bed catalytic cracking process with a catalyst (cyclic

catalyst regeneration), and then changed to the moving-bed catalytic cracking process (continuous catalyst regeneration). After that we arrived at the age of FCC development and enhancement.

The historical background and evaluation of these cracking processes developments are described in detail by J. L. Enos in his book, *Petroleum Progress and Profits*⁽¹⁾. From this book, the essential birth of the first FCC unit can be summarized as follows.

When the first FCC unit was developed around 1945, the fixed-bed Houdry process was still boasting of its own superiority for the catalytic cracking process. Further improvement of the Houdry process was realized by developing the moving-bed catalytic cracking process (TCC and Houdry Flow processes). On the other hand, companies that took up the challenge of developing a new process which would supersede the Houdry process included Standard Oil (New Jersey), M. W. Kellogg, Standard Oil (Indiana), British Petroleum, Royal Dutch/Shell Group, Texaco, and UOP. These companies promoted research on catalytic cracking with the common objective of new process development. These same companies also had patent rights and technical information in common possession, and formed the world's largest scientific and engineering manpower group at the time, employing about 1000 personnel in all.

Major R&D tasks of this group were: shortening catalytic contact time in a catalytic reaction; equalizing temperature in the catalyst bed; and moving a large volume of catalyst efficiently. During these development activities, catalyst fluidization technology attracted their attention. Furthermore, for military reasons at the initial stage of World War II, the pace of development of equipment and construction was much speeded up.

In 1940, at the Baton Rouge Refinery of Standard Oil (Louisiana), a 100-BPSD pilot plant was constructed, and achieved satisfactory results in tests of a fluid-solid-moving system. The test results were immediately adopted in the design of the actual plant. The first FCC unit of 12000 BPSD thus started operation in 1942. This was called the 'Upflow Type' (Model I) as shown in Figure 5.62 (a), and was the type in which catalysts rise in the reactor and regenerator and exit from the vessel tops.

Later, in 1944, the diameters of the reactor and regenerator were expanded, and separation of catalysts from vapour was carried out inside the vessels. The catalyst were further fluidized in the dense phase, and the flow was improved so that catalysts were withdrawn downward from the vessel bottoms. This was called the 'Downflow Type' (Model II) as shown in Figure 5.62 (b), and became the prototype configuration of present-day FCC reactors and regenerators. In addition, the shapes of catalysts were improved, and small spherical shapes came into use, significantly decreasing catalyst attrition and improving cyclone efficiency.

In Model I, the economical C/O ratio (catalyst/oil) was about 3 at the maximum limit, but in Model II it was possible to design the ratio technically

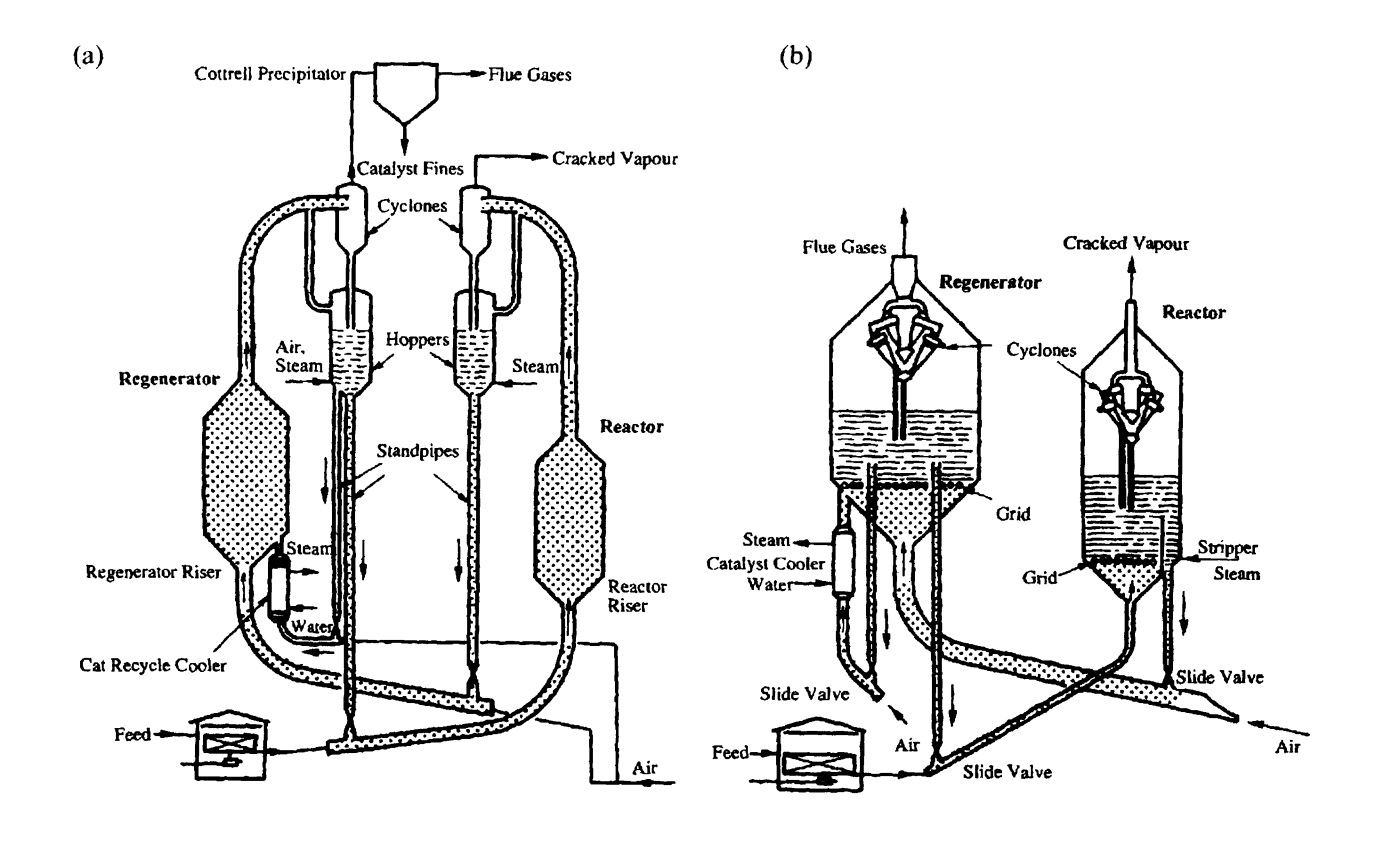


Figure 5.62 Configuration of early FCC units (model I type and II type)⁽⁴⁾. (a) Up-flow type FCC unit (Model I Type). (b) Down-flow type FCC unit (Model II type).

and economically within the range 3-30. Later in 1946, Model III of the pressure-balance type was developed by M. W. Kellogg. On the other hand, the first stacked-type FCC unit of UOP design started operation in 1947. Later, in 1951, the first M. W. Kellogg ortho-flow type of FCC commenced operation. Standard Oil (New Jersey) also created a new type of unit called Model IV by modifying Model II, with the first Model IV unit going into operation in 1952.

More than 50 years have passed since the birth of the first FCC unit. In the meantime, FCC technologies have been significantly advanced with improvements in reactor design, catalyst, and processing system. Today, in the 1990s, the most modern FCC units, as discussed in Section 5.5.4, are in use.

5.5.1 OUTLINE OF THE FCC PROCESS⁽³⁾

5.5.1.1 FCC and RFCC

In the past, vacuum gas oil (VGO) was the main feedstock for an FCC unit. However, more recently (since the late 1980s), residual oils such as atmospheric residue (AR) are feedstocks for FCC units with improvement and development of FCC catalysts and processing systems. In general, an FCC unit which can process residual oils is called a Residue FCC unit (RFCC unit) to define its difference from a conventional FCC unit. However, the basic processing principle of an RFCC unit is the same as that of an FCC unit (conventional FCC unit), although the feedstock types are different. Therefore, here we will define FCC units as including RFCC units and consider a wide range of feedstocks including residual oils.

5.5.1.2 FCC Process Principle and Flow Scheme

Figure 5.63 shows the general configuration of the latest FCC process with reaction mechanism, heat balance, and unit system flow.

The FCC unit consists of two major sections: one is the reaction section (feed oil catalytic cracking/catalyst regeneration) and the other is the work-up section (reactor effluent products' separation treatment). These two major sections are comprised of five process sections: (1) catalytic cracking/regeneration section; (2) regenerator flue gas power recovery/heat recovery section; (3) main fractionation section; (4) gas recovery section; and (5) dry gas, LPG and gasoline treatment section.

(1) Catalytic cracking/regeneration section

Feedstock contact with the circulating high-temperature solid catalysts with an average particle size of $60\,\mu m$ at the bottom of a reactor called a riser reactor, and after quick vaporization, the catalytic cracking reaction is achieved within several seconds during an upward flow in the riser reactor. The reaction

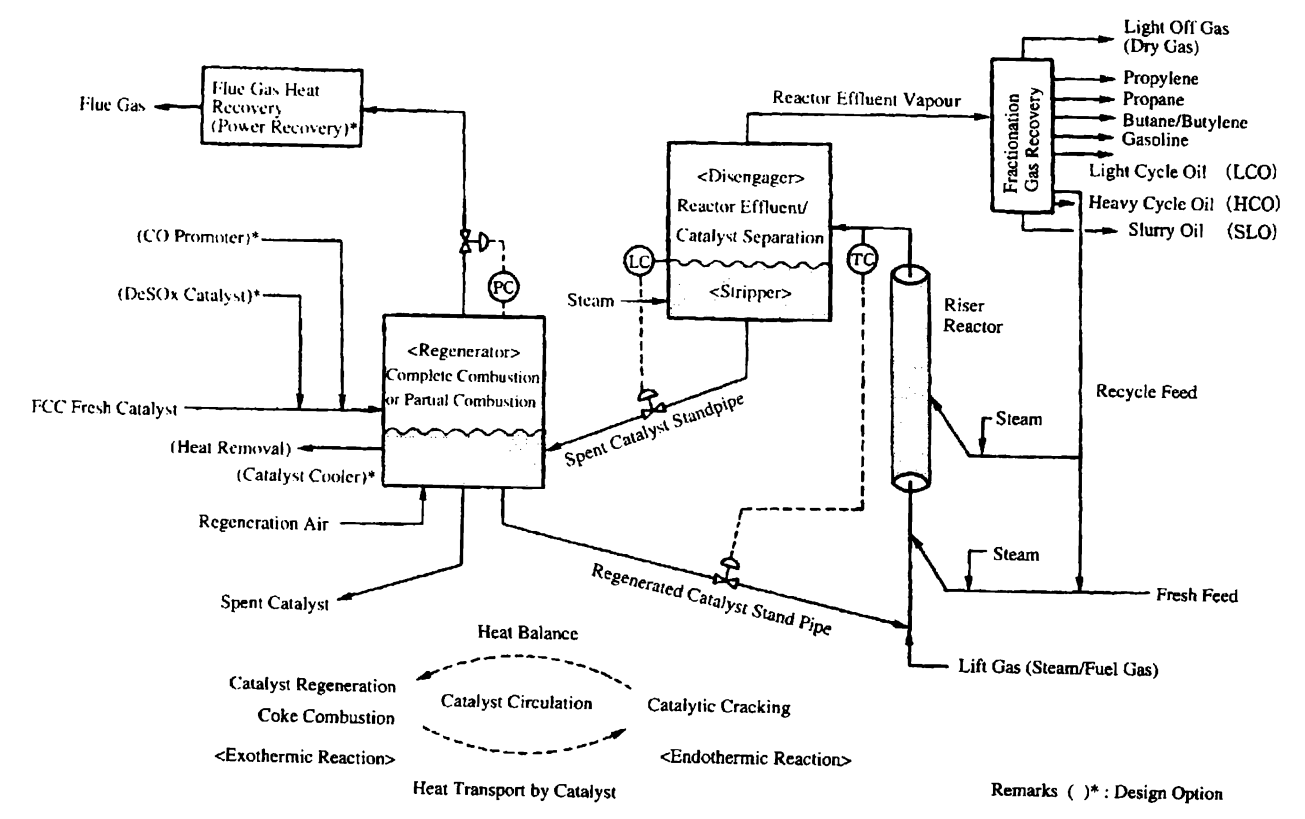


Figure 5.63 Configuration of fluid catalytic cracking (FCC) process⁽³⁾.

temperature is in the range 490-540 °C. Cracking reactions are described in detail in Sections 5.5.2 and 5.5.3.

Coke (composed of C, H, S) produced in the cracking reaction is burned off in the regenerator, and then the catalyst is regenerated. Coke contains hydrogen at 5–8 wt%, and the balance is almost all carbon. When coke is burnt, the catalyst bed temperature is increased due to the great heat generated. This regenerated hot catalyst can supply the heat needed for feed oil vaporization and the catalytic cracking reaction (endothermic reaction). The regeneration temperature is in the range 650–780 °C. The overall equation for the coke-burning reaction in the regenerator is expressed by the following six equations.

$$C + O_2 \rightarrow CO_2$$
 $2H + 1/2 O_2 \rightarrow H_2O$
 $C + 1/2 O_2 \rightarrow CO$ $S + O_2 \rightarrow SO_2$
 $CO + 1/2 O_2 \rightarrow CO_2$ $SO_2 + 1/2 O_2 \rightarrow SO_3$

In the regenerator, coke is burnt by partial combustion or complete combustion. In the partial combustion mode, flue gas containing CO is withdrawn from the regenerator overhead, and then CO in the flue gas is burnt to CO_2 in the downstream CO boiler. On the other hand, in the complete combustion mode, the flue gas contains CO at less than 0.05 vol%.

As an option, a specific catalyst which has the function of SO_x removal (MeO:DeSO_x catalyst) will be injected into the regenerator. In this case, the reaction for SO_x removal is as follows (Me stands for a basic metal).

$$MeO + SO_3 \rightarrow MeSO_4$$
 (regenerator)
 $MeSO_4 + 4H_2 \rightarrow MeO + H_2S + 3H_2O$ (reactor)

so when SO_x in the regenerator is changed to $MeSO_4$ by oxidation reaction, then this $MeSO_4$, contained in the regenerated catalyst, is sent to the reactor, where it is converted to H_2S by reduction (reaction). This converted H_2S is recovered as elementary sulphur in the downstream refining process unit.

The catalyst is fluidized in both the reactor and regenerator, and is circulated continuously between these vessels through stand-pipes like a liquid handled with pressure balance. The mechanism of catalyst circulation is described in detail in Section 5.5.3. The flow rate of the catalyst circulating from the regenerator is adjusted to keep the reaction temperature constant (reaction heat is supplied by the circulating hot catalyst). The catalyst circulation rate is estimated at about 20 t/min for a 30 000 BPSD FCC unit, although this depends on feedstock properties and reaction conditions. This flow rate means that 1200 t/h, a large amount of catalyst, is circulating in the reaction equipment.

In order to keep FCC catalyst activity constant, several tons of the equilibrium catalyst are withdrawn from the regenerator; on the other hand, almost the same quantity of fresh catalyst is introduced into the regenerator. Configurations of the reactor and regenerator and the internal configuration of the reaction equipment are different, in line with each process licenser's design. Details of their design features are discussed in Sections 5.5.3 and 5.5.4.

(2) Regenerator flue gas power recovery and heat recovery

Reactions for catalytic cracking and catalyst regeneration are performed at a higher temperature, and pressure for these reactions is relatively low (reactor: 0.2–0.25 MPa; regenerator: 0.25–0.3 MPa).

The power recovery system has recently been applied to a modern FCC unit in many cases to recover energy from the regenerator flue gas.

(3) Main fractionation and (4) Gas recovery

Reactor effluent vapour withdrawn from the reactor top is sent to the main fractionation and gas recovery sections, where it is separated into dry gas, C₃ and C₄ LPG, gasoline, cracked gas oil, and cracked residue.

(5) Dry gas, LPG and gasoline treatment

Dry gas (C_2 and lighter gas) will contain H_2S produced by the cracking reaction as well as other impurities such as N_2 , CO_2 , O_2 , CO, which are entrained by the circulating catalyst, although in small quantities. LPG will contain H_2S and mercaptan impurities. H_2S in dry gas and LPG streams are removed by an amine solution with a washing operation in an amine treatment unit, and the mercaptans in the LPG stream are removed by a caustic soda solution (NaOH solution) with a washing operation in a caustic treatment unit.

5.5.1.3 Feedstock and Products

5.5.1.3.1 Feedstock

In the past, vacuum gas oil (VGO) was the main feedstock for an FCC unit. However, as already described, heavier residual oil has been considered a feedstock for an FCC unit since the late 1980s, but only residual oil feedstocks, which can be processed economically, are actually considered to be suitable feedstocks.

In other words, the preferred feedstock can be cracked with no difficulty from the standpoint of process performance in terms of coke yield, catalyst consumption and utility consumption, while obtaining the desired product yields. Representative feedstocks and their properties are shown in Table 5.12. In general, most feedstocks have impurities which will affect FCC operation performance. Therefore, the feedstocks are evaluated on the basis of their

Table 5.12 Feedsto	ock properties	of FCC unit
--------------------	----------------	-------------

	Middle East desulphurized vacuum gas oil	South East atmospheric residue
Specific gravity (15/4 °C)	0.8956	0.8890
API°	26.3	27.5
Gas oil fraction (GO) [wt%] < boiling point 343 °C ⁻ >	7.0	4.0
VGO fraction (VGO) [wt%] < boiling point 343-538 °C ⁻ >	88.5	52.5
Vacuum residue fraction (VR) [wt%] < boiling point 538 °C ⁺ >	4.5	43.5
Carbon residue (CCR) [wt%]	0.2	4.2
Sulphur [wt%]	0.4	0.11
Nitrogen [wt%]	0.064	0.19
Metals [wt ppm]		
Nickel (Ni)	0.26	17.0
Vanadium (V)	0.15	0.5

impurities. How these impurities can affect FCC performance is discussed below.

(1) Sulphur

Sulphur itself is not harmful to FCC cracking reaction performance. However, sulphur in a feedstock will be distributed into the cracked products. When sulphur content is high in the feedstock, it means the sulphur will be high in the gasoline product. Sulphur distributed into coke will be atmospherically disposed of as SO_x contained in flue gas from the regenerator. Therefore, recent hydrotreatment of FCC feedstocks is usually carried out not only to reduce SO_x emission in the flue gas and sulphur in the gasoline product, but also to improve the gasoline product yield.

(2) Conradson Carbon Residue (CCR)

Heavier feedstocks contain aromatics which have very high boiling-point fractions and can easily turn into coke. CCR is used as the index for this aromatic content in feedstock. In the case of a straight-run VGO fraction, a maximum of 0.5 wt% CCR will be present when fractionation performance is done well. However, residual oils will contain CCR in a range of 5–10 wt%. When the CCR content in feedstock is high, coke yield will be increased. This means more air for regeneration is required. That, in turn, will cause some difficulty in heat balance between the reactor and regenerator sections.

In order to cope with this higher coke yield, catalyst performance for lower coke yield has been much improved recently, and equipment design has also

been much improved, with a catalyst cooler put into practical use to remove excess heat in the regenerator. Furthermore, two-stage regeneration technology has been adopted for heat balance for the regenerator.

Therefore, a certain amount of CCR can be tolerated in feedstock. However, pretreatment (such as hydrotreating, thermal cracking, and solvent deasphalting) will be required when the CCR content is above 10 wt%.

(3) Heavy metals (metals)

When heavy metals such nickel (Ni) and vanadium (V) compounds are contained in a feedstock, they will accumulate on a circulating catalyst. VGO will contain only 1–2 ppm when fractionation performance goes well, but the residual oil will sometimes contain several tens of ppm wt depending on the type of feedstock.

Nickel and vanadium will have a negative effect on catalyst activity and selectivity as described in Section 5.5.3.

Therefore, these heavy metals will cause a higher catalyst consumption in an FCC unit. In general, when both sulphur and CCR content is high in a feed-stock, the heavy metal content will likewise be high. The same pretreatment applied for sulphur and CCR removal will also be effective for metal removal.

(4) Nitrogen

An FCC catalyst has a certain acidity. Nitrogen, especially basic nitrogen, will neutralize this acidity, resulting in catalyst deactivation. Hydrotreatment as described above is effective for nitrogen removal.

(5) Sodium (Na)

Residual oil feedstock may contain a certain amount of sodium (Na) depending on the feedstock type. Na is a basic material and will neutralize the acid in the catalyst as basic nitrogen does, causing catalyst deactivation. Therefore, the Na content must be kept below a certain limit.

5.5.1.3.2 Products

As the result of a catalytic cracking reaction, cracked effluent vapour, including H_2S , methane and other light cracked gases, is withdrawn from the reactor top. This vapour contains small amounts of inert gases entrained in the circulating catalyst from the regenerator. The following products are obtained by distillation and treatment processes.

- (1) Dry gas (ethane and lighter gas): used for fuel gas.
- (2) C₃ LPG (propylene and propane mixture): further separated into propylene and propane depending on usage.
- (3) C₄ LPG (butene and butane mixture): used for fuel LPG, and otherwise used for feedstocks for MTBE and alkylate production. These will finally contribute to more gasoline production and increase the gasoline octane number.

- (4) Gasoline: used as a gasoline blending component, it shows a relatively lower boiling point among gasoline blending components, and has a high octane number. The motor octane number (MON) is relatively lower than the research octane number (RON), since many olefin compounds are present.
- (5) Cracked gas oil (LCO: Light Cycle Oil): used for blending components for diesel oil and fuel oil. However, in Japan, this is mainly used for A fuel oil due to its lower cetane index. LCO has sometimes been used recently as a diesel blending component after hydrotreatment.
- (6) Cracked residues (HCO/SLO: Heavy Cycle Oil/Slurry Oil): used as fuel oil blending components.

Figure 5.64 shows reaction yields of products vs. conversion level for two kinds of feedstocks. Conversion level and reaction conditions (reaction temperature, Cat./Oil ratio, etc.) to obtain the desired product yield pattern are discussed in Section 5.5.3.

5.5.2 BASIC THEORY OF FLUID CATALYTIC CRACKING

5.5.2.1 Catalytic Cracking Reaction⁽⁵⁻⁷⁾

The catalytic cracking reaction has been investigated for a long time and interpreted as a reaction with intermediates of carbenium ions which are produced on the acid sites of a catalyst surface.

The main reaction schemes of catalytic cracking are considered to progress with the following reaction mechanism.

(1) Initiation

$$R_1 - CH = CH - R_2 + HZ \rightarrow R_1 - CH_2 - CH^+ - R_2 + Z^-$$
Brønsted site Carbenium ion

or

$$R_1 - CH_2 - CH_2 - R_2 + L^+ \rightarrow R_1 - CH_2 - CH^+ - R_2 + HL$$

Lewis site Carbenium ion

(2) Proton exchange

$$R_1 - CH_2 - CH^+ - R_2 + R_3 - CH_2 - CH_2 - R_4$$

 $\rightarrow R_1 - CH_2 - CH_2 - R_2 + R_3 - CH_2 - CH^+ - R_4$

(3) Cracking

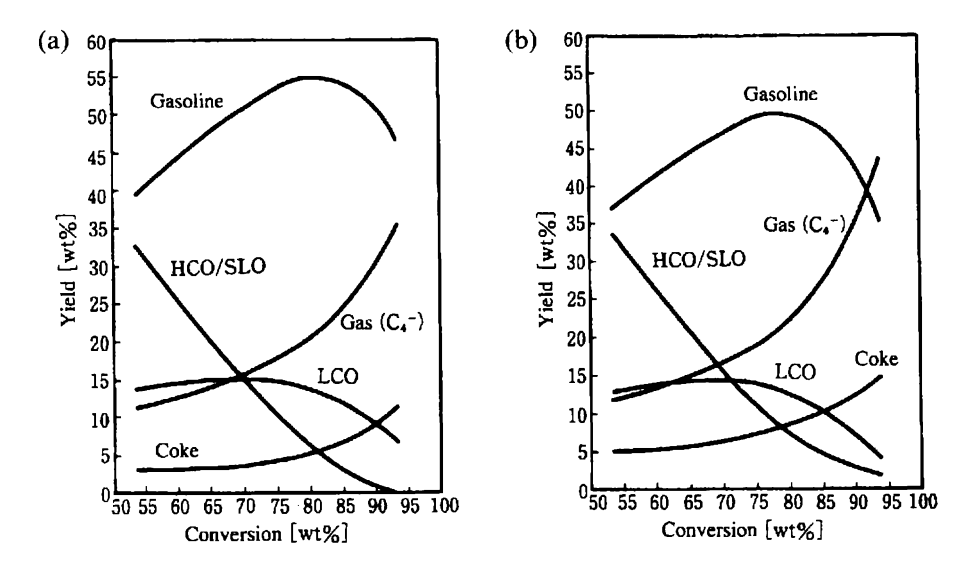


Figure 5.64 Conversion and reaction yield pattern of FCC unit. (a) Middle east. Desulphurized vacuum gas oil (HT VGO). (b) South east. Atmospheric residue (SR-AR).

This cracking mechanism is called β scission, because the scission of the carbon bond is brought about in the β position to the carbonium ion. The carbonium ion R_3^+ produced brings about the following reactions of (2) and (3).

An alternative reaction mechanism is proposed for strong acid sites of a catalyst.

(1') Initiation

$$R_1 - CH_2 - CH_2 - R_2 + HZ \rightarrow R_1 - CH_2 - CH_3^+ - R_2 + Z^-$$

Brønsted site Carbonium ion

(2') Production of carbenium ion

$$R_1 - CH_2 - CH_3^+ - R_2 \rightarrow R_1 - CH_2 - CH_1^+ - R_2 + H_2$$

(3') Cracking

$$R_1 - CH_2 - CH_3^+ - R_2 \rightarrow R_1^+ + CH_3 - CH_2 - R_2$$

The carbenium ions of $R_1 - CH_2 - CH^+ - R_2$ and R_1^+ consecutively bring about reactions (2) and (3) described above.

Carbenium ions make products rich in variety with other reactions as follows.

(4) Isomerization

$$R-CH_2-CH_2-CH^+-CH_3 \longrightarrow R-CH_2-C^+-CH_3$$

The FCC product distribution with high yields of isoparaffins and isoolefins results from isomerization on an acidic catalyst, but isomerization is not expected in a pyrolytic reaction.

$$CH_3-CH^+-(CH_2)_3-CH=CH-CH_3$$

$$CH_3$$

$$CH_3$$

$$CH_2$$

$$CH_3$$

$$CH_4$$

$$CH_4$$

$$CH_2$$

$$CH_2$$

(5) Cyclization

The following hydrogen transfer reaction is also important to explain the results of high yields of aromatic products.

(6) Hydrogen transfer

$$3C_nH_{2n} + C_mH_{2m} \rightarrow 3C_nH_{2n+2} + C_mH_{2m-6}$$

Olefins Naphthenes Paraffins Aromatics

Reactions (1)–(3) and (1')–(3') are the main reaction schemes in catalytic reactions to determine the cracking rate or yields of cracked products such as gasoline. On the other hand, reactions (4)–(6) affect the properties of cracked products such as the octane number of gasoline or the cetane number of cracked gas oil. Discussion is detailed in the next section on the catalyst, because those aspects are closely related to catalyst performance.

5.5.2.2 Catalytic Cracking Catalyst⁽⁸⁾

Amorphous silica-alumina catalysts were employed in the process when FCC was developed for the first time. The process required a large-volume reactor or a long residence time, because this catalyst has a low cracking activity with low acidity. Cracking activity was tremendously improved with zeolite employed as a catalyst in the 1960s. The cracking was found to be completed in the riser tube employed as a catalyst transfer line. The FCC process was then developed from a dense-phase bed reactor process into a lean-phase riser reactor process.

Requirements of catalyst performance cover a wide range of functions.

5.5.2.2.1 Hydrothermal Stability at Elevated Temperature

The activity of a cracking catalyst can be totally fouled in a reaction by the adsorption of condensed aromatics (coke) on its surface. Catalyst activity recovers by burning off the coke in the regenerator. On the other hand, the steam produced in this procedure gradually deactivates the catalyst by removing Al from crystal sites to render the zeolite catalyst amorphous. In general Y-zeolite is the Na type as is. It is weak in catalytic activity and hydrothermal stability. Sodium contained in Y-zeolite is removed or ion-exchanged by elements of the rare earth group (RE) to improve its characteristics as a catalyst. Recently, the USY (Ultra-Stable Y) catalyst is in common use. Sodium is firstly ion-exchanged by ammonia and Al is removed to an extent to give it hydrothermal stability. The USY catalyst, which is further ion-exchanged partially to RE, is much appreciated in the process because of its improved stability.

5.5.2.2.2 Higher Octane Requirement

Gasoline octane numbers are defined as RON in a low-speed condition and MON in high speed for antiknock indexes. The representative octane numbers of gasoline components are tabulated in Table 5.13. FCC gasoline is high in olefin content, as assumed from the cracking path defined by Eq (3), and the octane number depends mostly on the olefin content. This indicates that hydrogen transfer defined by Eq (6) should be suppressed in reactions to avoid olefin saturation. RE-zeolite is apt to accelerate hydrogen transfer, although it has a higher hydrothermal stability. It results in a lower octane number and a higher coke output. The USY catalyst is preferable from that standpoint.

N-paraffins in a gasoline fraction are not favourable components, because they are so low in octane number. The ZSM-5 type of zeolite is commonly used to selectively remove those n-paraffins from gasoline by cracking them into LPG fractions. The ZSM-5 type of zeolite has a smaller pore size than Y-zeolite. It allows n-paraffins to selectively diffuse into its pores and has a higher cracking activity.

More yields of isoparaffins and isoolefins are expected by the reaction defined by equation (4), isomerization of n-paraffins, because the tertiary carbenium ion is the most stable one. One report shows that reduction of non-frame aluminium is favourable to isomerization.

5.5.2.2.3 Metal Resistance

Nickel and vanadium compounds accumulate on the catalyst while the catalyst is circulated in use, because they are contained in FCC feedstocks such as vacuum gas oil or residual oil. Nickel does not deactivate the cracking activity of a cracking catalyst, but has a dehydrogenation activity. More hydrogen

Table 5.13 Octane numbers of representative gasoline components⁽⁷⁾

Hydrocarbon	Carbon number	Blending octane numbers RON MON		
Paraffins				
n-Butane	4	113	114	
n-Pentane	5	62	67	
2-Methylbutane	5	99	104	
n-Hexane	6	19	22	
2,2-Dimethylbutane	6	89	97	
n-Heptane	7	0	0	
2,2,3-Trimethylbutane	7	113	113	
2,2,4-Trimethylpentane	8	100	100	
Olefins				
1-Pentene	5	152	135	
2-Methyl-2-butene	5	176	141	
4-Methyl-2-butene	6	130	128	
2,2,4-Trimethyl-1-pentene	8	164	153	
Aromatics				
Benzene	6	99	91	
Toluene	7	124	112	
o-Xylene	8	120	103	

Octane number: octane number of pure hydrocarbons

Blending octane number: numbers for estimating octane number after blending

production affects the performance of the gas compressor installed downstream in the FCC process. Sometimes the procedure of nickel passivation is employed with antimony or bismuth compounds added to turn accumulated nickel into a nickel alloy in order to reduce nickel's dehydrogenation activity.

Accumulated vanadium deactivates zeolite activity by destroying its crystal structure through the removal of oxygen from zeolite. Zeolite steadily loses its activity according to the amount of vanadium accumulation on the catalyst. Various ideas on how to trap vanadium compounds in the matrix portion of the catalyst have been proposed to suppress vanadium compounds to diffuse into zeolite micropores.

The FCC process is recently defined as a residual oil upgrading process, and the limit of total metal accumulation on an equilibrium catalyst is tolerable up to 10 000 ppm, improved from the several thousands ppm in conventional FCC processes. A more metal-resistant catalyst is required to reduce catalyst consumption in the instance of more inferior feedstocks.

5.5.2.2.4 Bottom Conversion Characteristics

Residual oil has a huge molecular size as shown in Figure 5.65 as an average structural model. It is not allowed to diffuse into the micropores of Y-zeolite as

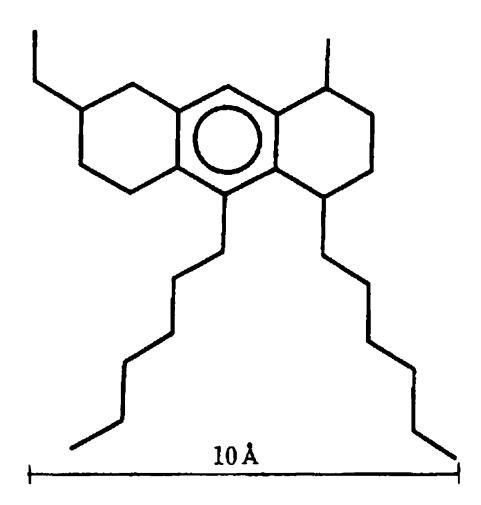


Figure 5.65 Hypothetical chemical structure model of hydrotreated residual oil⁽⁹⁾.

shown in the structural model of Figure 5.66. The residual oil should be cracked in advanced in the portion of the catalyst that has relatively large pores. The precracking role is expected in the matrix portion of the catalyst or the mesopores of zeolite created by the dealuminating process (such pores as B, C; pore C is too big to have a sufficient surface area, so pore B, with the proper size for precracking residual oils, is required). This suppresses the undesirable pyrolysis reaction of residual oils and leads to less coke make and more gasoline yield⁽⁹⁾.

On the contrary, less surface area on the matrix portion of the catalyst is required to reduce coke make in cracking vacuum gas oils with a small molecular size.

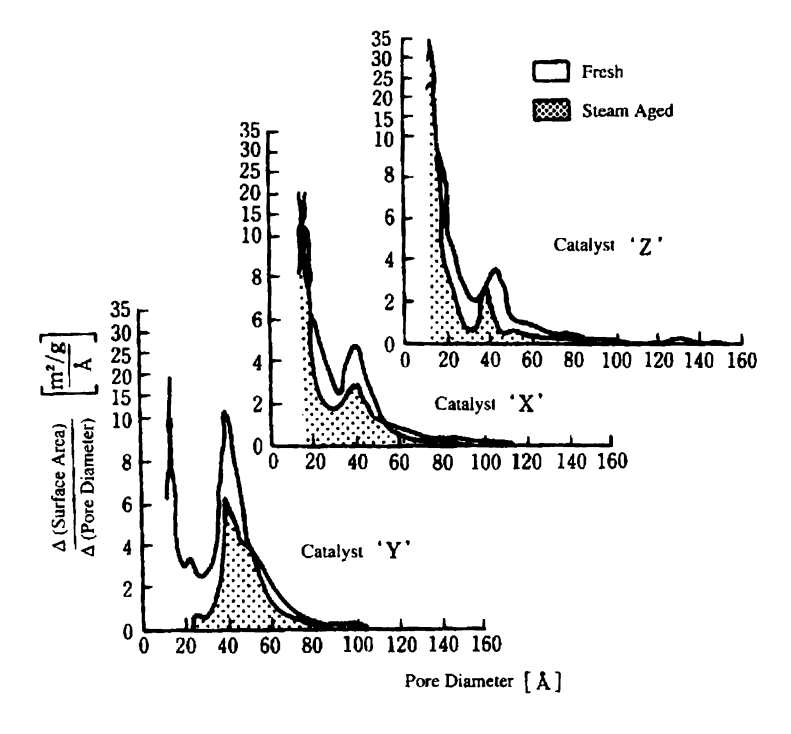
As discussed here, choice can be very flexible, but it is still important to choose FCC catalysts with properties suited to the varieties of feedstocks in a process.

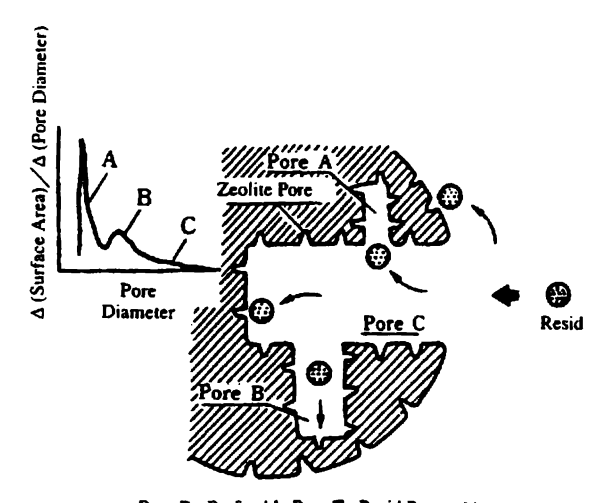
5.5.2.2.5 Coke-burning Ability

An oxygenation catalyst with a small amount of precious metal (Pt), defined as a CO promoter, is added to accelerate oxygenation of carbon monoxide and to remove coke on the catalyst efficiently by burning it off in the regenerator.

5.5.2.2.6 Desulphurization Ability

The sulphur in coke, which derives from sulphur compounds in feedstocks, is released as sulphur dioxide (SO₂) from the regenerator after it is oxygenated.





Pore B: Preferable Pore To Resid Precracking 9)

Figure 5.66 Micro-pore distribution of FCC catalyst including matrix portion⁽⁹⁾.

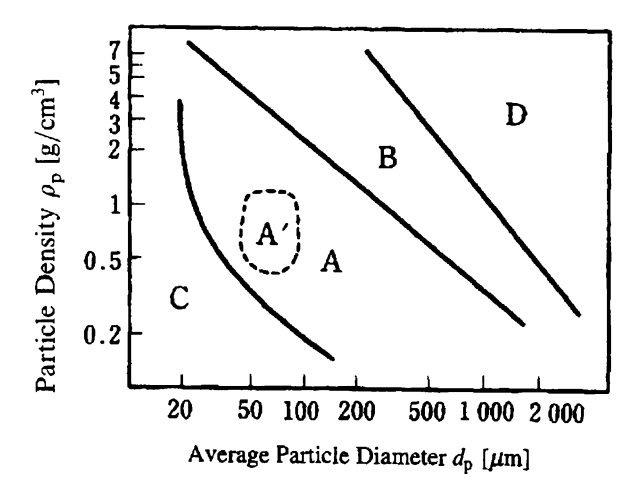


Figure 5.67 The Geldart classification of FCC catalyst particles(10,11).

When a catalyst containing basic metals is employed in the process, sulphur dioxide, as discussed in 5.5.1.2, is trapped on the catalyst and taken into the reaction system after it is further oxygenated to metal sulphates. The metal sulphates are then easily reduced to hydrogen sulphide, which can be recovered in the downstream portion of the process.

5.5.2.2.7 Fluidization Characteristics(10,11)

The FCC catalyst is commonly converted into particles by spray-drying a mixture of ca. 30% zeolite with amorphous silica-alumina. Figure 5.67 shows the Geldart Chart, which classifies particles from group A to D according to particle diameter and density. Catalyst particles should be manufactured in a range of A (or more desirably A') to have suitable fluid characteristics.

Table 5.14 shows the representative properties of FCC catalysts in the market. The average particle diameter falls within a range $67-74 \,\mu\text{m}$. A certain number of particles with relatively small diameters is contained in the distribution of particle diameter to improve fluidity. Higher resistance to attrition loss is also required for long-term circulating use.

5.5.3 THEORETICAL DISCUSSION OF FCC REACTOR DESIGN

5.5.3.1 Circulating Fluidized Bed Model⁽¹²⁻¹⁵⁾

Fluidized beds are defined by the flow regimes shown in Figure 5.68 according to their condition of fluidity. Such fluidized conditions are predicted from their solid and gas properties and their linear gas velocity as discussed in Figure 4.32 (see 4.3.2.4.4).

Table 5.14 FCC catalyst properties

		A-manufacturer		B-manufacturer (1)		B-manufacturer (2)	
		Fresh catalyst	Equilibrium catalyst	Fresh catalyst	Equilibrium catalyst	Fresh catalyst	Equilibrium catalyst
Chemical composi	tions						
Al ₂ O ₃	[wt%]	38.3	35.4	38.3	39.0	25.8	25.9
$R\tilde{E}_2\tilde{O}_3$	[wt%]	0.4	0.5	1.7	2.0	1.0	0.9
C	[wt%]		0.12		0.06		0.04
Na	[wt%]	0.32	0.24	0.23	0.18	0.20	0.23
Fe	[wt%]	0.25	0.43			_	
V	[ppm]		3268		117		1890
Ni	[ppm]		2582		315		1610
Cu	[ppm]		20				_
Physical properties							
Surface area	$[m^2g^{-1}]$	252	168	224	140	310	162
Bulk density	$[g cm^{-3}]$	0.86	0.88	0.77	0.87	0.76	0.82
Particle diamete					• • • • • • • • • • • • • • • • • • • •		****
$20 \mu \mathrm{m} >$	[wt%]	2	1	2	0	1	0
$40 \mu \mathrm{m} >$	[wt%]	17	10	14	7	17	2
$60 \mu \mathrm{m} >$	[wt%]	36		_			
$80 \mu \mathrm{m} >$	[wt%]	60	63	55	58	65	61
$105 \mu \mathrm{m} >$	[wt%]	_		76	81	86	88
Average diamete		69	70	74	79	67	74
Pore volume	[ml g ⁻¹]		. •	0.244	· <u>-</u>		
Attrition index of catalyst manu	depending on	0.33		< 5	_	< 5	_

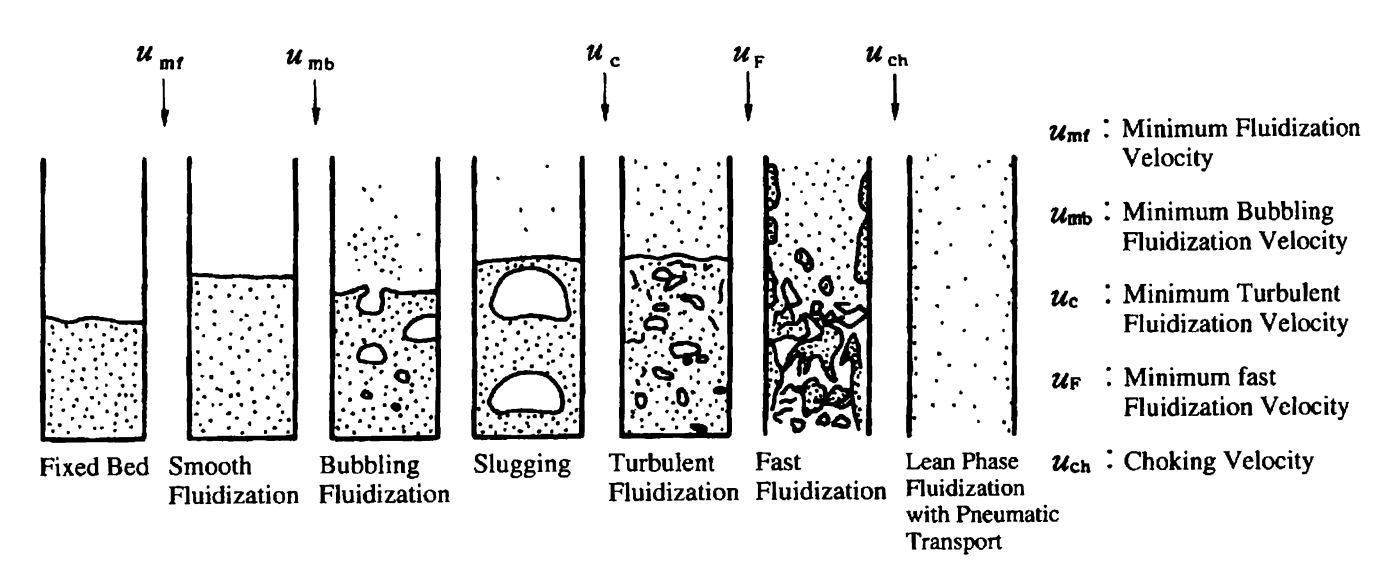


Figure 5.68 Classification of fluidization forms⁽¹²⁾.

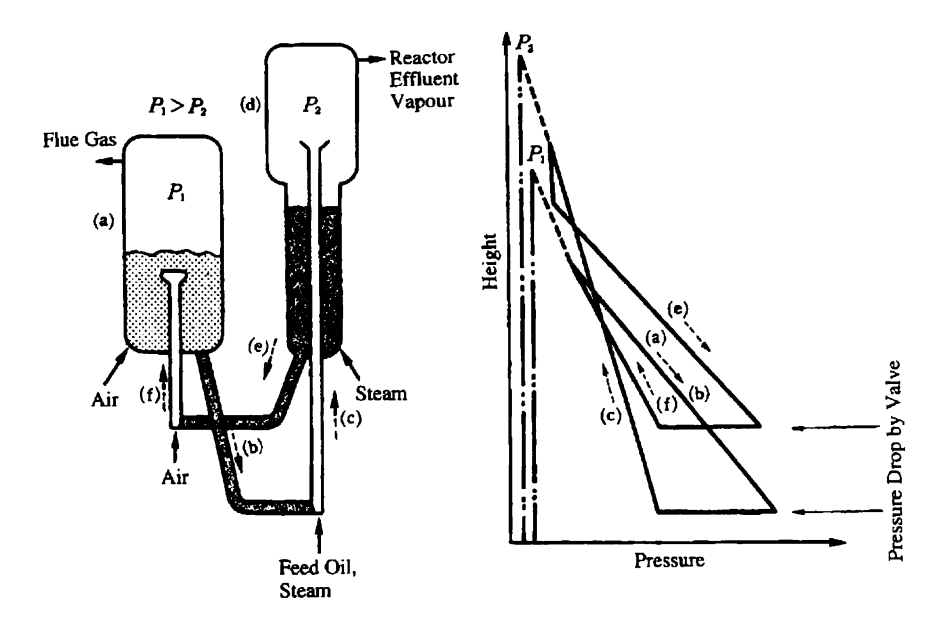


Figure 5.69 Pressure balance in FCC reactor system (side by side type).

Figures 5.69 and 5.70 show simplified sketches of the main equipment in two of the most representative types of FCC units, where different fluidized conditions are observed in different zones.

Turbulent fluidization is employed in the regenerator (a) to attain a uniform burning temperature in the bed. This is a single-stage, back-mixed reactor if defined by the CSTR Model.

The riser section as a reactor (c) has a lean-phase fluidization condition for pneumatic transport. The flow is almost a plug flow with the least degree of back mixing. Residence time is several seconds. The ratio of gas to solid velocity (gas rising velocity/solid rising velocity) is almost 1. This means that the concentration of catalyst particles in the riser is determined by the catalyst/oil ratio. The contact efficiency of gas with particles is nearly 100%.

The catalyst is transported from regenerator to riser by a pressure gradient. The transportation line (b) is kept in a condition of bubbling fluidization to attain smooth transport of the catalyst.

In the stripper (e), steam is injected from the bottom to vaporize and recover heavy oils and reduce coke make, which is adsorbed on the catalyst surface. The fluidized condition is one of bubbling fluidization. Sometimes a multistage counter-current contactor is employed.

Since the total pressure of a reactor system represented by the section of solid vapour separation (d) is lower than that of a regenerator (a), the pressure

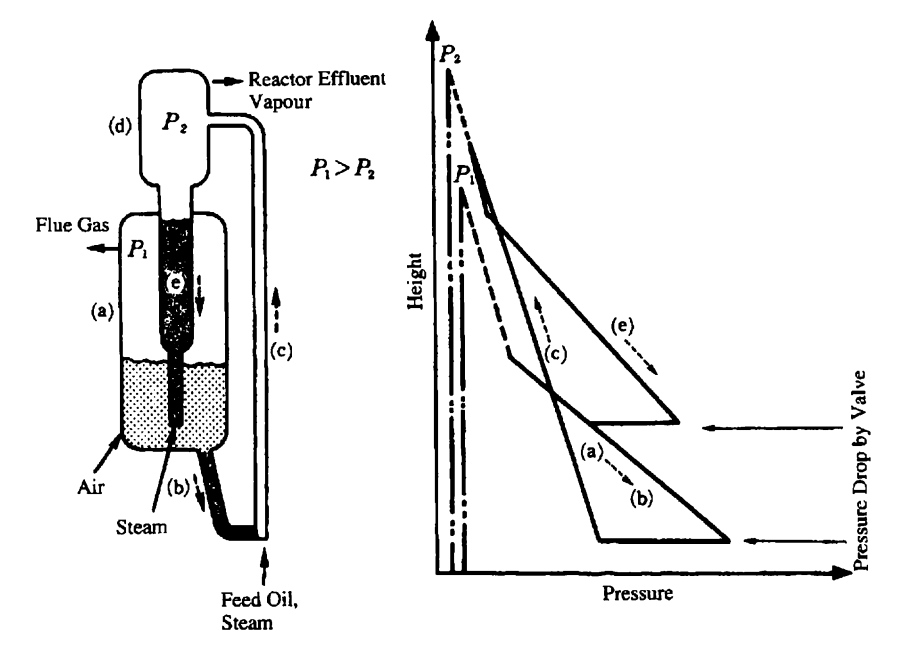


Figure 5.70 Pressure balance in FCC reactor system (stack type)⁽¹⁴⁾.

of the lift line (f) bottom in the case of an FCC units shown in Figure 5.69 (side-by-side type) must be lower than that of the stripper (e) bottom by keeping the lift line in a fast-fluidized bed condition with a lower catalyst density. This system makes it possible to transport the catalyst from a lower to higher pressure section. Such a lift line is not needed in the case of the FCC unit shown in Figure 5.70 (stack type), where the stripper itself is located in a position higher than the regenerator.

As is clear in the above discussion, the catalyst circulation depends on the pressure balances among each of the sections in the unit. For any circulating fluidized bed process, there is a section at a certain height with a dense phase formed in the bed like the stripper section (e) already described, where the particles are transported downward by gravity from a lower to higher pressure section against a pressure gradient. The pressure profile is shown in Figure 5.69 and 5.70 along each section of the FCC unit. The pressure balances are predicted basically from the static pressure, which is determined by a bed density and its height, and pressure drops in the section where particles are transported with a high velocity in a line like that in the riser tube. In practical design, the higher static pressure is given than that required in the higher pressure section and the flow rate of catalyst particles is adjusted by controlling a valve such as a slide valve.

The bed density required to calculate pressure balance is predicted from the particle concentration and void fraction of the bed. The pressure drops derived from the flow along the riser can be approximately predicted as a two-phase flow of particles and gas⁽¹²⁾.

An example of a procedure for estimating the void fraction of the bed is shown below.

(1) Volume fraction of bubbles in a bubbling fluidized bed The volume fraction of bubbles is calculated with the assumption of a twophase theory that bubbles are formed in the amount of gas flow above the minimum gas flow required for fluidization (minimum fluidizing velocity).

$$\varepsilon_{\rm b} = (u_{\rm O} - u_{\rm mf})/u_{\rm b}$$

where

 ε_b : gas bubbles hold-up u_0 : superficial gas velocity u_b : bubble rising velocity $u_{\rm mf}$: minimum fluidizing velocity

(2) Void fraction of lean-phase fluidization with pneumatic transport The gas and particle slip velocity is regarded as equivalent to the terminal

velocity of the particle.

 $u_{\rm sl} = u_{\rm O}/\varepsilon - v_{\rm O}/(1-\varepsilon) = u_{\rm t}$

ε: void fraction

 $v_{\rm O}$: superficial velocity of particle

u_{sl}: slip velocityu_t: terminal velocity

In a simpler procedure, the velocities of gas and particles can be assumed to be equivalent.

$$u_{\rm O}/\varepsilon = v_{\rm O}/(1-\varepsilon)$$

Fluidization technology theory seems to lag behind practical experience because of its complexity. Many theories or equations related to states of fluidization have been proposed, but most are experimental equations and are valid only in restricted systems. It is recommendable to confirm them in experimental ways under given conditions and with given particles before applying them in practical use.

5.5.3.2 Reaction Engineering Model

A reactor simulation was recently carried out for optimal operation of the FCC process as well as for the basic design of the unit.

A simplified lumping model is commonly employed for the reactor design, because the actual reaction in an FCC process is so complicated and because so many components are involved in the reaction.

5.5.3.2.1 Reaction Model for Catalytic Cracking(17-20)

A lumping model is commonly employed in reaction systems involving many actual components such as petroleum fractions. In the model, hypothetical components are arbitrarily defined, for instance, by the cuts of boiling points. Reaction rates are determined for those concentrations of lumped components. The three-lump model and ten-lump model proposed by V. W. Weekman are famed as catalytic cracking models. Here we discuss the six-lump model developed for catalytic reaction of residual oils.

C_1 : VGO/HCO	vacuum gas oil or heavy recycle oil
	bp. 343-538 °C (650-1000 °F) fraction
C_2 : VR/SLO	vacuum residue or cracked residual oil or slurry oil
- ,	bp. 538 °C ⁺ (1000 °F ⁺) fraction
C_3 :	C_4^- gas
C_4 :	gasoline, C ₅ to bp. 221 °C (430 °F) fraction
C ₅ : LCO	cracked gas oil or light cycle oil, bp. 221-343 °C
-	(430–650 °F) fraction
C ₆ : Coke	

The product distributions in the catalytic cracking of residual oils are obtained as shown in Figure 5.64 of the previous section according to reaction progress. They indicate that catalytic cracking is a representative reaction with both parallel and consecutive reactions. In the reaction model shown in Figure 5.71, cracking of VGO (C_1) and VR (C_2) , which are feedstock fractions, is defined as a second-order reaction and consecutive cracking of cracked products such as LCO (C_5) and gasoline (C_4) is defined as a first-order reaction. The cracking rates of lumped components i and j are defined as $K_iC_i^l$ and $K_jC_j^m$. The probability of producing component i by cracking component j is defined as P_{ji} . The production rate of component i is then described as follows.

$$dC_i/dt = -K_iC_i^l + \sum_i K_j P_{ji}C_j^m$$

Catalyst deactivation by coke deposition on the catalyst is defined as follows as a function of catalyst residence time t_C in the reactor.

$$K' = K \exp(-K_{\rm A}t_{\rm C})$$

Here a degree of catalyst deactivation C_A is defined as the ratio of K' to K.

$$C_{\rm A} = K'/K = \exp(-K_{\rm A}t_{\rm C})$$

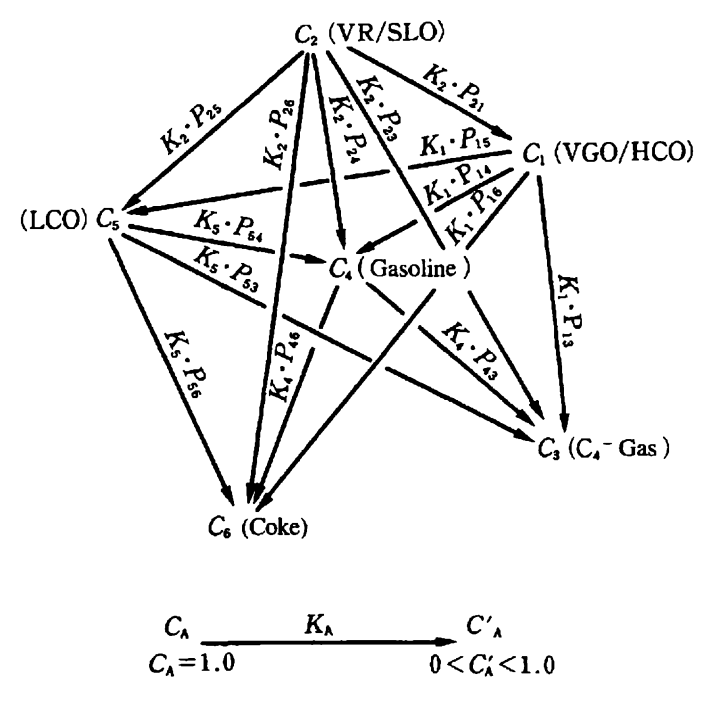


Figure 5.71 FCC reaction mechanism model.

This leads to the following equation of catalyst deactivation rate.

$$dC_A/dt_C = -K_AC_A$$

With the above definition newly employed in the catalyst deactivation model, the handling of catalyst deactivation is easier in a case in which the catalyst has a residence time distribution in the reaction system. If catalyst deactivation defined as $C_{\rm A}$ is considered to be common to all cracking rates, the cracking rate constant is predicted at the arbitrary residence time of the catalyst in the reactor as follows.

$$K_i' = K_i C_A$$

5.5.3.2.2 Reactor Model

Back mixing in an FCC reactor is essentially based on its shape. If the degree of back mixing is large, selectivity to produce gasoline is reduced to some extent and higher yields of coke and gas are obtained. The reactor model should be provided with a function such as one that simulates the reactions affected by

$$U_{\mathsf{R}} = \begin{array}{c} 1 & 2 \\ U_{\mathsf{C}} & & & \\ & &$$

Figure 5.72 Multi-stage CSTR model⁽¹⁷⁾.

back mixing in the reactor. Figure 5.72 shows a multi-stage CSTR model as an example of simulating the reaction with a back-mixing effect in the reactor.

Let a mass flux of feed oil and circulating catalyst be $U_{\rm H}$ and $U_{\rm C}$, respectively. The mass balances of each component and the catalyst activity are described as follows.

$$U_{H}(C_{1f} - C_{1}) = \frac{Z}{n} C_{A}(K_{1}C_{1}^{2} - K_{2}P_{21}C_{2}^{2})$$

$$U_{H}(C_{2f} - C_{2}) = \frac{Z}{n} C_{A}K_{2}C_{2}^{2}$$

$$U_{H}(C_{3f} - C_{3}) = -\frac{Z}{n} C_{A}(K_{1}P_{13}C_{1}^{2} + K_{2}P_{23}C_{2}^{2} + K_{4}P_{43}C_{4} + K_{5}P_{53}C_{5})$$

$$U_{H}(C_{4f} - C_{4}) = \frac{Z}{n} C_{A}\{K_{4}C_{4} - (K_{1}P_{14}C_{1}^{2} + K_{2}P_{24}C_{2}^{2} + K_{5}P_{54}C_{5})\}$$

$$U_{H}(C_{5f} - C_{5}) = \frac{Z}{n} C_{A}\{K_{5}C_{5} - (K_{1}P_{15}C_{1}^{2} + K_{2}P_{25}C_{2}^{2})\}$$

$$U_{H}(C_{6f} - C_{6}) = -\frac{Z}{n} C_{A}(K_{1}P_{16}C_{1}^{2} + K_{2}P_{26}C_{2}^{2} + K_{4}P_{46}C_{4} + K_{5}P_{56}C_{5})$$

$$U_{c}(C_{Af} - C_{A}) = \frac{Z}{n} K_{A}C_{A}$$

The last equation predicts the residual activity of a deactivated catalyst. In this case of a multi-stage CSTR model, the solutions are obtained analytically. WHSV (Weight Hourly Space Velocity) and cat/oil ratio, the most important parameters in the circulating fluidized bed reactor, are represented as follows with the variables used in the previous model.

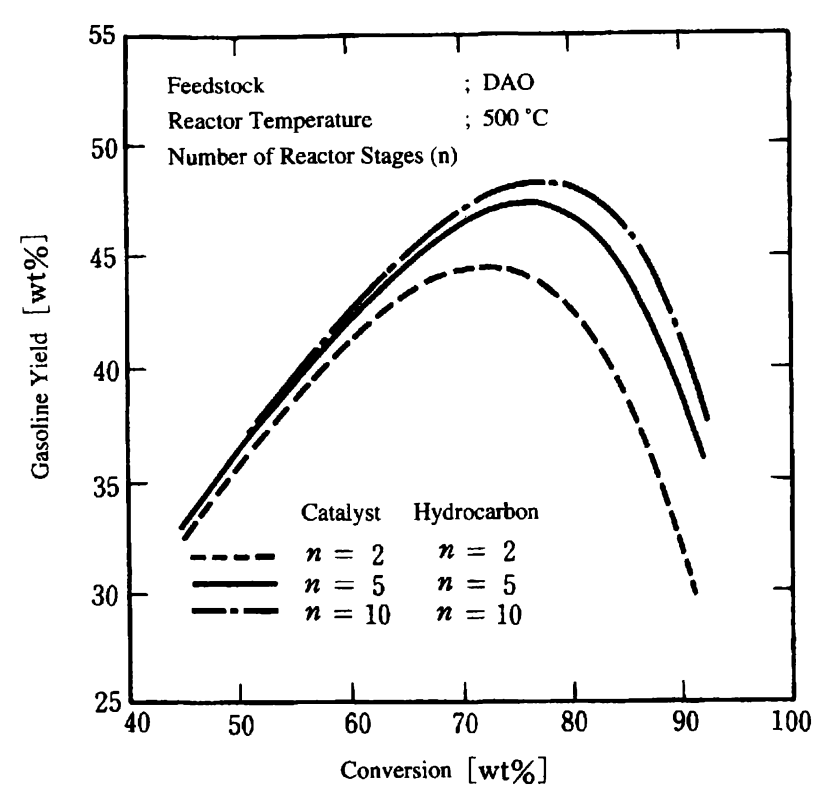


Figure 5.73 Effect of the number of reactor stages on gasoline selectivity⁽¹⁷⁾.

WHSV =
$$U_{\rm H}/Z/\rho_{\rm C}/(1-\varepsilon)$$

cat/oil ratio = $U_{\rm C}/U_{\rm H}$
 $\rho_{\rm C}$: catalyst particle density [kg/m³]

The effect of back mixing on the reactor can be predicted with the reactor model shown in Figure 5.73. Selectivity to produce gasoline is greatly affected by back mixing. The old-fashioned type of FCC process had a dense-phase reactor bed of large volume, but the latest progress in catalyst performance has made it possible to complete cracking in the riser as discussed above. A degree of back mixing in the dense-phase bed reactor of the former process is estimated in two stages at most by the CSTR model, but a modern reactor of the riser type has a much lower degree of back mixing, equivalent to approximately five to ten stages in a CSTR model. It is well understood that the modern FCC process produces a gasoline with a tremendously higher selectivity than that obtained in the old days, owing to processing advancements as well as improvements in cracking catalysts.

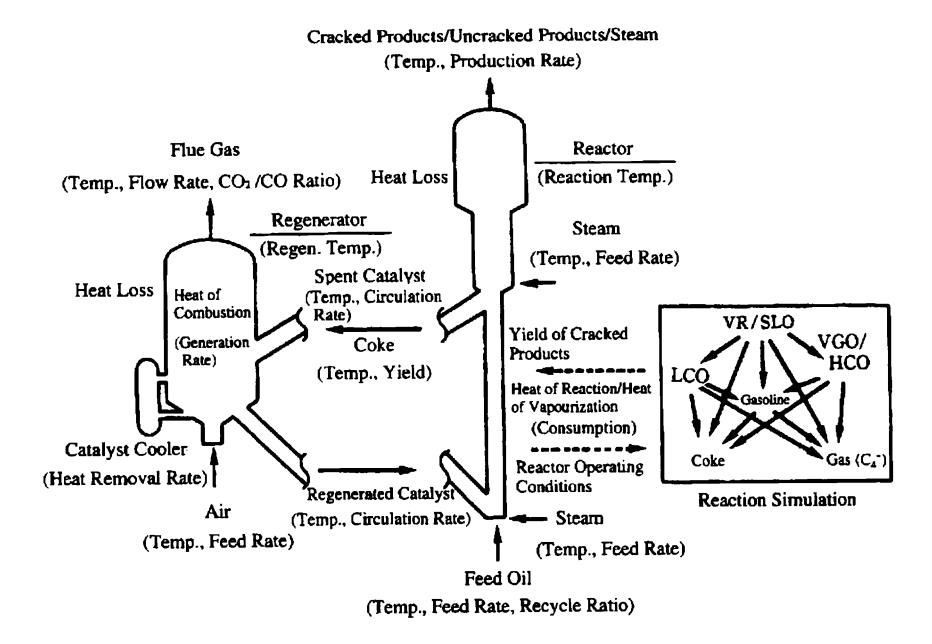


Figure 5.74 Heat balance in FCC unit.

5.5.3.2.3 Simulation Model of the FCC Unit

In the FCC unit, the combustion heat which is generated in the regeneration of coked catalyst is effectively utilized as the reaction heat required for cracking. In the simulation model of the FCC unit, the heat balance calculation is also essential, and is carried out with the circulating catalyst as the heat carrier as illustrated in Figure 5.74.

The example shows how to increase the catalyst circulation rate to raise the reaction temperature according to Figure 5.74. When the catalyst circulation rate is raised, the reaction temperature is raised, with more heat input to the reactor system. The cracking rate is then increased, with more coke deposition on the catalyst. More air feed to the regenerator is needed to remove the increased amount of coke by burning usually while maintaining the CO/CO_2 ratio $(CO/CO_2 = 0)$ is in a case of complete coke combustion). The residual coke on the regenerated catalyst is analysed as the index to sustain a certain degree of catalyst regeneration. When the CO/CO_2 ratio drops, the other operating conditions of the unit must be adjusted, because it means the condition of coke-burning would be shifting to the state of complete combustion with an increase of catalyst temperature in the regenerator exceeding the upper limit. The ways of adjusting (decreasing) the catalyst circulating rate, or of cutting feed oil preheating temperature are actually employed. More steam

generation is an alternative way to do this in a regenerator equipped with a catalyst cooler.

Although catalytic cracking itself is an endothermic reaction, the FCC unit may seem to be an apparently unstable system, because it has combustion in the regenerator section as an exothermic reaction with large heat release. However, with controlled air feed to the regenerator, the unit system will not run away, because the catalyst will not properly regenerate due to more coke deposition in an increased cracking condition. The catalyst will be deactivated by residual coke to a lower conversion rate. The FCC process is thus considered an auto-stable system in itself.

5.5.3.2.4 Effects of Operating Conditions

(1) Reaction temperature and cat/oil ratio

The cat/oil ratio is designed approximately in the range of three to nine. It is closely correlated with reaction temperature, and the effect is complicated when observed in practical operation. As discussed in a previous section, more conversion than expected is obtained when only the cat/oil ratio is increased under a condition in which a certain conversion rate has been attained, because the heat input into the reactor is then increased.

It is necessary to cut the regenerator temperature using a catalyst cooler or to cut a preheat temperature when the cat/oil ratio needs to be increased at the same conversion rate. Under a condition of increased cat/oil ratio, a more favourable reaction is achieved, with lower gas and coke make and improved gasoline selectivity, resulting in more catalytic than pyrolytic reaction in the reactor. There is less catalyst deactivation or less catalyst-coking under a lower residence time for the catalyst in the reactor, and a lower reaction temperature. When a lesser coke yield is observed with a higher cat/oil ratio, more regenerator temperature cutting is expected, and a much higher cat/oil ratio is possible even in a unit without a catalyst cooler.

(2) WHSV, contact time

A reaction is completed in the riser tube reactor in the latest type of FCC unit, and the residence time in the riser is a few seconds. The WHSV, representing the reaction time in a catalytic reaction, is approximately $100 \, h^{-1}$ with a zeolite catalyst employed. The catalyst loses its activity rapidly within a short residence time in the riser. The relationship between WHSV and conversion is not simple in the reaction of an FCC process. Conversion will not increase simply with a decrease in WHSV (increase in residence time of feed hydrocarbon in the reactor) with the cat/oil ratio kept constant because, at the same time, the residence time of catalyst in the reactor is also increased and the catalyst is more deactivated, resulting in lowered average activity. On the contrary, increasing WHSV to add more capacity does not result in a much lower conversion if

cat/oil is kept constant. The FCC process has flexible characteristics, so a conversion does not vary much, even with WHSV changes, under a constant cat/oil condition.

(3) Recycling

Heavy crackates can be recycled to extinction in the FCC process. The yield pattern is then improved by a recycling operation, but coke make is increased. A recycling operation has not been needed recently, because selectivity in gasoline production has been improved by advanced catalyst performance. A recycling operation is carried out only when a light feedstock is employed with a small amount of CCR, with more coke make required to keep the unit heatbalanced.

(4) Pressure

A lower pressure is preferable in catalytic cracking. In practical design the system pressure of a reactor section is determined by the cumulative pressure drops required in the work-up sections (separation and refining sections).

Hydrocarbon partial pressure in the reactor section: all of the hydrocarbon, accompanied by the catalyst, which is sent to the regenerator from the reactor section is called coke for convenience. However, most of this so called coke is still oil consisting of polyaromatics with a relatively high boiling point. In the RFCC, where designing is done for residual oil feed with a high potential of coke make, designs to reduce coke make are employed by reducing total pressure in the reactor section or reducing hydrocarbon partial pressure by injecting steam to vaporize hydrocarbons with a high boiling point in the reactor section and then recover them as a liquid product.

Steam partial pressure in the regenerator section: steam is generated during coke combustion as well as injected into the regenerator from outside for bed fluidization. A high steam partial pressure in the regenerator results in destruction of the zeolite structure of the catalyst at an elevated temperature. This in turn results in more catalyst consumption to maintain activity. It is a much-appreciated operation to strip out high boiling point hydrocarbons while keeping high hydrogen content in the reactor section to reduce steam partial pressure in the regenerator and also to reduce coke formation itself.

(5) Catalyst activity

In the FCC process, catalyst activity is managed from the standpoint of deactivation by hydrothermal destruction of zeolite and metal accumulation on the catalyst, rather than by coke deposit on the catalyst in the reactor. The regenerated catalyst circulating in the system is called E-cat (Equilibrium catalyst), and its activity is called equilibrium activity. This equilibrium activity

is managed by analysing a conversion of the standard feed oil by E-cat in the small fixed-bed reactor called MAT (Micro-Activity Tst unit).

The equilibrium catalyst is automatically drawn out of the system after it has been pulverized to a size so small by attrition that a cyclone cannot capture it. In the conventional FCC process, new catalyst was added in line with the amount of this loss by attrition. Recently, and especially in the RFCC process, equilibrium catalyst is positively withdrawn and new catalyst added to increase equilibrium activity against any loss of activity occurring during operation, because rapid deactivation is observed with metal accumulation on the catalyst.

5.5.4 PRACTICE OF FCC REACTOR DESIGN

5.5.4.1 Reactor Types and Their Configurations

Reactor types and their configurations differ in terms of each process licenser's design. At present (in 1996), the major FCC process licensers that provide the most modern design technology for FCC units are these seven companies⁽³⁾:

UOP (USA)⁽²¹⁾
M. W. Kellogg (USA)⁽²²⁾
Shell (Netherlands)^(23,24)
Exxon (USA)⁽²⁷⁾
Texaco (USA)⁽³⁰⁾

Stone and Webster Engineering (USA)⁽²⁵⁾

IFP France⁽²⁶⁾
Exxon (USA)⁽²⁷⁾
Texaco (USA)⁽³⁰⁾

The reaction equipment for an FCC unit basically consists of two reactors. One is the reactor (called a reactor with integration of a riser reactor, disengager and stripper), and the other one is the regenerator. The layouts of FCC reactors can be classified into two types of configurations. One is the side-by-side configuration shown in Figure 5.69 and the other one is the stacked configuration shown in Figure 5.70. For regenerator design at present, the two-stage regenerator configuration is sometimes adopted. In general, first-stage and second-stage regenerators are stacked. Figure 5.75 shows an example of stacked regenerators with the first-stage regenerator installed above or below the second-stage regenerator. Figure 5.76 shows two representative FCC configurations of a side-by-side unit (UOP) and a stacked unit (M. W. Kellogg) as examples.

5.5.4.2 Elementary Technologies for Reactor Design^(3,28)

When a reactor is designed, it is important to consider how to derive maximum performance from the given FCC catalyst. Major elements of reactor design will now be explained.

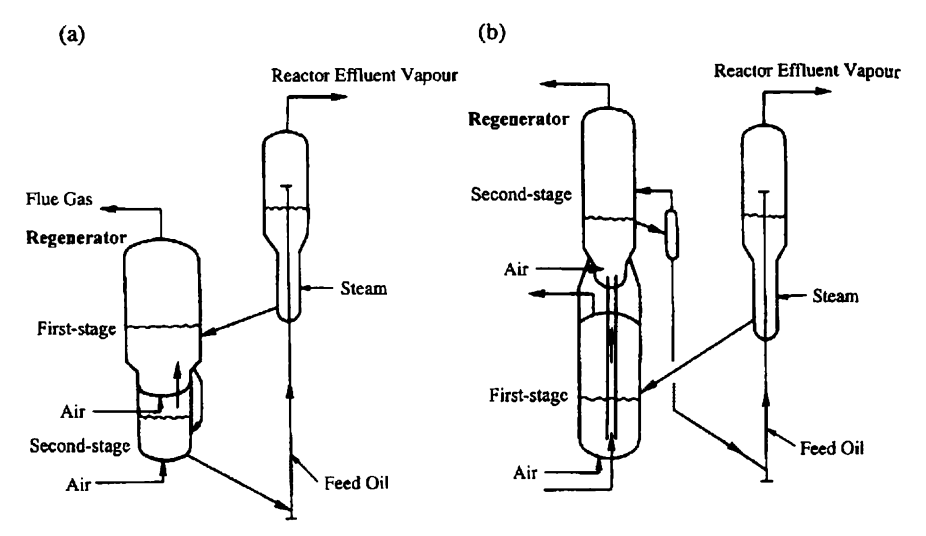


Figure 5.75 Configuration of two-stage regeneration style FCC. (a) Second-stage regenerator located below first-stage regenerator⁽²¹⁾. (b) Second-stage regenerator located above first-stage regenerator^(25,26).

5.5.4.2.1 Feed Injection System

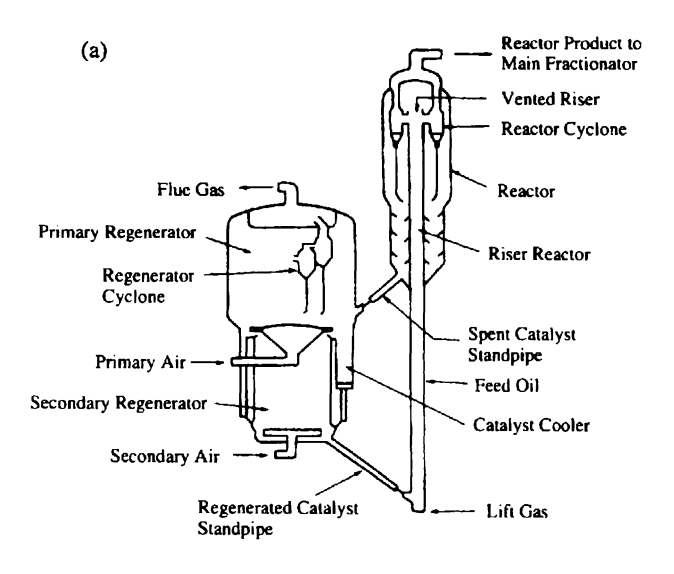
A catalytic cracking reaction will be performed in the vapour phase, so it is essential to vaporize quickly in the riser reactor before commencing a catalytic cracking reaction, in order to avoid thermal cracking in the liquid phase, which will cause poor reaction selectivity. Feed oil is injected into the riser after preheating. It is important to improve contact efficiency between the feed oil and the catalyst in the riser, especially when residual oils are processed in an FCC unit.

Before a catalyst is brought into contact with a feedstock, special design considerations should ensure an equal catalyst distribution in the riser reactor's bottom section with catalyst prefluidization under dense-phase conditions.

On the other hand, for feed nozzle design, the key point is how to atomize and distribute feed oil equally on the catalyst. In the past, a single-feed nozzle system was applied; however, current design tends to adopt a multi-feed nozzle system. In both designs, steam is used to reduce hydrocarbon's partial pressure for easier vaporization of heavy feed oils.

5.5.4.2.2 Separation System at Riser Outlet

As already described, the cracking reaction should be completed within several seconds. To avoid overcracking at the riser outlet, the reactor's effluent vapour and catalyst must be separated quickly and effectively. Residence time of the reactor's effluent vapour at the disengager must also be minimized.



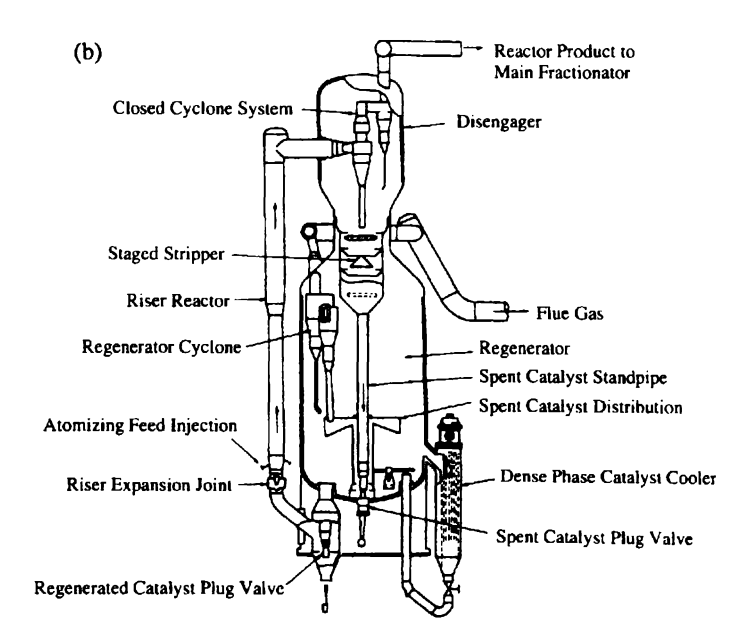


Figure 5.76 Configuration of reactor (reactor/regenerator) for FCC unit. (a) UOP RCC: two-stage regeneration style⁽²¹⁾. (b) Kellogg RFCC converter⁽²²⁾ (stacked type FCC).

There are two types of separation systems:

- (a) Open Cyclone System: as shown in Figure 5.76 (a), the reactor effluent enters the first-stage cyclone after it is separated from the catalyst at the riser outlet.
- (b) Closed Cyclone System: as shown in Figure 5.76 (b), the reactor's effluent vapour from the first-stage cyclone located at the riser outlet enters the second-stage cyclone by direct connection to the first-stage cyclone.

5.5.4.2.3 Stripping System

The catalyst in the stripper section is kept in a fluidized condition, and the hydrocarbons absorbed or entrained by the circulating catalyst are removed as much as possible by steam stripping. With steam stripping, the coke-burning load in the regenerator is decreased. Since steam is used as the stripping medium, design considerations in a stripping system (i.e., a two-stage stripping system) and the internal configuration (i.e., a number of baffles and some internal components) are needed to improve stripping efficiency.

5.5.4.2.4 Spent Catalyst Distribution System

In order to achieve equal catalyst regeneration, the catalyst circulating from the stripper should be equally distributed in the regenerator in combination with the air distribution system in which coke-burning air is introduced at the bottom of the regenerator. In the case of Kellogg's design shown in Figure 5.76 (b), the air and catalyst are contacted by a counter-current flow, and the spent catalyst is distributed equally from the top of the catalyst bed level through the spent catalyst distributor with six arms located at the regenerator's centre.

In another type of FCC process, the spent catalyst is introduced into the regenerator's bottom section from a side-entry nozzle where the catalyst is in contact with the air by a co-current flow. In still another type of FCC process, counter-current flow contact between the catalyst and the air is performed when the catalyst is introduced into the top of the catalyst level in the regenerator.

5.5.4.2.5 Air Distribution System

In order to achieve equal catalyst regeneration, the following technical targets should be considered in design of an air distribution system for coke-burning. The design should:

- (a) cover the regenerator's whole cross-sectional area
- (b) equalize air velocity in the regenerator as much as possible

- (c) control air velocity at the air-jet nozzle outlets to avoid catalyst attrition
- (d) prevent erosion of equipment by fluidized catalyst
- (e) minimize thermal and mechanical stress when operating conditions change
- (f) provide for operation flexibility to cover a wide range of air-flow rate.

The pipe grid type, dome (or plate) type and ring type are considered the design options for the air distributor.

5.5.4.2.6 Catalyst Cooling System

It may be necessary to adjust reaction yield in order to reduce coke yield, or to adopt some advanced heat balance technologies when residual feed will be processed.

Application of a catalyst cooler for the regenerator and the two-stage regeneration system will provide for good heat balance for residual feed processing.

In a catalyst cooler, steam is generated by heat removal. In past design, a bed coil in the regenerator and an upflow or dilute-phase type of catalyst cooler (catalyst flow inside tubes) externally located at the regenerator are sometimes adopted. However, in the latest designing, the downflow and dense-phase types of catalyst coolers (catalyst flow through the shell side) are mainly used as shown in Figure 5.76.

5.5.5 MATERIAL BALANCE AND HEAT BALANCE AROUND REACTORS⁽²⁹⁾

In Figure 5.74 the simulation model for heat balance in the FCC unit (reactor and regenerator sections) is explained. Here a more practical explanation of material and heat balance is presented. Material and heat balance around the reactor and regenerator is summarized below.

5.5.5.1 Material Balance

Reactor

n • Feedstock (fresh feed, recycle feed)

- Injection steam to feedstock (for atomizing and purging)
- Stripping steam to the stripper
- Regenerated catalyst (circulating catalyst).

Out • Cracked reactor effluent vapour

- Recycle oil vapour
- Spent catalyst (circulating catalyst including coke)
- Steam in the cracked reactor's effluent vapour.

Regenerator

- In Circulating spent catalyst (including coke)
 - Air for coke-burning.
- Out Regenerator flue gas
 - Circulating regenerated catalyst.

5.5.5.2 Heat Balance

Reactor

- Heat of feed oils (fresh and recycle feeds) at preheat conditions (liquid phase)
 - Heat of steam injected to feed oils and steam for stripping
 - Heat of circulating regenerated catalyst
 - Heat of coke absorption by catalyst (coke produced in the riser reactor).
- Out Heat of feed oil vapours (fresh and recycle) at the reactor outlet temperature
 - Heat of reaction
 - Heat of circulating spent catalyst at the reactor outlet temperature
 - Heat of injection steam and stripping steam at the reactor outlet temperature
 - Heat loss at the reactor section (radiation loss).

Regenerator

- In Heat of circulating spent catalyst at the regenerator inlet temperature
 - Heat of air for coke-burning at the regenerator inlet temperature
- Out Heat of flue gas at the regenerator outlet temperature
 - Heat of circulating regenerated catalyst from the regenerator
 - Heat of coke desorption from catalyst
 - Heat loss at the regenerator section (radiation loss)
 - Heat of removal by the catalyst cooler (if catalyst cooler is applied).

Example 5.15

The following operating data were obtained from an FCC unit which is now in actual operation.

Operating data:

• Combustion air to the regenerator (dry basis: excluding water fraction)

flow rate 117 160 kg/h temperature 200 °C Composition of the regenerator flue gas (dry basis: excluding water fraction)

O_2	0.3 vol%	SO_2	0.1 vol%
CO	3.1 vol%	N_2	81.6 vol%
CO_2	14.9 vol%		

Regenerator flue gas temperature
 Regenerator catalyst bed temperature (regenerated catalyst temperature)
 Spent catalyst (from the stripper to the regenerator) temperature

(1) With coke combustion balance calculation around the regenerator, estimate coke yield as wt% on the basis of fresh feed oil; (2) then estimate the flow rate of the circulationg catalyst [t/min].

Note: Capacity of the FCC unit is $30\,000$ BPSD (1bbl = $0.159\,kl$), and the specific gravity of the feed oil is 0.915 ($15/4\,^{\circ}C$).

Solution

(1) Calculation of coke yield (based on fresh feed oil)
The coke-burning rate is calculated by the material balance around the regenerator from the standpoint of analytical data on flue gas composition and the rate at which air is consumed for regeneration.

Step 1 Confirm flue gas composition (dry basis)

Composition	vol% (mol%)
O_2	0.3
CO	3.1
CO_2	14.9
SO_2	0.1
N_2	81.6
Total	100.0

Step 2 Flow rate of regeneration air A_f is calculated below, when the air's average molecular weight is 29. $A_f = 117\,160/29 = 4040\,\text{kmol/h}$

Step 3 N_2 flow rate in the regeneration air equals N_2 flow rate in the flue gas; therefore, the flow rate of the regenerator flue gas, RG_f (kmol/h), is $A_f \times (79.1)/(100) = RG_f \times (81.6)/(100)$

Then $RG_f = 3916 \, kmol/h$

Step 4 Total flow rate of the regenerator flue gas and composition are known, so the per-component balance of the regenerator flue gas is calculated as shown below.

Composition	vol%	mol. fraction	kmol/h
O_2	0.3	0.003	11.7
CO	3.1	0.031	121.4
CO_2	14.9	0.149	583.5
SO_2	0.1	0.001	3.9
N_2	81.6	0.816	3195.0
Total	100.0	1.000	3916.0

Step 5 Water fraction H_2O produced by the coke-burning reaction is obtained on the basis of the oxygen balanced required for cokeburning.

$$O_{2\,in}$$
 (regeneration air) = $A_f \times (20.9)/(100)$ = 844.4 kmol/h $O_{2\,out}$ (remaining O_2 in the coke-burning reaction + O_2 consumed for CO , CO_2 , and SO_2 production) = 11.7 + $(0.5) \times (121.4) + 583.5 + 3.9 = 659.8$ kmol/h $C + 1/2 O_2 = CO$ $C + O_2 = CO_2$ $S + O_2 = SO_2$

Therefore, it can be understood that the differential O_2 rate between the inlet and outlet around the regenerator $(844.4-659.8=184.6\,\mathrm{kmol/h})$ is consumed for the burning reaction of the hydrogen (H) in the coke.

Quantity of water fraction (H_2O) produced by the coke-burning reaction is obtained by $H_2 + 1/2 O_2 = H_2O$,

 H_2O produced = $2 \times (differential \ O_2 \ rate) = 369.2 kmol/h$

Composition of coke	Atomic weight	kmol/h	kg/h
C	12.00	121.4 + 583.5 = 704.8	8459
H	1.01	369.2×2	746
S	32.1	3.9	125
Total = coke-	burning rate	\mathbf{K}_{f}	9330

Step 6 Coke-burning rate is calculated from the flue gas composition rate.

This results in a coke-burning rate at 9330 kg/h (9.33 t/h). Weight flow rate of feed oil is $(30\,000/24) \times 0.159 \times 0.915 = 181.9 \,t/h$ So the coke yield on fresh feed is obtained as $(9.33/181.9) \times 100 = 5.12 \,wt\%$.

(2) Catalyst circulation rate

Heat balance calculation is based on the following steps 7-14, and then the catalyst circulation rate is calculated.

Step 7 Heat of combustion by coke-burning

Reaction of	Combustion heat	Flow rate	Heat rate
coke combustion	$\times 10^6 kJ/kmol$	mkol/h	$\times 10^6 kJ/h$
$C \rightarrow CO$	0.109	121.4	13.2
$C \rightarrow CO_2$	0.393	583.5	229.3
$S \rightarrow SO_2$	0.293	3.9	1.1
$H \rightarrow H_2O$	0.237	369.2	88.2
Total			331.8

Generated heat by coke combustion = $331.8 \times 10^6 \, kJ/h$

Step 8 Heat of coke entering the regenerator, K_h Reactor temperature $520 \,^{\circ}C$ Heat of coke = $(K_f) \times (c_{Dk}) \times (RX_t - DA_t)$ cpk : specific heat of coke 2.1 kJ/kg K

RX₁: reactor temperature (temperature of catalyst entering the regenerator) [°C]

DA: base temperature [°C]

Heat of coke $K_h = (9330) \times (2.1) \times (520 - 15) = 9.9 \times 10^6 \, kJ$

Step 9 Heat of air entering the regenerator, Ah

 $A_h = (A_f) \times (c_{pa}) \times (AB_t - DA_t)$

c_{pa}: specific heat of air, 29.6 kJ/kmol K

 \overrightarrow{AB}_t : temperature of regeneration air (at air blower outlet) [°C]

 $A_h = (4040) \times (29.6) \times (200 - 15) = 22.1 \times 10^6 \, kJ/h$

Step 10 Total heat input to the regenerator (excluding circulating catalyst)

		$Heat \times 10^6 kJ/h$
Heat in	Heat of combustion by coke-burning	331.8
	Heat of coke	9.9
	Heat of regeneration air	22.1
	Total	363.8

Step 11 Heat of regenerator glue gas

RG₁: regenerator temperature 700°C

Temperature difference from the base temperature $(15^{\circ}C)$

685°C

Composition	Flow rate kmol/h	Specific heat kJ/kmol K	Heat $\times 10^6 kJ/h$
O_2	11.7	31.8	0.25
CO	121.4	30.7	2.54
CO_2	583.5	46.9	18.78
SO_2	3.9	48.0	0.13
N_2	3 195.0	32.6	71.34
H_2O	369.2	37.0	9.36
Total	4 285.2		102.40

Step 12 Heat loss such as radiation heat from the regenerator

Heat loss is calculated from the size of the regenerator and the type of
equipment material; however, in this sample problem, 6% of total
combustion heat is assumed as heat loss.

Heat $loss = (0.06) \times (331.8) = 19.9 \times 10^6 \, kJ/h$.

Step 13 Heat transferred to the circulating catalyst, $H_{cat} \times 10^6 \, kJ/h$ $H_{cat} = Heat$ input to regenerator—heat output from regenerator.

Note: for the above calculation, heat input/out on the circulating catalyst is excluded.

		$Heat \times 10^6 kJ/h$
Heat in	From Step 10	363.8
Heat out	Regenerator flue gas	102.4
	Heat loss	19.9
Heat tran	sferred to catalyst, $H_{cat} =$	241.5

Step 14 CCR (Cat. Circulation Rate) [t/min]

Temperature of regenerator catalyst bed, RG_{bt} 690°C $H_{cat} = (CCR) \times (60) \times (c_{pcat}) \times (RG_{bt} - RX_t)/(1000)$ c_{pcat} : specific heat of circulating catalyst, 1.11 kJ/kg K 241.5 = $(CCR) \times (60) \times (1.11) \times (690 - 520)/(1000)$ CCR = 21.3 t/min.

References

- (1) J. L. Enos (translated by F. Kato and M. Kitamura from Petroleum Progress and Profits), Oil Industry and Technical Innovation, Saiwai Shobo (1972).
- (2) CATALAGRAM, published by Davison Chemical Division, W. R. GRACE Corp.
- (3) H. Minami, Petrotech, 16(5), 397 (1993).
- (4) R. Schaefer (Shell), Memorandum Concerning History of FCC (1989).
- (5) B. G. Gates, et al. (translation by T. Kei), Chemistry of Catalytic Processes, Tokyo, Kagaku Dojin (1984).
- (6) B. W. Wojciechowski and A. Corma, Catalytic Cracking, Marcel Dekker (1986).
- (7) J. Scherzer, Octane-Enhancing Zeolitic FCC Catalyst, Marcel Dekker (1990).
- (8) J. Briswas and I. E. Maxwell, Appl. Catal., 63, 197 (1990).
- (9) S. Sato, et al., JPI, 29, 1, 60 (1986).
- (10) D. Geldard, Powder Technol., 7, 285 (1973); 19, 133 (1978).
- (11) T. Miyauti, et al., Adv. Chem. Eng., 11, 275 (1981).
- (12) SCEJ Edition, Fluidized Bed Reactor-Industrial Practices and New Technologies, Kagaku Kogyosha (1988).
- (13) M. Horio, Funtai Kogyo Kyokai Shi, 23, 80 (1986).
- (14) D. Kunii, Fluidization Engineering, Nikkan Kogyo Shimbunsha (1962).
- (15) D. Kunii and O. Levenspiel, *Fluidization Engineering*, second edition, Butterworth-Heinemann (1991).
- (16) SCEJ Edition, Chemical Engineer's Handbook, fifth edition, 269 (1988).
- (17) T. Takatsuka, et al., JPI, 27, 6, 533 (1984).
- (18) D. M. Nace, et al., Ind. Eng. Chem. Proc. Des. Dev., 10, 530 (1971).

- (19) V. W. Weekman, et al., Ind. Eng. Chem. Proc. Des. Dev., 7, 90 (1968).
- (20) S. M. Jacob, et al., AIChE J., 22, 701 (1976).
- (21) B. Okamura, Petrotech, 13(12), 1015 (1990).
- (22) N. Khono, Petrotech, 13(11), 914 (1990).
- (23) T. Tanaka, Petrotech, 13(11), 912 (1990).
- (24) F. H. H. Khouw, et al. (Shell), Shell Residue FCC Challenges and Opportunities in a Changing Environment, JPI Refining Conference (1992).
- (25) A. R. Johnson, et al. (S&W), Advances in Residual Oil FCC, JPI Refining Conference (1992).
- (26) Y. Shida, Petrotech, 13(12), 1017 (1990).
- (27) D. C. Draemel, et al. (Exxon), FLEXICRACKING III R ER&E's Latest Cat. Cracking Design, JPI Refining Conference (1992).
- (28) T. Ishiyama, Petrotech, 16(5), 405 (1993).
- (29) E. Piere, Hydrocarbon Processing, Feb., 39 (1983).
- (30) R. J. Glendinning, et al., Advancements in Process and Control Technologies Improve FCC Profitability, JPI Refining Conference (1994).

CHAPTER 5.6

Wet Flue Gas Desulphurization

HIROSHI YANAGIOKA and TERUO SUGIYA

Chiyoda Corporation, Japan

The global environmental problems of air pollution have been recognized and addressed to protect the survival of nature and the activity of humankind. Acid rain is of particular concern as a global problem of air pollution which is primarily caused by sulphur oxides. In reducing the amount of sulphur oxides, desulphurization processes have been utilized. Fuel oil desulphurization has been actively promoted to reduce the content of sulphur compounds in fuel. Flue gas desulphurization has also performed an important role to remove the sulphur oxides directly discharged from combustion of fuel oil and coal, and has therefore contributed in the fight against air pollution. The technology of flue gas desulphurization has been improved to reduce those pollutants efficiently.

Since sulphur dioxides in flue gas tend to be acidic, neutralization processes are employed for the reactions with alkaline substances such as sodium hydroxide, ammonia, magnesium hydroxide, calcium hydroxide and calcium carbonate or limestone.

The major processes for flue gas desulphurization are classified as follows:

- (1) Dry process
 - Flue gas is treated at the temperature of the boiler outlet without injection of water.
- (2) Semi-dry process
 - Flue gas is treated under a spray of water to keep the temperature higher than its saturation temperature.
- (3) Wet process Sulphur oxides in the flue gas are absorbed in aqueous solution and treated at the saturation temperature.

The wet process named as the wet-limestone process has the advantage of using inexpensive limestone as a neutralizing agent, to produce saleable gypsum and

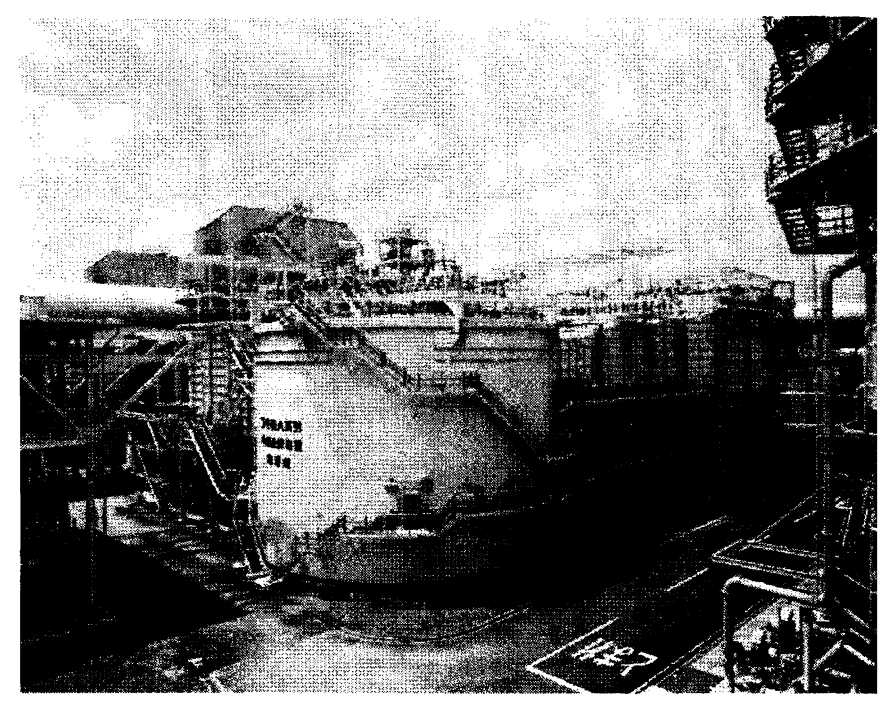


Figure 5.77 A JBR unit for a large industrial boiler plant (courtesy of Chubu Elect. Power K. K.).

to remove sulphur dioxides at high efficiency. In the process, a reactor callethe Jet Bubbling Reactor (JBR) is installed to perform the neutralization sulphur dioxides with limestone and to produce gypsum.

In this chapter, as an example of wet flue gas desulphurization, the we limestone processes are described, especially with respect to the chemic reactions and reactor design in $JBR^{(1,2)}$.

Figure 5.77 shows a JBR unit applied to a large industrial boiler plant.

5.6.1 PROCESS DESCRIPTION

Figure 5.78 shows an example of a simplified flow diagram for the Jet Bubblin flue gas desulphurization process.

Flue gas from a boiler enters a gas-to-gas heater (GGH) at 120–150 °C and then cooled down to 90–100 °C by exchanging the heat of the desulphuriz flue gas for heat recovery. The cooled flue gas then contacts directly with mak up water and the circulating gypsum slurry to be cooled down further up to t adiabatic saturation temperature, by the heat of evaporation of water.

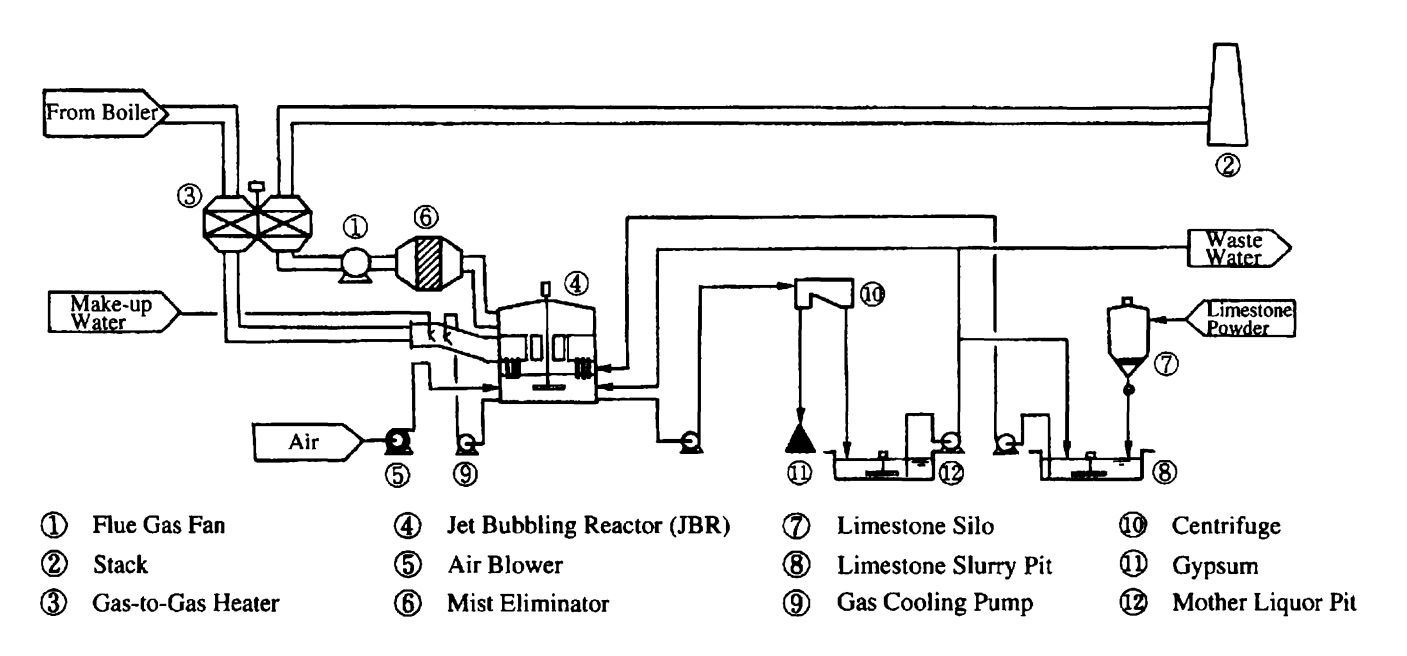


Figure 5.78 Simplified flow diagram of a flue gas desulphurization process.

The cooled flue gas enters the JBR, where sulphur dioxide in the flue gas is absorbed in alkali solution. Fly ash is also removed in the JBR. The desulphurized flue gas passing through a mist eliminator to remove entrained droplets, is boosted up by a flue gas fan, reheated in the GGH and finally discharged from a stack to the atmosphere.

The absorbed sulphur dioxide is changed to sulphite in the aqueous slurry, and the sulphite is oxidized to form sulphate by the air through an air blower. The sulphate is neutralized simultaneously by the ground limestone fed as an aqueous slurry, giving birth to gypsum crystals. The gypsum crystals are allowed to grow in the presence of a sufficient concentration of seed crystals.

The limestone slurry, which is prepared in a pit to give a constant concentration of limestone in an aqueous solution, is fed to the JBR with an amount of chemical equivalent to the absorbed sulphur dioxide.

The gypsum produced in the form of a slurry is discharged from the JBR by a slurry pump, and then sent to a centrifuge for de-watering. The water content of gypsum is usually decreased to about 10 wt%. The gypsum is then conveyed to a storage as the by-product of flue gas desulphurization.

5.6.2 STRUCTURE OF JBR

A cross-sectional view of the fundamental structure of JBR is shown in Figure 5.79.

5.6.2.1 Gas Phase

The flue gas first enters an enclosed plenum chamber structured between an upper deck plate and a lower deck plate, and is then uniformly distributed

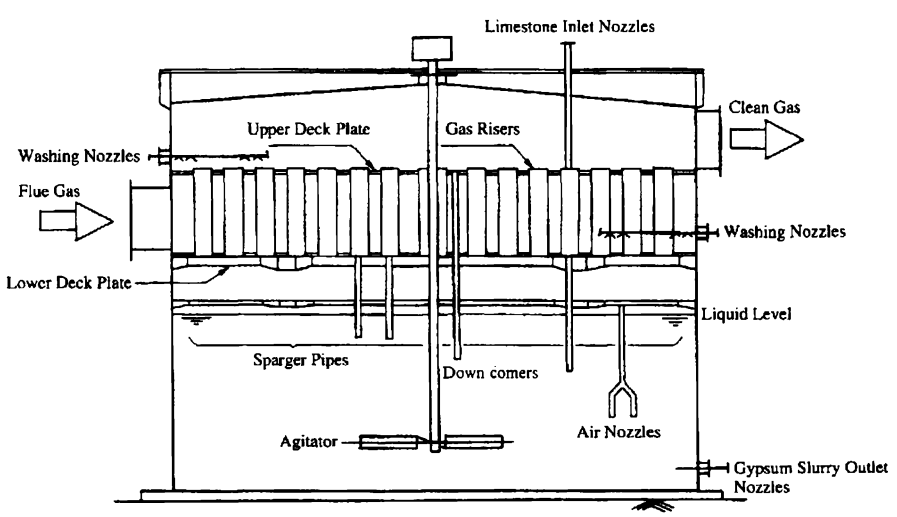


Figure 5.79 Typical structure of JBR.

through the sparger pipes or stand pipes that are perpendicularly disposed to the lower deck plate. The flue gas flows downwards through the spargers, and bubbles out into the slurry from the openings that are positioned at several hundreds of millimetres under the surface of the liquid. The gas bubbles, which are about several millimetres in diameter, form a jet bubbling zone in which gas hold-up is from 0.5 to 0.8·SO₂ in the flue gas is absorbed to the slurry as the flue gas passes through the jet bubbling zone. The space velocity of the flue gas is typically 1.5–2.8 m/s, depending on the required efficiency of SO₂ removal.

Separation of gas from liquid occurs in a space above the jet bubbling zone. The desulphurized gas then flows upwards through the gas risers that pass through both the lower and upper deck plates. Entrained liquid droplets contained in the gas are further disengaged in a second plenum above the upper deck plate. The cleaned flue gas leaves the JBR and enters a mist eliminator for the final separation of fine droplets.

5.6.2.2 Liquid Phase

Neutralization, sulphite oxidation, and crystal growth occur in the liquid zone located below the openings of the sparger pipes. Limestone is introduced through the inlet of an aqueous slurry of ground limestone for the purpose of neutralization. Oxidation air is supplied through the air nozzles.

An agitator positioned at the centre of the JBR, mixes those reactants sufficiently and also prevents the precipitation of gypsum on the bottom plate of the JBR. The gypsum is constantly produced in the liquid zone.

5.6.3 CHEMICAL REACTIONS IN JBR

5.6.3.1 Gas-liquid-solid Reactions

Figure 5.80 illustrates a schematic diagram for a number of reactions occurring in the gas, liquid and solid phases in the JBR.

In the upper froth layer or jet bubbling zone, SO₂ from the flue gas is absorbed into the slurry to form sulphite, which in turn reacts with dissolved oxygen in the lower liquid zone to form sulphate.

The produced sulphate further reacts with the limestone fed at the liquid zone to produce gypsum. Gypsum crystals grow to large sizes in the presence of sufficient seed crystals.

The overall reaction equation in the JBR is thus given by:

$$SO_2(g) + 2H_2O(l) + 1/2 O_2(g) + CaCO_3(s) \rightarrow CaSO_4 \cdot 2H_2O(s) + CO_2(g)$$
(5.35)

Equation (5.35) involves three phases: the gas phase (SO₂, O₂, CO₂): the liquid phase (H₂O) and solid phase (CaCO₃, CaSO₄ \cdot 2H₂O). Heterogeneous

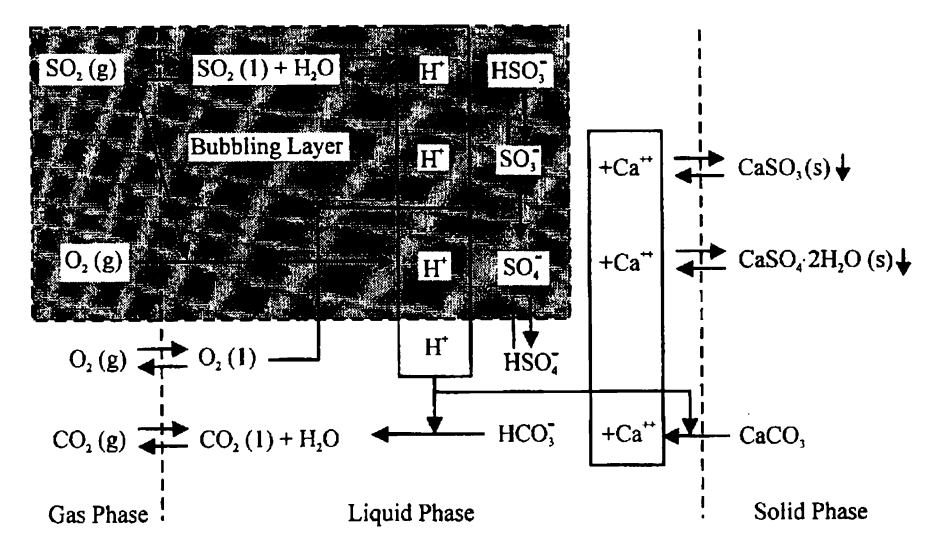


Figure 5.80 Schematic diagram for reactions in the JBR.

reactions occurring at the gas-liquid and liquid-solid interfaces are rate-determining steps. When treating typical flue gas from boilers, the above reaction proceeds at approximately atmospheric pressure and a temperature of about $50\,^{\circ}\text{C}$.

5.6.3.2 Absorption of SO₂

Absorption and dissolution of SO₂ are considered as reactions on the liquidgas interface, and can be represented by physical absorption of SO₂ into water and two steps of dissociation equilibrium.

$$SO_2(g) \to SO_2(l) \tag{5.36}$$

$$SO_2(1) + H_2O(1) \rightleftharpoons H^+ + HSO_3^-$$
 (5.37)

$$HSO_3^- \rightleftharpoons H^+ + SO_3^{2-} \tag{5.38}$$

Henry's law holds between $P_{SO_2}^*$, equilibrium partial pressure of SO_2 in the gas phase and $SO_2(1)$, concentration of SO_2 in the liquid phase. That is,

$$H_{SO_2} = P_{SO_2}^* / [SO_2(l)]$$
 (5.39)

where H_{SO_2} denotes Henry's constant.

Equilibrium relationships for dissociation of sulphites in solution are expressed by:

$$K_1 = [H^+] \times [HSO_3^-]/[SO_2(I)]$$
 (5.40)

$$K_2 = [H^+] \times [SO_3^{2-}]/[HSO_3^-]$$
 (5.41)

where K_1 , and K_2 are equilibrium constants.

In combination with the above three equations, a liquid-gas equilibrium relationship is obtained as:

$$P_{SO_2}^* = \frac{H_{SO_2}}{1 + \frac{K_1}{[H^+]} + \frac{K_1 K_2}{[H^+]^2}} \times C_{SO_2}$$
 (5.42)

where C_{SO_2} represents the total concentration of sulphites, that is, ([SO₂(l)+[HSO₃]+[SO₃²]). It is noted that according to this relationship, $P_{SO_2}^*$ decreases with decreasing C_{SO_3} and decreasing [H⁺].

Since the diffusion of SO₂ through the gas film at the gas-liquid interface is the rate-determining step, the rate of SO₂ absorption from flue gas can be expressed by:

$$r_{SO_2}(g) = K_G a (P_{SO_2} - P_{SO_2}^*)$$
 (5.43)

where $K_G a$ = overall gas-side mass transfer coefficient.

It can be found from this equation that the rate of SO_2 absorption increases as $P_{SO_2}^*$ decreases, and that C_{SO_2} and $[H^+]$ should be decreased in order to increase the required rate of SO_2 absorption.

In practice, the combined uses of both oxidation by air and neutralization by limestone decrease both C_{SO_2} and $[H^+]$, and result in the effective achievement of SO_2 absorption in the JBR.

5.6.3.3 Physical Absorption of O₂ and Oxidation of Sulphite⁽³⁾

Oxidation of sulphite by air is represented by the following equations:

$$O_2(g) \to O_2(l) \tag{5.44}$$

$$O_2(1) + 2SO_2(1) \rightarrow 2SO_3$$
 (5.45)

$$O_2(1) + 2HSO_3^- \rightarrow 2SO_4^- + H_2O$$
 (5.46)

$$O_2(1) + 2SO_3^{2-} \rightarrow 2SO_4^{2-}$$
 (5.47)

Physical absorption of oxygen from air is considered to be liquid-film diffusion controlled, and the rate of absorption is expressed by:

$$r_{\rm O_2} = k_{\rm L} a (C_{\rm O_2}^* - C_{\rm O_2}) = k_{\rm L} a (P_{\rm O_2}/H_{\rm O_2} - C_{\rm O_2})$$
 (5.48)

where H_{O_2} and $k_L a$ denote Henry's law constant and liquid-side mass transfer coefficient for O_2 , respectively.

Since the rate of sulphite oxidation in the liquid phase is much greater than the rate of physical absorption of O_2 , it can be handled in this system where the overall rate of oxidation is approximately $r_{O_2} = K_L a P_{O_2} / H_{O_2}$.

In practice, the overall rate of oxidation can be obtained from experimental data. For example, using calcium sulphite as the component to be oxidized, the following equation was obtained from a series of such experiments.

$$r_{\rm O_2} = k\pi P_{\rm O_2} (C_{\rm SO_2})^{0.5} \exp(0.135 \text{pH} - 2840/RT)$$
 (5.49)

It is interesting to note that several parts per million of ferric ions in the absorbent accelerate the rate of oxidation. The ferric components, which are usually contained in limestone as one of its impurities, can dissolve in an acidic solution to generate ferric ions.

Example 5.16: Estimation of SO₂ removal efficiency

In a JBR a flue gas with flow rate G_M and partial pressure P_{SO_2} enters sparger pipes and bubbles out into the absorbent to form the bubbling zone (height is Z_f). Derive a theoretical equation for expressing SO_2 removal efficiency in the JBR.

Solution

Referring to Figure 5.81, a material balance around an infinitesimal length Z-Z+dZ with the rate of SO_2 absorption represented by Eq. (5.43) gives the following basic equation:

$$G_m d(P_{SO}, /\pi) = K_G a(P_{SO}, -P_{SO}^*) dZ$$
 (5.50)

In the jet bubbling zone, it is assumed that the liquid phase is in complete mixing, while the gas phase is in piston flow, and that $\mathbf{P}_{SO_2}^*$ is constant. The boundary conditions are:

$$P_{SO_2} = P_{SO_2 in} \text{ at } Z = 0 \text{ and } P_{SO_2} = P_{SO_2 out} \text{ at } Z = Z_f$$
 (5.51)

Integration Eq. (5.50) with the boundary conditions,

$$\ln \frac{P_{SO_2out} - P_{SO_2}^*}{P_{SO_2in} - P_{SO_2}^*} = -\frac{K_G a \pi}{G_M} Z_f$$
 (5.52)

Hence, the SO_2 removal efficiency is defined as $\eta = I - P_{SO_2out}/P_{SO_2in}$. η is obtained from Eq. (5.52):

$$\eta = \left(1 - \frac{P_{SO_2}^*}{P_{SO_2m}}\right) \left(1 - exp\left(-\frac{K_G a \pi}{G_M} Z_f\right)\right)$$
 (5.53)

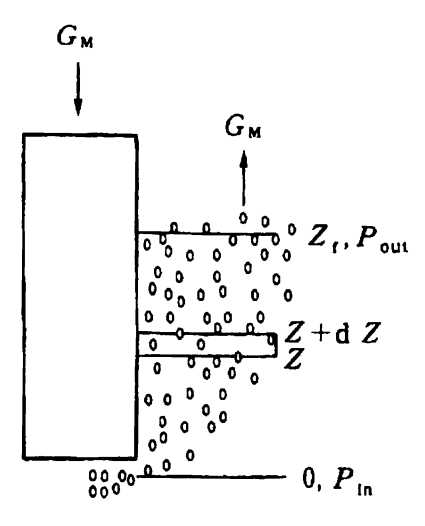


Figure 5.81 Gas absorption in the bubbling zone.

Since $P_{SO_2}^*$ is much smaller than P_{SO_2in} , the first term of the above equation can be taken as unity and the SO_2 removal efficiency η can be approximated as:

$$\eta = 1 - exp\left(-\frac{K_G a \pi}{G_M} Z_f\right)$$
 (5.54)

In actual operating conditions, K_G is a function of gas flow rate G_M , absorbent acidity pH, and inlet SO_2 partial pressure P_{SO_2in} . Several empirical equations have been obtained as a function of these variables. The following equation is one of such equations:

$$\eta = I - \exp(-k(pH)^{a}(P_{SO_{2}})^{-b}(G_{M})^{-c}(\Delta P)^{d})$$
 (5.55)

where ΔP is the flue gas pressure drop through the JBR. It is noted that the ΔP is equivalent to the submerged depth of sparger pipes when it is expressed in units of length. Figure 5.82 shows a relationship of ΔP versus SO_2 removal efficiency at the specific JBR operating conditions of $P_{SO_2in}=1100$ ppm, $G_M=400 \ Nm^3/h/sparger$, and pH=4.5.

In practical operation, the SO_2 removal efficiency can be controlled by varying the submerged depth of spargers.

5.6.3.4 Dissolution of Limestone and Neutralization Reaction

The dissolution of limestone and the neutralization reaction are represented by the following equations:

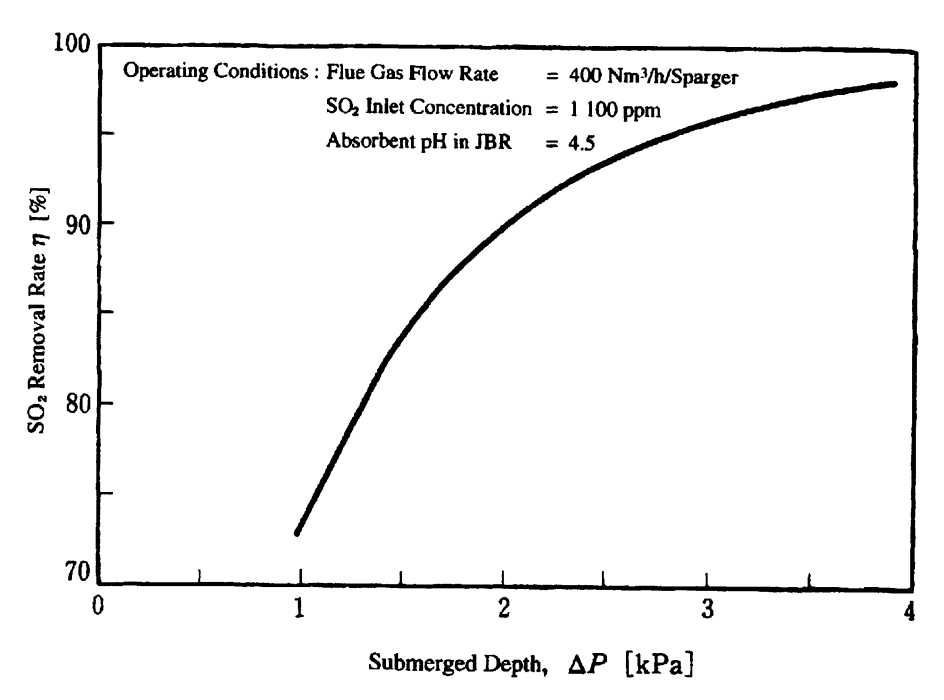


Figure 5.82 Relationship of ΔP vs. SO₂ removal rate.

$$CaCO_3(s) \rightarrow CaCO_3(l)$$
 (5.56)

$$CaCO_3(l) + 2H^+ + SO_4^{2-} + H_2O \rightarrow CaSO_4 \cdot 2H_2O(l) + CO_2(l)$$
 (5.57)

$$CO_2(l) \rightarrow CO_2(g)$$
 (5.58)

The neutralization reaction of limestone with hydrogen ion, as represented by Eq. (5.57), is a much faster reaction between acid and alkali than the dissolution of limestone, as represented by Eq. (5.56), since the diffusion of limestone from solid surface to liquid phase is the rate-determining step. Therefore, the consumption rate of limestone can be expressed in the following equation:

$$-r_{\text{CaCO}_3} = K_{\text{L}}a[\text{H}^+] \tag{5.59}$$

Figure 5.83 shows the result of experiments in which the neutralization reactions were conducted with varying residence times in the jet bubbling zone using the limestone that had been ground over 90% passed under a 200 mesh size screen. Note that lower pH operation can be provide a higher utilization of limestone.

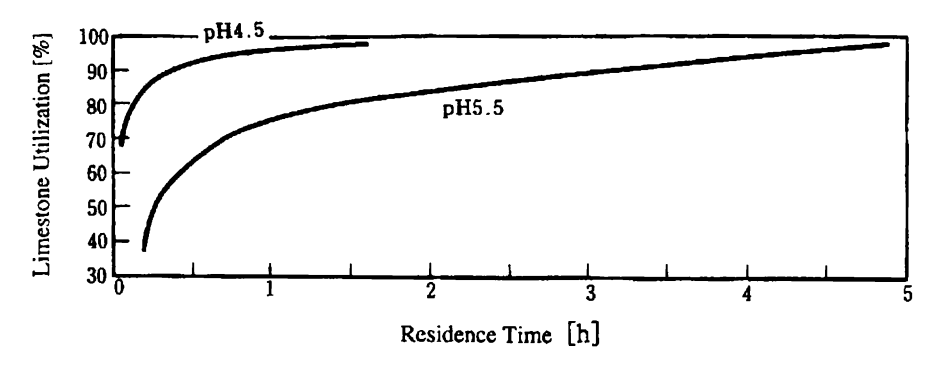


Figure 5.83 Effect of residence time for limestone utilization.

5.6.3.5 Production and Crystal Growth of Gypsum

Gypsum is produced by the diffusion from the supersaturated solution to the crystal surface.

$$CaSO_4 \cdot 2H_2O(1) \rightarrow CaSO_4 \cdot 2H_2O(s)$$
 (5.60)

The rate of production is expressed by the following equation that is proportional to the surface area of gypsum crystal (C_s) and the degree of supersaturation.

$$r_{\text{CaSO}_{4}\cdot 2\text{H},O} = k_{\text{s}}C_{\text{s}}\Delta C \tag{5.61}$$

Gypsum crystals in the supersaturated solution grow in two steps: one is diffusion of the solute from the liquid side to the crystal surface, and the other is alignment of diffused solute at the crystal lattice. The mean diameter of crystals is governed by the residence time ($\theta = 10$ –20 hours) of gypsum slurry in the JBR.

Figure 5.84 shows a particle size distribution of gypsum obtained in the JBR. However, the distribution is not always uniform, because those particle sizes depend on the distribution of residence time and the rate of crystal growth of each particle.

It is noted that when the degree of the supersaturation is over 1.3-1.4, the crystals of gypsum tend to deposit on the reactor wall as scale, since the formation rate of crystal is faster than the growth rate. In order to prevent this scaling problem, the degree of supersaturation should be maintained with the gypsum concentration as high as possible (20-30 wt%) in the JBR.

Example 5.17: Unreacted limestone in product gypsum

In order to utilize the product gypsum for wallboard or other building materials, it is necessary to meet certain specifications which limit the amount of impurities in

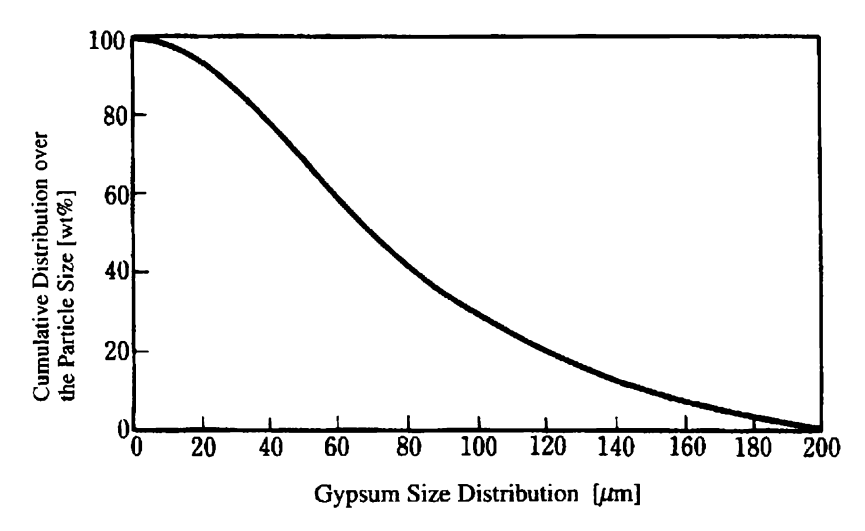


Figure 5.84 An example of gypsum size distribution.

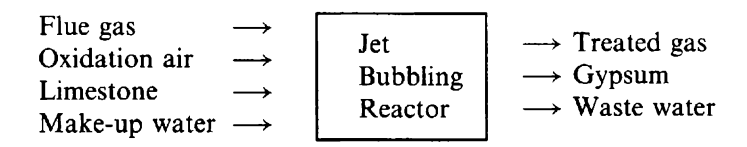
the gypsum. To meet the specification, calculate the unreacted limestone concentration in the gypsum varying pH values. Assume that the residence time in the bubbling zone is 1.5 hours.

Solution

According to Figure 5.83, the utilization of limestone at pH 4.5 and pH 5.5 with a residence time of 1.5 hours is 97% and 80%, respectively. Therefore, the concentration of unreacted limestone in the gypsum is $(100-97)\times100/172=1.72\%$ at pH 4.5 and $(100-80)\times100/172=11.6\%$ at pH 5.5.

5.6.4 HEAT AND MATERIAL BALANCE AROUND THE REACTOR

Input and output streams around the JBR are shown in the following figure.



In a steady state, there is no accumulation of heat and materials, and a material balance gives Σ (material in) = Σ (material out) and Σ (enthalpy in) = Σ (enthalpy out).

In the JBR, however, there are a temperature change, a phase change of water (vaporization and condensation accompanying with absorption and release of latent heat), and a chemical change for the chemical components as given in the following equation:

$$SO_2(g) + 2H_2O(l) + 1/2O_2(g) + CaCO_3(s) \rightarrow CaSO_4 \cdot 2H_2O(s) + CO_2(g)$$
(5.35)

$$\Delta H = -335 \text{ kJ/mol}$$
 (exothermic reaction)

In particular, a vapour-liquid equilibrium relationship of water must be satisfied so that the partial pressure of water vapour P_{H_2O} in the treated gas is equal to equilibrium vapour pressure of water $P_{H_2O}^*$.

Based on the chemical stoichiometry in Eq. (5.35) and the equilibrium relationship, the process conditions such as flow rate, temperature and pressure can be calculated by the mass and heat balances.

Example 5.18: Consumption of limestome and amount of vaporized water

A modern city with a population of one million generally needs $1000\,MW$ size electric power stations. Assume that a wet-type flue gas desulphurization plant (SO_2 removal rate 95%) is going to be constructed for a $350\,MW$ coal-fired boiler in the power plant. Determine the required amounts of water, limestone and produced gypsum.

Assume that the flow rate of the flue gas is $1050\,000\,Nm^3/h$, and the compositions of H_2O , N_2 , O_2 , SO_2 are 6.00, 75.41, 11.47 and $0.11\,vol\%$, respectively. The flue gas enters the JBR at $130\,^{\circ}C$ and $3.5\,kPaG$. The specific heat of the flue gas is $1.0\,kJ/Nm^3/^{\circ}C$ and the latent heat of water is $2260\,kJ/kg$.

Solution

The required amount of limestone (as $CaCO_3$, mw = 100) with 97% of limestone utilization at pH 4.5 in the JBR is calculated as follows:

$$1050\,000 \times 0.0011 \times 0.95/22.4 \times 100/0.97 = 5049 \,[\,kg/h\,].$$

The production rate of gypsum (as $CaSO_4 \cdot 2H_2O$, mw = 172) is:

$$5049 \times 0.97 \times 172/100 = 8242 [kg/h].$$

Let W [kg/h] be water for vaporization, and T [°C] be the temperature reached after adiabatic cooling, then the heat balance around JBR gives:

$$1050\,000 \times (130 - T) \times 1.0 = W \times 2260$$

On the other hand, the partial pressure of water vapour P_{H_2O} is:

$$(1050\ 000\times\ 0.06 + \text{W}/18 \times 22.4)/(1050\ 000 + \text{W}/18 \times 22.4) \times (101.3 + 3.5)\ [kPa]$$

Now, let us solve the above simultaneous equations using the trial and error method. Assuming $T = 47^{\circ}C$, we obtain:

$$W = 1050\,000 \times (130 - 47) \times 1.0/2260 = 38\,562 \,[\,kg/h\,]$$

$$\mathbf{P}_{H_2O} = (1050\,000 \times 0.06 + 38\,562/18 \times 22.4)/(1050\,000 + 38\,562/18 \times 22.4) \times (101.3 + 3.5) = 10.593\,[\,kPa\,].$$

Referring to the Steam Table, we find that the saturated vapour pressure $P_{H_2O}^*$ is 10.612 kPa at 47°C, which is very close to $P_{H_2O} = 10.593$. Thus, the assumed T = 47°C is checked. Therefore, the amount of water required for evaporation is $38\,562\,kg/h$.

Example 5.19: Diameter and height of JBR

Determine the size of the JBR given in example 5.18. Assume the amount of oxidation air is three times the stoichiometric requirement.

Solution

The flow rate of the flue gas saturated with water vapour is:

$$1050\,000 + 38\,562/18 \times 22.4 = 1097\,988\,[\,Nm^3/h\,],$$

and the flow rate of the treated flue gas is:

$$1097988 + 1050000 \times 0.0011 \times 0.95 \times 0.5 \times 3/0.21 = 1105825 [Nm^3/h].$$

Referring to Figure 5.85, we find that this JBR can be applied to the flue gas having SO_2 concentration = 1100 ppm at pH = 4.5. Since the gas flow rate per sparger is 400 Nm³/h at the inlet of the JBR, the number of spargers is calculated to be 1097 988/400 = 2745 pieces. Let these sparger tubes be arranged with a square pitch of 0.2 metre, and the required area for this arrangement becomes $0.2 \times 0.2 \times 2745 \cong 110 \,\text{m}^2$. Considering the area for the gas risers, the cross-sectional area of the JBR is taken as $110 \times 1.2 = 132 \,\text{m}^2$. Therefore, the diameter of the JBR is $\sqrt{(132/0.785)} = 12.9 \,\text{m}$.

The amount of gypsum slurry with content of 20 wt% is $8424/0.2 = 42\ 120\ kg/h$, and the volumetric flow rate of slurry withdrawn from the JBR is about $40\ m^3/h$. Let the residence time of the gypsum slurry be taken as 16 hours, then the liquid volume in the JBR is $40\times16=640\ m^3$. Therefore, the liquid height of the JBR is $640/132=4.8\ m$.

Since the gas velocity is usually taken as $15-20\,\text{m/s}$, it is calculated that the height of the inlet and outlet chambers is 2.6 m of each and 5.2 m as the total. Add another height of 1.0 m above the jet bubbling zone for the purpose of mist separation, then the total height of the JBR gas phase is 6.2 m. Thus, the required height of the JBR is $4.8+6.2=11.0\,\text{m}$. Further, add a design allowance of 1.0 m due to the fluctuation of the flue gas. The total height of the JBR is $12.0\,\text{m}$.

5.6.5 REACTIVE IMPURITIES IN THE FLUE GAS

5.6.5.1 Sulphur Trioxide

Sulphur trioxide (SO₃) in the flue gas usually contains about 1-2% in sulphur oxide. By cooling, SO₃ reacts with co-existing H_2O to form H_2SO_4 .

$$SO_3 + H_2O \rightarrow H_2SO_4 \tag{5.62}$$

At the acid dew point, the resulting H₂SO₄ condenses to form SO₃ mist or small particles of H₂SO₄, which is corrosive against common carbon steel.

Figure 5.85 shows a relationship between concentration of condensed sulphuric acid and temperature with SO_3 and H_2O concentration. The material of GGH should be selected in consideration of existing sulphuric acid (SO_3 mist) at the high-temperature side of GGH outlet.

5.6.5.2 Chlorides

Coal-fired flue gas usually contains about 50 ppm of gaseous HCl, which is removed from the flue gas as follows:

$$HCl(g) \rightarrow HCl(l)$$
 (5.63)

$$2HCl(l) + CaCO3(l) \rightarrow CaCl2(l) + H2O(l) CO2(g) \uparrow$$
 (5.64)

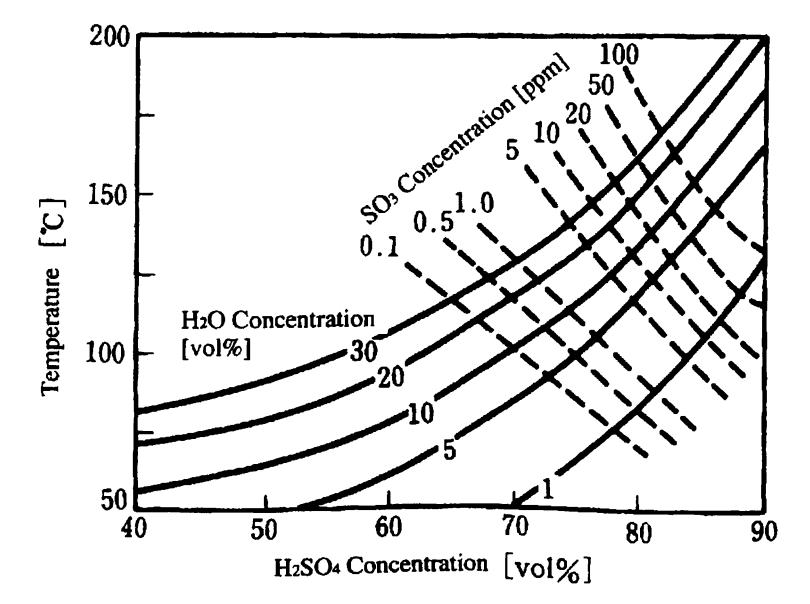


Figure 5.85 Relation between dew point and concentrations of SO_3 and H_2O in the flue gas.

Removal rate of gaseous HCl is typically over 99%.

Stainless steels are susceptible to pitting corrosion when chloride ions exist in the absorbent. Careful selection of materials and control of HCl concentration in the absorbent are necessary.

5.6.5.3 Fluorides

Coal-fired flue gas usually contains gaseous HF of the order of 30 ppm and removed as CaF₂ as follows:

$$HF(g) \rightarrow HF(l)$$
 (5.65)

$$2HF(l) + CaCO_3(l) \rightarrow CaF_2(s) \downarrow H_2O(l) CO_2(g) \uparrow \qquad (5.66)$$

Removal rate of gaseous HF is over 98% in the JBR reactor system.

It should be noted that fluorides sometimes form inactive compounds with limestone in the presence of aluminium ions, which may block the formation of gypsum. This loss of reactive limestone can be avoided by the addition of alkali (Na or Mg) to the absorbent. It is, however, known that such inactive compounds are less likely to form at lower pH operation.

5.6.5.4 Intermediate Compounds between NO_r and SO₂

Flue gas contains NO_x of the order of 50-400 ppm, depending on the types of fuel and whether or not a $DeNO_x$ plant is installed before the FGD plant. Several percentages of NO_x are absorbed to the absorbent to form nitrates and/or nitrites.

Nitrites react with sulphites to form various types of intermediate compounds (N-S compounds) as shown in Figure 5.86. The N-S compounds end up in the waste water from the FGD plant with a concentration of the order of a few parts per million, and some of the N-S compounds are detected as COD (Chemical Oxygen Demand). A special unit for decomposing the N-S compounds can be installed as required in the waste water treatment facilities.

5.6.5.5 Sulphur Oxides Having Different Valences

The oxidation process by air is usually effective to convert sulphite with a valence of +4 to sulphate with a valence of +6, but part of the sulphite is found to stay less oxidized, forming dithiosulphate with a valence of +5 as represented by the following reaction:

$$2HSO_3^- + 1/2O_2 \to S_2O_6^{2-} + H_2O$$
 (5.67)

with the rate of reaction given by:

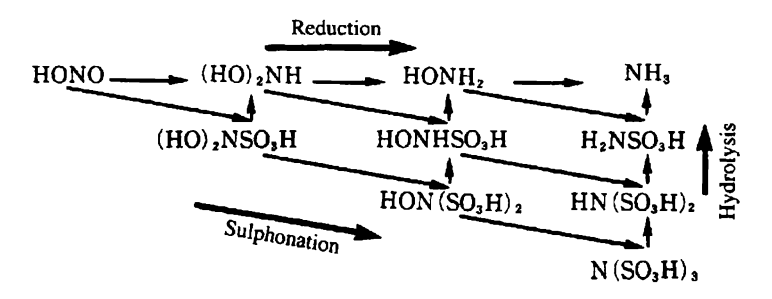


Figure 5.86 Reactions of NO_x and SO_2

$$r_{S_2O_6} = k(C_{SO_2})^2(C_{O_2})$$
 (5.68)

Dithiosulphate as the COD component is difficult to decompose in conventional waste water treating facilities. Its removal can effectively be achieved by thermal decomposition and adsorption using ion exchange resins.

5.6.6 APPLICABLE MATERIALS FOR THE WET FGD PLANT

In the wet desulphurization plant, suitable materials of construction should be selected for various equipment and their parts, in consideration of corrosive gas and liquid, erosive slurry, continuous operation, ease of maintenance, overall economics and so on. In Table 5.15 are shown the main equipment and its parts for the JBR type FGD plant, and also the materials of construction.

Table 5.15 Examples of materials of construction in JBR FGD plant

Service		Major materials of construction
GGH	Element Casing	Enamel-coated carbon steels S-TEN and C.S. + flakeglass reinforced plastic lining
Gas cooling zone	Vessel Spray nozzle	C.S. + FLRP lining FRP and ceramics
JBR	Reactor Deck-gas riser Spager Inner Pipes	C.S. + FLRP lining or 317 L S.S. or FRP solid FRP PVC FRP, 317 L S.S.
Vessels	Tank Pit	C.S. + FLRP lining or FRP solid Concrete + acid resistant lining
Gas cooling pump	Impeller Casing	Hastelloy C-276 or equivalent F.C. + rubber lining

References

- (1) Power, 134 (Oct), 156 (1990).
- (2) Power, 138 (Apr), 42 (1994).
- (3) Y. Kogawa, AIChE, Spring National Meeting, Paper No. 901 (1983).

Index

Absorptivity 66	Bubbling fluidized bed 77
Activation energy, feeding 17–18	bacoming hardined out '/
Adsorption equilibrium 29	Cascade control system 195
Adsorption rate 30	Catalyst role 22–3
Akita-Yoshida expression 127	Catalyst fold 22–3 Catalyst cracking catalyst. See Fluid
Ammonia plant reformer, sulphur	catalytic cracking (FCC)
poisoning in 262–3	Catalytic reactions 18, 81 rate 28
Ammonia synthesis 24	solid 32–3
Amorphous silica-alumina catalysts 347	
Archimedes number 124	Catalytic reforming 298
Aromatics, formation 229	Chemical engineering 105-6
Arrhenius equation 32	Chemical kinetics 3
Arrhenius plot 31	Chemical processes 7
Asahi Denka process 277	Chemical reaction engineering 3–8
Autocatalytic reaction 186	Chemical reaction rate control (CRC)
Auto-oxidation reactions 8	119
Autothermal operation 188	Chemical reactions 1
Average molecular weight (AMW) 274	classification 19
Aviation jet fuel 301	dynamic analysis 183–209
Avogadro's number 31	equilibrium 2
	factors governing 2
Batch/semi-batch (semi-continuous)/	kinetic characteristics 35
continuous systems 144	rate of 3
Batch stirred tank reactor	theory 2-3
design 84-91	types 17–38, 35
guidelines 200, 202, 203	Chemical reactors
optimal temperature profiles 201	design. See Reactor design
Batch-type reactors 4, 5, 83	types 71-81
Bessel differential equation 57	Chemical thermodynamics 10
Bessel function 57	Chemical Vapour Decomposition (CVD)
Bisphenol A (BPA) 273, 276, 277	reaction 101, 102
Black body radiation 65	Chlorides in flue gas 391-2
Boltzmann constant 31, 66	Circulating bubble column 79
Boundary conditions 50, 53, 57	Circulating fluidized bed 77
Breeding reactions of micro-organisms	CO ₂ reforming 267–9
34–5	Co-current/counter-current/cross-current
BTX 214, 231	systems 146–53
Bubble column 79	Coke formation 229–30
circulating 79	Column reactor 73
with agitator 79	with circulation 73
with outside circulation 79	Combustion reaction 18, 20, 38

Complete mixing/incomplete mixing/plug Diffusion flux 41, 42 flow systems 145-6 theorem 42 Complex reactions 18-19, 36-8, 86 Diffusion of vapour 41 heterogeneous 97-102 Discrete element method 113 homogeneous 97-102 Dispersed phase modelling 113-20 Computer fluid mechanics 107 Down flow type reactor 75 Computer graphics 107 Drag coefficient 124, 125 Concentration boundary layer 51 Dynamic analysis, chemical reactions Concentration driving force 44 183-209 Concerted reactions 228 Dynamics of steady states 167-70 Conduction of heat 39 Conradson carbon residue (CCR) 343-4 E-cat (equilibrium catalyst) 364 Consecutive reactions 38 Eddy diffusion 166-7 effect of concentration 200-2 Eddy diffusivity 132-5 effect of temperature 202-3 Electrochemical reactions 18 Constant volume batch stirred tank kinetic characteristics 35 reactor 85 Elementary reactions 18–20 governing equations 86 rate 28 Constant volume system Energy efficiency 26–8 governing equations 84–93 Energy equation 50, 57, 58 non-isothermal operation 90-1 Entrained flow/separate flow systems Contacting mode parameters 123 144-5 Continuity equation 49 Enzymes 33 Continuous flow type reactors 4, 5 Enzymic reactions 33-4 Continuous stirred tank reactor (CSTR) Epichlorohydrine (ECH) 273, 276, 277 83, 111, 113, 295 Epoxide equivalent (WPE) 274 cause and effect relationships 190, 191 Epoxy resin production 11, 212, 273-95 comparison with tubular reactor 95-6 agitation 281 design 91-4 batch operation 282-3 dynamics 184 ECH/BPA ratio 279 guidelines 202 elementary reactions 275–6 multi-stage 93, 200, 202-3, 359-60 first-stage reactor design 285-92 graphical solution 93-4 hydrolystable chlorine 293–5 Continuous tubular reactor, optimal industrial processes 276-9 structures 199 NaOH injection 281 Control systems. See Reactor control one-stage reaction process 277-9 Cooling type reactor 75 one-step process 277 Cracking furnace. See Naphtha cracking process operating factors 279-81 CVD (Chemical Vapour Decomposition) reaction model 281-2 reaction 101, 102 reaction pressure 280 reaction temperature 280 reaction time 279 Darnköhler number 112 second-stage reaction 281 second-stage reactor design 292-5 Database 3 simulation using reaction model 283-5 Desorption rate 30 Desulphurization 350-1, 377-94 two-step process 277, 278 Diesel fuels 301 water concentration in reacting liquid

280 - 1

Epoxy resins 273–4 BPA-type 273–4, 277

Diffusion 40–2

Diffusion coefficient 61, 96

Diffusion equation 50

Epoxy resins (continued)	flow scheme 339
quality parameters 274-5	fluidization forms 354
Epoxy value (EC) 274, 280	gas recovery 342
Equation of motion 49	general configuration 339
Equilibrium constant 21, 26–8	heat balance 370-5
Equilibrium products 23	heat recovery 342
Ergun's equation 128	historical background 337
Evaporation of drop in gas phase 60-1	main fractionation 342
Exothermic reaction 11, 185	material balance 369-70
cause and effect relationship 186	multi-stage CSTR model 359-60
hysteresis in 169	outline of process 339–45
	pressure 363-4
	process principle 339
Fick's law of diffusion 40	products 344-5
First-stage azeotropic reactor 11	reaction engineering model 357-64
Fixed bed reactor	reaction temperature 362
MAT 364	reactor design
thermometer allocation in 204	elementary technologies 365-9
Fixed beds, formation 74	practice 364-9
Flue gas desulphurization 14–15,	theory 352-64
377–94	reactor types and configurations 364-5
flow diagram 379	recycling 363
Fluid catalytic cracking (FCC) 13–14,	regenerator flue gas power recovery
77, 212, 298, 335–76	342
air distribution system 368	role in refining industry 336
basic theory 345-51	separation system at riser outlet 367
cat/oil ratio 362-3	simulation model 361-2
catalyst activity 364	spent catalyst distribution system 368
catalyst cooling system 368–9	stripping system 367
catalyst properties 353	technologies 13–14
catalytic cracking catalyst 347–51	WHSV 363
bottom conversion characteristics	Fluid mechanics 107
349–50	Fluidization
coke-burning ability 350	of powder bed 128
desulphurization ability 350-1	powder classification for 130 Fluidized bed reactors 188
fluidization characteristics 351	Fluidized bed reactors 188 flow conditions 173
higher octane requirement 348	Fluidized beds 76–8
hydrothermal stability at elevated temperature 348	circulating 77
metal resistance 348–9	three-phase 78
catalytic cracking reaction 345–9	two-phase theory 174
catalytic cracking/regeneration section	Fluorides in flue gas 392
339–42	Force balance 124
circulating fluidized bed model 352-7	Fourier number 63
configuration of early units 338	Fourier's law of heat conduction 39
contact time 363	Free radical chain reaction mechanism
dry gas, LPG and gasoline treatment	227–8
342	Fuel oils 302-4
effects of operating conditions 362-4	
feed injection system 367	Gas exchange coefficient 130-2
feedstock 342-6	Gas-liquid contactor 78-80

Gas-liquid interfaces 135	High mass flux effect 55-6
Gas-liquid tubular reactor 79	Homogeneous complex reactions 97–102
Gas-solid reactors 188	Homogeneous reactions, rate equations
Gasoline 301	31–2
Gibbs free energy relationship 23	Homogeneous reactors 71–3
Gibbs standard formation free energy 21	design 83–103
Graetz number 57, 59	Hydrocracking 297
Graetz problem 58	Hydrodenitrification kinetics for
Grain aggregate systems 163-6 Gypsum production and crystal growth	California coker gas oil 312
387	Hydrodesulphurization 310, 312 Hydrogen manufacturing 11, 247
361	Hydrogen plant
Hadamard condition 62	process flow diagram 249
Hadamard flow 59–60, 62	reformer design 257–9
Hadamard-Rybczynski theory 125	Hydrogenation catalysts 12
Heat balance 48, 83–4	Hydrolysable chlorine (PCL) 275
fluid catalytic cracking (FCC) 370–5	Hydroprocessing 298
Jet Bubbling Reactor (JBR) 388-90	catalyst types 306
single burning particle 168	operating conditions 309
tubular steam reforming 256	process description 309-10
Heat exchange 27	schematic process arrangement 309
Heat of reaction 21, 25	see also Catalytic reforming; Hydro-
Heat radiation 65-6	cracking; Hydrotreating
Heat transfer 4	Hydrotreating 12-13, 212, 297-334
exact solutions 53-5	applications 297
governing equations 49–50	catalysts 307
in laminar boundary layer along flat	chemical reactions 304-7
plate 49–56	feedstocks 298
inside circular tube	history 297
in laminar flow 56-9	objectives 298–304
with parabolic velocity profile	process fundamentals 304–10
(Graetz problem) 58–9	reaction kinetics 307–8
with uniform velocity profile 57–8	vacuum gas oil (VGO)
of drop in stationary gas 61	catalyst management 328–31
of group of particles and void function 63-4	catalyst volume 319–23
	catalysts 314–17
physical interpretation of dimensionless groups used in correlation 50-2	design feedstock 318 equilibrium 313-14
rate 57, 58	future trends 332-3
rate equations 39-43	heats of reaction 310–12
transfer number for 56	instrumentation 328
Heat transfer coefficient 48	material balance 319
overall 48	materials of construction 326-7
Heat transfer-controlled reaction systems	operation 328-31
4	optimum L/D ratio 327–8
Heavy metals in feedstock 344	pressure drop 325
Heterogeneous complex reactions	pressure vessels, wall thickness 325-6
97–102	process conditions 317
Heterogeneous reactions, rate equations	process control 328
32–5	process flow diagram 319
Heterogeneous reactors 74–81	reactions 310-14

Hydrotreating (continued) vacuum gas oil (VGO) (continued)	Liquid hourly space velocity (LHSV) 12, 319
	Liquid-liquid interfaces 135
reactor design 317-28 safety procedures 331-2	Liquid-phase reactions 81
space velocity 319–23	Low-sulphur fuel oil (LSFO) 298
Hysteresis in exothermic reaction systems	LPG 298
169	Lube oils 301–2
109	Lumped-parameter reactor 204
Intermediate cooling type reactor 75	Europeu-parameter reactor 204
Intermediate cooling type reactor 75 Intramolecular decomposition 228	Magaz mining condition 166.7
Irreversible reactions 24–5	Macro-mixing condition 166–7
	Mass flux 42, 44
Irrigated packed column 78	Mass transfer 4
Isolated spherical solid particle behaviour 124	continuous phase, of bubbles or drops in liquid phase 62
Isothermal reactions 153	dispersed phase 62-3
	exact solutions 53-5
Japan, petrochemical complexes in	governing equations 49-50
213–16	in laminar boundary layer along flat
Jet Bubbling Reactor (JBR) 14-15, 378	plate 49–56
absorption of SO ₂ 382-3	of bubbles, drops and particles 59-64
chemical reactions 381-8	of group of particles and void function
consumption of limestone and amount	63–4
of vaporized water 389-90	overall coefficient 44-8
diameter and height 390	physical interpretation of dimensionless
dissolution of limestone 385-6	groups used in correlation 50-2
estimation of SO ₂ removal rate 384	Mass transfer coefficients 43–8
gas-liquid-solid reactions 381-2	dimensionless groups 46
gypsum production and crystal growth	overall, and concentration profiles 47
387	various definitions 46
heat balance 388-90	Mass transfer control (MTC) 119
material balance 388-90	Mass transfer volumetric coefficient
neutralization reaction 385-6	130-2
oxidation of sulphite 383-4	MAT (Micro-Activity Tst unit) 364
physical absorption of O ₂ 383-4	Material balance 83-4
structure 380-1	fluid catalytic cracking (FCC) 369-70
unreacted limestone in product	hydrotreating of vacuum gas oil
gypsum 387–8	(VGO) 319
6,1	Jet Bubbling Reactor (JBR) 388-90
Kerosene 301	Measuring instruments, optimal alloca-
Kinetic severity function (KSF) 230-2	tion 203-4
Kinetic theory of gases 40	Membrane reactors 80-1
Kirchhoff's law 66	Michaelis-Menten reaction rate equation
Kunudsen diffusivity 162	33
,	Micro-mixing condition 166-7
Lagrange multipliers 205	Micro-organisms, breeding reactions of
Langmuir adsorption isotherm 29	34–5
Langmuir's model 29	Minimum fluidization velocity 128
Langmuir's rate equation 33	Mixed flow tank reactor 5
Lateral reactor 73	Mixing, complete/incomplete 145-6
Le Chatelier-Braun law 27	Mixing characteristics 183-5
Liquid fluidized bed 78	Molar diffusion flux 41

Molecular diffusion 166-7	technological trends 218
Molecular dynamics 3	technology trend 243-5
Monochromatic emissivity 66	typical configuration 219
Monochromatic radiation 65, 66	feed property 239
Monte Carlo method 113	feedstock properties vs yields 243
Moving beds 74–6	hot section 221-2
Multi-particle systems behaviour 125-7	quench and heat recovery 222-4
Multiphase processes, governing equa-	reaction model for yield estimation
tions for state variables of each	230-6
phase 108-13	reaction parameters and yields 239-43
Multiphase reaction processes 144-70	residence times vs yields 239-40
alternatives to state of interface 135-44	simulation method based on reaction
and chemical engineering 105-6	model 231-6
concepts 135-70	simulation results 239-43
contacting systems with porous mate-	treatment of cracked gas 221-2
rial 142–4	typical yields of once-through cracking
features of planning and design 105-8	215
model description 108-35	see also Thermal cracking
systems with flat interfaces 136–7	Newton-Laphson's method 93
systems with forced mechanical disper-	Nitrogen in feedstock 344
sion 141–2	Nitrogen-sulphur intermediate
systems with one or more phases	compounds in flue gas 392
dispersed 137–8	NO _x intermediate compounds in flue gas
systems with stabilized dispersions	392
138–41	Non-constant volume operation,
Multiphase reactors 105–81	governing equations 90
development 170–7	Nusselt number 52
interface 135	radict number 32
reasons for adopting 106–8	Olefins
scale-up 170–7	production 213
structures 144–70	reactions with radicals 228-9
Multi-stage cell model and continuous	Operating conditions 26–8
	Operating conditions 20-6
model relationship 121-3	Parabalia valosity profile 50
Multi-stage continuous stirred tank	Parabolic velocity profile 59
reactor (CSTR) 93, 293, 359–60 guidelines 200, 202–3	Parallel diffusion systems 155-8 Parallel reactions 38, 155-8
*	effect of reactant concentration
Multi-stage CSTR model 359-60	197–200
NaOH/BPA ratio 279	effect of temperature 200
Naphtha cracking 8–9, 212–45	Pelet numbers 96
coil outlet pressure (COP) vs yields 241	Petrochemical complexes in Japan
coil outlet temperature (COT) vs yields	213–16
242–3	Petroleum refining, block-flow scheme
cold section 221–2	335
cracking furnace 217-21	Phenomenological kinetics 3
chemical composition of radiant coil	Photochemical reactions 17
materials 221	kinetic characteristics 35
coil outlet pressure (COP) 244	reaction rates 36
coil outlet temperature (COT) 244	PID control system 192-4, 195
design procedure 236-9	Plasma chemical reactions 35
radiant tube and coil 219-21	kinetic characteristics 35

Plate distillation column 81 science and engineering 1-2 Plug flow reactor (PFR) 111, 113 target 83 Plug flow systems 145-6 see also specific applications and types Plug flow tubular reactor 5 Reactor dynamics Polycondensation reactions 11 and mixing characteristics 183-5 Polymerization 186 classification 183 Polymerization degree 274 definition 183 Population balance 113-20 Reactor optimization 194-209 Prandtl number 51, 54, 61 classification of problems 194-7 Proportional coefficient 30 optimal allocation of measuring instruments 203-4 solution to minimization problem with Quasi-Newton method 206-8 constraints 204-8 Reactor stability 185–8 Reactors Radial flow type reactor 75 basic concepts 5 Radiant heat transfer 65-8 comparison of characteristics 6 governing equations 66-7 types 4–8 Radiation 65-6 Recycling operation 188, 363 Ranz-Marshall correlation 61, 62 Reflectivity 66 Rate-determining step 36–7 Reforming catalyst 10 Rate equations Residual oil fluidized catalytic cracking chemical reactions 35-6 (RFCC) process 14, 339, 364 heat transfer 39-43 Reversible reactions 24-5 heterogeneous reactions 32-5 Reynolds number 50, 61 homogeneous reactions 31-2 Riser reactor 339 Reacting systems, patterning 38 Runge-Kutta Method 89–90 Reaction modelling 36 Reaction progress, direction 21-2 Reaction rate constant 119 Schmidt number 51, 54, 61 Reaction rates 28-36 Schottky diffusion 162 factors governing 30-6 Second-stage solvent reactor 11 photochemical reactions 36 Self-thermal-exchange reactor 75 predications 3 Semi-batch/cross-current contacting tubular reactor 98 systems 151-3 Reactor control 188-94 Series diffusion systems 158–63 determination of functional relation-Series reaction systems 158-63 Sherwood number 51, 52, 58, 59, 159 ships 192-4 Similarity transformation 52-3 optimal control problems 196, 208-9 selection of controlled variables 190 SO₂ removal 382-3 selection of manipulated variables 192 Sodium in feedstock 344 Reactor design Solid dispersed systems basic equations 83 behaviour 127-30 basis for 4 flow regimes 129 factors 19-21 Spouted bed 77 for industrial processes 8-15 Spray column 78 fundamentals 69 Stability of steady states 167–70 industrial reactors 211 Stangeland chart 300, 302 Statics of steady states 167-70 methodology 4 optimal design guidelines 196-203 Steam reforming process. See Tubular

steam reforming

optimal design problem 196

Stefan-Boltzmann law 66	dynamics 185
Stirred tank reactor 72-3, 83	flow velocity distribution 187–8
dynamics 185	gas-phase reactions with constant
mixing of fluid 187	pressure in 96
relationships between manipulated and	governing equations 94–5
controlled variables 193	guidelines 202
see also Batch stirred tank reactor;	mixing of fluid 187
Continuous stirred tank reactor	plug flow 5
(CSTR)	reaction rate 98
Stream lines of gas around bubble 131	Tubular steam reforming 9–11, 212,
STY (space time yield) 11	247–71
Sulphur in feedstock 343	alternatives 269–70
Sulphur oxides in flue gas 392–3	carbon-free operation 266
Sulphur poisoning in ammonia plant	carbon formation 264–7
reformer 262–3	carbon limits 264–7
Sulphur trioxide in flue gas 391	catalyst 259-61
Surface reactions 153–66	catalyst effective activity 263 catalyst particle size 260-1
Tank reactor 7–8	characteristic temperature, conversion, reaction rate and catalyst
Temperature control systems 195	effectiveness factor profiles 254
Temperature dependency 37, 102	CO ₂ reforming 267-9
Terminal velocity 124	effectiveness factor 259
Thermal cracking 213	enthalpy of formation 255
mechanism 226–30	equilibrium calculations 251–2
thermodynamics 224–5	equilibrium constants 250
see also Naphtha cracking	heat balance 256
Thermal radiation 65	heat transferred per unit time and unit
Thermal reactions 18, 31	volume of catalyst 257
Thermochemical reactions, kinetic char-	higher hydrocabons 269
acteristics 35	history 247–8
Thermodynamics 10, 27	poisoning 262–3
Thermometer allocation in fixed bed	reaction rate 259-61
reactor 204	reactions 248-52
Thiele number 157	reformer furnace 252-9
Three-phase contactor 80	reformer tubes 253, 256
Three-phase fluidized bed 78	tube coils 254
Tons per calendar day (TPCD) 318	
Tons per stream day (TPSD) 318	Unidirectional diffusion 42
Transfer line exchanger (TLE) 224, 225	Uniform reactions 153-66
Transfer number	Unstable phenomena 185-7
for heat transfer 56	•
for mass transfer 55	Vacuum gas oil (VGO) 298, 303
Transfer processes, relations with 38	hydrotreating. See Vacuum gas oil
Transmissivity 66	(VGO)
Tube-wall reactor 81	Velocity profile 56, 59
Tubular reactor 7, 71-2, 81, 83	Void fraction 128, 356-7
comparison with continuous stirred	Void function 63–4
tank reactor 95-6	
continuous 199	Weight hourly space velocity (WHSV)
design 94-6	360

Wet flue gas desulphurization 212, 377-94 materials of construction 393 process description 378-80 reactive impurities 391-3
Wetted-wall column 78

Whisker coke formation 229 WHSV (weight hourly space velocity) 360

Ziegler-Natta catalyst 18 Zone reactions 153-66